UNIVERSITY OF CAMBRIDGE

The role of macrophage intracellular lipid partitioning in glucose and lipid homeostasis during obesity

Kasparas Petkevicius

Wolfson College

This dissertation is submitted for the degree of
Doctor of Philosophy

Department of Clinical Biochemistry &
Institute of Metabolic Science
University of Cambridge

Supervisor: Professor Antonio Vidal-Puig

March 2018

Declaration

This dissertation is the result of my own work and includes nothing which is the outcome of work done in collaboration except as declared in the Preface and specified in the text.

It is not substantially the same as any that I have submitted, or, is being concurrently submitted for a degree or diploma or other qualification at the University of Cambridge or any other University or similar institution except as declared in the Preface and specified in the text. I further state that no substantial part of my dissertation has already been submitted, or, is being concurrently submitted for any such degree, diploma or other qualification at the University of Cambridge or any other University or similar institution except as declared in the Preface and specified in the text.

This dissertation does not exceed 60,000 words.

Signed:

Date:

Summary

Obesity-associated metabolic disorders are amongst the most prevalent causes of death worldwide. Understanding how obesity leads to the development of the Metabolic Syndrome (MetS) and cardiovascular disease (CVD) will enable the development of novel therapies that dissociate obesity from its cardiometabolic complications.

Our laboratory views the functional capacity of white adipose tissue (WAT), the organ designed for safe lipid storage, as a key factor in the development of MetS and CVD. At a genetically-defined stage of the **aberrant WAT expansion** that occurs during obesity, adipocytes undergo a **functional failure**, resulting in an impaired control of serum free fatty acid (FFA) concentration. In such setting, FFAs and their metabolic derivatives accumulate in other organs, where they cause **lipotoxicity**, leading to the development of insulin resistance and CVD. We therefore aim to understand the **pathophysiological mechanisms that induce adipocyte dysfunction**.

The past two decades of research have established the immune system as an important regulator of WAT function. The number of adipose tissue macrophages (ATMs), the most abundant immune cell type in WAT, increases during obesity, resulting in WAT inflammation. Multiple genetic and pharmacological intervention studies of murine models of obesity have assigned a causal link between ATM pro-inflammatory activation and WAT dysfunction. However, while the propagation of inflammation in ATMs during obesity has been extensively studied, **factors triggering ATM inflammatory activation are less clear**.

Recently, our lab has observed lipid accumulation in the ATMs isolated from obese mice. Lipid-laden ATMs were pro-inflammatory, leading us to **hypothesise that aberrant lipid build-up in macrophages triggers WAT inflammation during obesity**. This thesis expands on the initial findings from our lab and describes two novel mechanisms that potentially contribute to lipid-induced inflammatory activation of ATMs.

In **chapter 3**, **the role of *de novo* phosphatidylcholine (PC) synthesis pathway during lipotoxicity in macrophages** is addressed. The first part of the chapter demonstrates that lipotoxic environment increased *de novo* PC synthesis rate in bone marrow-derived macrophages (BMDMs) and ATMs, and that loss of rate-limiting enzyme in *de novo* PC synthesis pathway, **CTP:phosphocholine cytidylyltransferase α (CCTα)** diminished saturated FFA-induced inflammation in BMDMs. In the second part, I show that macrophage-specific CCTα deletion did not impact on the development of WAT inflammation or systemic insulin resistance, but had a minor benefitial effect on hepatic gene transcription during obesity.

Chapter 4 develops on recent observations of interactions between **sympathetic nerves and macrophages** in WAT. In the first part of the chapter, I demonstrate that stimulating **β2-adrenergic receptor (β2AR)**, the main receptor for sympathetic neurotransmitter **norepinephrine** in macrophages, enhanced intracellular triglyceride storage by up-regulating diacylglycerol O-acyltransferase 1 (*Dgat1*) gene expression in BMDMs. The second part of the chapter shows that macrophage-specific β2AR deletion did not modulate systemic glucose and lipid metabolism during obesity, but mice lacking β2ARs in macrophages demonstrated augmented hepatic glucose production on a chow diet. Furthermore, systemic β2AR blockade or macrophage-specific β2AR deletion in mice did not affect the thermogenic response to cold exposure.

Chapter 5 includes the characterisation of β2AR stimulation-induced changes to the global cellular proteome of BMDMs, and a subsequent validation of the role of candidate transcription factors in regulating β2AR agonism-induced gene expression in BMDMs.

Table of contents

Acknowledgements

My special thanks to my supervisor **Professor Toni Vidal-Puig** for allowing me to join his laboratory. I am most grateful to him for the creative freedom and all the opportunities I have been given throughout my PhD, which was critical for my scientific development. I am also thankful for Toni's regular advice during my PhD, which facilitated my professional and personal development. Furthermore, thanks to Toni for taking interest in my future scientific career.

Huge thanks to **Dr. Samuel Virtue** for his guidance and support throughout my PhD. Sam not only gave me a solid technical background in laboratory techniques and animal work, but also taught me his unconventional ways of thinking about animal physiology and experimental design.

I am also thankful to all the members of the **TVP lab** for supporting me during my PhD and making my stay in the laboratory enjoyable. In particular, thanks to **Dr. Guillaume Bidault** for his frequent assistance in my experiments and scientific advice; **Dr. Michele Vacca, Dr. Vanessa Pellegrinelli, Dr. Sergio Rodriguez-Cuenca, Dr. Stefania Carobbio, Dr. Vivian Peirce, Mr. Mark Campbell** and **Mr. Martin Dale** for their help and advice; to **Mrs. Agnes Lukasik** for genotyping my mice.

Many thanks to **Mr. Daniel Hart**, **Miss Jade Bacon**, **Mrs. Sarah Grocott**, **Miss Haidee Pit** and **Mr. Harry Hellmers** for taking excellent care of all my experimental animals; to **Ms. Charley Beresford** and **Mrs. Laura McKinven** for setting up my animal breedings and weaning the litters; and to **Dr. Amy Warner**, **Miss Hannah Webber** and **Dr. Anne Mcgavigan** for their assistance in ordering animals and writing study plans.

I am very grateful to my collaborator **Prof. Kathryn Lilley** for allowing me to perform a large-scale proteomics analysis in her laboratory, and to **Dr. Houjiang Zhou** from her group for supervising me through the sample preparation for proteomics and for analysing my samples by LC-MS/MS. Also thanks to **Mr. Aurelien Dugourd** from **Prof. Julio Saez-Rodriguez**'s group for performing bioinformatics analysis of the proteomics data.

Many thanks to **Mr. Hong Liu** and **Prof. Gerard Karsenty** for donating me *Adrb2*-floxed mice and coordinating their shipment to the UK.

I am also grateful to **Dr. Susan Fitzpatrick** and to **Prof. Randall Johnson** for providing me with the bones from macrophage-specific *Hif1a* and *Hif2a* knockout mice.

Huge thanks to the **Wellcome Trust** and the **British Heart Foundation** for funding my PhD.

Finally, thanks to my girlfriend **Karine**, my sister **Justina**, my parents **Renata** and **Valdas**, my grandparents **Jakaterina, Saulius, Irena** and my late grandfather **Jonas** for their continuous love, support and encouragement throughout my PhD.

Contributions of collaborators

Some of the figures in the *Introduction* were provided by **Dr. Guillaume Bidault**, **Dr. Vanessa Pellegrinelli** and **Dr. Vivian Peirce**, as indicated in legend.

Some of the preliminary data presented in *Chapter 3* was acquired by **Dr. Xavier Prieur, Dr. Crystal Mok** and **Dr. Guillaume Bidault**, as indicated in legend. Some of the preliminary data in *Chapter 3* was analysed by **Dr. Samuel Virtue** and a PhD student **Mr. Cankut Cubuk** from **Prof. Joaquin Dopazo**'s group, as indicated in legend.

Dr. Guillaume Bidault performed flow cytometry analysis of the experiment presented in *Chapter 3*.

Dr. Samuel Virtue provided substantial assistance in optimising and performing *in vivo* macrophage-to-liver phosphatidylcholine transfer assay presented in *Chapter 3*.

Disease Model Core staff **Mr. Daniel Hart**, **Miss Jade Bacon**, **Mrs. Sarah Grocott**, **Miss Haidee Pit** and **Mr. Harry Hellmers** performed animal husbandry, animal and diet weighing, and set up energy expenditure experiments presented in *Chapters 3 and 4*.

All serum biochemical measurements presented in *Chapters 3 and 4* were performed by **Cambridge University Hospitals NHS Foundation Trust Core Biochemical Assay Laboratory**.

Dr. Samuel Virtue and **Dr. Anne Mcgavigan** performed hyperinsulinaemic-euglycaemic clamp experiments and subsequent analyses presented in *Chapter 4*.

Dr. Houjiang Zhou from **Prof. Kathryn Lilley**'s group provided substantial technical assistance in sample preparation for quantitative proteomics. **Dr. Houjiang Zhou** performed LC-MS/MS analysis for quantitative proteomics. Bioinformatics analysis of quantititave proteomics experiment presented in *Chapter 5* was performed by a PhD student **Mr. Aurelien Dugourd** from **Prof. Julio Saez-Rodriguez**'s group.

Seahorse analyses and mitochondrial reactive oxygen species measurement in BMDMs presented in *Chapter 5* were performed by **Dr. Guillaume Bidault**.

Setting up of breedings and weaning of experimental animals were performed by **Ms. Charley Beresford** and **Mrs. Laura McKinven**. All animal genotyping was performed by **Mrs. Agnes Lukasik**.

Abbreviations

2-DG	2-deoxyglucose
α1AR	α1-adrenergic receptor
α2AR	α2-adrenergic receptor
ABC	ATP-binding cassette
AC	adenylyl cyclase
ACAT1	acyl-CoA:cholesterol acyltransferase 1
ACSL	acyl-CoA synthetase
ADRP	adipose differentiation-related protein
AKR	aldo-keto reductase
ALDH	aldehyde dehydrogenase
ALT	alanine transaminase
ANCOVA	analysis of covariance
ANGPTL4	angiopoietin-like 4
APOA	apoliprotein A
APOB	apoliprotein B
ARG1	arginase 1
AST	aspartate transaminase
ATF1	activating transcription factor 1
ATGL	adipose triglyceride lipase
ATM	adipose tissue macrophage
ATP	adenosine triphosphate
AUC	area under curve
β1AR	β1-adrenergic receptor
β2AR	β2-adrenergic receptor

β3AR	β3-adrenergic receptor
BAT	brown adipose tissue
BMDM	bone marrow-derived macrophage
BMI	body-mass index
BMP	bone morphogenic protein
bp	base pair
BSA	bovine serum albumin
cAMP	cyclic adenosine monophosphate
CBP	CREB-binding protein
CCL	CC chemokine ligand
CCR	CC chemokine ligand receptor
CCT	CTP:phosphocholine citidyltransferase
CHOP	C/EBP homologous protein
CLS	crown-like structure
CLS	cardiolipin
CoA	coenzyme A
COMT	catechol-O-methyltransferase
COX	cyclooxygenase
CPT	carnitine palmitoyltransferase
CRE	cAMP-responsive element
CREB	cAMP-responsive element-binding protein
CRTC	CREB-regulated transcription coactivator
CSF-1	colony stimulating factor-1
CVD	cardiovascular disease
c-Src	proto-oncogene tyrosine-protein kinase Src
DAG	diacylglycerol

DAMP	damage-associated molecular pattern
DBH	dopamine b-hydroxylase
DGAT	diacylglycerol acyltransferase
DHA	docosahexaenoic acid
DNA	deoxyribonucleic acid
DNL	*de novo* lipogenesis
dpm	disintegrations per minute
DUSP1	dual specificity phosphatase
EAE	experimental autoimmune encephalitis
ECAR	extracellular acidification rate
ECM	extracellular matrix
ECT	CTP:phosphoethanolamine citidyltransferase
EE	energy expenditure
ELISA	enzyme-linked immunosorbent assay
ELOVL	Elongation of very long chain fatty acids
EPA	eicosapentaenoic acid
ER	endoplasmic reticulum
ERK	extracellular signal-regulated kinase
eWAT	epididymal white adipose tissue
FABP	fatty acid-binding protein
FADS	fatty acid desaturase
FAME	fatty acid methyl ester
FAO	fatty acid oxidation
FASN	fatty acid synthase
FATP	fatty acid transport protein
FBP1	fructose-1,6-bisphosphatase 1

FBS	fetal bovine serum
FFA	free fatty acid
G6PC	glucose-6-phosphatase
GC	gas chromatography
GDF3	growth differentiation factor-3
GIR	glucose infusion rate
GNMT	Glycine N-methyltransferase
GO	Gene Ontology
GPR/GPCR	G protein-coupled receptor
GPX	glutathione peroxidase
GRK	GPCR kinase
GTT	glucose tolerance test
GWAS	genome-wide association study
gWAT	gonadal white adipose tissue
HDAC4	histone deacetylase 4
HDL	high-density lipoprotein
HFD	high-fat diet
HGP	hepatic glucose production
HIF	hypoxia-inducible factor
IBD	inflammatory bowel disease
IKK	IκB kinase
IL	interleukin
IRE1α	inositol-requiring enzyme 1α
IRF	interferon regulatory factor
ITT	insulin tolerance test
JNK	c-Jun N-terminal kinase

KLF	Krüppel-like factor
LAL	lysosomal acid lipase
LC	liquid chromatography
LCAT	lecithin-cholesterol acyltransferase
LDL	low-density lipoprotein
LO	lipoxygenase
LPCAT	acyl-CoA:lysophosphatidylcholine acyltransferase
LPL	lipoprotein lipase
LPS	lipopolysacharide
LSC	liquid scintillation counting
LTT	lipid tolerance test
LXR	liver X receptor
MACS	magnetic-activated cell sorting
MAO	monoamine oxidase
MAPK	mitogen-activated protein kinase
MAT	monoamine transporter
MAT1A	methionine adenosyltransferase 1A
MCP1	monocyte chemotactic protein 1
MCT4	monocarboxylate transporter 4
MetS	Metabolic Syndrome
MGL1	macrophage lectin 1
mRNA	messenger ribonucleic acid
MS	mass spectrometry
MSK	mitogen and stress activated protein kinase
MUFA	monounsaturated fatty acid
NADPH	nicotinamide adenine dinucleotide phosphate

NASH	non-alcoholic steatohepatitis
NCoR	nuclear receptor co-repressor
NE	norepinephrine
NET	norepinephrine transporter
NF-κB	nuclear factor-kappa B
NLR	Nod-like receptor
OCR	oxygen consumption rate
OxPhos	oxidative phosphorylation
PA	phosphatidic acid
PAMP	pathogen-associated molecular pattern
PBS	phosphate-buffered saline
PC	phosphatidylcholine
PCK1	phosphoenolpyruvate carboxykinase 1
PCR	polymerase chain reaction
Pcyt1	CTP:phosphocholine citidyltransferase (gene)
Pcyt2	CTP:phosphoethanolamine citidyltransferase (gene)
PE	phosphatidylethanolamine
PEMT	phosphatidylethanolamine N-methyltransferase
PGC1	PPAR coactivator 1
PI	phosphatidylinositol
PKA	protein kinase A
PKC	protein kinase C
PLTP	phospholipid transfer protein
PPAR	peroxisome proliferator-activated receptor
PRR	pattern recognition receptor
PS	phosphatidylserine

PTDSS	phosphatidylserine Synthase
PUFA	polyunsaturated fatty acid
qRT-PCR	quantitative real-time PCR
RER	respiratory exchange ratio
ROS	reactive oxygen species
RPKM	reads per kilobase per milion mapped reads
RPMI	Roswell Park Memorial Institute
RQ	respiratory quotient
RT	room temperature
RXR	retinoid X receptor
SAM	S-adenosylmethionine
SAM	sympathetic-associated macrophage
SCAP	SREBP-cleavage activating protein
SCD	stearoyl-CoA desaturase
scWAT	subcutaneous white adipose tissue
SEM	standard error of mean
SERCA	sarco/endoplasmic reticulum Ca^{2+}-ATPase
SIK	salt-inducible kinase
SIM	single ion monitoring
SM	sphingomyelin
SNP	single nucleotide polymorphism
SNS	sympathetic nervous system
SP1	specificity protein 1
SPE	solid phase extraction
SREBP	sterol regulatory element-binding protein
SVF	stromal vascular fraction

TANK	TRAF family member-associated NF-κB activator
TBK1	TANK binding kinase 1
TCA	tricarboxylic acid
TG	triglyceride
TH	tyrosine hydroxylase
THBS1	thrombospondin 1
TLC	thin layer chromatography
TLR	toll-like receptor
TNFα	tumour necrosis factor α
UCP1	uncoupling protein 1
VEGFA	vascular endothelial growth factor A
vLDL	very low-density lipoprotein
VSN	variance stabilisation normalisation
vWAT	visceral white adipose tissue
WAT	white adipose tissue
WT	Wild-type
XBP1	X-box binding protein 1
ZT	Zeitgeber time

1 Introduction

1.1 Adipose tissue inflammation and the development of insulin resistance

1.1.1 Obesity and Metabolic Syndrome

Obesity has reached epidemic proportions worldwide, with around 670 million people having a body-mass index (BMI) over 30 kg/m^2 and clinically defined as being obese[1]. Obesity is widely associated with the range of metabolic dysfunctions, including insulin resistance, high blood pressure and dyslipidaemia, which are collectively termed the Metabolic Syndrome (MetS)[2,3]. Individuals with MetS exhibit a substantially greater risk of developing type-2 diabetes and cardiovascular disease (CVD) compared to the general population[4]. Both type-2 diabetes and CVD are amongst the highest causes of mortality in the world, with 8.76 million of deaths per year attributed to ischaemic heart disease (#1 cause of death globally), 6.24 million – to stroke (#2 cause) and 1.59 million – to type-2 diabetes (#6 cause)[5]. Furthermore, treating patients with mentioned diseases represent a substantial financial burden on health care systems worldwide[5].

Current weight loss interventions, such as diet, exercise and pharmaceuticals, as well as therapeutic strategies targeting MetS have all had limited success[6]. While bariatric surgery can dramatically reduce the body weight and improve metabolic status of the patient, it is generally expensive and there are numerous risks and complications involved, such as bowel obstruction, gallstones, ulcers and subsequent malnutrition[7]. Therefore, deeper understanding of pathophysiological mechanisms driving MetS is required for the development of novel treatments.

1.1.2 Obesity is caused by positive energy balance

The obesity epidemic is caused by increased food intake and a more sedentary lifestyle observed in modern humans[8]. These two factors can be viewed as increased energy input and decreased energy output, resulting in a positive energy balance. Like all living organisms, animals store excess energy as chemical bonds in the form of carbohydrates and fats. Positive energy balance in mammals predominantly manifests in the form of fatty acids, which are physiologically stored as calorie-dense triglycerides (TGs) in white adipose tissue (WAT)[9].

The ability to store energy as lipids allowed animals to survive through prolonged periods of food scarcity and thus was evolutionarily conserved[10]. However, low food abundance is no longer a threat to modern humans living in developed countries, rendering such evolutionary adaptation obsolete and damaging from the health and environmental points of view. The feeding behaviour and energy expenditure of humans is still governed by genetic mechanisms shaped through millions of years of evolution[10]. The 'thrifty gene' hypothesis[11] thus states that genes which enabled individuals to efficiently collect and process food to deposit fat during periods of food abundance in order to provide energy during periods of food shortage are now acting as the main drivers of obesity in the current environment. While high degree of heritability (approximately 60-80%) of BMI estimated by monozygotic twin studies supports this hypothesis[12,13], it is still being questioned by the scientific community, with main counterargument being the fact that the majority of the population remains lean despite the overabundance of food[14,15]. Indeed, it has been suggested that over the course of evolution, humans have been under pressure to remain lean in the obesogenic environments in order to decrease the risk of predation. Individuals storing more fat may be less manoeuvrable and slower to evade predators and hence higher fat storage increases predation mortality[16-18].

Amongst all brain regions involved in regulating energy balance in vertebrates, hypothalamus has a central role[19]. It consists of multiple nuclei of neurons that infer the energy status of the animal by directly sensing circulating nutrients and by integrating signals from peripheral hormones. The fine balance of orexigenic and anorectic stimuli in hypothalamus lead to the stimulation of foraging behaviour in a fasted state[19]. Most genes linked to an increased BMI by large-scale genome-wide association studies (GWAS) are thus thought to play a direct role in energy balance sensing in hypothalamus[20,21].

1.1.3 Distribution of adipose tissues in humans and mice

Two functionally and morphologically distinct types of adipose tissue exist in most mammals – white and brown. WAT can be further divided into two main distinctive types according to their anatomical location – subcutaneous (scWAT) and visceral (vWAT)[22]. scWAT is located between skin and muscle layers, and is primarily found in the abdomen and gluteofemoral region in humans[22] (Figure 1-1 B). vWAT surrounds and cushions inner organs in the abdominal cavity and consists of omental, mesenteric, retroperitoneal, gonadal (gWAT, attached to the uterus and ovaries in females and epididymis and testis in men) and epicardial depots in humans[22] (Figure 1-1 B). Mice have two main scWAT depots – anterior (located in the head and neck region) and flank (located in the upper leg region), and four vWAT depots – mesenteric, retroperitoneal, perirenal and gonadal (epididymal or eWAT in male mice)[22] (Figure 1-1 A). Epididymal WAT depots are substantially larger in mice than in humans.

Two main depots of brown adipose tissue (BAT) exist – interscapular and mediastinal in mice[23], and supraclavicular and subscapular in humans[24] (Figure 1-1 A,B).

The most commonly studied representative adipose tissue depots in mice are inguinal (flank) scWAT, gWAT and interscapular BAT (Figure 1-1 A). They are also the only adipose tissue depots investigated in this thesis.

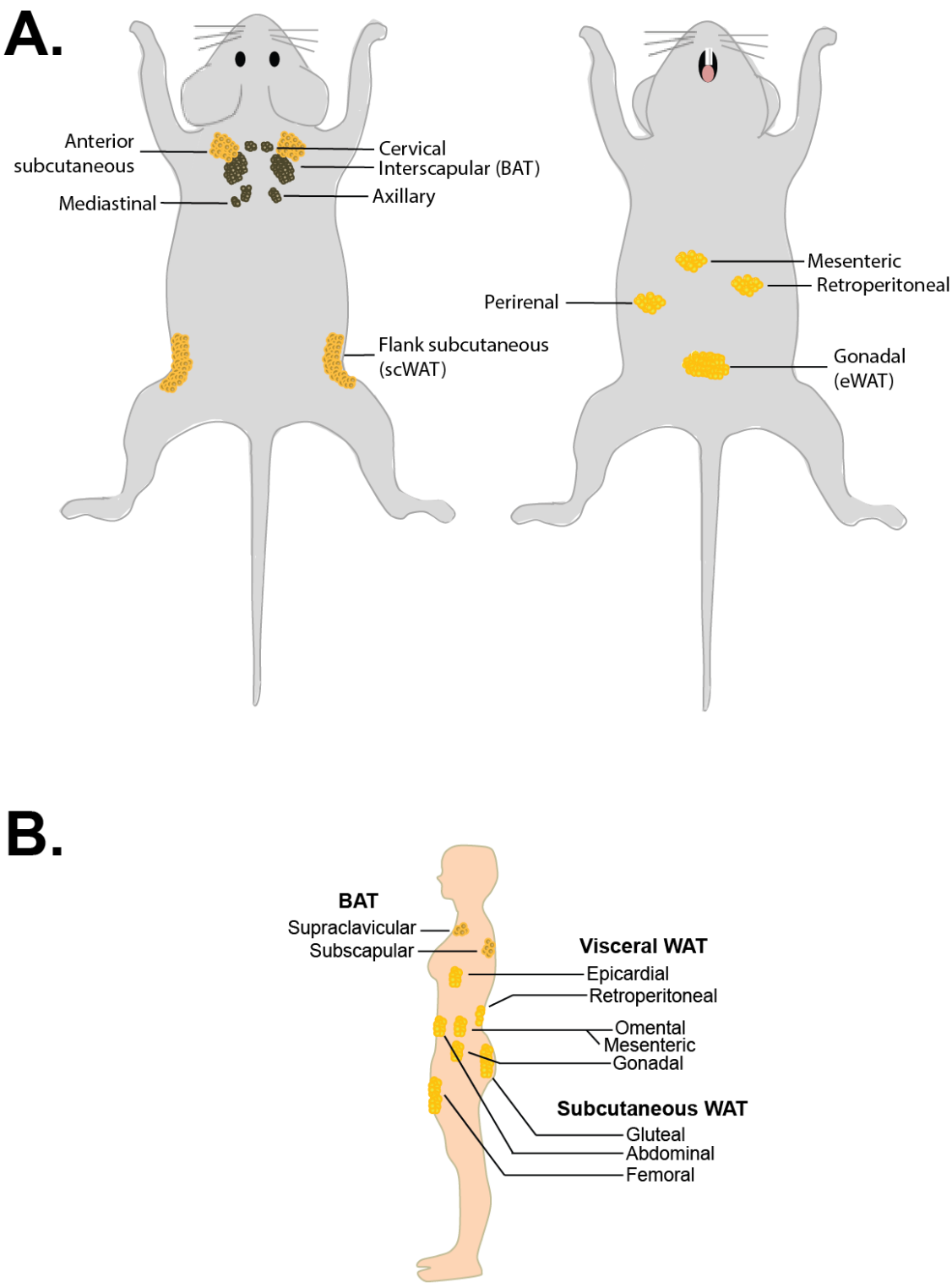

Figure 1-1. Distribution of white and brown adipose tissue depots in mice and humans.

*Anatomical location of indicated WAT and BAT depots in (**A**) mice and (**B**) humans. In (**A**), depots indicated as BAT, scWAT and eWAT were analysed as representative depots for each type of adipose tissue in this thesis. Figure provided by Dr. Vanessa Pellegrinelli and Dr. Vivian Peirce.*

1.1.4 Functions of WAT

WAT is a connective tissue with the adipocyte being its parenchymal cell[25]. The primary functions of adipocytes are postprandial energy storage as TGs in lipid droplets and the release of this energy as free fatty acids (FFAs) via the process of lipolysis in a fasted state. Both of these processes are tightly regulated by multiple local and peripheral signals, including hormones, cytokines, neurotransmitters and lipid mediators, all converging on the adipocyte[25].

1.1.4.1 Postprandial lipid clearance role of WAT

Meal ingestion leads to an increased serum glucose and lipid concentration. Postprandial circulating lipids are predominantly TGs and cholesterol esters packaged into chylomicrons by intestinal epithelial cells, and very low- and low-density lipoproteins (vLDL and LDL) released by hepatocytes following chylomicron delivery to the liver[26]. Pancreatic beta cells directly respond to increased serum glucose by secreting insulin into the circulation, which signals to multiple tissues to promote glucose disposal. While the majority of glucose is taken up by muscle and liver to form glycogen in an insulin-dependent manner[27], WAT responds to insulin by secreting lipoprotein lipase (LPL). LPL is anchored to the extracellular side of the plasma membrane, where it digests chylomicrons and vLDL and liberates FFAs[28]. Insulin simultaneously promotes FFA uptake and esterification in adipocytes, therefore reducing postprandial lipid load[28] (Figure 1-2). Furthermore, adipocytes also contribute to the normalisation of postprandial glucose concentration by taking up glucose via insulin-regulated glucose transporter GLUT4 and converting it to FFAs through the process of *de novo* lipogenesis (DNL)[28] (Figure 1-2). Overall, WAT plays a major role in the resolution of a postprandial state.

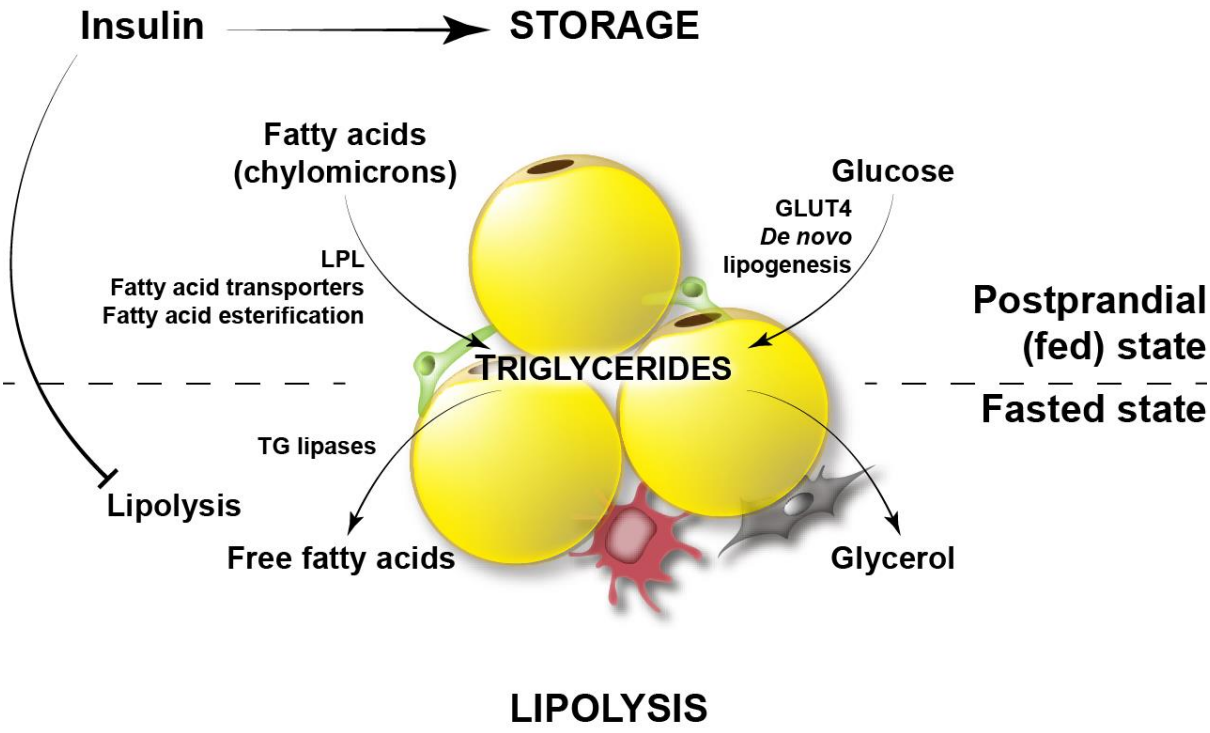

Figure 1-2. Energy storage and lipolysis functions of WAT.

The top part of the figure illustrates the processes occurring in WAT in a postprandial state, while the bottom part – in the fasted state of the animal. Figure provided by Dr. Guillaume Bidault.

1.1.4.2 Basal and on-demand systemic energy supply role of WAT

WAT maintains a consistent FFA supply to other organs by basal lipolysis, which is greatly supressed by insulin in a postprandial state[29] (Figure 1-2). During states when the energy requirement of tissues cannot be maintained solely by circulating glucose and basal lipolysis, the hypothalamus signals to WAT via sympathetic nervous system (SNS) to promote on-demand lipolysis[29]. The SNS can deliver the signal directly to WAT in a form of norepinephrine (NE) released locally from bundles of sympathetic nerves, or indirectly by promoting the release of epinephrine into circulation by chromaffin cells of the adrenal medulla. Both NE and epinephrine act on β-adrenergic receptors on adipocytes, initiating an intracellular signalling cascade that rapidly culminates in TG hydrolysis and FFA release[29].

1.1.4.3 Role of WAT in circadian nutrient metabolism

All animals exhibit a circadian pattern of feeding, sleeping and other biological activities[30]. Diurnal animals, such as humans, are active during the light phase of the day and sleep during the dark phase, while nocturnal animals behave in the opposite

manner. The majority of foraging and food consumption occurs during the active phase for any given species[30]. This temporal imbalance causes WAT to predominantly store lipids during the active phase, and release them into circulation during the resting phase[31]. Most other tissues have also adapted to this paradigm by utilising glucose as a fuel when it is readily available in the active phase, and then switching to fatty acid oxidation (FAO) when glucose availability is reduced in the resting phase[31]. WAT therefore was instrumental for efficient animal adaptation to circadian rhythmicity.

1.1.4.4 Energy storage and insulating roles of WAT

Environments with high degree of seasonal temperature variation typically only provide adequate food supply during the warm period of the year. Consequently, most mammals living in such environments display a circannual pattern of food intake, with a vast majority of calories ingested during summer. This period of hyperphagia in mammals is also signified by a massive expansion of WAT, leading to the development of muscle insulin resistance and increased circulating insulin levels[32]. Such dynamic WAT expansion allows mammals to enter a state of hibernation in winter, when food availability is sparse and TGs stored in adipocytes become the sole source of energy until spring[32]. Increased scWAT content also serve an insulating function that conserves energy required for thermogenesis[32]. WAT therefore allowed animals to inhabit continental climate areas without the need of circannual migration.

1.1.4.5 Endocrine role of WAT

Besides its aforementioned primary functions, WAT is also an endocrine organ, secreting specific hormones termed adipokines into circulation[33]. Leptin was the first adipokine to be discovered in 1994[34], and since then it has been prescribed a plethora of roles, including suppression of appetite[35,36] and activation of the SNS output to adipose tissues in hypothalamus[37,38], promotion of FAO in muscle[39] and inhibition of bone formation[40]. Mouse and human homozygous carriers of inactivating mutations in leptin gene (ob/ob mouse strain) are hyperphagic and become obese early in life[34,41], which can be reversed by supplementation with exogenous leptin[36,42]. Adiponectin is another abundant circulating adipokine mediating peripheral insulin sensitivity[43]. Adiponectin-deficient mice are more insulin resistant despite having the same fat mass as controls[44]. Besides leptin and adiponectin, multiple other adipokines with important roles in metabolic homeostasis and pathophysiology have been identified[33], which are beyond the scope of this thesis.

1.1.5 Functions of BAT

Like white adipocytes, brown adipocytes in BAT contain TG-rich lipid droplets. However, they have substantially more mitochondrial mass than white adipocytes and express uncoupling protein 1 (UCP1)[45]. In most cells, oxidation of energy substrates culminates in the mitochondrial electron transport chain, which utilises the bond-dissociation energy to transport the protons from mitochondrial matrix to intermembrane space, creating a proton gradient and energy potential across the inner mitochondrial membrane. Adenosine triphosphate (ATP) synthase and UCP1 are both localised on the inner mitochondrial membrane and allow the protons to leak back to the mitochondrial matrix[45]. ATP synthase couples this dissipation of energy potential to the production of ATP, which serves as an energy donor to fuel most cellular reactions. UCP1 does not couple the proton leak to a chemical reaction, therefore membrane potential energy is dissipated as heat[45]. BAT utilises fatty acids stored in lipid droplets, as well circulating glucose and FFAs for UCP1-dependent heat production, which warms blood circulating through BAT and is then dispersed through the rest of the body[45]. In order to facilitate high rates of FAO for fuel production, brown adipocytes contain substantially smaller lipid droplets than white adipocytes, which allows lipolysis to occur more rapidly due to increased lipid droplet surface area to volume ratio[23].

Ability to produce heat by activating BAT allows mammals to live in the environments below their thermoneutral temperature (the temperature in which the heat produced by basal metabolic reactions is sufficient to maintain core body temperature of the animal) without the need of constant shivering. Cold environmental temperature of the animal is mainly sensed by peripheral sensory neurons that signal to the hypothalamus, which then rapidly increases SNS outflow to BAT[45]. NE released from sympathetic nerves acts on β-adrenergic receptors on brown adipocytes, initiating lipolysis, FAO and UCP1-dependent heat production[45]. Prolonged cold exposure also results in BAT expansion and the recruitment of brown adipocytes in scWAT, a process often referred to as scWAT browning or beiging[45].

Recent reports describing functional BAT in adult humans sparked an interest in BAT activation as a potential therapy for weight loss[46] and improved systemic glucose homeostasis[47]. Genetic and pharmacological mouse models of increased BAT

activation and scWAT browning are leaner when fed obesogenic diets due to the increased oxidation of fatty acids that would otherwise accumulate in WAT[46]. However, current mechanistic knowledge of BAT activation and scWAT browning in mice and humans is still premature for the development of successful weight loss therapeutics that would not have detrimental off-target effects. As both endogenous (epinephrine and NE) and pharmacological β-adrenergic receptor agonists elicit systemic effects beyond thermogenesis, including increased heart rate and blood pressure, the main challenge in the development of successful weight loss therapies is to selectively increase β-adrenergic signalling in BAT without directly affecting other tissues[48].

1.1.6 Adipose tissue expandability hypothesis

Postprandial WAT expansion is typically counteracted by lipolysis-mediated WAT contraction in the fasted state. Due to the frequent variability in feeding and fasting periods (as discussed in 1.1.2 and 1.1.4), WAT evolved the capacity to expand greatly beyond its regular size, being able to buffer serum lipid concentrations postpradially even after prolonged periods of hyperphagia[49]. As a result, all other animal tissues have evolved in a small, WAT-buffered range of serum lipid concentration, and were under no constraints to develop adaptations to elevated levels of extracellular lipids present for prolonged periods of time[49].

The majority of obese individuals with MetS were initially lean with normally functioning WAT. Similarly, the WAT of genetically obese ob/ob mice at young ages, or of Wild-type (WT) mice before the administration of obesogenic diets, is able to appropriately take up and release FFAs. Obesogenic environments leads to hyperphagia in mice and humans, which results in a continuous WAT expansion without prolonged fasting periods. However, a genetically-defined limit to a WAT expansion[50] occurs when adipocytes become desensitised to a postprandial increase in circulating insulin, leading to impairments in FFA uptake and suppression of basal lipolysis[51]. Other metabolic organs, such as liver, muscle and kidney, are then subjected to chronically elevated circulating FFA concentrations and start to accumulate lipids[51]. Aberrant ectopic lipid accumulation causes lipid-induced toxicity (lipotoxicity), leading to impaired tissue function, particularly the inability to respond to insulin appropriately[51]. Initially, systemic insulin resistance is compensated for by the expansion of pancreatic beta cell mass and their elevated insulin production[52]. However, exhaustive insulin

production leads to apoptosis of beta cells, resulting in the loss of blood glucose level control and the development of type-2 diabetes[52]. Elevated serum lipid concentrations also promote the development of arterial plaques, thus directly contributing to the development of atherosclerosis[53].

The adipose tissue expandability hypothesis is supported by human and animal models of both increased and decreased WAT expansion capacity. Approximately 20-30% of obese human population do not exhibit symptoms of MetS, attributed to their improved WAT function[54]. Similarly, ob/ob mice overexpressing the globular domain of adiponectin demonstrate elevated WAT mass, but decreased ectopic lipid accumulation and improved systemic insulin sensitivity compared to ob/ob controls[55]. Conversely, specific genetic mutations cause lipodystrophy in humans, characterised by decreased or complete ablation of WAT mass and severe systemic insulin resistance[56]. Recapitulating such mutations in mice also impairs WAT expansion and leads to ectopic lipid deposition and the development of insulin resistance[57]. Currently, there is a lack of in-depth mechanistic understanding of how maximal WAT expansion capacity is regulated.

1.1.7 Adipose tissue inflammation

Expansion and contraction of most tissues, including WAT, requires modification of extracellular environment. As the size of the adipocytes taking up FFAs increases, the extracellular matrix (ECM) needs to be degraded to accommodate enlarged cells[58]. Furthermore, appropriate tissue expansion requires coordinated increase in vascularisation in order to maintain sufficient tissue oxygenation and nutrient supply. Formation and degradation of ECM and vascularisation processes are tightly regulated by the immune system within a tissue[58]. Coincident with its dynamic remodelling, WAT is enriched in immune cells that adopt a regulatory (anti-inflammatory) and tissue remodelling profile in metabolically healthy animals[58]. However, in obesity WAT becomes infiltrated with pro-inflammatory immune cells and exhibits low-grade sterile inflammation[59,60], as observed in other pathogen-free inflammatory diseases, such as rheumatoid arthritis or atherosclerosis[61].

While a part of the scientific community regards the sterile inflammation merely as a symptom of impaired WAT function[62], the overwhelming evidence from animal studies indicates a causative role for the immune system in the development of insulin resistance and MetS[61]. Multiple mouse models where cells of the innate or adaptive immune system had been genetically targeted demonstrated altered metabolic profile during obesity[63]. However, the evolutionary role of the immune system in the maintenance of healthy WAT function and during aberrant expansion remains unclear[61]. This thesis will focus on macrophages, the most abundant immune cell of adipose tissue, and will discuss their role in initiating and propagating WAT inflammation and insulin resistance.

1.2 Macrophages and the development of adipose tissue inflammation

1.2.1 Macrophage biology

1.2.1.1 Homeostatic roles of tissue macrophages

The macrophage is a type of leukocyte (white blood cell) of the innate immune system, highly specialised in phagocytosis (a process of cell engulfing a solid particle) of dying cells, microbes, foreign substances and cellular debris[64]. Macrophages continually monitor their environment by intra-tissue movement and macropinocytosis (non-selective uptake of water-soluble extracellular material), identify local environmental changes via a multitude of cell surface and intracellular receptors and respond to such changes by direct phagocytosis or initiation of an immune response[64]. Millions of cells at the end of their lifespan are eliminated every day from a healthy organism in a way that does not trigger damage but is instead part of a homeostatic clearance programme that involves engulfment by macrophages[65]. Sensing and phagocytosis of apoptotic cells thus maintains macrophages in the anti-inflammatory state[65]. However, recognition of environmental changes that do not typically occur in healthy tissue, such as the presence of bacterial components or elevated concentrations of intracellular metabolites in the extracellular milieu (indicating non-apoptotic, uncontrolled cell death), triggers macrophage inflammatory activation, which will be discussed in more detail further.

Besides the aforementioned functions, macrophages have acquired roles specific to the tissues they reside in. For example, Kupffer cells (liver-resident macrophages) perform erythrophagocytosis (engulfment of red blood cells at the end of their lifespan) and process and release iron into circulation, ensuring systemic iron homeostasis[66]. Alveolar macrophages (located in the lung) degrade pulmonary surfactant released by type 2 alveolar cells, maintaining adequate surfactant levels[67]. Loss of this degradation process leads to the development of pulmonary alveolar proteinosis, a disease characterised by abnormal surfactant accumulation, interfering with the ability of the lung to exchange oxygen and carbon dioxide from the blood[67]. Microglia (brain macrophages) are instrumental in modifying neuronal synaptic transmission and plasticity required for learning[68] and memory formation[69]. Overall, most tissues rely on resident macrophages to maintain their appropriate function.

1.2.1.2 Macrophage development

In the past, monocytes and macrophages were viewed as part of the continuum forming mononuclear phagocyte system[70]. According to this system, macrophages are fully differentiated cells that have lost proliferative potential and are constantly replenished by circulating monocytes produced by bone marrow-derived myeloid progenitors. However, recent lineage tracing[71-75] and parabiosis[76-79] experiments have found that most tissue macrophages, including Langerhans cells (epidermal macrophages), microglia, alveolar macrophages and Kupffer cells are renewed independently of circulating precursors in adult mice. Multiple fate-mapping studies have now established that most tissue macrophages are seeded during foetal development from precursors located in the extra-embryonic yolk sac[72,80], or from foetal liver macrophages without passing through a monocyte intermediate[81].

A model of macrophage development strictly linking tissue-resident macrophage identity to embryonic origin has shortcomings as well. Depending on the study, Kupffer cells, splenic red pulp macrophages and peritoneal macrophages display a degree of engraftment of circulating monocytes during adulthood[82,83], indicating that embryonic precursors may not be the only source of resident macrophages. Furthermore, circulating monocytes that contribute to tissue macrophage populations are capable of acquiring nearly identical phenotypes to their counterparts of embryonic origin[84-86]. Finally, bone marrow-derived precursors can rapidly repopulate tissues after the

ablation of resident macrophages by irradiating mice[87]. These observations catalysed the proposition of 'niche' hypothesis[88], which suggests that each tissue has a limited number of available macrophage niches that are tightly regulated by chemotactic and growth factors produced by parenchymal cells. Once all niches are occupied by foetal macrophages capable of self-maintenance, circulating monocyte can only differentiate into a tissue macrophage when a niche is vacated. During tissue expansion or injury, the number of niches increase substantially, and are populated by the most competitive progenitors – either locally proliferating macrophages of embryonic origin, circulating monocytes, or both[88]. This model is supported by experiments demonstrating macrophage plasticity – the ability to rapidly acquire a phenotype specific to the resident tissue, despite having a different tissue of origin[86]. Overall, the local tissue environment, rather than the cellular origin, is the major determinant of a macrophage phenotype.

Immune cells within tissues are predominantly identified by their surface protein marker expression. Most tissue macrophages of embryonic origin are classified by their high expression of adhesion receptor EMR1 (F4/80) and intermediate expression of integrin alpha M (CD11b) ($F4/80^{hi}$, $Cd11b^{int}$)[89]. Most macrophages differentiated from circulating monocytes are $F4/80^{int-hi}$, $Cd11b^{hi}$ [89].

1.2.1.3 Macrophage polarisation

Innate immune cells, including macrophages, form the first line of defence against invading pathogens. While the variety of existing pathogens is virtually endless, different classes of pathogens express shared features characteristic of that class, called pathogen-associated molecular patterns (PAMPs)[90]. Similarly, every type of pathogen-free tissue damage has a distinctive molecular signature called a damage-associated molecular pattern (DAMP). Macrophages recognise PAMPs and DAMPs by pattern recognition receptors (PRRs) and initiate an appropriate immune response[90]. While multiple membrane-bound and cytosolic PRRs exist, only toll-like receptors (TLRs) and Nod-like receptors (NLRs) will be discussed here due to their importance in the development of WAT inflammation.

Humans and mice have ten and twelve different TLRs, respectively. All TLRs localise on the plasma membrane, with the exception of TLRs 3, 7 and 9, which are found in the endosomes[90]. TLRs recognise a multitude of PAMPs, including the sensing of various bacterial components by TLRs 1, 2, 4, 5, and 11 and viral nucleic acids by TLRs 3, 7, 8, and 9[90]. Binding of a PAMP to a TLR initiates an intracellular signalling cascade, culminating in the activation of nuclear factor-kappa B (NF-κB) or interferon regulatory factor (IRF) transcription factors that mediate the expression of genes encoding inflammatory cytokines, such as tumour necrosis factor alpha (TNFα) and interleukin-6 (IL-6)[90]. TLR stimulation also results in a dramatic change in macrophage phenotype, characterised by altered cell shape, motility, protein expression, membrane lipid composition and intracellular metabolism[90]. These changes are further modulated by released inflammatory cytokines signalling back to cytokine receptors on macrophages in an autocrine manner, or by various molecules released from neighbouring immune and non-immune cells signalling to macrophages in a paracrine manner[90]. Once integrated, all signalling inputs polarise macrophages to a specific phenotype. Classical macrophage activation, or acquisition of M1 polarisation (or inflammatory activation, as will be often referred to in this thesis), occurs in response to stimulation with bacterial antigens, such as lipopolysaccharide (LPS), which activates macrophages via the TLR4 receptor[91]. M1-polarised macrophages specialise at engulfing and eliminating bacteria by respiratory burst, which involves membrane-localised production of reactive oxygen species (ROS), directed to oxidise bacterial membranes and proteins[91].

Besides direct initiation of inflammatory cytokine release, TLR stimulation also leads to the production of a subset of cytoplasmic NLRs, namely NLRP1, NLRP3 and NLRC4, and their assembly into oligomeric structures called inflammasomes[90]. Upon their activation, inflammasomes trigger a caspase-1-mediated inflammatory cascade, culminating in the maturation and release of the cytokines interleukin-1β (IL-1β) and interleukin-18 (IL-18)[90]. IL-1β is a potent mediator of both local and systemic pro-inflammatory responses, and is responsible for the febrile response (fever) to an infection by acting on temperature-sensing hypothalamic neurons[92]. Prolonged inflammasome activation ultimately leads to pyroptosis, a form of programmed cell death distinct from apoptosis, involving cell swelling, bursting and release of DAMPS, such as ATP and deoxyribonucleic acid (DNA) into extracellular space, thus further

propagating the immune response[93]. Inflammasomes are activated by a variety of PAMPs and DAMPs, including ATP, viruses, bacterial toxins, cholesterol crystals and low intracellular potassium concentrations[94].

Once the pathogen is eliminated and tissue damage is contained, inflammation has to be resolved in order prevent any further unnecessary damage to host cells. The second phase of the response to TLR signalling is the re-polarisation of macrophages to a resolution, or M2b state[91]. Resolution phase macrophages are characterised by the production of vast amounts of anti-inflammatory cytokines, such as interleukin-10 (IL-10) and interleukin-1 receptor antagonist (IL-1RA), that potently diminish local inflammatory response, allowing a tissue to return to its normal state[91].

Not all invading pathogens cause pro-inflammatory immune responses. Certain types of microorganisms (including helminths, saprophytic mycobacteria and lactobacilli) have often been present in tissues throughout mammalian evolution. In many cases, it was more energy-efficient for the host to allow these microorganisms to parasitise a negligible amount of nutrients than to expend energy eliminating them[95]. Therefore, presence of parasites in a tissue invokes an immunomudulatory response, which leads to secretion of multiple anti-inflammatory molecules, including cytokines interleukin-4 (IL-4) and interleukin-13 (IL-13) that polarise macrophages to M2a state[96]. M2a, or alternatively activated macrophages contribute to encapsulation and containment of parasites[96]. Coincidentally, macrophages present in a healthy, pathogen-free tissue are also M2a-polarised, and such polarisation state is known to be important for their tissue-remodelling activity[91].

The high incidence of sterile inflammatory disorders, such as allergies, arthritis and type-1 diabetes in modern society lead to the postulation of ‘the hygiene hypothesis’[97], which states that increased sterility of modern environments is responsible for the emergence of the pathogen-free inflammatory diseases. It is supported by the fact that individuals raised in a farm-like environment, characterised by a frequent presence of animal- and soil-borne pathogens were less susceptible to developing allergies than individuals raised in cities[98]. A formulation of ‘the hygiene hypothesis’ called ‘Old Friends hypothesis’ reasons that tissue parasites are important for appropriate function

of the immune system in mammals[95,99]. A continuous presence of tissue parasites throughout mammalian evolution have produced a symbiotic relationship, in which parasites utilise nutrients from the host, and the host relies on parasites for immune system development[99]. Such hypotheses have led to the development of helminthic therapies, involving a deliberate infestation of individuals with a helminth or their egg in order to treat sterile inflammatory disorders, such as Crohn's disease or inflammatory bowel disease (IBD)[100-102]. Helminth infection has also been successful in alleviating the symptoms of MetS in mice, as will be discussed further in this thesis (1.2.2.4).

1.2.1.4 The role of cell metabolism in macrophage polarisation

As already illustrated by the evolutionary choice of mammals to contain, rather than eliminate parasites, inflammation is an energetically costly process. Consequently, the intrinsic metabolism of immune cells has to be fine-tuned for nutrient conservation. Until recently, the metabolic reprogramming of macrophages and other immune cells upon activation was thought to be merely a consequence of their polarisation, occurring in order to sustain their energy requirements[103]. However, recent research has extensively shown that macrophage polarisation can be altered by modulating their intrinsic metabolism.

Most cells can adapt to hypoxia (low environmental oxygen levels) by engaging in anaerobic metabolism[104]. Under normoxic conditions, most cells utilise the monomers of all macronutrients, including glucose, amino acids and fatty acids to fuel the mitochondrial tricarboxylic acid (TCA) cycle for the production of ATP by oxidative phosphorylation (OxPhos)[105]. OxPhos cannot be performed in hypoxia, therefore cells switch to anaerobic glycolysis to generate ATP and convert pyruvate to lactate instead of oxidising it in mitochondria[104]. Anaerobic glycolysis produces 2 ATP molecules per glucose molecule, which is only about 5% of its energy potential achievable by OxPhos (38 ATP molecules)[105]. However, the rate of ATP production by anaerobic glycolysis is approximately 100 times greater than by OxPhos[105].

In specific cases, such as high intensity exercise, cells utilise glycolysis for ATP synthesis under conditions of normoxia in order to accelerate the rate of ATP

production[106]. Cancer cells also switch their metabolism to anaerobic glycolysis due to their defective mitochondria in a process called Warburg effect[107,108]. The Warburg effect rapidly occurs in classically activated macrophages, which dramatically increase glucose uptake to fuel both the glycolysis pathway for ATP production, and the pentose phosphate pathway to generate reductive potential in the form of reduced nicotinamide adenine dinucleotide phosphate (NADPH) required for the respiratory burst[103]. Rather than exhibiting mitochondrial dysfunction, M1 macrophages repurpose their mitochondria for the production of ROS, which augments macrophage bactericidal activity[109] and acts as an intracellular signal to further propagate inflammatory gene expression[110]. Competitively inhibiting glycolysis using the metabolically inert pathway intermediate 2-deoxyglucose (2-DG) or by scavenging mitochondrial ROS using antioxidants prevents the acquisition of a pro-inflammatory phenotype in macrophages[103,110,111].

Anaerobic glycolysis during M1 polarisation is not sustainable due to excessive ROS-induced damage to intracellular proteins and lipids, and macrophages either revert back to ATP generation by OxPhos during the acquisition of the resolution phenotype[112-114] or undergo cell death[115]. OxPhos is also a predominant form of ATP generation in M2a-polarised tissue macrophages[112]. Blocking OxPhos by mitochondrial respiratory chain inhibitors prevents the polarisation of macrophages to a M2a state in response to IL-4 and exacerbates their pro-inflammatory phenotype upon classical activation[116]. While the oxidation of glucose, amino acids and fatty acids has been described to fuel OxPhos in M2 macrophages[113,117], fatty acid oxidation (FAO) is thought to play a key role in M2 polarisation[116] and will be discussed further in this thesis (1.3.1.4).

1.2.2 The role of macrophages in adipose tissue inflammation

1.2.2.1 The development and roles of adipose tissue macrophages

As for their counterparts in other tissues, adipose tissue macrophages (ATMs) have been shown to develop from bone marrow-independent progenitors without a monocyte intermediate in frogs and mice[118,119]. ATMs exhibit a typical tissue macrophage behaviour, including efferocytosis of adipocytes and remodelling of the ECM[120]. Even though ATMs display a substantially different gene expression profile to

other tissue macrophages[121], only a few specialised functions for ATMs have been proposed, and will be discussed further in this thesis.

Regulation of adipocyte insulin sensitivity by ATMs. Similar to the relationship between other tissue macrophages and their parenchymal cells, ATMs can influence the behaviour of adipocytes through paracrine signalling. Secretion of different pro-inflammatory cytokines, such as TNFα and IL-1β by ATMs are known to reduce the responsiveness of adipocytes to insulin[122-127]. Furthermore, TNFα can also inhibit adipocyte differentiation from precursor cells[128-130]. Therefore, release of inflammatory cytokines from ATMs has to be tightly controlled in order to maintain appropriate WAT function. Elevated secretion of inflammatory mediators within WAT predominantly occurs because of two non-exclusive reasons – expansion of the ATM population or an altered balance of M1 and M2 macrophages within the ATM population[120]. Both of these processes have been observed in WAT during obesity and will be discussed further.

It is not fully clear why ATMs have evolved the ability to regulate adipocyte responsiveness to insulin. One hypothesis is that during acute infection, nutrients are diverted away from the metabolic organs (such as WAT and muscle) towards immune cells that require substantial amounts of energy to fight invading pathogens (as discussed in 1.2.1.4)[131,132]. In support of such hypothesis, genetic mouse models with hyper-inflammatory and over-proliferative myeloid cells exhibit fat loss due to excessive glucose uptake by myeloid cells[133]. Furthermore, some acute and chronic inflammatory diseases in humans, including chronic obstructive pulmonary disease and sepsis, are associated with cachexia[134].

Regulation of WAT lipolysis by ATMs. Upon the induction of on-demand lipolysis by fasting or in response to pharmacological activation of adipocyte β-adrenergic receptors, ATMs have been shown to accumulate lipid droplets[135,136]. ATMs have therefore been suggested to buffer lipids released from adipose tissues[137,138], and such a hypothesis has been supported by a study showing that pharmacological depletion of ATMs increases the rate of FFA release from WAT[135]. However, it is still unclear whether ATMs directly reduce the rate of lipolysis by taking up FFAs immediately after

release, and/or indirectly by secreting factors that inhibit adipocyte lipolysis. Furthermore, the physiological significance of such inhibitory mechanism has not yet been discussed or demonstrated. As β-adrenergic receptor-dependent lipolysis is known to occur in short bursts (approximately 9 pulses of FFA release per hour)[139], a speculative role for lipid accumulation in ATMs could be the reduction of serum FFA oscillations by lipid uptake during the burst release phase, and lipid release to circulation in-between bursts.

1.2.2.2 ATM recruitment to WAT

ATM recruitment during WAT lipolysis. Prolonged fasting and pharmacologically-induced lipolysis has both been shown to promote[135,140] or have no effect[136] on ATM accumulation in WAT. Lipolysis-induced expansion of the ATM population is dependent on the recruitment of bone marrow monocytes by the release of monocyte chemotactic protein 1 (MCP1 or CCL2) from WAT[135]. Intact adipocyte lipolytic machinery is also crucial for this process, as ATM recruitment does not occur in fasted mice lacking adipose triglyceride lipase (ATGL)[135,140], an enzyme catalysing the initial step in TG hydrolysis. However, the physiological importance of ATM recruitment during fasting is unclear, as mice deficient in CCL2 receptor (CCR2) do not exhibit differences in blood glucose or FFAs compared to WT controls[141]. Browning of scWAT upon cold exposure has also been associated with and dependent on monocyte recruitment to scWAT and will be discussed further in this thesis (1.4.2).

ATM recruitment during WAT expansion. WAT expansion during obesity leads to a dramatic increase of the ATM population, with macrophages representing approximately 50% of total cells in hypertrophic WAT[59]. This increase is attributed mainly to infiltration of circulating monocytes[142], but the proliferation of local ATMs has also been demonstrated[143-147]. Several chemokines have been implicated in monocyte chemotaxis to adipose tissues, of which the most well studied is the CCL2, acting via CCR2[141,148,149]. Utilising an *Fabp4* promoter to overexpress *Ccl2* transgenically specifically in adipose tissues causes macrophage recruitment and the development of the MetS in mice fed a standard chow diet[148]. Conversely, disrupting CCL2 signalling by genetic deletion[150] or pharmacological antagonism of CCR2[151] prevents monocyte infiltration to WAT during obesity and reduces the symptoms of MetS in mice. RANTES-CCR5[152], CXCL5-CXCR2[153] and CX3CL1-CX3CR1[154] chemokine-receptor

pairs have also been similarly shown to contribute to the progression of WAT inflammation and insulin resistance. Overall, animal studies indicate that preventing monocyte infiltration to WAT during obesity prevents the development of WAT inflammation and MetS.

While increased ATM proliferation precedes monocyte infiltration during WAT expansion, the pathological role of this increase in the number of ATMs is unclear. Some reports suggest that CCR2 and an inflammatory cytokine osteopontin directly increase ATM proliferation rate during obesity, leading to WAT inflammation and insulin resistance[145,147]. Other studies argue for an anti-inflammatory role for the expansion of the local ATM population, mediated by IL-4 signalling[146,155]. Further studies focusing on WAT expansion during early stages of obesity are thus required to understand the metabolic effects of ATM proliferation.

Despite numerous studies investigating the metabolic consequences of disturbed ATM recruitment to WAT, the *physiological trigger* for this process during the onset of obesity is less clear. It is evident that the occurrence of a specific set of events induce an immune response in WAT that precedes ATM proliferation and monocyte infiltration[156,157]. However, the exact nature of these events and their chronological occurrence leading to WAT dysfunction is not yet understood. Deciphering the mechanisms initiating inflammation in WAT during obesity is crucial for understanding the physiological importance of WAT inflammation and might hold a key for MetS therapy.

1.2.2.3 Inflammatory activation of ATMs during obesity

The vast majority of ATMs localise directly next to dying adipocytes during obesity, forming crown-like structures (CLS)[158]. Multiple ATMs are required to efficiently process a single dying adipocyte due to their substantial differences in size. Macrophages in CLS collectively form an acidic extracellular compartment surrounding the adipocyte by secreting intact lysosomes (cellular organelles containing digestive enzymes)[159]. Adipocyte TGs are digested extracellularly by lysosomal acid lipase (LAL), and liberated FFAs are taken up and esterified by CLS macrophages, which

become lipid-laden, resembling foam cells found in advanced atherosclerotic plaques[159,160].

Based on the vast abundance of CLS in dysfunctional WAT during obesity, adipocyte death has been suggested to be the initiator of inflammation and monocyte recruitment[161]. Indeed, a model of artificially induced adipocyte apoptosis by targeted activation of caspase-8 results in monocyte infiltration and CLS formation[162]. However, mouse models in which adipocyte survival is genetically modulated do not uniformly exhibit alterations in WAT inflammatory profile[163]. Furthermore, caspase-8-induced adipocyte death results in a robust increase in M2, but not M1 ATM population size[162], suggesting that there are factors regulating inflammatory activation of ATMs beyond adipocyte death.

PRRs and their downstream intracellular signalling cascades in macrophages unquestionably plays a role in ATM inflammatory activation during obesity. Both whole body and macrophage-specific genetic ablation of either TLR4[164,165], NLRP3[166,167] or TLR4 adaptor protein MYD88[168,169] protected mice from developing MetS during obesity. Similarly, genetically inhibiting enzymes that transduce inflammatory signals to transcription factors, such as p38 mitogen-activated protein kinase (p38 MAPK)[170] and c-Jun N-terminal kinases 1,2 (JNK1,2)[171] prevents obesity-induced WAT inflammation and systemic insulin resistance. Finally, a multitude of transcription factors mediating macrophage polarisation and inflammatory cytokine gene transcription, including peroxisome proliferator-activated receptor gamma (PPARγ)[172] and kruppel-like factor 4 (KLF4)[173] have been reported to play a role in the development of WAT dysfunction and insulin resistance[131,132].

The list of genetically validated molecular mechanisms acting in ATMs to perpetrate inflammation during obesity exceeds the volume of this thesis. Instead, here I will predominantly focus on the factors that *initiate* inflammatory ATM activation. As obesity-related adipocyte dysfunction leads to a lipid spillover in other tissues, the major trigger for WAT inflammation is thought to be aberrant lipid accumulation in ATMs. How lipids and their metabolism affect the phenotype of macrophages will be discussed in 1.3.

1.2.2.4 Therapies targeting WAT inflammation to alleviate insulin resistance during obesity

Since the discovery of obesity-induced WAT inflammation, anti-inflammatory interventions were proposed as therapies to alleviate insulin resistance and improve systemic metabolism in obese individuals. One potential advantage in utilising existing anti-inflammatory drugs to treat MetS is the knowledge of their clinical effects in humans, acquired from the treatment of sterile inflammatory disorders, such as rheumatoid arthritis. Amlexanox, a clinically approved drug to treat asthma and allergic rhinitis, has been shown to effectively reduce body weight and insulin resistance in obese mice by inhibiting kinases TRAF family member-associated NF-κB activator (TANK) binding kinase 1 (TBK1) and IκB kinase ε (IKKε) that are involved in inflammatory signal transduction[174]. Furthermore, amlexanox improved insulin sensitivity and hepatic steatosis in a subset of patients with type-2 diabetes, which had been characterised by increased WAT inflammatory gene expression compared to non-responders prior to the drug treatment[175]. The results of amlexanox clinical trial suggests that small-molecule anti-inflammatory drugs could be used to treat MetS in humans exhibiting particularly high degree of WAT inflammation. Treatment of obese non-diabetic patients with another small-molecule inhibitor salsalate, which targets the same arm of inflammatory signalling pathway, namely blocks NF-κB activation by IKKβ, resulted in a reduced fasting blood glucose and increased adiponectin levels, thus indicating improved WAT function[176-179].

Monoclonal anti-TNFα antibodies (such as adalimumab or infliximab) and recombinant IL-1 receptor antagonists (such as anakinra) have shown mixed results in the improvement of insulin sensitivity in humans. Studies that investigated the side effects of TNFα antagonists in patients with rheumatoid arthritis found that prolonged treatment reduced basal insulin and glucose levels, indicating an enhanced insulin sensitivity[180]. On the other hand, clinical trials designed to address the efficacy of TNFα and IL1-β antibody-based antagonists and IL-1 receptor blockers on insulin sensitivity in patients with type-2 diabetes showed little to no significant effects[181-184]. However, some clinical trials targeting inflammatory cytokines in insulin resistant individuals suffered from lack of statistical power, and larger scale trials are currently ongoing[185].

As an alternative to targeting pro-inflammatory macrophage pathways, therapies enhancing M2 polarisation of ATMs were successful in alleviating MetS symptoms in murine models of obesity. Helminth infection, leading to increased alternatively activated WAT macrophage population enhanced glucose tolerance in obese mice[186,187]. Furthermore, soil-transmitted helminth-infected humans had lower fasting plasma insulin levels compared to uninfected controls, suggesting an improved insulin sensitivity[188,189]. Finally, delivery of liposome-bound IL-10 into macrophages *in vivo* reduced WAT inflammation, serum lipid concentration and hepatic steatosis in obese mice[190]. Overall, while the interventions promoting ATM M2 polarisation have shown promising results in the insulin-resistant mice, future studies in humans will need to be conducted to verify their translatability.

In accordance with our knowledge regarding the link between WAT inflammation and insulin resistance, the vast majority of anti-inflammatory therapies against MetS were designed to limit the existing inflammatory reaction without removing its pathophysiological trigger. As multiple macrophage inflammatory signalling cascades have been implicated in the development of WAT inflammation, selectively blocking only one of them might not be sufficient to alleviate the inflammatory response. Therefore, a deeper understanding of the mechanisms leading to ATM inflammatory activation might enable the design of pharmaceuticals specifically blocking the *inflammatory initiation phase*, which would consequently reduce the activity of all downstream inflammatory pathways and be potentially more effective in treating MetS in humans.

1.3 The role of lipids in regulating macrophage function

1.3.1 The role of FFAs and sterols in regulating macrophage function

1.3.1.1 Cellular fluxes and metabolism of free fatty acids and sterols

In addition to their previously discussed energy storage function, FFAs also serve a major role as building material for membranes. Cholesterol and its metabolic derivatives are a part of a sterol family of lipids that cannot be burned for energetic purposes, and their predominant function is membrane synthesis[26]. Cellular membranes are some of the most basic features of life. Plasma membrane polarity and hydrophobicity enable cellular identity by preventing the concentration-mediated diffusion of multiple different molecules into and out of a cell. Appropriate cell function thus requires the maintenance of cell membrane integrity, which is ensured by a tight regulation of membrane synthesis, degradation and remodelling. As FFAs and cholesterol are essential for membrane formation, their import, synthesis, export, storage and breakdown are under strict control by multiple intracellular and extracellular cues[26]. Unsurprisingly, FFAs and cholesterol themselves have acquired a multitude of signalling roles during evolution, regulating metabolic and other aspects of cell function. In this section, an overview of all major metabolic pathways involving FFAs will be provided. This should enable the reader to place the specific lipid metabolism routes that will be discussed subsequently into a global map of cellular lipid metabolism.

Figure 1-3 summarises the intracellular routes of FFAs and cholesterol in macrophages. Circulating FFAs are bound to serum albumin or present as TGs in lipoprotein particles. Once hydrolysed by LPL, FFAs enter cells via fatty acid translocase CD36 or fatty acid transport proteins (FATP). Prior to participating in most metabolic pathways, FFAs have to be activated by forming a high-energy thioester bond with a cofactor coenzyme A (CoA), which is catalysed by a family of long-chain fatty acyl-CoA synthetase (ACSL) enzymes[26]. There are 5 different ACSL isoforms in mammals, and each one of them is thought to direct FFA to specific metabolic fates[191]. Furthermore, FATP proteins ligate CoA to FFA upon its entry to a cell. Hydrolysis of fatty acyl-CoA (FA-CoA) thioester bond provides energy for fatty acid esterification and remodelling processes[26]. Ultimately, FA-CoAs can be oxidised in mitochondria to yield acetyl-CoA (that can subsequently enter the TCA cycle) or esterified to a glycerol backbone to form diacylglycerol (DAG), which is a precursor for phospholipid and TG

synthesis[26]. Alternatively, they can be esterified to a sterol moiety to form cholesterol esters or to an amino acid serine to enter ceramide synthesis pathway[26].

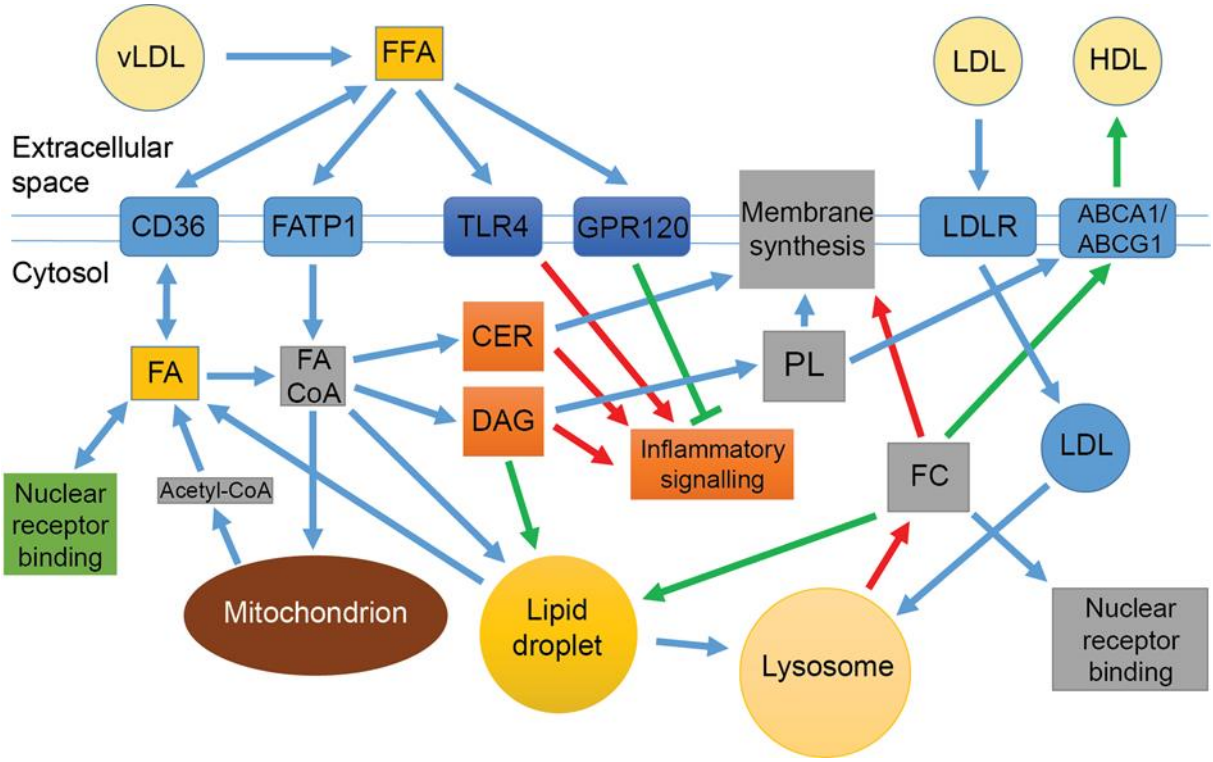

Figure 1-3. A simplified overview of cellular fatty acid and sterol metabolism. *PL, phospholipid; FC, free cholesterol; CER, ceramide; FA, fatty acid. Green arrows/boxes indicate pathways and processes that have been shown to be beneficial, and red arrows/boxes – pathways and molecules that are detrimental in the ATMs during obesity.*

Sterols reach cells as fatty-acyl esters in LDL particles, which are internalised and directed to lysosomes, where LAL liberates free cholesterol that can then be used for membrane synthesis in its free form, or after re-esterification to a fatty acid[26].

Most cells, including macrophages, can synthesise fatty acids and cholesterol *de novo* from the end product of glycolysis pathway, acetyl-CoA[26]. Acetyl-CoA can be carboxylated to form malonyl-CoA, which is then used as a substrate for fatty acid synthase (FASN), a multimeric enzyme that produces a saturated fatty acid with an acyl chain of 16 carbons (palmitate) from 8 malonyl-CoA molecules after multiple rounds of elongation reactions[26]. Similarly, sterols are generated from acetyl-CoA through multiple enzymatic steps, which are catalysed by proteins of mevalonate pathway[26].

There are approximately 50 known fatty acids in nature, out of which around 30 can be found in mice and humans. As the end product of DNL is palmitate, the remaining fatty acids are formed by subsequent palmitate remodelling or acquired from dietary sources[26]. The main sources of DNL-derived FFAs in mammals are liver and WAT, but most cells have the capacity to synthesise specific FFAs based on their needs[26]. Two predominant modifications can be applied to a fatty acyl chains – elongation and desaturation. The former process adds two extra carbons to the fatty acid, making it longer and more hydrophobic, while the latter introduces a double bond at a specific location within the fatty acyl chain, creating a kink in the molecule. Longer and more saturated fatty acids decrease membrane fluidity, therefore an appropriate balance of fatty acyl chain length and unsaturation needs to be maintained to ensure correct membrane function[26]. When not referred to by their common names, a numeric description of fatty acids will be used in this thesis, where a fatty acid with a chain length of x carbons, y double bonds and the position of the first double bond being z carbons from the methyl end of the acyl chain will be called Cx:ynz.

While the overall fatty acid remodelling pathway map is complex, the synthesis of the most abundant fatty acids is catalysed by only several enzymes in mammals. Palmitatoyl-CoA can be elongated to C18:0 (stearate) by members of Elongation of very long chain fatty acids (ELOVL) enzyme family, out of which the main isoform in liver, WAT and macrophages is ELOVL6 (Figure 1-4)[192]. Palmitatoyl-CoA and stearoyl-CoA can be desaturated to form monounsaturated fatty acids (MUFAs) C16:1n9 (palmitoleate) and C18:1n9 (oleate) respectively by stearoyl-CoA desaturases (SCDs) (Figure 1-4)[193]. The main SCD isoform in liver and WAT is SCD1, while macrophages demonstrate both SCD1 and SCD2 activities[193]. The only source of C18:2n6 (linoleic acid) and C18:3n3 (α-linolenic acid) is diet, as they cannot be derived from palmitate in humans and mice[26]. The CoA esters of these essential fatty acids are substrates of different ELOVL and fatty acid desaturase (FADS) enzymes, which catalyse the formation of multiple polyunsaturated fatty acids (PUFAs) through several elongation and desaturation steps (Figure 1-4). C18:2n6, C20:4n6 (arachidonic acid), C20:5n3 (eicosapentaenoic acid or EPA) and C22:6n3 (docosahexaenoic acid or DHA) are the most abundant PUFAs in the phospholipids of most cells, including macrophages[26].

Fatty acids are also present in a cell in their free, unesterified form, bound to members of fatty acid-binding protein (FABP) family. FABPs and sterol-binding proteins

solubilise FFAs and free sterols, therefore allowing them to diffuse through cytoplasm and nucleus[194]. FFAs and sterols act as ligands for transcription factors of nuclear receptor family, regulating the transcription of genes involved in lipid metabolism and other related cellular processes[26].

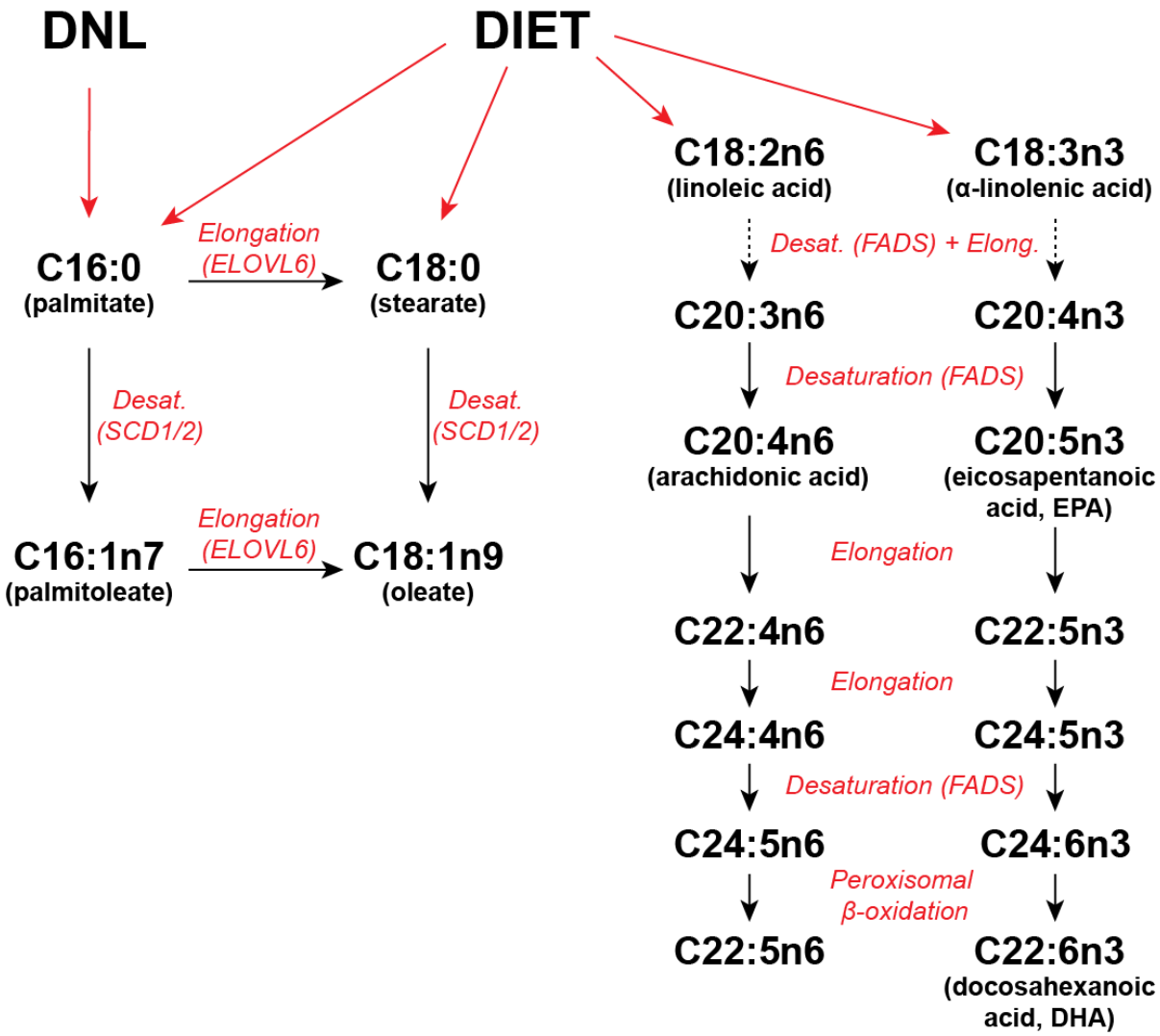

Figure 1-4. Mammalian fatty acid remodelling pathways.

Cellular palmitate can be derived from both DNL and diet, while the only source of linoleic and α-linolenic acids is diet. The final step of 22:5n6 and 22:6n3 biosynthesis involves the hydrolysis of 2 carbons from the acyl chain by peroxisomal β-oxidation.

1.3.1.2 The role of fatty acid, sterol and DAG signalling in regulating macrophage function

Pro-inflammatory signalling of palmitate. A major structural component of the LPS molecule is lipid A, consisting of two phosphorylated glycosamine molecules linked with six fatty acyl chains[195]. As the fatty acyl components of LPS are saturated and between 10 and 16 carbons long, endogenous palmitate is hypothesised to be a ligand for TLR4 due to its structural resemblance to the hydrophobic moiety of lipid A[196,197]. Indeed, multiple studies have demonstrated TLR-dependent inflammatory activation of macrophages by palmitate, characterised by activation of JNK and p38 MAPK signalling pathways and induction of NF-κB-dependent gene transcription[164,198-201]. Furthermore, TLR4-knockout mice are protected against developing insulin resistance following acute intravenous infusion of lipids or after prolonged feeding with high-fat diet[164]. Deletion of the *Tlr4* gene in hematopoietic cells also improves WAT inflammation and insulin sensitivity in obese mice[202]. However, some studies argue against the ability of palmitate to stimulate TLR4, suggesting that an endotoxin contamination present in bovine serum albumin, which is used for solubilisation of palmitate in cell culture studies, is responsible for the activation of the TLR4 pathway upon palmitate treatment[203]. Others have proposed that an endogenous circulating protein fetuin-A is an essential component of TLR4 signalling complex, and is required for palmitate-mediated TLR4 activation[204]. Overall, while the precise mechanism is not yet clear, the majority of the field agrees with the pro-inflammatory properties of palmitate.

Intracellular DAG signalling. Diacylglycerol is a metabolic intermediate in phospholipid and TG synthesis pathways (Figure 1-3). It is also produced in response to specific extracellular signalling cues and act as second messenger within a cell, mainly involved in binding and activating protein kinase C (PKC)[205]. Once active, PKC promotes differentiation and M1 polarisation in macrophages[206,207], and is also known to supress insulin signalling in metabolically relevant tissues, such as liver and muscle[208]. Dyslipidaemia observed during obesity leads to DAG accumulation within hepatocytes and myocytes (muscle cells), which is hypothesised to drive the development of insulin resistance[208]. Genetic deletion of enzymes involved in DAG biosynthesis leads to improved metabolic profile in obese mice[208]. While it has not been directly addressed, DAG accumulation and subsequent PKC activation is also thought to be involved in ATM inflammatory activation during obesity[209].

Anti-inflammatory signalling of unsaturated FFAs. Supplementing diets with unsaturated fatty acid-containing lipids has been long known to improve systemic nutrient metabolism in mice and humans[210]. MUFAs and PUFAs demonstrate anti-inflammatory effects through the activation of cell surface and nuclear receptors. G protein-coupled receptor 120 (GPR120) is hypothesised to be the cell surface sensor of unsaturated fatty acids[211]. MUFAs and PUFAs, but not SFAs can bind to GPR120 with varying affinities and stimulate the activation of its downstream pathway[212]. GPR120 genetic deletion does not affect WAT inflammation and insulin resistance in obese mice[212]. However, while dietary supplementation with PUFAs improves systemic insulin sensitivity during obesity, their beneficial effect is lost in whole body and hematopoietic cell-specific *Gpr120* knockout mice[212]. Furthermore, other study has found that loss of GPR120 function leads to increased body mass in mice fed an obesogenic diet by increasing food intake[213]. In line with such finding, a deleterious mutation of *GPR120* gene, leading to reduced receptor signalling activity, has been linked to increased BMI in humans[213]. Other cell surface FFA receptors, such as GPR40 and GPR43 have also been implicated in macrophage immunomodulation[214]. However, their agonists are short chain fatty acids derived from gut bacterial metabolism, which will not be covered in this thesis.

Activation of nuclear receptors by FFAs. FFA and sterol sensing in the nucleus is critical for shaping the phenotype of macrophages. Transcription factors of PPAR family are activated by unsaturated fatty acids and regulate cellular FFA uptake, storage and oxidation.[215] Macrophages deficient in their most abundant PPAR isoform PPARγ are incapable of polarising to M2a state, and macrophage-specific PPARγ knockout mice are more susceptible to developing insulin resistance during obesity[172]. Oxysterols, modified forms of cholesterol, are endogenous ligands of liver X receptor α and β (LXRα and LXRβ) transcription factors, which reduce cellular cholesterol levels by regulating the expression of enzymes involved in cholesterol uptake and efflux, such as LDL receptor (LDLR), ATP-binding cassette transporter 1 (ABCA1) and ATP-binding cassette sub-family G member 1 (ABCG1)[216]. In macrophages, LXRs have been shown to induce *Elovl5, Fads2* and *Scd2* gene transcription, leading to elevated intracellular production of unsaturated fatty acids[217,218]. Enhancing macrophage LXR activity by genetically removing either nuclear receptor co-repressor 1 (NCoR)[218] or FABP4 (aP2)[219] results in increased production of unsaturated fatty acids, thus improving the inflammatory and metabolic profile of obese mice. PUFAs promote the

resolution of inflammation in macrophages by uncoupling NF-κB binding to DNA from its transcriptional activity via an unknown mechanism[218,220].

Until recently, PPARs and LXRs have been thought to be the predominant transcription factors linking fatty acid metabolism and inflammation in macrophages. However, a time-course analysis of FFAs in macrophages following their inflammatory activation have revealed that the levels of unsaturated FFAs are reduced during the initial, pro-inflammatory phase after TLR stimulation, but are restored to the original state during the resolution phase[220]. Such reinduction of unsaturated FFA biosynthesis is mediated by a transcription factor sterol regulatory element-binding protein 1 (SREBP1), and it has been shown to mediate the resolution of inflammation in cultured macrophages and mice by catalysing the production of anti-inflammatory MUFAs and PUFAs[220]. How SREBP1 is activated during macrophage inflammatory activation remains to be investigated.

1.3.1.3 The role of membrane saturation in regulating macrophage function

Cell shape, motility and membrane-bound protein function depends on the fatty acid composition of cellular membranes[26]. Cells have therefore evolved numerous mechanisms to sense changes in membrane fluidity and normalise it, if necessary[26]. As most of intracellular lipid synthesis and remodelling occurs in the endoplasmic reticulum (ER), it is also where lipid-sensing proteins predominantly localise, including the inactive forms of SREBP transcriptions factors[26]. Inactive SREBPs are present in an ER-bound protein complex that perceives the membrane lipid composition[221]. The SREBP2 complex is a cellular cholesterol sensor, and when the membrane cholesterol levels drop, SREBP2 is proteolytically cleaved and transported into the nucleus, where it drives the transcription of genes encoding mevalonate pathway enzymes[221]. SREBP1 is also regulated by post-translational cleavage, which is inhibited by high ER PUFA levels[192]. Other factors that activate SREBP1 will be discussed further in this thesis (1.3.3.5).

One of the main functions of the ER is folding and post-translational modification of newly synthesised proteins. Cells contain the machinery to sense the states when the demand for protein synthesis exceeds the capacity of the ER enzymes to facilitate protein folding[222]. In these conditions of ER overload, cells have been termed to exhibit ER stress. ER stress invokes an adaptive unfolded protein response (UPR), which is

conserved from worms to mammals and lead to the expansion of ER and biosynthesis of multiple chaperone proteins that facilitate protein folding[222]. Interestingly, altered ER membrane lipid composition also leads to ER stress and UPR activation independently of cellular proteostasis[223-225].

Obesity has been shown to promote ER stress in multiple cell types, including hepatocytes[226], pancreatic β cells[227], adipocytes[228,229], hypothalamic neurons[230] and ATMs[231]. In many cases, obesity-related ER stress is thought to be a consequence of altered systemic lipid metabolism, associated with increased accumulation of intracellular lipids. The precise cellular mechanism linking lipid accumulation and ER stress is not fully understood, but the elevated saturation of ER membranes has been suggested to be involved[224,225]. Indeed, treating cells with high concentrations of palmitate leads to a profound ER stress response due to increased ER membrane saturation[232]. Consequently, numerous studies have utilised prolonged incubations with palmitate to model obesity-mediated ER stress in cell culture[232]. Such a modelling system has been proven to be successful in many cases, as genetic models that exhibit reduced ER stress in response to palmitate *in vitro* often have a diminished ER stress response during obesity *in vivo*. However, it is not yet clear whether saturated fatty acids are responsible for ER stress development during obesity.

Animal genetic models uniformly favour a causal role of macrophage ER stress for the development of inflammation and insulin resistance during obesity[231,233,234]. The expression of proteins co-ordinating cellular ER stress response, namely C/EBP homologous protein (CHOP) transcription factor, which promotes apoptosis, and inositol-requiring enzyme 1α (IRE1α), which catalyses the splicing-mediated activation of X-box binding protein 1 (XBP1)-encoding mRNA, are increased in ATMs during obesity[231]. Systemic CHOP deficiency prevents the development of insulin resistance in response to an obesogenic diet by maintaining ATMs in an M2 polarisation state[234]. Macrophage-specific IRE1α deletion leads to an improved metabolic profile by increasing systemic energy expenditure, thus attenuating weight gain during high-fat feeding[231]. Pharmacologically targeting macrophage IRE1α also decreases inflammation in atherosclerotic plaques, resulting in alleviated atherosclerosis[235]. While palmitate is known to induce ER stress in cultured macrophages[233], the mechanisms that promote the ER stress response in ATMs or plaque macrophages are not clear.

1.3.1.4 The role of FAO in regulating macrophage function

Contrary to anaerobic glycolysis, which can generate ATP at a very high rate and low efficiency, FAO is characterised by a low rate, but high efficiency of ATP synthesis[105]. Due to their reduced and anhydrous state, fatty acids are the most efficient energy source in the body, capable of producing 9 kilocalories (kcal) of energy per gram, compared to 4 kcal/g for carbohydrates[105]. Therefore, from a systemic point of view, it is more beneficial for a multicellular organism to restrict anaerobic glycolysis to cells with high energy expenditure, while having cells with low energy demand be preferentially fuelled by FAO. Such biological adaptation is also reflected in macrophage biology, where M1-polarised macrophages utilise glucose to maintain their high bioenergetic needs, and M2 macrophages that do not require fast rates of ATP production operate on FAO[236]. Interestingly, during the initial phase of the acquisition of M2 polarisation, macrophages exhibit an increased glycolytic flux that is diminished when the polarisation is accomplished[103,237]. Blocking glycolysis in macrophages during exposure to M2-polarising agents prevents the development of M2 polarisation[238]. Therefore, current literature suggests that regardless of the inflammatory nature of the trigger, the initial period of macrophage activation, characterised by energy-demanding processes (such as chromatin remodelling and gene transcription, protein expression and membrane remodelling), is fuelled by energy derived from glycolysis[116,117].

Recently published findings have suggested that FAO is not only a consequence of a change in the cellular phenotype in M2-polarised macrophages, but also plays a causal role in the acquisition of M2 polarisation[238]. A mechanism has been proposed, where exogenous and endogenous fatty acids in macrophages are initially stored as TGs in lipid droplets before being hydrolysed in the lysosomes by LAL and shuttled to the mitochondria for β-oxidation[238]. Inhibiting this process by genetically deleting LAL, or pharmacologically inhibiting carnitine palmitoyltransferase I (CPT1), a mitochondrial FFA transporter (catalysing the initial step in FFA import, namely esterification of a fatty acid to carnitine), blocks FAO and prevents the development of M2 macrophages[238]. However, these findings have recently been challenged by a genetic deletion of CPT2 (catalysing the hydrolysis of fatty acyl-carnitine within mitochondria) in macrophages, which results in impaired FAO but does not affect the acquisition of M2 polarisation[239]. Overall, it is now thought that FAO in M2 macrophages is a consequence, rather than

a cause of a change in the phenotype, and that pharmacological CPT1 inhibitor etomoxir blocks M2 polarisation via a yet unknown off-target effect[239].

Similarly to how excess FFAs can be systemically eliminated via oxidation in BAT during obesity, increasing the FAO capacity of a cell has been shown to be protective during lipotoxicity by decreasing the intracellular lipid load. Overexpression of myocyte CPT1 isoform (*Cpt1b*) in skeletal muscle alleviates insulin resistance in high-fat diet-fed rats by reducing intramuscular TG and DAG accumulation[240]. Liver-specific overexpression of hepatic CPT1 isoform (*Cpt1a*) also improved the metabolic profile of obese mice, potentially due to a decreased hepatic DAG and ceramide concentrations[241]. Similarly, enhancing FAO by *Cpt1a* overexpression in macrophages *in vitro* reduces palmitate-induced inflammation[242], while genetic deletion of *Cpt1a* in macrophages exacerbates saturated FFA-mediated ER stress and inflammatory activation[243]. However, FAO does not appear to be important in ATMs during obesity, as the loss of CPT2 and resulting loss of FAO in macrophages does not potentiate the development WAT inflammation or insulin resistance during high-fat feeding of mice[244].

1.3.2 The role of lipid droplets in regulating macrophage function

1.3.2.1 Formation and function of intracellular lipid droplets

Due to their hydrophobicity, TGs and cholesterol esters spontaneously group together and form droplets when present in an aqueous phase[245]. Similarly, most cells exist as emulsions, containing lipid droplets mainly consisting of TGs and cholesterol esters dispersed in the aqueous cytoplasm[245]. However, intracellular lipid droplets are membrane-enveloped organelles that do not arise spontaneously. Instead, their formation, stability and function is under strict control by intracellular signalling mechanisms[245]. Such regulation enables a wide variety of lipid droplet properties to be observed within the same animal. For example, white adipocytes in mammals each contain a single large lipid droplet, while brown adipocytes have multiple small lipid droplets. As obesity is a disorder related to excessive and abnormal TG storage, accumulation of lipid droplets in multiple cell types have been described to play a role in the development of MetS[246].

In eukaryotes, lipid droplets are formed *de novo* in the ER, where TG and cholesterol-synthesising enzymes predominantly localise[245] (Figure 1-5). *De novo* TG biosynthesis in most cells is performed via a Kennedy pathway, involving the esterification of two

fatty acyl-CoAs to glycerolphosphate and the hydrolysis of the phosphate group from the glycerol moiety to form DAGs[245]. DAGs can then be used for phospholipid (as will be described further) or TG biosynthesis. The final step of TG biosynthesis, the esterification of a fatty acyl-CoA to DAG, is catalysed by the diacylglycerol acyltransferase (DGAT) enzymes DGAT1 and DGAT2 (Figure 1-5)[245]. While both DGATs catalyse the same reaction, they share no sequence similarity and thus evolved independently from each other. Consequently, they exhibit different structures, subcellular localisations, substrate preferences, tissue and cellular distribution and physiological roles[245].

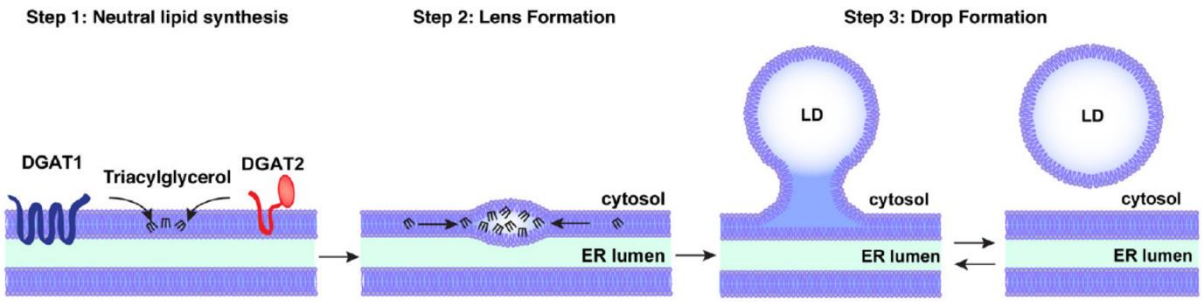

Figure 1-5. A step-wise simplified model of lipid droplet formation.
Figure taken from Wilfling et al[247].

DGAT1 is found exclusively in the ER, where it can esterify fatty acyl-CoAs to a number of substrates, including DAG, monoacylglycerol, retinol, long-chain alcohols[248] and cholesterol[249], although TG synthesis appears to be its predominant function[250]. DGAT1 plays an important role in esterifying excess extracellular lipids and has been suggested to reduce lipotoxicity-induced ER stress[250,251]. TGs and cholesterol esters are relatively inert molecules. Therefore, when ER is faced with a lipid overload, one of the physiological responses is to direct the excess lipids for 'safe' storage within the lipid droplets[252]. Enzymes involved in TG biosynthesis are under XBP1 transcriptional control in the liver and are up-regulated in response to ER-stress mediated activation of IRE1α[253]. Furthermore, cells deficient in DGAT1 undergo apoptosis after a prolonged incubation with oleate, which is otherwise well-tolerated in WT cells[251]. Physiologically, *Dgat1* knockout mice are viable and have functional WAT[254]. Interestingly, these mice are resistant to high-fat diet-induced obesity and insulin resistance[254], and also exhibit a longer lifespan on a chow diet than WT controls[255].

Such a beneficial metabolic profile is mainly attributed to DGAT1 deficiency in the enterocytes (intestinal epithelial cells), which leads to an impaired postprandial lipid absorption[256,257]. Paradoxically, *Dgat1* overexpression in muscle[258] or heart[259] also improves insulin sensitivity in obese animals by reducing tissue DAG levels. Furthermore, overexpressing *Dgat1* in WAT[260] or liver[261] increases the respective tissue weight by promoting lipid storage. However, such DGAT1-dependent WAT expansion or liver steatosis is dissociated from any metabolic impairments related to ectopic lipid accumulation observed during obesity[260,261]. Overall, *Dgat1* overexpression models demonstrate that appropriate intracellular lipid storage has no adverse metabolic effects, and thus provide elegant support for both the adipose tissue expandability and lipotoxicity hypotheses.

DGAT2 is thought to synthesise TGs predominantly from fatty acid substrates derived from DNL[262-265]. In contrast to DGAT1, DGAT2 is localised to both the ER and lipid droplets. Furthermore, while lipid droplets generated by DGAT1 are relatively small and of constant size, DGAT2-containing lipid droplets demonstrate further growth after budding off the ER[266]. Therefore, small lipid droplets are generally thought to be synthesised by DGAT1, and large lipid droplets – by DGAT2[266]. *Dgat2* knockout mice die shortly after birth due to a defect in skin barrier function[267]. These mice also exhibit lipopenia (lack of circulating lipids), indicating that DGAT2 is the main TG-synthesising enzyme in mammals[267].

1.3.2.2 The role of lipid droplets in regulating macrophage function

Lipid droplets in macrophages have been predominantly studied in the context of bacterial and parasitic infections or pathophysiological disorders, such as atherosclerosis[268,269]. Lipid droplet formation in macrophages in response to a bacterial infection is thought to be dependent on TLR signalling[269]. Lipid droplet-containing macrophages found in atherosclerotic plaques are termed foam cells and are derived from the uptake of oxidised LDL particles. Interestingly, individuals carrying polymorphisms attenuating TLR4 signalling have reduced risk of developing atherosclerosis, while being more susceptible to bacterial infections[270]. Based on these observations, recent reports have established a link between macrophage inflammatory activation and lipid droplet formation[269].

Prolonged stimulation with LPS has been shown to promote TG-containing lipid droplet formation in macrophages in the absence of exogenous lipids[271-274]. Furthermore, macrophages activated with LPS accumulated approximately 3-fold more TGs or cholesterol esters when incubated with TG-containing particles or LDL, respectively[271]. LPS has also been described to reduce the rate of lipolysis, thus leading to TG retention in lipid-laden macrophages[274]. So far, the mechanisms mediating increased TG accumulation during macrophage inflammatory activation have been predominantly based on the molecular characterisation of lipid-laden and M1-polarised macrophages[203,271,272,274-276]. LPS has been observed to induce the expression of DGAT2 and other enzymes of the Kennedy pathway, ACSL1, multiple FABP proteins and lipid droplet-coating adipose differentiation-related protein (ADRP)[272,274,276]. Therefore, it is thought that LPS promotes fatty acid storage by increasing the expression of genes related to fatty acid uptake, TG synthesis and lipid droplet formation and decreasing lipolytic and FAO gene transcription[238,272]. However, a recent report has suggested that LPS-induced lipid accumulation in macrophages is driven entirely by the increased rate of culture medium acidification, occurring due to elevated lactate production by highly glycolytic inflammatory macrophages[273]. Indeed, simply manipulating the extracellular pH of macrophages is sufficient to induce lipid accumulation[273]. Interestingly, macrophages have been shown to create an acidic extracellular compartment to digest aggregated lipoproteins in atherosclerotic plaques[277], or dying adipocytes in WAT[159]. However, the mechanisms of pH-mediated intracellular lipid storage are unclear.

One of the main functions of lipid droplets in macrophages is the storage of inflammatory lipid mediator precursors[268]. During their inflammatory activation, macrophages produce fatty acid-derived eicosanoids that, depending on their type, either propagate or alleviate local inflammation[278]. Enzymes that generate eicosanoids, including lipoxygenases (LO) and cyclooxygenases (COX), have been shown to localise on lipid droplet membranes in macrophages[268,279]. Macrophage inflammatory activation promotes the release of precursor fatty acids from the lipid droplets, including arachidonic acid, EPA and DHA, that are then used for the synthesis of a multitude of eicosanoids, including leukotrienes, prostaglandins and resolvins[278]. Increased lipid droplet formation is thus thought to enhance the capacity for eicosanoid formation in macrophages. Indeed, significant correlations between lipid droplet

formation and enhanced generation of both LO- and COX-derived eicosanoids have been observed[279-282].

Similar to atherosclerotic foam cells, ATMs isolated from obese mice exhibit increased intracellular lipid droplet content[283]. Obesity has also been linked to an increased lysosomal biogenesis in the ATMs[160,284,285]. As ATMs digest dying adipocytes, a logical assumption is that macrophage lipid accumulation stems from FFAs released from extracellular TG hydrolysis. Indeed, sequestering of lipids released from digested adipocytes, thus buffering the release of hydrolysed FFAs into the circulation, is one of the proposed roles of ATM lipid droplets[137,138]. As already discussed in 1.2.2.1, such a buffering mechanism might not be restricted to the FFAs released from dying adipocytes, but also to FFAs liberated during on-demand lipolysis. In line with this, depleting macrophages from the obese adipose tissues increases the rate of FFA release into the circulation, while inhibiting lysosomal lipolysis of the intracellular lipid droplets in the ATMs reduces WAT lipolysis in obese animals[284]. However, the fatty acid composition of TGs found in ATMs is distinct to the fatty acid composition of adipocytes in the WAT isolated from ob/ob mice[283]. In particular, ATM lipid droplets exhibit an enrichment of MUFAs and PUFAs relative to adipocytes[283], suggesting that ATMs do not simply store the contents of a dead adipocyte, but rather selectively buffer the release of unsaturated fatty acids into the circulation. The physiological role of such selective storage of FFAs in the ATMs remains to be investigated.

While lipid droplet accumulation in macrophages is normally associated with pathophysiological states, it can be considered as an adaptive and protective cellular response against lipid-induced toxicity and inflammation. It is also important to emphasise that lipid droplets represent only the 'visible' spectrum of intracellular lipids, namely TGs and cholesterol esters, which are relatively biologically inert. In contrast, DAGs[286], ceramides[287] and saturated FFAs are invisible to lipid dyes but display potent intracellular reactivity. The relative importance between these two types of lipids in macrophages is emphasised by a genetic model of *Dgat1* overexpression[209]. *Dgat1*-overexpressing macrophages are protected against palmitate-induced inflammation, despite exhibiting increased TG accumulation in response to FFA treatment[209]. Interestingly, increased DGAT1 activity also reduces the inflammatory activation of macrophages in response to LPS stimulation[209]. Importantly, myeloid cell-specific overexpression of *Dgat1* reduces WAT inflammation and improves the metabolic

profile in mice after prolonged high-fat feeding[209]. Furthermore, DGAT1 deficiency in myeloid cells leads to an increased systemic inflammation in a mouse model of atherosclerosis[288]. However, lack of DGAT1 activity does not impact saturated fatty acid-induced ER stress[233] or oxidised LDL-induced inflammation[288] in macrophages. Finally, while pharmacological PPARγ agonists have been shown to promote *Dgat1* expression in cultured macrophages[209], the physiological factors regulating *Dgat1* transcription in macrophages *in vivo* have not yet been described.

1.3.2.3 The role of lipid droplets during hypoxia and anaerobic metabolism

Hypoxia has been long known to promote lipid droplet accumulation in multiple cell types[289-291]. Cancer cells exhibiting high rates of anaerobic glycolysis also have increased lipid droplet content[292]. Multiple mechanisms contribute to hypoxia-induced lipid droplet formation, including increased DNL[293,294], elevated exogenous fatty acid uptake[295-297] and decreased FAO[298]. While different cells rely on separate mechanisms to coordinate TG accumulation during hypoxia, hypoxia-inducible factor (HIF) proteins appear to be necessary for lipid droplet formation in a low oxygen environment or in cancer cells[297].

The HIF family of transcription factors contain 6 members, among which the most studied proteins are HIF1α and HIF2α, encoded by *Hif1a* and *Epas1* genes, respectively[299]. Under normoxia, HIFs are continuously degraded by ubiquitin-dependent targeting for proteosomal degradation[299]. Hypoxia stabilises HIFs in the nucleus, leading to the transcription of genes related to glycolytic metabolism (*Glut1*), angiogenesis (vascular endothelial growth factor A, *Vegfa*) and lipid metabolism (*Adrp*, *Cd36*)[299]. HIF1α activity is also important for the induction of Warburg effect and the survival of multiple cancer cells[300]. Similarly, the switch to anaerobic glycolysis in LPS-activated macrophages and subsequent inflammatory gene expression is mediated by HIF1α[111,114,301].

The functional roles of lipid droplets during hypoxia, in cancer cells and LPS-activated macrophages are speculative. Firstly, it has been suggested that lipid droplets ensure ER homeostasis during the conditions of cellular stress. The synthesis of the most abundant unsaturated fatty acid oleate within the cell by SCD enzymes requires oxygen as an electron acceptor[26]. In hypoxia, the metabolic flux through SCD1 is supressed, leading to increased exogenous MUFA uptake[295]. The storage of MUFAs

in lipid droplets during hypoxia might provide a stable cellular source of MUFAs, when their *de novo* synthesis capacity is limited, thus alleviating the pressure of lipogenesis and lipid remodelling from the ER.

Secondly, lipid droplets have been ascribed an antioxidant role[302]. Reprogramming of cellular metabolism during hypoxia, in cancer cells or in LPS-treated macrophages is associated with an increased production of ROS[110,303,304]. ROS-induced lipid peroxidation is detrimental for cell survival. Consequently, cells have evolved multiple mechanisms to prevent the formation of lipid peroxides. For example, glutathione peroxidases (GPX) are a family of enzymes that catalyse the glutathione-mediated reduction of oxidised lipids back to their native state[305]. Recently, GPX4 activity has been shown to be essential for cancer cell survival by allowing the membrane integrity and functionality to be maintained during the metabolic state with a high rate of ROS production[306,307]. As lipid droplets are hydrophobic, they protect unsaturated fatty acids from ROS, which are mainly hydrophilic and propagate through the aqueous cytosol. It has been reported that during physiological states of hypoxia in *Drosophila* brain, glial cells relocate unsaturated fatty acids from their membranes to the lipid droplets in order to avoid lipid peroxidation[302]. Such adaptive processes allow successful neuron development, and preventing glial lipid droplet formation by *Dgat1* knockdown impairs brain development in *Drosophila*[302].

1.3.3 The role of phospholipids in regulating macrophage function

1.3.3.1 Cellular pathways of phospholipid biosynthesis

Figure 1-6 illustrates the simplified intracellular pathways of phospholipid synthesis. The biosynthesis of aqueous precursors for phosphatidylcholine (PC) and phosphatidylethanolamine (PE) occurs in cytosol and nucleus[26]. DAGs are synthesised *de novo* from glycerol and FFAs in the ER[26]. The addition of choline and ethanolamine headgroups onto DAGs (to synthesise PC and PE, respectively) is catalysed in the ER, or directly on the membranes of cellular organelles, such as the nucleus, mitochondria or lipid droplet[26]. PC can then be further modified by a headgroup exchange between choline and serine to form phosphatidylserine (PS) in the ER, or by switching the DAG moiety to a ceramide to form sphingomyelin (SM) in the Golgi apparatus[26]. PE can also be modified into PS or tri-methylated to form PC in the ER. *De novo* cardiolipin (CL) synthesis occurs in mitochondria, where PS can also be decarboxylated to form PE[26]. Finally, phosphatidylinositol (PI) is synthesised in the

ER and further modified by phosphorylation in the Golgi apparatus to form phosphoinositides, which play an important effector role in G protein-coupled receptor (GPCR) signalling[26].

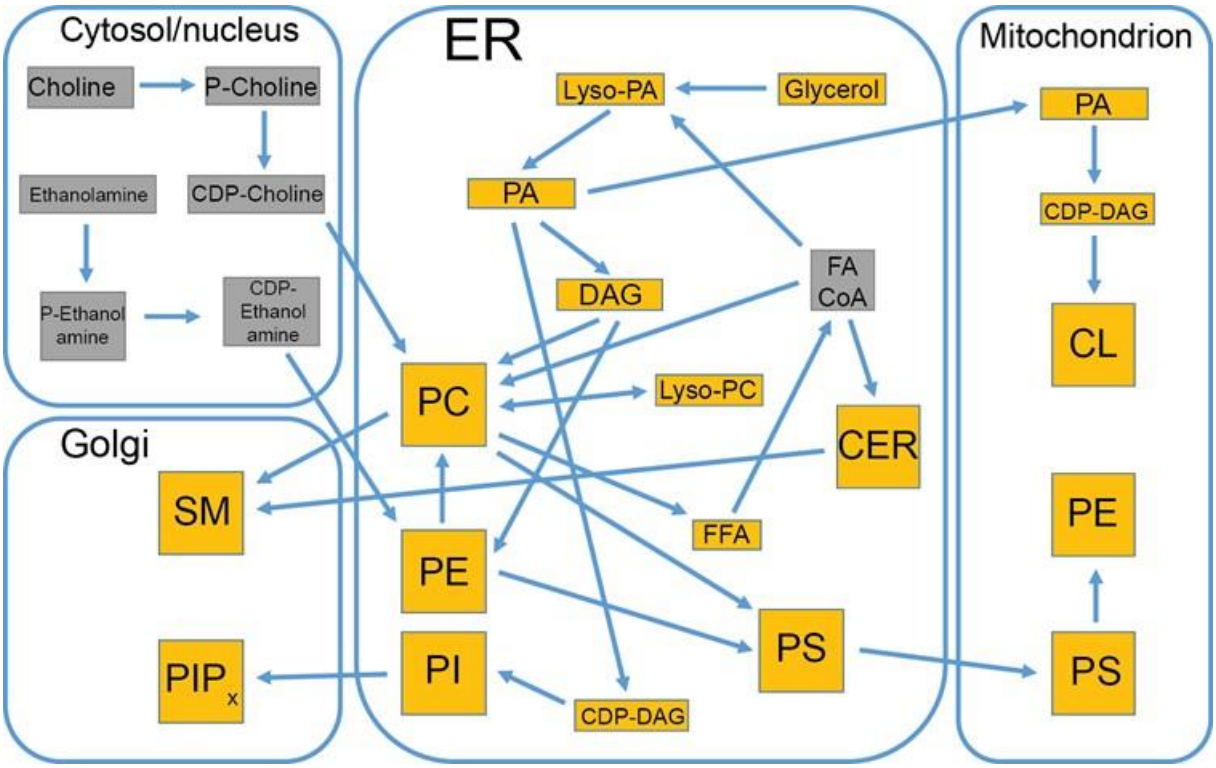

Figure 1-6. Simplified map of cellular phospholipid biosynthesis pathways.

Phospholipids can be degraded by phospholipases that cleave the headgroup together with the phosphate moiety to form DAGs, or without removing the phosphate to produce phosphatidic acid (PA)[26]. Furthermore, circulating lipoproteins contain intact phospholipids that can also be taken up or removed from a cell via lipoprotein internalisation or secretion[26]. Finally, PC can be removed from the liver into the bile, where it acts as a surfactant to aid the digestion of lipids[26].

1.3.3.2 Cellular PC and PE biosynthesis pathways

PC and PE constitute the vast majority of intracellular phospholipids[26]. Their *de novo* biosynthesis proceeds mainly via the Kennedy pathway, which is summarised in Figure 1-7. Firstly, phospholipid polar-group precursors ethanolamine and choline are phosphorylated by ethanolamine and choline kinases, respectively[26]. Phophoethanolamine and phosphocholine are then attached to a cytidine phosphate

by CTP:phosphoethanolamine and CTP:phosphocholine citidyltransferases (ECT and CCT, respectively)[26]. The final step of PE and PC formation is catalysed by DAG:CDP-ethanolamine and –choline phosphotransferases, which replace the cytidine phosphate with DAG moiety[26].

PE can also be converted to PC in three subsequent methylation reactions catalysed by phosphatidylethanolamine N-methyltransferase (PEMT)[26]. This reaction is particularly relevant in the liver, where it produces approximately 30% of overall PC content[308]. However, as PEMT activity is thought to not be functionally relevant in macrophages[309], the biological importance of PE to PC conversion will not be discussed here.

The enzymes of the Kennedy pathway can significantly overlap in their substrate usage. For example, several choline kinase isoforms have been reported to phosphorylate ethanolamine and specific phosphotransferases can catalyse the formation of both PC and PE from their respective precursors[310-312]. Conversely, ECT and CCT are highly specific for phosphoethanolamine and phosphocholine, respectively[313]. Furthermore, the reactions catalysed by ECT and CCT have been shown to be rate-limiting, as most cells contain high levels of their respective substrates and almost no products[314-316]. Consequently, the enzymatic activities of both ECT and CCT are highly regulated, as will be discussed in 1.3.3.3. However, some reports have suggested that the cellular availability of ethanolamine, choline or DAG can limit *de novo* PE and PC synthesis rate[317,318]. Macrophages also exhibit functional regulation of the choline transporter and increase their rate of choline uptake when the demand for PC biosynthesis is high[319]. Therefore, it is not yet clear whether the regulation of choline transport or CCT enzymatic activity physiologically modulates the rate of PC biosynthesis in macrophages. However, it is likely that both processes play a role in ensuring cellular PC homeostasis, and their relative importance is context-dependent. Due to the observed regulation of CCT in ATMs, as will become evident in the results section of this thesis, here I will only discuss the role of CCT in regulating cellular PC levels.

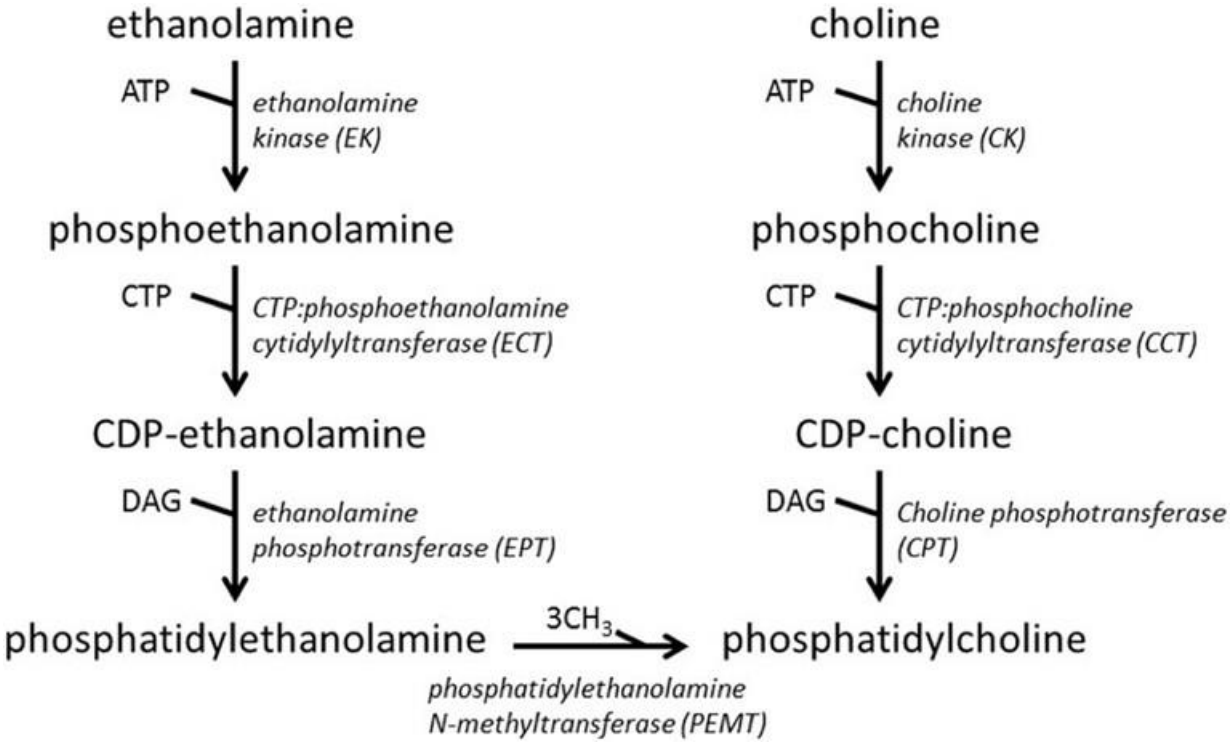

Figure 1-7. Kennedy pathway of de novo PC and PE biosynthesis.
Figure taken from Pulido et al[320]*.*

Finally, most phospholipids synthesised *de novo* can be subsequently remodelled via Lands cycle[26]. It involves the hydrolysis of a single fatty acyl moiety from membrane phospholipids to form lysophospholipids (phospholipids with a single fatty acyl chain) and an esterification of different fatty acyl-CoAs to the newly formed lysophospholipids[26]. Acyl-CoA:lysophosphatidylcholine acyltransferases (LPCATs) represent a family of enzymes that catalyse the esterification of fatty acyl-CoAs to lysoPCs. While the *de novo* PC synthesis pathway is required to generate the bulk of membrane PCs, the activity of LPCATs is thought to be important for ensuring the diversity of cellular PC species[321,322]. There are 4 LPCAT enzymes in mammals, with each of them having a different preference towards esterifying specific acyl-CoAs[323]. The best-characterised LPCAT enzyme in macrophages is LPCAT3, which is responsible for the incorporation of PUFAs into lysoPCs[324]. *Lpcat3*-deficient macrophages exhibit enhanced pro-inflammatory response to LPS due to decreased esterification of arachidonic acid into membranes, resulting in increased intracellular levels of free arachidonic acid[324]. Macrophages lacking LPCAT3 enzyme thus produce higher levels of arachidonic acid-derived prostanglandins in repose to LPS, leading to augmented inflammatory activation[324].

1.3.3.3 Regulation and importance of CCT for cell function

PC is the most abundant phospholipid species, corresponding to approximately 50% of total cellular phospholipids in a typical mammalian cell[313]. Similarly, PC is the major phospholipid in all mammalian cellular organelles, particularly in the ER, where it can make up nearly 60% of all phospholipids[313]. Due to its high biological importance, PC synthesis is strictly controlled by transcriptional and post-translational regulation of CCT[325].

Two CCT-encoding genes are present in mammalian genome, namely *Pcyt1a* and *Pcyt1b*[326]. *Pcyt1a* encodes the CCT isoform CCTα, while *Pcyt1b* mRNA is alternatively spliced to produce CCTβ2 and CCTβ3 isoforms in mice, and CCTβ1 and CCTβ2 in humans[327,328]. CCTα is ubiquitously expressed, and both CCTβ enzymes are predominantly found in the brain and gonads[329]. In most peripheral tissues, including macrophages, CCTα is approximately 10 times more abundant than CCTβ, making it responsible for nearly all cellular CCT catalytic activity[329]. The importance of CCTα is emphasised by the *Pcyt1a* global knockout mouse, which exhibits embryonic lethality as early as 3.5 days post coitum due to a failure of progression from a morula to a blastocyst, where a high rate of PC synthesis is required to fuel the membrane formation of the rapidly dividing embryo[330]. In contrast, systemic deletion of the CCTβ2 splice variant is well-tolerated, with female sterility resulting from gonadal failure being the only observed phenotype, likely occurring due to a high expression of CCTβ2 in gonads[331]. Interestingly, humans homozygous for inactivating mutations in the coding region of *Pcyt1a* have recently been reported[332-335]. In some cases, biallelic loss of a functional *Pcyt1a* gene resulted in congenital lipodystrophy and fatty liver disease[335], while other deleterious mutations caused spondylometaphyseal dysplasia with cone-rod dystrophy, characterised by short stature, altered bone structure and visual impairment, caused by cone-rod loss[332-334]. At present, it is not yet clear how humans lacking CCTα activity can develop and survive until adulthood, and why the mutations in *Pcyt1a* coding sequence manifest in the aforementioned, and not other tissue dysfunctions.

CCTα activity is primarily regulated post-translationally[336]. The main mechanism leading to an increased rate of CCT activity is the translocation of the soluble inactive form to membranes, where it becomes activated[337-340]. Such membrane binding-

dependent activation requires an amphipathic helix domain of CCTα, which senses hydrophobic properties of the membrane and mediates the docking of the enzyme[341,342]. Conditions that promote CCTα membrane binding include low membrane PC[343,344] or high membrane FFA[337] and DAG[345] levels. Upon binding, the curvature stress stored in membranes is sufficient to induce a profound conformation change in CCTα, thus promoting its enzymatic activity[346,347].

CCTα is also regulated by phosphorylation and proteosomal degradation. The C-terminal domain of the enzyme contains 16 serine phosphorylation sites[348-350]. However, mutating all residues to alanine does not affect CCTα membrane binding[349]. Interestingly, phosphorylation of serine 315 by extracellular signal-regulated kinases 1 and 2 (ERK1/2) can inhibit CCTα activity in lung epithelial cells[351], while phosphorylation of CCTα in macrophages, occurring predominantly due to phosphatase inhibition, increases its activation[352]. In quiescent B cells, CCTα is continuously synthesised and targeted for proteosomal degradation[353]. Upon stimulation with LPS, proteosomal CCTα degradation is inhibited, leading to an increased rate of PC biosynthesis required for the clonal expansion of B cells[353]. In an alveolar epithelial cell line, TNFα stimulation promotes CCTα ubiquitination and subsequent proteosomal degradation[354].

Pcyt1a gene exhibits a complex transcriptional regulation, with multiple transcription factors regulating its expression. Perhaps the best-studied physiological control of *Pcyt1a* gene expression is the cell cycle. During the synthesis or S phase of the cell cycle, when DNA replication occurs, transcription factor specificity protein 1 (Sp1) increases *Pcyt1a* gene transcription, which is performed in order to ensure sufficient capacity for PC synthesis during the subsequent division phase of cell cycle[355-357]. Deprivation of choline results in decreased PC levels and a cell cycle arrest at G_1 phase, which is a preparatory step for the S phase, in multiple cell lines[356,358,359]. In the murine macrophage cell line BAC1.2F5, the cell cycle can be arrested at G_1 phase by removing macrophage colony stimulating factor-1 (CSF-1) from the culture medium[360]. Readdition of CSF-1 has been shown to engage the cell cycle and increase *Pcyt1a* mRNA by 4-fold[361]. However, the increase in mRNA expression was not caused by an increased rate of transcription, but by a decreased rate of mRNA degradation in macrophages[361].

Multiple studies have reported SREBP1-dependent positive regulation of *Pcyt1a* transcription[362-365]. However, a subsequent study has suggested that SREBP1 increases CCTα activity indirectly by promoting *de novo* fatty acid biosynthesis, thus elevating the substrate supply for PC biosynthesis[366]. Similarly, loading cultured cells with fatty acids has been previously shown to increase PC biosynthesis[337,367]. As increased intracellular DAG levels can also activate CCTα[345], at present it is not clear if it is the fatty acids themselves, or their DAG metabolic derivatives that mediate increased CCTα activity.

Finally, an ER-stress mediated increase in XBP1 activity has been shown to promote ER expansion, driven by increased PC biosynthesis[353,368,369]. Overexpressing spliced *Xbp1* in fibroblasts also leads to elevated CCTα activity[369]. Interestingly, active XBP1 did not change *Pcyt1a* mRNA levels, but enhanced the rate of CCTα protein translation via an unknown mechanism[369].

1.3.3.4 The role of PC biosynthesis in regulating macrophage function

While PC is the most abundant phospholipid in monocytes, these cells also contain high cellular levels of free cholesterol[370]. During the process of monocyte to macrophage differentiation, cellular cholesterol levels exhibit a 3-fold decrease and PC abundance increases by nearly 2-fold[370]. This dramatic change is cellular lipid composition is driven by an activation of SREBP1 transcriptional activity, leading to an elevated FASN, SCD1, ELOVL6, FADS1 and FADS2 enzyme-encoding gene expression[370]. In contrast, SREBP2 target gene expression and free cholesterol levels are decreased in mature macrophages compared to monocytes[370]. Increased DNL and fatty acid remodelling in differentiating monocytes is coupled to up-regulated PC and PE synthesis[370]. However, the mRNA levels of enzymes involved in PC and PE formation do not change during macrophage differentiation, indicating a post-transcriptional regulation of CCT and ECT activity[370]. Finally, inhibiting FASN or SREBP1 reduces the rate of PC and PE production and drastically impairs macrophage differentiation[370].

The requirement of high membrane PC levels for macrophage function is explained by macrophage morphology. During their differentiation from monocytes, macrophages increase in size nearly 3-fold[370]. Furthermore, they expand their ER and Golgi apparatus[370], both of which contain high PC levels[313]. Finally, macrophages contain

numerous philopodia and exhibit dynamic changes in their membranes, particularly during phagocytosis[371]. The biophysical properties of PC allow for membrane kinks to occur, which are associated with the initial step of phagocytosis[372].

Surprisingly, the macrophage-specific *Pcyt1a* knockout mouse has normal levels of peritoneal macrophages[309,373]. Furthermore, *Pcyt1a*-deficient peritoneal macrophages exhibit similar appearance, migration and phagocytosis capacity as WT cells, indicating intact macrophage differentiation[373]. Similarly, loss of *Pcyt1a* in hepatocytes[374] or lung epithelial cells[375] does not affect their development. The residual CCT catalytic activity in CCTα-null cells is thought to occur due to compensatory up-regulation of CCTβ2 isoform[309,374], which could provide a sufficient rate of PC synthesis to allow unimpaired cellular differentiation. Alternatively, circulating lipoproteins can also supply substantial amounts of PC to primary cells and tissues[376]. While macrophages lacking *Pcyt1a* gene exhibit normal function in the basal state, they fail to mount an appropriate response to specific challenges, as summarised below.

PC metabolism in macrophages has been studied most comprehensively with regards to cholesterol uptake and cholesterol-induced ER stress. In advanced atherosclerosis, plaque rupture and thrombotic vascular occlusion is thought to occur, at least in part, due to the death of lipid-laden macrophages within the plaque[377]. As these foam cells are known to accumulate large amounts of free cholesterol[378-381], and as excess intracellular free cholesterol leads to macrophage cell death[382,383], adaptive mechanisms that protect macrophages from cholesterol-induced death are of high therapeutic interest.

Loading cultured macrophages with acetylated LDL to model plaque foam cell formation is relatively well-tolerated, as excess intracellular cholesterol is esterified in the ER to form cholesterol esters that are safely stored in lipid droplets[384]. Inhibiting the enzyme that catalyses cholesterol esterification, acyl-CoA:cholesterol acyltransferase 1 (ACAT1), promotes free cholesterol retention in the ER[382,383]. Elevated free cholesterol levels result in a rapid ER expansion, which requires an increased rate of PC synthesis[385]. Such compensatory PC synthesis is not accompanied by increased *Pcyt1a* transcription, but by post-translation activation of the CCTα enzyme[352,386]. PC levels in plaque-residing foam cells also positively

correlate with the severity of atherosclerosis[386,387]. In response to loading with acetylated LDL in the presence of ACAT1 inhibitor, CCTα-null peritoneal macrophages exhibited a profound cell death, likely due to their inability to provide sufficient PC for ER expansion[309]. Surprisingly, despite the generation of a macrophage-specific *Pcyt1a* knockout mouse and the observed failure of macrophages to adapt to free cholesterol loading *in vitro* being published nearly two decades ago[309], no follow-up studies regarding the susceptibility of this mouse model to atherosclerosis have been published yet.

In LPS-activated macrophages, synthesised cytokines need to be exported outside the cell predominantly via Golgi apparatus[388]. The formation of secretory vesicles in Golgi requires phospholipid synthesis[388]. After a prolonged stimulation with LPS, *Pcyt1a*-deficient macrophages exhibit reduced PC and elevated DAG levels, consistent with their inability to provide adequate amounts of CTP:phosphocholine for DAG:CDP–choline phosphotransferase[373]. Consequently, cytokines that rely on the Golgi for secretion, such as TNFα and IL-6, accumulate intracellularly in CCTα-null macrophages during LPS challenge, while IL-1β release, which is Golgi-independent, is unimpaired[373]. Furthermore, macrophage-specific *Pcyt1a* knockout mice exhibit increased mortality due to impaired cytokine release during bacterial infection of the lung[373]. Defects in cytokine secretion in *Pcyt1a*-deficient macrophages can be restored by providing exogenous lyso-PC and elevating DAG levels alone does not inhibit the release of TNFα, indicating that PC formation is the limiting factor for cytokine release in CCTα-null cells[373].

1.3.3.5 The role of membrane phospholipid and cholesterol composition in regulating cellular function

Besides the aforementioned cases where high rates of phospholipid (including PC) synthesis are required to enable intrinsic and adaptive cellular processes, a change in membrane PC content alone does not necessarily lead to functional membrane alterations. Instead, membrane fluidity and permeability are predominantly influenced by the relative ratio of different phospholipid and sterol species[26]. As each phospholipid species elicits a divergent effect on the physical properties of membranes, the interactions between all phospholipids and sterols determines the overall cellular membrane fluidity and integrity[26]. However, considering the relative effect of each structural lipid on membrane fluidity and integrity requires complex mathematical

modelling. Furthermore, even state-of-the-art lipidomic tools can only detect a subset of cellular phospholipids and sterols, preventing visualisation of the full complexity of membrane lipid biology[389]. Therefore, most studies investigating membrane lipid composition predominantly focus on the interactions between a few major membrane lipid species[389]. In this section, only the relationships between membrane PC and PE, cholesterol and total phospholipid will be considered.

PC and PE substantially differ in their structure due to their headgroup size[26]. PCs contain a large polar choline moiety and form cylindrical structures, while PEs acquire a conical shape due to their small ethanolamine headgroup[26] (Figure 1-8). Because of their different shape, PC and PE are asymmetrically distributed in the plasma membrane – PC is predominantly found in the outer leaflet, whereas PE is localised in the inner leaflet[313]. Such asymmetry enables the curvature, while maintaining membrane integrity (Figure 1-8).

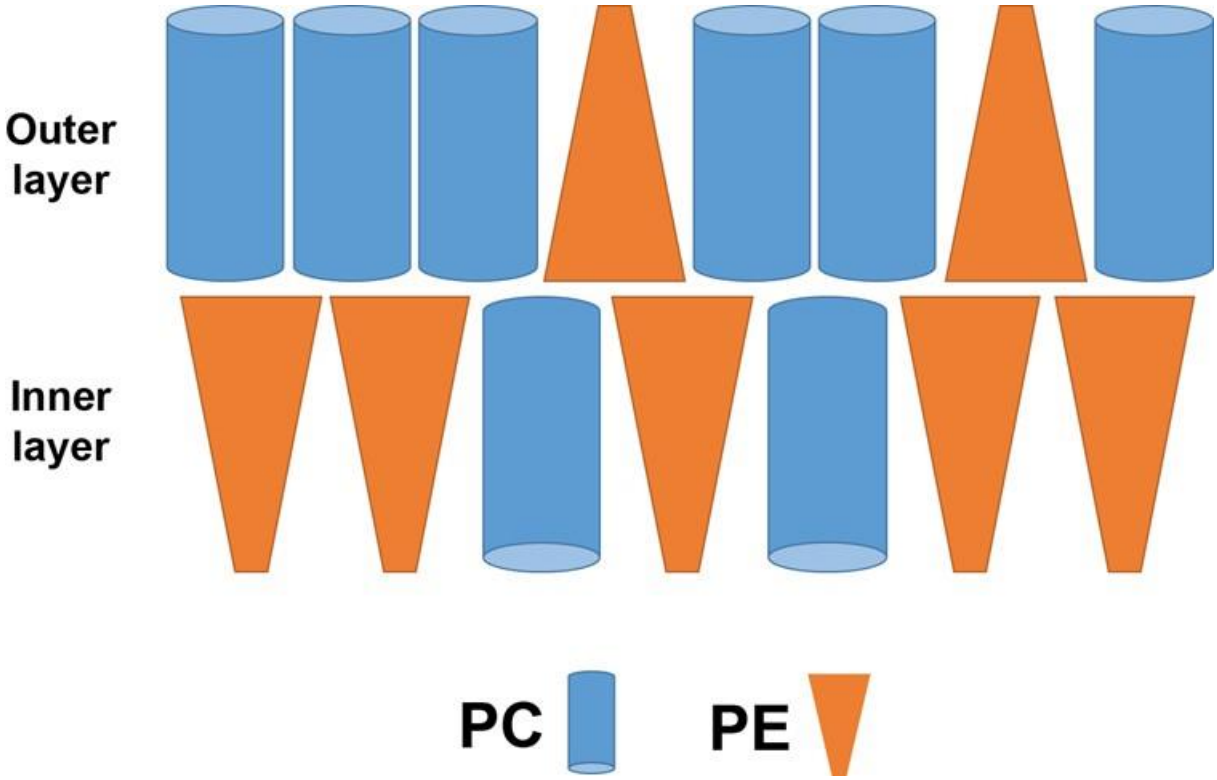

Figure 1-8. Simplified visualisation of PC and PE structures and their distribution within plasma membrane bilayer.

Appropriate PC:PE molar ratio (approximately 3 in most mammalian cells) needs to be maintained to ensure the integrity and function of cellular membranes. Perhaps the most elegant illustration of the importance of PC:PE ratio is the expansion of the lipid droplet. As lipid droplets have monolayer membranes, elevated PC:PE ratio is required to allow for the curvature of the membranes, particularly those of small lipid droplets, where surface area to volume ratio is relatively high[246]. During lipid droplet expansion, CCTα has been shown to localise onto lipid droplet membranes to directly supply the substrates for PC synthesis[367]. Genetic deletion of *Pcyt1a* homologue in Drosophila cells or *Pcyt1a* in mouse macrophages induces a failure to provide adequate PC levels during the growth lipid droplets and lowers the PC:PE ratio of lipid droplet membranes[367]. Lower membrane PC:PE ratio leads to the coalescence of many small lipid droplets to a few large ones, as an attempt to minimise the membrane tension by reducing droplet surface area to volume ratio[367].

Abnormally low hepatic PC:PE ratios have been associated with liver dysfunction[376]. It has been estimated that PC comprises 60-80% of the membrane phospholipids of TG-rich lipoproteins, including vLDL secreted by the liver[26]. The initial step of vLDL synthesis in the hepatocytes involves the lipidation of carrier protein apoliprotein B (apoB) in the ER, resulting in the formation of nascent vLDL particle[390,391]. Insufficient PC levels during apoB lipidation lead to low PC:PE ratio in nascent vLDL, which leads to its proteosomal degradation[392,393]. The physiological importance of this process is reflected by dietary choline deficiency, which promotes the development of hepatic steatosis in rodents[394-396] and humans[397,398] due to reduced vLDL secretion. Similarly, circulating TG concentrations in fasted hepatocyte-specific *Pemt* or *Pcyt1a* knockout mice are approximately 50% lower than in WT animals[374,399].

Another manifestation of low PC:PE ratio is the loss of hepatic plasma membrane integrity[400]. *Pemt* knockout animals fed choline-deficient diet are devoid of any PC synthesis and rapidly develop non-alcoholic steatohepatitis (NASH) and liver failure, which is attributed to increased plasma membrane permeability and subsequent liver damage[400]. NASH patients also exhibit a lower hepatic PC:PE ratio than healthy controls[400].

Low membrane PC:PE ratio leads to SREBP1 activation in worms and mammals[401]. While SREBPs are typically activated by the lipid-binding chaperone SREBP-cleavage

activating protein (SCAP), which transports SREBPs to Golgi for proteolytic cleavage in response to low ER levels of cholesterol or PUFAs[221], PC:PE ratio-dependent SREBP activation does not require SCAP[401,402]. Instead, low PC:PE ratio mediates the relocalisation of SREBP-cleaving proteases from the Golgi to the ER via a retrograde protein transport mechanism[401,402]. Consistent with the cellular observations, liver-specific *Pcyt1a* knockout mice exhibit increased hepatic SREBP1 processing and SREBP1 target gene expression[401]. Therefore, another potential mechanism linking low PC:PE ratio and liver steatosis is SREBP1 activation and a subsequent increase in DNL.

Interestingly, abnormally high hepatic PC:PE ratio has also been linked to the development of liver steatosis in mice[226,403]. While increased SREBP1 target gene expression is a known causal feature of hepatic steatosis, a recent study has shown that the expression of genes related to phospholipid metabolism is also altered in the livers of ob/ob animals[226]. Mainly, ob/ob mice have increased hepatic *Pcyt1a* and *Pemt*, but reduced *Pcyt2* expression, encoding PE-synthesising ECT enzyme[226]. These gene expression changes functionally lead to an elevated PC:PE ratio of hepatic ER membranes, resulting in a disrupted function of sarco/endoplasmic reticulum Ca^{2+}ATPase (SERCA)[226], which transports calcium from the cytosol into the ER. Diminished SERCA activity induces a profound ER-stress response, causing hepatic lipid accumulation and insulin resistance in ob/ob mice[226]. Normalising hepatic PC:PE ratio by liver-specific deletion of *Pemt* alleviates hepatic steatosis and improves the metabolic profile of ob/ob animals[226].

DAGs produced from the degradation of phospholipids by phospholipases can be subsequently utilised for TG biosynthesis (Figure 1-9). Strikingly, approximately 65% of the hepatic TG pool has been estimated to be derived from PC in a lean mouse[404]. Half of the PC-derived TG pool reaches the liver in the form of high-density lipoprotein (HDL) particles[404] that carry the excess peripheral cholesterol to be excreted via the reverse cholesterol transport pathway.

Glycine N-methyltransferase (GNMT) is an enzyme that negatively regulates the synthesis of S-adenosylmethionine (SAM), which is a methyl donor utilised in PE to PC conversation by PEMT (Figure 1-9). While disrupting hepatic PEMT activity by genetic deletion of methionine adenosyltransferase 1A (MAT1A), which catalyses SAM

formation, leads to hepatic steatosis due to impaired vLDL release[405], enhanced PEMT activity caused by *Gnmt* gene knockout also promotes liver steatosis[403]. Increased PC formation in *Gnmt*-deficient mice causes elevated hepatic TG levels by promoting the metabolic flux through PC to DAG to TG conversion pathway[403] (Figure 1-9).

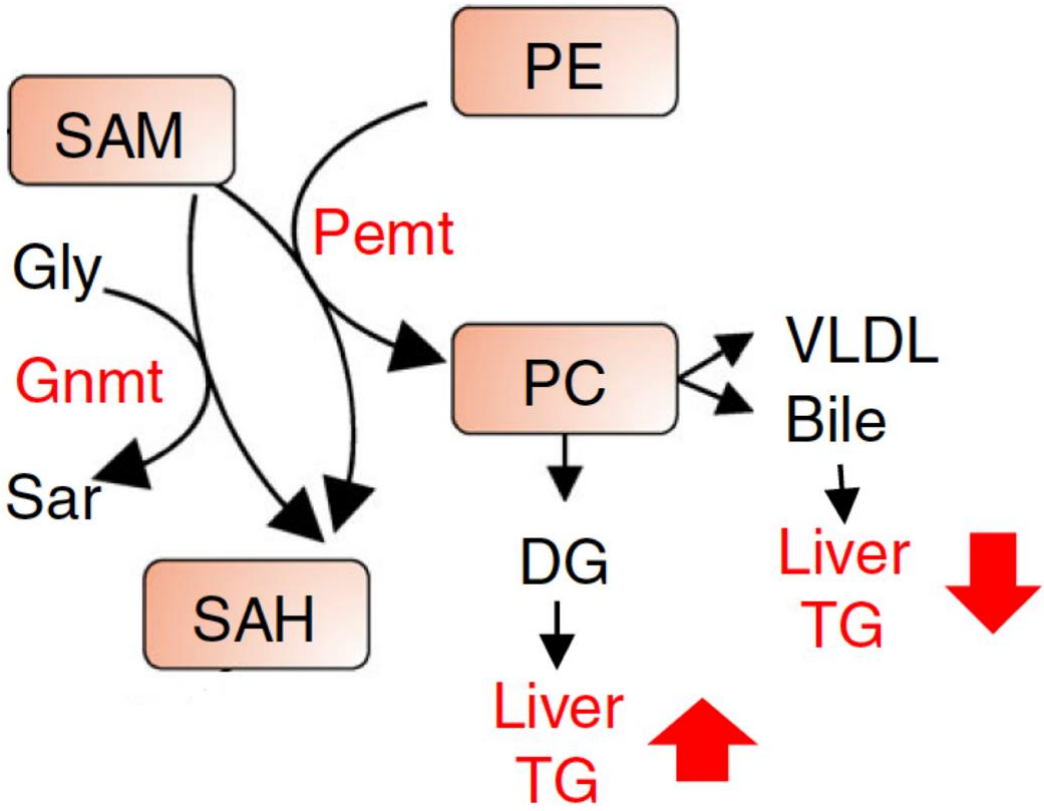

Figure 1-9. Simplified relationship between hepatic PC and TG levels.
GNMT negatively regulates SAM levels by catalysing the synthesis of N-methylglycine (sarcosine, Sar) from glycine (Gly) and converting SAM to S-adenosylhomocysteine (SAH). Figure adapted from Kim et al[406].

Cholesterol is an important regulator of membrane fluidity, as its hydrophobic properties and relatively small size allows it to integrate in the gaps between membrane phospholipids[407]. While still debated by some researchers, cellular plasma membranes are thought to contain areas with high cholesterol:phospholipid ratios[407]. These areas, termed lipid rafts, have increased structural order due to a reduced membrane fluidity. A highly ordered environment is required for the appropriate activity of multiple plasma membrane proteins, including TLR4[408] and proto-oncogene tyrosine-protein kinase Src (c-Src)[409], an up-stream activator of JNK signalling.

Saturated fatty acids have been reported to promote insulin resistance by altering the distribution of membrane lipid rafts[409]. Treating cells with palmitate stabilises c-Src within lipid rafts, leading to hyperactivation of JNK signalling and subsequent insulin resistance[409]. Unsaturated fatty acids exert an opposite effect by preventing c-Src membrane repartitioning[409]. Importantly, adipose tissues isolated from high-fat diet-induced obese mice exhibit c-Src stabilisation within lipid rafts, activation of JNK pathway and diminished insulin signalling[409]. In macrophages, fatty acids derived from endogenous fatty acid synthesis have been shown to selectively incorporate into lipid rafts[408]. LPS- or palmitate-mediated inflammatory activation of macrophages increases FASN protein expression and the rate of *de novo* fatty acid synthesis, which is important for the stabilisation of TLR4 within lipid rafts[408]. Consequently, macrophages deficient in the FASN-encoding gene *Fasn* have diminished inflammatory activation following stimulation with LPS or palmitate[408]. Importantly, macrophage-specific *Fasn* knockout mice exhibit reduced WAT inflammation and improved systemic insulin resistance after prolonged high-fat feeding[408]. Treating FASN-deficient macrophages with cholesterol, but not exogenous palmitate, restores plasma membrane lipid rafts and rescues defective TLR4 signalling[408]. How macrophages discriminate endogenous DNL-derived fatty acids from the exogenous fatty acids taken up from the extracellular space remains to be investigated.

1.4 Interactions between macrophages and the SNS

1.4.1 Overview of the link between nervous and immune system

The SNS is one of the main regulators of systemic lipid metabolism. Due to its ability of rapidly promoting WAT lipolysis, BAT FAO and UCP1-dependent energy dissipation, multiple therapies that activate SNS or mimic SNS action in tissues have been proposed to treat obesity[47]. While the majority of research regarding this topic is focused on understanding the neuronal networks in the brain that regulate sympathetic tone in adipose tissues, or mapping the adrenergic signalling pathways in the adipocytes that link SNS activity with its functional outcomes, ATMs have also been reported to play a role in regulating SNS output to WAT and BAT[410]. Therefore, in this section of the chapter I will summarise the literature describing the function of macrophages in regulating WAT SNS tone, and also the role of the SNS in regulating macrophage function in multiple tissues.

The initial observations of sympathetic neurotransmitters modulating the activation of innate immune cells were made more than 100 years ago[411]. Since then, all major immune organs, including spleen, lymph nodes and bone marrow have been demonstrated to have sympathetic innervation[412]. SNS activity in immune organs has been shown to regulate nearly all aspects of immune cell function, including the mobilisation of bone marrow cells into the circulation, leukocyte recruitment and adhesion, cytokine release and bacterial killing[413]. As the interactions between nervous and immune systems constitute a separate field of neuroimmunology, the summary of which would vastly exceed the capacity of this thesis, here I will focus my discussion on the findings related to the relationship between sympathetic nerves and macrophages.

1.4.2 Regulation of tissue sympathetic tone by macrophages

1.4.2.1 Secretion of NE by tissue macrophages

Immune cells were first reported to produce catecholamines more than two decades ago[414]. Pharmacological inhibition of tyrosine hydroxylase (TH), a rate-limiting enzyme in the biosynthesis of dopamine and NE, was shown to reduce catecholamine levels in lymphocyte extracts, suggesting an endogenous nature of catecholamine production in immune cells[414]. Subsequently, macrophages were demonstrated to express the mRNA encoding TH and dopamine β-hydroxylase (DBH)[415,416], an enzyme converting

dopamine to NE. Furthermore, the transcript levels of NE-synthesising enzymes and NE secretion into the medium were increased in cultured macrophages in response to LPS stimulation. Importantly, the inhibitory effects of α2-adrenergic receptor (α2AR) blockade on lung inflammation in response to lung injury persisted even when sympathetic nerve endings or T cells were ablated from the periphery[416], suggesting that macrophages were releasing NE in order to potentiate lung damage-induced inflammation. A more recent report ascribed a pathogenic role to NE released from macrophages during experimental autoimmune encephalitis (EAE), the rodent model of multiple sclerosis[417]. Genetic deletion of a gene encoding the transcription factor NR4A1 was shown to enhance the expression of *Th* in macrophages, resulting in accelerated infiltration of leukocytes into the central nervous system and disease exacerbation[417].

A major shift in the field of metabolism occurred several years ago, when M2 ATMs were observed to produce NE during cold exposure in mice[418]. Strikingly, macrophage-specific genetic deletion of the IL-4 receptor, or systemic pharmacological ablation of macrophages rendered mice cold-intolerant due to their inability to activate non-shivering thermogenesis on demand[418]. Subsequent studies utilising different mouse models confirmed the role of M2-polarised ATMs in the direct regulation of scWAT browning, but not BAT activation via local NE production[419]. Cold exposure was shown to promote monocyte recruitment to scWAT in a CCR2-dependent manner[419,420] and to induce ATM M2 polarisation by engaging their IL-4 receptor[419]. Genetically modifying the ATM phenotype was sufficient to affect scWAT browning during obesity, leading to an altered energy balance observed in multiple studies[231,421,422].

However, the studies regarding endogenous NE production by ATMs were recently challenged by multiple laboratories, which could not detect the expression of TH or measure detectable NE production in M2-polarised macrophages *in vitro* or in ATMs *in vivo*[423-425]. Furthermore, hematopoietic deletion of the *Th* gene was demonstrated to have no effect on adipose tissue function or energy balance on a chow or HFD[423]. However, due to the multiple independent observations of altered energy balance in macrophage-targeted genetic models, the role of macrophages in regulating WAT SNS tone was not dismissed, but rather deemed necessary of further investigation[423].

1.4.2.2 Regulation of sympathetic nerve function by tissue macrophages

Perhaps the main reason that fuelled the hypothesis of ATMs regulating WAT browning by NE production was that at the time, scWAT was thought to be poorly innervated, with only 2-15 % of adipocytes being in contact with sympathetic fibres[426,427]. However, state-of-the-art techniques have established that scWAT has a great abundance of SNS neurons, with nearly every adipocyte having a direct access to a nerve axon[38,428]. Based on these findings, macrophages are more likely to modulate tissue SNS tone by interacting with NE-producing nerves, rather than synthesising NE endogenously.

Microglia are known to mediate nerve development in the brain[429]. Peripheral macrophages have also been implicated in injury-mediated peripheral nerve repair in different organisms[430-432]. Multiple macrophage-derived neurotrophic factors have been shown to guide the axons of regenerating nerves[433,434]. Microglia and brain inflammation have also been suggested to play a role in the development of neurodegenerative disorders, such as Parkinson's[435] and Alzheimer's[436] diseases, indicating both beneficial and detrimental functions of macrophages in regulating nerve function.

Recent studies have shown that tissue macrophage-nerve interactions are required for an appropriate intestinal function. Macrophages present in the intestinal muscle were shown to regulate peristaltic activity of the colon by secreting bone morphogenic protein 2 (BMP2), which directly stimulated enteric neurons and altered the pattern of smooth muscle contractions[437]. In turn, enteric neurons released CSF1 that was required for local macrophage development[437]. Furthermore, sympathetic nerves located in small intestinal muscle were demonstrated to be activated upon gut bacterial infection[438]. NE released from activated SNS neurons acted on β2-adrenergic receptors (β2ARs) of macrophages residing in intestinal muscle and polarised them to an M2 phenotype, which was suggested to mediate the resolution of intestinal inflammation[438].

Direct interactions between sympathetic nerves and macrophages in adipose tissues have also been recently observed by multiple groups. CX3CR1-positive macrophages in BAT were shown to regulate the branching of SNS neurons in developing BAT by expressing a signalling molecule plexin-A4[425]. Genetic deletion of a transcriptional regulator MECP2 in macrophages resulted in elevated plexin-A4 expression, which

acted on a neuronal semaphorin-6A receptor, leading to increased SNS nerve repulsion and impaired BAT innervation[425]. CX3CR1-positive cell-specific *Mecp2* gene knockout mice displayed spontaneous obesity during adulthood, which was attributed to their impaired BAT function[425]. Macrophages localised directly next to sympathetic nerves in eWAT and scWAT were also demonstrated in two independent studies[424,439], which reported the ability of macrophages to take up and catabolise NE released from SNS neurons, as will be summarised in 1.4.2.3. Finally, while not visually demonstrating the presence of macrophage-nerve interactions in WAT, other studies showed the capacity of ATMs to directly respond to NE stimulation and will be presented in 1.4.3.

1.4.2.3 NE degradation by macrophages

Like most endogenous receptor agonists, the signalling of monoamines is limited by their reuptake and degradation[440]. In brain, the synaptic concentrations of monoamines are regulated by the activity of monoamine transporters (MATs), which catalyse the reuptake of monoamines to the pre-synaptic neuron[440]. Serotonin, dopamine and NE have their own respective classes of MATs, out of which norepinephrine transporter (NET, also known as solute carrier family 6 member 2 (SLC6A2)) mediates the internalisation of NE[441]. Once taken up, NE is degraded in three sequential enzymatic steps as illustrated in Figure 1-10. NE is initially oxidised by monoamine oxidase (MAO) and methylated by catechol-O-methyltransferase (COMT), before being converted to metabolically inert products vanillylmandelic acid and 3-methoxy-4-hydoxyphenylglycol that are excreted in urine[440]. MAO also catalyses the oxidation of serotonin and dopamine, thus mediating their degradation[440].

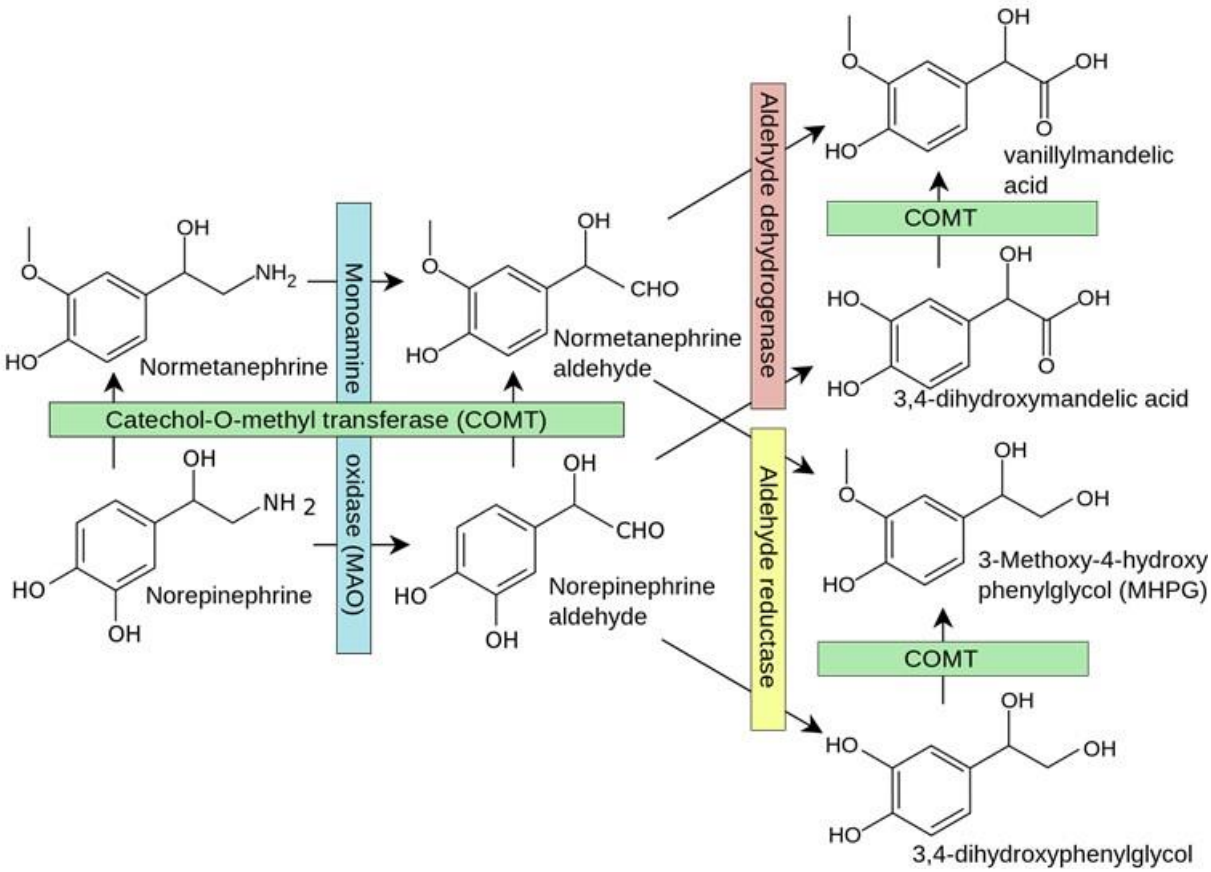

Figure 1-10. Norepinephrine degradation pathway.

Figure taken from Mikael Häggström[442]*.*

The monoamine theory of depression postulates that the underlying pathophysiological basis of depression is reduced brain monoamine levels[443]. Based on this theory, the inhibitors of MAO were successfully developed into clinical anti-depressants[444]. Furthermore, clinical and recreational drugs that affect concentration, activity, mood and pleasure mainly target monoamine uptake (Prozac, Ritalin, Adderall, amphetamine and its metabolic derivatives, and cocaine) and degradation (moclobemide)[445]. Finally, polymorphisms in the *Maoa* gene (encoding the MAOA isoform), that result in decreased MAOA enzymatic activity, have been linked to aggression, anti-social behaviour and mood disorders[446-448]. Overall, cellular neurotransmitter uptake and degradation plays a key role in regulating monoamine signalling in brain.

Interestingly, SLC6A2 has been found to be expressed in periphery. NE signalling to osteoblasts is known to decrease bone mass. Genetic deletion of *Slc6a2* has been reported to increase NE availability in bone, leading to reduced bone formation[449].

Similarly, pharmacological blockade of SLC6A2 induced bone loss in WT mice[449]. Peritoneal macrophages also exhibited the ability to rapidly take up and degrade NE *in vitro*[450]. Surprisingly, the NE uptake into peritoneal macrophages was independent of SLC6A2, as it could not be inhibited pharmacologically with cocaine[450]. Even though these findings have been made over three decades ago, the molecular mechanisms mediating NE uptake into peritoneal macrophages and the physiological importance of this process are still unknown.

Recently, ATMs have been reported to reduce SNS tone in WAT by taking up and degrading NE[424,439]. A group investigating molecular mechanisms driving aging-related impairment in WAT lipolysis discovered that ATMs isolated from aged mice expressed high levels of MAOA, COMT and aldehyde dehydrogenase and reductase enzymes and were limiting NE signalling to the adipocyte β-adrenergic receptors[439]. The development of monoamine degradation programme in ATMs during aging was mediated by the NLRP3 inflammasome-dependent up-regulation of a transcription factor growth differentiation factor-3 (GDF3)[439]. Dysfunctional fasting- or exogenous NE-induced lipolysis in WAT explants from aged animals could be restored by genetic *Nlrp3* gene deletion, or pharmacological MAOA inhibition[439]. An independent study found that scWAT contained a distinct group of ATMs that directly associated with sympathetic nerves[424]. This ATM population, termed sympathetic-associated macrophages (SAMs), expressed SLC6A2 and MAOA proteins and showed a capacity to take up and metabolise NE *ex vivo*[424]. Furthermore, SAMs became highly pro-inflammatory during obesity[424]. Importantly, *Slc6a2* knockout in hematopoietic cells increased BAT activation and scWAT browning in response to cold exposure, and resulted in a reduced rate of body weight gain during high-fat feeding of mice, suggesting that SAM-dependent NE catabolism is a physiologically relevant process[424]. The environmental factors that promote the SAM phenotype in macrophages remain to be investigated[451]. Overall, recent studies have established the specialised role of adipose tissue-resident macrophages in limiting NE signalling to adipocytes, thus opening a novel research area with a potential to develop novel anti-obesity therapies.

1.4.3 β-adrenergic receptor signalling in macrophages

1.4.3.1 The roles of adrenergic receptors in regulating macrophage function

All catecholamines signal through membrane-bound GPCRs. NE and epinephrine specifically target a subset of GPCRs called adrenergic receptors, which can be further subdivided to α1, α2, β1, β2 and β3-adrenergic receptors. Each adrenergic receptor has specific signalling properties due to their discrete G protein coupling. In general, α_1-adrenergic receptors are coupled to G_q proteins, which upon activation promote membrane phospholipase C activity, leading to increased intracellular second messenger DAG and inositol triphosphate concentrations that subsequently activate PKC[452]. β-adrenergic receptors are mainly coupled to G_s proteins, which generate the second messenger cAMP upon activation, and their signalling will be discussed in 1.4.3.3. α2ARs are coupled to G_i proteins that inhibit the production of cAMP, thus antagonising the activity of β-adrenergic receptors[453].

Most mammalian cells have a distinct adrenergic receptor expression profile, and the cellular response to NE or adrenaline is mediated by the integrated signalling from all cell surface adrenergic receptors[454]. For example, adipocytes mainly express α_2 and β_3 adrenergic receptors[455]. Therefore, the production of a key effector molecule cAMP that regulates the intracellular lipolytic activity is decided by the relative balance of activatory β_3-adrenergic receptor stimulation, and inhibitory α_2-adrenergic receptor stimulation[455].

All tissue macrophages predominantly express β2AR (encoded by *Adrb2*), and β2AR is the best-characterised adrenergic receptor in the immune system[456]. Infections lead to high circulating concentrations of TNFα, IL-1β and IL-6, all of which stimulate hypothalamic neurons and increase SNS tone in relevant target tissues, including lymphoid organs and sites of inflammation[456]. NE released in inflamed tissues act on β2ARs, which rapidly supresses the immune response by increasing intracellular cAMP levels in the immune cells, including macrophages. Such a negative feedback circuit ensures an appropriate resolution of inflammation and restoration of immune system homeostasis after pathogen clearance. Numerous reports over the past three decades have documented an anti-inflammatory role of β2AR stimulation in macrophages[456]. Pharmacological β2AR inhibition during systemic LPS challenge has been reported to dramatically decrease animal survival rate due to an exacerbated

septic shock[457]. Furthermore, conditioning humans in the conditions of extreme cold has been reported to profoundly reduce the systemic levels of inflammatory mediators in response to intravenous administration of LPS, which has been attributed to increased circulating NE and epinephrine concentrations in conditioned individuals[458]. ATMs have been suggested to be maintained in an M2 polarisation state due to SNS activity in WAT that acts via ATM β2ARs[459]. Surgical denervation of WAT dramatically reduces tissue NE content and leads to increased WAT inflammation in chow-fed mice[459]. Conversely, elevating SNS activity in WAT by systemic leptin administration results in increased WAT NE concentration and reduced inflammation[460]. Finally, stimulating or antagonising macrophage α2ARs (which counteract β2AR activity) has been shown to promote or inhibit the secretion of pro-inflammatory cytokines, respectively[461,462].

Interestingly, while there is an overwhelming evidence for an anti-inflammatory role of β2ARs in macrophages, a few reports have described the potentiating effect of β2AR activation in macrophage inflammatory activation. Stimulating LPS-macrophages with β2AR agonist has been demonstrated to elevate IL-6 and IL-1β production in an ERK and p38 signalling-dependent manner[463]. Furthermore, acute exposure to a particulate matter-containing air (an experimental model of air pollution) is known to cause cardiovascular thrombosis, which is mediated by IL-6 released from alveolar macrophages[464,465]. Particulate matter inhalation has been shown to promote the systemic release of catecholamines that engage β2ARs on lung macrophages and stimulate IL-6 secretion in a mitochondrial ROS-dependent manner[465]. Macrophage-specific genetic loss, or pharmacological β2AR inhibition in mice confers protection against particulate matter-induced IL-6 release and development of arterial thrombosis[465].

The reason for such discrepant findings on the modulation of inflammatory response in macrophages by β2AR agonism is unclear. It has been suggested that the outcome of β2AR signalling in macrophages can be context-dependent[456]. Therefore, the choice of inflammatory stimulus, macrophage subtype, culturing conditions and incubation periods might all affect the observed outcome of β2AR activation[456]. As the overall physiological role of the SNS is to ‘adapt’ the target tissue to the environmental

conditions and the intrinsic state of the animal, it could explain why some studies report a pro-inflammatory, and others an immunomodulatory role of β2AR in macrophages.

β-adrenergic signalling has been also demonstrated to stimulate immune cell mobilisation from the bone marrow and to guide circulating macrophage progenitors to the relevant tissues. The levels of circulating hematopoietic stem cells (HSCs), which give rise to all myeloid cells, exhibit circadian oscillations in mice and humans[466,467]. Such circadian fluctuations of HSC mobilisation from the bone marrow are regulated by NE secreted from the bone marrow SNS nerves that acts on the β3ARs of the bone marrow stromal cells[466]. Chronic environmental stress leads to increased circulatory HSC levels via the same mechanism[468]. NE released from the SNS nerve terminals in tissues can also act as chemoattractant for circulating monocytes. Stimulation of β2AR on monocytes and macrophages promotes their chemotaxis *in vitro*[469]. Furthermore, β2AR stimulation has been shown to induce CCR2 expression in macrophages[470]. β2AR-deficient macrophages fail to migrate to the heart following acute injury[470,471], and mice carrying a myeloid cell-specific *Adrb2* deletion display 100% mortality following myocardial infarction, compared to approximately 20% mortality observed in WT mice[471]. Finally, β1AR- and β2AR-deficient bone marrow exhibits reduced engraftment of the colon compared to WT bone-marrow following transplantation into irradiated WT mice, leading to impaired intestinal barrier integrity and an altered gut microbiome[472]. Overall, despite several conflicting reports in the literature, macrophage β2AR activation has been ascribed anti-inflammatory and chemoattractive roles by multiple studies.

1.4.3.2 Murine genetic models of β2AR deficiency

Besides already mentioned myeloid cell-specific knockout models, β2AR deficiency has also been investigated in other tissues. A whole-body *Adrb2* knockout mouse exhibits normal development and has normal resting heart rate and blood pressure[473]. However, they become hypertensive during exercise and demonstrate an elevated hypertensive response to epinephrine compared with WT mice[473]. Interestingly, β2AR-deficient animals can still exercise normally and actually have a greater total exercise capacity than WT controls, which could be attributed to their lower respiratory exchange ratio during exercise, indicating increased FAO[473]. In support of this, *Adrb2* knockouts have lower fat mass on chow diet than WT mice[473]. Subsequent study have

showed that β2AR-deficient animals have elevated retinal TNFα levels, leading to the development of a diabetic retinopathy[474]. Furthermore, *Adrb2* knockout mice display hyperinsulinaemia in the fasted state[475]. This observation is contrary to the potentiating effect of β2AR signalling on insulin secretion in pancreatic β cells[476]. A separate investigation has found that β2AR-deficient mice exhibit marked glucose intolerance due to defective insulin secretion[476]. Aging-induced impairments in glucose-stimulated insulin secretion have also been linked with reduced β2AR levels in pancreatic islets, and genetic overexpression of *Adrb2* in the β cells of aged mice prevents the development of aging-related glucose intolerance[476].

β2AR signalling in osteoblasts (bone-forming cell) is essential for appropriate bone formation. Leptin has been shown to regulate bone formation by centrally modulating SNS tone in bones[40,477]. Stimulation of the β2AR in osteoblasts by NE inhibits osteoblast proliferation and promotes bone resorption[478]. Consequently, pharmacological or genetic inhibition of β2AR signalling leads to an increase in bone mass[40,477]. Conversely, systemic administration of β2AR agonists decreases bone formation, increases bone resorption, and results in an overall bone loss[40,477,479].

Hepatocyte β2AR signalling regulates liver nutrient metabolism. Liver-specific *Adrb2* overexpression elevates hepatic levels of gluconeogenic enzymes and decreases liver glycogen content[480]. Similarly, systemic administration of β2AR pharmacological agonists leads to a reduction, while β2AR blockers promote an increase in hepatic glycogen levels in mice and humans[480,481]. β2AR agonists also increase hepatic lipid accumulation in mice through a mechanism that is independent of WAT lipolysis[482]. Furthermore, hepatic β2AR expression and liver steatosis are increased in aged mice[482]. The age-related increase in hepatic TG accumulation observed in WT mice is attenuated in β2AR knockout animals, leading to improved glucose tolerance compared to controls[483].

Overall, the variety of phenotypes observed in different genetic models of tissue-specific β2AR deficiency indicates that β2AR signalling has unique tissue and cell type-dependent functions. This variety is perhaps expected, given the multitude of regulatory roles that SNS has in nearly every mammalian tissue[484]. Importantly, such observations suggest that cell-specific *Adrb2* knockout models should be preferentially

utilised to investigate the importance of β2AR signalling in a specific cell type, in order to avoid the confounding effects of the loss of β2ARs in other tissues.

1.4.3.3 β-adrenergic receptor signalling pathway

Figure 1-11 depicts the canonical response to $G\alpha_s$-coupled receptor agonism in a simplified manner. In response to agonist stimulation, $G\alpha_s$-coupled GCPRs release the α domain of the G protein, which then binds to adenylyl cyclase (AC) and increases its catalytic activity, leading to an elevated intracellular cyclic adenosine monophosphate (cAMP) concentration[485]. cAMP acts as a second messenger by modulating the activity of multiple down-stream effector enzymes, including protein kinase A (PKA). Once activated, PKA translocates into the nucleus, where it phosphorylates cAMP-responsive element-binding protein (CREB) and promotes CREB-dependent gene transcription[485].

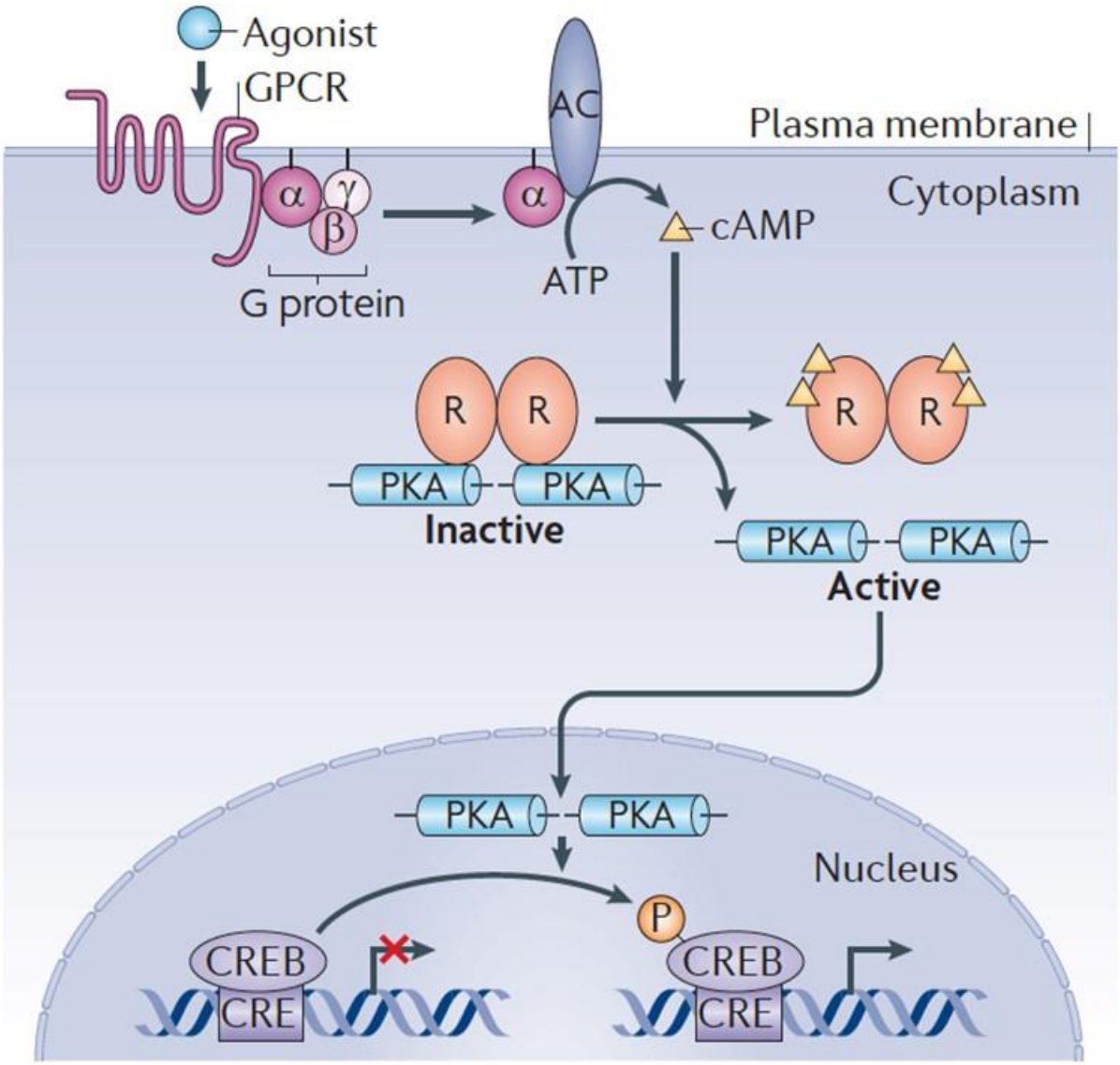

Figure 1-11. Canonical G_{as}-coupled receptor signalling pathway.

Upon GPCR activation, cAMP produced by AC binds to the regulatory subunits (R) of PKA, liberating the catalytic subunits and allowing their translocation into the nucleus. Figure taken from Altarejos and Montminy[485]*.*

PKA also phosphorylates other proteins in a cell type-dependent manner[486]. For example, adipocytes express high levels of a lipid droplet-binding protein perilipin-1[487]. In a basal state, perilipin-1 coats the surface of a lipid droplet, thus preventing the intracellular TG lipases from accessing stored TGs[487]. However, in response to adipocyte β-adrenergic stimulation, active PKA phosphorylates perilipin-1, leading to its altered conformation that allows ATGL- and HSL-mediated lipolysis to occur[487]. HSL is also directly phosphorylated by PKA, which increases its lipolytic activity[488].

Specific GPCRs, including β2AR, also exhibit *non-canonical intracellular signalling*. After a prolonged stimulation or in response to high extracellular agonist concentrations, GPCRs are phosphorylated by GPCR kinases (GRKs)[489]. Phosphorylation by GRKs recruits arrestin proteins, which bind to GPCRs and promote their internalisation by clathrin-dependent endocytosis, thus limiting the surface availability and signalling of the receptor[489]. Upon internalisation, the GPCR-arrestin complex is either recycled and returned to the plasma membrane, or targeted to lysosomes for degradation[489]. Interestingly, internalised GPCR-arrestin complex has been reported to signal from endosomes, leading to the activation of multiple downstream signalling molecules, including ERK[489].

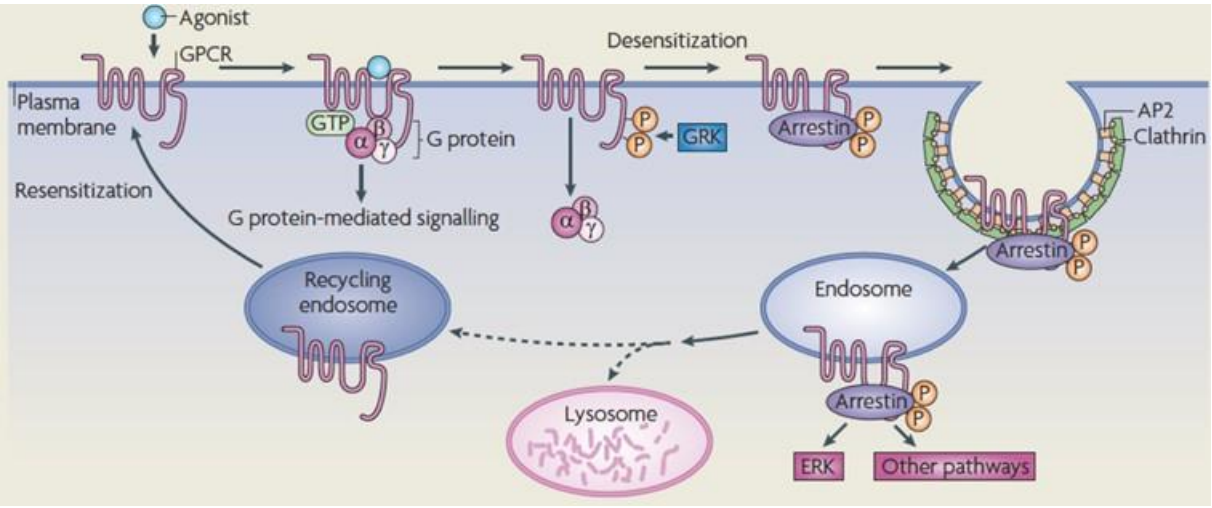

Figure 1-12. GPCR internalisation and β-arrestin-dependent signalling.
Figure taken from Ritter and Hall[489].

1.4.3.4 The roles of cAMP and CREB in regulating macrophage function

The CREB family of transcription factors include CREB, cAMP response element modulator (CREM) and activating transcription factor 1 (ATF1)[485]. Several protein kinases, including PKA, PKC and calmodulin kinases, can phosphorylate CREB at its transcription activating site, serine-133[485]. Once phosphorylated, CREB binds to its coactivators CREB-binding protein (CBP) or p300 and initiate the transcription of its target genes[485].

CREB has been ascribed an anti-inflammatory role in macrophages. The resolution phase of inflammation in macrophages is predominantly controlled by cAMP[490,491]. Inhibiting cAMP production converts resolution phase macrophages back to an M1 phenotype, whereas enhancing intracellular cAMP levels in M1 macrophages induces the resolution phenotype prematurely during bacterial infection[490]. Similarly to CREB, the optimal activity of the M1 polarisation-driving transcription factor NF-κB requires its interaction with CBP/p300[492]. As both phosphorylated CREB and NF-κB subunit RelA binds to the same region of CBP/p300, it has been proposed that NF-κB activity is inhibited by activated CREB through competition for limiting amounts of CBP/p300[493,494]. The relative physiological contribution of such a transcriptional-competition mechanism to the overall anti-inflammatory role of CREB has not yet been investigated.

The gene encoding the main cytokine mediating the resolution of inflammation, *Il10*, is under the transcriptional control of CREB[495]. During inflammation, TLR stimulation leads to the activation of ERK and p38 kinases, which phosphorylate and activate mitogen and stress activated protein kinases (MSK) 1 and 2[496]. MSKs then phosphorylate CREB to promote IL-10 production, thus limiting macrophage inflammatory activation[496]. Interestingly, recent studies have found that CREB Ser133 phosphorylation is required, but not sufficient for *Il10* transcription[497,498]. The transcriptional induction of a subset of CREB target genes, including *Il10*, is also dependent on the binding of CREB-regulated transcription coactivators (CRTCs) to the CREB-CBP/p300 protein complex[485]. In the basal state, CRTCs are phosphorylated by salt-inducible kinases (SIKs), leading to their sequestering in the cytoplasm[485]. When intracellular cAMP levels are increased, PKA catalyses inhibitory phosphorylation of SIKs, resulting in a decreased CRTC phosphorylation. Dephosphorylated CRTC then translocates into the nucleus and binds to CREB[485]. G_{as}-coupled GPCRs have been shown to drive the formation of resolution phase macrophages by PKA-SIK-CRTC pathway-dependent IL-10 secretion and autocrine signalling[498]. Furthermore, pharmacologically inhibiting SIKs during TLR stimulation also promotes the M2b macrophage polarisation[497].

CREB and cAMP have an anti-inflammatory role in ATMs during obesity. Compared to genotype controls, macrophage-specific *Creb1* knockout (encoding the major CREB isoform in macrophages) mice exhibit augmented WAT inflammation, glucose

intolerance and insulin resistance after prolonged high-fat feeding[499]. Furthermore, elevated WAT SNS tone leads to cAMP-dependent inhibition of SIKs in ATMs[460]. Like CRTCs, histone deacetylase 4 (HDAC4) is sequestered in the cytoplasm due to its inhibitory phosphorylation by SIKs. Therefore, cAMP-mediated inhibition of SIKs promotes HDAC4 nuclear translocation, which modifies the chromatin structure to enable the resolution phase transcriptional programme in macrophages[460]. Macrophage-specific *Hdac4* knockout mice exhibit increased body weight, fat mass, WAT inflammation and insulin resistance after high-fat feeding, compared to genotype controls[460]. Finally, genetic variants in *HDAC4* gene have been associated with obesity in humans, suggesting that cAMP signalling in ATMs might regulate energy balance in humans[460].

1.4.3.5 The role of β-arrestins in regulating macrophage function

Compared to G_{as}-mediated cAMP signalling, the role of β-arrestin signalling in macrophages is less clear. Macrophages express β-arrestins 1 and 2, both of which have been reported to interact with β2AR in other cell types[500,501]. Upon their internalisation, both β-arrestins have been reported to directly bind and prevent the activation of NF-κB[502,503]. However, other studies have showed that β-arrestins positively regulate NF-κB activity[504,505]. β-arrestin 1 has also been found to interact with CREB and enhance its transcriptional activity[506]. In cultured macrophages, β-arrestin 2 has been reported to inhibit LPS-induced cytokine production[507,508]. Finally, knockdown of β-arrestins 1 and 2 drastically decreases macrophage chemotaxis *in vitro*[509]. Furthermore, β2AR-mediated CCR2 expression in macrophages is dependent on β-arrestin 2 signalling *in vivo*[470].

β-arrestin signalling is metabolically beneficial during obesity. Mice deficient in β-arrestin 1 gain more weight and develop exacerbated WAT inflammation and insulin resistance than controls on high-fat diet[510,511]. Conversely, transgenic overexpression of β-arrestin-1 reduces diet-induced obesity and improves glucose tolerance and systemic insulin sensitivity[510]. Similarly, hepatic β-arrestin 2 expression is greatly reduced in obese animals, and systemic β-arrestin 2 deficiency leads to a worsened metabolic phenotype after prolonged high-fat feeding[512]. Hepatocyte-specific *Arrb2* deletion (encoding β-arrestin 2) greatly increases liver GPCR signalling, resulting in diminished insulin sensitivity and impaired systemic glucose metabolism[513]. Liver-

specific overexpression of *Arrb2* reduces hepatic GPCR signalling and protects mice against the metabolic complications during obesity[513].

At present, it is not clear whether β-arrestins play an anti-inflammatory role in ATMs during obesity. It has been shown that GPR120 exerts its anti-inflammatory effects through β-arrestin 2-mediated suppression of an inflammatory signalling cascade downstream of TLRs[212]. However, no studies have investigated the metabolic profiles of mice with macrophage-specific β-arrestin 1 or 2 deficiencies.

1.4.4 The associations of human *ADRB2* gene polymorphisms with obesity and metabolic complications

ADRB2 gene has been sequenced in multiple human populations and more than 80 different polymorphisms have been identified[514]. Two nonsynonymous single nucleotide polymorphisms (SNPs) resulting in amino acid changes in the 16 position (arginine to glycine, Arg16Gly) and the 27 position (glutamic acid to glutamine, Glu27Gln) are common with observed minor allele frequencies of 40-50%[514]. *In vitro* characterisation of *ADRB2* mutants demonstrated that the Gly16 variant increased the agonist-stimulated internalisation of β2AR, whereas Gln27 isoform did not show any effects on receptor expression or signalling[515,516]. A third nonsynonymous SNP encoding an amino acid change in the 164 position (threonine to isoleucine, Thr164Ile) occurs with a minor allele frequency of 1-3%[514]. The Ile164 isoform is approximately four times less responsive to agonist-induced stimulation than the Thr164 isoform *in vitro*[517]. These three *ADRB2* polymorphisms have been associated with multiple disorders, including asthma, hypertension, obesity and type-2 diabetes[514]. Furthermore, *ADRB2* SNP carriers display altered pharmacokinetics to β2AR therapeutic agonists[514]. Here, only the major findings related to the metabolic effects of *ADRB2* variants will be summarised.

Association studies of the Arg16Gly SNP with obesity and type-2 diabetes have reported conflicting results. The Arg16 variant has been linked to a minor increase in the risk of type-2 diabetes development in two different populations[518,519]. Furthermore, the Arg16 variant has also been found to correlate with BMI in several investigations[520-522]. In contrast, other studies have reported a significant association between the Gly16 variant and insulin resistance[523,524]. Among individuals with

hypertriglyceridaemia, individuals homozygous for the Arg16 variant had higher circulating total cholesterol and LDL-cholesterol levels[525].

Similarly to Arg16Gly, the studies investigating the association of the Gln27Glu variant with metabolic outcomes have reported positive[522,526], negative[527,528] or no association[518,519,529] with type-2 diabetes in different populations. In the presence of the Arg16 variant, Gln27 variant-carriers show an increased risk of obesity, while other studies have showed either a positive[530-532] or no association[533] of the Glu27 variant with BMI.

The largest study on *ADRB2* polymorphisms to date (64,000 individuals) reported no associations with either of the *ADRB2* SNPs with type-2 diabetes[534]. In this study, out of 3 variants only the Thr164Ile was linked to an increased risk of obesity[534]. Furthermore, no large population GWAS studies have yet associated SNPs in the *ADRB2* gene with obesity or type-2 diabetes. It is therefore possible that the published significant associations between *ADRB2* variants and metabolic disorders stem from a small number of individuals in the study groups, and the significant effects disappear in large cohorts of individuals.

1.5 Central hypothesis and aims of thesis

The research strategy of our laboratory has been largely shaped by 'adipose tissue expandability' hypothesis (1.1.6), stating that when the adipose tissue reaches its limit of expansion, lipids fail to be stored in adipocytes and start to accumulate in other cell types. Such aberrant ectopic lipid accumulation promotes lipotoxicity, which is the driving cause of obesity-related cardiometabolic complications.

Within adipose tissue itself, in a lean healthy state, the lipid flux into and within ATMs is tightly regulated by extracellular signalling cues, and lipid availability is controlled by appropriately-functioning adipocytes. In obesity, adipocyte dysfunction causes aberrant lipid accumulation in ATMs. Furthermore, obesity dysregulates extracellular signals that control ATM intracellular lipid metabolism, leading to a shift from biologically inert (TGs, CEs) to biologically active (PCs, DAGs, ceramides, sterols) lipid species within ATMs.

Central hypothesis: qualitative repartitioning of intracellular lipid species triggers the pro-inflammatory activation of ATMs, leading to the development of systemic insulin resistance.

The proposed central hypothesis will be investigated in 3 aims, each of them representing a separate results chapter of this thesis:

First, multiple studies presented in the introduction illustrate the importance of intracellular lipid metabolism and membrane lipid composition for an appropriate cell function. While altered PC:PE ratio has been observed in multiple tissues during obesity, no reports regarding fatty acid- or obesity-induced alterations in macrophage PC:PE ratio currently exist. Therefore, in the first results chapter of this thesis (**Chapter 3**), I will aim to characterise the effects of obesity on ATM PC and PE metabolism, and explore the mechanistic link between the cellular PC:PE ratio and macrophage inflammatory activation by saturated fatty acids.

Secondly, the effect of sympathetic nerve activity on ATMs is poorly understood. Importantly, the direct metabolic consequences of the loss of NE sensing by ATMs have not yet been described, as all the previous reports investigating the role of SNS in the regulation of WAT inflammation have manipulated the overall SNS output to

WAT, and have thus targeted all of the cell types present in the tissue. Furthermore, the molecular mechanisms mediating lipid accumulation in ATMs during fasting are unclear. Therefore, in the second results chapter (**Chapter 4**) I will aim to characterise the effects of NE stimulation on macrophage lipid partitioning and saturated fatty acid-induced inflammation, and to understand the role of NE signalling in ATMs in the regulation of WAT inflammation and systemic metabolism.

In the third results chapter (**Chapter 5**), I will aim to describe the intracellular signalling and transcriptional mechanisms underlying the phenotypic changes in macrophage nutrient metabolism occurring in response to β2AR stimulation.

2 Materials and methods

2.1 Materials

Details of compounds used in animal and cell experiments are summarised in Table 2-1.

Compound name	Source	Catalogue number
E. coli lipopolysaccharide (LPS)	Sigma	L4391
Interleukin-4 (IL-4)	Peprotech	214-14
(±)-Norepinephrine (+)- bitartrate salt	Sigma	A0937
Fenoterol hydrobromide	Sigma	F1016
ICI-118,511	Tocris	0821
HG-9-91-01	BioVision	B1849
2-deoxyglucose	Sigma	D8375
Chetomin	Sigma	C9623
A922500	Cayman	10012708
Bafilomycin A1	Sigma	B1793
Orlistat	Sigma	O4139
Human insulin (Actrapid)	Novo Nordisk	ADE138C (Obtained from a pharmacy)
Glucose (20% solution)	CIMR	n/a
Fentanyl	Martindale Pharma	PL 00156/0038
Midazolam (Hypnovel)	Roche	PL00031/0126
Acepromazine	Novartis	GTIN5037694004606
Methyl-[^{3}H]- choline chloride	Perkin Elmer	NET109250UC
D-[3-^{3}H]- glucose	Perkin Elmer	NET331A250UC
[1-^{14}C]- palmitic acid	Perkin Elmer	NEC075H050UC
[1-^{14}C]- oleic acid	Perkin Elmer	NEC317050UC
[1,2-^{14}C]- acetic acid, sodium salt	Perkin Elmer	NEC553250UC
[1-^{13}C]- oleic acid	CIL	CLM-149
Palmitic acid	Cayman	1000627
Oleic acid	Cayman	90260
L-Carnitine hydrochloride	Sigma	C0283
Oligomycin A	Sigma	75351
FCCP	Sigma	C2920
Rotenone	Sigma	R8875
Antimycin A1	Sigma	A8674
Etomoxir	Sigma	E1905

Table 2-1. Compounds and their sources.

2.2 *In vivo* methods

2.2.1 Animal care

Unless otherwise indicated, mice were housed 3-5 per-cage in a temperature-controlled room (21°C) with a 12 h light/dark cycle, with 'lights on' corresponding to 6 am. Animals had *ad-libitum* access to food and water. All animal protocols were conducted in accordance with the UK Home Office and Cambridge University ethical guidelines.

2.2.2 Animal diets

Nutritional composition of diets are summarised in Table 2-2. A standard chow diet was administered to animals from weaning. For HFD studies, a specified HFD was administered to the animals *ad-libitum* from 8 weeks of age for the indicated period of time.

Diet name	Diet ID	Manufacturer	Carbohydrate	Protein	Lipid
Standard chow	DS-105	Safe diets	64.3	22.4	13.3
HFD 45%	D12451	Research diets	35.0	20.0	45.0
HFD 60%	D12492	Research diets	20.0	20.0	60.0

Table 2-2. Nutritional composition of animal diets.

Nutrient values correspond to the percentage of the total energy content of the diet.

2.2.3 Animal models

Animal age, gender, diet, housing temperature, and genetic background is described in legend, where applicable.

WT mice used for generation of bone marrow-derived macrophages and temperature, diet and compound administration studies were male on a C57Bl/6J genetic background (bought from Charles River, UK).

For all macrophage-specific gene deletion studies, animals were crossed to a mouse model expressing Cre recombinase from bacteriophage P1 under LysM promoter (LysM-Cre). This model was generated by replacing a single allele of *Lyz2* gene with the coding sequence of Cre recombinase as described[535] and was gifted to us on a mixed C57Bl/6J, 129/Sv genetic background by Dr. Suzanne Jackowski. LysM-Cre line was backcrossed to a C57Bl6/J genetic background using Marker-Assisted

Accelerated Backcrossing (MAX-BAX, Charles River, UK) technology until SNP genotyping confirmed >99% background purity.

Macrophage-specific *Pcyt1a* knockout mouse was generated by crossing a mouse model containing *loxP* sequences surrounding *Pcyt1a* alleles (Pcyt1a$^{fl/fl}$) to the LysM-Cre mouse. Pcyt1a$^{fl/fl}$ mouse was generated by Prof. Ira Tabas and Dr. Susan Jackowski as described[309], and was gifted to us on a mixed C57Bl/6J, 129/Sv genetic background by Dr. Suzanne Jackowski. Pcyt1a$^{fl/fl}$ line was backcrossed to a pure C57Bl6/J genetic background as described for LysM-Cre line above.

Macrophage-specific *Adrb2* knockout mouse was generated by crossing a mouse model containing *loxP* sequences surrounding *Adrb2* alleles (Adrb2$^{fl/fl}$) to the LysM-Cre mouse. Adrb2$^{fl/fl}$ mouse was generated by Prof. Florent Elefteriou and Prof. Gerard Karsenty as described[536], and was gifted to us by Prof. Gerard Karsenty on a pure C57Bl/6J genetic background.

Femur and tibia bones from macrophage-specific *Hif1a*[301] and *Hif2a*[537] knockout mice (LysM-Cre Hif1a exon2$^{fl/fl}$ and LysM-Cre Hif2a exon2$^{fl/fl}$, respectively) and littermate floxed controls were gifted to us by Prof. Randall Johnson on a pure C57Bl/6J genetic background.

All experimental macrophage-specific knockout mice were produced by crossing LysM$^{+/+}$ with LysM$^{+/Cre}$ animals on a floxed/floxed background, yielding a 1:1 Mendelian ratio of control (floxed/floxed LysM$^{+/+}$) to knockout (floxed/floxed LysM$^{+/Cre}$) offspring.

2.2.4 Blood sampling

All blood samples were taken from tail vein of unrestrained animals directly into glass capillary tubes. At the end of each study, terminal blood samples were collected into blood collection tubes (0103, Vetlab) by cardiac puncture immediately after sacrifice. Blood samples were kept on ice before centrifuging at >10,000 g for 5 min. Serum was then collected and stored at -80°C for subsequent analyses.

2.2.5 Cold exposure

For 72 h of cold exposure, animals in their home cages were placed in the temperature-controlled room set at 5°C (50% relative humidity). Weighing and blood sampling of

cold-exposed mice was performed in the same room. For 24 h of cold exposure, mice were placed in a temperature-controlled cabinet set at 10 °C (50% relative humidity) and culled immediately after leaving the cabinet.

2.2.6 Indirect calorimetry

Energy expenditure (EE) and respiratory quotient (RQ) were calculated from data gathered from single-housed mice fed *ad-libitum* by a custom-made monitoring system (Creative Scientific UK). The monitoring system calculated oxygen and carbon dioxide concentrations at 18-minute intervals, with flow rates set to 400 ml/min. EE was calculated from oxygen consumption and carbon dioxide production measured over a 48 h period using modified Weir equation[538] (EE J/min = 15.818 x VO_2 (ml/min) + 5.176 x VCO_2 (ml/min)). EE was compared between genotypes using analysis of covariance (ANCOVA) with body weight as a covariate.

2.2.7 Food intake and faecal excretion analyses

Daily food intake and faecal excretion were assessed by single-housing mice in cages containing liners and manually weighing food pellets and crumbs (food intake), and faeces (excretion).

2.2.8 Glucose tolerance tests

Mice were fasted for 16 h from 4 pm to 8 am. Mice were single-housed at least 1 h prior to being injected intraperitoneally with 1 mg/kg glucose. Blood samples for glucose measurement were taken at 0, 10, 20, 30, 60, 90 and 120 min after the injection.

2.2.9 Insulin tolerance tests

Mice were fasted for 6 h from 8 am to 2 pm. Mice we single-housed at least 1 h prior to being injected intraperitoneally with 0.75 IU/kg of human insulin. Insulin dose of 1 IU/kg was used for HFD-fed mice. Blood samples for glucose measurement were taken at 0, 10, 20, 30, 60, 90 and 120 min after the injection.

2.2.10 Lipid tolerance tests

Mice were fasted for 16 h from 4 pm to 8 am. Mice we single-housed at least one hour prior to being administered with 200 μl of olive oil by oral gavage. Blood samples for glucose measurement were taken at 0, 1, 2, 4 and 8 h after injection.

2.2.11 Compound injection studies

In order to block β2-adrenergic receptor signalling, mice were injected intraperitoneally with 500 μg of ICI-118,551 for the period indicated in legend.

2.2.12 Hyperinsulinaemic-euglycaemic clamps

All clamp studies were performed by Dr. Sam Virtue and Dr. Anne Mcgavigan. Mice were fasted for 16 h from 4 pm to 8 am. Animals were anaesthetised by subcutaneously injecting 11 ml/kg of the following combination of drugs: fentanyl (0.03125 mg/ml), midazolam (0.625 mg/ml) and acepromazine (0.625 mg/ml). Once unconscious, mice were placed on temperature controlled heating pads (Harvard Apparatus) and their core body temperature was maintained at 37°C. Catheters were placed in the tail veins connected to two separate syringe pumps. Mice underwent a basal infusion period with 231 kBq/ml [3-^{3}H]-glucose, 3 mg/ml sodium citrate in 0.9% NaCl solution, infused at 100 μl/h for 90 min. A bolus of 30 μl of hyperinsulinaemic infusate (basal infusate + 0.11 mU/ml human insulin) was then administered to initiate hyperinsulinaemia, and the hyperinsulinaemic infusate continued to be administered at 100 μl/h for at least 90 min. Immediately after initiation of hyperinsulinaemia, 12.5% glucose, 3 mg/ml sodium citrate in 0.9% NaCl solution was infused at a variable rate in order to clamp glucose at the basal level. Blood glucose was measured every 5 min for 90 min and glucose infusion rate (GIR) was adjusted until mice had stable blood glucose values that were +/- 0.5 mM of their initial values. Serum samples were collected for the determination of specific activity at the end of basal and hyperinsulinaemic states.

Radioactivity in serum was measured by mixing 10 μl of serum sample with 90 μl PBS, before adding 100 μl 20% trichloroacetic acid to precipitate proteins. Samples were then centrifuged at 16,000 g for 10 min, and 160 μl of the supernatant was transferred to a clean tube and air-dried at 95 °C. Dried samples were resuspended in 100 μl of water, 90 μl of the sample was transferred to 4 ml of scintillation liquid (SG-BXX-24, Lab Logic) and subjected to liquid scintillation counting (LSC).

Steady state clamp GIR was considered to be the average of GIRs at 70, 80 and 90 min following insulin infusion. Steady state kinetic parameters were calculated as follows:

- Glucose specific activity (dpm/μmol) = plasma specific activity (dpm/ml) / glucose concentration (mM).

- Glucose turnover (R_d, μmol/min) = rate of radiolabelled glucose infusion / glucose specific activity.

- GIR was calculated based on the rate of 12.5% glucose solution infusion and expressed as μmol/ml.

- Hepatic glucose production (HGP, μmol/ml) in a basal state was equal to R_d, in hyperinsulinaemic state it was equal to R_d – GIR.

2.2.13 Macrophage-to-liver PC transport assay

BMDMs were plated in 6-well plates and cellular PC was labelled by incubating cells in the presence of 0.074 MBq/ml methyl-[3H]- choline chloride in the medium for 24 h. Cells were then washed, detached using ice-cold Dulbecco's phosphate buffered saline (PBS, D8537, Sigma) containing 1 mM EDTA and manually counted. Cells were centrifuged at 500 g, 4°C for 5 min and re-suspended in PBS at the concentration of 10^6 cells/200 µl. Specific activity of cells was determined by lysing 10^5 cells in 100 µl of PBS containing 1% Triton^{TM} X-100 (X100, Sigma), adding the lysates to scintillation vials containing 5 ml of Hionic-Fluor scintillation liquid (6013319, Perkin-Elmer) and subjecting them to LSC.

10^6 BMDMs containing approximately $2x10^6$ dpm were injected into each mouse, and blood samples were collected at 3, 6 and 24 h. Serum HDL fraction was isolated by using LDL and vLDL precipitation buffer according to manufacturer's instructions (ab105138, Abcam). Radioactivity was determined in total and in HDL lipid and aqueous fractions of serum by lipid extraction as described in 2.5.7. 24 h later, mice

were sacrificed and liver, brain, brown adipose tissue and spleen were collected. Dounce homogeniser was used to homogenise approximately 100 mg of each tissue directly in the scintillation vials containing 5 ml of Hionic-Fluor scintillation liquid. Radioactivity in each tissue was measured by LSC and all counts were expressed as percentage values of the amount (dpm) injected.

2.2.14 Serum biochemistry

Blood glucose was measured using an AlphaTRAK 2 (Zoetis) glucose meter and strips. All serum biochemistry analysis was performed in Keith Burling's Core Biochemical Assay Laboratory using the following commercially available kits: TG (Siemens Healthcare), cholesterol and HDL (Dade-Behring), free choline (Abcam), FFA (1138175001, Roche), ALT and AST (Siemens Healthcare) were measured enzymatically. LDL concentration was calculated using the Friedwald formula ([LDL] = [Cholesterol] – [HDL] – [TG]/2.2). Insulin was measured using electrochemical luminescence immunoassay (K152BZC, MesoScale Discovery).

2.3 *Ex vivo* methods

2.3.1 Isolation of peritoneal macrophages

Immediately after sacrifice, 5 ml of PBS containing 0.5 mM EDTA was injected into palpitate peritoneal cavity. As much liquid as possible was recovered, and the procedure was repeated two more times with fresh PBS containing 0.5 mM EDTA. Pooled lavages were centrifuged at 400 g, 4° for 5 min and pellets were frozen for subsequent analysis.

2.3.2 Isolation of alveolar macrophages

Immediately after sacrifice, 800 µl of PBS containing 0.5 mM EDTA was injected into lungs. As much liquid as possible was recovered, and the procedure was repeated two more times with fresh PBS containing 0.5 mM EDTA. Suspension was centrifuged at 400 g, 4° for 5 min and pellets were frozen for subsequent analysis.

2.3.3 Adipose tissue fractionation

Adipose tissues were removed after sacrifice, chopped thoroughly and re-suspended in 10 ml digestion solution containing 7 ml Hanks' Balanced Salt Solution (HBSS, H9269, Sigma), 0.23 g bovine serum albumin (BSA, A9418, Sigma), and 20 mg

collagenase type II (C6885, Sigma), filtered through 0.22 µm membrane. The digestion was performed at 37°C for 20 min, with shaking at 100 rpm. The digestion mixture was then passed through a 100 µm cell strainer (352360, Falcon) into a fresh tube and incubated at room temperature for 10 min, allowing the adipocyte fraction to layer on the surface. Adipocyte fraction was collected by pipetting and frozen for subsequent analysis. The remaining solution was centrifuged at 400 g, 4° for 5 min and pellet was re-suspended in 1 ml of pre-cooled (at 4°C) selection buffer (2 mM EDTA, 0.5% bovine serum albumin in PBS). Total cell number was determined by manual counting. Cell suspension was centrifuged at 400 g, 4° for 5 min and pellet was re-suspended in 90 µl of selection buffer and 10 µl of CD11b micro-beads (130049601, Miltenyi Biotec) per 10^7 cells. Cell suspension was mixed and incubated for 15 min at 4°C. Cells were then washed by adding 3 ml of selection buffer and centrifuged at 400 g, 4° for 5 min. Pellet was re-suspended in 500 µl of selection buffer and loaded onto a MACS LS column (130-042-401, Miltenyi Biotec) placed in the magnetic field of a MACS separator (Miltenyi Biotec) and flow-through was collected in a fresh tube. The column was then washed thrice with 3 ml of selection buffer. The total effluent contained unlabelled cells and corresponded to the adipose tissue stromal vascular fraction (SVF). The LS column was then removed from the MACS separator and placed in a fresh collection tube. The labelled cells were eluted using 5 ml of selection buffer and corresponded to adipose tissue macrophage (ATM) fraction. Both SVF and ATM fractions were centrifuged at 400 g, 4° for 5 min and pellets were frozen and stored at -80°C for subsequent analysis.

2.3.4 Isolation of Kupffer cells

The composition of solutions used in the procedure of Kupffer cell isolation are summarised in Table 2-3. All solutions were made in-house one day before the experiment and their pH was adjusted to 7.4 before sterile-filtering.

Immediately after sacrifice, the liver was perfused through the portal vein with SC-1 at 37°C for 5 min at a flow rate of 7.5 ml/min. Subsequently, the liver was perfused with sterile-filtered SC-2 containing 0.5 mg/ml Pronase E (107433, Merck Millipore) for 5 min at a flow rate of 7.5 mL/min, and then with sterile-filtered SC-2 containing 0.25 mg/ml Collagenase P (COLLP-RO, Sigma). After the final perfusion, liver was excised and placed in a glass beaker with 120 ml of sterile-filtered SC2 containing 0.4 mg/ml Pronase E, 0.4 mg/ml Collagenase P and 2 mg/ml DNAse I (10104159001, Sigma).

Liver was dissected into small pieces with scissors before sealing the beaker with tin foil and incubating the suspension at 37°C for 20 min. During the first 10 min of incubation, a single drop of 1 M NaOH was added every 2 min. During the last 10 min of incubation, a single drop of 1 M NaOH was added every 5 min. Suspension was then divided evenly between 3 50 ml Flacon tubes and they were complemented with SC-2 until full. All tubes were centrifuged at 25 g, room temperature for 3 min and pellets were discarded. Supernatants were centrifuged again at 25 g, room temperature for 3 min and pellets were discarded. Supernatants were then centrifuged at 350 g, room temperature for 10 min, resulting pellets were re-suspended in 50 ml of PBS and centrifuged at 350 g, room temperature for 10 min. Kupffer cells from pellets were isolated by magnetic CD11b micro-beads as described in 2.3.3.

Chemical name	**SC-1**	**SC-2**
NaCl	8000	8000
KCl	400	400
NaH_2PO_4	75.5	75.5
Na_2HPO_4	120.5	120.5
$NaHCO_3$	350	350
$CaCl_2$. 2 H_2O	-	560
HEPES	2380	2380
EGTA	190	-
D-(+)-Glucose	900	-
Phenol red	6	6

Table 2-3. Composition of solutions used in the procedure of Kupffer cell isolation. *Concentrations for all chemicals are indicated in mg/l.*

2.4 *In vitro* methods

2.4.1 Culture and differentiation of bone-marrow derived macrophages

Femur and tibia bones from WT mice were isolated and cleaned, and 10 ml of Roswell Park Memorial Institute Medium (RPMI)-1640 (Sigma) was flushed through each bone using a syringe. Bone marrow cells were counted manually, pelleted by centrifugation, and re-suspended in RPMI-1640 with 20-30% L929 conditioned medium, 10% heat-inactivated FBS (Gibco, Thermo Fisher Scientific) and 100 U/ml penicillin-streptomycin (Thermo Fisher Scientific) (macrophage differentiation medium). To differentiate into macrophages, cells were seeded in 10 cm non-culture treated plates (Falcon) at a density of $5x10^6$ cells per plate per 10 ml of macrophage differentiation medium and cultured for 7 days at 37ºC in 5% CO_2. On day 5 of differentiation, medium was removed and 10 ml of fresh macrophage differentiation medium was added to each plate. On day 7 of differentiation, macrophages were detached using ice-cold

PBS containing 1 mM EDTA, counted manually, centrifuged at 500 g, room temperature for 5 min and re-suspended in macrophage differentiation medium at the concentration of $5x10^5$ cells/ml. Immediately after, cells were plated for experiments at the following densities: 100 μl of cell suspension per well of 96-well plate, 500 μl/well of 24-well plate, 1 ml/well of 12-well plate, 2 ml/well of 6-well plate and 10 ml per 10 cm plate. Cells were incubated for at least 24 h after plating before conducting experiments.

To make L929 conditioned medium, L929 cells (CCL-1, ATCC) were seeded in DMEM supplemented with 10% heat-inactivated FBS, 100 U/ml penicillin-streptomycin and 2 mM L-glutamine (Sigma) at a density of 500,000 cells per 50 ml of medium per T175 tissue culture flask. Medium was harvested after 1 week of culture, and then 50 mL of fresh DMEM supplemented with 10% heat-inactivated FBS, 100 U/ml penicillin-streptomycin and 2 mM L-glutamine was added onto cells and harvested 1 week later. Batches obtained after the first and second weeks of culture were mixed at a 1:1 ratio, aliquoted and stored at -20°C.

Detection of Mycoplasma in cell cultures was not performed.

2.4.2 Cell stimulations

All BMDM stimulations were performed in macrophage differentiation medium for periods indicated in legend. To polarise BMDMs to M1 or M2 state, they were treated for 24 h with 100 ng/ml LPS, or 10 μM IL-4 respectively. In co-stimulation experiments, adrenergic receptor agonists were added 5 min before stimulating macrophages with LPS or IL-4. In all inhibitor and antagonist studies, inhibitors/antagonists were added 30-60 min prior to stimulation.

All fatty acid treatments were done using FFAs conjugated to BSA (fatty acid and endotoxin free, A8806, Sigma). The conjugation was performed by preparing a sterile-filtered 1% BSA solution in macrophage differentiation medium. Both 1% BSA medium and concentrated fatty acid solution (100 mM of fatty acid in ethanol) were heated at 60°C before adding fatty acid solution dropwise into 1% BSA medium in order to make a medium containing 1 mM fatty acid and 1% BSA. This medium was then sonicated until it became completely clear and used for stimulations on the same day without sterile filtering. FFA-free BSA solution was used as a control.

2.4.3 Stable isotope and radioisotope labelling

For radiolabelling experiments, radioisotope tracers were dissolved in macrophage differentiation medium at the following concentrations: 0.074 MBq/ml for methyl-[^{3}H] choline chloride, 0.006 MBq/ml for [1-^{14}C]-palmitic and oleic acids and 0.148 MBq/ml for [1-^{14}C] acetic acid. BMDMs were plated at the standard densities in 24-well plates for choline incorporation, fatty acid oxidation, lipid uptake and lipolysis assays and in 6-well plates for lipid analysis by thin-layer chromatography.

Radioactivity in total cells was determined by lysing cells in 100 µl of PBS containing 1% Triton^{TM} X-100, adding the lysate to scintillation vial containing 5 ml of Hionic-Fluor scintillation liquid and subjecting it to LSC. Radioactivity in culture medium was determined by adding 100 µl of cell culture supernatant to scintillation vial containing 5 ml of Hionic-Fluor scintillation liquid and subjecting it to LSC. Radioactivity in cellular lipids was analysed as described in 2.5.7.

For stable isotope labelling experiments, BMDMs were treated with BSA-[1-^{13}C] oleic acid conjugate as described in 2.4.2 and cellular lipids were analysed as described in 2.5.

2.4.4 Fatty acid oxidation assay

FAO assay was adapted from a published protocol[539]. BMDMs were treated as described in the legend before washing them with PBS and incubating in the presence of FAO medium (DMEM containing 12.5 mM HEPES, 1 mM L-carnitine, 0.3% BSA and 100 µM palmitate or 100 µM oleate, radiolabelled as described in 2.4.3). 0 h NE and etomoxir treatments were performed after the medium change. Plates were then immediately sealed with parafilm M and placed at 37 °C for 3 h.

Meanwhile, CO_2 traps were prepared by adding 200 µl of concentrated HCl into the 1.5 ml Eppendorf tubes containing paper discs, wetted with 20 µl of 1 M NaOH, in the inner side of their lids. Once the FAO reaction finished, 400 µl of medium from BMDMs were transferred into the CO_2 traps, lids were immediately closed and tubes were incubated for 1 h at room temperature, allowing CO_2 to escape the medium and react with NaOH in the paper disc. Paper discs were then transferred to scintillation vials containing 5 ml of Hionic-Fluor scintillation liquid and subjected to LSC. FAO rate was

expressed as fold change by dividing the specific activity of the paper discs from treated cells to that of untreated controls.

2.4.5 Confocal microscopy

Before plating BMDMs, sterile glass coverslips were added into each well of culture plates. After culturing, medium was aspirated, cells were washed once with PBS and fixed with 4% formalin solution for 10 min. Fixed cells were washed twice with PBS for 20 min and simultaneously stained with BODIPY 493/503 for neutral lipids (D3922, Thermofisher Scientific) and Hoechst 33342 (B2261, Sigma) for nuclei at the concentrations recommended by manufacturer, followed by three 20 min washes with PBS. Coverslips with stained cells were mounted on microscopy slides using Fluoromount (F4680, Sigma) and imaged using Zeiss LSM 510 Meta Confocal microscope (Carl Zeiss). Excitation/emission spectra were 497/505 nm for BODIPY and 392/440 nm for Hoechst 33342.

2.4.6 Flow cytometry

On day 7 of differentiation, BMDMs were detached as described in 2.4.1 and 10^6 cells were centrifuged at 400 g, 4 °C for 5 min and resuspended in 200 μl of staining buffer (PBS, 1mM EDTA, 3% heat-inactivated FBS) in 5 ml round-bottom tubes (352054, Falcon) and maintained on ice during subsequent manipulations. For the quantification of cell death, detached BMDMs were pooled with the tissue culture supernatants containing floating dead cells. 10^6 Cells were stained with LIVE/DEAD dye (L10119, Invitrogen) according to the manufacturer's instructions and centrifuged at 400 g, 4 °C for 5 min. Cells were resuspended in 200 μl of staining buffer and non-specific antibody binding was blocked with 5 μg/ml of anti-CD16/32 (Clone 93, Biolegend) for 20 min. BMDMs were then centrifuged at 400 g, 4 °C for 5 min, resuspended in 200 μl of staining buffer and stained with the following antibodies: anti-CD11b (M1/70, BD biosciences), anti-F4/80 (BM8, Biolegend), anti-CD301 (LOM-14, Biolegend), anti-CD206 (C068C2, Biolegend) for 30 min. Cells were then washed thrice by resuspending in 300 μl of staining buffer and centrifuging at 400 g, 4 °C for 5 min. Finally, cells were resuspended in 300 μl of staining buffer and analysed on LSRFortessa (BD Biosciences) flow cytometer with FACS Diva software. Data was analysed using TreeStar FlowJo software (Version vX0.7), by calculating median fluorescence intensity of each marker in the live cell population. Data acquisition and analysis was performed by Dr. Guillaume Bidault.

2.4.7 Measurement of oxygen-consumption rate and extracellular acidification rate

BMDMs were plated in XF-96 cell culture plates (101085-004, Agilent) at a density of 50,000 cells per well. On the day of experiment, cells were washed with PBS and 180 µl of XF assay medium (modified DMEM, pH 7.4 (102365-100, Agilent), supplemented with 2 mM L-glutamine and 10 mM glucose) was added to each well. Plate was then incubated for 1 h at 37°C in the atmospheric gas environment. Real-time measurements of oxygen-consumption rate (OCR) and extracellular acidification rate (ECAR) were performed using an XF-96 Extracellular Flux Analyzer (Agilent) according to manufacturer's instructions. All drugs used during the assay were diluted in the XF assay medium and injected automatically by the XF-96 Extracellular Flux Analyzer. Assays were performed by Dr. Guillaume Bidault.

2.4.8 Measurement of intracellular and mitochondrial ROS production

BMDMs were seeded at a density of 50,000 cells per well in a black 96-well plate and stimulated as indicated in legend. Cells were then washed with warm RPMI medium and incubated at 37°C with 5 µM MitoSox (mitochondrial superoxide indicator, M36008, Thermofisher Scientific) for 15 min. Cells were counterstained with Hoechst 33342 for 15 min to normalise for DNA input, and a non-stained well was used to correct for auto-fluorescence signal from each condition. After three washes with warm RPMI medium, fluorescence intensity was determined using a Tecan Infinite M1000 Pro Plate reader set to measure the excitation/emission spectra at 510/580 nm for MitoSox and 350/488 nm for Hoechst 33342. Assays were performed by Dr. Guillaume Bidault.

2.5 Analytical methods

2.5.1 Extraction and quantification of RNA

RNA from cell samples (except adipocytes) was extracted using Rneasy Plus Mini kit (74106, Qiagen) following manufacturers' instructions. 30 µl of RNAse-free water was used for elution. Rneasy Plus Micro kit (74004, Qiagen) was used to extract RNA from adipose tissue macrophage fractions, with 14 µl of RNAse-free water used for elution.

RNA from tissues and adipocytes was harvested by adding 1 ml of RNA Stat-60 reagent (Tel-Test) to approximately 100 mg of frozen tissue placed in a Lysing Matrix D tube (MP Biomedicals). Samples were homogenised using a FastPrep homogeniser

(MP Biomedicals) for 2 x 45 s at 5.5 m/s and centrifuged at 14,000 g for 5 min to pellet debris. The aqueous phase was transferred to a fresh tube containing 200 µl chloroform. Samples were mixed and centrifuged at 14,000 g, 4°C for 15 min. The clear upper phase containing RNA was removed and precipitated by mixing it with 500 µl isopropanol and incubating at room temperature for 10 min. Samples were centrifuged at 14,000 g, 4°C for 10 min and supernatants were discarded. RNA pellets were then washed with 70% ethanol, air-dried and re-suspended in 100 µl of RNAse-free water.

RNA concentration and purity was determined using Nanodrop ND-1000 spectrophotometer (Thermofisher Scientific). The absorbance was measured at 260 nm against RNAse-free water. A single A260 unit was assumed to be equal to 40 µg/mL of RNA. All RNA samples were stored at -80°C for subsequent processing.

2.5.2 Quantitative real-time polymerase chain reaction (qRT-PCR)

Complementary DNA (cDNA) was generated using Promega reagents in a 20 µl reaction as follows: 500 ng RNA was added to 1 x M-MLV reverse transcriptase master mix (M351A) with 2.5 mM $MgCl_2$ (A351B), 1.25 mM dNTPs (U151B), and 5 µg/mL random hexamers (C118A), and denatured at 65°C for 5 min before being transferred directly to ice in order to prevent the reassembly of the secondary structures of RNA. After the addition of 1 µL of M-MLV reverse transcriptase (M170b), the reaction was incubated at 37°C for 1 h for cDNA synthesis and 95°C for 5 min for enzyme denaturation. cDNA was diluted 75-fold in RNAse-free water and stored at -20°C.

qRT-PCR was performed in a 13 µL reaction with 5 µl of diluted cDNA, 6.5 µl of 2x TaqMan or SYBR Green reagent (Applied Biosystems), 1.3 µl of 3 mM forward and reverse primer mix (including 1.5 mM of probe for TaqMan reactions) and 0.2 µl of RNAse-free water according to the default manufacturer's protocol (Applied Biosystems). Primer sequences are described in Table 2-4. Reactions were run in duplicate for each sample and quantified using the ABI Prism 7900 sequence detection system (Applied Biosystems). Duplicates were checked for reproducibility, and then averaged; 'no reverse transcriptase' controls were included to check for genomic DNA contamination, and 'no template' controls were included to check for the formation of primer dimers. Product specificity was determined using a dissociation curve for SYBR green reactions. A standard curve generated from a pool of all cDNA samples was

used for quantification. The expression of genes of interest was normalized using BestKeeper method to the geometric average of 3-4 housekeeping genes (*18s*, *36b4*, *Actb*, and *Tbp*), and data was expressed as arbitrary units.

Gene	Forward primer (5'-3')	Reverse primer (5'-3')	Probe (5'-3')
18s	CGGCTACCACATCCAAGGAA	GCTGGAATTACCGCGGCT	GAGGGCAAGTCTGGTGCCAG
36b4	AGATGCAGCAGATCCGCAT	GTTCTTGCCCATCAGCACC	
Abca1	TCCTCATCCTCGTCATTCAAA	GGACTTGGTAGGACGGAACCT	
Abcg1	GCTGTGCGTTTTGTGCTGTT	TGCAGCTCCAATCAGTAGTCCTAA	
Acsl1	CAAACCAGCCCTATGAGTGGAT	CAGCCCGGAGCCTATGC	
Acsl4	GACAGGCCAGTGTGAACGTATC	GCCAAAGGTAAGTAGCCAATATATGTG	
Actb	GCTCTGGCTCCTAGCACCAT	GCCACCGATCCACACAGAGT	ATCAAGATCATTGCTCCTCCTGAGCGC
Adrb1	TATCGAATCATCCGAGACGTACAG	TCCCAACTCCTCCTAAACTTTCC	
Adrb2	TGGTGGTGATGGTCTTTGTC	GTCTTGAGGGCTTTGTGCTC	
Adrb3	CCAGCCAGCCCTGTTGA	GGACGCGCACCTTCATAGC	
Adrp	TCATCCAGAAGCTGGAGCCA	GCAGTCTTTCCTCCATCCTGTC	
Angptl4	AAGATGACCCAGCTCATTGG	ATCACTGTCCAGCCTCCATC	
Apoa1	GCGGCAGAGACTATGTGTCC	CAGTTTTCCAGGAGATTCAGGT	
Arg1	CTCCAAGCCAAAGTCCTTAGAG	AGGAGCTGTCATTAGGGACATC	
Atgl	CGCCTCTCGAAGGCTCTCT	TGTAGCCCTGTTTGCACATCTC	
Ccr2	ACCTGTAAATGCCATGCAAGT	TGTCTTCCATTTCCTTTGATTTG	
Cd11b	CAGACAGGAAGTAGCAGCTCCT	CTGGTCATGTTGATGAAGGTGCT	
Cd11c	GGCTATCAAGCATGTCATAACAGAAC	CCCCTTGTTTTCTCCCATCAG	
Cd206	GCATGGGTTTTACTGCTACTTGATT	CAGGAATGCTTGTTCATATCTGTCTT	
Cd36	GCCAAGCTATTGCGACATGA	TCTCAATGTCCGAGACTTTTCA	CACAGACGCAGCCTCCTTTCC
Chop	CCACCACACCTGAAAGCAGAA	AGGTGAAAGGCAGGGACTCA	CTGGTCCACGTGCAGTCATGGCA
Cidea	GTGGACACAGAGGAGTTCTTT	GTCGAAGGTGACTCTGGCTATTC	ACAGAAATGGACACCGGG

Cox2	CCCTGAAGCCGTACACATCA	GTCACTGTAGAGGGCTTTCAATTCT	TTGAAGAACTTACAGGAGAGAAGGAAATGGCTG
Cpt1a	AGGGCTGCACTCCTGGAAG	CACGATAAGCCAGCTGGAGG	
Cpt1b	GCGTGCCAGCCACAATTC	TCCATGCGGTAATATGCTTCAT	
Dgat1	AGGTTCTCTAAAAATAACCTTGCATT	TCGTGGTATCCTGAATTGGTG	
Dgat2	GGCGCTACTTCCGAGACTAC	TGGTCAGCAGGTTGTGTGTC	
Dio2	TGCGCTGTGTCTGGAACAG	CTGGAATTGGGAGCATCTTCA	
Dusp1	GTGCCTGACAGTGCAGAATC	CACTGCCCAGGTACAGGAAG	
Elovl3	AAGGTTGTTGAACTGGGA CGA C	GTGGTGGTACCAGTGGACAAA	
Elovl6	TGCAGGAAAACTGGAAGAAGTCT	ATGCCGACCACCAAAGATAAA	
F4/80	CAGATACAGCAATGCCAAGCA	GATTGTGAAGGTAGCATTCACAAGTG	
Fabp4	CACCGCAGACGACAGGAAG	GCACCTGCACCAGGGC	TGAAGAGCATCATAACCCTAGATGGCGG
Fads1	TGCACCCCCTCTTCTTCGCC	AGGCTGGGGGTCCGATGAGG	
Fasn	GCCCAGACAGAGAAGAGGCA	CTGACTCGGGCAACTTCCC	GGAGGAGGTGGTGATAGCCGGTATGTC
Fatp1	CGTTTCGATGGTTATGTTAGTGACA	CATCACTAGCACGTCACCTGAGA	
Fatp2	GCGTGCCTCAACTACAACATT	CCTCCTCCACAGCTTCTTGT	
Fatp5	AGGGTTTTTGCATTCCTGTG	TTGGTTCTTTCGAACCTTGG	
Fbp1	GACCCTGCCATCAATGAGTATCT	CCACATACCGGGCACCATAG	
Fizz1	GGGATGACTGCTACTGGGTG	TCAACGAGTAAGCACAGGCA	
G6pc	CCAACCACAAGATGACGTTCA	ACTCTTGCTATCTTTCGAGGAAAGA	AAAGCCAACGTATGGATTCCGGTGT
Glut1	GACCCTGCACCTCATTGG	GATGCTCAGATAGGACATCCAAG	
Glut4	ACTCATTCTTGGACGGTTCCTC	CACCCCGAAGATGAGTGGG	TGGCGCCTACTCAGGGCTAACATCA
Gnmt	GCTGGACGTAGCCTGTGG	CACGCTCATCACGCTGAA	
Got2	TGGAGTCACAGCTGAAGATCTTG	CACCTCTTGCAACCATTGCTT	
Hif1a	GCACTAGACAAAGTTCACCTGAGA	CGCTATCCACATCAAAGCAA	
Hif1a exon 2	CGGCGAAGCAAAGAGTCTGAAG	GATGGTGAGCCTCATAACAGAAGC	
Hif2a	CCAGGAGCTCAAAAGGTGTC	CAGGTAAGGCTCGAACGATG	

Hif2a exon2	ACAATGACAGCTGACAAGGAG	TTGTTGTAGACTCTCACTTGCCC	
Hsl	GGAGCACTACAAACGCAACGA	TCGGCCACCGGTAAAGAG	CAGGCCTCAGTGTGACCGCCAGTT
Il10	CAGAGCCACATGCTCCTAGA	TGTCCAGCTGGTCCTTTGTT	
Il1b	TGGGCCTCAAAGGAAAGAAT	CAGGCTTGTGCTCTGCTTGT	
Il6	ACACATGTTCTCTGGGAAATCGT	AAGTGCATCATCGTTGTTCATACA	
Klf4	CGGGAAGGGAGAAGACACT	GAGTTCCTCACGCCAACG	
Lcat	GGCTGAACTCAGTAACCACACA	TTGGCTTCTAGCCGATTCC	
Lipa	AAGGCTGCACCATAGGTTTCA	GGCAAGCGTCCCAATTGA	
Lpl	TGGAGAAGCCATCCGTGTG	TCATGCGAGCACTTCACCAG	TGCAGAGAGAGGACTCGGAGACGTGG
Maoa	CGGATATTCTCAGTCACCAATG	ATTTGGCCAGAGCCACCTA	
Mat1a	ATCTGAGGCGCTCTGGTGT	CCTGCATGTACTGAACTGTTACCT	
Mcp1	AGGTCCCTGTCATGCTTCTG	GCTGCTGGTGATCCTCTTGT	
Mgl1	AGGTCCCTGTCATGCTTCTG	GCTGCTGGTGATCCTCTTGT	
Msr1	GGGAGTGTAGGCGGATCA	GGAGATGATAGTAGGGTGCTCTG	
Nlrp3	CCCTTGGAGACACAGGACTC	GAGGCTGCAGTTGTCTAATTCC	
Nr4a1	CTGTCCGCTCTGGTCCTC	AATGCGATTCTGCAGCTCTT	
Pck1	TGTGGGCGATGACATTGC	TGGCATTTGGATTTGTCTTCAC	TATCAACCCAGAAAACGGGTTTTTTG
Pcyt1a	TCTGCAGGGAGCGATGATG	TGTGGAGATACCTTCTGTCCTCTGT	TATAAGCACATCAAGGACGCAGGCATGTT
Pcyt1b	CAGTGCCAAGCACCTCATGA	GGCCTATCAACTGGTGTTCCTAA	
Pcyt2	GCTGCTCCCTACGTCACC	CGTCTACTGTCAGCGTGATGTC	
Pemt	TCTGCATCCTGCTTTTGAACA	TGGGCTGGCTCATCATAGC	
Pgc1a	AACCACACCCACAGGATCAGA	CTCTTCGCTTTATTGCTCCATGA	CAAACCCTGCCATTGTTAAGACCGAGAA
Pisd	TTGCCTCTTCAGGCAGGT	CGCAGCAGGAACAAGGAT	
Pltp	GCTTCTGAGGGCCACCTAC	TTCAGCTTCAGTGGGGAGTT	
Ptdss1	GTTAGCATTCCCCAATGGTC	CCAAAAACCATTCGCCATA	
Ptdss2	CCATTTTCCAGACCTCATCC	TGAGAAACAATTCGTAGACCACA	

Scd1	CTTGCGGATCTTCCTTATCATT	GATCTCGGGCCCATTCG	ACCATGGCGTTCCAGAATGACGTGT
Srb1	GCCCATCATCTGCCAACT	TCCTGGGAGCCCTTTTTACT	
Srebp1c	GCCATGGATTGCACATTTGA	GGCCCGGGAAGTCACTG	GACATGCTCCAGCTCATCAACAACCAAG
Tbp	CAAACCCAGAATTGTTCTCCTT	ATGTGGTCTTCCTGAATCCCT	
Thbs1	CACCTCTCCGGGTTACTGAG	GCAACAGGAACAGGACACCTA	
Tnf	CATCTTCTCAAAATTCGAGTGACAA	TGGGAGTAGACAAGGTACAACCC	CACGTCGTAGCAAACCACCAAGTGGA
Ucp1	CCCGCTGGACACTGCC	ACCTAATGGTACTGGAAGCCTGG	AAGTCCGCCTTCAGATCCAAGGTGAAG
Xbp1 spl.	AGCTTTTACGGGAGAAAACTCA	GCCTGCACCTGCTGCG	
Xbp1 tot.	ACACGCTTGGGAATGGACAC	CCATGGGAAGATGTTCTGGG	
Ym1	AGAAGGGAGTTTCAAACCTGGT	GTCTTGCTCATGTGTGTAAGTGA	

Table 2-4. Sequences of primers used in this thesis.

FAM/TAMRA reporter and quencher detection system was used for genes with indicated probe sequences, and SYBR was used for the remaining genes.

2.5.3 Protein extraction and quantification

BMDMs were treated as described in legend, washed once with ice-cold PBS and lysed in ice-cold RIPA buffer (50 mM Tris-HCl, 150 mM NaCl, 1 mM EDTA, 0.1% SDS, 0.5% sodium deoxycholate, 1% NP-40, pH 7.4) containing Pierce™ protease and phosphatase inhibitors (88668, Thermofisher Scientific). 150 µl of RIPA buffer was used to lyse 10^6 cells. Lysates were collected and centrifuged at 14,000 g, 4°C for 10 min to remove cell debris.

Protein concentration was determined by DC Protein assay (5000111, Biorad) according to manufacturer's instructions.

2.5.4 Western blotting

Protein lysates were diluted in NuPAGE™ LDS sample buffer (NP0007, Thermofisher Scientific) containing 2.5% 2-mercaptoethanol and boiled at 95°C for 5 min. 10 µg of protein was then separated by electrophoresis using NuPAGE™ SDS-polyacrylamide gels (Thermofisher Scientific) and transferred to nitrocellulose membranes using the iBlot® Dry Blotting System (Thermofisher Scientific). Membranes were blocked for 1 h in 5% fat-free milk (Marvel) or 5% BSA in Tris-buffered saline containing 0.05% Tween

(TBST) at room temperature, and incubated overnight at 4°C with the appropriate primary antibody (Table 2-5). Bound primary antibodies were detected using peroxidase-coupled secondary anti-rabbit antibody (7074, Cell signalling) and enhanced chemiluminescence (WBLUF0500, Millipore). Blots were exposed digitally using the ChemiDoc MP System (Bio-Rad), and bands were quantified using Image Lab™ software (Bio-Rad). The expression of proteins was normalised to a housekeeping protein (β-actin), and the phosphorylation status was determined by normalising to a respective total protein. All protein quantification data is expressed as arbitrary units.

Antibody (Host species)	**Source (Clone ID)**	**Dilution (diluent)**
CREB (Rabbit)	Cell signalling (48H2)	1:1000 (3% milk in TBST)
P-Ser133 CREB (Rabbit)	Cell signalling (87G3)	1:1000 (3% BSA in TBST)
B-actin (Rabbit)	Abcam	1:5000 (3% milk in TBST)
Pcyt1a (Rabbit)	Abcam (EPR3940(2))	1:2500 (3% milk in TBST)
P-Thr183/Tyr185 JNK (Rabbit)	Cell signalling (9251)	1:1000 (3% BSA in TBST)
JNK (Rabbit)	Cell signalling (9252)	1:1000 (3% milk in TBST)
P-Thr180/Tyr182 p38 MAPK (Rabbit)	Cell signalling (D3F9)	1:1000 (3% BSA in TBST)
P38 MAPK (Rabbit)	Cell signalling (9212)	1:1000 (3% milk in TBST)

Table 2-5. Antibodies used in this thesis.

2.5.5 Enzyme-linked immunosorbent assay (ELISA)

BMDMs were treated as described in the legend and culture supernatants were collected. IL-1β ELISA (DY401, R&D Systems) was performed on the culture supernatants according to manufacturer's instructions.

2.5.6 Hepatic glycogen and glucose measurement

Hepatic glycogen and free glucose content was determined using enzymatic glycogen assay kit (ab65620, Abcam) according to manufacturer's instructions.

2.5.7 Lipid extraction

Total lipids from frozen tissue, plasma and cells were extracted using a modified Folch extraction method[540]. Glass pipettes were used throughout the procedure in order to avoid plastic-bound lipid contamination. 1.2 ml of HPCL-grade chloroform:methanol

2:1 v/v mixture was added to samples in a Lysing Matrix D tube (MP Biomedicals). Where applicable, appropriate amounts (calculated by approximating the average abundance of every fatty acid within neutral and phospholipid fraction in the sample and adding matching amounts of neutral and phospholipid standard) of glyceryl heptadecanoate (neutral lipid standard, T2151, Sigma) and 1,2-dinonadecanoyl-sn-glycero-3-phosphocholine (phospholipid standard, 850367, Avanti Polar Lipids) were included in extraction mixture as internal standards. Tissue samples were homogenised using a FastPrep homogeniser for 2 x 45 s at 5.5 m/s, centrifuged at 14,000 g for 5 min to pellet debris and transferred to fresh 2 ml Eppendorf tubes. Cell and plasma samples were homogenised by vortexing for 15 s and were not centrifuged. 240 µl of HPLC-grade water was added to each sample before vortexing for 2 min and centrifuging at 16,000 g for 10 min. 700 µl of the lower lipid fraction was transferred to a 7 ml glass tube. A second extraction was performed by adding 700 µl of fresh HPLC-grade chloroform followed by vortexing and centrifugation as above. 900 µl of lower lipid fraction was collected and pooled with the first 700µl fraction (total 1600µl). Collected lipid fractions were dried under nitrogen stream. Where applicable, dried lipid weight was determined by measuring the difference of glass vial weight before and after the extraction. Tissue lipid content was then determined by dividing the dried lipid weight by the wet weight of tissue used for extraction. Dried lipids were stored at -20°C for subsequent processing, or re-suspended in 100 µl chloroform, transferred to scintillation vials containing 5 ml of Opti-Fluor scintillation liquid (6013199, Perkin Elmer) and subjected to LSC.

2.5.8 Total lipid fractionation to neutral and phospholipid fractions

Lipids were fractionated into neutral and phospholipids by solid phase extraction (SPE). Glass pipettes were used throughout the procedure in order to avoid plastic-bound lipid contamination. Dried lipids were re-suspended in 1 ml chloroform and applied to aminopropyl (NH_2) solid-phase extraction columns (Bond Elut, 12113014, Agilent) placed in a hermetic glass SPE tank connected to a vacuum pump. The flow-through containing neutral lipids was collected along with two subsequent washes with 1 ml chloroform into fresh 7 ml glass vials. Phospholipids bound to the column were eluted with 2 ml of HPLC-grade chloroform:methanol 2:1 v/v solution into fresh 7 ml glass vials. Collected neutral and phospholipid fractions were dried under nitrogen stream and stored at -20°C for subsequent analysis.

2.5.9 Thin-layer chromatography

BMDMs were treated in 6-well plates as indicated in legend and lipids were labelled as described in 2.4.3. Lipids from cells were extracted as described in 2.5.7 and solubilised in 50 µl of HPLC-grade chloroform. 20 µl of lipids were then spotted at the bottom of 20 cm x 20 cm thin layer chromatography (TLC) silica plates (Z292974, Sigma). TLC plates were placed into hermetic glass chambers containing 250 ml of one of the following solutions: 65:25:4 chloroform:methanol:ammonium hydroxide v/v for phospholipid separation, or 80:20:1 hexane:diethyl ether:acetic acid v/v for neutral lipid separation. Plates were allowed to develop until the solvent front was approximately 2 cm below the top of the plate. Plates were dried under laminar flow and incubated with radiographic films (47410, Fujifilm) in the dark for 1-3 days at room temperature. Radiographic films were developed using automated film developer and scanned. ImageJ software (NIH) was used to calculate the density of the bands on scanned radiograms.

After radiogram was obtained, plates were sprayed with a total lipid dye (0.005% primuline (206865, Sigma) in acetone:water 4:1 v/v), then dried under laminar flow and imaged digitally under the UV light using the ChemiDoc MP System (Bio-Rad).

In order to quantify radioactivity in a sample, the same amount (20 µl) of lipids was transferred to a scintillation vial containing 5 ml of Opti-Fluor scintillation liquid and subjected to LSC.

2.5.10 Microsomal preparation

BMDMs were treated as indicated in legend. 10^7 BMDMs were re-suspended in 5 ml of homogenising buffer (10 mM Tis-HCl, 0.25 M sucrose, 1 mM EDTA, pH 7.0) containing Pierce™ protease and phosphatase inhibitors and homogenized in a Potter-Elvehjam tissue grinder with PTFE pestle at 1000 rpm for 2 min on ice. The homogenate was transferred to 6.5 ml ultracentrifuge tubes (344088, Beckman Coulter) and sequentially centrifuged using 50.4 Ti rotor (347299, Beckman Coulter) as follows: 10 min at 700 g, 10 min at 8000 g and 10 min at 17,000 g, all at 4°C. The supernatant was then transferred to a fresh tube and the pellet was discarded. The supernatant was centrifuged at 105,000 g, 4°C for 45 min. The supernatant was then discarded and the pellet containing microsomes was re-suspended in 5 ml of centrifugation buffer (20 mM Tris-HCl, 0.4 M KCl, pH 7.4). The suspension was

centrifuged for at 105,000 g, 4°C for 5 min. The supernatant was discarded and the pellet containing microsomes was re-suspended in 50 µl of 0.1 M Tris-HCl (pH 7.4). Protein concentration of the microsomal preparation was quantified by DC protein assay (Biorad) before aliquoting and storing microsomes at -80 °C.

2.5.11 Gas chromatography-mass spectrometry

2.5.11.1 Quantitative analysis of fatty acid methyl esters (FAMEs)

In order to derive FFAs and esterified fatty acids from complex lipids into FAMEs, 750 µl of HPLC-grade chloroform: methanol 1:1 v/v solution was added to previously dried lipids in 7 ml glass vials. 125 µl of 10% boron trifluoride in methanol (134821, Sigma) was then added into each vial. Vials were sealed and incubated in an oven at 80°C for 90 min in order to hydrolyse fatty acid-glycerol and fatty acid-cholesterol ester bonds and form FAMEs. Samples were allowed to cool, and 1 ml of HPLC-grade n-Hexane and 500 µl of HPLC-grade water were added. Samples were briefly vortexed and centrifuged at 2000 g using benchtop centrifuge. The upper organic layer was transferred into 2 ml gas chromatography glass vials and dried under nitrogen stream.

Gas chromatography-mass spectrometry was performed with Agilent 7890B gas chromatography system linked to Agilent 5977A mass spectrometer, using AS3000 auto sampler. A TR-FAME column (length: 30 m, inter diameter: 0.25 mm, film size: 0.25 µm, 260M142P, Thermofisher Scientific) was used with helium as carrier gas. Inlet temperature was set at 230°C. Dried FAME samples were re-suspended in HPLC-grade n-Hexane (100 µl of solvent was used for BMDM samples and 1 ml – for tissue samples). 1 µl of this solution was injected for analysis. The oven programme used for separation is detailed in Table 2-6. If the height of any FAME peaks exceeded 10^8 units, sample was re-injected with 10:1 – 100:1 split ratio. Identification of FAME peaks was based on retention time and made by comparison with those in external standards (Food industry FAME mix, 35077, Restek).

Oven ramp rate (°C/min)	Oven temperature (°C)	Hold time (min)
-	100	2
25	150	0
2.5	162	3.8
4.5	173	5.0
5.0	210	0
40	230	0.5

Table 2-6. Oven temperature programme used for FAME separation by gas chromatography. *Carrier gas flow was set to 1.5 ml/min.*

Peak integration and quantification was performed using MassHunter Workstation Quantitative Analysis software (version B.07.00, Agilent). Specific high-abundance ions from total ion chromatogram were chosen to calculate each fatty acid peak. The peak area values for each fatty acid were then normalised to the peak area value of internal standard in that sample and expressed as units/mg tissue or units/10^6 cells. When relative changes in lipids were analysed, values were expressed in molar percentages by dividing the area of each peak by the sum of all peak areas for a given sample. This analysis accounted for differences in total lipids between samples.

2.5.11.2 Microsomal DGAT activity assay

Microsomal DGAT activity assay protocol was adapted from a recent publication[541]. Eppendorf tubes containing 100 µl of DGAT reaction mixtures (50 µM of palmitoyl-CoA (870716P, Avanti Polar Lipids), 50 µM of oleoyl-CoA (870719P, Avanti Polar Lipids), 333 µM sn-1,2-dioctanoylglycerol (800800O, Avanti Polar Lipids), 200 mM HEPES, 3.2 mM MgCl2, pH 7.4) were prepared. Reactions were initiated by adding 10 µg of microsomes (diluted in 20 µl of water) into the reaction mixtures. 'No acyl-CoA' and 'no microsome' controls were included in each assay. Tubes were incubated at 30°C for 10 min and reactions were quenched by transferring them to 2 ml glass vials containing 1 ml of HPLC-grade chloroform: methanol 2:1 v/v solution. 280 µl of 100 mM acetic acid were then added to each vial. Vials were vortexed for 2 min and centrifuged at 1,500 g, room temperature for 5 min. Lower phase containing neutral lipids was transferred to fresh 2 ml glass vials and samples were dried under nitrogen flow.

Gas chromatography-mass spectrometry was performed using DB-5 column (Agilent), with helium as carrier gas. Dried lipids were re-suspended in 60 µl of HPLC-grade isooctane and 1 µl of solution was injected splitless for analysis. Flow rate was set to 2 ml/min and inlet temperature was 315 °C. The oven programme was as follows: initial oven temperature was set to 150°C, then temperature was increased at a rate of 15°C/min until it reached 315°C, where it was maintained for an additional 18 min. Mass spectrometry detection was set to single ion monitoring (SIM) mode, with ions 127.0, 327.0, 439.0 and 469.0 being monitored at a dwell time of 50 ms/ion.

Peak integration and quantification was performed using MassHunter Workstation Quantitative Analysis software (version B.07.00, Agilent). 327.0 ion was used to quantify the peaks, and ions 439.0 and 469.0 were used as qualifiers to identify 1,2-dioctanoyl-3-palmitoyl-glycerol and 1,2-dioctanoyl-3-oleoyl-glycerol, respectively. 'No acyl-CoA' and 'no microsome' controls were used to verify the 1,2-dioctanoyl-3-palmitoyl-glycerol and 1,2-dioctanoyl-3-oleoyl-glycerol peaks. Relative DGAT activity was calculated by dividing the peak area of stimulated BMDMs by the peak area of control BMDMs, and expressed as fold change from control.

2.5.12 Sample preparation for quantitative proteomics

BMDMs were plated in 10 cm plates and stimulated as described in legend. Protein was extracted and quantified as described in 2.5.3. 100 µg of protein from each sample was reduced, alkylated and precipitated as follows: each sample was diluted to 100 µl in 1 M triethylammonium bicarbonate (TEAB, 90114, Thermofisher Scientific). Disulphide bonds were reduced by adding 5 µl of 200 mM tris(2-carboxyethyl)phosphine (646547, Sigma) and incubating samples at 37 °C for 1 h. Cysteine residues were then alkylated by adding 5 µl of 375 mM iodoacetamide (90034, Thermofisher Scientific) and incubating at room temperature for 30 min. Proteins were then precipitated by adding 500 µl of ice-cold acetone and incubating overnight at -20°C. Precipitated proteins were then pelleted by centrifugation at 10,000g, 4°C for 10 min, supernatants were discarded and pellets were air-dried for 10 min at room temperature. Samples were stored at -80°C.

Pellets were solubilised in 100 µl of 100 mM HEPES buffer (pH 8.5) and digested with sequencing grade trypsin (V5111, Promega) with a 1:40 enzyme:protein ratio at 37°C for 1 h. An additional aliquot of trypsin at 1:40 concentration was added and samples were incubated overnight at 37 °C. Trypsin digests were centrifuged at 13,000 g for 5 min to remove any insoluble matter and dried by vacuum centrifugation.

Peptide samples were re-suspended in 100 µl of 100 mM HEPES buffer (pH 8.5). Each sample was then labelled with unique mass tag according to manufacturer's instructions (TMT10plex™, 90110, Thermofisher Scientific). Once labelled, samples were combined and dried by vacuum centrifugation. Labelled peptides were desalted using Sep-Pak C18 solid phase extraction cartridges according to manufacturer's instructions (WAT054955, Waters). The eluate from cartridges was dried by vacuum

centrifugation and re-suspended in 100 µl of 20 mM HPLC-grade ammonium formate (pH 10.0) and 4% HPLC-grade acetonitrile v/v solution for high pH reversed-phase liquid chromatography.

2.5.13 Quantitative proteomics by liquid chromatography-mass spectrometry

Sample fractionation by high pH reverse-phase liquid chromatography and subsequent analysis of each eluted fraction (10 fractions in total) by mass spectrometry was performed in the lab of Prof. Kathryn Lilley by Dr. Houjiang Zhou. Analysis parameters and equipment used is described in detail in a methods section of a recent publication from Prof. Lilley's group[542]. The full raw list of detected proteins (including the number and abundance of peptides detected) is deposited in the University of Cambridge data repository and can be accessed via the following link: https://doi.org/10.17863/CAM.28046 .

2.6 Statistical analysis and graphical representation of data

All data from experiments is represented as a mean, with error bars showing standard error of the mean and the number of replicates stated in legend. Some data is represented as a fold-change, and it is stated in legend to what value the data represented was normalised to generate the fold-change. Statistical tests used are also stated in legend. A student's t-test was used to compare two groups; one-way analysis of variance (ANOVA) was used to compare more than 2 groups, followed by Bonferonni's post-hoc test. Where more than one factor influenced the variable being measured, 2-way ANOVA was used to test for a significant effect of each factor as well as an interaction between factors. For assessment of EE or clamp GIR, ANCOVA was used to correct for the animal's body weight. In these cases, significance was defined as $p < 0.05$.

Statistical and pathway analysis of proteomics data was performed by a PhD student Aurelien Dugourd from Prof. Saez-Rodriguez group. Variance stabilisation normalisation (VSN) method was applied to normalise the protein expression levels between samples[543]. Differential statistical analysis was performed using LIMMA package[544]. For the prediction of biological pathways, processes and transcription factors, PIANO analysis[545] was performed with the following ontologies: c2 canonical

pathways (version 6, Molecular Signatures database (v6, msigDB)), c5 biological processes (v6, msigDB) and transcription factor regulons (provided by Dr. Luz Garcia).

In this thesis, all statistical tests were performed and graphs were generated using GraphPad Prism 6 software. Graphs and figures were edited for presentation using Adobe Illustrator CC 2015 software.

2.7 Metabolizer algorithm

The methodology of the Metabolizer algorithm used to analyse microarray data has been described in detail in a recent publication[546]. In a simplified manner, the algorithm uses defined Kegg pathway modules to infer the theoretical flux through metabolic pathways, solely based on the expression levels of genes that encode the enzymes constituting the pathway.

3 The role of *de novo* PC synthesis during lipid-induced inflammation in macrophages

3.1 Introduction

3.1.1 Preliminary data

Our laboratory previously characterised ATMs isolated from WT and ob/ob mice at two metabolically distinct time points of their lifespan. At the first time point (corresponding to 5 weeks of age), ob/ob animals were rapidly gaining fat mass due to their hyperphagia, but still displayed normal glycaemia and mild hyperinsulinemia [283]. Therefore, WAT sampled from 5-week-old ob/ob mice provided a snapshot of rapid, healthy WAT expansion and remodelling processes. By the second time point (16 weeks of age), ob/ob mice had decelerated their fat mass expansion and had already developed WAT inflammation and dysfunction, followed by pronounced glucose intolerance and dyslipidaemia[283]. Comparative analysis of these two time points simultaneously could enable us to compare the behaviour of ATMs in a healthy and dysfunctional WAT and identify molecular mechanisms that potentially cause WAT inflammation and insulin resistance.

One striking observation arising from transcriptomic and lipidomic analysis of ATMs was their specific regulation of genes related to M2 polarisation and lipid remodelling. When compared to age-matched WT controls, 5-week-old ob/ob ATMs had markedly increased mRNA levels of M2 macrophage markers and lipid metabolism genes *Elovl6*, *Scd1* and *Dgat1 (*Figure 3-1 A,B), all of which have been described to reduce lipotoxic effects of exogenous saturated FFAs on macrophages [209,219]. Interestingly, ATMs isolated from 16-week-old ob/ob mice showed an opposite phenotype, with down-regulation of genes encoding M2 polarisation markers and lipid metabolism enzymes compared to WT controls (Figure 3-1 A,B). Furthermore, the development of the transcriptional signature observed at 16 weeks of age co-occurred with an intracellular accumulation of lipids in ob/ob ATMs (Figure 3-1 C). As pharmacologically enhancing adipocyte storage capacity resulted in a reduction in ATM lipid accumulation and enhancement of M2 polarisation in ob/ob mice, this study concluded that adipocyte dysfunction lead to lipid accumulation within ATMs that caused their inflammatory activation[283]. While a reduction in the expression of *Elovl6, Scd1* and *Dgat1* in 16-week-old ob/ob ATMs could potentially explain their inability to handle increased

amounts of intracellular lipids, this study did not identify any molecular mechanisms linking intracellular lipid accumulation to the inflammatory activation of ATMs.

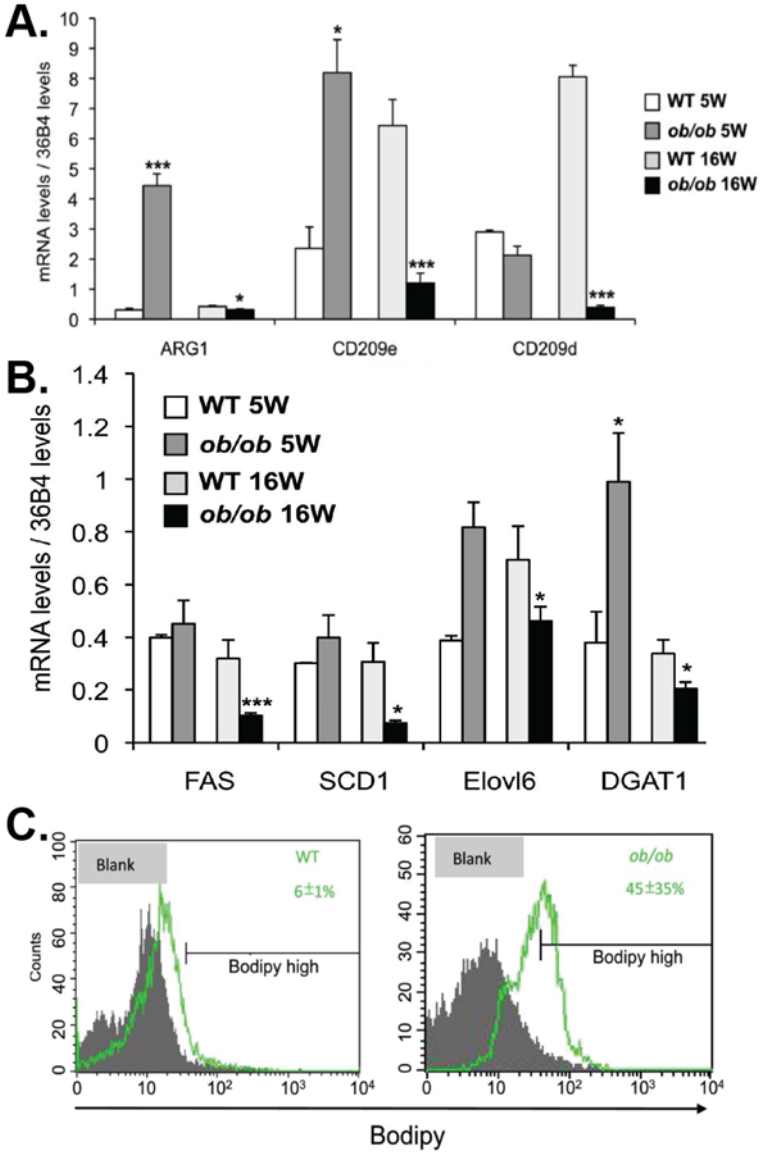

Figure 3-1. Phenotypic analysis of ATMs isolated from 5- and 16- week-old WT and ob/ob mice.

*mRNA levels of M2 polarisation markers (**A**) and lipid metabolism enzymes (**B**) in ATMs isolated from 5-week-old WT (n=4, white bars) and ob/ob (n=5, dark grey bars), and 16-week-old WT (n=6, light grey bars) and ob/ob (n=9, black bars) male mice. Gene expression has been measured by qPCR as described[283]. **C.** Flow cytometry analysis of Cd11b-positive cells from WAT stained with intracellular lipid dye Bodipy. *, *** p < 0.05 compared to WT using student's t-test. All graphs are presented as published in Prieur et al.[283].*

Following the publication of the study by Prieur *et al*., lipidomic data was reanalysed to compare the total measured abundances of complex lipid species between ATMs isolated from WT and ob/ob eWAT. As the predominant phospholipid species in mammalian cells, including macrophages is PC^{370}, the fact that PE was the most abundant measured lipid indicated incomplete detection coverage of the ATM phospholipidome (Figure 3-2 A). However, out of all measured lipids, the measured PE species were reduced and no change in the abundance of measured PC species was observed in the ATMs from ob/ob mice, resulting in an elevated PC to PE molar ratio (Figure 3-2 A).

Transcriptomic data published in Prieur *et al.* study was also reanalysed using *Metabolizer algorithm*, which predicted the activity of cellular metabolic pathways based on changes of the expression of genes encoding the enzymes constituting each pathway. The activity of Kegg module M00090, which encompasses all the enzymes of *de novo* PC synthesis pathway (Figure 1-7), was down-regulated in 5-week-old, but increased in 16-week-old ATMs from ob/ob compared to age matched WT mice (Figure 3-2 B). Module M00092, representing the genes encoding the enzymes constituting *de novo* PE synthesis pathway (Figure 1-7) was not affected by genotype (Figure 3-2 C), suggesting that observed increase in PC to PE ratio in 16-week-old ATMs was likely driven by increased *de novo* PC synthesis, rather than decreased PE production. Importantly, as the fluidity of cellular membranes is determined by the relative ratios, rather than the absolute amounts of individual lipid species, an observed increase in PC to PE ratio was suggestive of altered membrane physical properties and likely to contribute to an altered phenotype of ob/ob ATMs.

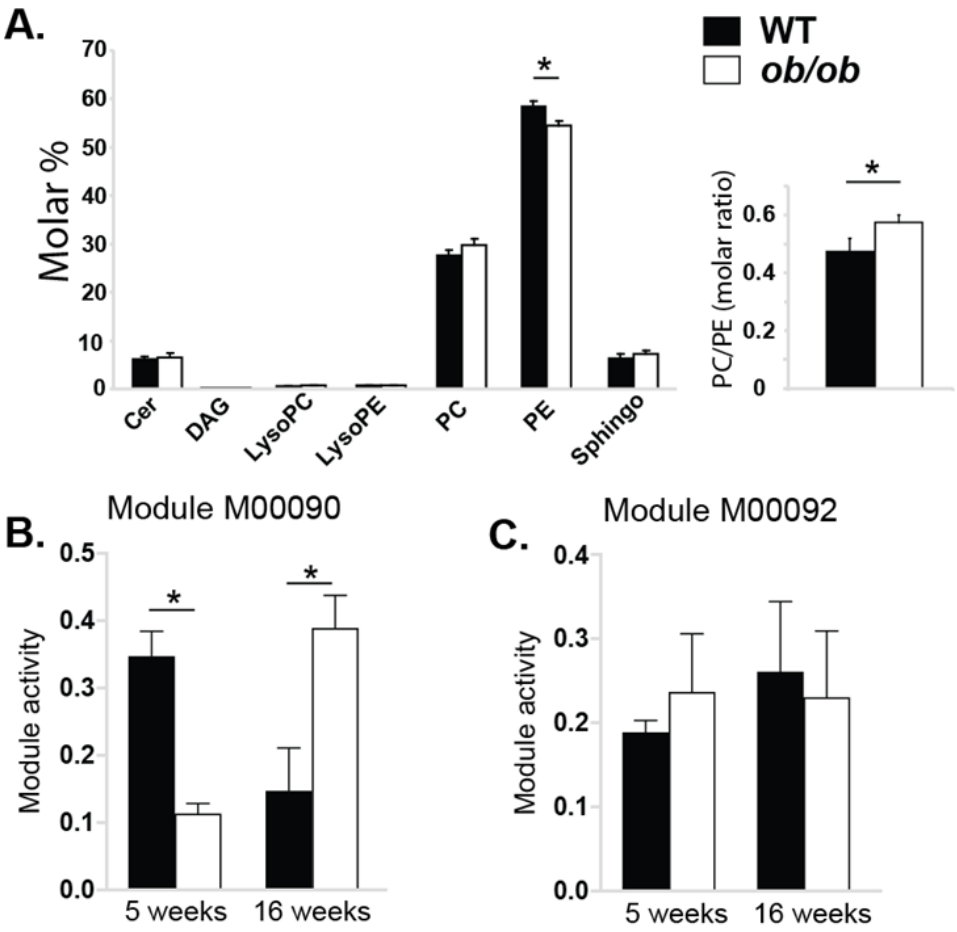

Figure 3-2. Concentrations of lipid species and the activity of transcriptional modules of phospholipid biosynthesis in ATMs isolated from 5- and 16- week-old WT and ob/ob mice.

*ATMs isolated from 5- and 16-week-old WT and ob/ob mice were subjected to transcriptomic and lipidomic analyses as described. A. Concentrations of measured complex lipid species in ATMs isolated from 16-week-old WT (n=3, black bars) and ob/ob (n=6, white bars) male mice, expressed as molar percentages of total measured lipids. B. The activity of Kegg module M00090 (PC biosynthesis), calculated based on transcriptional changes of genes involved in de novo PC synthesis pathway that were measured by microarray in ATMs isolated from 5- and 16-week-old WT and ob/ob male mice (n=4 /group). C. The activity of Kegg module M00092 (PE biosynthesis), calculated based on transcriptional changes of genes involved in de novo PE synthesis pathway that were measured as in (B). * p < 0.05 compared to WT using student's t-test. ATM isolation and omics analyses were performed as part of a published study managed by Dr. Xavier Prieur. Lipidomics data was re-analysed as molar percentages by Dr. Sam Virtue. Kegg module activity was assessed by a PhD student Cankut Cubuk from Prof. Joaquin Dopazo's group.*

Validation of the expression of genes encoding PC-synthesising enzymes by RT-qPCR revealed a two-fold increase in the transcript levels of rate-limiting enzyme CCTα in 16-week-old ob/ob ATMs (Figure 3-3 A), and a marked suppression of *Pcyt1b* transcription in 5-week-old ob/ob ATMs compared to WT controls (Figure 3-3 B). An independent experiment involving a bone-marrow transplant of WT donor bone-marrow into irradiated WT or ob/ob host mice, showed a similar increase in *Pcyt1a* transcription in ATMs isolated from ob/ob hosts at 20 weeks of age (Figure 3-3 C).

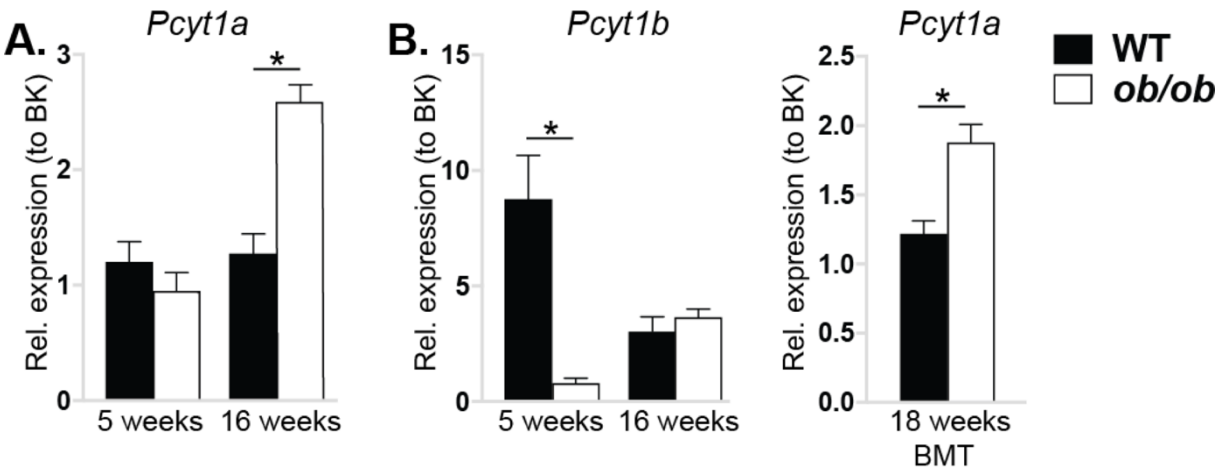

Figure 3-3. Expression of de novo PC biosynthesis genes in ATMs isolated from 5-, 16- and 18-week-old WT and ob/ob mice.

*Pcyt1a (**A**) and Pcyt1b (**B**) mRNA levels (normalised to BestKeeper) in ATMs isolated from 5-week-old WT (n=4, black bars) and ob/ob (n=5, white bars), and 16-week-old WT (n=6, black bars) and ob/ob (n=9, white bars) male mice. **C.** Pcyt1a mRNA levels in ATMs isolated from 20-week-old WT (n=7, black bars) and ob/ob (n=7, white bars) female mice that had been irradiated at 8 weeks of age and reconstituted with bone marrow cells isolated from WT mice. ATMs in (**A** and **B**) were isolated as part of published study managed by Dr. Xavier Prieur. ATMs in (**C**) were isolated and analysis was performed by Dr. Guillaume Bidault. * p < 0.05 compared to WT using 2-way ANOVA with Tukey's multiple comparisons test (**A** and **B**) or student's t-test (**C**).*

3.1.2 Research questions and aims

Overall, the observations from the study of Prieur *et al.* and *post hoc* analyses indicated an inverse relationship between *de novo* PC synthesis and M2 polarisation, as well as lipid remodelling in ATMs. During healthy adipose tissue expansion, as portrayed by 5-week-old ob/ob WAT, ATMs adopt an M2 phenotype and enhance their fatty acid remodelling, but reduce the rate of *de novo* PC biosynthesis (**Error! Reference source not found.**). However, in the dysfunctional WAT of 16-week-old ob/ob mice, ATM population exhibits a shift from M2 to M1 polarisation, co-occurring with increased intracellular lipid accumulation, down-regulation of fatty acid remodelling gene transcription and increase in PC:PE ratio (**Error! Reference source not found.**). Altogether, **dysfunctional WAT creates a lipotoxic and inflammatory milieu, leading to increased PC biosynthesis in ATMs.** The research questions of this chapter can thus be formulated as follows:

1) Is an increased *de novo* PC biosynthesis in ATMs during obesity an adaptive mechanism that limits WAT inflammation? 2) Alternatively, does the increase in *de novo* PC biosynthesis in ATMs during obesity promote ER stress and WAT inflammation?

Based on the presented literature on PC metabolism in different cell types, elevated *de novo* PC synthesis in macrophages can be speculated to either have a protective or a detrimental role during obesity. On the one hand, increased PC levels may enable ATMs to function in a lipotoxic environment by providing membrane biosynthetic material for lipid droplet formation and lipid partitioning towards inert FFA storage, thus alleviating ER from excessive lipid load and reducing ER stress and inflammation. On the other hand, increased *de novo* PC synthesis may lead to increased rate of saturated fatty acid incorporation to ER membranes, thus causing ER stress and pro-inflammatory activation of ATMs[233].

In this chapter, I will aim to answer my proposed questions in two objectives:

Objective 1. **To investigate the functional impact of reduced *de novo* PC biosynthesis on macrophage function in a lipotoxic environment *in vitro***. This will be performed using BMDM as a model cell, with the initial attempt to understand how *de novo* PC biosynthesis is regulated by lipotoxic and

inflammatory stimuli in macrophages *in vitro*. Subsequently, BMDMs from mice with macrophage-specific *Pcyt1a* deletion will be utilised to assess the impact of reduced *de novo* PC biosynthesis on the response of macrophages to lipotoxic stimuli.

Objective 2. **To assess the impact of reduced macrophage *de novo* PC biosynthesis on the function of metabolic tissues in lean and obese states *in vivo*.** To address this, I will investigate the metabolic profile of mice lacking *Pcyt1a* gene in macrophages both in healthy, chow-fed state and after prolonged feeding with high-fat diet in order to induce insulin resistance and dyslipidaemia. Furthermore, ATMs, whole WAT and livers will be analysed for metabolic and inflammatory gene markers.

I will ultimately combine the evidence gathered from both objectives to draw a model explaining the role of *de novo* PC biosynthesis in mediating the inflammatory activation of ATMs during obesity. This model will hopefully contribute to the global objective of providing an overall understanding of physiological processes leading to the development of WAT dysfunction and insulin resistance, and will complement current mechanisms emphasising the importance of ATM lipid metabolism for appropriate WAT function, particularly macrophage fatty acid synthesis[408] and lipid remodelling[219].

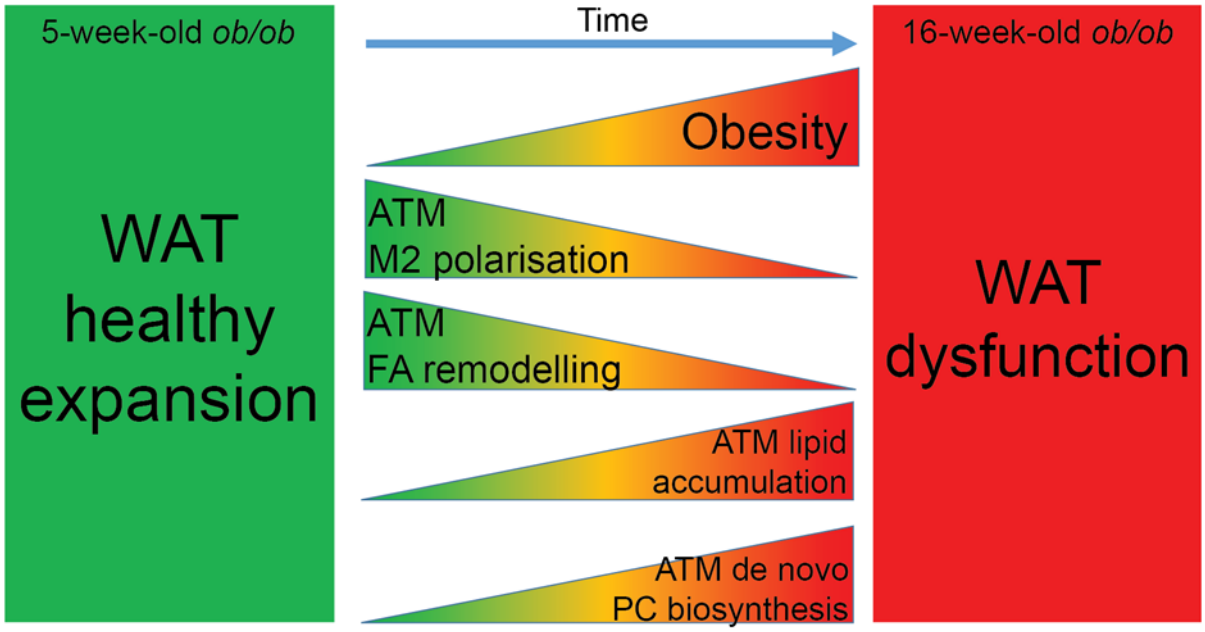

Figure 3-4. Schematic representation of changes in ATM phenotype over time in ob/ob mice.

3.2 Results

3.2.1 The role of *Pcyt1a* in palmitate-induced ER stress and inflammation in BMDMs

3.2.1.1 LPS and exogenous fatty acids increased *de novo* PC biosynthesis in macrophages

Rationale and results. The majority of choline-containing lipids are PC species, and the remaining minority are sphingolipids, which are synthesised from PC precursors. Therefore, the only way hydrophilic choline can be incorporated into hydrophobic lipid fraction is via *de novo* PC biosynthesis. Consequently, measuring the appearance of radiolabelled choline in lipid fraction over time is a good readout of the rate of *de novo* PC biosynthesis. Furthermore, as CCTα is a rate-limiting enzyme in *de novo* PC biosynthesis pathway, this method can be considered as a proxy for the real-time assessment of CCTα enzymatic activity in living cells.

A previous study showed that *de novo* PC biosynthesis is required for cytokine secretion following LPS stimulation[373]. However, the rate of choline incorporation to PC was not affected during the initial 6 h period of LPS stimulation[373]. To validate this finding, I stimulated BMDMs with LPS and immediately tracked the incorporation of radiolabelled choline into total cellular lipids. Contrary to the published result[373], I observed a nearly two-fold increase in *de novo* PC formation during the initial 2 h period following macrophage TLR4 stimulation (Figure 3-5 A).

Loading cells with exogenous fatty acids has been reported to increase PC biosynthesis in order to generate membranes for newly formed lipid droplets[367]. Oleate has been shown to more readily lead to lipid droplet formation, compared to palmitate[547]. Consistently, I observed an approximately 3-fold increase in *de novo* PC synthesis during the first 2 h following the exposure of BMDMs to oleate (Figure 3-5 B). Interestingly, equimolar dose of palmitate also resulted in a smaller increase in PC biosynthesis despite having little to no effect on BODIPY-stained lipid droplet formation (Figure 3-5 B, data not shown). Furthermore, the increase in *de novo* PC formation rate in BMDMs was directly proportional to the concentration of palmitate in culture medium (Figure 3-5 C). As palmitate concentrations exceeding 100 μM have been routinely used in the literature to model lipotoxicity in macrophages *in vitro*, I chose to investigate the importance of *de novo* PC biosynthesis for the development of ER stress and inflammation **in response to palmitate**.

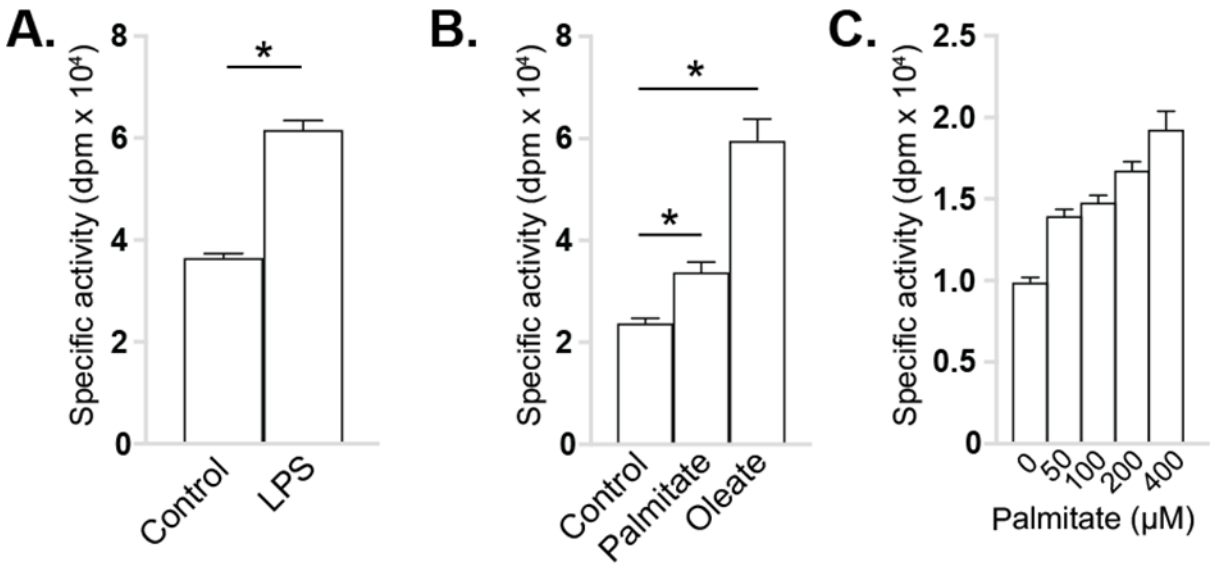

Figure 3-5. Incorporation of choline into lipids after BMDM stimulation with LPS or fatty acids.

*Specific activity of total cellular lipids of WT BMDMs treated with either 100 ng/ml LPS for 2 h (**A**), 100 μM palmitate or 100 μM oleate for 2 h (**B**) or indicated concentrations of palmitate for 2 h (**C**) in the presence of methyl-[^{3}H] choline chloride tracer. N=4 mice/experiment. * $p < 0.05$ compared to control using student's t-test (**A**), 1-way ANOVA with Dunnett's multiple comparisons test (**B**). Means in (**C**) are significantly different when tested using 1-way ANOVA with a post hoc test for left-to-right linear trend (significant differences are not visually indicated). All mice were of C57Bl/6J genetic background.*

3.2.1.2 *Pcyt1a* gene deletion did not affect the differentiation of BMDMs

Rationale and results. One previous study has utilised Pcyt1a$^{fl/fl}$ BMDMs, where *Pcyt1a* gene was excised at the end of the differentiation by exogenously adding cell-penetrating Cre recombinase protein[367]. However, so far no studies have characterised the differentiation capacity of BMDMs obtained from LysM-Cre Pcyt1a$^{fl/fl}$ mice. As this model has been previously shown to have appropriate numbers of functional peritoneal macrophages[373], I did not expect it to have an impaired BMDM differentiation. Indeed, the protein expression of macrophage surface markers F4/80, CD11b, CD206 and CD301 was not affected by the presence of *Cre* gene in the *LysM* locus on Pcyt1a$^{fl/fl}$ background after 7 days of BMDM differentiation (Figure 3-6 A). The expression of macrophage surface marker genes was also similar between genotypes, with the exception of CD206, which was down-regulated in BMDMs from LysM-Cre Pcyt1a$^{fl/fl}$ mice (Figure 3-6 B).

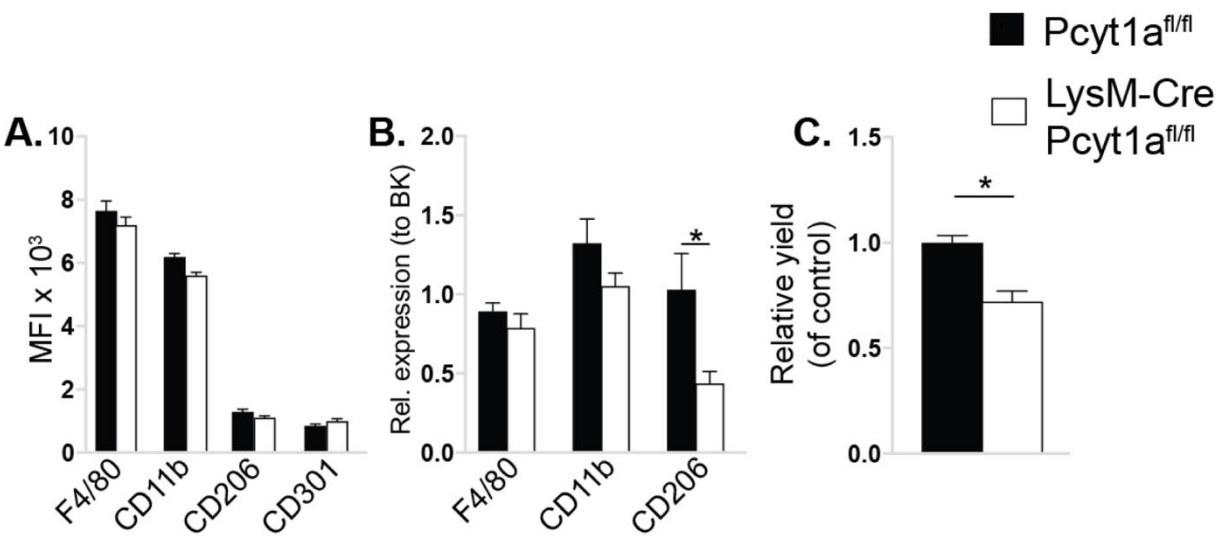

Figure 3-6. Differentiation efficiency of BMDMs from LysM-Cre Pcyt1a$^{fl/fl}$ mice. ***(A)*** *Flow cytometry analysis of F4/80, CD11b, CD206 and CD301 macrophage surface marker expression in differentiated BMDMs from Pcyt1af$^{l/fl}$ (black bars) and Pcyt1a$^{fl/fl}$ LysM-Cre (white bars) mice. (**B**) mRNA levels (normalised to BestKeeper) of F4/80, Cd11b, Cd206 in differentiated BMDMs from Pcyt1af$^{l/fl}$ and Pcyt1a$^{fl/fl}$ LysM-Cre mice. (**C**) Relative yield of differentiated BMDMs from Pcyt1a$^{fl/fl}$ LysM-Cre compared to Pcyt1af$^{l/fl}$ mice. (**A**) N=5 Pcyt1af$^{l/fl}$ and 3 Pcyt1a$^{fl/fl}$ LysM-Cre, n=4 mice/group (**B** and **C**). All mice were of C57Bl/6J genetic background. * p < 0.05 compared to Pcyt1a$^{fl/fl}$ using student's t-test.*

A typical BMDM differentiation method involves plating an even number (approximately 5 million) of bone marrow cells in each plate and normally allows obtaining around 10 million BMDMs per plate after 7 days of culturing. However, I noticed that bone marrow cells from LysM-Cre Pcyt1a$^{fl/fl}$ produced approximately 30% less of mature BMDMs compared to Pcyt1a$^{fl/fl}$ controls in three independent cultures (Figure 3-6 C, representative result of three cultures).

Conclusion. CCTα deficiency did not affect BMDM differentiation but reduced the yield of mature BMDMs.

3.2.1.3 *Pcyt1a* gene deletion reduced CCTα protein levels and decreased the basal rate of choline, palmitate and acetate incorporation into BMDM lipids

Rationale and results. Next, I investigated the CCTα deletion efficiency in LysM-Cre Pcyt1a$^{fl/fl}$ BMDMs. The action of Cre recombinase on *Pcyt1a* gene locus in macrophages was previously shown to be not completely penetrant, resulting in a mixed population of *Pcyt1a*-expressing (approximately 20-30% of population) and *Pcyt1a*-deficient cells (approximately 70-80% of population)[373]. While I did not analyse individual cells, I also found approximately 70% reduction in *Pcyt1a* mRNA levels in LysM-Cre Pcyt1a$^{fl/fl}$ BMDMs compared to controls on mixed C57Bl/6J, 129/Sv genetic background (Figure 3-37 C, same genetic background as published previously[373]), and approximately 50% reduction on pure C57Bl/6J genetic background (Figure 3-7 A). CCTα protein levels were reduced by approximately 70% in LysM-Cre Pcyt1a$^{fl/fl}$ BMDMs on pure C57Bl/6J genetic background (Figure 3-7 B, C). The rate of choline incorporation to cellular lipids was reduced by approximately 50% and 30% on mixed C57Bl/6J, 129/Sv and pure C57Bl/6J genetic backgrounds, respectively (Figure 3-37 B, Figure 3-7 D). The reduction of *de novo* PC biosynthesis in LysM-Cre Pcyt1a$^{fl/fl}$ BMDMs was accompanied by a small reduction in palmitate incorporation, and approximately 30% decrease in acetate incorporation to cellular lipids, indicating reduced rate of total fatty acid synthesis on a pure C57Bl/6J genetic background (Figure 3-7 D).

Despite observing a more potent decrease in *Pcyt1a* mRNA and *de novo* PC biosynthesis in LysM-Cre Pcyt1a$^{fl/fl}$ BMDMs on mixed C57Bl/6J, 129/Sv, compared to a pure C57Bl/6J genetic background, I chose to perform all *in vitro* experiments on a

pure C57Bl/6J genetic background. The rationale for this decision was that most murine metabolic phenotyping studies involve the use of C57Bl/6J mice, having all experiments performed on the same background would ensure a higher reproducibility of our work.

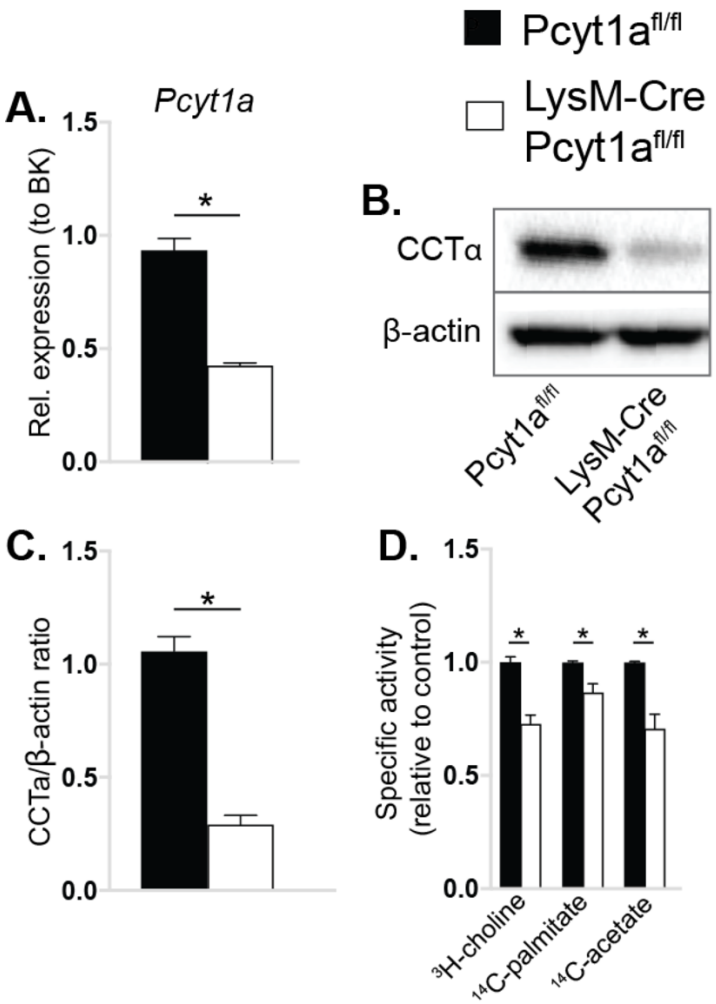

Figure 3-7. Validation of CCTα deletion in BMDMs from LysM-Cre Pcyt1a$^{fl/fl}$ mice. *Pcyt1a mRNA (normalised to BestKeeper) (**A**), representative Western blots (**B**) and quantification of CCTα relative to β-actin protein levels (**C**) in differentiated BMDMs from Pcyt1a$^{fl/fl}$ (black bars) and Pcyt1a$^{fl/fl}$ LysM-Cre (white bars) mice. (**D**) Incorporation of ^{3}H-choline, ^{14}C-palmitate and ^{14}C-acetate, present at tracer amounts in the medium for 3 h, into cellular lipids of unstimulated BMDMs from Pcyt1a$^{fl/fl}$ and Pcyt1a$^{fl/fl}$ LysM-Cre mice. N=5 Pcyt1a$^{fl/fl}$ and 3 Pcyt1a$^{fl/fl}$ LysM-Cre (**A** and **C**), n=4 mice/group (**D**). All mice were of C57Bl/6J genetic background. * p < 0.05 compared to Pcyt1a$^{fl/fl}$ using student's t-test.*

3.2.1.4 *Pcyt1a* gene deletion did not affect LPS-induced JNK phosphorylation in BMDMs

Rationale. Ablation of cellular fatty acid synthesis has been previously shown to result in impaired JNK phosphorylation in response to LPS[408]. I have confirmed the published observation that stimulating BMDMs with LPS increased the rate of fatty acid synthesis (Figure 3-8 B). As LPS-induced fatty acid synthesis and *de novo* PC synthesis were reduced to a similar extent in LysM-Cre Pcyt1a$^{fl/fl}$ BMDMs (Figure 3-8 A, B), I hypothesised that *de novo*-synthesised fatty acids are utilised by *de novo* PC biosynthesis pathway to generate PC. I therefore investigated whether *Pcyt1a* deletion resulted in impaired LPS-induced JNK phosphorylation, as reported for BMDMs deficient in *Fasn* gene[408].

Results. Despite having reduced rate of fatty acid synthesis, LysM-Cre Pcyt1a$^{fl/fl}$ BMDMs did not show an impairment in JNK phosphorylation after acute LPS treatment compared to controls (Figure 3-8 C, D).

Conclusion. This result indicated that TLR4-JNK signalling pathway was intact in LysM-Cre Pcyt1a$^{fl/fl}$ BMDMs.

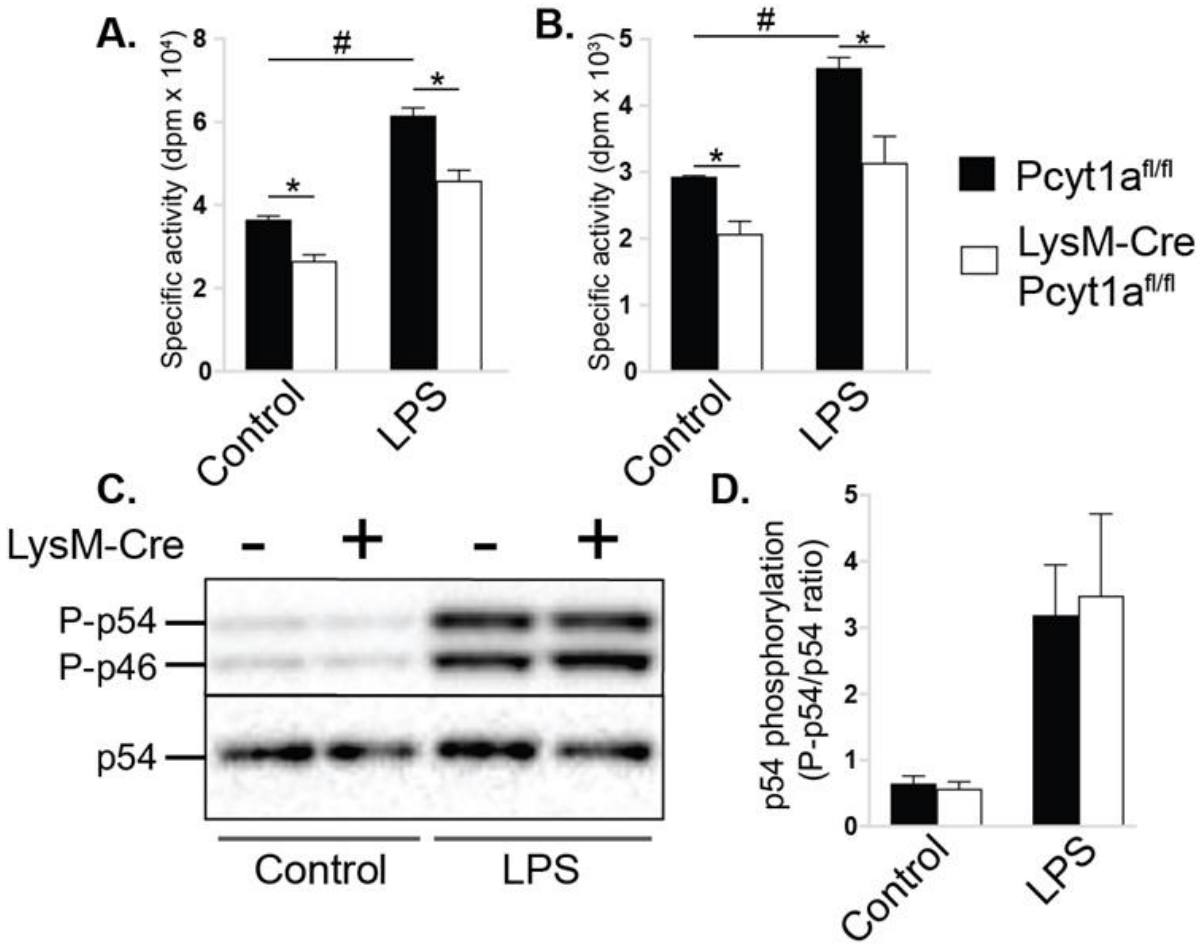

Figure 3-8. Induction of fatty acid synthesis and phosphorylation of JNK in response to LPS in BMDMs from LysM-Cre Pcyt1a$^{fl/fl}$ mice.

*Incorporation of ^{3}H-choline (**A**) and ^{14}C-acetate (**B**) tracers into cellular lipids of Pcyt1a$^{fl/fl}$ (black bars) and Pcyt1a$^{fl/fl}$ LysM-Cre (white bars) BMDMs during the stimulation with 100 ng/ml LPS for 3 h. Representative Western blots (**C**) and quantification of phosphorylated JNK splicing form p54 relative to total p54 protein levels (**D**) in Pcyt1a$^{fl/fl}$ and Pcyt1a$^{fl/fl}$ LysM-Cre BMDMs stimulated with 100 ng/ml LPS for 30 min. N=4 mice/group. * $p < 0.05$ compared to Pcyt1a$^{fl/fl}$ and # < 0.05 compared to unstimulated control using 2-way ANOVA with Bonferroni's multiple comparisons test. All mice were of C57Bl/6J genetic background.*

3.2.1.5 *Pcyt1a* gene deletion resulted in formation of giant lipid droplets without affecting TG biosynthesis in oleate-treated BMDMs

Rationale. Decreased rate of *de novo* PC biosynthesis has been previously reported to result in giant lipid droplets after loading cells with oleate.

Results. I confirmed this observation in LysM-Cre Pcyt1a$^{fl/fl}$ BMDMs exposed to oleate in order to induce lipid droplet formation (Figure 3-9 A). As intracellular TG storage is known to play a protective role during palmitate-induced lipotoxicity[209], I investigated whether increased size of lipid droplets in BMDMs had any effect on their capacity to synthesise TGs. LysM-Cre Pcyt1a$^{fl/fl}$ BMDMs incorporated the same amount of oleate in the TG fraction as controls, despite having substantially larger lipid droplets (Figure 3-9 B, C).

Conclusion. Any potential changes in lipotoxicity-mediated stress and inflammation caused by reduced PC synthesis in BMDMs are not likely to be due to altered TG storage capacity.

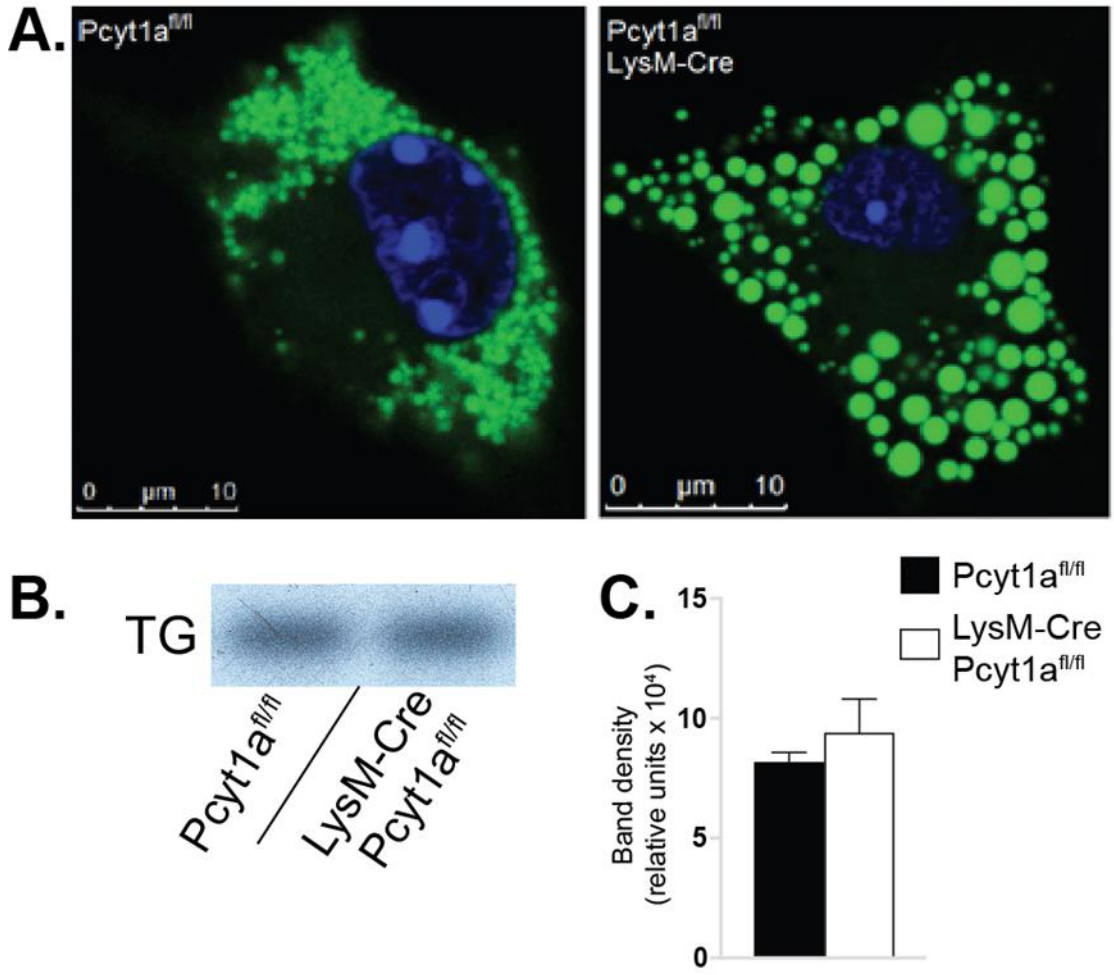

Figure 3-9. Formation of lipid droplets and intracellular triglycerides in response to oleate in BMDMs from LysM-Cre Pcyt1a$^{fl/fl}$ mice.

A. *Representative confocal microscopy image of Pcyt1a$^{fl/fl}$ and Pcyt1a$^{fl/fl}$ LysM-Cre BMDMs stained with BODIPY (green) or Hoechst 33342 (blue) after 16 h incubation in the presence of 100 µM oleate. Representative radiogram (**B**) and quantification (**C**) of TG fraction of neutral lipids separated by TLC from Pcyt1a$^{fl/fl}$ (n=5, black bars) and Pcyt1a$^{fl/fl}$ LysM-Cre (n=3, white bars) BMDMs treated with 100 µM oleate for 16 h in the presence of ^{14}C-oleate tracer. Mice were of mixed C57Bl/6J, 129/Sv (**A**) and pure C57Bl/6J genetic background (**B, C**).*

3.2.1.6 *Pcyt1a* gene deletion supressed cellular stress signalling and *Tnf* gene expression in palmitate-treated BMDMs

Rationale. Having established that reduced PC synthesis did not affect TLR4-JNK signalling axis and fatty acid partitioning to TGs, I next assessed the response of *Pcyt1a*-deficient macrophages to a lipotoxic insult.

Results. I treated LysM-Cre Pcyt1a$^{fl/fl}$ BMDMs with increasing concentrations (0, 200, 400 and 600 μM) of palmitate for a prolonged period of time. Both 400 and 600 μM concentrations of palmitate were potently cytotoxic, and the amount of viable cells after treatment with 600 μM palmitate was not sufficient for protein analysis. As expected, palmitate caused the activating phosphorylation of stress-responsive MAPKs JNK (both splicing isoforms p54 and p46) and p38 in control macrophages in a dose-dependent manner (Figure 3-10 A-D). However, LysM-Cre Pcyt1a$^{fl/fl}$ BMDMs showed a marked reduction in JNK and p38 phosphorylation following palmitate treatment compared to controls (Figure 3-10 A-D). Similarly, induction of *Tnf* gene expression by 400 and 600 μM palmitate was supressed in *Pcyt1a*-deficient BMDMs (Figure 3-10 E).

Conclusion. *Pcyt1a*-deficient BMDMs exhibited diminished inflammatory activation in response to palmitate.

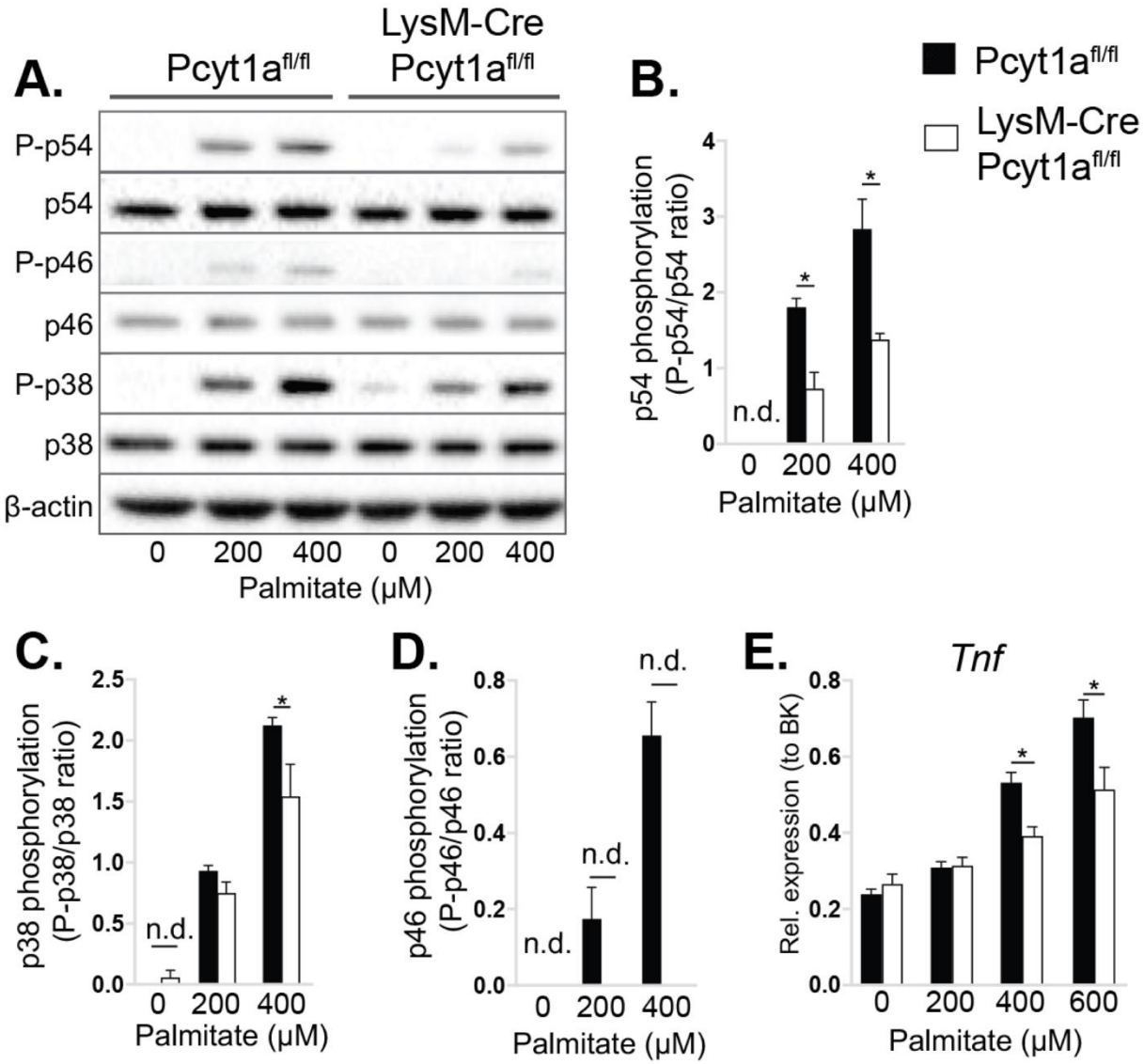

Figure 3-10. Inflammatory activation of BMDMs from LysM-Cre Pcyt1a$^{fl/fl}$ mice in response to prolonged incubation with palmitate.

*Representative Western blots (**A**) and quantification of phosphorylated JNK splicing forms p54 and p46 and phosphorylated p38 MAPK relative to respective total protein levels (**B-D**) in Pcyt1a$^{fl/fl}$ (black bars) and Pcyt1a$^{fl/fl}$ LysM-Cre (white bars) BMDMs treated with 0, 200 or 400 μM palmitate for 16 h. **E.** Tnf mRNA levels (normalised to BestKeeper) in Pcyt1a$^{fl/fl}$ and Pcyt1a$^{fl/fl}$ LysM-Cre BMDMs treated with 0, 200, 400 or 600 μM palmitate for 16 h. N=5 Pcyt1a$^{fl/fl}$ and 3 Pcyt1a$^{fl/fl}$ LysM-Cre mice. * $p < 0.05$ compared to Pcyt1a$^{fl/fl}$ using 2-way ANOVA with Bonferroni's multiple comparisons test. N.d. indicates undetectable protein level, where significant differences were not assessed. All mice were of C57Bl/6J genetic background.*

3.2.1.7 *Pcyt1a* gene deletion alleviated palmitate-induced cell death of BMDMs

Rationale. As I have observed profound cell death of BMDMs after a prolonged treatment with high doses (>200 μM) of palmitate, I decided to assess whether *Pcyt1a* deletion affected the cytotoxicity of palmitate in BMDMs using flow cytometry.

Results. I treated LysM-Cre Pcyt1a$^{fl/fl}$ and control BMDMs with increasing concentrations of palmitate overnight. As already observed in 3.2.1.6, palmitate caused cell death in BMDMs in a dose-dependent manner (Figure 3-11). However, cell death was attenuated in LysM-Cre Pcyt1a$^{fl/fl}$ BMDMs treated with 250 μM and 500 μM palmitate, compared to control cells (Figure 3-11).

Conclusion. *Pcyt1a*-deficient BMDMs were less susceptible to cell death in response to a prolonged treatment with 250 and 500 μM palmitate than controls.

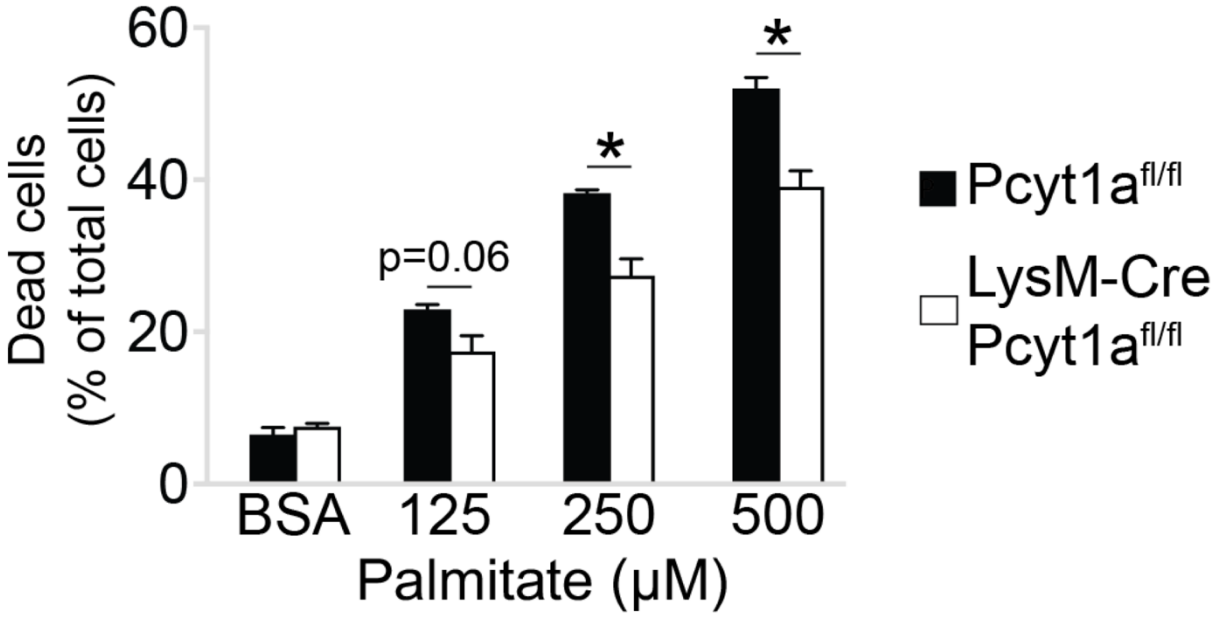

Figure 3-11. Cell death of BMDMs from LysM-Cre Pcyt1a$^{fl/fl}$ mice in response to prolonged incubation with palmitate.

*Flow cytometry quantification of cell death (expressed as a percentage of LIVE/DEAD dye-positive cells relative to total BMDM population) in Pcyt1a$^{fl/fl}$ (black bars, n=4) and Pcyt1a$^{fl/fl}$ LysM-Cre (white bars, n=4) BMDMs treated with BSA or 125, 250 or 500 μM palmitate for 16 h. * p < 0.05 compared to Pcyt1a$^{fl/fl}$ using 2-way ANOVA with Bonferroni's multiple comparisons test. All mice were of C57Bl/6J genetic background.*

3.2.1.8 *Pcyt1a* gene deletion did not affect the rate of ER stress development following palmitate treatment, but reduced ER stress and *Tnf* gene expression after prolonged palmitate treatment

Rationale. Palmitate has been shown to exert some of its inflammatory effects in macrophages by causing ER stress[548]. I therefore decided to investigate whether diminished inflammatory and stress activation of *Pcyt1a*-deficient BMDMs was caused by a reduced rate of ER stress development.

Results. I chose 250 μM concentration of palmitate for this experiment, as my previous results indicated that it potently induces ER stress without having a major effect on cell viability (data not shown). I treated LysM-Cre Pcyt1a$^{fl/fl}$ BMDMs with palmitate for different lengths of time (0, 1, 2, 4, 6 and 8 h) and measured the induction of *Chop* transcription and *Xbp1* mRNA splicing as markers of ER stress. As expected, palmitate induced a transcriptional ER stress response in a time-dependent manner in control cells (Figure 3-12 B, C). LysM-Cre Pcyt1a$^{fl/fl}$ BMDMs exhibited increased basal transcription of ER stress markers, as it has been reported previously for different cell types with impaired *de novo* PC biosynthesis[223] (Figure 3-12 B, C). However, *Pcyt1a*-deficient BMDMs developed ER stress in response to palmitate at the same rate as controls (Figure 3-12 B, C). Acute induction of *Tnf* transcription in response to palmitate, likely driven by TLR4 activation, was also similar in both genotypes, with LysM-Cre Pcyt1a$^{fl/fl}$ BMDMs showing only minor reduction in *Tnf* message levels 4 h post stimulation (Figure 3-12 A).

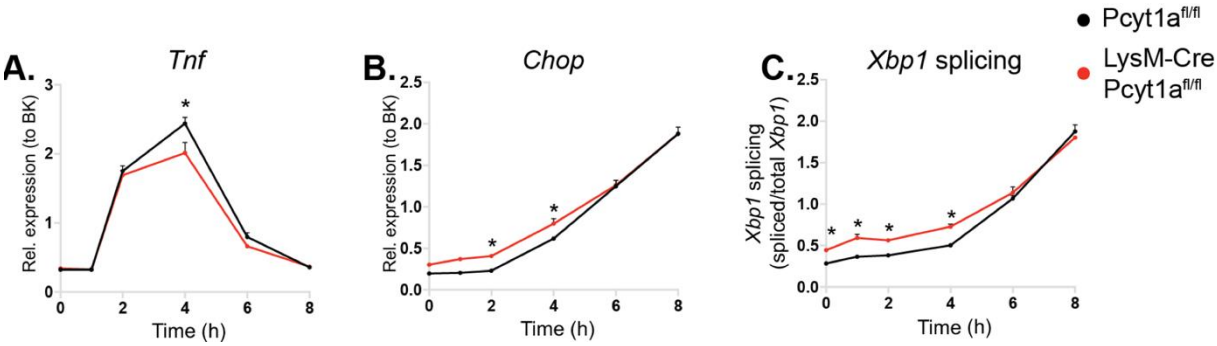

Figure 3-12. Inflammatory activation and development of ER stress in BMDMs from LysM-Cre Pcyt1a$^{fl/fl}$ mice in response to acute treatment with palmitate.

*mRNA levels (normalised to BestKeeper) of Tnf (**A**), Chop (**B**) and the ratio of spliced to total Xbp1 mRNA levels (**C**) in Pcyt1a$^{fl/fl}$ (black lines, n=4) and Pcyt1a$^{fl/fl}$ LysM-Cre (red lines, n=4) BMDMs treated with 250 μM palmitate for 0, 2, 4, 6 and 8 h in a reverse time-course manner. T=0 h were treated with BSA for 8 h. * p < 0.05 compared to Pcyt1a$^{fl/fl}$ using 2-way ANOVA with Bonferroni's multiple comparisons test. All mice were of C57Bl/6J genetic background.*

Interestingly, LysM-Cre Pcyt1a$^{fl/fl}$ BMDMs showed a reduction in ER stress markers and *Tnf* mRNA compared to controls following the exposure to 250 μM palmitate for a **prolonged period of time** (Figure 3-13 A-C).

Conclusion. Reduced PC biosynthesis in macrophages alleviated ER stress during chronic, but not acute lipotoxic stress.

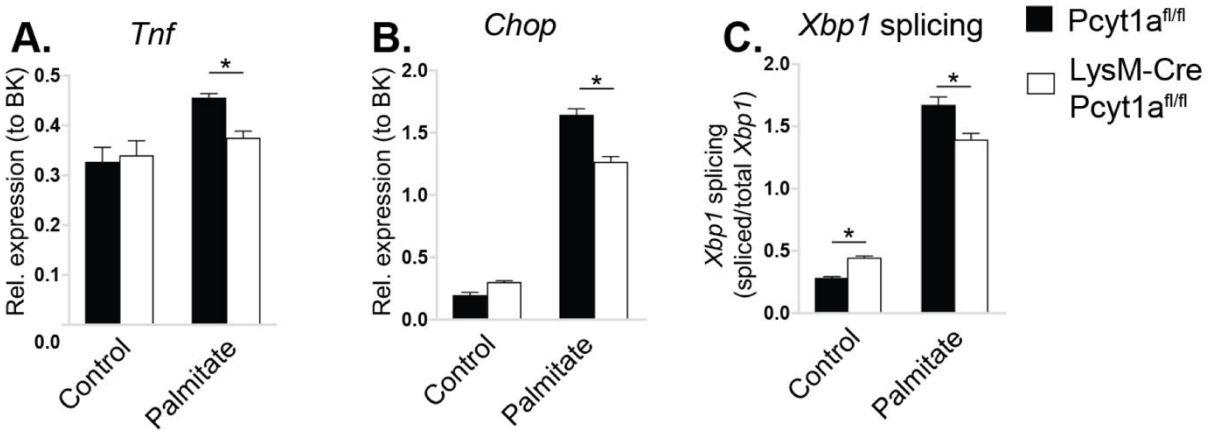

Figure 3-13. Inflammatory activation and development of ER stress in BMDMs from LysM-Cre Pcyt1a$^{fl/fl}$ mice in response to prolonged treatment with palmitate. *mRNA levels (normalised to BestKeeper) of Tnf (**A**), Chop (**B**) and the ratio of spliced to total Xbp1 mRNA levels (**C**) in Pcyt1a$^{fl/fl}$ (black bars, n=4) and Pcyt1a$^{fl/fl}$ LysM-Cre (white bars, n=4) BMDMs treated with 250 μM palmitate for 24 h. * p < 0.05 compared to Pcyt1a$^{fl/fl}$ using 2-way ANOVA with Bonferroni's multiple comparisons test. All mice were of C57Bl/6J genetic background.*

3.2.1.9 *Pcyt1a* gene deletion did not affect the rate of palmitate incorporation to cellular PC in palmitate-treated BMDMs

Rationale. CCTα inhibition has been previously suggested to reduce the rate of saturated fatty acid incorporation to membrane PC, which would concomitantly slow down the rate of ER stress development[233]. I have already shown that in the unstimulated state, *Pcyt1a*-deficient BMDMs incorporated palmitate to cellular lipids at a lower rate than controls (Figure 3-7 D). However, cells can shuttle fatty acids to phospholipids through *de novo* biosynthesis or lipid remodelling pathways, and the relative contribution of each pathway might depend on the exogenous fatty acid concentration. Therefore, I investigated whether reduced ER stress and inflammatory activation following the treatment with high concentration of palmitate was due to its impaired incorporation to PC in LysM-Cre Pcyt1a$^{fl/fl}$ BMDMs.

Results. I treated cells with 250 μM palmitate and traced its movement into PC fraction. However, despite having reduced basal rate of palmitate incorporation into cellular lipids, *Pcyt1a*-deficient BMDMs esterified palmitate to PC and total lipids at the same rate as controls (Figure 3-14 A-C).

I then tested whether a prolonged treatment of LysM-Cre Pcyt1a$^{fl/fl}$ BMDMs with fatty acids resulted in palmitate re-partitioning from PC fraction. As it has been reported previously, a larger amount of palmitate appeared in PC fraction than oleate[233] (Figure 3-15 A,B). However, neither of the fatty acids showed a difference in the total amount incorporated into a PC fraction after prolonged treatment between LysM-Cre Pcyt1a$^{fl/fl}$ BMDMs and controls (Figure 3-15 A,B).

Conclusion. This finding indicated that the rate of palmitate esterification to membrane phospholipids does not link reduced *de novo* PC biosynthesis to diminished induction of ER stress and inflammation during chronic treatment with palmitate.

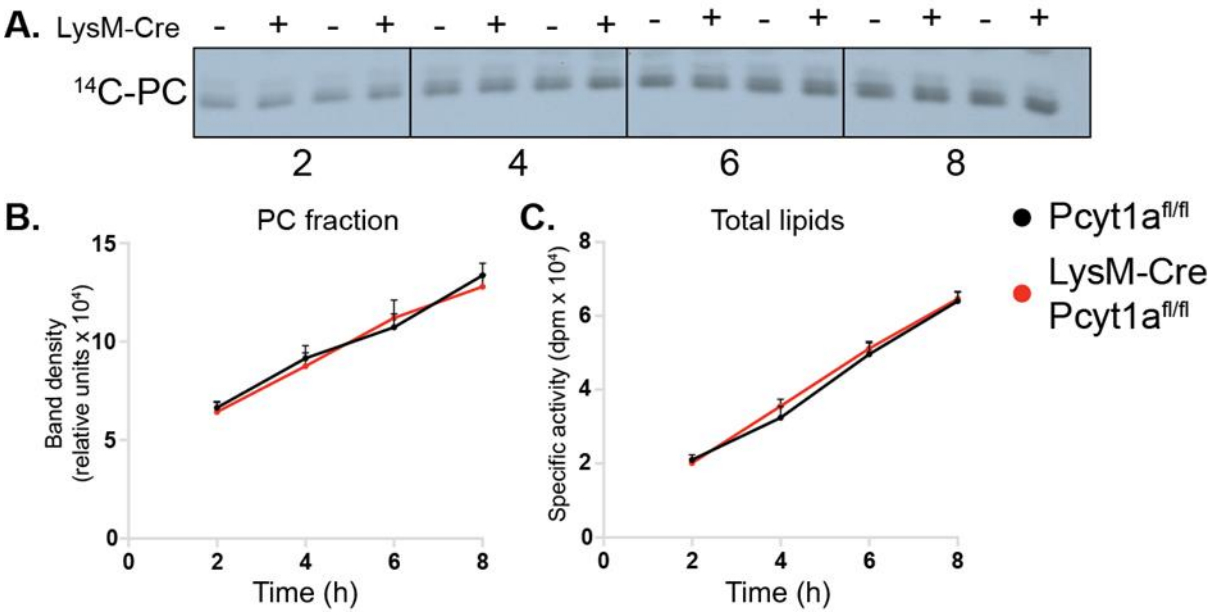

Figure 3-14. Incorporation of palmitate into lipids in BMDMs from LysM-Cre Pcyt1a$^{fl/fl}$ mice in response to acute treatment with palmitate.

*Representative radiogram (**A**) and quantification (**B**) of PC fraction of phospholipids separated by TLC from Pcyt1a$^{fl/fl}$ (black lines) and Pcyt1a$^{fl/fl}$ LysM-Cre (red lines) BMDMs treated with 250 μM palmitate for 2, 4, 6 and 8 h in the presence of ^{14}C-palmitate tracer. (**C**) Specific activity of total lipids from Pcyt1a$^{fl/fl}$ and Pcyt1a$^{fl/fl}$ LysM-Cre BMDMs treated as in (**A** and **B**). N=4 mice/group. All mice were of C57Bl/6J genetic background.*

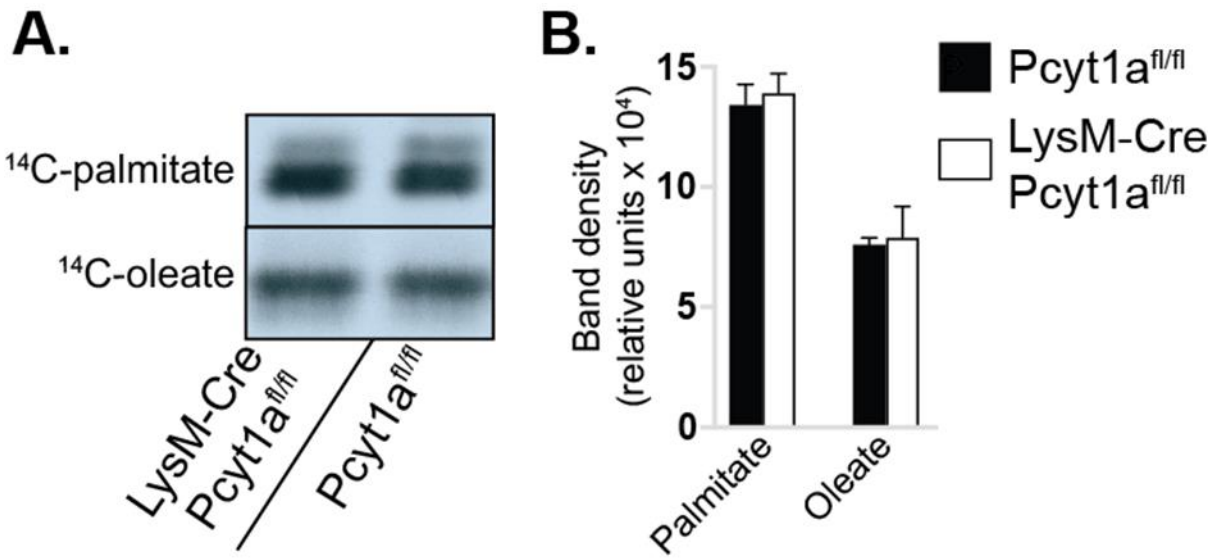

Figure 3-15. Incorporation of fatty acids into lipids in BMDMs from LysM-Cre Pcyt1a$^{fl/fl}$ mice after prolonged incubation with palmitate and oleate.

*Representative radiogram (**A**) and quantification (**B**) of PC fraction of phospholipids separated by TLC from Pcyt1a$^{fl/fl}$ (black bars, n=5) and Pcyt1a$^{fl/fl}$ LysM-Cre (white bars, n=3) BMDMs treated with 100 μM palmitate or 100 μM oleate for 16 h in the presence of respective ^{14}C-labelled tracer. All mice were of C57Bl/6J genetic background.*

3.2.1.10 *Pcyt1a* gene deletion diminished the suppression of fatty acid remodelling gene transcription after prolonged treatment with palmitate

Rationale. Elongation and desaturation of fatty acids by macrophages have been ascribed a protective role during LPS and palmitate-induced inflammation[219,220]. One of the major transcription factors regulating the expression of fatty acid remodelling genes in macrophages is SREBP1[220]. Interestingly, reduced cellular PC levels can lead to the induction of SREBP1 transcriptional activity[401,402]. I therefore investigated whether *Pcyt1a*-deficient BMDMs had altered regulation of SREBP1-target genes *Elovl6, Scd1* and *Fads1* that encode fatty acid elongation and desaturation enzymes.

Results. As observed in ATMs isolated from 16-week-old ob/ob mice, prolonged treatment with palmitate down-regulated fatty acid remodelling gene expression, suggesting a diminished SREBP1 transcriptional activity (Figure 3-16). When compared to controls, LysM-Cre Pcyt1a$^{fl/fl}$ BMDMs showed higher expression of *Elovl6* and *Fads1*, and no change in *Scd1* mRNA levels after a prolonged treatment with palmitate (Figure 3-16).

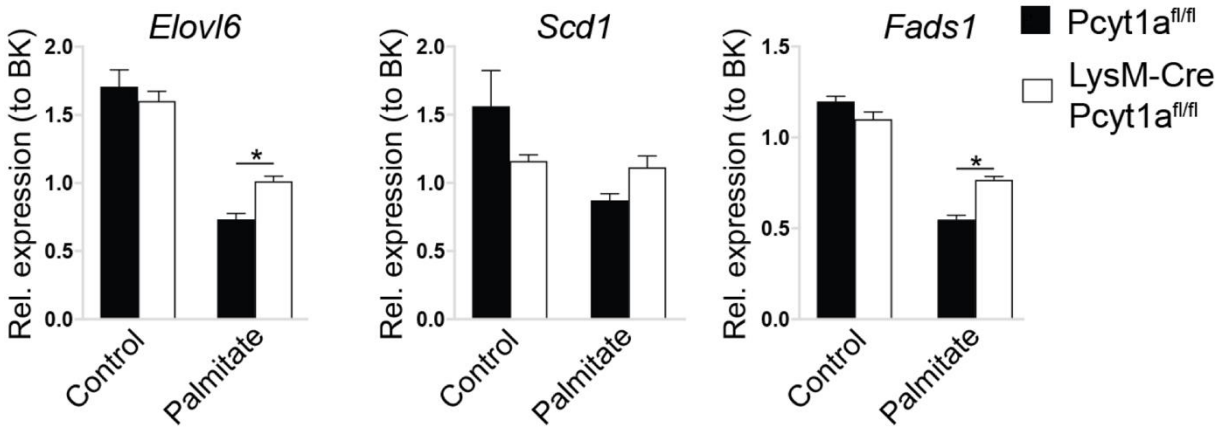

Figure 3-16. Fatty acid remodelling gene transcription in BMDMs from LysM-Cre Pcyt1a$^{fl/fl}$ mice after prolonged incubation with palmitate.

*mRNA levels (normalised to BestKeeper) of Elovl6, Scd1 and Fads1 in Pcyt1a$^{fl/fl}$ (black bars, n=4) and Pcyt1a$^{fl/fl}$ LysM-Cre (white bars, n=4) BMDMs treated with 250 μM palmitate for 24 h. * p < 0.05 compared to Pcyt1a$^{fl/fl}$ using 2-way ANOVA with Bonferroni's multiple comparisons test. All mice were of C57Bl/6J genetic background.*

Rationale. Next, I checked whether BMDMs had a capacity to elongate and/or desaturate palmitate present at a high extracellular concentration. I treated cells with 100 μM of 1-^{13}C palmitate isotope. Labelling first carbon of the molecule allowed me to monitor palmitate elongation and desaturation, as these processes do not modify the carboxyl-end of fatty acids.

***Results*.** As expected, I observed a dramatic increase in 1-^{13}C palmitate to endogenous 1-^{12}C palmitate ratio after a prolonged incubation of BMDMs with stably-labelled palmitate, indicating its incorporation to phospholipids (Figure 3-17). Treatment with labelled palmitate also resulted in the formation of labelled palmitoleate (C16:1n7) and stearate (C18:0), respective desaturation and elongation reaction products of palmitate (Figure 3-17).

Conclusion. These findings indicated that BMDMs are functionally capable of remodelling exogenous fatty acids present at lipotoxic concentrations, and also suggested that maintained transcription of fatty acid remodelling enzymes in *Pcyt1a*-deficient BMDMs after prolonged treatment with palmitate could explain reduced ER stress and inflammation.

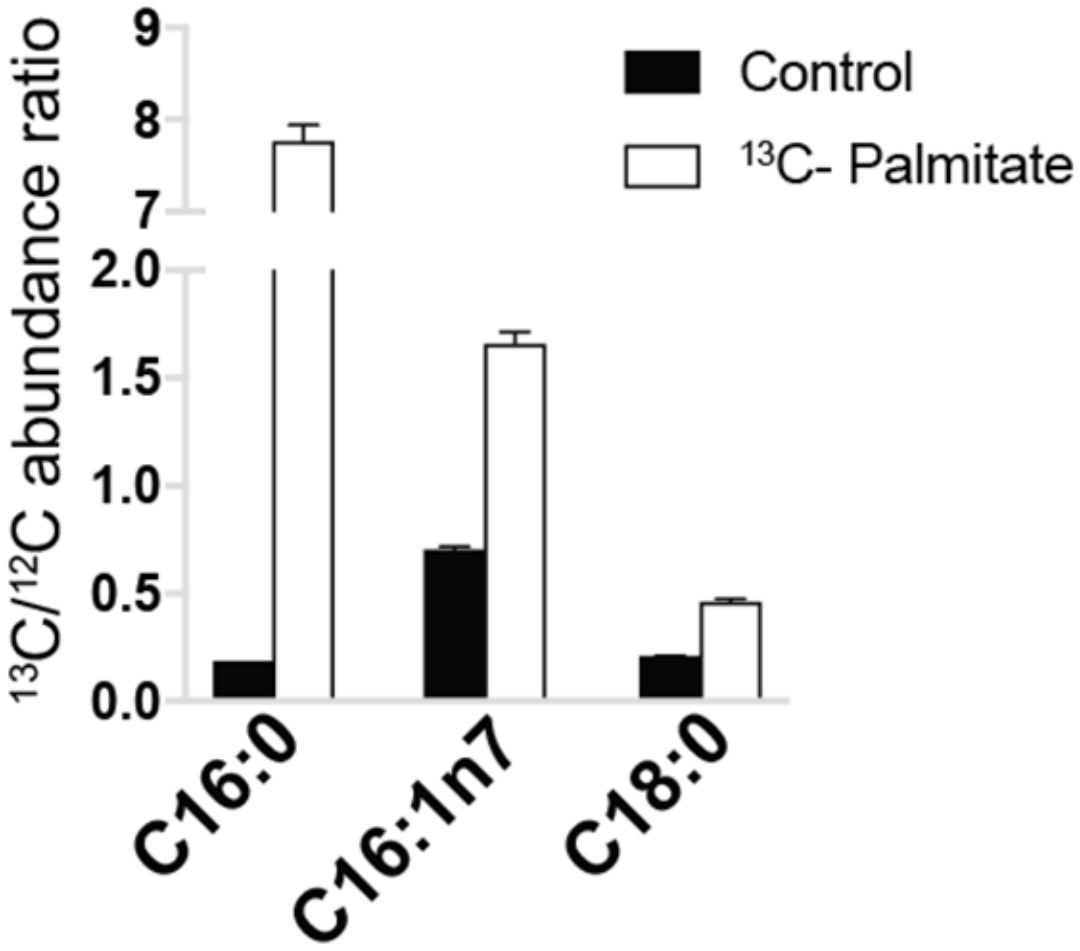

Figure 3-17. Remodelling of exogenous palmitate in BMDMs.

Ratio of 1-^{13}C to 1-^{12}C isotopes of C16:0, C16:1n7 and C18:0 fatty acids measured by GC-MS in lipids of BMDMs treated with 100 μM 1-^{13}C palmitate for 16 h. N=4 mice. Significant differences are not indicated. All mice were of C57Bl/6J genetic background.

3.2.2 The importance of *Pcyt1a* in macrophages for glucose and lipid metabolism of lean and obese mice on mixed C57Bl/6J, 129/Sv genetic background

3.2.2.1 The rationale for experimental methodology performed for *in vivo* metabolic phenotyping of LysM-Cre Pcyt1a$^{fl/fl}$ mice

Dietary treatments and housing conditions. LysM-Cre Pcyt1a$^{fl/fl}$ mice have been previously studied in vivo[373], but none of their metabolic characteristics have been described yet. I decided to use 45% kcal HFD (manufactured by Research Diets) to induce obesity and insulin resistance because it had been routinely used by our group to model HFD-induced obesity. HFD was administered to animals from 8 weeks of age, as previous results from our group suggested that mice of this age developed insulin resistance at a faster rate than mice fed HFD immediately after weaning at 4 weeks of age (data not shown). High-fat feeding continued for 8 weeks before mice were subjected to metabolic testing, as this period is sufficient to induce insulin resistance and WAT inflammation in WT animals[283]. Mice were individually housed a week prior to initial energy balance analysis in order to acclimatise them to the experimental conditions of metabolic cages and reduce stress response during the analysis. Mice remained single housed during the remaining period of metabolic testing, as re-housing them in groups was likely to result in fighting. Finally, mice were culled for tissues at 20 weeks of age, having been fed HFD for 12 consecutive weeks.

Glucose and insulin tolerance tests were primarily done to assess muscle glucose uptake and hepatic glucose production. **Lipid tolerance** test was a readout for intestinal lipid absorption rate and WAT lipid uptake. Serum biochemicals were measured to provide insight on liver, muscle, adipose tissue, pancreatic beta cell and intestinal function. Finally, gene transcription analysis of WAT fractions, whole WAT and livers were performed to investigate inflammation, insulin signalling and nutrient metabolism of each cell fraction or organ.

Power analysis. I chose to study 8 mice per group, because previous work from our lab indicated that such sample number was sufficient to observe a significant difference of 20% between groups in metabolic tests with 80% confidence. In this and the following chapter, sample size of less than 8 animals per group in any metabolic studies was either due to unexpected animal loss, or a *post hoc* decision to exclude mice from analysis that were statistical outliers for multiple metabolic characteristics.

All metabolic analyses of chow-fed control group of Pcyt1a$^{fl/fl}$ and LysM-Cre Pcyt1a$^{fl/fl}$ mice were performed at the same age as HFD-fed group to account for aging effects. However, chow and HFD groups were analysed in two separate batches. Importantly, as my main aim was to identify phenotypic differences between Pcyt1a$^{fl/fl}$ and LysM-Cre Pcyt1a$^{fl/fl}$ mice, only genotype was used as a dependent variable in statistical analysis, as distinguishing the diet from batch effects would be difficult. In graphs containing data from both chow and HFD mice, such grouping was solely done to illustrate the directionality of diet-induced change of a presented parameter, and not for statistical comparison of chow and HFD groups.

3.2.2.2 Macrophage-specific *Pcyt1a* deletion did not affect total energy balance of chow-fed mice on mixed genetic background

Rationale. I initially investigated whether deficiency of *Pcyt1a* in macrophages affected any components of energy balance of chow-fed mice.

Results. Genotype had no effect on body weight, chow consumption or average energy expenditure at 16 weeks of age, when mice were analysed in metabolic cages (Figure 3-18 A,B,C).

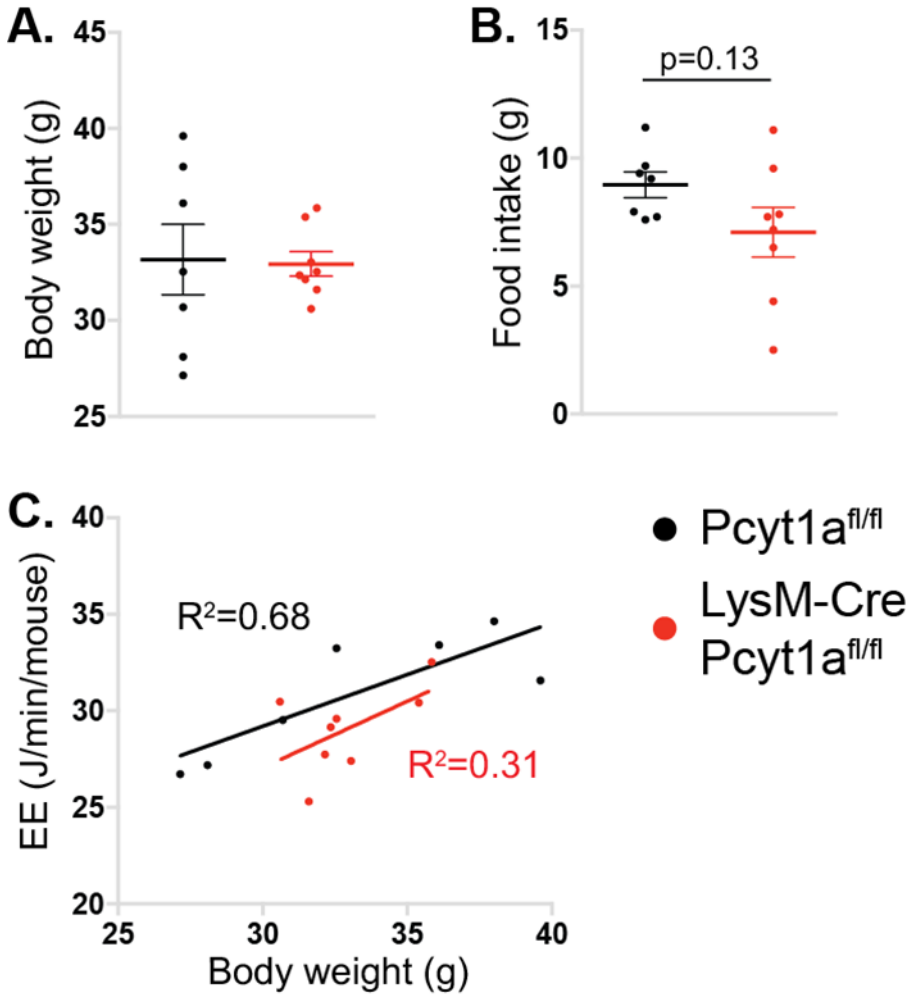

Figure 3-18. Food intake and energy expenditure of chow-fed Pcyt1a$^{fl/fl}$ and LysM-Cre Pcyt1a$^{fl/fl}$ mice on mixed genetic background.

*Body weight (**A**), food intake (**B**) and average energy expenditure plotted against body weight assessed over 48 h in Pcyt1a$^{fl/fl}$ (black dots, n=7) and Pcyt1a$^{fl/fl}$ LysM-Cre (red dots, n=8) 16-week-old male mice on mixed C57Bl/6J, 129/Sv background. Statistical significance was assessed by student's t-test (**A** and **B**) or one-way ANCOVA (**C**).*

3.2.2.3 Macrophage-specific *Pcyt1a* deletion did not affect serum metabolite concentrations of chow-fed mice on mixed genetic background

Results. Chow-fed LysM-Cre Pcyt1a$^{fl/fl}$ animals exhibited normal serum concentrations of insulin, FFAs, TGs, lipoprotein-bound cholesterol and choline in the fed state (Table 3-1). Overnight fasting elevated FFAs and reduced insulin and TGs to the same level in both genotypes (Table 3-1). Blood glucose levels were not affected by fasting or genotype on a chow diet (Table 3-1).

Feeding state	Random fed		Fasted overnight	
Genotype	**Pcyt1a$^{fl/fl}$**	**LysM-Cre Pcyt1a$^{fl/fl}$**	**Pcyt1a$^{fl/fl}$**	**LysM-Cre Pcyt1a$^{fl/fl}$**
Glucose (mM)	10.86 ± 0.56	10.76 ± 0.38	10.16 ± 0.77	10.61 ± 0.50
Insulin (µg/L)	1.33 ± 0.3	1.71 ± 0.41	0.44 ± 0.08	0.46 ± 0.09
FFA (mM)	1.12 ± 0.08	1.11 ± 0.13	1.46 ± 0.19	1.36 ± 0.13
TG (mM)	2.24 ± 0.18	2.13 ± 0.25	1.60 ± 0.12	1.70 ± 0.23
Total cholesterol (mM)	3.89 ± 0.37	3.56 ± 0.21	-	-
HDL cholesterol (mM)	2.30 ± 0.24	2.09 ± 0.13	-	-
LDL cholesterol (mM)	0.57 ± 0.09	0.51 ± 0.07	-	-
Total choline (µM)	45.14 ± 1.60	47.85 ± 3.33	-	-

Table 3-1. Serum biochemistry of chow-fed Pcyt1a$^{fl/fl}$ and LysM-Cre Pcyt1a$^{fl/fl}$ mice on mixed genetic background in a random-fed state or after overnight fast. *Concentrations of serum biochemicals are expressed as means ± SEM. N=7 Pcyt1a$^{fl/fl}$, n=8 LysM-Cre Pcyt1a$^{fl/fl}$ 16-20-week-old male mice on mixed C57Bl/6J, 129/Sv background.*

3.2.2.4 Macrophage-specific *Pcyt1a* deletion did not impact glucose, insulin and lipid tolerance of chow-fed mice on mixed genetic background

Results. Following exogenous administration of glucose, chow-fed LysM-Cre Pcyt1a$^{fl/fl}$ mice were able to normalise serum glucose concentration at the same rate as controls (Figure 3-19 A,B). There were no differences in insulin-mediated serum glucose uptake between genotypes (Figure 3-19 C,D). Finally, both groups showed similar serum TG concentration curves following gavage with olive oil (Figure 3-19 E,F).

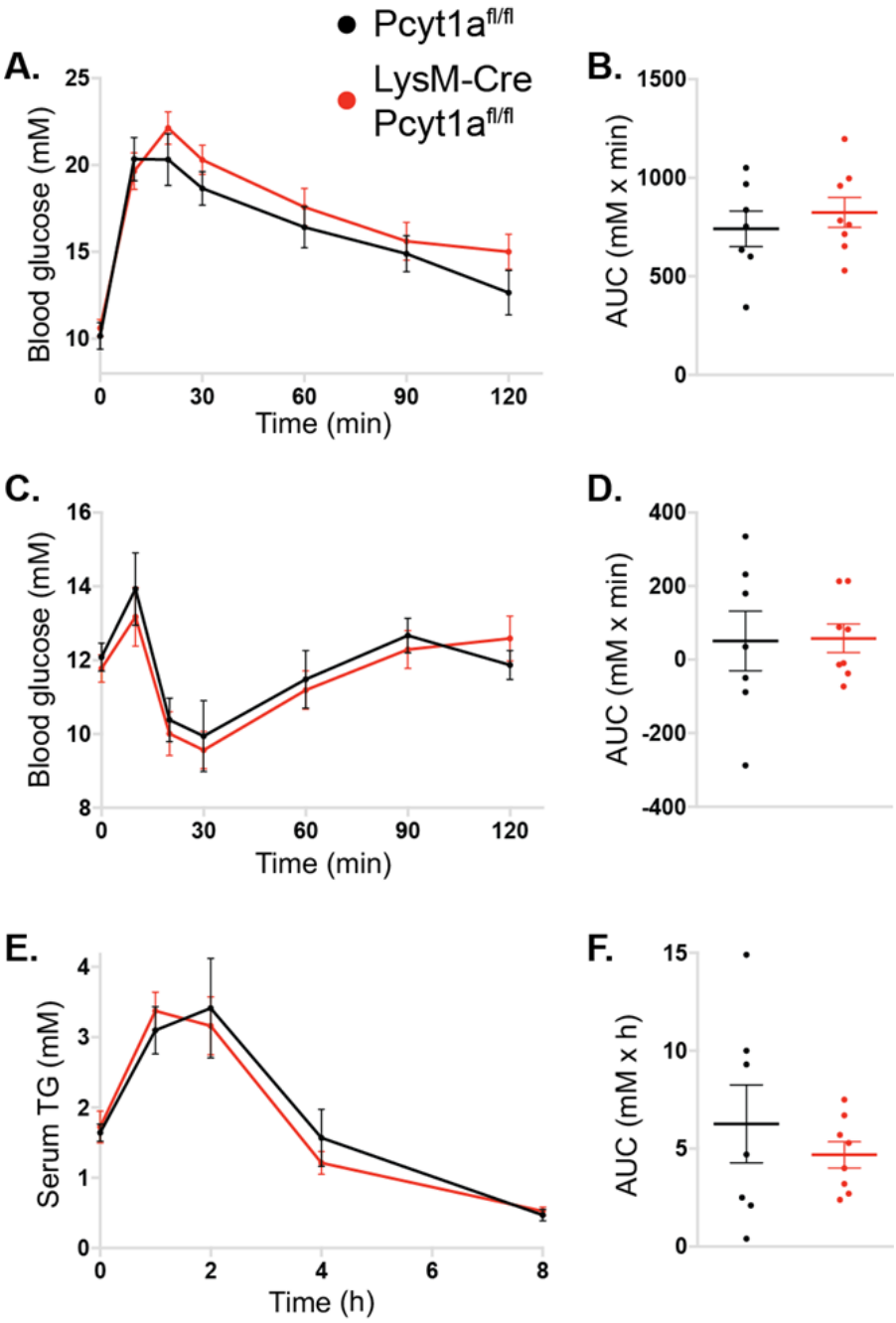

Figure 3-19. Glucose, insulin and lipid tolerance tests of chow-fed Pcyt1a$^{fl/fl}$ and LysM-Cre Pcyt1a$^{fl/fl}$ mice on mixed genetic background.

*Blood glucose concentration curves (**A**) and AUC (**B**) of mice injected with 1 mg/kg glucose at T=0 min after an overnight fast. Blood glucose concentration curves (**C**) and AUC (**D**) of mice injected with 0.75 IU/kg insulin at T=0 after 6 h fast. Serum TG concentration curves (**E**) and AUC (**F**) of mice administered with 200 μl of olive oil by oral gavage at T=0 after overnight fast. N=7 Pcyt1a$^{fl/fl}$ (black lines/dots) and n=8 LysM-Cre Pcyt1a$^{fl/fl}$ (red lines/dots)16-19-week-old male mice on mixed C57Bl/6J, 129/Sv background. Statistical significance was assessed by student's t-test (**B, D, F**).*

3.2.2.5 Macrophage-specific *Pcyt1a* deletion did not affect the weights of metabolic tissues of chow-fed mice on mixed genetic background

Results. Chow-fed LysM-Cre Pcyt1a$^{fl/fl}$ animals had similar body weight as controls at the end of the study (Figure 3-20 A). The expression of *Pcyt1a* in macrophages did not affect the weight of BAT, scWAT, eWAT and liver, relative to total body weight (Figure 3-20 B-E).

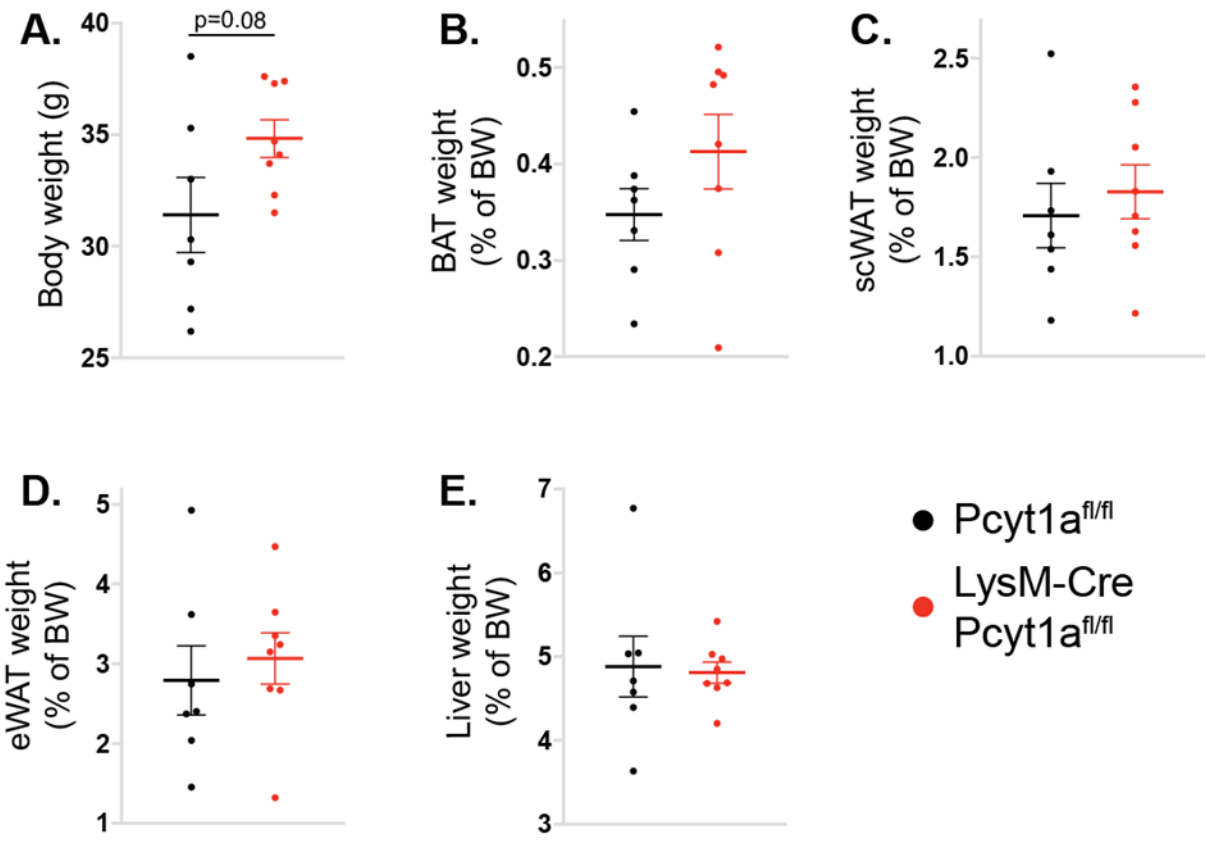

Figure 3-20. Tissue weights of chow-fed Pcyt1a$^{fl/fl}$ and LysM-Cre Pcyt1a$^{fl/fl}$ mice on mixed genetic background.

*Body weight (**A**) and weights of BAT (**B**), scWAT (**C**), eWAT (**D**) and liver (**E**), expressed as a percentage of body weight of Pcyt1a$^{fl/fl}$ (n=7, black dots) and LysM-Cre Pcyt1a$^{fl/fl}$ (n=8, red dots) 20-week-old male mice on mixed C57Bl/6J, 129/Sv background culled in a random fed state. Statistical significance was assessed by student's t-test.*

3.2.2.6 Macrophage-specific *Pcyt1a* deletion did not affect total energy balance of HFD-fed mice on mixed genetic background

Results. Animals of both genotypes had similar body weight after 8 weeks of high-fat feeding (Figure 3-21 A). There were no differences between HFD-fed LysM-Cre Pcyt1a$^{fl/fl}$ animals and controls in food intake and energy expenditure during 48 h of metabolic cage analysis (Figure 3-21 B,C).

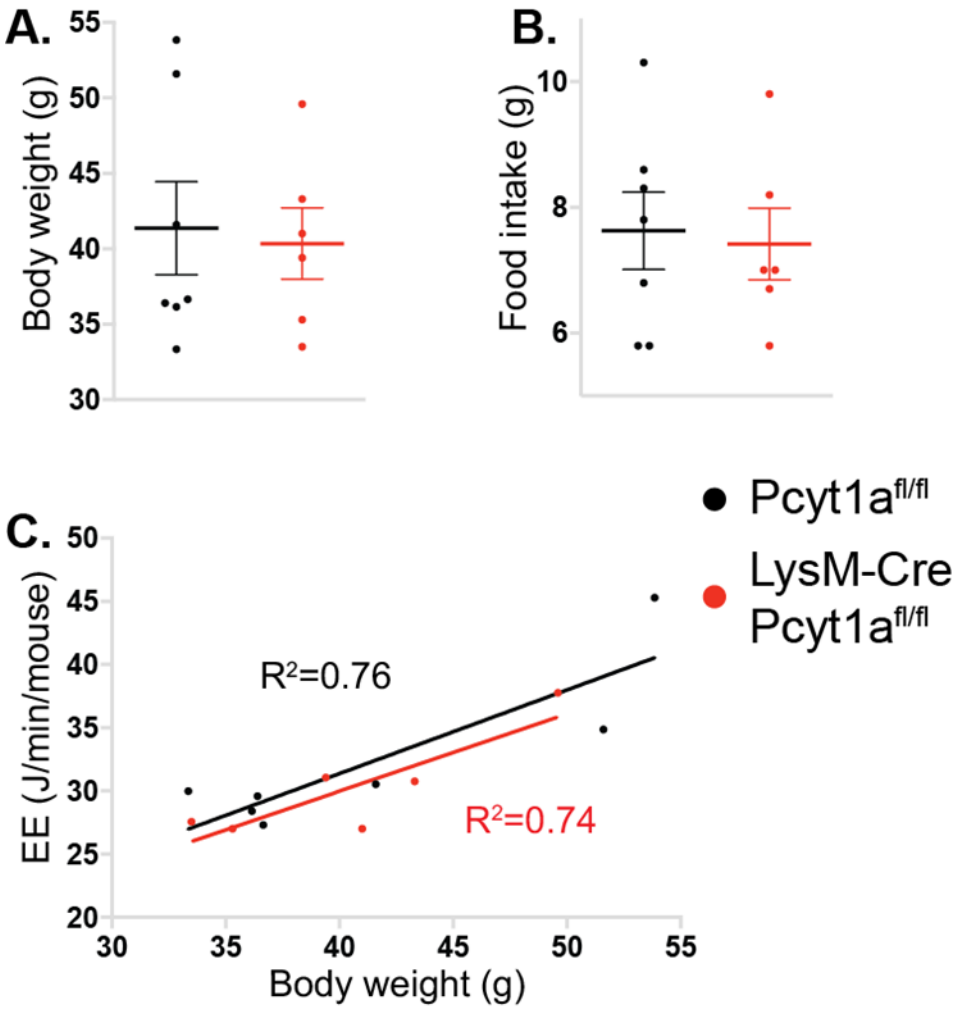

Figure 3-21. Food intake and energy expenditure of HFD-fed Pcyt1a$^{fl/fl}$ and LysM-Cre Pcyt1a$^{fl/fl}$ mice on mixed genetic background.

*Body weight (**A**), food intake (**B**) and average energy expenditure plotted against body weight assessed over 48 h in Pcyt1a$^{fl/fl}$ (black dots, n=7) and Pcyt1a$^{fl/fl}$ LysM-Cre (red dots, n=6) 16-week-old male mice on mixed C57Bl/6J, 129/Sv background, fed a 45% kcal fat diet (D12451) from 8 weeks of age. Statistical significance was assessed by student's t-test (**A** and **B**) or one-way ANCOVA (**C**).*

3.2.2.7 Macrophage-specific *Pcyt1a* deletion did not affect serum metabolite concentrations of HFD-fed mice on mixed genetic background

Results. Serum concentrations of insulin, FFAs, TGs, lipoprotein-bound cholesterol and choline in LysM-Cre Pcyt1a$^{fl/fl}$ animals in the fed state were equivalent to controls (Table 3-2). Overnight fasting elevated FFAs and reduced insulin to the same level in both genotypes (Table 3-2). Serum TGs and blood glucose levels were not affected by fasting or genotype after HFD (Table 3-2).

Feeding state	Random fed		Fasted overnight	
Genotype	**Pcyt1a$^{fl/fl}$**	**LysM-Cre Pcyt1a$^{fl/fl}$**	**Pcyt1a$^{fl/fl}$**	**LysM-Cre Pcyt1a$^{fl/fl}$**
Glucose (mM)	9.96 ± 0.64	9.87 ± 0.71	9.81 ± 0.50	9.40 ± 0.63
Insulin (µg/L)	4.56 ± 1.70	12.99 ± 9.16	0.53 ± 0.13	0.57 ± 0.20
FFA (mM)	0.83 ± 0.18	0.71 ± 0.07	1.05 ± 0.1	1.05 ± 0.05
TG (mM)	1.40 ± 0.24	1.48 ± 0.28	1.50 ± 0.11	1.50 ± 0.14
Total cholesterol (mM)	6.39 ± 0.28	6.63 ± 0.38	-	-
HDL cholesterol (mM)	3.05 ± 0.17	3.19 ± 0.12	-	-
LDL cholesterol (mM)	2.7 ± 0.19	2.77 ± 0.32	-	-
Total choline (µM)	59.94 ± 7.92	57.07 ± 2.73	-	-

Table 3-2. Serum biochemistry of HFD-fed Pcyt1a$^{fl/fl}$ and LysM-Cre Pcyt1a$^{fl/fl}$ mice on mixed genetic background in a random-fed state or after overnight fast.
Concentrations of serum biochemicals are expressed as means ± SEM. N=7 Pcyt1a$^{fl/fl}$, n=6 LysM-Cre Pcyt1a$^{fl/fl}$ 16-20-week-old male mice on mixed C57Bl/6J, 129/Sv background, fed a 45% kcal fat diet (D12451) from 8 weeks of age.

3.2.2.8 Macrophage-specific *Pcyt1a* deletion did not impact the glucose, insulin and lipid tolerance of HFD-fed mice on mixed genetic background

Results. LysM-Cre Pcyt1a$^{fl/fl}$ mice showed a similar serum glucose clearance rate as controls on HFD (Figure 3-22 A,B). No genotype-mediated effect on insulin-mediated circulating glucose uptake was observed in HFD-fed mice (Figure 3-22 C,D). Finally, HFD-fed LysM-Cre Pcyt1a$^{fl/fl}$ mice had comparable serum TG concentration curves to controls following olive oil ingestion (Figure 3-22 E,F).

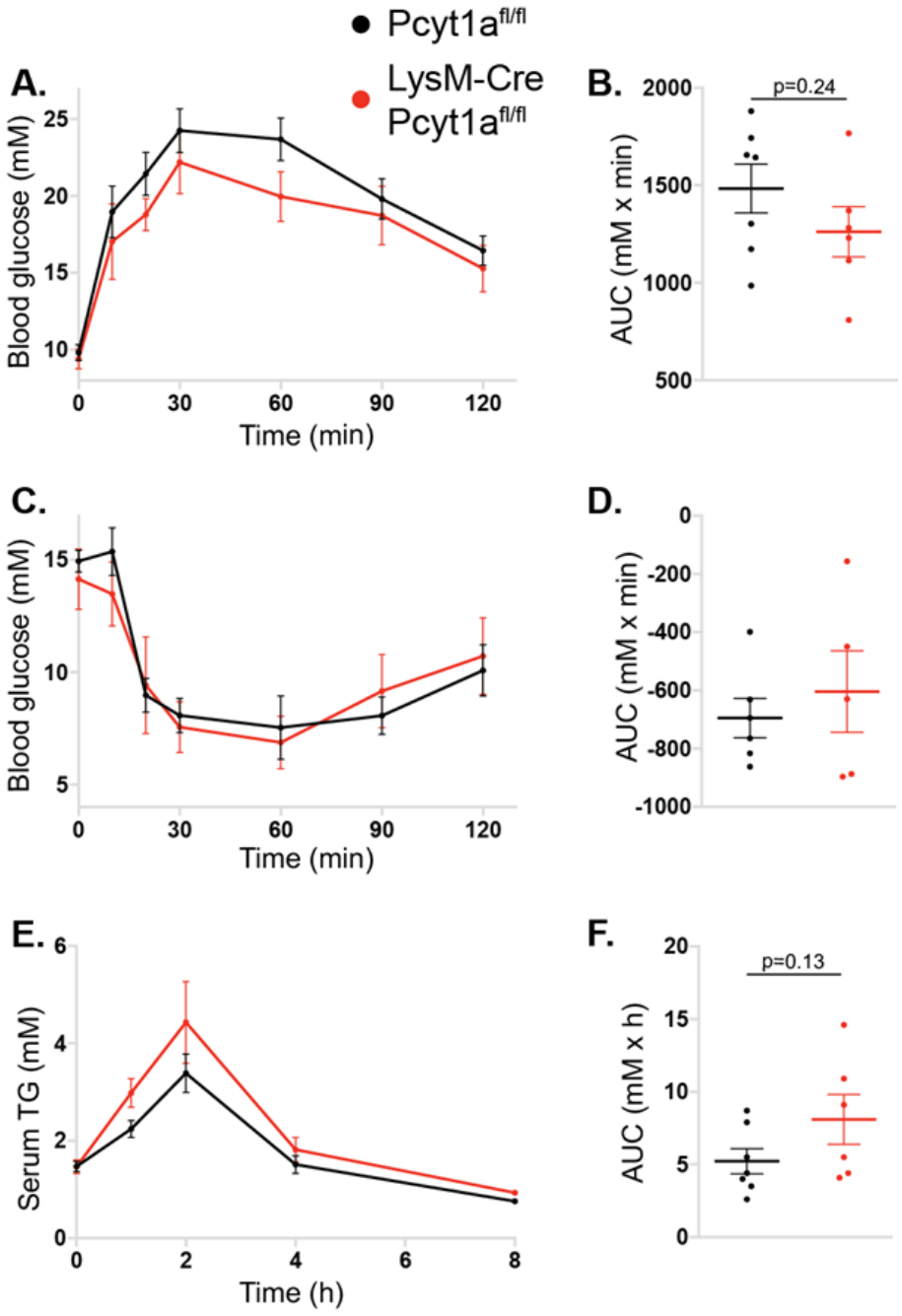

Figure 3-22. Glucose, insulin and lipid tolerance tests of HFD-fed Pcyt1a$^{fl/fl}$ and LysM-Cre Pcyt1a$^{fl/fl}$ mice on mixed genetic background.

*Blood glucose concentration curves (**A**) and AUC (**B**) of mice injected with 1 mg/kg glucose at T=0 min after an overnight fast. Blood glucose concentration curves (**C**) and AUC (**D**) of mice injected with 1 IU/kg insulin at T=0 after 6 h fast. Serum TG concentration curves (**E**) and AUC (**F**) of mice administered with 200 μl of olive oil by oral gavage at T=0 after overnight fast. N=7 Pcyt1a$^{fl/fl}$ (black lines/dots) and n=6 LysM-Cre Pcyt1a$^{fl/fl}$ (red lines/dots)16-19-week-old male mice on mixed C57Bl/6J, 129/Sv background, fed a 45% kcal fat diet (D12451) from 8 weeks of age. Statistical significance was assessed by student's t-test (**B, D, F**).*

3.2.2.9 Macrophage-specific *Pcyt1a* deletion had no effect on the metabolic tissue weights of HFD-fed mice on mixed genetic background

Results. Genotype had no effect on body weight at the end of the study (Figure 3-23 A). The weights of adipose tissue depots were unchanged in HFD-fed LysM-Cre Pcyt1a$^{fl/fl}$ animals, when normalised to the total body weight and compared to controls (Figure 3-23 B-D). Liver to body weight ratio showed a high degree of variability after high-fat feeding, and was not different between genotypes (Figure 3-23 E).

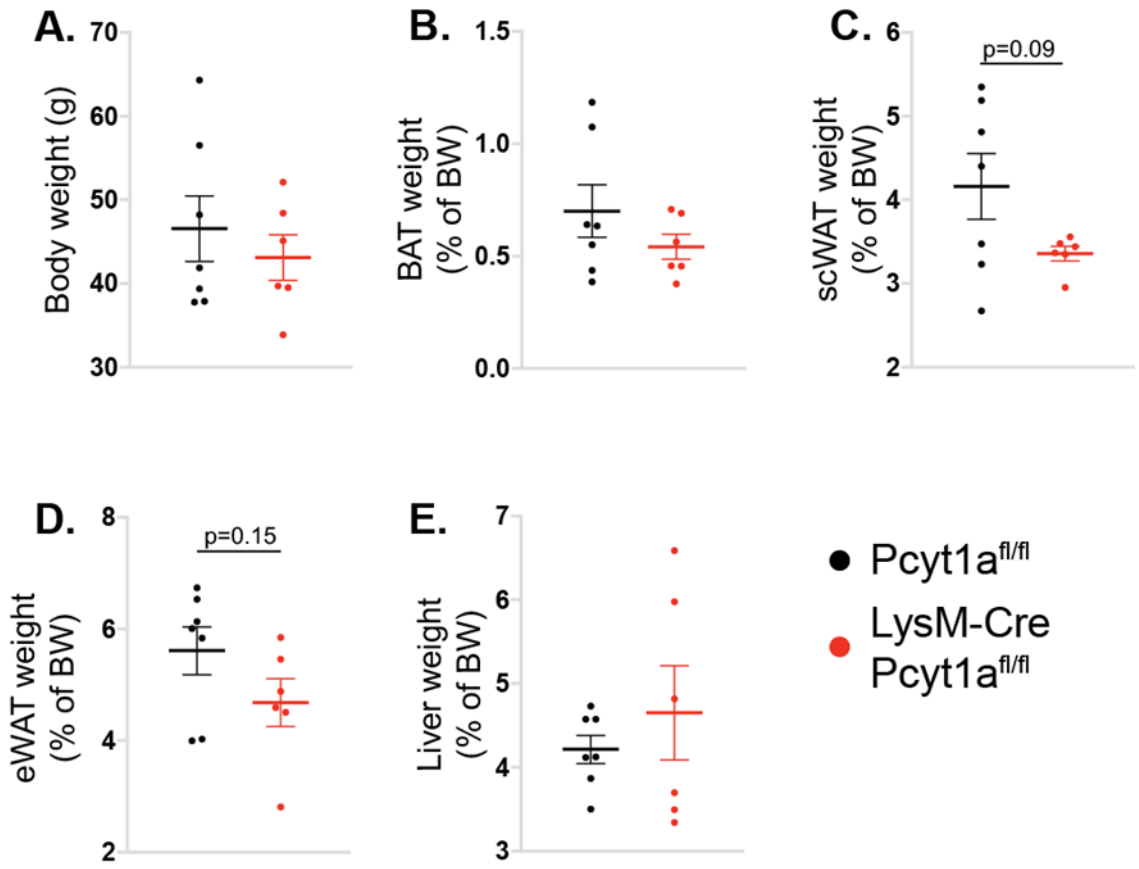

Figure 3-23. Tissue weights of HFD-fed Pcyt1a$^{fl/fl}$ and LysM-Cre Pcyt1a$^{fl/fl}$ mice on mixed genetic background.

*Body weight (**A**) and weights of BAT (**B**), scWAT (**C**), eWAT (**D**) and liver (**E**), expressed as a percentage of body weight of Pcyt1a$^{fl/fl}$ (n=7, black dots) and LysM-Cre Pcyt1a$^{fl/fl}$ (n=6, red dots) 20-week-old male mice on mixed C57Bl/6J, 129/Sv background, fed a 45% kcal fat diet (D12451) from 8 weeks of age and culled in a random fed state.*

3.2.2.10 Macrophage-specific *Pcyt1a* deletion had no major effect on eWAT gene expression in chow-fed mice on mixed genetic background

Method. At the end of study, eWATs from all mice were digested and ATMs were isolated using CD11b-positive purification. Gene expression in adipocytes, ATMs and the pool of remaining eWAT cells (CD11b-negative fraction) was compared between LysM-Cre Pcyt1a$^{fl/fl}$ animals and controls.

Results. As expected, presence of Cre recombinase in LysM allele reduced *Pcyt1a* expression by approximately 50% in ATMs, but not other eWAT cell types (Figure 3-24 A). Genotype had no effect on the expression of genes encoding *de novo* PC biosynthesis enzymes CCTβ and PEMT, lipid metabolic enzyme LAL and lipid droplet-associated protein ADRP in any eWAT cell fraction (Figure 3-24 A). As I have already observed in BMDMs, *Pcyt1a* gene deficiency increased ER stress-related transcription of *Chop* and decreased surface marker *Cd206* gene expression in ATMs (Figure 3-24 A,B). Besides increased *Arg1* gene expression in the adipocyte and CD11b-negative fractions, genotype had no effect on the expression of measured immune system-related genes (Figure 3-24 B).

3.2.2.11 Macrophage-specific *Pcyt1a* deletion had no major effect on eWAT gene expression in HFD-fed mice on mixed genetic background

Results. eWATs isolated from HFD-fed groups were analysed in the same manner as described in 3.2.2.10. *Pcyt1a* transcription was also reduced by approximately 50% in ATMs from LysM-Cre Pcyt1a$^{fl/fl}$ mice compared to controls (Figure 3-25 A). eWAT adipocytes from LysM-Cre Pcyt1a$^{fl/fl}$ animals exhibited elevated expression of genes *Cd36* and *Abca1*, encoding enzymes involved in fatty acid transport and reverse cholesterol export (Figure 3-25 A). However, no other measured metabolic and immune system-related genes showed a genotype-mediated regulation in eWAT fractions on HFD (Figure 3-25 A,B).

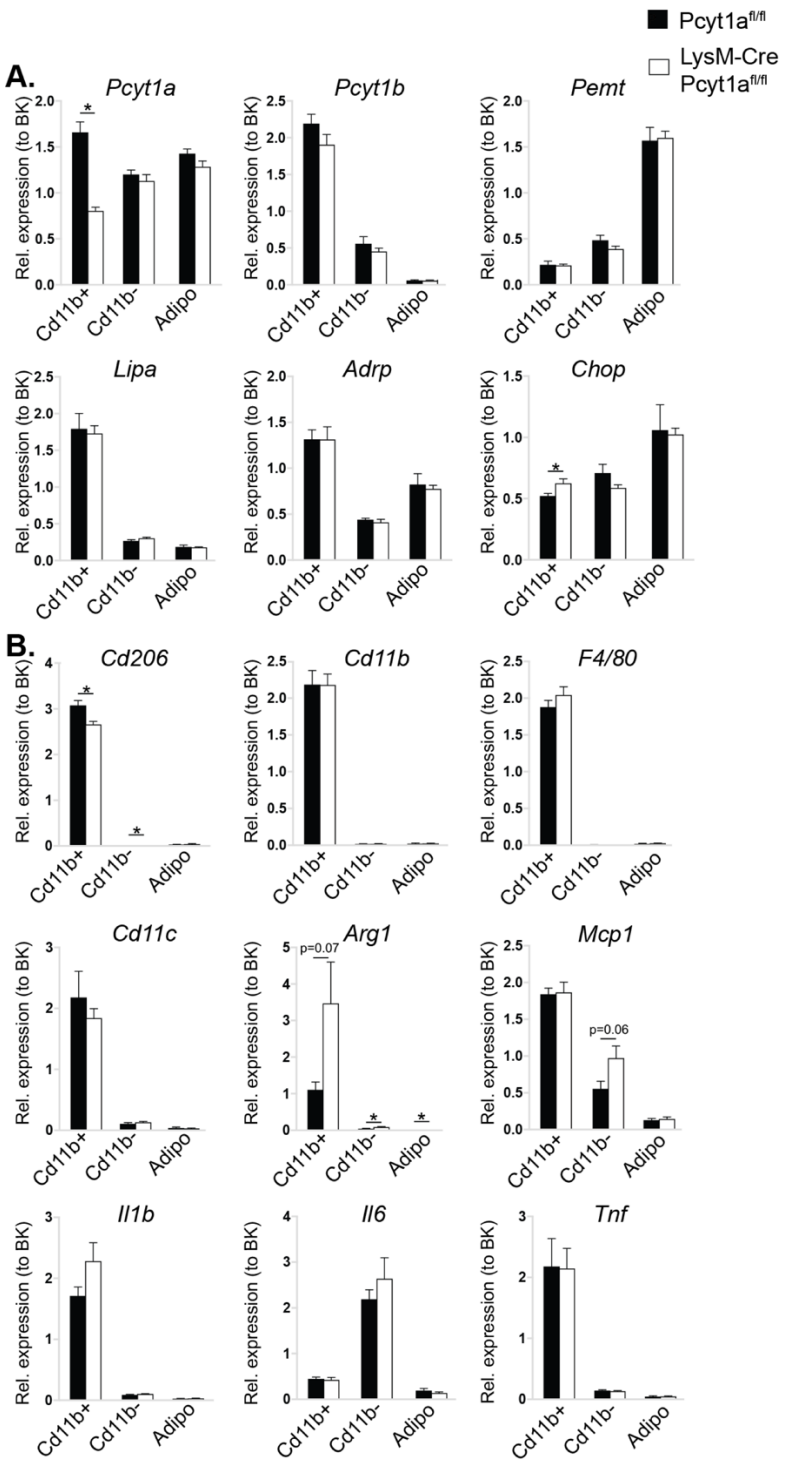

Figure 3-24. Gene expression analysis of eWAT cell fractions isolated from chow-fed Pcyt1a$^{fl/fl}$ and LysM-Cre Pcyt1a$^{fl/fl}$ mice on mixed genetic background. *mRNA levels (normalised to BestKeeper) of metabolic genes Pcyt1a, Pcyt1b, Pemt, Lipa, Adrp, Chop (**A**) and immune system genes Cd206, Cd11b, F4/80, Cd11c, Arg1, Mcp1, Il1b, Il6, Tnf (**B**) from adipocyte, Cd11b-positive and Cd11b-negative fractions of eWAT isolated from Pcyt1a$^{fl/fl}$ (n=7, black bars) and LysM-Cre Pcyt1a$^{fl/fl}$ (n=8, white bars) 20-week-old male mice on mixed C57Bl/6J, 129/Sv background culled in a random fed state. * p < 0.05 compared to Pcyt1a$^{fl/fl}$ using student's t-test.*

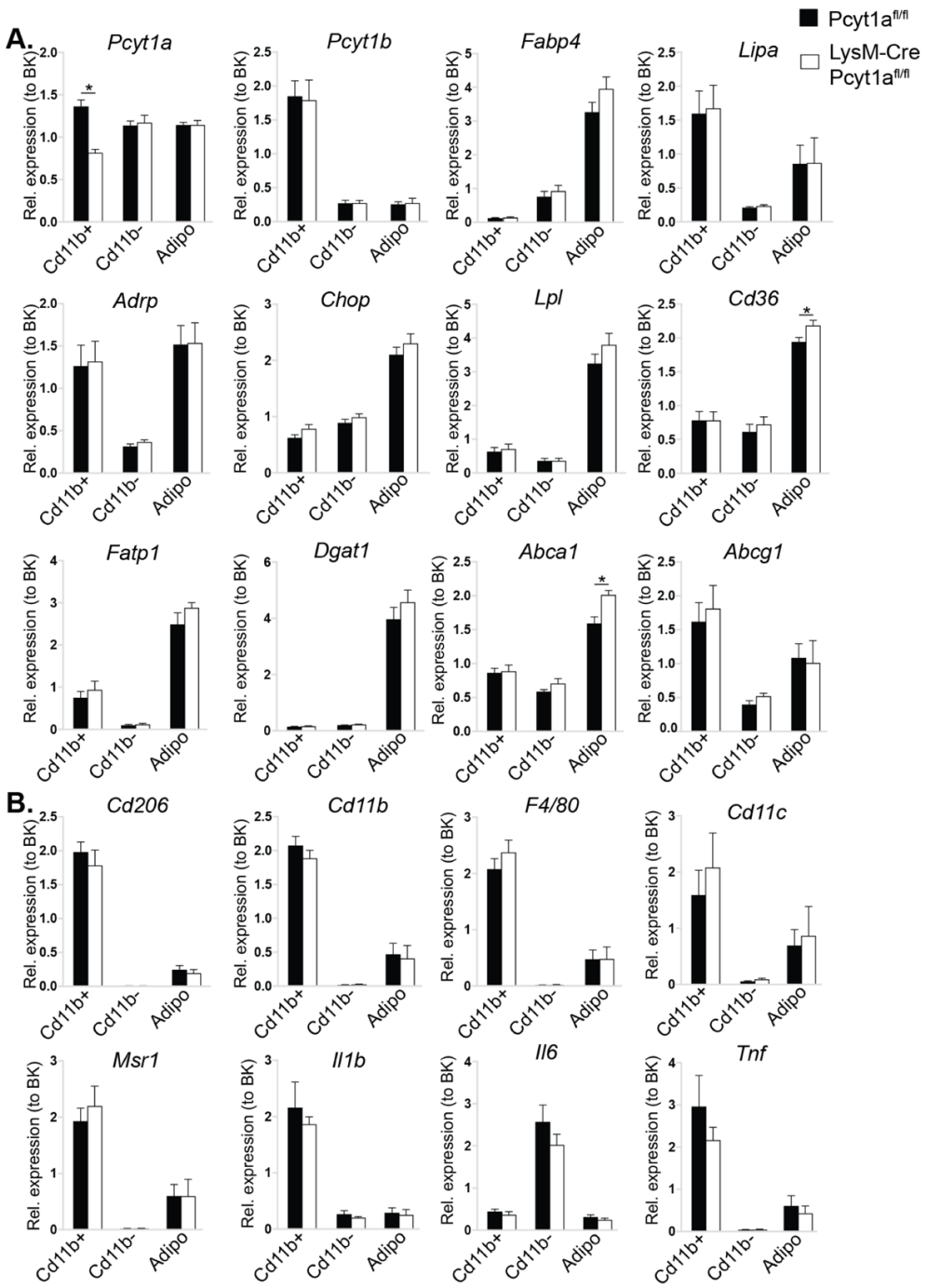

Figure 3-25. Gene expression analysis of eWAT cell fractions isolated from HFD-fed Pcyt1a$^{fl/fl}$ and LysM-Cre Pcyt1a$^{fl/fl}$ mice on mixed genetic background.

*mRNA levels (normalised to BestKeeper) of metabolic genes Pcyt1a, Pcyt1b, Fabp4, Lipa, Adrp, Chop, Lpl, Cd36, Fatp1, Dgat1, Abca1, Abcg1 (**A**) and immune system genes Cd206, Cd11b, F4/80, Cd11c, Msr1, Il1b, Il6, Tnf (**B**) from adipocyte, Cd11b-positive and Cd11b-negative fractions of eWAT isolated from Pcyt1a$^{fl/fl}$ (n=7, black bars) and LysM-Cre Pcyt1a$^{fl/fl}$ (n=6, white bars) 20-week-old male mice on mixed C57Bl/6J, 129/Sv background, fed a 45% kcal fat diet (D12451) from 8 weeks of age and culled in a random fed state. * $p < 0.05$ compared to Pcyt1a$^{fl/fl}$ using student's t-test.*

3.2.2.12 Macrophage-specific *Pcyt1a* deficiency resulted in a reduced hepatic gluconeogenic gene transcription in HFD-fed mice on mixed genetic background

Rationale. To investigate genotype effects on HFD-induced hepatic insulin resistance and inflammation, livers isolated from HFD-fed mice were assessed for macrophage marker and insulin-regulated metabolic gene expression.

Results. No differences were found between LysM-Cre Pcyt1a$^{fl/fl}$ and control animals in hepatic mRNA levels of macrophage markers and insulin-regulated metabolic genes (Figure 3-26 A). However, while genotype had no effect on gluconeogenic gene expression in chow-fed mice, LysM-Cre Pcyt1a$^{fl/fl}$ mice exhibited reductions in liver genes encoding gluconeogenic enzymes phosphoenolpyruvate carboxykinase (*Pck1*) and fructose-1,6- biphosphatase (*Fbp1*) after HFD compared to control mice (Figure 3-26 A).

3.2.2.13 Macrophage-specific *Pcyt1a* deficiency resulted in reduced hepatic lipid metabolism gene transcription in HFD-fed mice on mixed genetic background

Rationale. Reduced transcriptional signature of gluconeogenesis in LysM-Cre Pcyt1a$^{fl/fl}$ animals on HFD lead me to perform further hepatic gene expression analysis, focusing on lipid metabolism-related genes.

Results. Out of all measured FFA metabolism genes, *Dgat1* gene was reduced in LysM-Cre Pcyt1a$^{fl/fl}$ animals compared to controls on HFD (Figure 3-27 A). Similarly, the expression of phospholipid metabolism-related genes *Pcyt1a, Ptdss1* and *Mat1a* was lower in the livers of LysM-Cre Pcyt1a$^{fl/fl}$ mice on HFD (Figure 3-27 C). Finally, I observed genotype-dependent alterations in the levels of genes related to lipoprotein metabolism both on chow and HFD. Transcripts for LPL and APOA1, the main protein component of HDL particle, were reduced, while gene encoding phospholipid transfer protein (PLTP), which catalyses the transfer of PC from circulating vLDL to HDL, was increased in LysM-Cre Pcyt1a$^{fl/fl}$ animals on a chow diet (Figure 3-27 B). The levels of messages for angiopoietin-like 4 and lecithin-cholesterol acyltransferase (LCAT), enzyme mediating the formation of cholesterol esters from PC and free cholesterol, were lower in LysM-Cre Pcyt1a$^{fl/fl}$ mice than in controls on HFD (Figure 3-27 B).

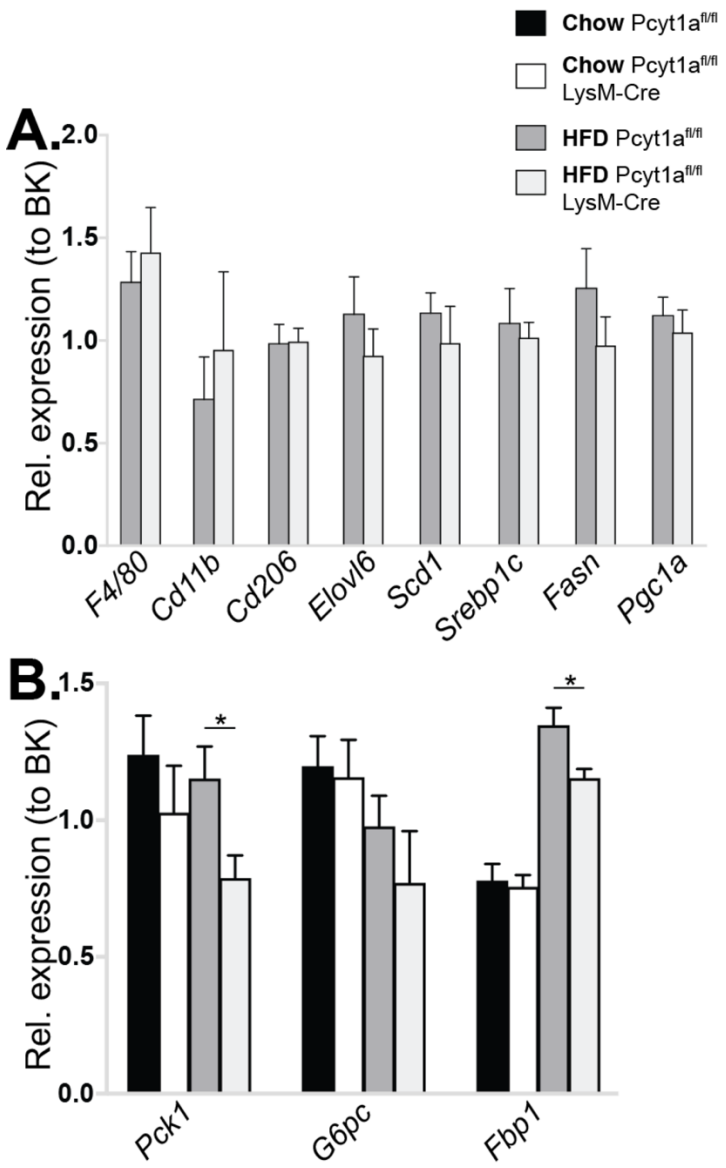

Figure 3-26. Insulin-regulated and immune system gene expression analysis of livers isolated from chow and HFD-fed Pcyt1a$^{fl/fl}$ and LysM-Cre Pcyt1a$^{fl/fl}$ mice on mixed genetic background.

A. *mRNA levels (normalised to BestKeeper) of immune system genes F4/80, Cd11b, Cd206 and insulin-regulated metabolic genes Elovl6, Scd1, Srebp1c, Fasn, Pgc1a in the livers isolated from Pcyt1a$^{fl/fl}$ (n=7, dark grey bars) and LysM-Cre Pcyt1a$^{fl/fl}$ (n=6, light grey bars) 20-week-old male mice on mixed C57Bl/6J, 129/Sv background, fed a 45% kcal fat diet (D12451) from 8 weeks of age and culled in a random fed state.* ***B.*** *mRNA levels of insulin-regulated gluconeogenic genes Pck1, G6pc and Fbp1 in the livers isolated from Pcyt1a$^{fl/fl}$ (n=7, black bars) and LysM-Cre Pcyt1a$^{fl/fl}$ (n=8, white bars) chow-fed 20-week-old male mice on mixed C57Bl/6J, 129/Sv background, and of the same genotypes fed 45% kcal fat diet (D12451) from 8 weeks of age (as in* ***A****), culled in a random fed state. * $p < 0.05$ compared to Pcyt1a$^{fl/fl}$ using student's t-test.*

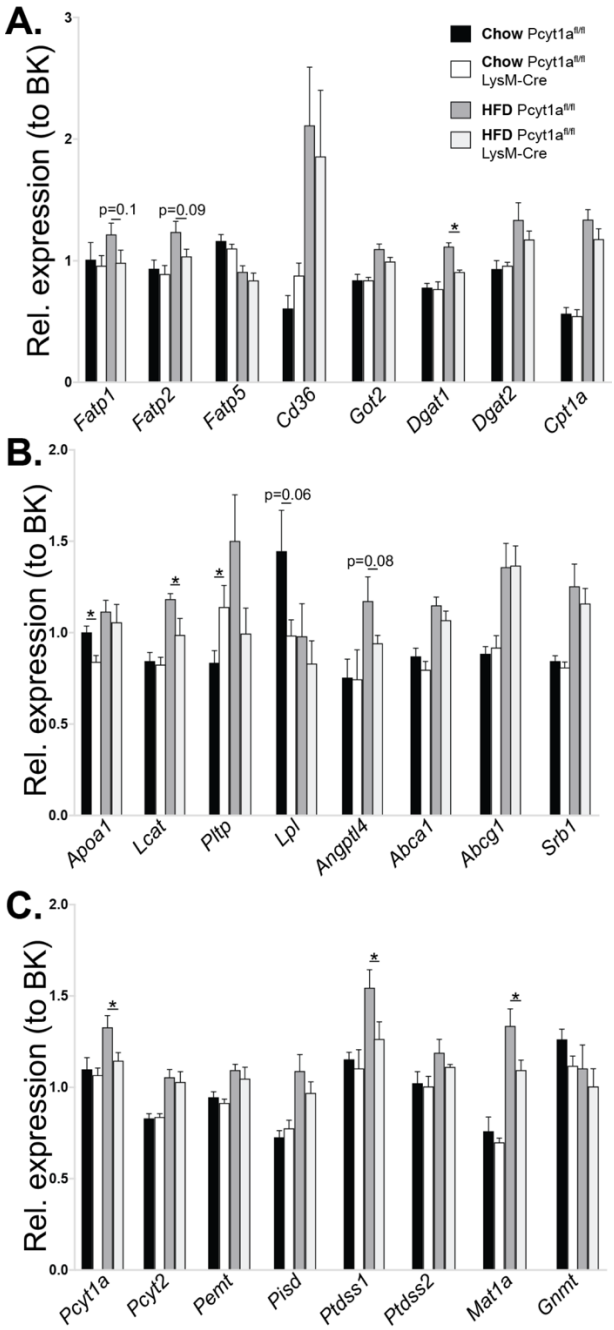

Figure 3-27. Metabolic gene expression analysis of livers isolated from chow and HFD-fed Pcyt1a$^{fl/fl}$ and LysM-Cre Pcyt1a$^{fl/fl}$ mice on mixed genetic background.

*mRNA levels (normalised to BestKeeper) of fatty acid metabolism genes Fatp1, Fatp2, Fatp5, Cd36, Got2, Dgat1, Dgat2, Cpt1a (**A**), lipoprotein metabolism genes Apoa1, Lcat, Pltp, Lpl, Angptl4, Abca1, Abcg1, Srb1 (**B**) and phospholipid metabolism genes Pcyt1a, Pcyt2, Pemt, Pisd, Ptdss1, Ptdss2, Mat1a, Gnmt (**C**) in the livers isolated from chow-fed Pcyt1a$^{fl/fl}$ (n=7, black bars), LysM-Cre Pcyt1a$^{fl/fl}$ (n=8, white bars) and HFD-fed Pcyt1a$^{fl/fl}$ (n=7, dark grey bars), LysM-Cre Pcyt1a$^{fl/fl}$ (n=6, light grey bars) 20-week-old male mice on mixed C57Bl/6J, 129/Sv background, culled in a random fed state. HFD-fed group received 45% kcal fat diet (D12451) from 8 weeks of age. * p < 0.05 compared to Pcyt1a$^{fl/fl}$ using student's t-test.*

3.2.2.14 Macrophage-specific *Pcyt1a* deficiency had no effect on liver lipid and glycogen content in chow- or HFD-fed mice on mixed genetic background

Results. In contrast to observed changes in hepatic gene transcription, I found no differences in hepatic lipid or glycogen content between LysM-Cre Pcyt1a$^{fl/fl}$ and control animals on either chow or HFD (Figure 3-28 A,B).

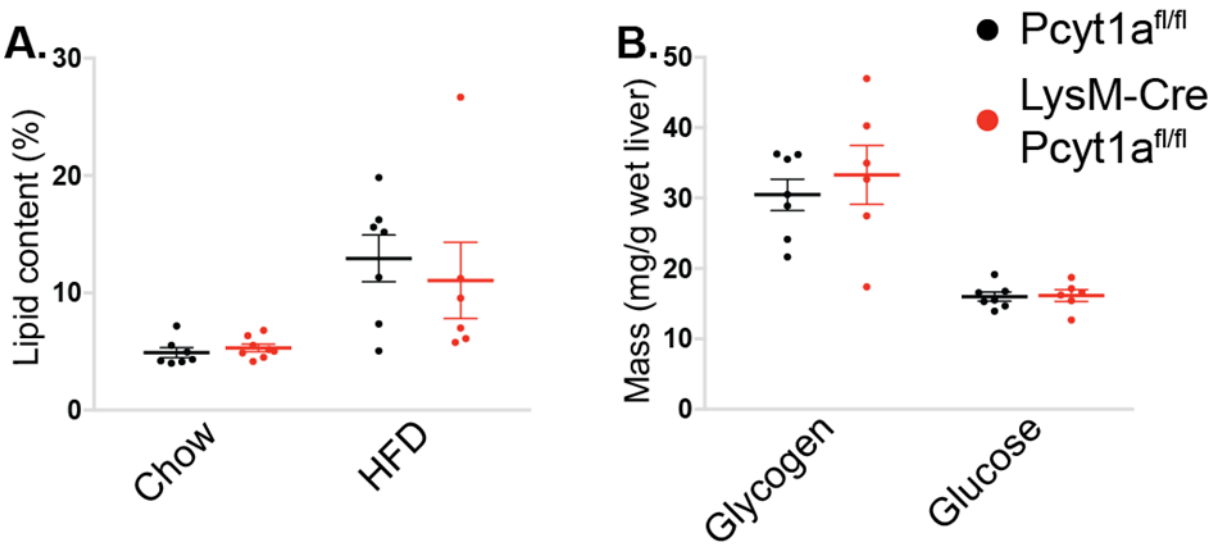

Figure 3-28. Hepatic lipid, glycogen and glucose levels in chow and HFD-fed Pcyt1a$^{fl/fl}$ and LysM-Cre Pcyt1a$^{fl/fl}$ mice on mixed genetic background.

A. *Total lipid weight (as percentage of tissue weight) of the livers isolated from chow-fed Pcyt1a$^{fl/fl}$ (n=7, black dots), LysM-Cre Pcyt1a$^{fl/fl}$ (n=8, red dots) and HFD-fed Pcyt1a$^{fl/fl}$ (n=7, black dots), LysM-Cre Pcyt1a$^{fl/fl}$ (n=6, red dots) 20-week-old male mice on mixed C57Bl/6J, 129/Sv background, culled in a random fed state.* ***B.*** *Glycogen and free glucose content of the livers isolated from HFD-fed Pcyt1a$^{fl/fl}$ (n=7, black dots) and LysM-Cre Pcyt1a$^{fl/fl}$ (n=6, red dots) 20-week-old male mice. HFD-fed group received 45% kcal fat diet (D12451) from 8 weeks of age.*

3.2.3 The importance of *Pcyt1a* in macrophages for glucose and lipid metabolism of lean and obese mice on a pure C57Bl/6J genetic background

3.2.3.1 The rationale for the changes of experimental settings for *in vivo* metabolic phenotyping of LysM-Cre Pcyt1a$^{fl/fl}$ mice on a pure C57Bl/6J genetic background

As metabolic phenotypic of LysM-Cre Pcyt1a$^{fl/fl}$ animals on C57Bl/6J genetic background was performed approximately 2 years after the results from the study on mixed genetic background were obtained, I decided to change a few experimental parameters, based on the initial results and published literature.

Dietary treatments. The most significant alteration in the phenotyping protocol was a change from 45% to 60% kcal fat obesogenic diet. Performing an unbiased literature analysis on the diets used to induce obesity and insulin resistance in animal models with immune cell-specific genetic modifications revealed that the vast majority of publications used D12492 (Research Diets) 60% kcal fat diet in their experiments. I therefore decided to utilise the same diet type to allow higher reproducibility of my results, and to be able to compare my data with other published observations.

As I did not observe any major effects of *Pcyt1a* deletion on ATM phenotype or WAT function on mixed genetic background, I decided to *omit lipid tolerance test* from the phenotyping protocol. Furthermore, instead of analysing each eWAT fraction individually, I measured gene transcription in whole eWAT.

I also decided to exclude lipoprotein and choline measurements from the analysis of serum biochemicals, as they were not affected by genotype on mixed genetic background. Instead I chose to quantify circulating **liver enzymes**, alanine and aspartate aminotransferases (ALT and AST, respectively), as a proxy for HFD-induced liver damage.

The remaining parameters remained as described in 3.2.2.1.

3.2.3.2 Macrophage-specific *Pcyt1a* deletion did not affect total energy balance of chow-fed mice on C57Bl/6J genetic background

Results. Genotype had no effect on body weight at 16 weeks of age, when mice were analysed in metabolic cages (Figure 3-29 A). Chow consumption and average energy expenditure were similar between LysM-Cre Pcyt1a$^{fl/fl}$ and control animals during 48 h of metabolic cage analysis (Figure 3-29 B,C).

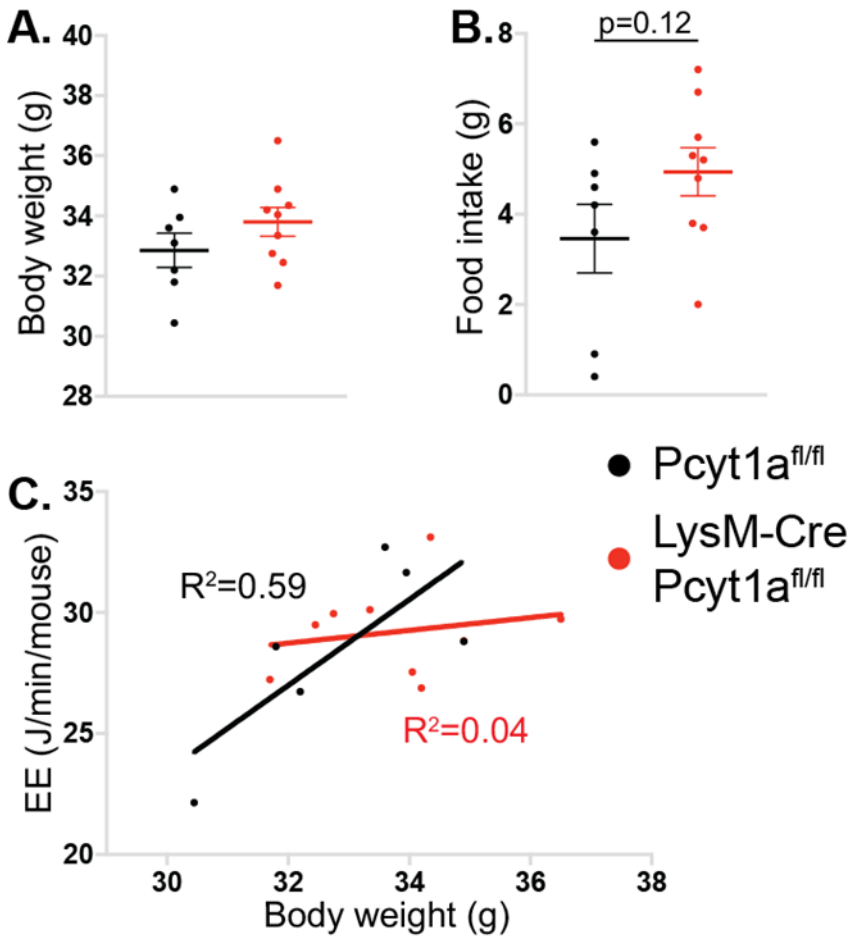

Figure 3-29. Food intake and energy expenditure of chow-fed Pcyt1a$^{fl/fl}$ and LysM-Cre Pcyt1a$^{fl/fl}$ mice on C57Bl/6J genetic background.

*Body weight (**A**), food intake (**B**) and average energy expenditure plotted against body weight assessed over 48 h in Pcyt1a$^{fl/fl}$ (black dots, n=7) and Pcyt1a$^{fl/fl}$ LysM-Cre (red dots, n=9) 16-week-old male mice on a pure C57Bl/6J background. Statistical significance was assessed by student's t-test (**A** and **B**) or one-way ANCOVA (**C**).*

3.2.3.3 Macrophage-specific *Pcyt1a* deletion did not affect serum metabolite concentrations of chow-fed mice on C57Bl/6J genetic background

Results. Serum concentrations of insulin, TGs and liver enzymes were not different between LysM-Cre Pcyt1a$^{fl/fl}$ mice and controls on chow diet (Table 3-3). Fasting potently supressed insulin levels in both genotypes (Table 3-3). Finally, genotype had no effect on the circulating levels of glucose and FFAs in either fed or fasted states (Table 3-3).

Feeding state	Random fed		Fasted overnight	
Genotype	**Pcyt1a$^{fl/fl}$**	**LysM-Cre Pcyt1a$^{fl/fl}$**	**Pcyt1a$^{fl/fl}$**	**LysM-Cre Pcyt1a$^{fl/fl}$**
Glucose (mM)	9.5 ± 0.44	10.47 ± 0.24	6.39 ± 0.35	5.8 ± 0.3
Insulin (µg/L)	1.34 ± 0.22	1.37 ± 0.24	0.11 ± 0.01	0.14 ± 0.02
FFA (mM)	1.34 ± 0.2	1.77 ± 0.12	1.06 ± 0.09	1.14 ± 0.09
TG (mM)	2.26 ± 0.28	2.47 ± 0.17	-	-
ALT (U/L)	72.29 ± 33.62	48.56 ± 12.16	-	-
AST (U/L)	483.71 ± 301.51	339.67 ± 151.04	-	-
ALT/AST ratio	0.24 ± 0.04	0.28 ± 0.05	-	-

Table 3-3. Serum biochemistry of chow-fed Pcyt1a$^{fl/fl}$ and LysM-Cre Pcyt1a$^{fl/fl}$ mice on C57Bl/6J genetic background in a random-fed state or after an overnight fast.

Concentrations of serum biochemicals are expressed as means ± SEM. N=7 Pcyt1a$^{fl/fl}$, n=9 LysM-Cre Pcyt1a$^{fl/fl}$ 16-19-week-old male mice on a pure C57Bl/6J background.

3.2.3.4 Macrophage-specific *Pcyt1a* deletion did not impact glucose and insulin tolerance of chow-fed mice on C57Bl/6J genetic background

Results. Following exogenous administration of glucose, chow-fed LysM-Cre Pcyt1a$^{fl/fl}$ mice were able to normalise serum glucose concentration at the same rate as controls (Figure 3-30 A,B). There were no differences in insulin-mediated serum glucose uptake between genotypes (Figure 3-30 C,D).

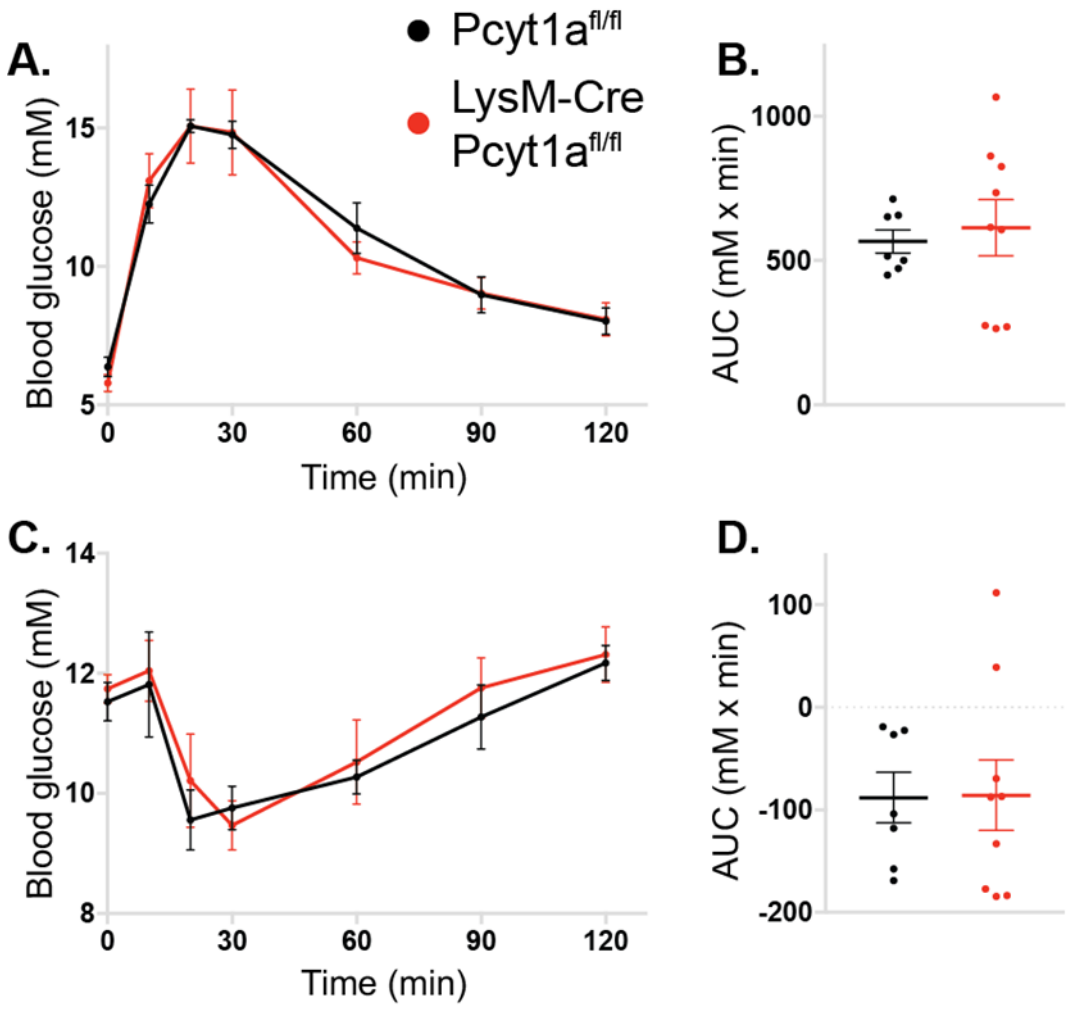

Figure 3-30. Glucose and insulin tolerance tests of chow-fed Pcyt1a$^{fl/fl}$ and LysM-Cre Pcyt1a$^{fl/fl}$ mice on C57Bl/6J genetic background.

*Blood glucose concentration curves (**A**) and AUC (**B**) of mice injected with 1 mg/kg glucose at T=0 min after an overnight fast. Blood glucose concentration curves (**C**) and AUC (**D**) of mice injected with 0.75 IU/kg insulin at T=0 after 6 h fast. N=7 Pcyt1a$^{fl/fl}$ (black lines/dots) and n=9 LysM-Cre Pcyt1a$^{fl/fl}$ (red lines/dots)16-18-week-old male mice on a pure C57Bl/6J background. Statistical significance was assessed by student's t-test (**B, D**).*

3.2.3.5 Macrophage-specific *Pcyt1a* deletion did not affect the weights of metabolic tissues of chow-fed mice on C57Bl/6J genetic background

Results. There were no genotype-dependent differences in total body weight, and BAT-, scWAT-, eWAT- and liver-to-body weight ratios between chow-fed LysM-Cre Pcyt1a$^{fl/fl}$ and control mice in the fed state at the end of the study (Figure 3-31 A-E). However, there was a statistically significant outlier for the relative liver weight in the control group (Figure 3-31 E, 3.64% vs group average ± SEM of 5.04 ± 0.24%). As all the other measured parameters in the outlier mouse were within a normal range, it was not excluded from the analysis.

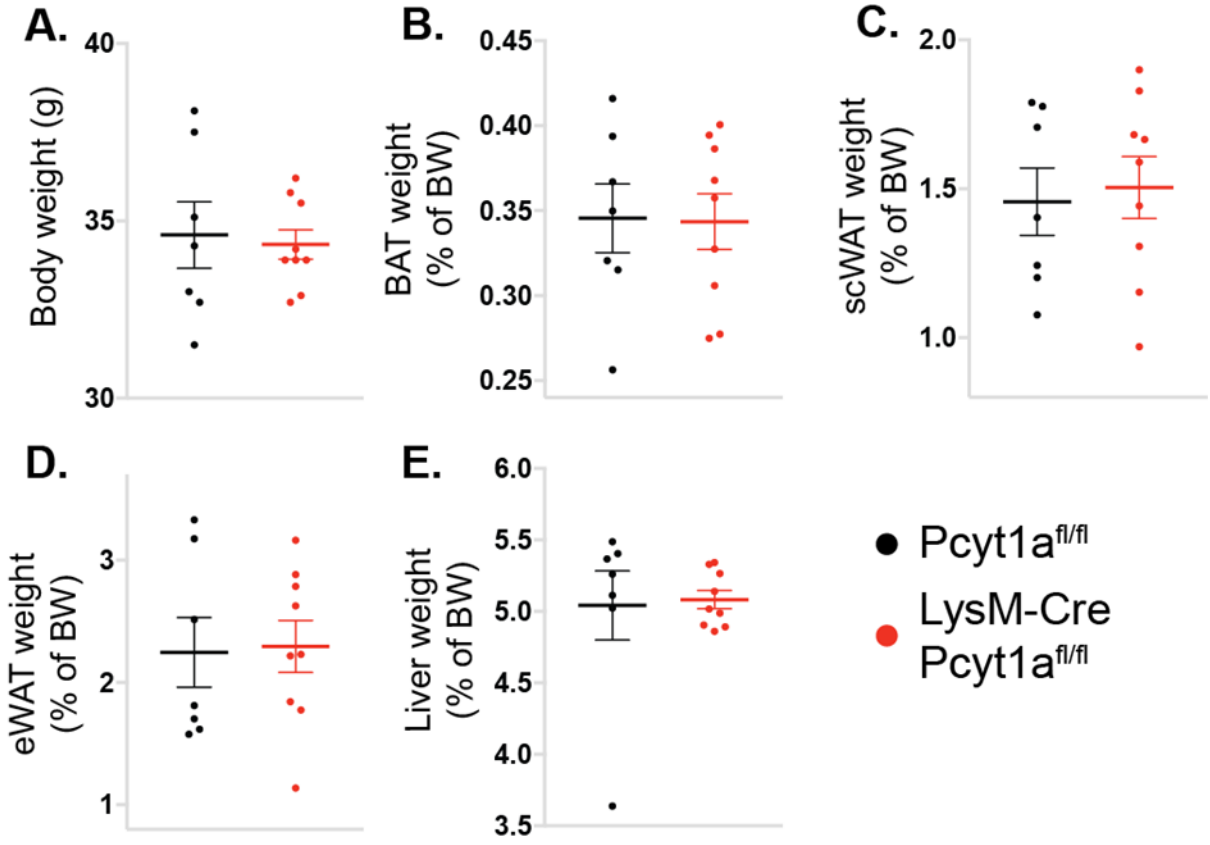

Figure 3-31. Tissue weights of chow-fed Pcyt1a$^{fl/fl}$ and LysM-Cre Pcyt1a$^{fl/fl}$ mice on C57Bl/6J genetic background.

*Body weight (**A**) and weights of BAT (**B**), scWAT (**C**), eWAT (**D**) and liver (**E**), expressed as a percentage of body weight of Pcyt1a$^{fl/fl}$ (n=7, black dots) and LysM-Cre Pcyt1a$^{fl/fl}$ (n=9, red dots) 20-week-old male mice on a pure C57Bl/6J background culled in a random fed state. Statistical significance was assessed by student's t-test.*

3.2.3.6 Macrophage-specific *Pcyt1a* deletion did not affect total energy balance of HFD-fed mice on C57Bl/6J genetic background

Results. HFD-fed LysM-Cre Pcyt1a$^{fl/fl}$ mice had similar body weights as controls at the start of metabolic cage analysis (Figure 3-29 A). No differences in food intake or average energy expenditure were observed between genotypes on HFD over 48 h of analysis (Figure 3-32 B,C).

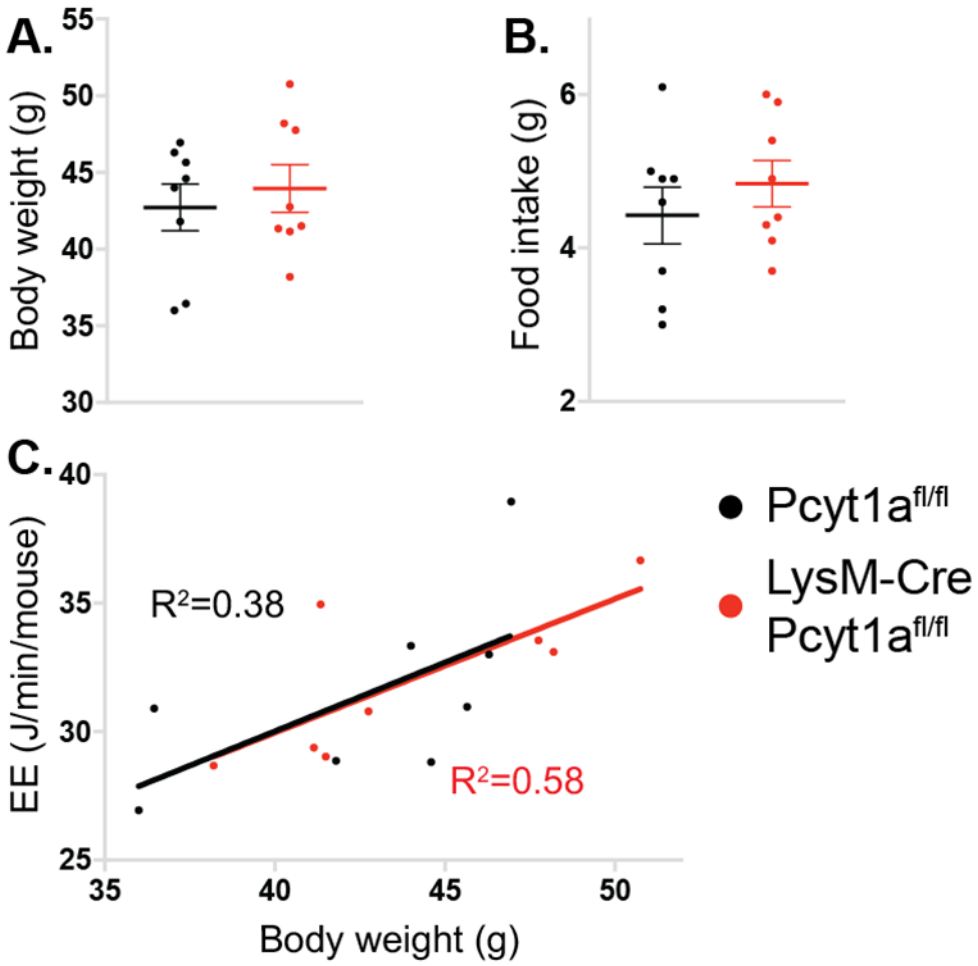

Figure 3-32. Food intake and energy expenditure of HFD-fed Pcyt1a$^{fl/fl}$ and LysM-Cre Pcyt1a$^{fl/fl}$ mice on C57Bl/6J genetic background.

*Body weight (**A**), food intake (**B**) and average energy expenditure plotted against body weight assessed over 48 h in Pcyt1a$^{fl/fl}$ (black dots, n=8) and Pcyt1a$^{fl/fl}$ LysM-Cre (red dots, n=8) 16-week-old male mice on a pure C57Bl/6J background, fed a 60% kcal fat diet (D12492) from 8 weeks of age. Statistical significance was assessed by student's t-test (**A** and **B**) or one-way ANCOVA (**C**).*

3.2.3.7 Macrophage-specific *Pcyt1a* deletion had no effect on serum metabolite concentrations of HFD-fed mice on C57Bl/6J genetic background

Results. Serum levels of glucose, insulin, FFAs, TGs and liver enzymes were not different in either fed or fasted states between genotypes on HFD (Table 3-4).

Feeding state	Random fed		Fasted overnight	
Genotype	**Pcyt1a$^{fl/fl}$**	**LysM-Cre Pcyt1a$^{fl/fl}$**	**Pcyt1a$^{fl/fl}$**	**LysM-Cre Pcyt1a$^{fl/fl}$**
Glucose (mM)	11.19 ± 0.24	11.6 ± 0.49	9.25 ± 0.25	8.76 ± 0.58
Insulin (µg/L)	3.75 ± 0.72	3.45 ± 0.83	0.74 ± 0.18	0.57 ± 0.13
FFA (mM)	1.07 ± 0.13	1.32 ± 0.04	1.62 ± 0.1	1.45 ± 0.07
TG (mM)	1.53 ± 0.15	1.47 ± 0.05	-	-
ALT (U/L)	122.88 ± 38.07	107.71 ± 23.78	-	-
AST (U/L)	289.38 ± 86.75	455.86 ± 177.7	-	-
ALT/AST ratio	0.45 ± 0.07	0.41 ± 0.1	-	-

Table 3-4. Serum biochemistry of HFD-fed Pcyt1a$^{fl/fl}$ and LysM-Cre Pcyt1a$^{fl/fl}$ mice on C57Bl/6J genetic background in a random-fed state or after overnight fast.
Concentrations of serum biochemicals are expressed as means ± SEM. N=8 Pcyt1a$^{fl/fl}$, n=8 LysM-Cre Pcyt1a$^{fl/fl}$ 16-19-week-old male mice on a pure C57Bl/6J background, fed a 60% kcal fat diet (D12492) from 8 weeks of age.

3.2.3.8 Macrophage-specific *Pcyt1a* deletion did not impact the glucose and insulin tolerance of HFD-fed mice on C57Bl/6J genetic background

Results. Both genotypes exhibited similar rates of blood glucose clearance following the administration of exogenous glucose (Figure 3-33 A,B). There were no differences in insulin-mediated serum glucose uptake between genotypes (Figure 3-33 C,D).

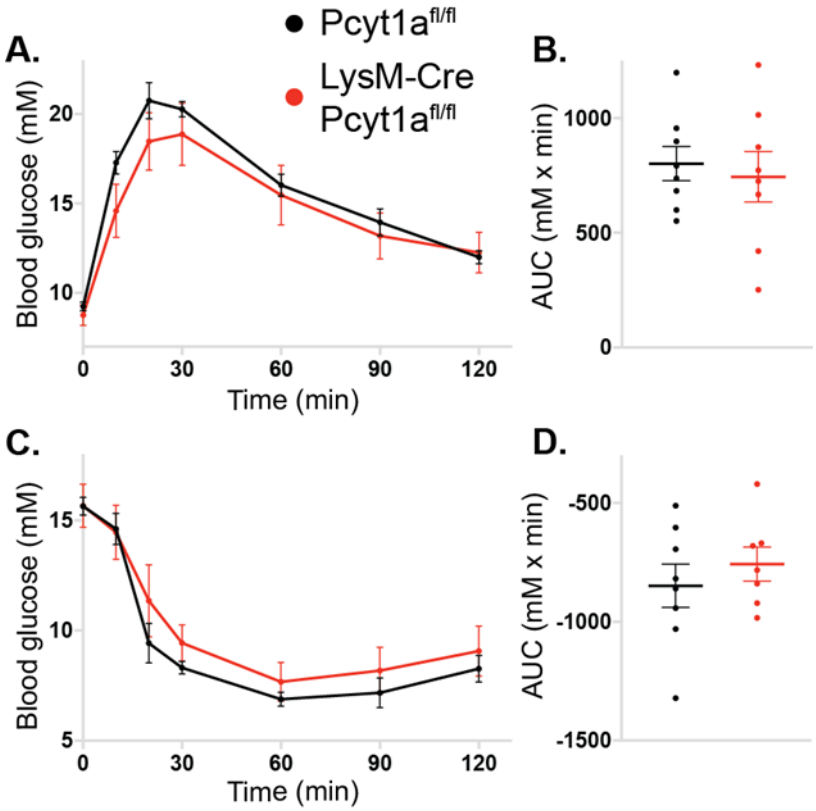

Figure 3-33. Glucose and insulin tolerance tests of HFD-fed Pcyt1a$^{fl/fl}$ and LysM-Cre Pcyt1a$^{fl/fl}$ mice on C57Bl/6J genetic background.

*Blood glucose concentration curves (**A**) and AUC (**B**) of mice injected with 1 mg/kg glucose at T=0 min after an overnight fast. Blood glucose concentration curves (**C**) and AUC (**D**) of mice injected with 1 IU/kg insulin at T=0 after 6 h fast. N=8 Pcyt1a$^{fl/fl}$ (black lines/dots) and n=7-8 LysM-Cre Pcyt1a$^{fl/fl}$ (red lines/dots)16-18-week-old male mice on a pure C57Bl/6J background, fed a 60% kcal fat diet (D12492) from 8 weeks of age. Statistical significance was assessed by student's t-test (**B, D**).*

3.2.3.9 Macrophage-specific *Pcyt1a* deletion did not affect the weights of metabolic tissues of HFD-fed mice on C57Bl/6J genetic background

Results. The expression of *Pcyt1a* in macrophages did not affect the total body weight or the weight of BAT, scWAT, eWAT and liver, relative to total body weight on HFD at the end of the study (Figure 3-34 A-E).

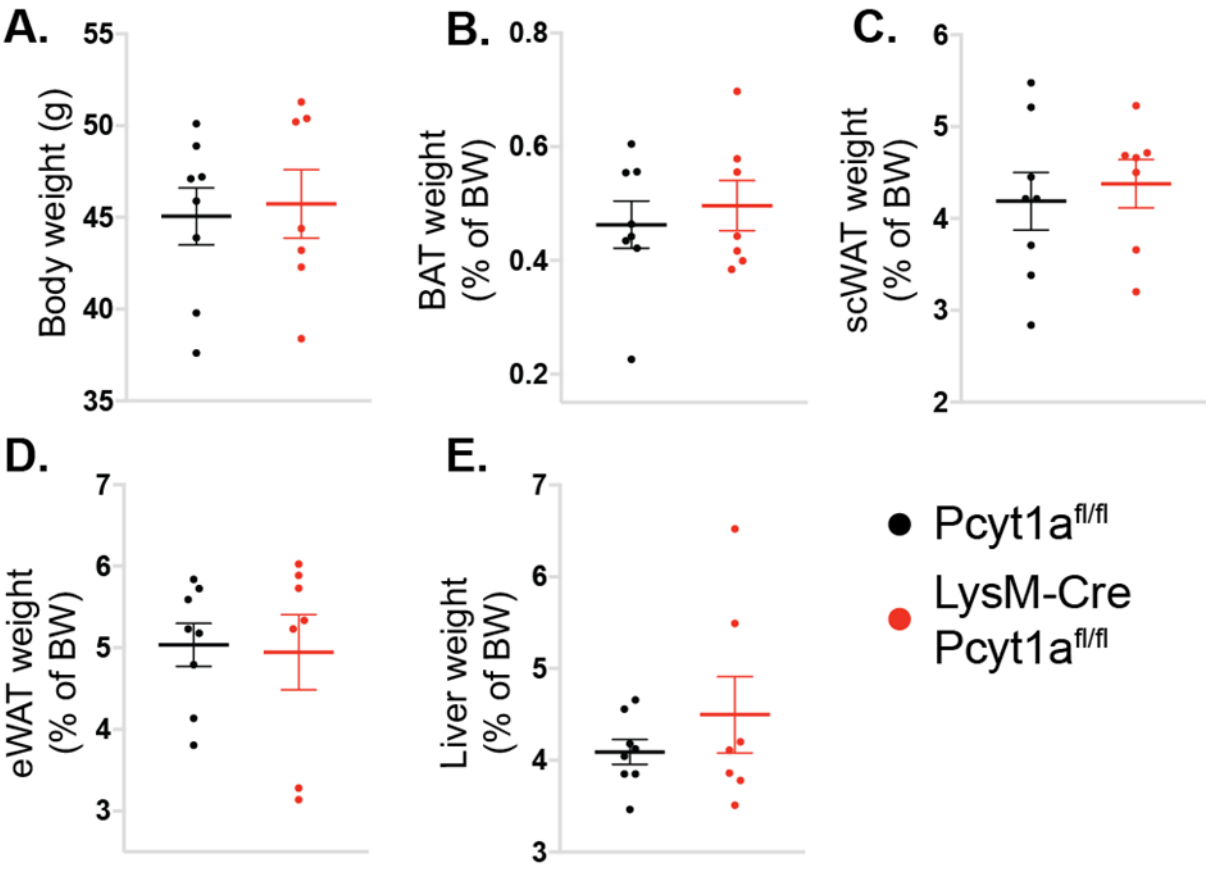

Figure 3-34. Tissue weights of HFD-fed Pcyt1a$^{fl/fl}$ and LysM-Cre Pcyt1a$^{fl/fl}$ mice on C57Bl/6J genetic background.

*Body weight (**A**) and weights of BAT (**B**), scWAT (**C**), eWAT (**D**) and liver (**E**), expressed as a percentage of body weight of Pcyt1a$^{fl/fl}$ (n=8, black dots) and LysM-Cre Pcyt1a$^{fl/fl}$ (n=7, red dots) 20-week-old male mice on a pure C57Bl/6J background, fed a 60% kcal fat diet (D12492) from 8 weeks of age and culled in a random fed state. Statistical significance was assessed by student's t-test.*

3.2.3.10 Macrophage-specific *Pcyt1a* deletion had no effect on eWAT gene expression in chow- and HFD-fed mice on C57Bl/6J genetic background

Results. No genotype-dependent differences were observed in either inflammatory or metabolic gene transcription in eWAT on chow or HFD (Figure 3-35 A,B).

3.2.3.11 Macrophage-specific *Pcyt1a* deficiency modestly reduced *G6pc* and *Dgat1* gene transcription in HFD-fed mice on C57Bl/6J genetic background

Results. The expression of hepatic inflammatory markers *F4/80*, *Cd11b* and *Tnf* was comparable between LysM-Cre Pcyt1a$^{fl/fl}$ and controls on HFD (

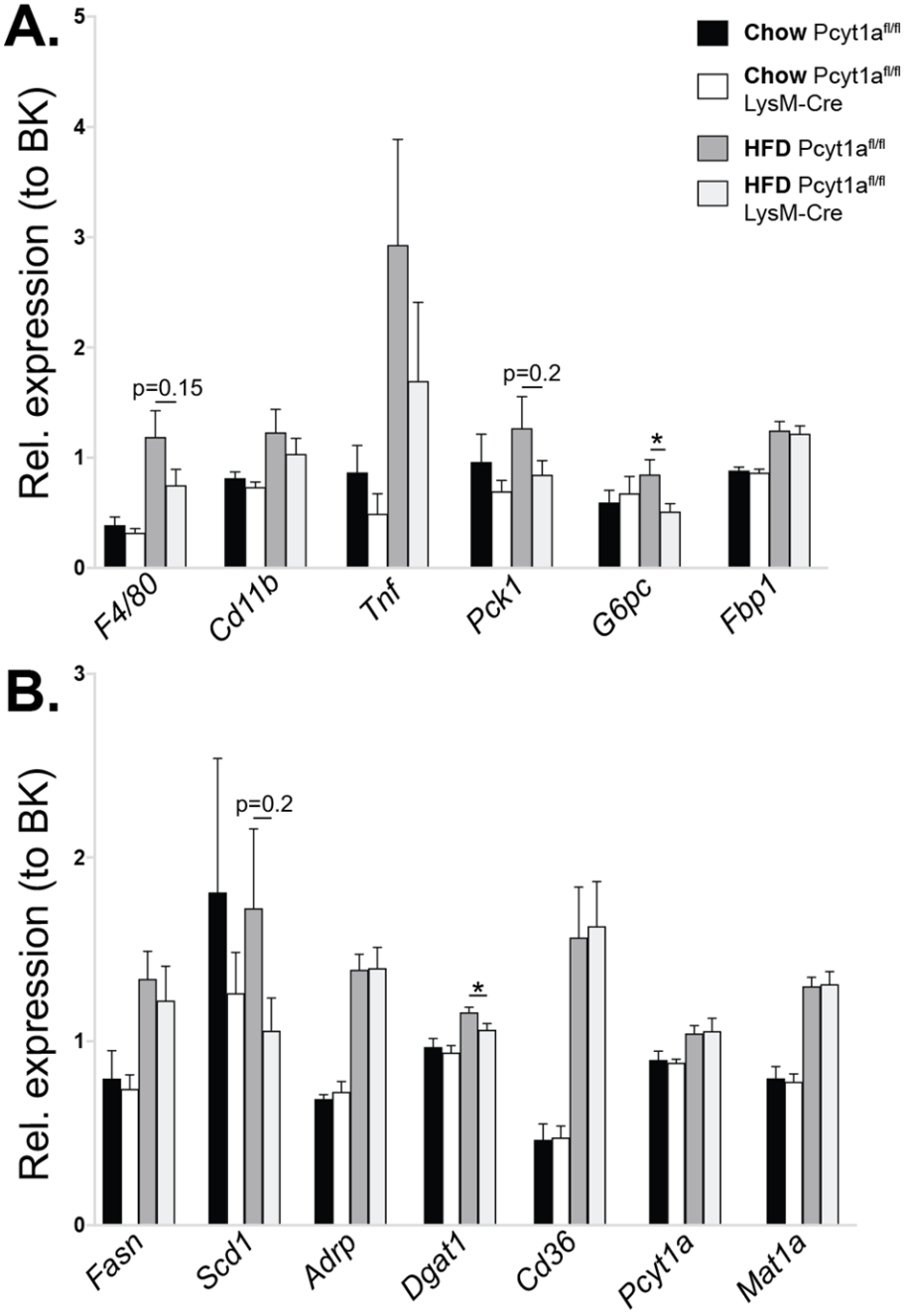

Figure 3-36 A). Similar to the results obtained on mixed genetic background, the expression of gluconeogenic gene *G6pc* was lower in LysM-Cre Pcyt1a$^{fl/fl}$ mice than in

control group on HFD, indicating a lower HGP rate (

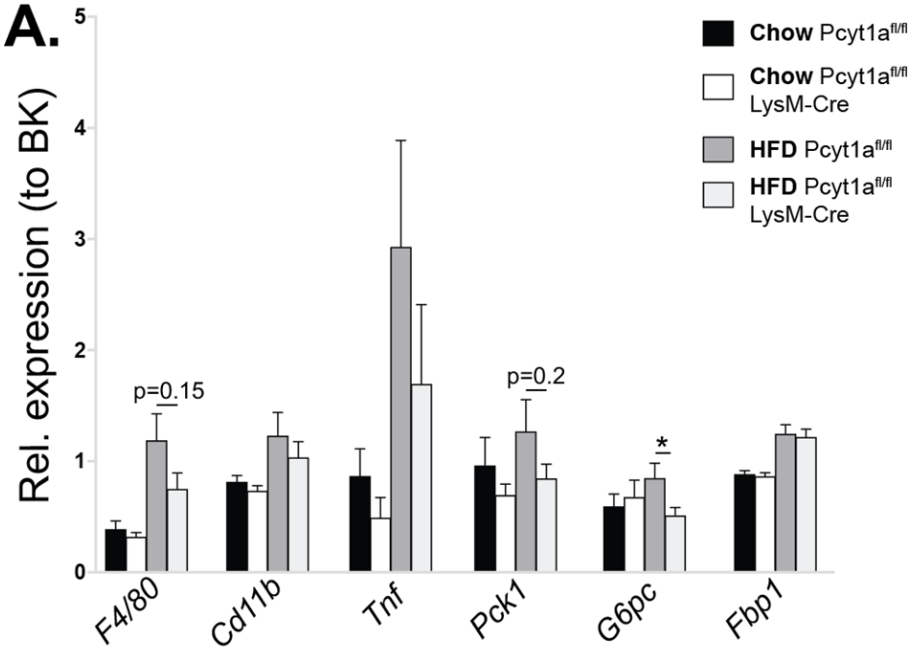

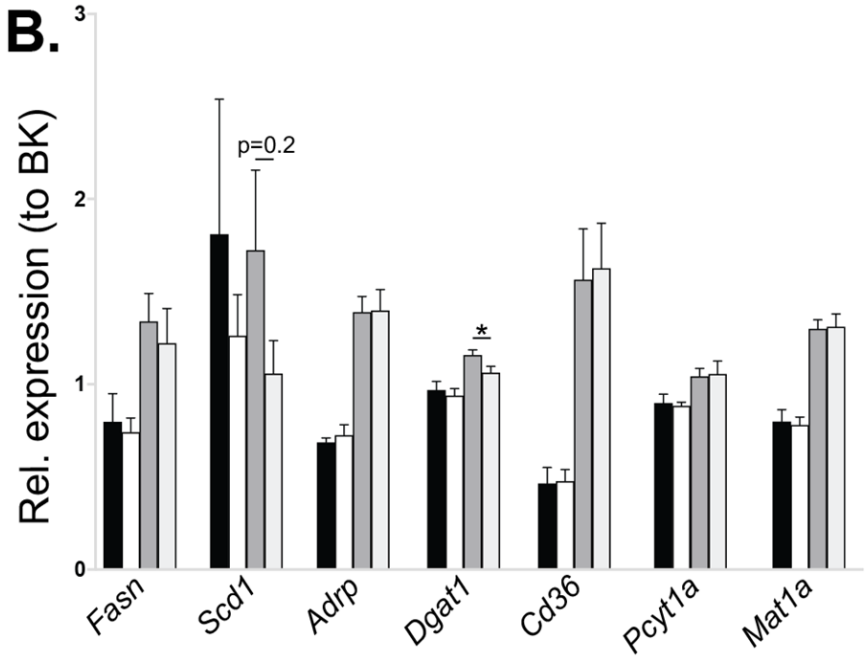

Figure 3-36 A). Finally, modest reduction in *Dgat1* was observed in LysM-Cre Pcyt1a$^{fl/fl}$ animals compared to controls on HFD (

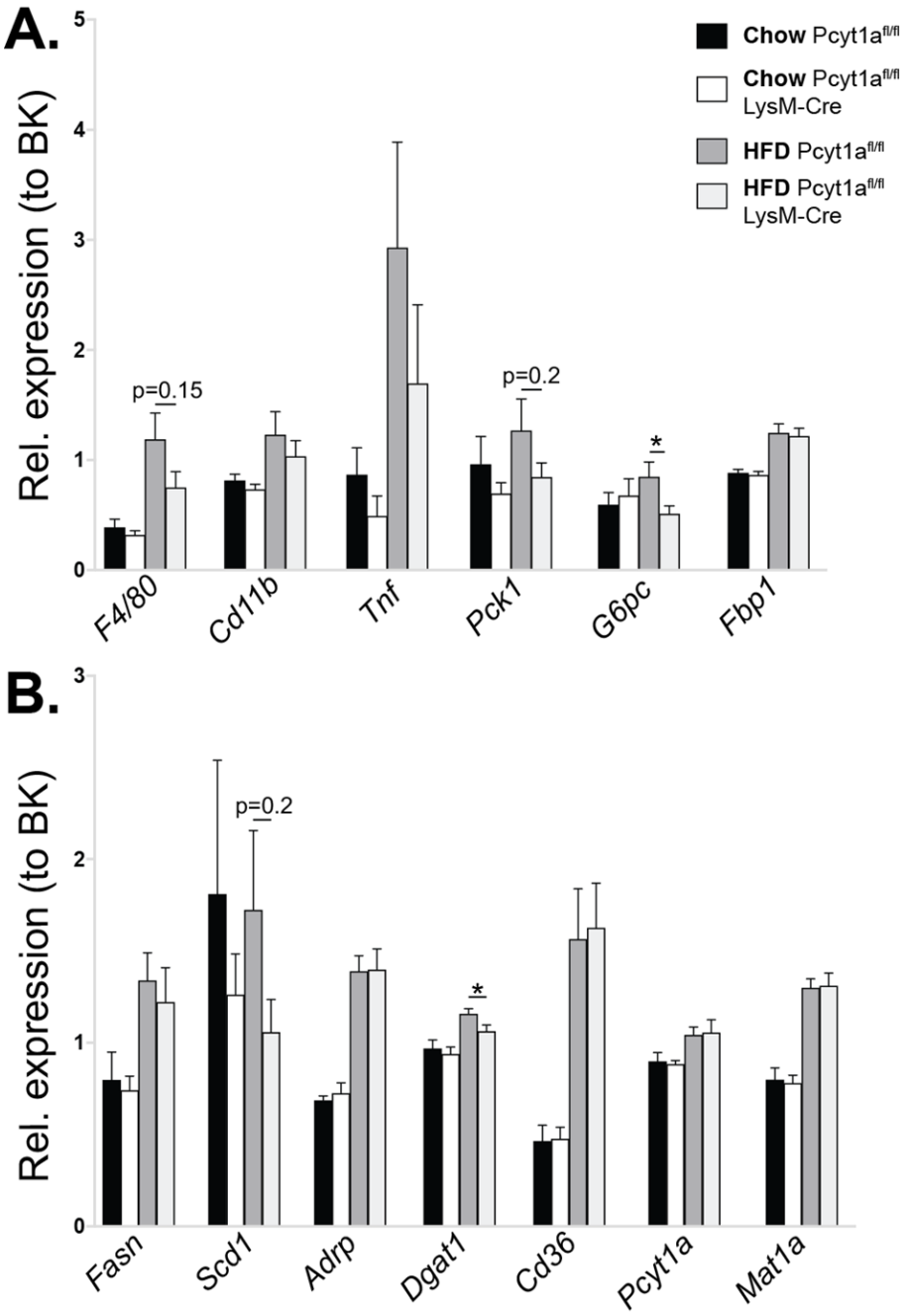

Figure 3-36 B).

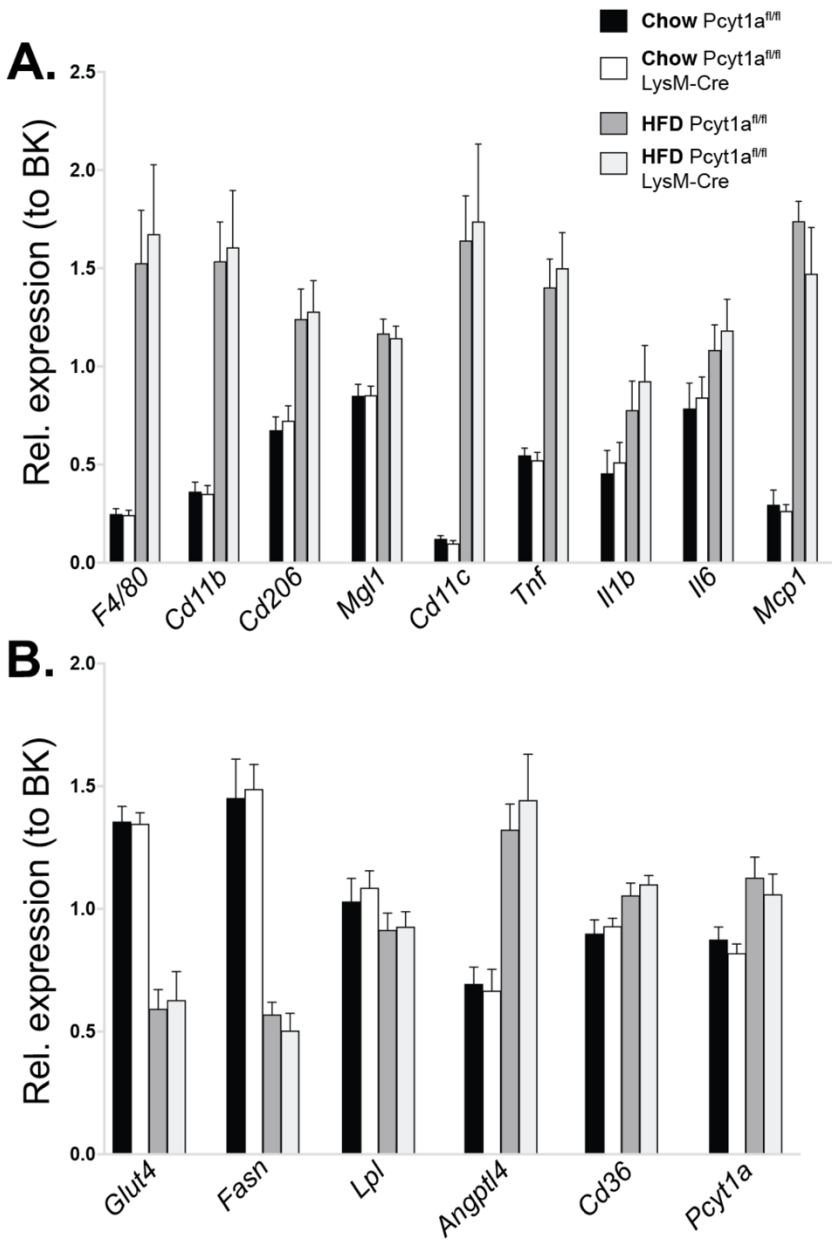

Figure 3-35. Immune system and metabolic gene expression analysis of eWATs isolated from chow and HFD-fed Pcyt1a$^{fl/fl}$ and LysM-Cre Pcyt1a$^{fl/fl}$ mice on C57Bl/6J genetic background.

*mRNA levels (normalised to BestKeeper) of immune system genes F4/80, Cd11b, Cd206, Mgl1, Cd11c, Tnf, Il1b, Il6, Mcp1 (**A**) and metabolic genes Glut4, Fasn, Lpl, Angptl4, Cd36, Pcyt1a (**B**) in the eWATs isolated from chow-fed Pcyt1a$^{fl/fl}$ (n=7, black bars), LysM-Cre Pcyt1a$^{fl/fl}$ (n=9, white bars) and HFD-fed Pcyt1a$^{fl/fl}$ (n=8, dark grey bars), LysM-Cre Pcyt1a$^{fl/fl}$ (n=7, light grey bars) 20-week-old male mice on a pure C57Bl/6J background, culled in a random fed state. HFD-fed group received 60% kcal fat diet (D12492) from 8 weeks of age. * p < 0.05 compared to Pcyt1a$^{fl/fl}$ using student's t-test.*

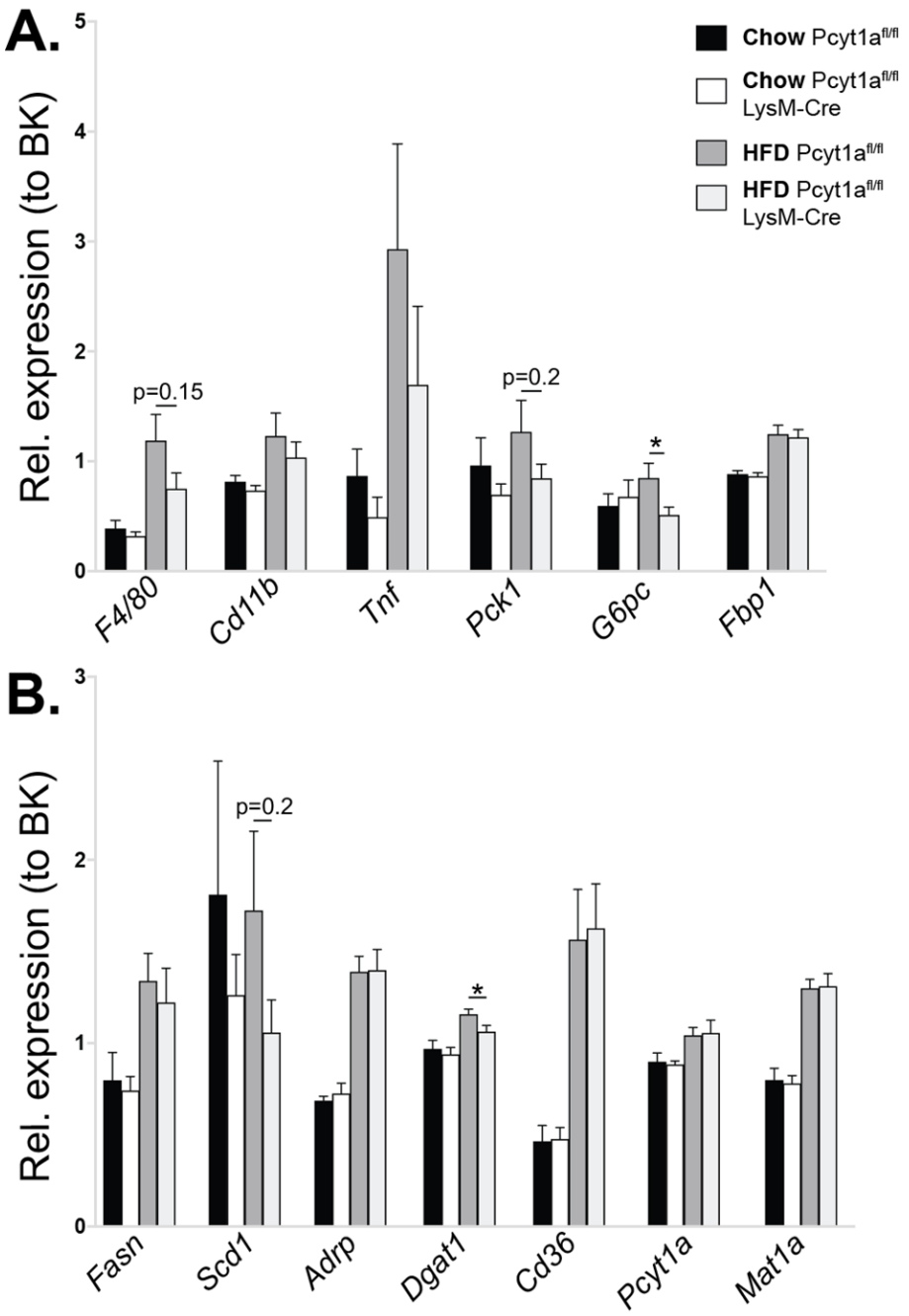

Figure 3-36. Immune system, gluconeogenic and lipid metabolism gene expression analysis of livers isolated from chow and HFD-fed Pcyt1a$^{fl/fl}$ and LysM-Cre Pcyt1a$^{fl/fl}$ mice on C57Bl/6J genetic background.

*mRNA levels (normalised to BestKeeper) of immune system genes F4/80, Cd11b, Tnf, gluconeogenic genes Pck1, G6pc, Fbp1 (**A**) and lipid metabolism genes Fasn, Scd1, Adrp, Dgat1, Cd36, Pcyt1a, Mat1a (**B**) in the livers isolated from chow-fed Pcyt1a$^{fl/fl}$ (n=7, black bars), LysM-Cre Pcyt1a$^{fl/fl}$ (n=9, white bars) and HFD-fed Pcyt1a$^{fl/fl}$ (n=8, dark grey bars), LysM-Cre Pcyt1a$^{fl/fl}$ (n=7, light grey bars) 20-week-old male mice on a pure C57Bl/6J background, culled in a random fed state. HFD-fed group received 60% kcal fat diet (D12492) from 8 weeks of age. * p < 0.05 compared to Pcyt1a$^{fl/fl}$ using student's t-test.*

3.2.4 The role of Pcyt1a in macrophages in mediating macrophage-to-liver PC transport

3.2.4.1 Rationale for performing macrophage-to-liver PC transport assay using LysM-Cre Pcyt1a$^{fl/fl}$ BMDMs

Rationale. Because I observed a transcriptional signature that is suggestive of a modest improvement in hepatic metabolism in obese LysM-Cre Pcyt1a$^{fl/fl}$ mice compared to controls without any major changes in eWAT or liver inflammation, I considered alternative ways that macrophages could affect hepatic metabolism.

All tissue macrophages transiently accumulate high levels of cholesterol through phagocytosis of dead cells, which is then transported to the liver via HDL particles for disposal. While HDL is classically viewed as a cholesterol-carrying lipoprotein, it contains large amounts of phospholipid that is also internalised by the liver[549]. Recently it has been shown that HDL-bound PC delivered to the liver contribute to the hepatic PC and TG pools[404]. As PC is the main lipid species in HDL, and reverse cholesterol transport to a premature HDL particle increases *de novo* PC synthesis rate in macrophages[550], I **hypothesised** that *Pcyt1a*-deficient macrophages might have an impaired PC transfer to APOA1 protein, thus decreased rate of HDL lipidation. LysM-Cre Pcyt1a$^{fl/fl}$ mice would consequently have a net reduction in PC delivery to the liver

that might result in a mild improvement in hepatic metabolism on HFD, supporting my

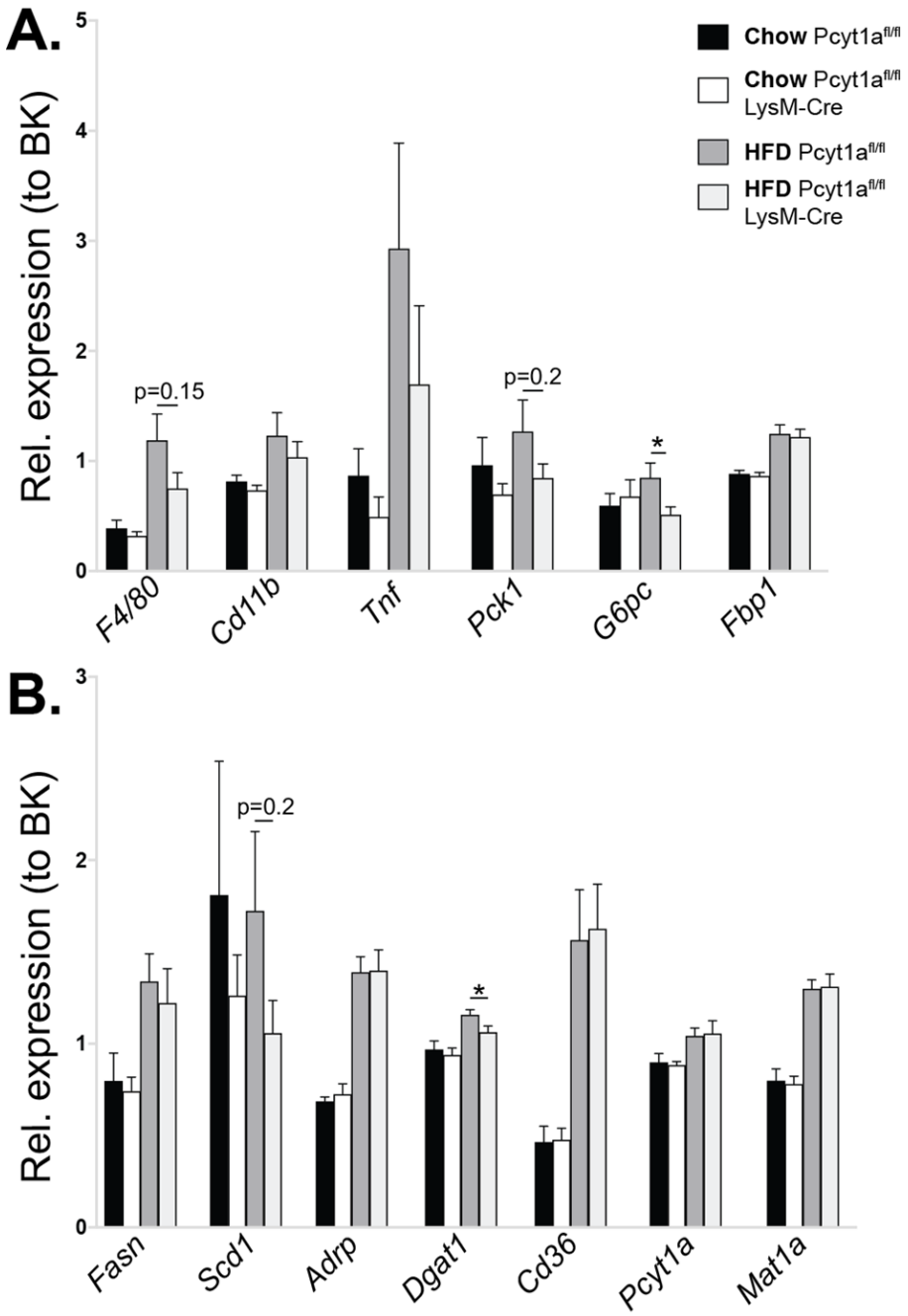

data (Figure 3-27, Figure 3-36). This hypothesis was supported by disrupted hepatic expression of genes involved in lipoprotein metabolism in LysM-Cre Pcyt1a$^{fl/fl}$ animals, namely *Apoa1*, which encodes the main protein component of HDL, and *Lcat* and *Pltp*, encoding enzymes responsible for PC transfer between lipoprotein particles (Figure 3-27 B).

Method. In order to directly demonstrate decreased macrophage-to-liver PC transport in LysM-Cre Pcyt1a$^{fl/fl}$ mice, I decided to establish a recently published assay that involves an intraperitoneal injection of ^{3}H-PC-labelled macrophages into host mice and tracing the appearance of radiolabel in the serum and liver[404].

3.2.4.2 Optimisation of PC radiolabelling and validation of donor BMDM phenotype for liver-to-macrophage PC transport assay

Rationale and optimisation. As a uniform PC labelling between LysM-Cre Pcyt1a$^{fl/fl}$ and control BMDMs was desired, I needed to take into account the difference in the rate of choline incorporation into the cellular PC fraction. Since *de novo* PC synthesis rate was approximately 50% lower in LysM-Cre Pcyt1a$^{fl/fl}$ BMDMs than controls (Figure 3-37 B), I considered increasing the specific activity of the medium used for labelling *Pcyt1a*-deficient cells by 50% to achieve the same radiolabel content in cells of both genotypes. Initially I validated that incorporation of labelled choline into the cells over 24 h was directly proportional to its specific activity in the media (Figure 3-37 A). Based on the linear relationship between specific activity in the labelling media and radiolabel incorporation to cells, I decided to use a medium with the specific activity of 0.06 MBq/ml to label controls, and of 0.12 MBq/ml to label LysM-Cre Pcyt1a$^{fl/fl}$ BMDMs. Indeed, 24 h of incubation with indicated media resulted in cells of both genotypes having a specific activity of approximately 1 dpm/cell.

Rationale. The expression of genes related to lipoprotein metabolism was analysed in cells that were used for macrophage-to-liver PC transport assay.

Results. *Pcyt1a* expression was reduced by approximately 70% in LysM-Cre Pcyt1a$^{fl/fl}$ BMDMs compared to controls (Figure 3-37 C). Transcript levels of *Abca1* and *Abcg1* genes, which encode proteins regulating cholesterol and phospholipid efflux from cells to HDL particles, were similar in *Pcyt1a*-deficient and control macrophages (Figure 3-37 C). Finally, the expression of genes encoding scavenger receptors that are involved in lipoprotein particle uptake was also influenced by genotype - LysM-Cre Pcyt1a$^{fl/fl}$ BMDMs had higher levels of *Cd36*, but lower levels of *Srb1* mRNA than controls (Figure 3-37 C).

3.2.4.3 *Pcyt1a* gene deletion did not affect the rate of PC release from macrophages into serum

Method. After 24 h of labelling, 2 millions of LysM-Cre Pcyt1a$^{fl/fl}$ and control donor BMDMs having a specific activity of 1 dpm/cell were injected into host WT mice. Serum samples from host mice were then taken at 3.5, 7 and 24 h post injection. LDL and vLDL particles were subsequently removed from serum samples by chemical precipitation, and processed samples were fractionated to lipid and aqueous phases.

Radioactivity measured in the lipid fraction corresponded to HDL-bound PC, while aqueous phase contained radiolabelled free choline released from degradation of PC by phospholipases.

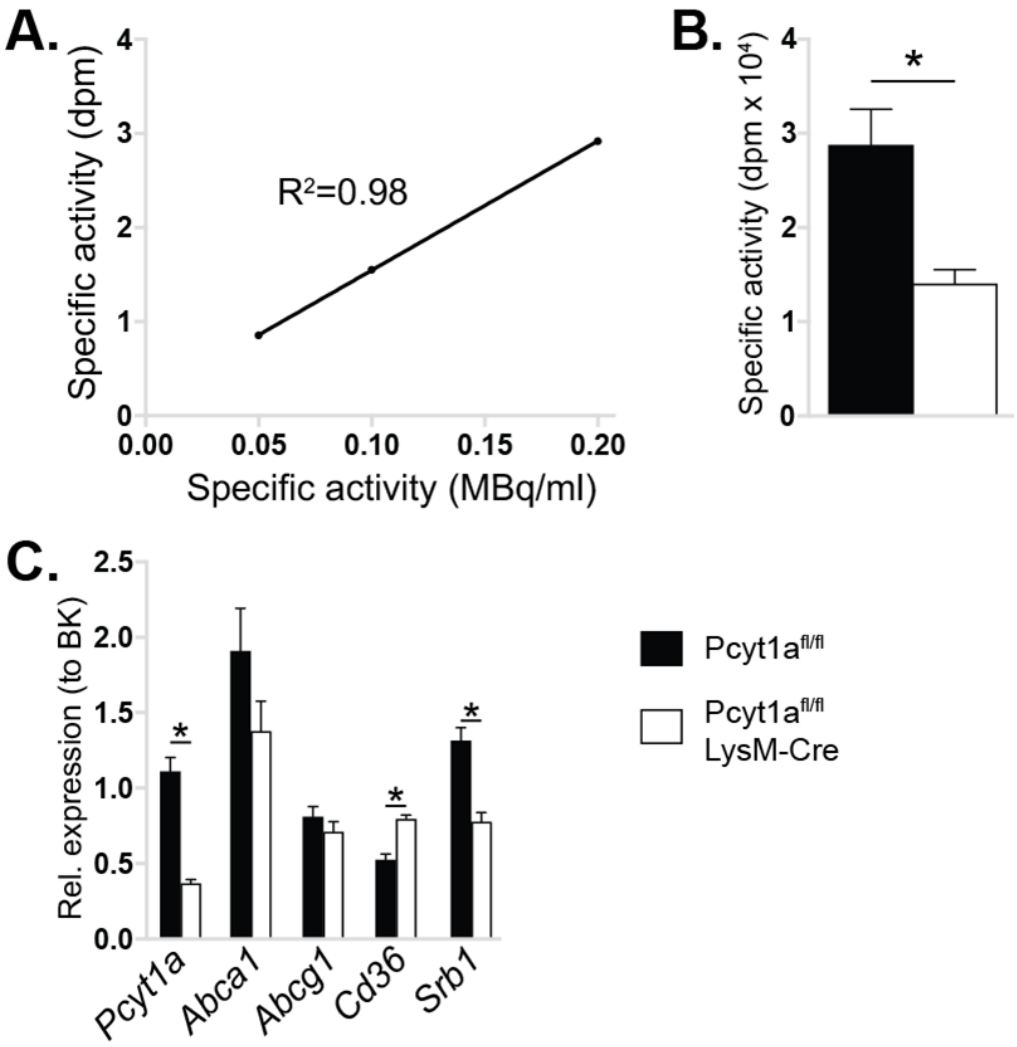

Figure 3-37. Optimisation of PC radiolabelling, de novo PC biosynthesis and lipoprotein metabolism gene expression in BMDMs from donor Pcyt1a$^{fl/fl}$ or LysM-Cre Pcyt1a$^{fl/fl}$ mice.

A. *Specific activity of WT BMDMs (expressed per single cell) cultured in the presence of 0.05, 0.1 and 0.2 MBq/ml ^{3}H-choline tracer for 24 h.* ***B.*** *Incorporation of ^{3}H-choline tracer into cellular lipids of unstimulated BMDMs from Pcyt1a$^{fl/fl}$ (black bars) and Pcyt1a$^{fl/fl}$ LysM-Cre (white bars) mice over 3 h.* ***C.*** *mRNA levels (normalised to BestKeeper) of phospholipid and lipoprotein metabolism genes Pcyt1a, Abca1, Abcg1, Cd36, Srb1 in unstimulated BMDMs from Pcyt1a$^{fl/fl}$ and Pcyt1a$^{fl/fl}$ LysM-Cre mice on mixed C57Bl/6J, 129/Sv background. N=4 mice/group. * p < 0.05 compared to Pcyt1a$^{fl/fl}$ using student's t-test.*

Results. Host mice injected with LysM-Cre Pcyt1a$^{fl/fl}$ BMDMs displayed a comparable rate of radioactivity appearance in total serum to controls (Figure 3-38 A). Mice carrying LysM-Cre Pcyt1a$^{fl/fl}$ BMDMs had slightly elevated radioactivity levels in the aqueous phase of the serum compared to controls at 24 h after injection (Figure 3-38 B). No differences in the rate of appearance of HDL-bound PC was observed between donor genotypes (Figure 3-38 C).

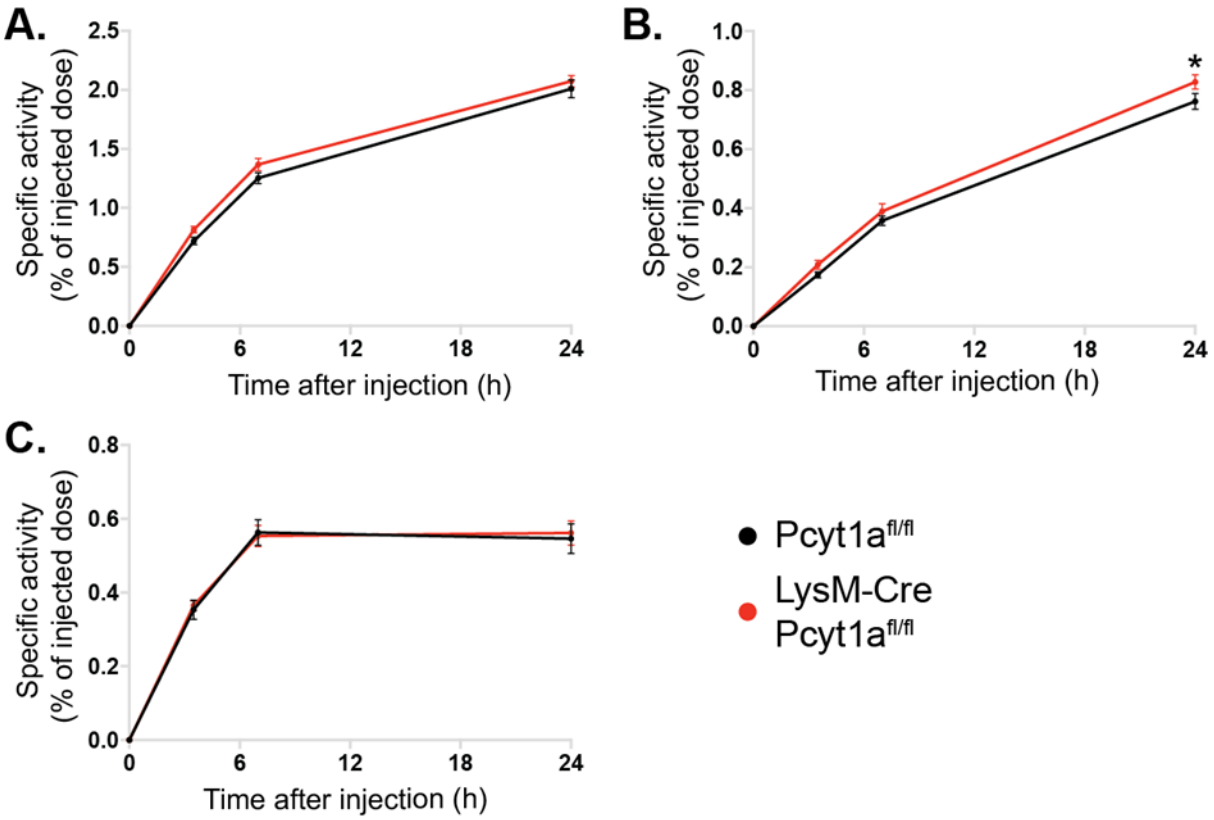

Figure 3-38. Presence of ^{3}H-choline tracer in the serum of mice after IP injection with ^{3}H-PC-labelled BMDMs from donor Pcyt1a$^{fl/fl}$ or LysM-Cre Pcyt1a$^{fl/fl}$ mice. *Host mice were injected with 10^{6} BMDMs with a total specific activity of 10^{6} dpm per mouse. Specific activity (expressed as percentage of injected dose) of total serum (**A**) and aqueous (**B**) and lipid (**C**) serum HDL fractions of WT 10-week-old female mice, 3.5, 7 and 24 h after injection with ^{3}H-PC-labelled BMDMs from donor Pcyt1a$^{fl/fl}$ (black lines) and LysM-Cre Pcyt1a$^{fl/fl}$ (red lines) 10-week-old female mice on mixed C57Bl/6J, 129/Sv background. N=4 donor BMDM mice/group, n=8 host mice/group (BMDMs from a single donor were injected into two WT hosts). * $p < 0.05$ compared to Pcyt1a$^{fl/fl}$ using 2-way ANOVA with Bonferroni's multiple comparisons test.*

3.2.4.4 *Pcyt1a* gene deletion did not affect the total PC delivery from macrophages into the liver

Rationale. 24 h after injection, host mice were culled and radioactivity levels were measured in the liver, spleen, brain and BAT in order to assess the cumulative delivery of PC from macrophages during the assay.

Results. No genotype-dependent differences in the radioactivity concentration or total tissue radioactivity levels were found in the liver, spleen or BAT between two groups (Figure 3-39 A,B). Host mice carrying LysM-Cre Pcyt1a$^{fl/fl}$ BMDMs had a minor increase in radioactivity concentration and total radioactivity amount in the brain, compared to controls (Figure 3-39 A,B).

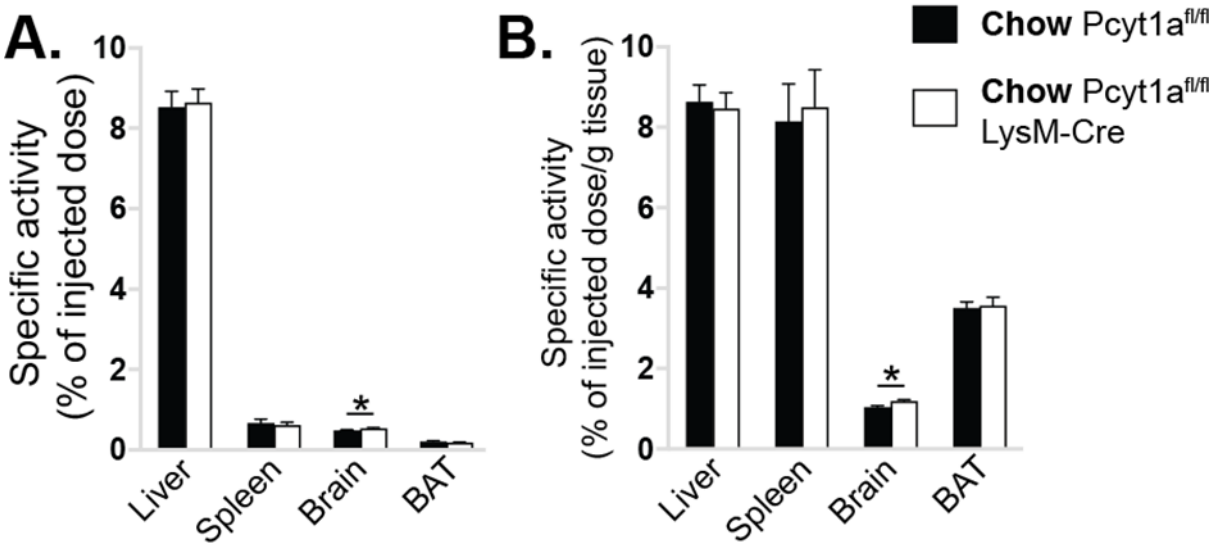

Figure 3-39. Presence of ^{3}H-choline tracer in the tissues of mice 24 h after IP injection with ^{3}H-PC-labelled BMDMs from donor Pcyt1a$^{fl/fl}$ or LysM-Cre Pcyt1a$^{fl/fl}$ mice.

*Host mice were injected with 10^6 BMDMs with a total specific activity of 10^6 dpm per mouse. Liver, spleen, brain and BAT were isolated 24 h after injection, homogenised and specific activity (expressed as a percentage of injected dose) was quantified and expressed as the total tissue amount (**A**) or amount per g of tissue (**B**). N=4 donor Pcyt1a$^{fl/fl}$ (black bars) and n= 4 donor LysM-Cre Pcyt1a$^{fl/fl}$ (white bars) 10-week-old female mice on mixed C57Bl/6J, 129/Sv background, n=8 10-week-old female host mice/group (BMDMs from a single donor were injected into two WT hosts). * $p < 0.05$ compared to Pcyt1a$^{fl/fl}$ using student's t-test.*

3.3 Discussion

This chapter describes how *de novo* PC biosynthesis in macrophages is linked to the development of ER stress and inflammation in response to saturated FFAs, and how it affects the metabolic health of a whole animal in lean and obese states. The study stemmed from the finding that *de novo* PC biosynthesis was increased in ATMs isolated from obese mice. The results obtained in this chapter were expected to expand the current view of how lipotoxicity leads to the inflammatory activation of ATMs during obesity. The main findings of this chapter were as follows:

1) LPS and lipotoxic concentrations of palmitate increased *de novo* PC synthesis in BMDMs.

2) *Pcyt1a*-deficient BMDMs had diminished inflammatory activation and ER stress after prolonged treatment with lipotoxic concentrations of palmitate.

3) LysM-Cre Pcyt1a$^{fl/fl}$ mice did not exhibit changes in WAT inflammation or systemic insulin sensitivity on chow or HFD, but demonstrated minor benefitial changes in hepatic gene expression on HFD.

3.3.1 *De novo* PC synthesis was increased in ATMs from obese mice and BMDMs stimulated with LPS and palmitate

While *de novo* PC synthesis in ATMs was not directly measured, I observed an increased *Pcyt1a* gene transcription and elevated PC:PE ratio in ATMs isolated from 16-week-old ob/ob mice compared to WT controls, indicating increased *de novo* PC synthesis rate. In future, a more direct validation of this finding could be performed by isolating ATMs from lean and obese mice and incubating them in the presence of radiolabelled choline in order to assess the rate of choline incorporation into PC. However, a previous study linking increased PC levels to ER stress and insulin resistance in the liver during obesity was also conducted without directly assessing hepatic *de novo* PC synthesis rate and solely relied on gene transcription and lipidomic analyses[226], suggesting that such parameters accurately reflect PC synthesis rate *in vivo*.

Contrary to a previous published observation[373], I found that LPS acutely increased *de novo* PC synthesis rate in macrophages. A difference in macrophage cell type

(thioglycolate-elicited peritoneal macrophages *versus* BMDMs) could potentially explain such discrepancy. Thioglycolate is known to induce inflammatory activation of peritoneal macrophages[551], and could potentially increase basal PC synthesis rate even after elicitation and prolonged culturing. Observed induction of PC synthesis after LPS treatment might therefore be blunted in thioglycolate-elicited macrophages.

In agreement with the previous study, I found that treating BMDMs with oleate increased *de novo* PC synthesis rate[367]. This was likely due to the oleate-induced lipid droplet formation and post-translational activation of CCTα. Importantly, I was first to observe an increase in *de novo* PC biosynthesis rate following the stimulation of BMDMs with palmitate. However, the effect size of palmitate stimulation compared to LPS or equimolar concentration of oleate on the induction of PC synthesis was substantially smaller. As palmitate has been previously shown to signal via TLR4 receptor[552], but also to weakly induce lipid droplet formation, it is unclear which of the two mentioned processes is responsible for palmitate-mediated increase in *de novo* PC synthesis rate in BMDMs. In the future, this question could be addressed by utilising TLR4-knockout BMDMs, in which all direct signalling effects of palmitate should be lost, and any changes in *de novo* PC synthesis rate could be attributed to the intracellular metabolic processing of palmitate. Alternatively, WT BMDMs could be treated with palmitate in the presence of DGAT1 inhibitor in order to block lipid droplet formation. If the increase in *de novo* PC synthesis persisted in this setting, then it would be most likely driven by the inflammatory signalling of palmitate.

3.3.2 *Pcyt1a*-deficient BMDMs did not exhibit impairments in differentiation, LPS signalling or palmitate incorporation to PC

Unlike most studies that investigated the importance of a metabolic enzyme for macrophage polarisation, I did not profile the phenotype of LPS-treated macrophages, because it has already been partially addressed in a previous study[373]. As *Pcyt1a*-deficient macrophages exhibited impaired Golgi-dependent secretion of inflammatory cytokines TNFα and IL-6, their M1 phenotype after prolonged LPS stimulation would most likely be different due to a lack of autocrine signalling by mentioned cytokines, as it has been observed in LPS-stimulated TNF receptor-deficient macrophages[553]. While in our experiments I also measured *Tnf* gene expression as a readout for palmitate-induced inflammation, published studies have observed that TNFα secretion induced by LPS is around 100 times higher than by palmitate[408]. As macrophages from LysM-

Cre Pcyt1a$^{fl/fl}$ animals exhibited an approximately two-fold reduction in LPS-induced TNFα secretion[373], I think that the remaining capacity of *de novo* PC synthesis must be sufficient to release TNFα from *Pcyt1a*-deficient macrophages in response to palmitate.

Importantly, in agreement with a previous study, I found the differentiation of *Pcyt1a*-deficient BMDMs to be intact[373]. It is also likely that the reduction in macrophage yield after differentiation is a compensatory mechanism for a reduced PC synthesis rate in LysM-Cre Pcyt1a$^{fl/fl}$ BMDMs. Since disrupting PC formation by inhibiting fatty acid synthesis has been shown to impair BMDM differentiation[370], it is unclear how *Pcyt1a*-deficient macrophages can maintain the differentiation capacity of WT cells. A likely explanation is that remaining *de novo* PC synthesis rate is sufficient to provide enough PC for differentiating *Pcyt1a*-deficient BMDMs. In future, I will compare whole lipidomes of LysM-Cre Pcyt1a$^{fl/fl}$ BMDMs and controls to further verify that *Pcyt1a* deficiency does not impair membrane phospholipid composition.

Macrophages lacking FASN enzyme exhibit impaired LPS-induced JNK activation due to altered lipid composition of membrane microdomains[408]. Despite observing reduced fatty acid synthesis rate in *Pcyt1a*-deficient macrophages, I found their JNK phosphorylation to be intact after LPS stimulation. One likely explanation for this discrepancy is that *Fasn* knockout macrophages have a substantially greater reduction in fatty acid synthesis rate compared to *Pcyt1a* knockouts, therefore possess defective lipid rafts within plasma membranes. However, it is also possible that FASN-deficient macrophages do not differentiate appropriately, as described in a separate study[370]. Impaired differentiation could also explain reduced phospholipid levels in lipid rafts and decreased JNK phosphorylation after LPS stimulation, but surprisingly macrophage differentiation markers were not analysed in the study[408]. Another important thing to note is that I have not assessed the composition of lipid rafts in *Pcyt1a* knockout BMDMs. While my experiments and a published report[373] indicate that TLR4 signalling is intact in *Pcyt1a*-deficient macrophages, in future, the lipid composition of membrane rafts can be directly measured using detergent-based isolation and LC-MS detection. Overall, *Pcyt1a*-deficient BMDMs had reduced fatty acid synthesis rate, but showed no impairments in JNK phosphorylation after LPS stimulation, indicating that reduced *de novo* PC biosynthesis did not affect TLR4-JNK signalling axis.

Contrary to a suggestion made by a recent study[233], I did not find *de novo* PC synthesis to be responsible for palmitate incorporation into the PC fraction of lipids when macrophages were treated with high concentrations of palmitate. However, I did observe reduced palmitate incorporation into cellular lipids in LysM-Cre Pcyt1a$^{fl/fl}$ BMDMs compared to controls in a basal state. Such discrepancy suggests a mechanism where *de novo* PC synthesis pathway in macrophages can utilise both endogenously and exogenously derived palmitate as a substrate in an unstimulated, homeostatic state. Once macrophages are exposed to atypically high palmitate concentrations, the Lands cycle most likely becomes responsible for rapid palmitate incorporation into PC fraction. The best studied LPCAT enzymes in macrophages are predominantly responsible for incorporating PUFAs into membrane PCs[554]. However, a potential Lands cycle enzyme mediating palmitate incorporation into membrane PCs in macrophages could be LPCAT1, which demonstrates a preference towards palmitoyl-CoA[323]. Cells lacking *Lpcat1* exhibit augmented apoptosis in response to high extracellular PUFA concentrations, due to the inability to maintain appropriate levels of membrane saturation[555]. Whether *Lpcat1*-deficient BMDMs are protected against palmitate-induced ER stress and inflammation could be investigated in future.

3.3.3 The relationship between cellular PC levels and FFA remodelling capacity and inflammation in palmitate-treated macrophages

The most striking findings obtained in the first part of this chapter are reduced ER stress, cell death and inflammation and greater expression of SREBP1-regulated fatty acid remodelling genes in LysM-Cre Pcyt1a$^{fl/fl}$ BMDMs compared to controls after prolonged incubation with palmitate. Induction of SREBP1-dependent gene transcription has been previously shown to have anti-inflammatory effects[219,220], therefore it is a likely mechanism that limits palmitate-induced inflammation in *Pcyt1a*-deficient macrophages. Alternatively, ER stress induced by prolonged palmitate treatment could indirectly cause inflammation by promoting cell death. Indeed, LysM-Cre Pcyt1a$^{fl/fl}$ BMDMs exhibit reduced cell death and inflammation in response to cytotoxic doses of palmitate. While it would be of interest to know whether palmitate-induced ER stress is directly coupled to pro-inflammatory signalling pathways, or promote inflammation indirectly by causing cell death, the important fact is that functionally *Pcyt1a*-deficient macrophages have reduced inflammatory activation in response to palmitate.

The observed decrease in SREBP1 target genes following prolonged treatment with palmitate is in line with current literature, which suggests that ER membrane saturation inhibits SREBP1 cleavage and activation[556]. However, LysM-Cre Pcyt1a$^{fl/fl}$ BMDMs are likely to demonstrate reduced SREBP1 inhibition via an alternative mechanism, involving the sensing of low PC levels within the ER[401,402]. It has been already described that while their basal PC concentration is normal, *Pcyt1a*-deficient macrophages are incapable of maintaining appropriate PC levels after prolonged treatment with LPS, when the demand for *de novo* PC biosynthesis is high[373] (Figure 3-40). A likely hypothesis is that **prolonged treatment with palmitate would also decrease PC levels in LysM-Cre Pcyt1a$^{fl/fl}$ BMDMs compared to controls, and thus lead to increased SREBP1 activation and diminished ER stress, cell death and inflammation compared to control cells**. However, three key experiments will be performed using *Pcyt1a*-deficient BMDMs and controls to further prove this hypothesis in future:

a) Cellular PC levels after prolonged treatment with palmitate will be quantified by lipidomic analysis.
b) SREBP1 activation after prolonged treatment with palmitate will be measured by Western blot.
c) Palmitate remodelling and overall fatty acid desaturation in response to prolonged treatment with palmitate will be assessed by lipidomic analysis.

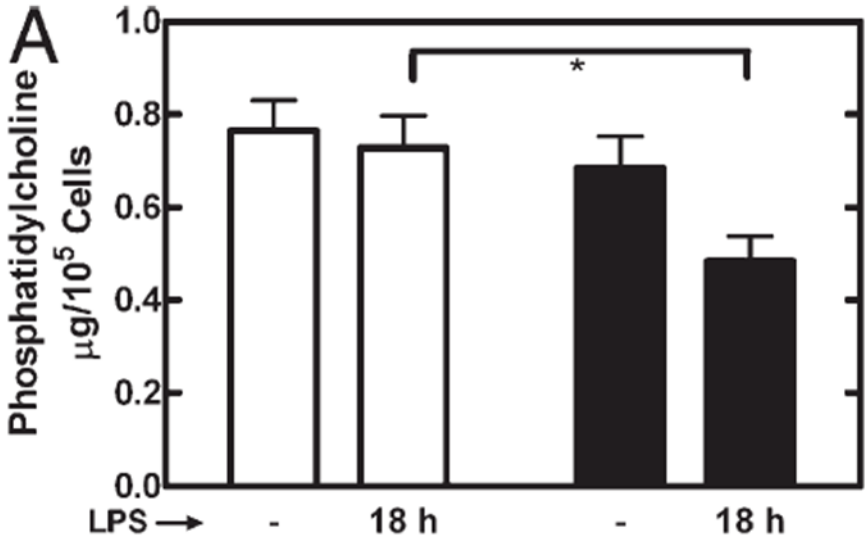

Figure 3-40. Reduced PC levels in Pcyt1a-deficient macrophages after prolonged LPS stimulation.

*Control (white) and LysM-Cre Pcyt1a$^{fl/fl}$ (black) thioglycolate-elicited peritoneal macrophages were incubated with 10 ng/ml LPS or without LPS for 18 h, and total lipids were extracted. PC was isolated by thin layer chromatography and quantified by flame ionization. Values were normalized to cell numbers. Data are the mean of determinations from at least two individual mice of each genotype. Error bars indicate mean ± SEM. *, P < 0.05 using 2-way ANOVA. Graph is presented as published by Tian et al*[373]*.*

If the results obtained from the suggested experiments were in line with proposed hypothesis, it would indicate a mechanism where **the capacity of a macrophage to maintain its PC levels in response to high saturated FFA concentrations is detrimental, resulting in reduced FFA remodelling activity and increased ER stress, cell death and inflammation** (Figure 3-41). Importantly, such model would be in line with the phenotype of ATMs isolated from WT and ob/ob animals at 5 and 16 weeks of age, where ***de novo*** **PC synthesis is inversely related to M2 polarisation and FFA remodelling gene transcription** (**Error! Reference source not found.**).

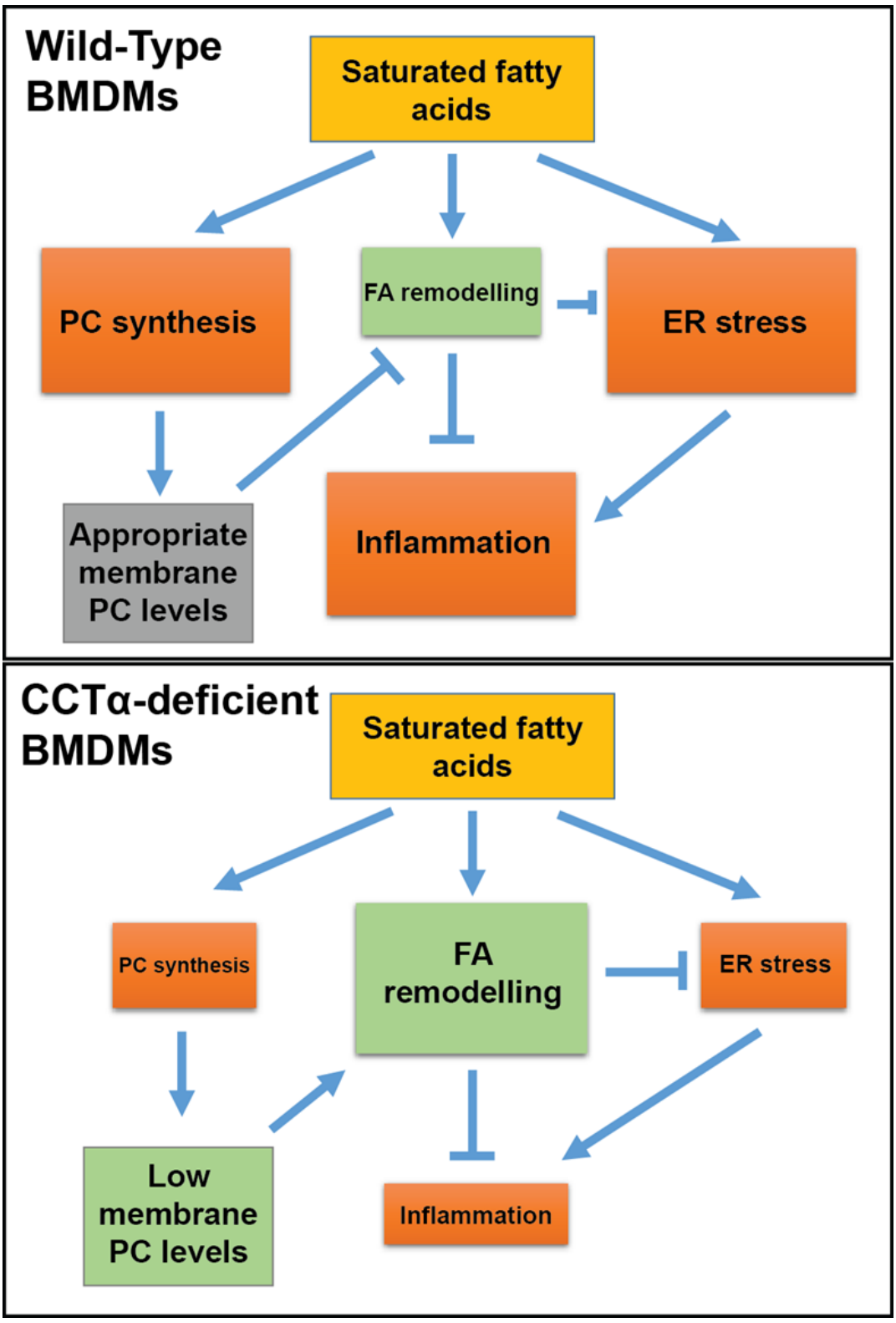

Figure 3-41. Schematic representation of a potential mechanism mediating reduced ER stress and inflammation observed in CCTα-deficient BMDMs after prolonged treatment with palmitate.

3.3.4 Macrophage-specific *Pcyt1a* deficiency did not alter WAT inflammation and systemic insulin sensitivity in lean or obese mice

Despite reducing ER stress and inflammatory activation in response to palmitate *in vitro*, macrophage-specific *Pcyt1a* deletion did not affect the inflammatory profile of eWAT during obesity *in vivo*. There are other examples in the literature in which genetically modified macrophages exhibit altered inflammatory profile *in vitro*, but genetic manipulation of macrophages *in vivo* does not affect WAT inflammation during obesity[557,558]. Owing to the complexity of pathophysiological mechanisms occurring during obesity, it is difficult to pinpoint a reason for such discrepancy between the behaviour of macrophages in the cell culture and adipose tissue. However, unaltered development of WAT inflammation in LysM-Cre Pcyt1a$^{fl/fl}$ animals can be attributed to:

a) **Incomplete deletion of *Pcyt1a* gene in the ATM population by CRE recombinase.** I observed approximately 50% reduction in *Pcyt1a* mRNA levels in ATMs isolated from in LysM-Cre Pcyt1a$^{fl/fl}$ mice on a mixed genetic background. As described by a previous publication[373], such reduction most likely indicates a presence of a mixed population, where one half of total cells express normal levels of *Pcyt1a* gene, and the other half lacks *Pcyt1a* transcript entirely. It is therefore plausible that having a functional anti-inflammatory mechanism in only half of the ATM population is insufficient to prevent the development of WAT inflammation. *Pcyt1a* deletion efficiency in ATMs might be improved by expressing CRE recombinase under a different promoter, such as *Csf1r* or *Cd11b*, instead of *Lysm*. Alternatively, LysM-Cre Pcyt1a$^{fl/fl}$ mice could be further crossed to Pcyt1a$^{+/-}$ line[330], and all *in vivo* experiments could be performed on Pcyt1a$^{+/-}$ background to further reduce *Pcyt1a* gene expression.

b) **Differences in eWAT inflammation induced by HFD and ob/ob genetic background.** I observed increased *Pcyt1a* transcription and elevated PC:PE levels in ob/ob ATMs compared to WT controls at 16 weeks of age. However, metabolic studies in this chapter were performed using a mouse model of HFD-induced obesity. There are multiple differences between genetically and diet-induced obese animal models, including their daily caloric intake, nutritional composition of food and endogenous effects of leptin. Importantly, the majority of fatty acyl chains in WAT isolated from of ob/ob mouse are derived from the

DNL, while HFD decrease DNL in WAT and promote the storage of dietary FFAs. As lipids within eWAT are hypothesised to trigger ATM inflammatory activation, the FFA composition of adipocytes is a likely determinant of the development of WAT inflammation. It is therefore plausible that the rate of *de novo* PC biosynthesis in ATMs is only increased in response to DNL-derived, and not dietary lipids. In future, I will analyse the total lipidome of ATMs isolated from mice after prolonged high-fat feeding to assess if their PC:PE ratio is increased compared to chow-fed controls. I will also transplant the bone marrow of LysM-Cre Pcyt1a$^{fl/fl}$ and control mice into ob/ob hosts to re-create the conditions under which elevated PC:PE ratio in ATMs was originally observed, in order to test whether *Pcyt1a*-deficient bone marrow could improve the metabolic profile of ob/ob animals.

c) **Poor *in vivo* translatability of findings observed in BMDMs treated with palmitate.** Despite being frequently utilised in the literature, the treatment of macrophages with high concentrations of palmitate in the absence of other FFAs does not fully reflect pathophysiological mechanisms occurring in WAT during obesity. Prolonged high-fat feeding results in elongation and desaturation of the fatty acyl chains in WAT[559], therefore ATMs are exposed to a mixture of FFAs that are predominantly unsaturated. It has been shown that even low doses of oleate can completely ablate the effects of palmitate on ER stress and inflammation *in vitro*[233]. Furthermore, treating macrophages with FFA mixture that resembles WAT fatty acyl composition does not induce ER stress and inflammation[136]. At present, it is not clear how complex FFA mixtures affect macrophages, but it is possible that the protective effect of reduced rate of PC synthesis only occurs in response to treatment with saturated FFAs. However, such question will not be answered until lipid-mediated ER stress and inflammation can be modelled *in vitro* in a physiological manner.

3.3.5 Macrophage-specific *Pcyt1a* deficiency modestly improved liver metabolic gene transcription during obesity

Despite not having any effect on WAT inflammation and systemic insulin sensitivity, *Pcyt1a* deletion in macrophages had a favourable outcome on liver metabolic gene transcription after high fat feeding on two different genetic backgrounds. There was a genetic background-dependent effect - LysM-Cre Pcyt1a$^{fl/fl}$ mice on mixed genetic

background exhibited a more pronounced down-regulation of hepatic genes related to gluconeogenesis and lipid metabolism on HFD compared to the same line on C57Bl/6J genetic background. A stronger impact on metabolic gene transcription on mixed genetic background could be attributed to a higher deletion efficiency of *Pcyt1a* gene (approximately 70% reduction of *Pcyt1a* mRNA in BMDMs on mixed genetic background vs 50% reduction on C57Bl/6J background).

The effect size of observed changes in hepatic gene expression between LysM-Cre Pcyt1a$^{fl/fl}$ and control animals is marginal. This is a likely reason why measured alterations in gene expression did not translate into changes in hepatic lipid content or have any effect on systemic glucose metabolism. An important thing to note is that I have investigated a macrophage-specific knockout mouse model, thus the impact on the whole body metabolism was expected to be lower compared to global gene knockout models. Furthermore, the deletion efficiency of *Pcyt1a* in ATMs was only around 50%, therefore the observed effect sizes likely underestimate the full biological importance of *de novo* PC biosynthesis in macrophages in regulating hepatic gene transcription during obesity.

As gluconeogenesis and FFA uptake are generally increased in the liver during fasting, hepatic mRNA measurements indicate that *Pcyt1a* in macrophages might play a role after high-fat feeding in the fasted state. As summarised in the introduction, ATMs accumulate lipids after prolonged fasting. Perhaps such lipid accumulation, combined with inflammatory milieu of eWAT during HFD, is sufficient to transiently create pathophysiological conditions where reduced rate of *de novo* PC synthesis provides a favourable ATM inflammatory profile. Unfortunately, I did not have tissues from HFD-fed LysM-Cre Pcyt1a$^{fl/fl}$ mice in the fasted state to assess WAT inflammation, which I will perform in future. Furthermore, I will perform hyperinsulinemic-euglycemic clamp analysis of HFD-fed mice lacking *Pcyt1a* in macrophages in the fasted state to accurately assess hepatic glucose production.

Alternatively, there might be other ways through which macrophages influence hepatic gene transcription during obesity. Even though lack of *Pcyt1a* in macrophages had no effect on liver inflammation after high-fat feeding on both genetic backgrounds, I cannot fully rule out Kupffer cells as mediators of the phenotypic differences between LysM-Cre Pcyt1a$^{fl/fl}$ and control mice. In future, I am planning to isolate Kupffer cells from

HFD-fed mice to compare their transcriptomes and lipidomes to controls from chow-fed animals. If they show any obesity-induced changes in PC metabolism, I will isolate Kupffer cells from LysM-Cre Pcyt1a$^{fl/fl}$ mice after high-fat feeding to analyse their inflammatory and metabolic profile.

Finally, hepatic gene transcription indicated altered lipoprotein metabolism in LysM-Cre Pcyt1a$^{fl/fl}$ animals. While they exhibited normal total, LDL- and HDL-bound serum cholesterol levels, it is plausible that the size or shape of their HDL particles was altered, leading to impaired reverse cholesterol transport. However, the results from our established *in vivo* assay did not suggest any genotype-dependent changes in macrophage-to-liver PC transport via HDL. One major issue with measuring PC transport to the liver is PC labelling – ^{3}H-choline, which I utilised in the assay, can be removed from PC by phospholipases and enter the circulation in its free form. This does not occur when macrophage-to-liver cholesterol transport is investigated, as mice and humans do not break down ^{14}C-cholesterol but excrete it. Based on the serum tracer levels, ^{3}H-choline predominantly appeared in the lipid phase at 3.5 and 7 h post injection, but there was no further elevation in the radioactivity concentration in lipid fraction from 7 to 24 h after injection, suggesting that any potential changes in serum or tissue tracer levels after 7 h are due to circulating free choline. Higher radioactivity levels in the serum and brain of mice 24 h after the injection with *Pcyt1a*-deficient BMDMs than controls could simply indicate increased free choline content of LysM-Cre Pcyt1a$^{fl/fl}$ macrophages. Overall, this assay could be improved by culling animals 7 h after injection, when the ^{3}H-choline is delivered to tissues predominantly as HDL-bound PC. However, since I did not observe any differences in HDL-^{3}H-PC appearance in serum between mice injected with LysM-Cre Pcyt1a$^{fl/fl}$ or control BMDMs, it is likely that macrophage-to-liver PC transport is not responsible for changes in hepatic gene transcription in this model.

3.3.6 Conclusions

In this chapter, I found that *de novo* PC synthesis was increased in ATMs isolated from obese mice and in BMDMs treated with saturated fatty acid palmitate. Lack of a rate-limiting enzyme in *de novo* PC synthesis pathway, CCTα, diminished palmitate-induced ER stress and inflammation in BMDMs by up-regulating SREBP1-dependent fatty acid remodelling gene transcription. Mice lacking *Pcyt1a* in macrophages did not exhibit any changes in WAT inflammation and function in lean and obese states, but had a hepatic transcriptional signature indicative of mildly improved glucose and lipid metabolism after high-fat feeding. Further experiments are required to validate a proposed anti-inflammatory mechanism in *Pcyt1a*-deficient BMDMs *in vitro*, and to understand the relationship between *de novo* PC synthesis in macrophages and the regulation of hepatic gene transcription *in vivo*.

4 The role of β2-adrenergic receptor in the regulation of adipose tissue macrophage function

4.1 Introduction

4.1.1 Early insights leading up to the project: β-adrenergic receptor activation in macrophages reduced their lipolysis rate

At the start of my degree, the paradigm of nerve-immune interactions had already been established, but there were no reports on the communication between SNS and macrophages within adipose tissues. Therefore, little preliminary data was available in the literature when I initiated this project in the first year of my degree.

My interest in macrophage β2AR was sparked from the insights obtained during the optimisation of a lipolysis assay in BMDMs. Lipolysis assays are routinely performed in our institute and involve culturing adipocytes with radiolabelled oleate overnight, then washing cells and incubating them in the fresh medium. The appearance of a radioactive tracer in the medium in an unstimulated state is a readout for basal lipolysis, and on-demand lipolysis is assessed by stimulating adipocytes with PKA activators immediately after the medium change. Surprisingly, during the initial assay optimization I found that forskolin, which promotes cAMP production by increasing adenylyl cyclase activity, suppressed the rate of oleate release from BMDMs (data not shown). In order to understand the mechanism for forskolin-mediated lipolysis suppression, I stimulated macrophages with insulin, which inhibits lipolysis in adipocytes, and forskolin, isoprenaline and CL-316,243, all of which promote on-demand adipocyte lipolysis by activating PKA. Quantification of the amount of oleate released in 4 h showed that isoprenaline reduced the rate of lipolysis in BMDMs, while other stimuli did not show an effect compared to unstimulated cells (Figure 4-1 A). I confirmed this finding by performing a dose-response experiment, which revealed that isoprenaline already suppressed FFA release in BMDMs at 10 nM (Figure 4-1 B). Therefore, my initial results revealed that activating β-adrenergic receptors in macrophages reduced their lipolysis rate.

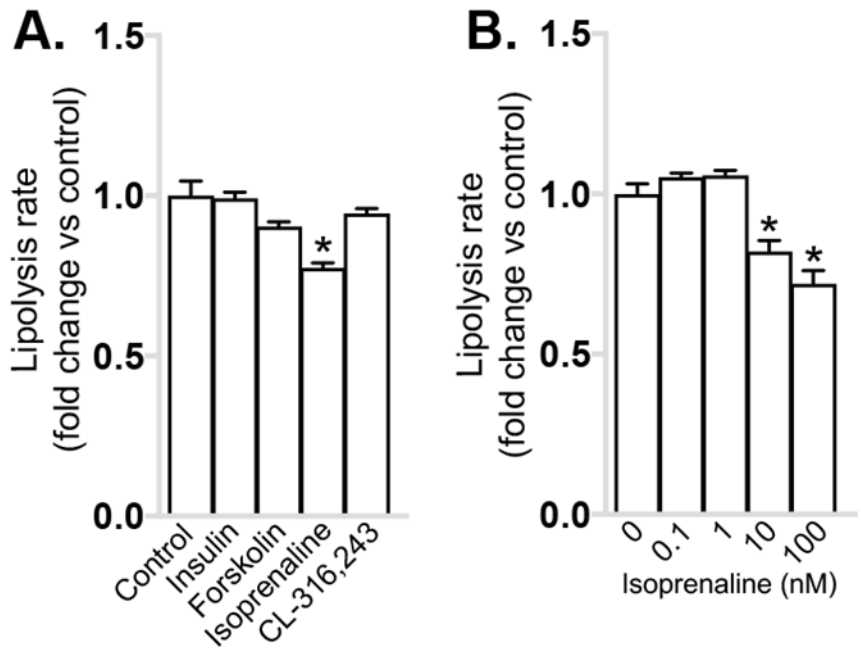

Figure 4-1. The effect of PKA activity modulators on the lipolysis rate in BMDMs. *Oleate release into the medium by BMDMs (pre-loaded with 250 μM oleate in the presence of ^{14}C-oleate tracer for 16 h) during 4 h post stimulation with (**A**) 100 nM insulin, 10 μM forskolin, 100 nM isoprenaline or 10 μM CL-316,243, or (**B**) indicated concentrations of isoprenaline. Lipolysis rate is expressed as specific activity of the medium of treated cells relative to untreated controls. N=4 mice/experiment. * p < 0.05 compared to control using one-way ANOVA with Bonferroni's multiple comparisons test.*

On the basis of this observation, together with the evidence that prolonged fasting leads to adipocyte lipolysis and lipid accumulation in ATMs[135,136] and given the fact that a mechanistic basis for such opposing effect has not yet been addressed, I hypothesised that NE released from nerve endings in WAT may play a dual role by activating lipolysis in adipocytes and inhibiting lipid release in ATMs. Therefore, I decided to gather more preliminary data that could justify studying the importance of β-adrenergic receptors in the regulation of ATM lipid metabolism.

4.1.2 Acquisition of preliminary data

4.1.2.1 β2AR activation increased TG storage in BMDMs

I initially sought to understand which isoform of β-adrenergic receptors may be the target of isoprenaline in BMDMs. Gene expression analysis revealed that *Adrb2* gene was transcribed, while *Adrb1* and *Adrb3* mRNA (encoding β1AR and β3AR,

respectively) could not be detected in BMDMs, suggesting that isoprenaline acted on β2AR.

In order to simulate a fasted state-like environment of ATMs, I treated BMDMs with NE for 10 min before placing them in the presence of 250 μM ^{13}C-oleate. The amount of exogenous oleate in the neutral lipid fraction of unstimulated cells was comparable between incubations lasting 8 and 24 h, suggesting that during initial 8 h of treatment BMDMs reached their limit of oleate storage within macrophage lipid droplets and did not further expand their TG pool (Figure 4-2). Interestingly, when macrophages were stimulated with NE, the amount of exogenous oleate was increased 2-fold after 8 h, and 3-fold after 24 h of incubation, indicating that NE enhanced TG storage capacity in BMDMs (Figure 4-2). Importantly, this stimulatory effect of NE was lost in the presence of β2AR-specific antagonist ICI-118,511, suggesting that NE modulated TG metabolism in BMDMs via its action on β2AR (Figure 4-2).

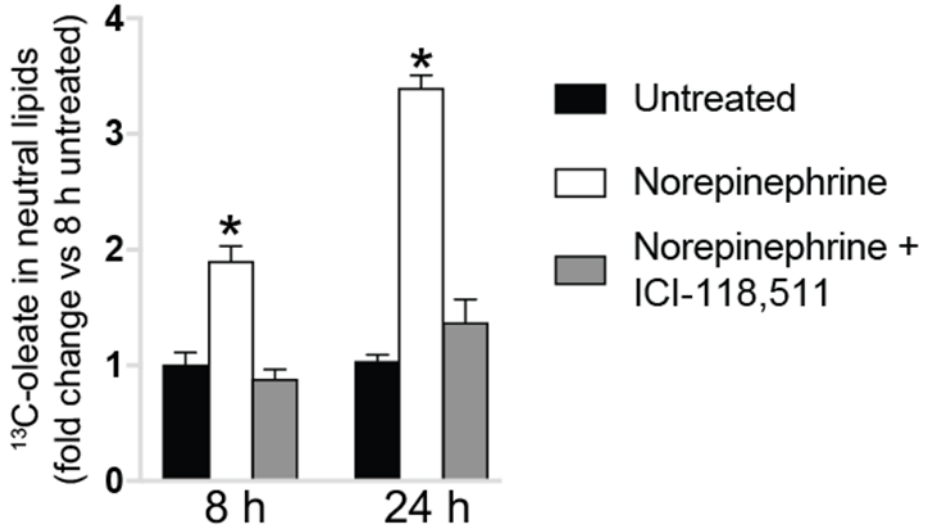

Figure 4-2. The effect of β2AR stimulation on the TG storage capacity in BMDMs. *GC-MS quantification of ^{13}C-oleate in the neutral lipid fraction of BMDMs stimulated with 1 μM NE (white bars) or with 1 μM NE and 1 μM ICI-118,511 (grey bars) for 10 min and then treated with 250 μM ^{13}C-oleate for 8 and 24 h. Values are normalised to the ^{13}C-oleate amount in the neutral lipid fraction of unstimulated cells (black bars) after 8 h of oleate loading. N=4 mice. * p < 0.05 compared to control at each time point using two-way ANOVA with Bonferroni's multiple comparisons test.*

4.1.2.2 Macrophage-activating stimuli down-regulated *Adrb2* gene expression in BMDMs

Next, I have investigated how different stimuli affected *Adrb2* gene expression in BMDMs. 1 h NE treatment reduced *Adrb2* mRNA levels in BMDMs, indicating a negative feedback on the receptor gene transcription upon its stimulation (Figure 4-3 A). This finding suggested that any potential reductions in *Adrb2* transcript observed *in vivo* might reflect elevated β2AR agonism at the time of sacrifice.

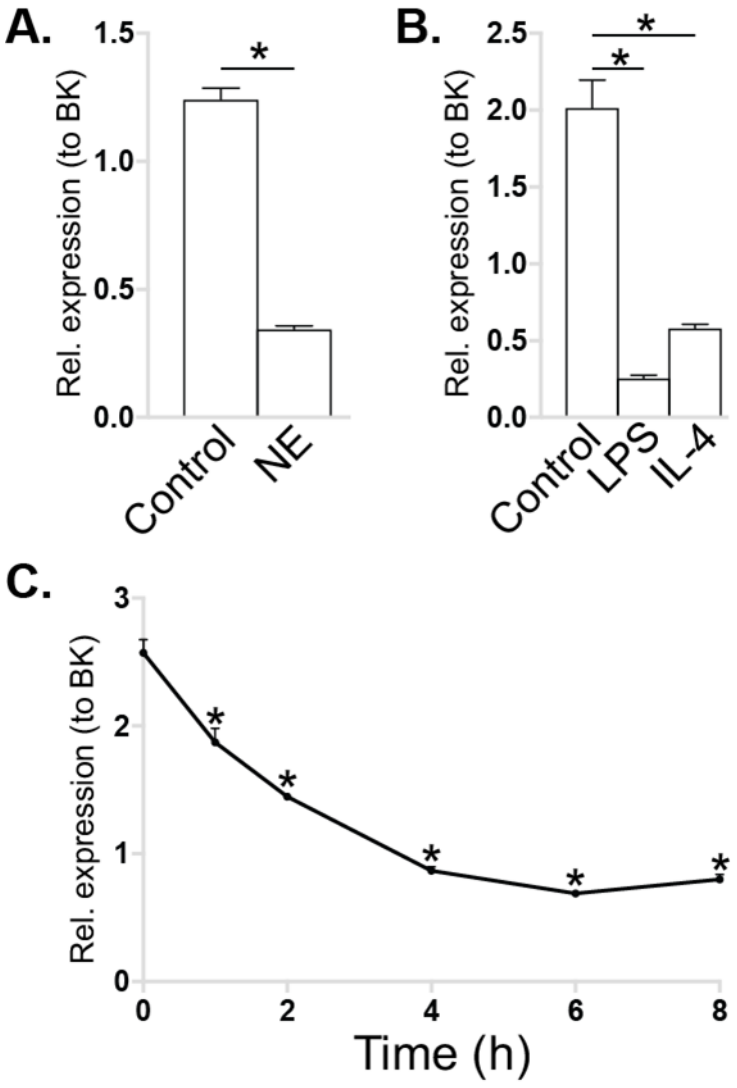

Figure 4-3. Regulation of Adrb2 gene transcription by NE, LPS, IL-4 and palmitate in BMDMs.

Adrb2 mRNA levels (normalised to BestKeeper) *in BMDMs treated with (**A**) 1 μM NE for 1 h, with (**B**) 100 ng/ml LPS or 10 μM IL-4 for 24 h, or with (**C**) 250 μM palmitate for indicated periods of time. N=4 mice/experiment. * p < 0.05 compared to 0 h using (**A**) student's t-test or (**B, C**) one-way ANOVA with Bonferroni's multiple comparisons test.*

Prolonged treatment with LPS and IL-4 potently decreased *Adrb2* transcription in BMDMs (Figure 4-3 B). High dose of palmitate also reduced *Adrb2* transcript levels in a time-dependent manner (Figure 4-3 C). **Overall, regardless of its inflammatory nature, macrophage activation suppressed *Adrb2* gene transcription**.

4.1.2.3 Characterisation of *Adrb2* gene expression in macrophages *in vivo*

In order to characterise the expression of *Adrb2* in different tissue macrophages, I isolated macrophages from lung, peritoneum, adipose tissues and liver, and included BMDMs for relative comparison. Compared to BMDMs, alveolar and peritoneal macrophages, **ATMs and liver CD11b-positive cells showed higher *Adrb2* mRNA levels** (Figure 4-4 A). Furthermore, as recently reported[459], ***Adrb2* gene expression was enriched in the ATM fraction within eWAT** (Figure 4-4 B).

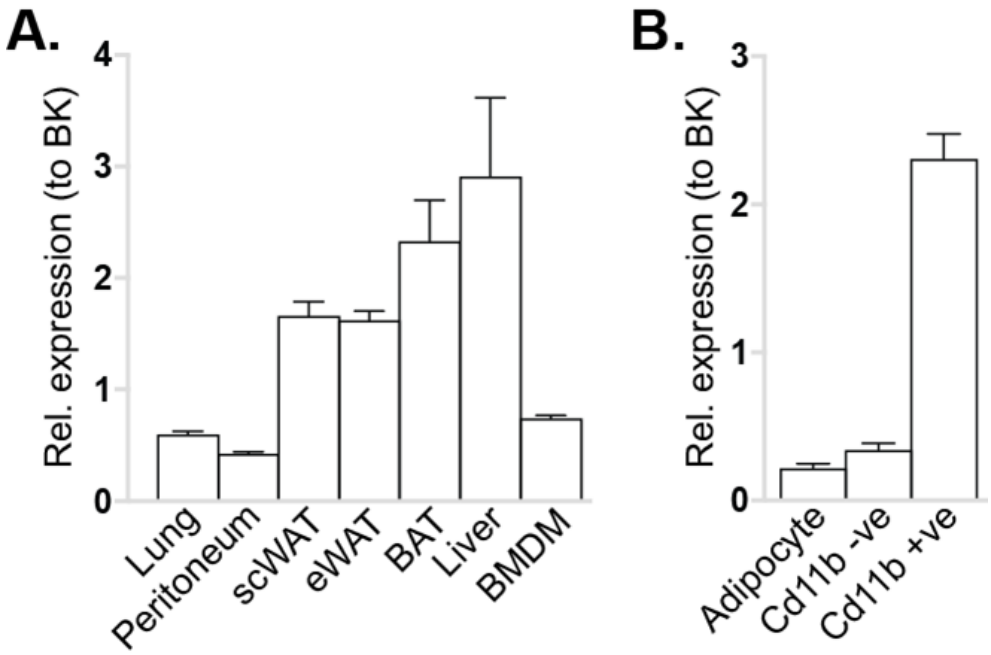

Figure 4-4. Adrb2 gene expression in tissue macrophages and eWAT cellular fractions.

Adrb2 mRNA levels (normalised to BestKeeper) *in (**A**) macrophages isolated from indicated tissues and BMDMs, or in (**B**) adipocyte, Cd11b-negative and Cd11b-positive eWAT cellular fractions. All macrophages in (**A**) were isolated from the same mice (8-week-old males, n=3, C57Bl/6J genetic background), with the exception of liver macrophages, which were isolated from separate age-, sex- and genetic background-matched animals (n=3). eWATs in (**B**) were isolated from 16-week-old males of C57Bl6/J genetic background (n=8). Statistical differences were not assessed.*

Next, I investigated whether 24 h of fasting could induce lipid accumulation in eWAT ATMs, as previously described[135,136]. Indeed, ATMs isolated from eWATs of fasted mice showed increased *Adrp* (also known as *Plin2*) mRNA levels compared to eWAT macrophages from fed mice, indicating increased amount of lipid droplets (Figure 4-5 A). However, fasting did not modulate *Adrb2* gene expression in ATMs (Figure 4-5 B).

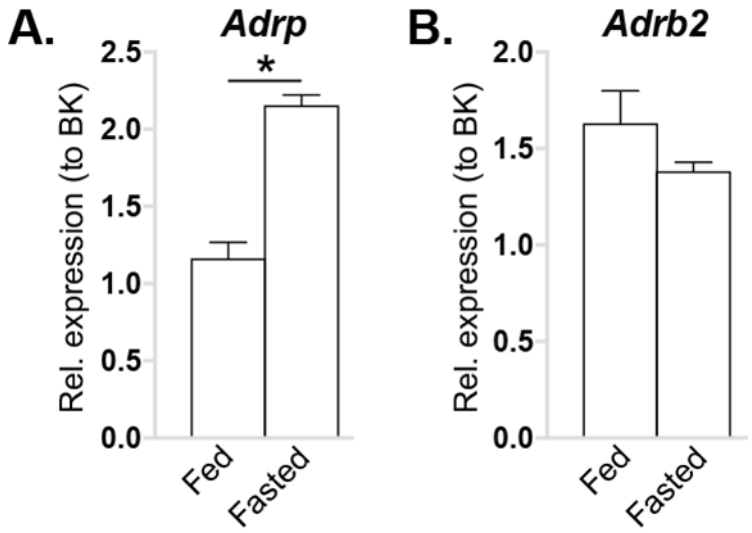

Figure 4-5. Adrp and Adrb2 gene expression in ATMs in fed and fasted states. *(**A**) Adrp (Plin2) and (**B**) Adrb2 mRNA levels* (normalised to BestKeeper) *in eWAT Cd11b-positive cells isolated from mice in a fed state or after 24 h of fasting. N=3 8-week-old C57Bl/6J males/condition. * p < 0.05 between two conditions using student's t-test.*

WAT function depends on the time of the day, where lipid storage predominates in the active phase and lipolysis - in the resting phase of the day. I therefore hypothesised that ATMs could be subjected to regular short periods of fasting-induced lipolysis every day. In order to validate this, I isolated scWAT cellular fractions at three distinct times of day. 9 am (3 h after lights on or zeitgeber time (ZT) 3) corresponded to an early period of resting phase, 3 pm (ZT 9) – to a late period of resting phase and 9 pm (ZT15) – to an early period of active phase. Increased SNS output to scWAT promotes its browning, which can be used as a molecular readout for local sympathetic nerve firing. As *Ucp1* mRNA in adipocytes is elevated upon NE stimulation[560], *Ucp1* gene expression in the adipocyte fraction can be used as a proxy for SNS activity in scWAT at the time of sacrifice.

Ucp1 and *Adrb3* genes showed highest levels of expression in the adipocytes at ZT3, indicating an elevated SNS output to scWAT during early period of resting phase (Figure 4-6 B). Interestingly, mRNA levels of *Adrp* and *Dgat1* were also increased at ZT3 in CD11b-positive cell fraction, suggesting that ATMs responded to enhanced local SNS activity by increasing their TG storage (Figure 4-6 A). Of relevance, *Adrb2* transcription in ATMs demonstrated an opposite regulation to *Ucp1* gene expression in adipocytes (Figure 4-6), indicating an activation-induced negative feedback on receptor gene transcription, as observed in BMDMs after the treatment with NE (Figure 4-3 A). **Overall, *Adrb2* mRNA in ATMs was regulated by feeding-fasting status of the animal, with the *Adrb2* transcript levels in the ATM fraction inversely correlating with the SNS output to scWAT**.

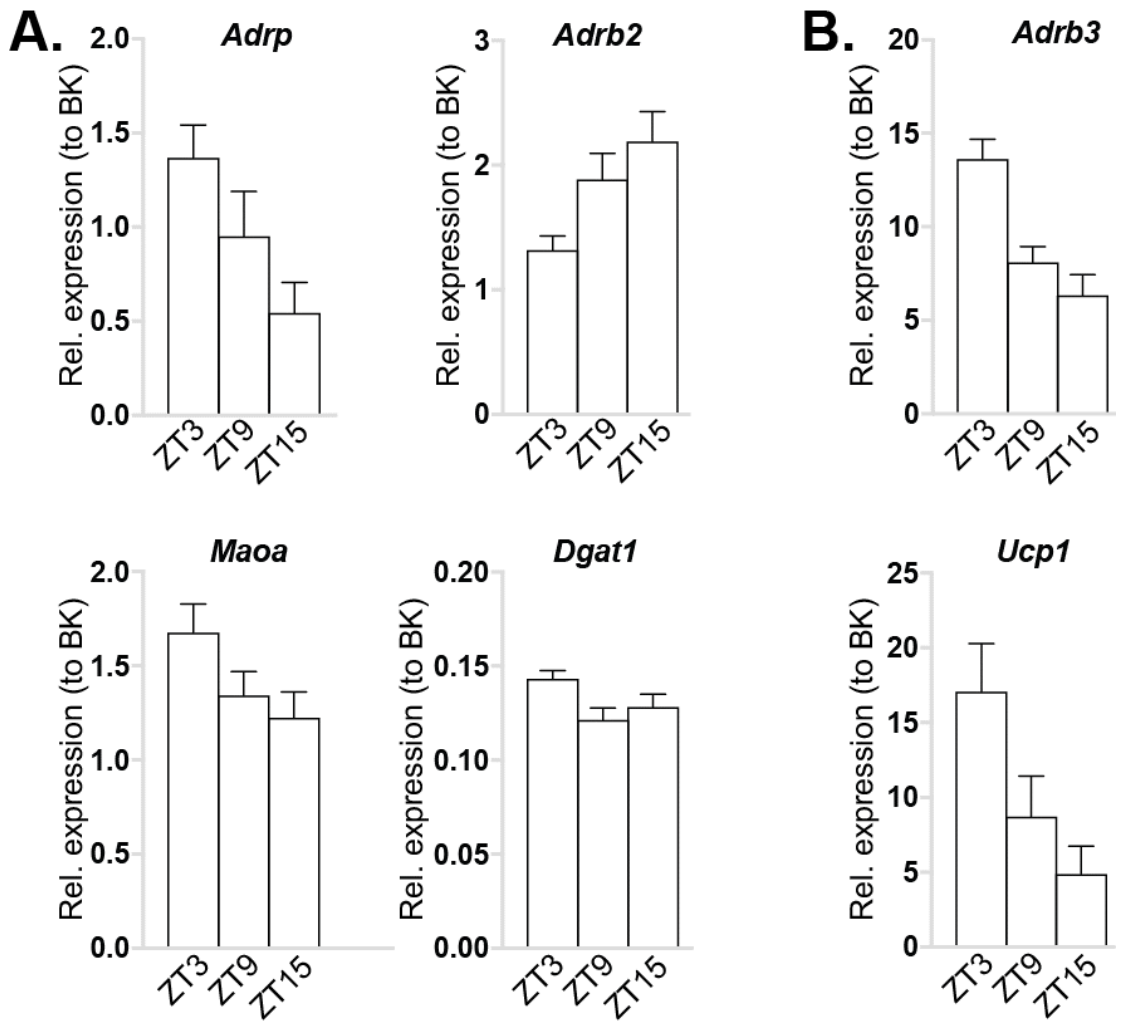

Figure 4-6. Time of day-dependent regulation of adrenergic and lipid metabolism gene transcription in ATMs and adipocytes.

*(**A**) Adrp, Adrb2, Maoa and Dgat1 mRNA levels* (normalised to BestKeeper) *in Cd11b-positive cell fraction, and (**B**) Adrb3 and Ucp1 mRNA levels* (normalised to BestKeeper) *in adipocyte fraction of scWATs isolated from mice at 9 am (ZT3), 3 pm (ZT9) and 9 pm (ZT15). Isolations were performed in two batches, with all time points in a single batch acquired on the same day. N=8 (two batches of 4) 8-week-old males of C57Bl/6J genetic background/time-point. All presented genes are significantly different ($p < 0.05$) for time variable when assessed by one-way ANOVA with Bonferroni's multiple comparisons test, with the exception of Maoa, where p=0.08.*

Chronic obesity is known to elevate peripheral SNS tone[561]. However, on-demand lipolysis in obese animals is supressed, in part due to adipocyte β-adrenergic receptor desensitisation[562]. Obesity has been previously shown to down-regulate *Adrb2* gene expression in ATMs[459]. In line with a published report[459], I found that prolonged high-

fat feeding increased pro-inflammatory cytokine *Tnf* and reduced M2 polarisation marker and *Adrb2* gene expression in macrophages isolated from eWAT (Figure 4-7). While it was not clear whether decreased *Adrb2* levels in ATMs during obesity are due to activation-induced receptor desensitisation, reduced β2AR-positive macrophage population or other unknown mechanisms, this finding indicated that **β2AR signalling in ATMs was affected by high-fat diet-induced obesity**.

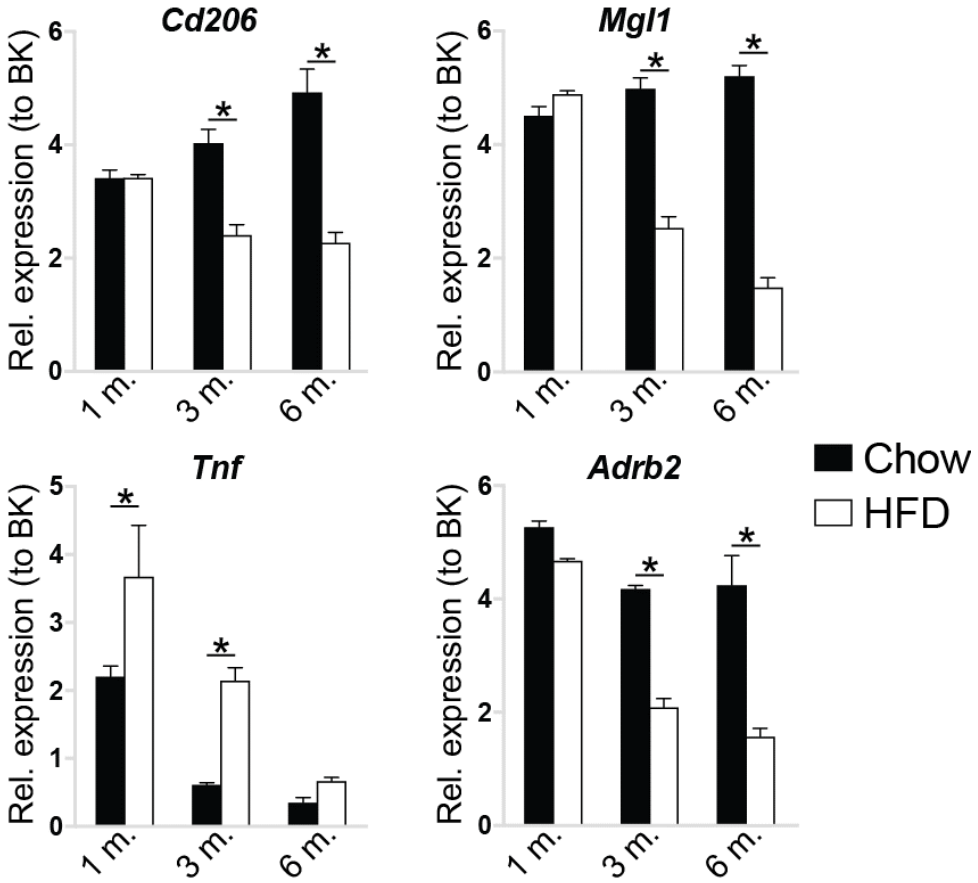

Figure 4-7. Expression of Adrb2 and macrophage polarisation marker genes in mice fed HFD for 1, 3 or 6 months.

The expression of M2 macrophage marker (Cd206, Mgl1), M1 macrophage marker (Tnf) and Adrb2 genes (normalised to BestKeeper) *in Cd11b-positive cell fraction of eWATs isolated from mice fed 45% kcal fat HFD (white bars) for 1, 3 or 6 months and from age-matched chow-fed controls (black bars). HFD was administered to mice from weaning. All mice were males of C57Bl/6J genetic background. N=4 (1 month chow), n=2 (1 month HFD), n=4 (3 months chow), n=5 (3 months HFD), n=2 (6 months chow), n=7 (6 months HFD). * p < 0.05 compared to chow-fed control at each time-point using two-way ANOVA with Bonferroni's multiple comparisons test. Tissue collections, cell isolations and RNA purifications were performed by a PhD student Crystal Mok.*

4.1.3 Research questions and aims

Overall, my ***preliminary data*** showed that macrophages isolated from WAT expressed high levels of *Adrb2* gene. Together with recent studies reporting a presence of sympathetic nerve-associated macrophages (SAMs) in BAT[425] and WAT[424,439], these findings suggested that the activity of β2AR-positive macrophages in a close proximity to sympathetic nerves within adipose tissues could be directly influenced by changes in the local sympathetic tone, similarly to intestinal macrophages[438]. The regulation of *Adrb2* expression in ATMs in a physiological and pathophysiological manner indicated that β2AR signalling could directly modulate ATM function *in vivo*. Furthermore, chemokine receptor property of β2AR[469,470] might be important for an appropriate localisation of SAMs to their neighbouring nerve fibres.

Despite extensive characterisation of changes in ATM lipid metabolism during obesity, physiological cues regulating macrophage lipid metabolism remain largely unknown. My preliminary results suggested that NE might regulate TG storage in ATMs in a physiological manner. In line with my findings, large scale gene transcription analysis from a recent report[424] showed that SAMs located in scWAT had higher expression levels of genes encoding TG-synthesising enzymes *Dgat1* and *Dgat2* than other analysed macrophage populations (Figure 4-8).

Finally, early experiments investigating circulating catecholamine clearance in living humans indicated that β-adrenergic receptor stimulation is required for efficient catecholamine degradation[563,564]. β2AR in SAMs might therefore act as a sensor for increased local SNS tone, leading to up-regulation of NE degradation machinery contributing to negative regulation of sympathetic nerve firing.

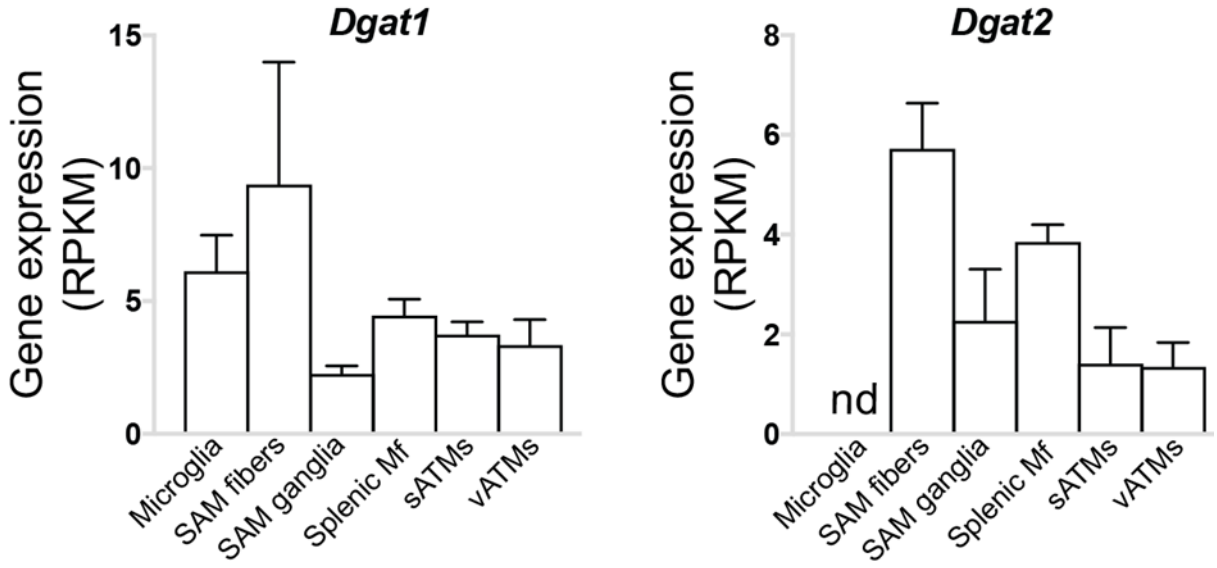

Figure 4-8. Expression of Dgat1 and Dgat2 genes in different tissue macrophage populations.

The expression of Dgat1 and Dgat2 genes in microglia (n=3), SAMs isolated from scWAT (SAM fibers) (n=2), SAMs isolated from superior cervical ganglia (SAM ganglia) (n=3), peritoneal (n=3), scWAT (n=2) and eWAT (n=2) ATMs. Macrophage populations were isolated and analysed as described in a recent report[424]*. Data was obtained from Gene Expression Omnibus database (GSE103847). Values are expressed as reads per kilobase of transcript per million of mapped reads (RPKM) + SEM. Statistical differences were not assessed.*

Based on the available literature and my preliminary data, the research questions of this chapter can be formulated as follows:

1) Does NE signalling via β2ARs in macrophages alleviate the pro-inflammatory effects of FFAs by partitioning them towards TG storage within lipid droplets? 2) Does β2AR signalling in macrophages affect the development of WAT inflammation and insulin resistance during obesity? 3) Do β2ARs in ATMs regulate SNS tone in WAT by mediating NE uptake and degradation?

The research questions of this chapter are summarised in Figure 4-8

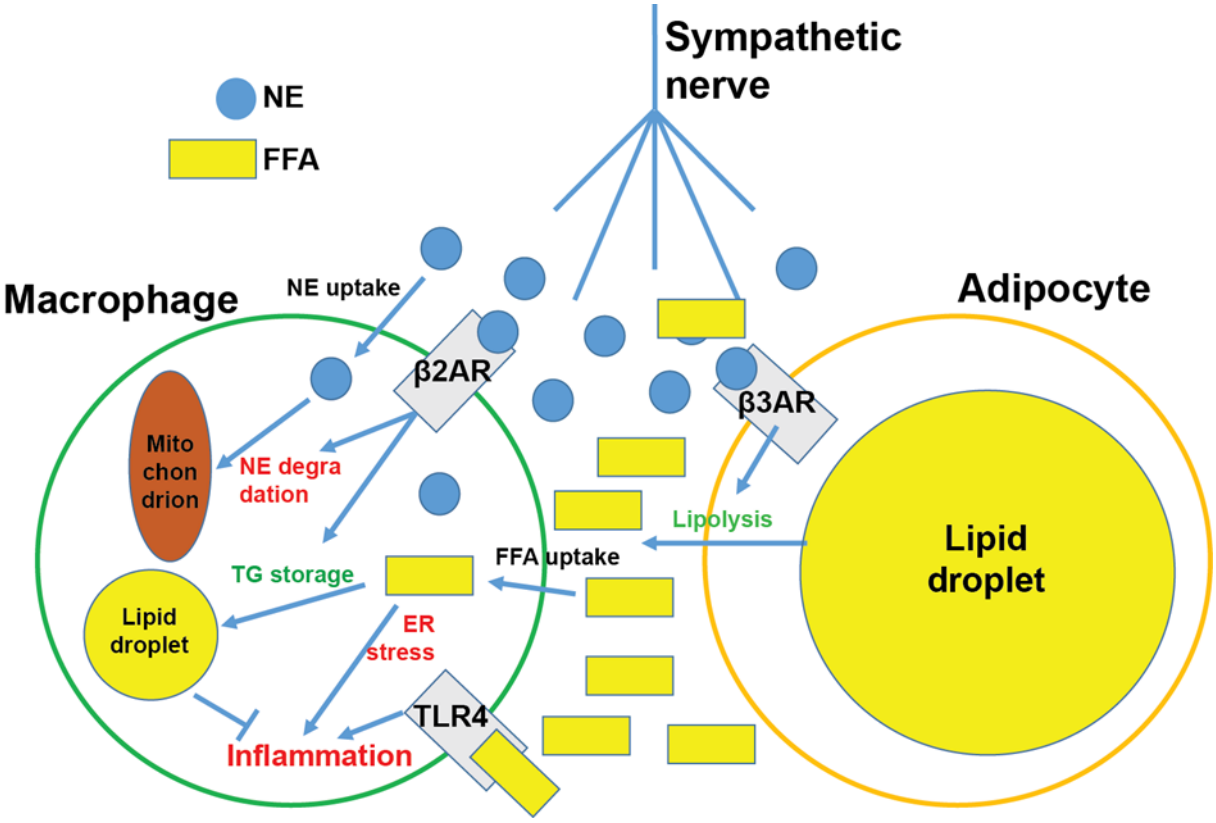

Figure 4-9. Schematic representation of a dual role of norepinephrine signalling in adipose tissues.

NE secreted from sympathetic nerves in adipose tissues simultaneously stimulate macrophage β2ARs and adipocyte β3ARs. β3AR stimulation promotes FFA release from adipocytes, while β2AR stimulation counteracts the inflammatory effects of FFAs by increasing TG storage, and enhances NE degradation in mitochondria. Pathways in green represent beneficial, while pathways in red – detrimental processes for WAT function that occur during obesity.

In this chapter, I will aim to address my research questions in two objectives:

***Objective 1*. To identify and characterise the molecular mechanisms through which β2AR activation leads to increased TG storage in macrophages and to determine whether β2AR activation can protect macrophages from palmitate-induced ER stress and inflammation**. This will be performed by tracing radiolabelled fatty acid fluxes within intracellular lipid pools of BMDMs treated with β2AR agonists.

Objective 2*. To assess the impact of the loss of macrophage β2AR signalling on the function of metabolic tissues in lean and obese states *in vivo. To address this, I will utilise a mouse model with macrophage-specific *Adrb2* deletion to study the metabolic effects of β2AR signalling in macrophages during states of elevated SNS tone in adipose tissues, namely cold exposure. I will also subject mice lacking β2AR in macrophages to prolonged high-fat feeding and assess their energy balance, glucose and lipid metabolism. Livers and adipose tissues from *in vivo* experiments will be analysed for metabolic and inflammatory gene expression in order to assess the importance of macrophage β2AR signalling for tissue metabolism and inflammation during states of elevated SNS tone and obesity.

Expected impact. The data obtained from both aims would be beneficial to the field of metabolism in multiple ways.

Firstly, unravelling a novel pathway regulating macrophage TG metabolism could contribute to our understanding of molecular mechanisms leading to the development of lipid-induced inflammation in macrophages observed during obesity and atherosclerosis.

Secondly, my findings would follow up on recent reports regarding nerve-macrophage interactions in small intestine and adipose tissues by providing an insight into how increased firing of neighbouring sympathetic neurons affect macrophage lipid metabolism.

Third, as human polymorphisms in the coding region of *ADRB2* gene have been linked to increased rates of obesity, dyslipidaemia and insulin resistance[514], this chapter could provide insight on the contribution of β2ARs in macrophages to the development of such metabolic traits in the *ADRB2* polymorphism carriers. Finally, β2AR is one of the best characterised GPCR, and there are numerous pharmaceuticals that agonise or block this receptor with high selectivity, including novel intracellular allosteric antagonists[565]. Therefore, depending on the results obtained from Objective 2, macrophage-specific targeting of β2AR could be considered as a therapeutic approach to treat obesity, MetS or other disorders in which SNS tone is altered.

4.2 Results

4.2.1 Molecular mechanisms driving increased TG accumulation in response to β2AR stimulation in BMDMs

4.2.1.1 β2AR agonist stimulated the transcription of CREB target genes, including *Dgat1* in BMDMs

***Rationale*.** Most publications regarding the effects of macrophage β2AR agonism have focused either on its immunomodulatory role during LPS treatment, or investigated the phenotype of macrophages that had been treated with β2AR agonist for a prolonged period of time (24 h). Since my preliminary experiments showed that β2AR activation suppressed lipolysis in BMDMs within the first 4 h of stimulation, I rationalised that the early signalling events leading up to changes in BMDM TG metabolism would be important. Thus I initially sought to understand the specificity and signalling kinetics of β2AR stimulation in BMDMs.

As β-adrenergic stimulation is well known to induce CREB phosphorylation and promote the expression of CREB target genes, I performed a time-course stimulation of BMDMs with the β2AR-specific agonist fenoterol in order to determine the kinetics of CREB-dependent gene transcription upon β2AR activation. As readouts for CREB transcriptional activity, I chose four CREB target genes with a known function in macrophages: a) *Nr4a1* (encoding transcription factor Nur77, which is a negative regulator of inflammation in macrophages); b) *Klf4* (encoding a transcription factor that promotes M2 polarisation in macrophages); c) *Cox2* (encoding an enzyme cyclooxygenase-2, involved in the synthesis of prostaglandins that diminish macrophage inflammatory activation); d) *Dusp1* (encoding an enzyme dual specificity protein phosphatase 1, which dephosphorylates JNK and p38 kinases, therefore limiting macrophage inflammatory activation).

***Results*.** All four canonical CREB target genes showed the same expression profile upon β2AR activation, characterised by a sharp immediate increase in mRNA levels that reached their peak of expression at approximately 1 h, and returned backed to baseline at approximately 3 h post stimulation (Figure 4-10). This finding indicated a rapid and transient activation of CREB-dependent gene transcription upon β2AR activation.

Next, I utilised CREB target gene prediction tool (http://natural.salk.edu/CREB/) to

identify enzymes involved in TG biosynthesis containing CRE sequence in their promoters. *Dgat1* gene was predicted to be regulated by CREB, which was also confirmed in a study demonstrating the up-regulation of DGAT1 protein expression through the recruitment of CREB-CRTC complex to *Dgat1* gene promoter in skeletal myocytes in response to isoprenaline[566]. Indeed, *Dgat1* mRNA levels increased following β2AR activation in BMDMs, peaking at 2 h and returning to baseline at 8 h post stimulation (Figure 4-10).

Furthermore, As recent reports have assigned a major role for LAL in macrophage lipolysis[238], I also measured *Lipa* gene expression in fenoterol-treated BMDMs. Consistent with a reduced rate of fatty acid release from lipid-laden BMDMs, β2AR activation progressively reduced *Lipa* transcript levels until 6 h post stimulation (Figure 4-10).

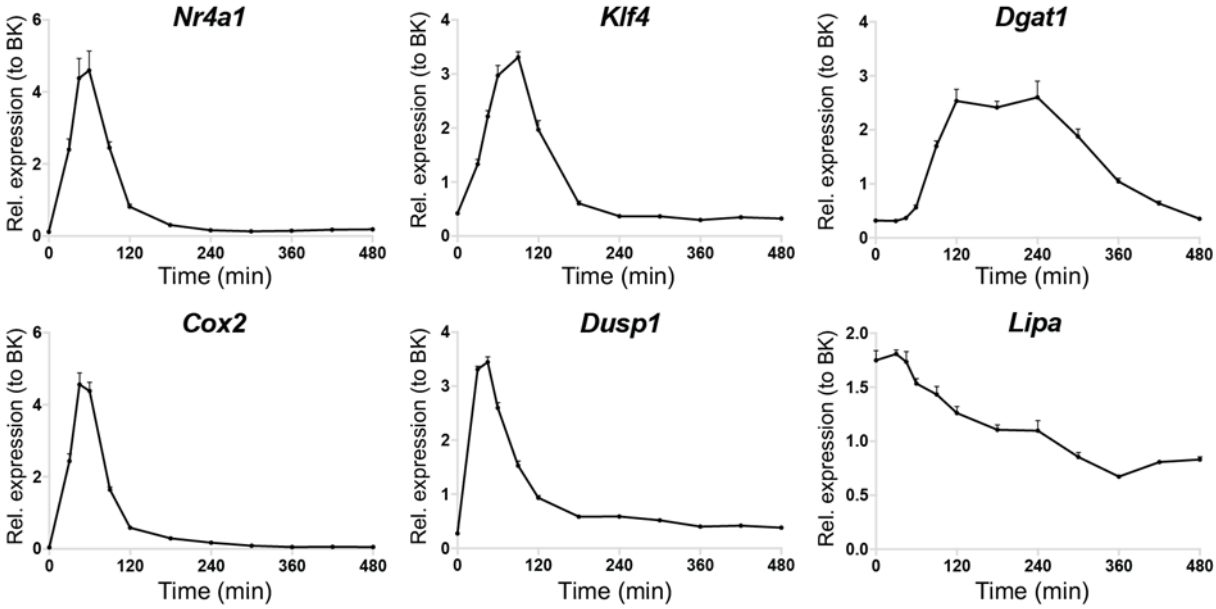

Figure 4-10. Regulation of CREB target gene transcription in BMDMs in response to β2AR stimulation by fenoterol.

Nr4a1, Cox2, Klf4, Dusp1, Dgat1 and Lipa mRNA levels (normalised to BestKeeper) *in BMDMs treated with 1 μM fenoterol for 0, 30, 45, 60, 90, 120, 180, 240, 300, 360, 420 or 480 min. N=4 mice. Statistical differences were not assessed.*

4.2.1.2 NE and fenoterol activated CREB transcription specifically via β2AR

***Rationale*.** In order to ensure that fenoterol specifically acted on β2ARs in BMDMs, and that the observed outcome on gene transcription and TG metabolism was not due to off-target effects, I studied BMDMs from mice lacking β2AR specifically in macrophages.

Results. Treating control BMDMs with fenoterol for 20 min potently induced the activatory phosphorylation of CREB and another cAMP-activated transcription factor ATF1 (Figure 4-11). Importantly, fenoterol had no effect on CREB and ATF1 phosphorylation in LysM-Cre Adrb2$^{fl/fl}$ BMDMs, indicating its specificity to β2ARs (Figure 4-11).

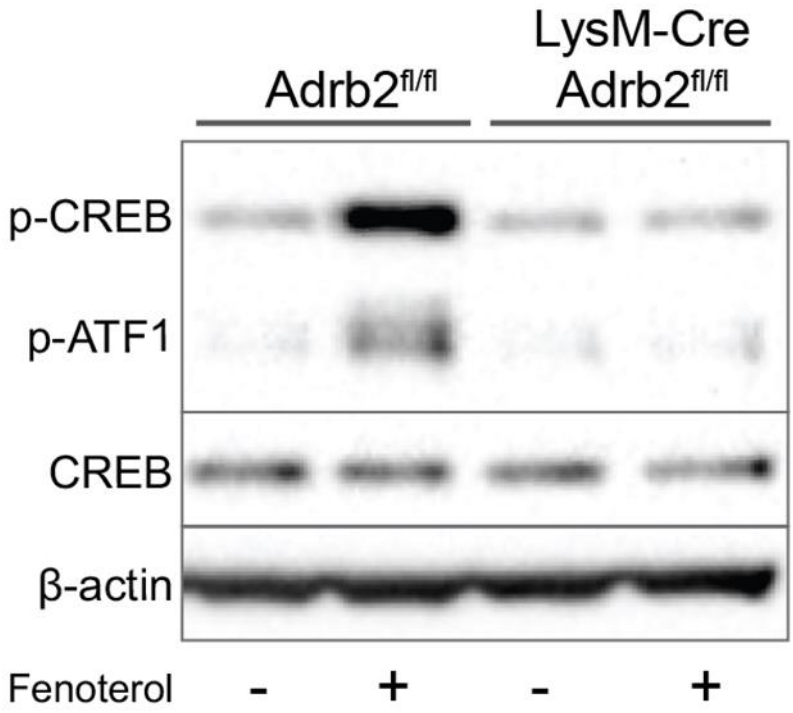

Figure 4-11. CREB phosphorylation in control and LysM-Cre Adrb2$^{fl/fl}$ BMDMs in response to β2AR stimulation by fenoterol.

Representative Western blots (out of 4 mice/group) of p-Ser133 CREB and p-Ser63 ATF1 (detected by the same antibody due to the sequence similarity surrounding phosphorylation sites), total CREB and β-actin proteins in Adrb2$^{fl/fl}$ and LysM-Cre Adrb2$^{fl/fl}$ BMDMs stimulated with 1 μM fenoterol for 20 min.

Next, I stimulated BMDMs with NE in the presence or absence of β2AR-specific antagonist ICI-118,511 to validate whether NE could invoke similar effects on gene transcription as fenoterol in a β2AR-specific manner. Indeed, treatment of NE mimicked the effects of fenoterol on *Dgat1* and *Lipa* gene transcription in BMDMs, and the observed response to NE was completely blocked in the presence of ICI-118,511 (Figure 4-12).

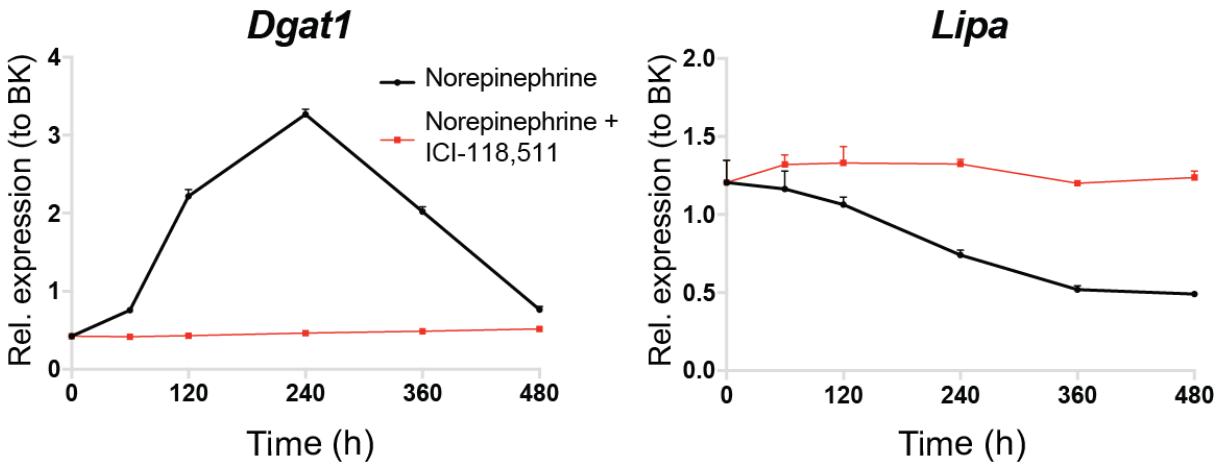

Figure 4-12. Regulation of Dgat1 and Lipa gene expression in BMDMs in response to β2AR stimulation by NE.

Dgat1 and Lipa mRNA levels (normalised to BestKeeper) in BMDMs treated with 1 μM NE alone (black lines) or 1 μM NE and 1 μM ICI-118,511 (red lines) for 0, 1, 2, 4, 6, and 8 h. N=4 mice. Statistical differences were not assessed.

Finally, I treated LysM-Cre Adrb2$^{fl/fl}$ and control BMDMs with fenoterol and different concentrations of NE and measured CREB target gene expression. While in control cells NE potently induced *Nr4a1* and *Dgat1* gene expression in a dose-dependent manner at 1 and 4 h, respectively, the effects of NE and fenoterol were completely absent in β2AR-deficient BMDMs (Figure 4-13 A,B).

***Conclusion*.** The effects of NE and fenoterol on CREB phosphorylation and gene transcription were specific to β2AR stimulation in BMDMs.

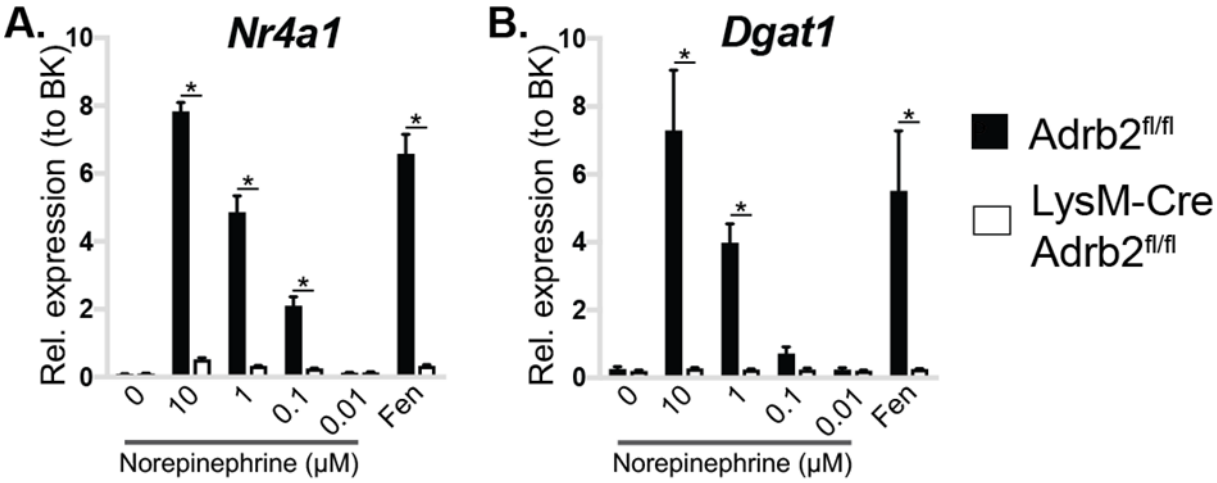

Figure 4-13. Nr4a1 and Dgat1 gene expression in LysM-Cre Adrb2$^{fl/fl}$ BMDMs stimulated with fenoterol and different doses of NE.

*(**A**) Nr4a1 mRNA levels (normalised to BestKeeper) after 1 h of stimulation, and (**B**) Dgat1 mRNA levels (normalised to BestKeeper) after 4 h of stimulation of Adrb2$^{fl/fl}$ (black bars) and LysM-Cre Adrb2$^{fl/fl}$ (white bars) BMDMs with indicated doses of NE or 1 μM fenoterol. N=4 mice/group. * p < 0.05 compared between genotypes using 2-way ANOVA with Bonferroni's multiple comparisons test.*

4.2.1.3 β2AR activation rapidly supressed the release of intracellular oleate in BMDMs independently of TG hydrolysis, lipophagy or re-esterification

Rationale. My preliminary experiments have already shown reduced release of intracellular oleate from BMDMs during initial 4 h after β2AR activation (Figure 4-1). However, these experiments were not informative in terms of kinetics of oleate release from BMDMs. In the attempt to understand how β2AR stimulation delays the kinetics of oleate release, I performed a frequent sampling of the medium from oleate-loaded BMDMs following β2AR activation.

***Results*.** As published previously[567], oleate release rate from unstimulated cells progressively reduced over time after medium change, which is a consequence of increased extracellular oleate concentration, leading to its increased rate of re-uptake and re-esterification (Figure 4-14 A,B).

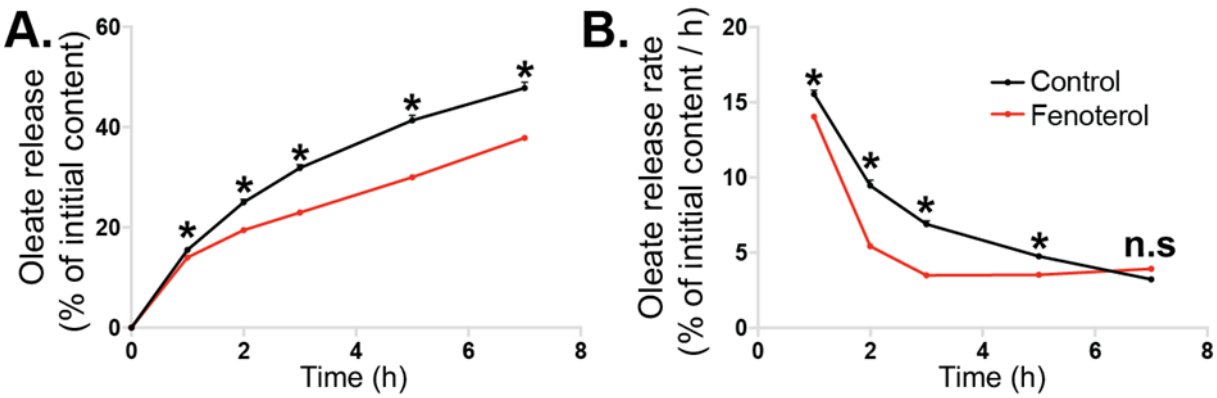

Figure 4-14. Kinetics of oleate release from BMDMs following β2AR activation. *Oleate release into the medium by BMDMs (pre-loaded with 250 μM oleate in the presence of ^{14}C-oleate tracer for 16 h) 1, 2, 3, 5 and 7 h post medium change in the presence (red lines) or absence (black lines) of 1 μM fenoterol. Lipolysis rate is expressed as (**A**) a percentage of specific activity measured in the medium at the time of sampling compared to total initial specific activity (the sum of the specific activity of the medium at the final time-point of sampling and total cellular specific activity), or as (**B**) a rate of oleate release (calculated by dividing the difference of specific activity in the medium between two subsequent time-points by the difference of sampling time between the same time-points). N=4 mice. T=0 represents background radioactivity. * p < 0.05 compared to control at each time-point using two-way ANOVA with Bonferroni's multiple comparisons test.*

The suppression of oleate release from BMDMs by β2AR activation was already evident at 1 h following medium change and stimulation with fenoterol (Figure 4-14 A). However, the most prominent change in oleate release rate occurred between 1 and 3 h after β2AR activation (Figure 4-14 B). The effects of NE on the oleate release rate from BMDMs were comparable to the effects of fenoterol, and they were prevented in the presence of β2AR-specific blocker, indicating a β2AR signalling-specific event (Figure 4-15 A).

***Rationale*.** In order to identify the intracellular processes that mediate the inhibitory effects of β2AR activation on oleate release, I utilised the following inhibitors: A922500, in order to inhibit DGAT1 and prevent the re-esterification of released oleate; orlistat, to inhibit TG lipases; bafilomycin A1, to block autophagy, thus preventing lipid droplet fusion with lysosomes (lipophagy).

***Results*.** As expected, inhibiting DGAT1 increased (Figure 4-15 B), while blocking autophagy and the action of TG lipases reduced the rate of oleate release from BMDMs (Figure 4-15 C,D). However, all the inhibitors still elicited an effect of comparable magnitude in β2AR agonist-treated BMDMs (Figure 4-15 B-D).

***Conclusion*.** The inhibitory action on oleate release by β2AR activation did not depend on facilitated fatty acid re-esterification, or inhibition of TG lipases or autophagy.

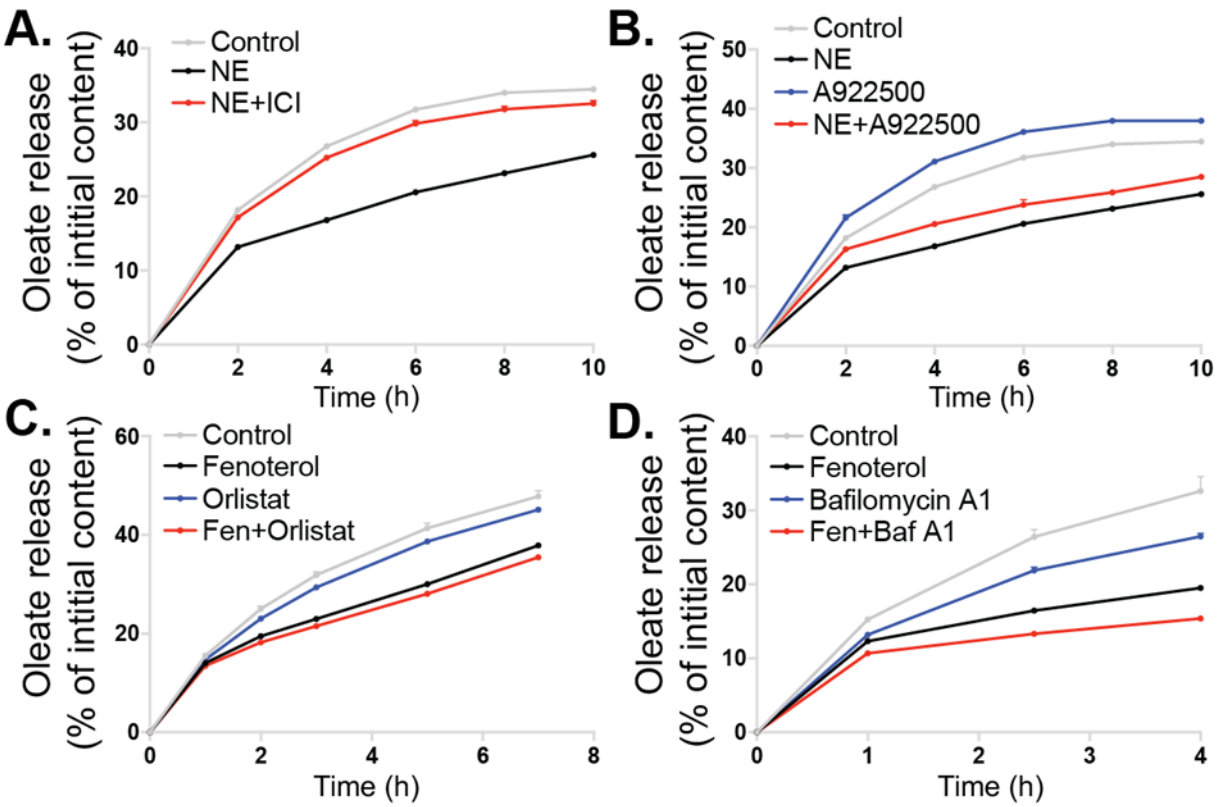

Figure 4-15. The effect of triglyceride synthesis, lipolysis and autophagy inhibitors on β2AR-mediated suppression of oleate release from BMDMs.

*Oleate release into the medium by BMDMs (pre-loaded with 250 μM oleate in the presence of ^{14}C-oleate tracer for 16 h) at indicated time-points post medium change. BMDMs were pre-treated with (**A**) 1 μM ICI-118,511, (**B**) 1 μM A922500, (**C**) 10 μM orlistat and (**D**) 100 nM bafilomycin A1 for 30 min before medium change and treatment with either (**A, B**) 1 μM NE or (**C, D**) 1 μM fenoterol. N=4 mice/experiment. Within each graph, grey lines represent control cells, and black, blue and red lines – stimulation with β2AR agonist alone, treatment with inhibitor alone, or co-treatment with β2AR agonist and inhibitor, respectively. In all graphs, each treatment was significantly different from every other treatment at all measured time-points (except T=0, which represents background radioactivity) when analysed using two-way ANOVA with Bonferroni's multiple comparisons test. Statistical differences are not visually indicated.*

4.2.1.4 Acute β2AR activation diminished oleate oxidation in BMDMs

***Rationale*.** As β2AR stimulation supressed the rate of intracellular oleate release, I wanted to evaluate whether activating β2AR could also decrease the rate of FAO in BMDMs. In order to test this, I optimised an assay to assess the rate of exogenous FAO in BMDMs, involving incubating cells with 100 μM of fatty acid containing ^{14}C-labelled tracer in a hermetically sealed plate in order to trap CO_2 in the medium. $^{14}CO_2$ can then be extracted from the medium and quantified, corresponding to complete β-oxidation of exogenous fatty acids, which predominantly occurs in mitochondria.

***Results*.** As expected, acute treatment with etomoxir (CPT1 inhibitor) reduced the rate of both palmitate and oleate oxidation, and prolonged LPS stimulation diminished the rate of oleate oxidation in BMDMs (Figure 4-16 A,B). Interestingly, while β2AR stimulation by NE did not affect the rate of palmitate oxidation, it rapidly decreased the rate of oleate oxidation (Figure 4-16 A,B).

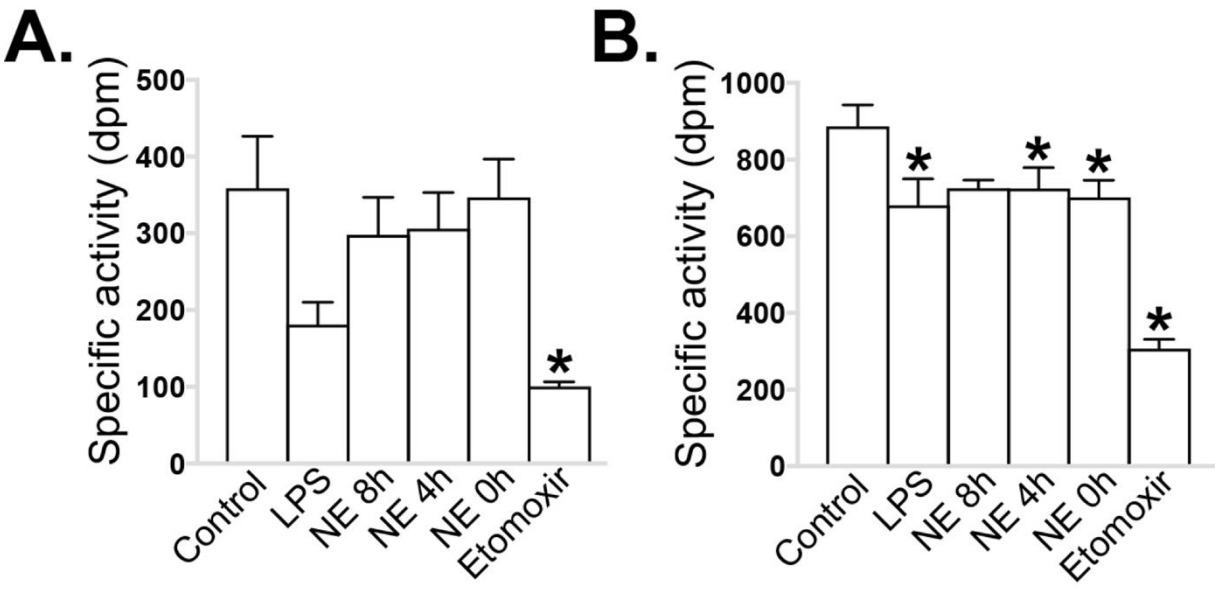

Figure 4-16. The oxidation of exogenous palmitate and oleate in response to β2AR activation in BMDMs.

*(**A**) 100 μM palmitate and (**B**) 100 μM oleate oxidation in WT BMDMs (n=4 mice), pre-treated with 100 ng/ml LPS for 24 h, 1 μM NE for 8, 4 or 0 h, or 100 μM etomoxir for 30 min and incubated for 3 h in a hermetic manner. Values are expressed as specific activity of captured $^{14}CO_2$ from the medium during 3 h incubation. * $p < 0.05$ compared to control using one-way ANOVA with Bonferroni's multiple comparisons test.*

4.2.1.5 β2AR activation increased TG storage in a predominantly DGAT1-dependent manner

***Rationale*.** My initial observations also included the increase in BMDM TG storage capacity in response to β2AR activation (Figure 4-2). However, as such effect was observed following 8 and 24 h of β2AR activation, it was not clear whether it occurred due to the same mechanism(s) that mediated the suppression of oleate release and/or oxidation from BMDMs (Figure 4-14, Figure 4-15), or via an alternative process.

As I have measured a substantial increase in *Dgat1* mRNA after β2AR stimulation, I decided to assess whether this transcriptional change also translated to an increased DGAT enzymatic activity. For this, I adapted a recently published gas chromatography-based assay, involving measuring fatty acyl-CoA esterification rate to sn-1,2-dioctanoylglycerol substrate in the presence of cellular microsomes[541]. Due to the distinct elution times of the reaction products sn-1,2-dioctanoyl-3-palmitoylglycerol and sn-1,2-dioctanoyl-3-oleoylglycerol, I was able to simultaneously measure the esterification rates of palmitoyl-CoA and oleoyl-CoA substrates in a single reaction. Furthermore, during the assay optimisation in BMDMs, I found that both palmitoyl-CoA and oleoyl-CoA esterification could be completely inhibited by DGAT1-selective inhibitor A922500, indicating a predominant role of DGAT1 isoform in catalysing TG condensation in BMDMs (data not shown).

***Results*.** Previous gene expression analysis of BMDMs treated with LPS or IL-4 for 24 h performed in our lab showed that *Dgat1* mRNA levels were not modulated by the polarisation of macrophages towards M1 or M2 states (data not shown). Consistent with such findings, DGAT activity towards palmitoyl-CoA and oleoyl-CoA was unchanged after prolonged treatment with LPS or IL-4, compared to untreated BMDMs (Figure 4-17 A,B). In line with an observed increase in *Dgat1* mRNA, I found a 2-fold increase in DGAT activity for both palmitoyl-CoA and oleoyl-CoA in BMDMs 8 h after β2AR activation (Figure 4-17 A,B). DGAT activity for both substrates remained elevated even 24 h after β2AR activation, showing a 50% increase compared to untreated BMDMs (Figure 4-17 A,B).

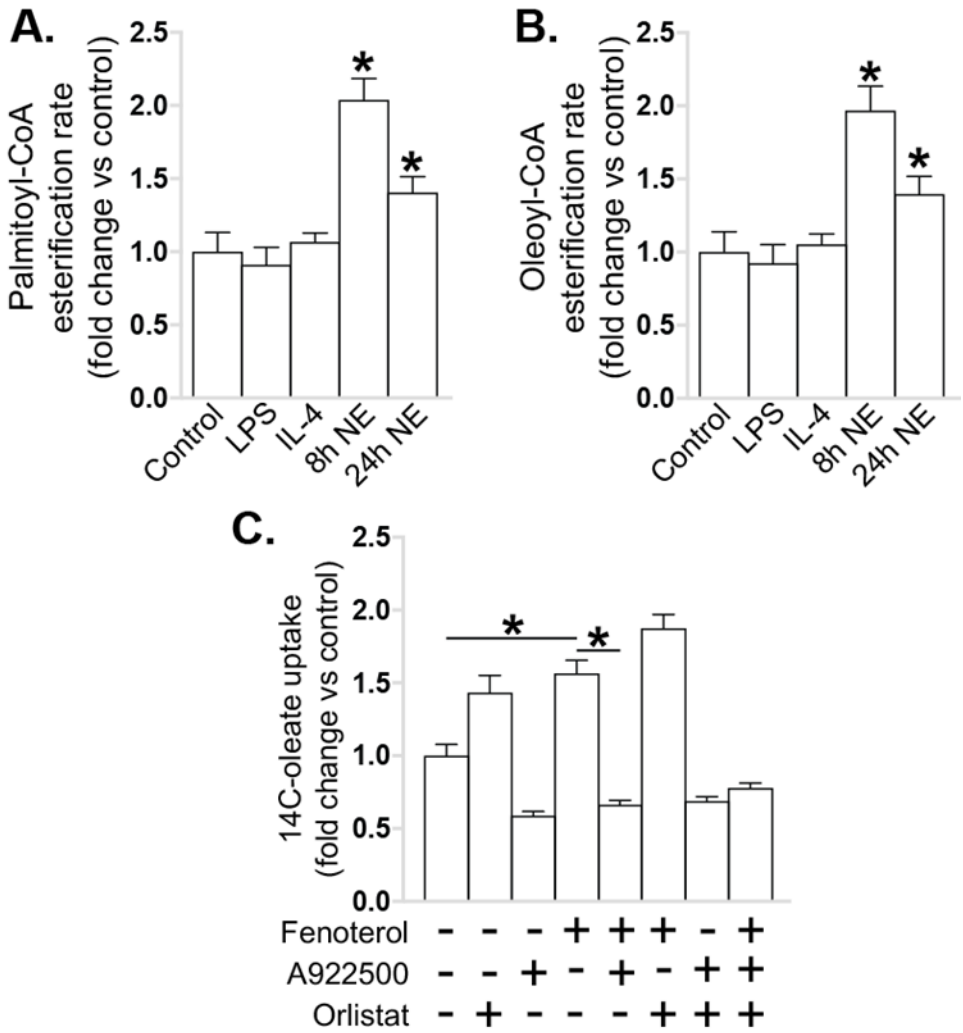

Figure 4-17. DGAT1 activity-dependent oleate uptake in BMDMs following β2AR activation.

*DGAT activity in the microsomal fraction of BMDMs stimulated with 100 ng/ml LPS or 10 μM IL-4 for 24 h, or 1 μM NE for 8 or 24 h, using (**A**) palmitoyl-CoA or (**B**) oleoyl-CoA as a substrate. Esterification rate is expressed as fold change from untreated cells. (**C**) Oleate uptake by BMDMs, stimulated with 1 μM fenoterol, 1 μM A922500 or 10 μM orlistat, as indicated below the graph, and treated with 250 μM oleate in the presence of ^{14}C-oleate tracer for 16 h. Oleate uptake is expressed as a fold change in specific activity of stimulated cells from unstimulated controls. N=4 mice/experiment. * p < 0.05 compared to (**A, B**) control or (**C**) between indicated columns using one-way ANOVA with Bonferroni's multiple comparisons test. In (**C**), the following comparisons were also significantly different but not visually indicated: Ctrl vs orl/ fen + orl; A922 vs every other column (except ctrl), fen vs A922 + orl/ fen + A922 + orl; fen + orl vs fen + A922/ A922 + orl/ fen + A922 + orl; fen + A922 vs fen + A922 + orl; A922 + orl vs fen + A922 + orl.*

***Rationale*.** Next, I wanted to investigate whether increased DGAT1 activity was mediating enhanced oleate uptake in β2AR agonist-treated BMDMs. To test this, I stimulated cells with fenoterol in the presence of DGAT1 inhibitor A922500. In order to rule out the role TG lipases as targets of β2AR action in BMDMs, I also co-treated the cells with β2AR agonist and orlistat.

***Results*.** As expected, blocking DGAT1 activity reduced the overall BMDM oleate uptake by approximately 50% (Figure 4-17 C). The remaining 50% of specific activity within the cell was likely due to oleate incorporation into phospholipids, as reported previously[233]. In contrast, orlistat enhanced exogenous oleate content within BMDMs by approximately 40%, presumably caused by an increased TG retention within intracellular lipid droplets (Figure 4-17 C). While fenoterol still invoked an increase in oleate uptake in the presence of A922500 and orlistat, the magnitude of the increase was greatly reduced when A922500 was present (Figure 4-17 C, 56% increase in fenoterol-treated cells compared to control, and 13% increase in fenoterol + A922500-treated cells compared to A922500 alone). Orlistat also diminished the magnitude of the increase in oleate uptake (Figure 4-17 C, 31% fenoterol + orlistat-treated cells compared to orlistat alone). Co-treatment of cells with A922500 and orlistat had a similar effect to A922500 treatment alone (Figure 4-17 C, 13% increase in fenoterol + A922500 + orlistat compared to A922500 + orlistat alone).

Conclusion. DGAT1 activity could account for the majority of β2AR agonism-elicited effects on the oleate uptake in BMDMs.

***Rationale*.** Finally, I decided to directly assess the effect of β2AR activation on BMDM TG storage, and whether it was mediated by increased DGAT1 activity. I stimulated BMDMs with fenoterol in the presence of A922500 and loaded them with radiolabelled palmitate and oleate.

***Results*.** β2AR activation or DGAT1 inhibition did not change the levels of intracellular FFAs or 1,3-DAGs in BMDMs loaded with either oleate or palmitate (total lipid staining, Figure 4-18, Figure 4-19). However, the radiolabelled FFA, 1,2- and 1,3-DAG species were increased in BMDMs following β2AR activation, suggesting an increased flux through lipid metabolic pathways that utilise such molecules as reaction intermediates (radiogram, Figure 4-18, Figure 4-19).

Consistent with my previous findings, I observed a profound increase in overall TG levels in BMDMs after β2AR activation and incubation with oleate, that could be mainly attributed to exogenous oleate incorporation, as indicated by increased TG radiolabelling (Figure 4-18). While TG amount in palmitate-treated cells was too low to be detected by primuline staining, the flux of ^{14}C-palmitate to intracellular TGs showed a similar pattern to ^{14}C-oleate (Figure 4-19). Fenoterol also promoted the incorporation of exogenous oleate and palmitate to CEs (radiogram, Figure 4-18, Figure 4-19). Interestingly, while the effects of β2AR agonism on palmitate incorporation to cellular TGs and CEs were completely blocked by A922500 (Figure 4-19), the esterification of exogenous oleate was still increased in fenoterol-treated cells when DGAT1 was inhibited (Figure 4-18).

***Conclusion*.** Overall, these findings indicated that β2AR activation potentiated palmitate incorporation in TGs in a DGAT1-dependent manner. However, oleate content in TGs was increased in both DGAT1-dependent and other unknown mechanism.

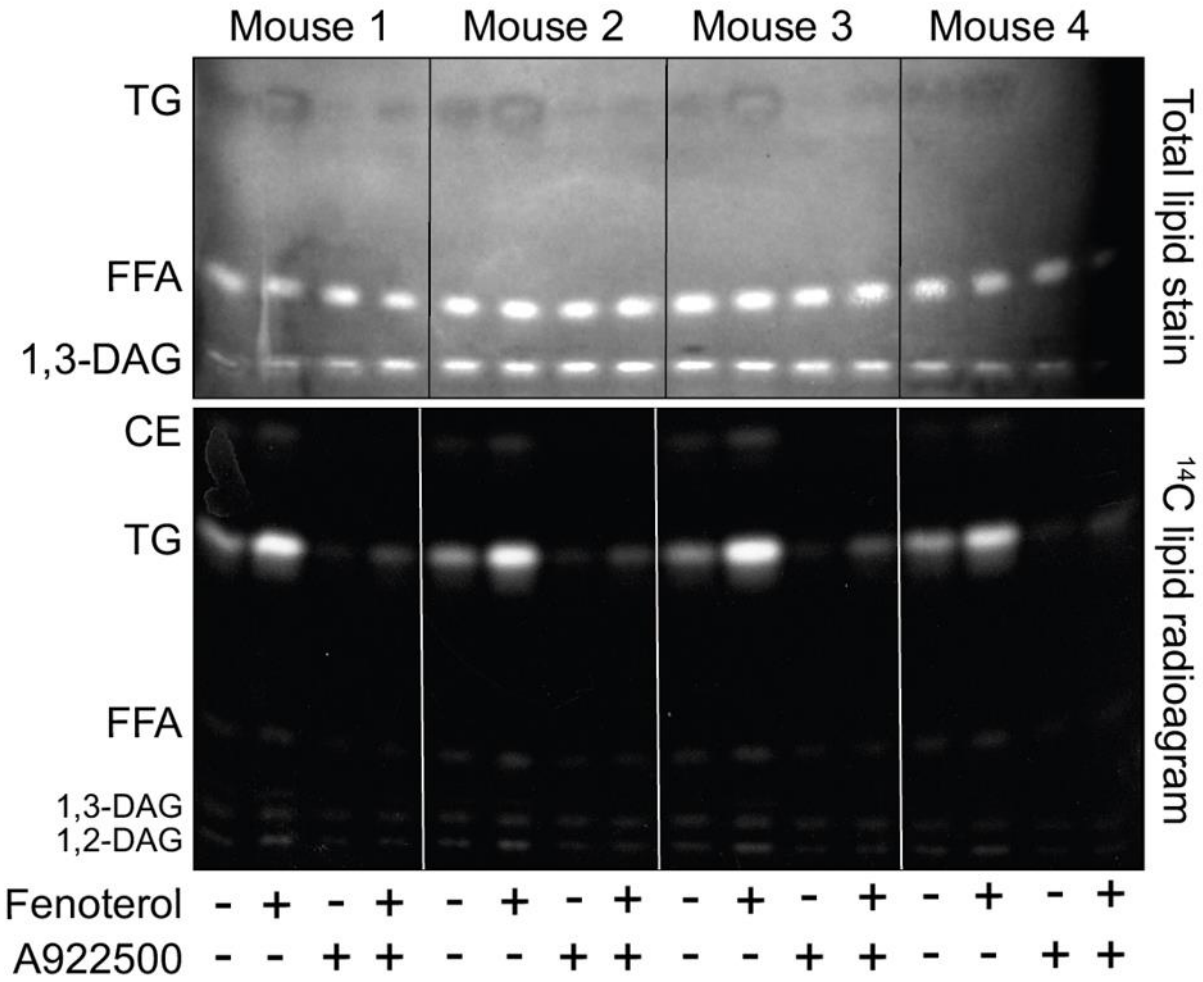

Figure 4-18. The effect of β2AR activation and DGAT1 inhibition on the flux of exogenous oleate through neutral lipids in BMDMs.

Total lipid stain (image above) and autoradiogram (image below) of the TLC plate containing separated neutral lipids isolated from BMDMs that had been stimulated with 1 μM fenoterol or 1 μM A922500 (as indicated below the graph) and then treated with 100 μM oleate containing ^{14}C-oleate tracer for 16 h. N=4 mice. The migration of the neutral lipid species indicated on the left side of the images were determined using chemical standards. CE and 1,2-DAG bands were not observed in the total lipid stain.

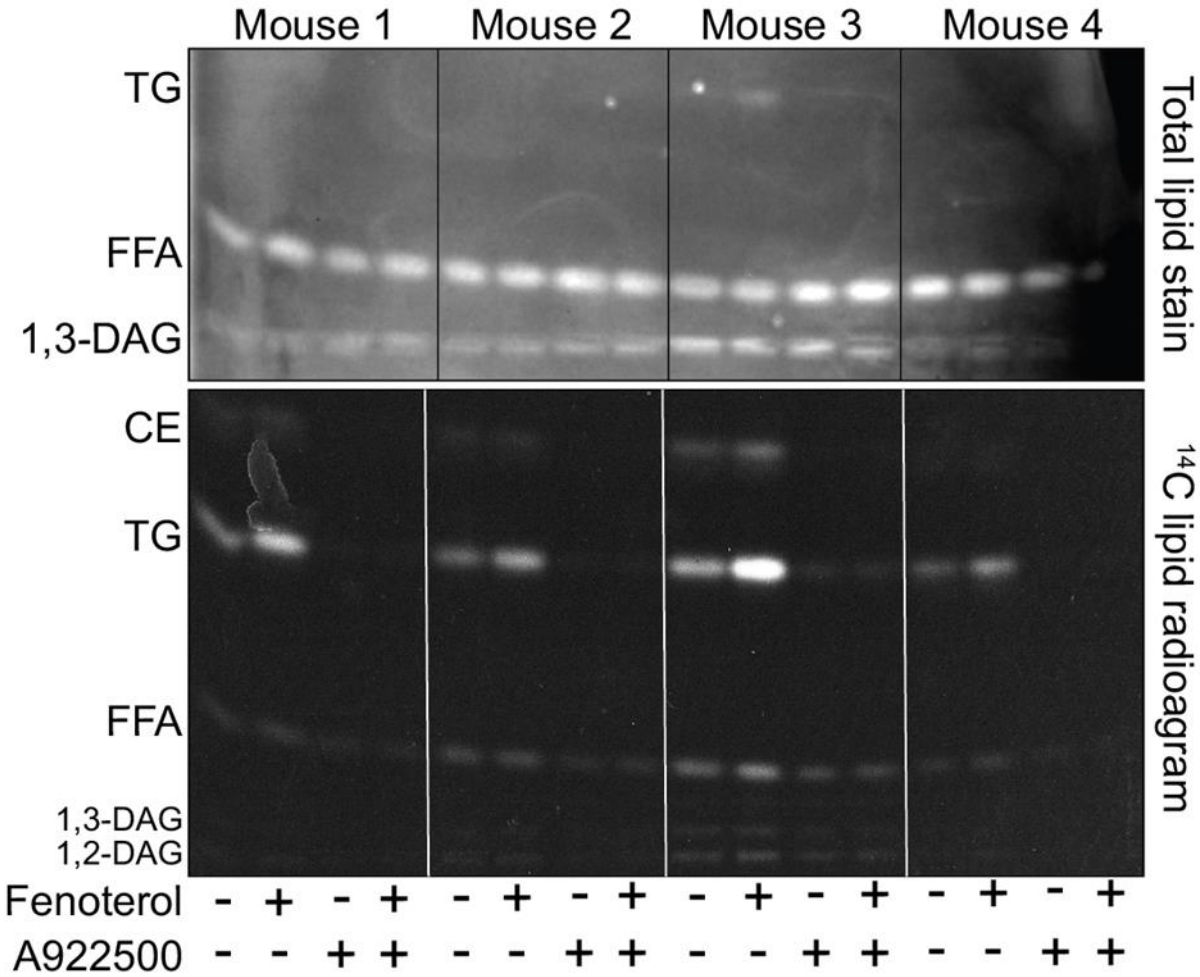

Figure 4-19. The effect of β2AR activation and DGAT1 inhibition on the flux of exogenous palmitate through neutral lipids in BMDMs.

Total lipid stain (image above) and autoradiogram (image below) of the TLC plate containing separated neutral lipids isolated from BMDMs that had been stimulated with 1 μM fenoterol or 1 μM A922500 (as indicated below the graph) and then treated with 100 μM palmitate containing ^{14}C-palmitate tracer for 16 h. N=4 mice. The migration of the neutral lipid species indicated on the left side of the images were determined using chemical standards. CE and 1,2-DAG bands were not observed in the total lipid stain.

4.2.1.6 β2AR activation decreased palmitate-induced inflammatory activation in BMDMs independently of ER stress or TG storage

Rationale. As my results have shown that β2AR activation promoted DGAT1-dependent lipid storage in BMDMs, and a similar magnitude of *Dgat1* transcriptional increase by genetic overexpression was previously described to prevent palmitate-induced inflammatory activation of macrophages[209], I decided to test whether β2AR stimulation could reduce the ER stress and inflammation in BMDMs treated with palmitate. I stimulated cells with fenoterol in the presence of A922500 before treating them with palmitate.

***Results*.** As I have already observed in the previous chapter, palmitate induced *Tnf* gene expression after 4 h of incubation, and *Tnf* mRNA returned to its basal levels after 8 h of incubation (Figure 4-20 A). β2AR activation completely diminished the peak in *Tnf* transcription, but such inhibitory effect could not be prevented by blocking DGAT1 (Figure 4-20 A). Furthermore, fenoterol did not reduce the rate of ER stress development in palmitate-treated BMDMs, as the expression of ER stress markers *Chop* and spliced *Xbp1* isoform was comparable in cells stimulated with β2AR agonist and controls in the presence of palmitate (Figure 4-20 A). Finally, while β2AR activation showed a modest reduction in *Chop* transcription, it did not affect *Xbp1* mRNA splicing in BMDMs after a prolonged incubation with palmitate, and *Chop* mRNA levels could not be restored to the level observed in controls in the presence of A922500 (Figure 4-20 B).

***Conclusion*.** Overall, I found that β2AR agonist diminished the early inflammatory activation, but not the development of ER stress in palmitate-treated BMDMs, and its early anti-inflammatory effect was independent of enhanced TG storage.

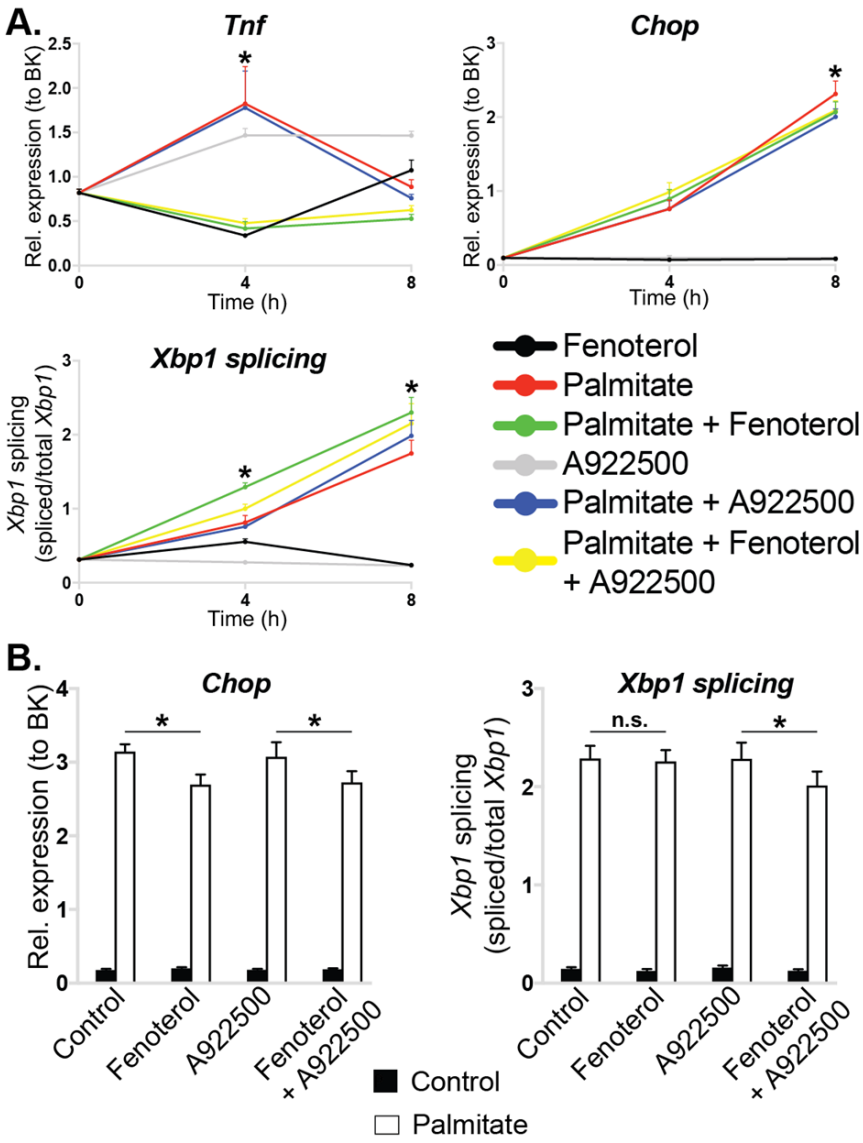

Figure 4-20. The effects of β2AR activation and DGAT1 inhibition on palmitate-induced ER stress and inflammatory activation of BMDMs.

(***A***) *Tnf and Chop mRNA* (normalised to BestKeeper)*, and the ratio of spliced to total Xbp1 mRNA levels in BMDMs treated with 1 μM fenoterol (black lines), 100 μM palmitate (red lines), 1 μM A922500 (grey lines), palmitate + fenoterol (green lines), palmitate + A922500 (blue lines), palmitate + fenoterol + A922500 (yellow lines). N=4 mice. * p < 0.05 compared between palmitate and palmitate + fenoterol at each time-point using two-way ANOVA with Bonferroni's multiple comparisons test.* (***B***) *Chop mRNA* (normalised to BestKeeper) *and the ratio of spliced to total Xbp1 mRNA levels in BMDMs treated with 1 μM fenoterol, 1 μM A922500 and fenoterol + A922500 (as indicated below the graphs) and then stimulated with 250 μM palmitate for 24 h. N=4 mice. * p < 0.05 compared between indicated treatments using two-way ANOVA with Bonferroni's multiple comparisons test.*

4.2.2 The importance of β2AR in macrophages for glucose and lipid metabolism on a pure C57Bl/6J genetic background

4.2.2.1 Macrophage-specific *Adrb2* deletion did not affect total energy balance of chow-fed mice

***Rationale*.** Prior to conducting any *in vivo* experiments designed to analyse specific metabolic traits, I decided to perform general metabolic phenotyping of LysM-Cre Adrb2$^{fl/fl}$ animals in order to understand how β2AR deficiency in macrophages affect systemic energy balance and glucose and lipid homeostasis on a chow diet or after prolonged high-fat feeding.

As one of the initial hypotheses was that β2AR might be important for limiting SNS outflow to the adipose tissues by regulating NE degradation in SAMs, that could in turn increase energy expenditure and reduce the body weight, I measured the body weight of the animals from the early post-weaning period (6 weeks of age) until the initial metabolic cage analysis (16 weeks of age).

Results. No differences in the body weight was observed throughout this period (Figure 4-21 A) or using metabolic cage analysis (Figure 4-21 B) between LysM-Cre Adrb2$^{fl/fl}$ and control mice. While genotype did not affect the food intake and energy expenditure during 48 h of measurement (Figure 4-21 C,D), some animals of both genotypes exhibited a profound stress response, indicated by the absence of chow consumption (Figure 4-21 C) and weight loss (not shown) during analysis. Average daily RER was similar between genotypes on a chow diet (Figure 4-21 E).

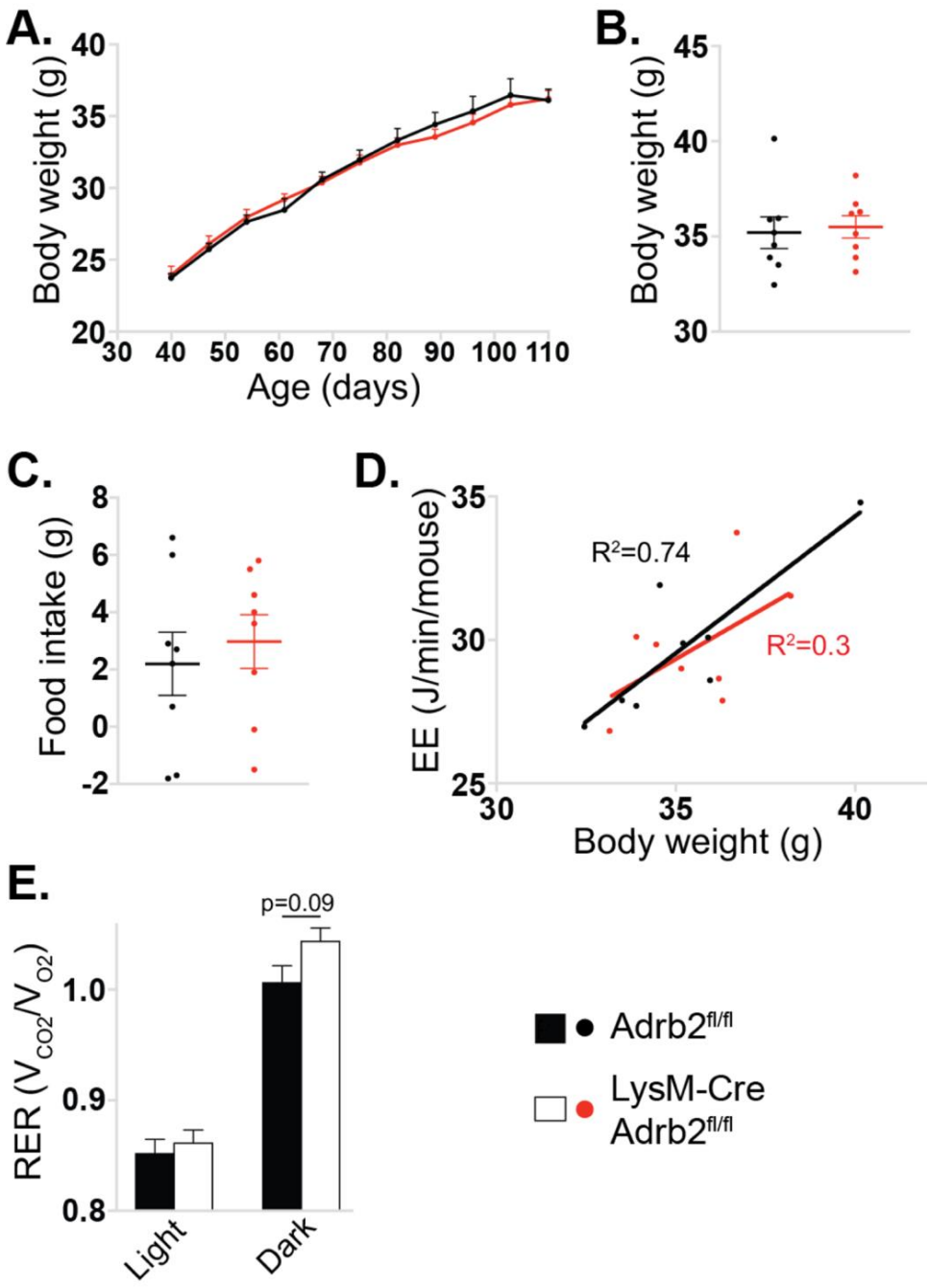

Figure 4-21. Body weight, food intake and energy expenditure of chow-fed Adrb2$^{fl/fl}$ and LysM-Cre Adrb2$^{fl/fl}$ mice.

*(**A**) Weekly body weight measurements prior to the study, and (**B**) body weight, (**C**) food intake, (**D**) average energy expenditure plotted against body weight and (**E**) average RER values during light and dark parts of the day assessed over 48 h in Adrb2$^{fl/fl}$ (black lines/dots/bars, n=8) and LysM-Cre Adrb2$^{fl/fl}$ (red lines/dots and white bars, n=8) 16-week-old male mice on a pure C57Bl/6J genetic background. Statistical differences between genotypes were assessed using two-way ANOVA with Bonferroni's multiple comparisons test (**A, E**) student's t-test (**B, C**) or one-way ANCOVA (**D**).*

4.2.2.2 Macrophage-specific *Adrb2* deletion increased the levels of circulating liver enzymes in chow-fed mice

Results. Chow-fed LysM-Cre Adrb2$^{fl/fl}$ animals and controls exhibited similar serum concentrations of glucose, insulin, FFAs and TGs in the fed state (Table 4-1). Unusually high measured FFA levels in both groups indicated a potential sample quality issue (Table 4-1). The levels of liver enzyme AST was elevated in LysM-Cre Adrb2$^{fl/fl}$ mice, with no change in the ALT to AST ratio compared to control group (Table 4-1). Finally, genotype did not affect the insulin, glucose and FFA concentration after an overnight fast (Table 4-1).

Feeding state	Random fed		Fasted overnight	
Genotype	**Adrb2$^{fl/fl}$**	**LysM-Cre Adrb2$^{fl/fl}$**	**Adrb2$^{fl/fl}$**	**LysM-Cre Adrb2$^{l/fl}$**
Glucose (mM)	8.63 ± 0.47	8.48 ± 0.22	6.00 ± 0.24	7.19 ± 0.58
Insulin (µg/L)	2.33 ± 0.86	1.41 ± 0.26	0.27 ± 0.03	0.29 ± 0.06
FFA (mM)	2.4 ± 0.24	2.94 ± 0.28	1.41 ± 0.11	1.29 ± 0.09
TG (mM)	2.36 ± 0.24	2.94 ± 0.28	-	-
ALT (U/L)	29.5 ± 2.64	120 ± 42.25	-	-
AST (U/L)	154 ± 40.09	473.38 ± 123.78*	-	-
ALT/AST ratio	0.24 ± 0.04	0.34 ± 0.11	-	-

Table 4-1. Serum biochemistry of chow-fed Adrb2$^{fl/fl}$ and LysM-Cre Adrb2$^{fl/fl}$ mice in a random-fed state or after overnight fast.

*Concentrations of serum biochemicals are expressed as means ± SEM. N=8 Adrb2$^{fl/fl}$, n=8 LysM-Cre Adrb2$^{fl/fl}$ 16-19-week-old male mice on a pure C57Bl/6J genetic background. * p < 0.05 compared between genotypes using student's t-test.*

4.2.2.3 Macrophage-specific *Adrb2* deletion improved systemic glucose clearance of chow-fed mice during GTT

Results. LysM-Cre Adrb2$^{fl/fl}$ animals exhibited a higher rate of glucose clearance from the blood during the GTT compared to control mice, as indicated by lower AUC (Figure 4-22 A,B). Furthermore, blood glucose concentration was higher in LysM-Cre Adrb2$^{fl/fl}$ mice after 6 h fast (average of 10.19 ± 0.26 in Adrb2$^{fl/fl}$ group vs 11.45 ± 0.41 in LysM-Cre Adrb2$^{fl/fl}$ group, p=0.02). However, both genotypes had comparable areas under curve during the ITT (Figure 4-22 C,D).

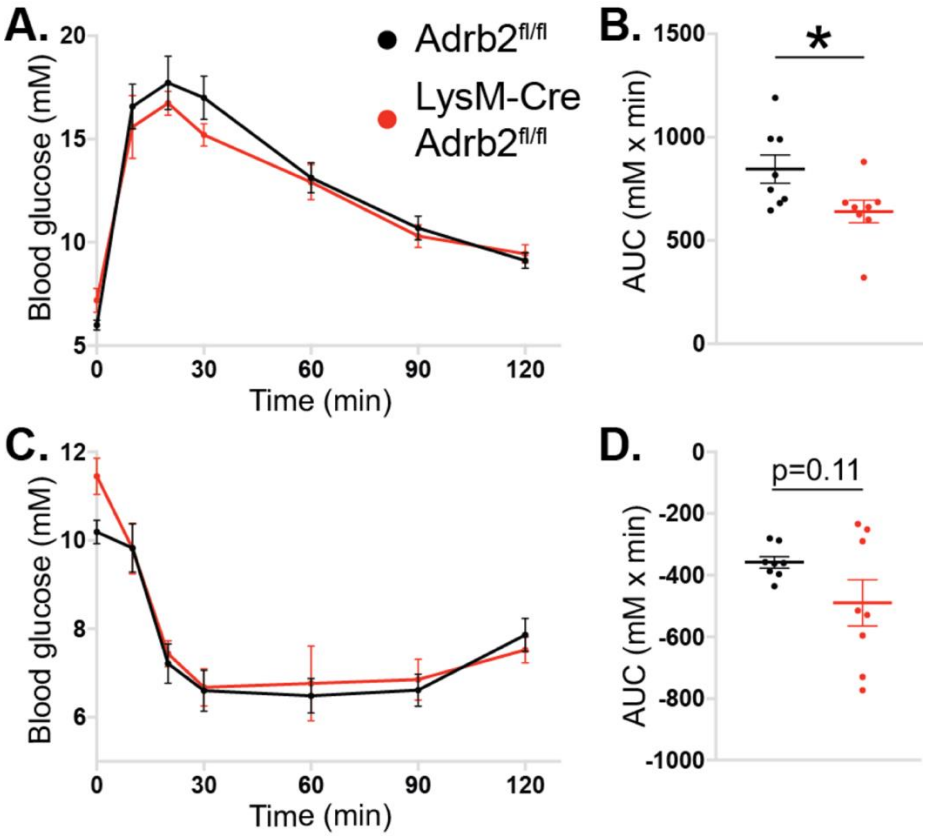

Figure 4-22. Glucose and insulin tolerance tests of chow-fed Adrb2$^{fl/fl}$ and LysM-Cre Adrb2$^{fl/fl}$ mice.

*Blood glucose concentration curves (**A**) and AUC (**B**) of mice injected with 1 mg/kg glucose at T=0 min after an overnight fast. Blood glucose concentration curves (**C**) and AUC (**D**) of mice injected with 0.75 IU/kg insulin at T=0 after 6 h fast. N=8 Adrb2$^{fl/fl}$ (black lines/dots) and n=8 LysM-Cre Adrb2$^{fl/fl}$ (red lines/dots) 16-18-week-old male mice on a pure C57Bl/6J background. * p < 0.05 compared between genotypes using student's t-test (**B, D**).*

4.2.2.4 Macrophage-specific *Adrb2* deletion tended to increase the liver weight of chow-fed mice

Results. There were no genotype-dependent differences in total body weight, and BAT-, scWAT-, eWAT- and liver-to-body weight ratios at the end of the study (Figure 4-23 A-E).

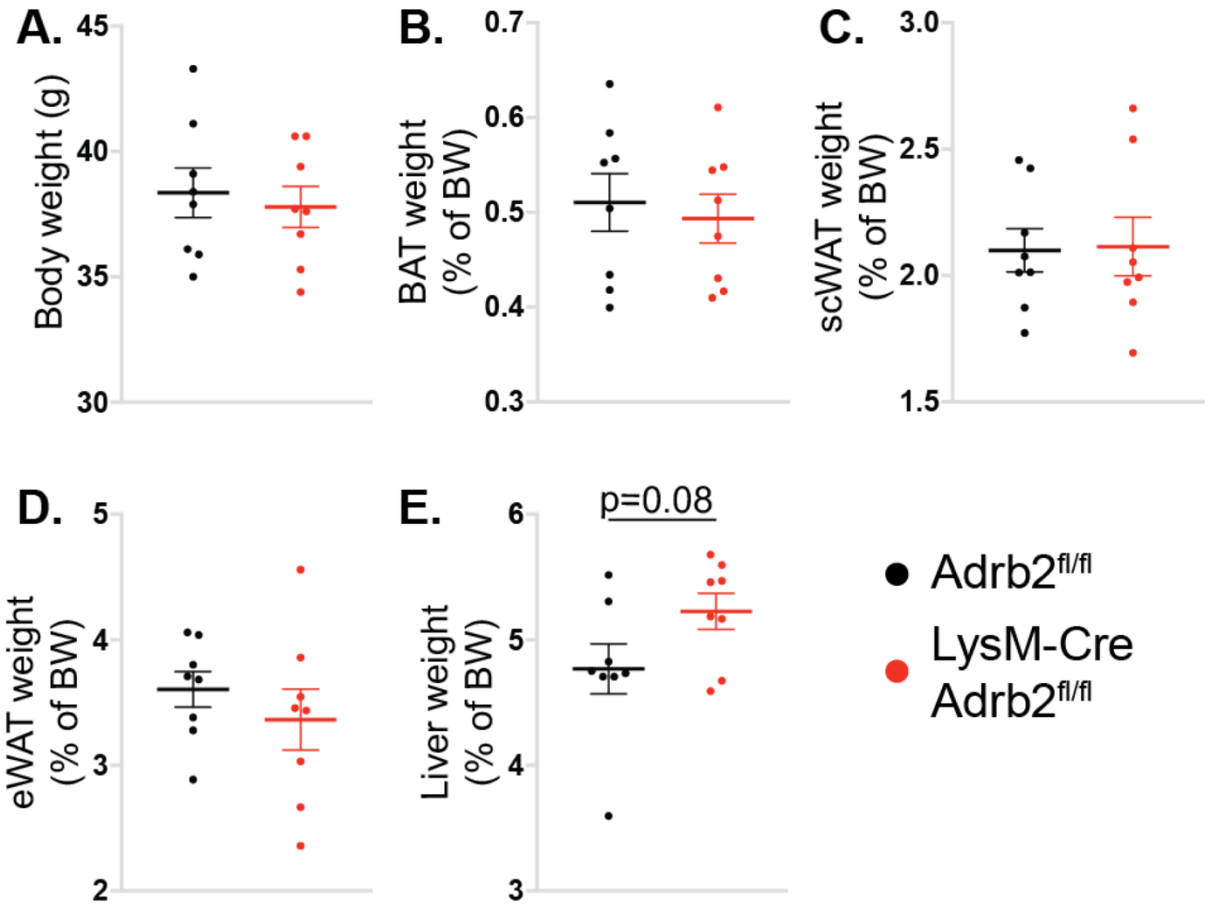

Figure 4-23. Tissue weights of chow-fed Adrb2$^{fl/fl}$ and LysM-Cre Adrb2$^{fl/fl}$ mice. *Body weight (**A**) and weights of BAT (**B**), scWAT (**C**), eWAT (**D**) and liver (**E**), expressed as a percentage of body weight of Adrb2$^{fl/fl}$ (n=8, black dots) and LysM-Cre Adrb2$^{fl/fl}$ (n=8, red dots) 19-week-old male mice on a pure C57Bl/6J background culled in a random fed state. Statistical significance was assessed using student's t-test.*

4.2.2.5 Macrophage-specific *Adrb2* deletion reduced the body weight gain during HFD in mice without affecting food intake or energy expenditure

Results. Animals of both genotypes weighed similarly at 8 weeks of age, when the high-fat feeding was initiated (Figure 4-24 A). LysM-Cre Adrb2$^{fl/fl}$ mice gained body weight at a lower rate than control group and exhibited a reduced total body weight after 7 weeks of HFD, and during the metabolic cage analysis (Figure 4-24 A-C). However, no genotype-dependent differences in food intake or energy expenditure were observed between groups during 48 h of analysis (Figure 4-24 D,E).

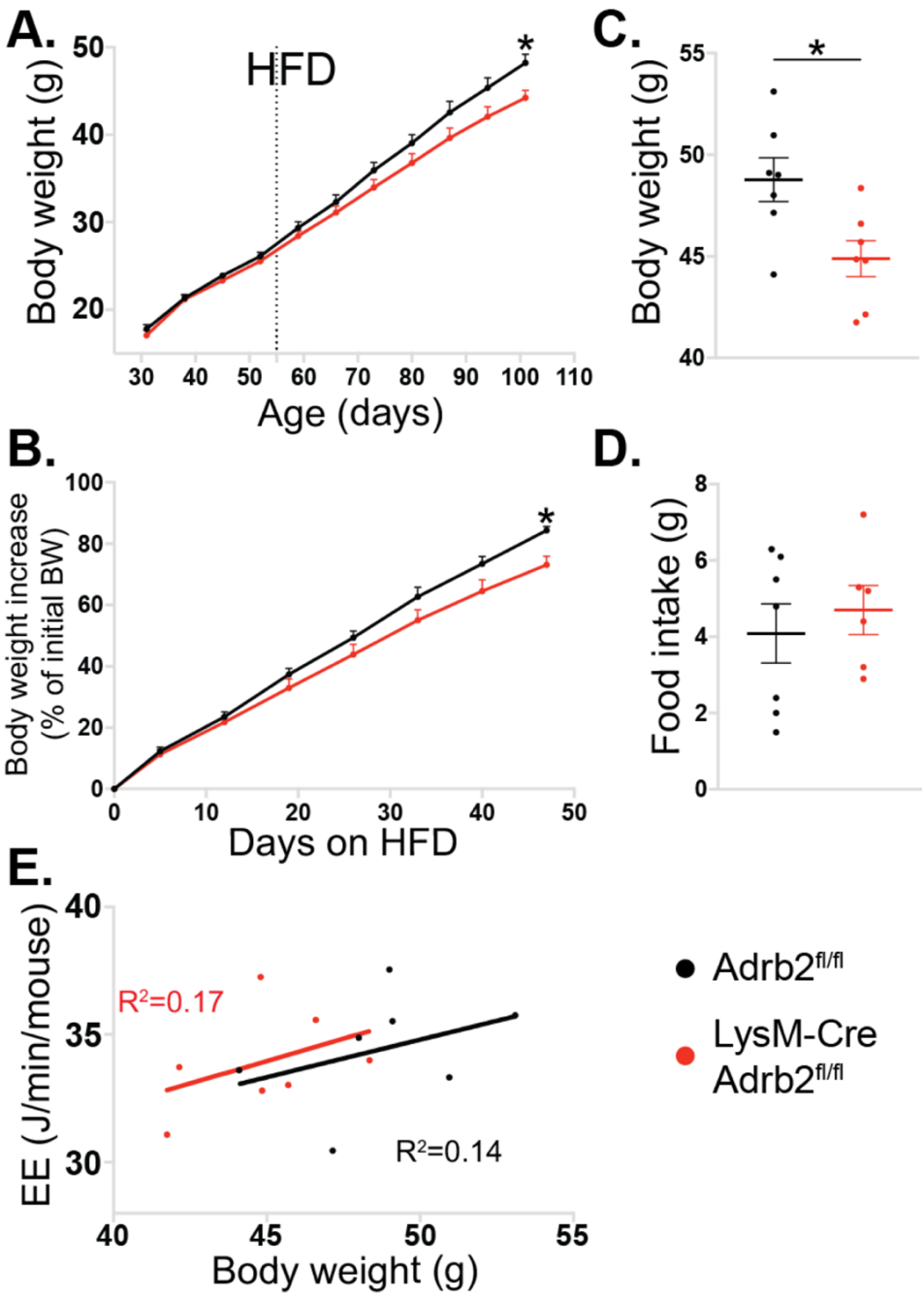

Figure 4-24. Body weight, food intake and energy expenditure of HFD-fed Adrb2$^{fl/fl}$ and LysM-Cre Adrb2$^{fl/fl}$ mice.

*Weekly body weight measurements prior to the study (dotted line indicates the switch from chow to HFD) expressed as (**A**) average body weight or as (**B**) percentage body weight increase from the start of HFD and (**C**) body weight, (**D**) food intake, (**E**) average energy expenditure plotted against body weight assessed over 48 h in Adrb2$^{fl/fl}$ (black lines/dots, n=7) and LysM-Cre Adrb2$^{fl/fl}$ (red lines/dots, n=7) 16-week-old male mice on a pure C57Bl/6J genetic background, fed a 60% kcal fat diet (D12492) from 8 weeks of age. * p < 0.05 compared between genotypes using two-way ANOVA with Bonferroni's multiple comparisons test (**A, B**) student's t-test (**C, D**) or one-way ANCOVA (**E**).*

4.2.2.6 Macrophage-specific *Adrb2* deletion had no effect on serum metabolite concentrations of HFD-fed mice

Results. Despite their lower body weight, LysM-Cre Adrb2$^{fl/fl}$ mice showed similar levels of serum glucose, insulin, TGs and FFAs in the fed state to controls (Table 4-2). No differences in serum ALT levels and ALT/AST ratio were observed between two groups (Table 4-2). Circulating glucose, insulin and FFA levels were similar between genotypes after overnight fast (Table 4-2).

Feeding state	Random fed		Fasted overnight	
Genotype	**Adrb2$^{fl/fl}$**	**LysM-Cre Adrb2$^{fl/fl}$**	**Adrb2$^{fl/fl}$**	**LysM-Cre Adrb2$^{l/fl}$**
Glucose (mM)	10.94 ± 0.66	10.27 ± 0.69	9.8 ± 0.44	9.3 ± 0.63
Insulin (µg/L)	8.48 ± 1.53	9.43 ± 3.1	1.25 ± 0.16	1.06 ± 0.25
FFA (mM)	1.05 ± 0.07	1.2 ± 0.09	0.7 ± 0.06	0.69 ± 0.08
TG (mM)	1.06 ± 0.06	1.25 ± 0.09	-	-
ALT (U/L)	191.71 ± 21.74	109.57 ± 37.85	-	-
AST (U/L)	255 ± 20.06	227 ± 59.05	-	-
ALT/AST ratio	0.81 ± 0.14	0.49 ± 0.08	-	-

Table 4-2. Serum biochemistry of HFD-fed Adrb2$^{fl/fl}$ and LysM-Cre Adrb2$^{fl/fl}$ mice in a random-fed state or after overnight fast.

Concentrations of serum biochemicals are expressed as means ± SEM. N=7 Adrb2$^{fl/fl}$, n=7 LysM-Cre Adrb2$^{fl/fl}$ 16-19-week-old male mice on a pure C57Bl/6J genetic background, fed a 60% kcal fat diet (D12492) from 8 weeks of age.

4.2.2.7 Macrophage-specific *Adrb2* deletion did not impact the glucose or insulin tolerance of HFD-fed mice

Results. LysM-Cre Adrb2$^{fl/fl}$ mice were leaner than HFD-fed controls during GTT and ITT (data not shown). However, following exogenous administration of glucose, they normalised serum glucose concentration at the same rate as controls (Figure 4-25 A,B). There were no differences in insulin-mediated serum glucose uptake between genotypes (Figure 4-25 C,D).

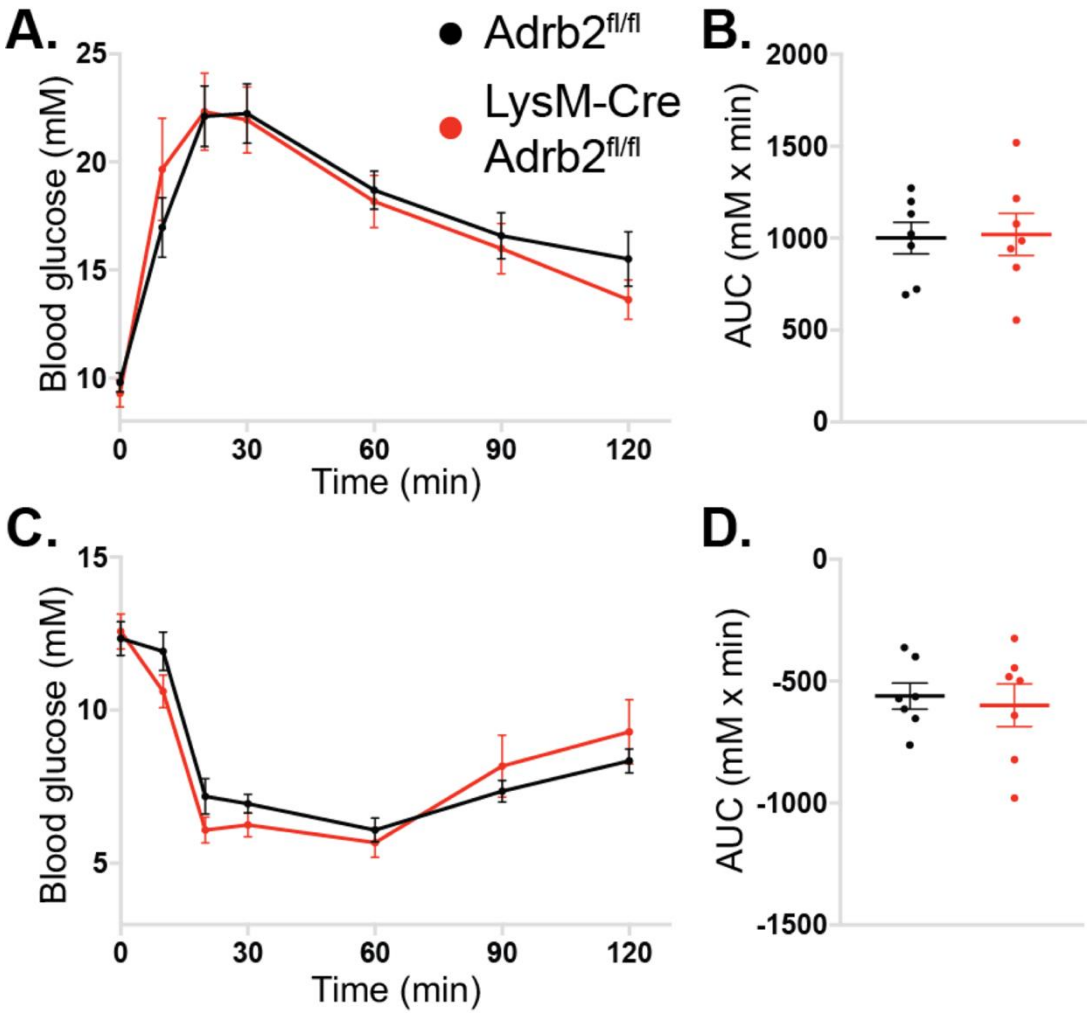

Figure 4-25. Glucose and insulin tolerance tests of HFD-fed Adrb2$^{fl/fl}$ and LysM-Cre Adrb2$^{fl/fl}$ mice.

*Blood glucose concentration curves (**A**) and AUC (**B**) of mice injected with 1 mg/kg glucose at T=0 min after an overnight fast. Blood glucose concentration curves (**C**) and AUC (**D**) of mice injected with 1 IU/kg insulin at T=0 after 6 h fast. N=7 Adrb2$^{fl/fl}$ (black lines/dots) and n=7 LysM-Cre Adrb2$^{fl/fl}$ (red lines/dots) 16-18-week-old male mice on a pure C57Bl/6J background, fed a 60% kcal fat diet (D12492) from 8 weeks of age. Statistical significance was assessed using student's t-test (**B, D**).*

4.2.2.8 Macrophage-specific *Adrb2* deletion reduced liver weight of HFD-fed mice

Results. LysM-Cre Adrb2$^{fl/fl}$ animals weighed approximately 8% less than controls at the end of the study (Figure 4-26 A). No differences in BAT-, scWAT-, and eWAT-to-body weight ratios were observed between genotypes (Figure 4-26 B,C). LysM-Cre Adrb2$^{fl/fl}$ group had a reduced liver-to-body weight ratio compared to control mice on HFD (Figure 4-26 D,E).

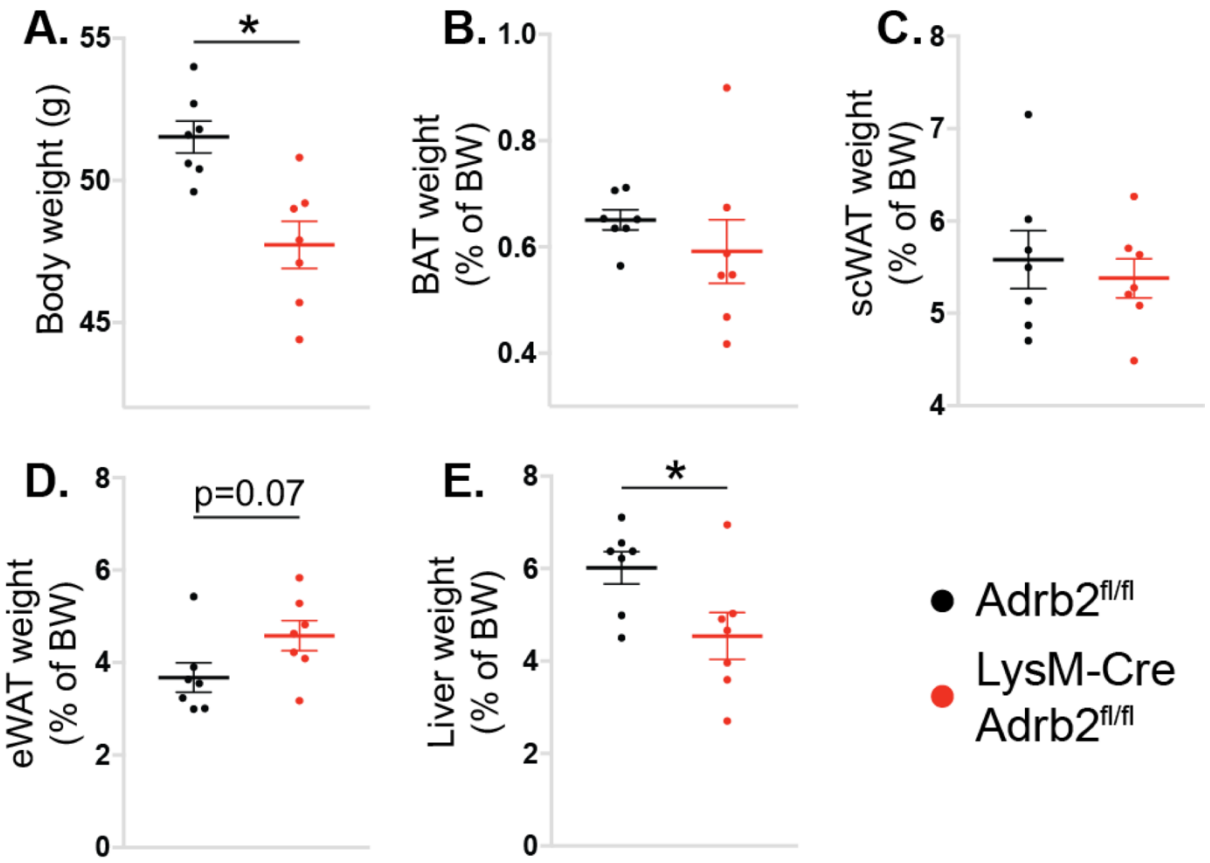

Figure 4-26. Tissue weights of HFD-fed Adrb2$^{fl/fl}$ and LysM-Cre Adrb2$^{fl/fl}$ mice. *(**A**) Body weight and weights of (**B**) BAT, (**C**) scWAT, eWAT (**D**) and liver (**E**), expressed as a percentage of body weight of Adrb2$^{fl/fl}$ (n=7, black dots) and LysM-Cre Adrb2$^{fl/fl}$ (n=7, red dots) 19-week-old male mice on a pure C57Bl/6J background, fed a 60% kcal fat diet (D12492) from 8 weeks of age and culled in a random fed state. * p < 0.05 compared between genotypes using student's t-test.*

4.2.2.9 Macrophage-specific *Adrb2* deletion reduced metabolic gene expression, but had no effect on the inflammatory gene expression in ATMs isolated from chow- or HFD-fed mice

Rationale. At the end of the study, eWATs isolated from both chow- and HFD-fed groups were digested and ATMs were isolated using CD11b-positive purification. Similarly to the previous chapter, tissues from chow and HFD groups were obtained at different times, therefore statistical comparisons were only performed between genotypes, and not between diets in any following tissue analyses. However, results from both diets were presented alongside in the same graphs in order to visualise the directional change of each analysed parameter during HFD.

***Results*.** High excision rate of *Adrb2* gene was observed, with ATMs isolated from LysM-Cre Adrb2$^{fl/fl}$ animals containing approximately 15% of *Adrb2* mRNA compared to the control levels in both chow- and HFD-fed groups (Figure 4-27 A). No compensatory increase in *Adrb1* transcription was observed in β2AR-deficient ATMs from chow- or HFD-fed groups (Figure 4-27 A). No differences in the expression of ATM inflammatory or M2 marker genes were observed between genotypes in either chow- or HFD-fed groups (Figure 4-27 A). Interestingly, while β2AR-deficient ATMs exhibited equivalent mRNA levels of metabolic genes to the control cells in chow-fed group, they showed lower expression of metabolic genes *Cd36*, *Dgat1*, *Acsl1*, *Acsl4*, *Pcyt1a* and *Glut1* compared to controls in HFD-fed group, indicating decreased lipid uptake (Figure 4-27 B). Finally, the expression of gene encoding moamine oxidase A was unchanged in β2AR-deficient ATMs compared to controls in chow or HFD groups (Figure 4-27 B).

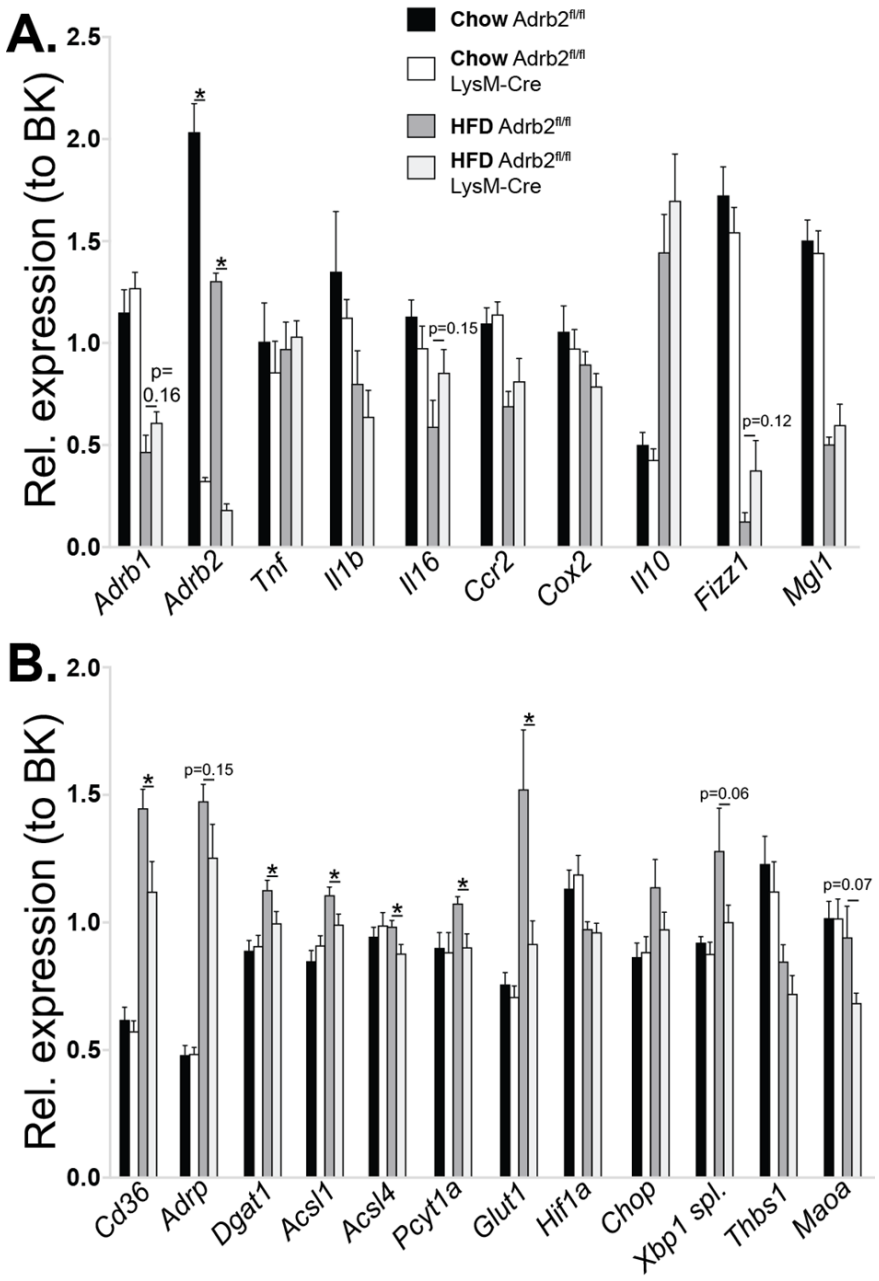

Figure 4-27. Gene expression analysis of eWAT ATMs isolated from chow and HFD-fed Adrb2$^{fl/fl}$ and LysM-Cre Adrb2$^{fl/fl}$ mice.

mRNA levels (normalised to BestKeeper) *of (**A**) Adrb1, Adrb2 and immune system genes Tnf, Il1b, Il6, Ccr2, Cox2, Il10, Fizz1 and Mgl1, (**B**) metabolic genes Cd36, Adrp, Dgat1, Acsl1, Acsl4, Pcyt1a, Glut1, Hif1a, Chop, Thbs1, Maoa and the ratio of spliced to total Xbp1 mRNA levels in CD11b-positive fraction of eWAT isolated from chow-fed Adrb2$^{fl/fl}$ (n=8, black bars), LysM-Cre Adrb2$^{fl/fl}$ (n=8, white bars) and HFD-fed Adrb2$^{fl/fl}$ (n=7, dark grey bars), LysM-Cre Adrb2$^{fl/fl}$ (n=7, light grey bars) 19-week-old male mice on a pure C57Bl/6J genetic background, culled in a random fed state. HFD-fed group received 60% kcal fat diet (D12492) from 8 weeks of age. * p < 0.05 compared to Adrb2$^{fl/fl}$ using student's t-test.*

4.2.2.10 Macrophage-specific *Adrb2* deletion had no major effect on scWAT and BAT gene expression in chow- or HFD-fed mice

Results. *Ucp1* mRNA levels were similar between genotypes in scWAT from chow- and HFD-fed groups, indicating that macrophage-specific β2AR deficiency did not impact the browning of WAT (Figure 4-28 A). Chow-fed LysM-Cre Adrb2$^{fl/fl}$ animals had increased *Cd206*, but similar *Cd11b*, *Pgc1a* and *Cidea* mRNA levels in scWAT compared to controls (Figure 4-28 A). On HFD, *Adrb3*, *Lpl*, *Glut4* and *Hsl* scWAT mRNA levels were comparable between the two groups (Figure 4-28 A). *Adrb2* mRNA in scWAT was similar in chow-fed, but was decreased in HFD-fed LysM-Cre Adrb2$^{fl/fl}$ mice, suggesting that nearly 50% of *Adrb2* expression in scWAT from HFD animals is derived from ATMs (Figure 4-28 A).

BAT from chow- and HFD-fed groups showed the same expression levels of *Ucp1*, *Adrb3*, *Cd36*, *Glut4* and *Hsl* between genotypes (Figure 4-28 B). LysM-Cre Adrb2$^{fl/fl}$ mice had lower *Atgl* mRNA on a chow diet. *Pgc1a*, *Cd206*, *Fatp1* and *Cpt1b* transcript levels were comparable on a HFD to controls (Figure 4-28 B). Similarly to the observations in scWAT, *Adrb2* expression was lower in the chow-fed LysM-Cre Adrb2$^{fl/fl}$ animals compared to controls, indicating that approximately 10% of *Adrb2* transcript levels in BAT are derived from the ATMs (Figure 4-28 B).

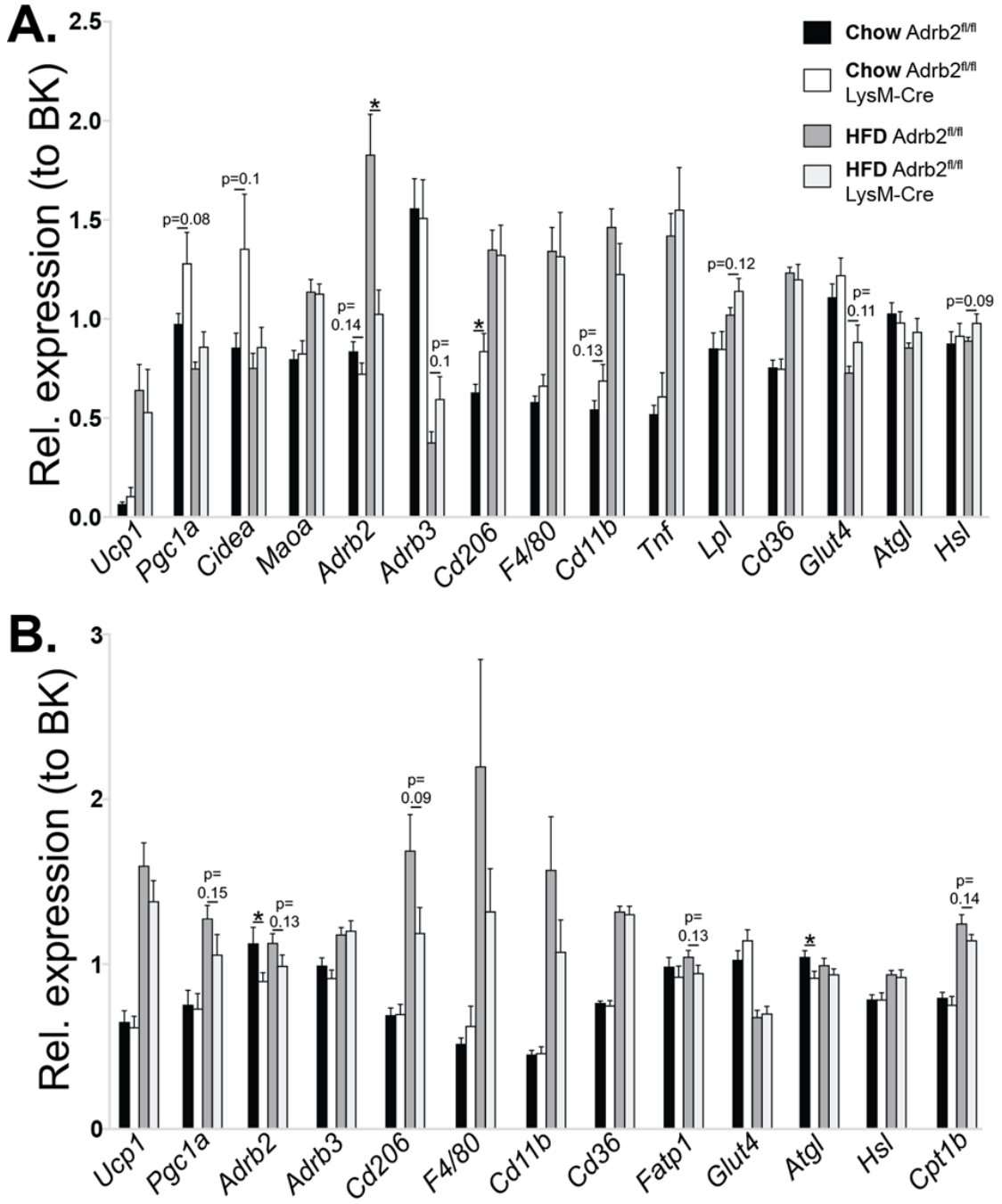

Figure 4-28. Gene expression analysis of scWAT and BAT isolated from chow and HFD-fed Adrb2$^{fl/fl}$ and LysM-Cre Adrb2$^{fl/fl}$ mice.

*(**A**) Ucp1, Pgc1a, Cidea, Maoa, Adrb2, Adrb3, Cd206, F4/80, Cd11b, Tnf, Lpl, Cd36, Glut4, Atgl and Hsl mRNA levels in scWAT and (**B**) Ucp1, Pgc1a, Adrb2, Adrb3, Cd206, F4/80, Cd11b, Cd36, Fatp1, Glut4, Atgl, Hsl and Cpt1b mRNA levels* (normalised to BestKeeper) *in BAT isolated from chow-fed Adrb2$^{fl/fl}$ (n=8, black bars), LysM-Cre Adrb2$^{fl/fl}$ (n=8, white bars) and HFD-fed Adrb2$^{fl/fl}$ (n=7, dark grey bars), LysM-Cre Adrb2$^{fl/fl}$ (n=7, light grey bars) 19-week-old male mice on a pure C57Bl/6J genetic background, culled in a random fed state. HFD-fed group received 60% kcal fat diet (D12492) from 8 weeks of age. * p < 0.05 compared to Adrb2$^{fl/fl}$ using student's t-test.*

4.2.2.11 Macrophage-specific *Adrb2* deletion increased hepatic *Fasn* mRNA in chow-fed mice, but had no major impact on hepatic gene expression in HFD-fed mice

Results. Livers from chow-fed LysM-Cre Adrb2$^{fl/fl}$ animals expressed higher levels of *Fasn* gene, but showed no differences in the mRNA levels of other metabolic or immune system genes compared to controls (Figure 4-29). On a HFD, β2AR deficiency in macrophages did not affect the expression of metabolic or immune system genes (Figure 4-29). Similarly to the adipose tissues, *Adrb2* mRNA was lower in LysM-Cre Adrb2$^{fl/fl}$ animals on both diets, indicating that approximately 20% and 40% of hepatic *Adrb2* expression is derived from Kupffer cells on a chow and HFD, respectively (Figure 4-29).

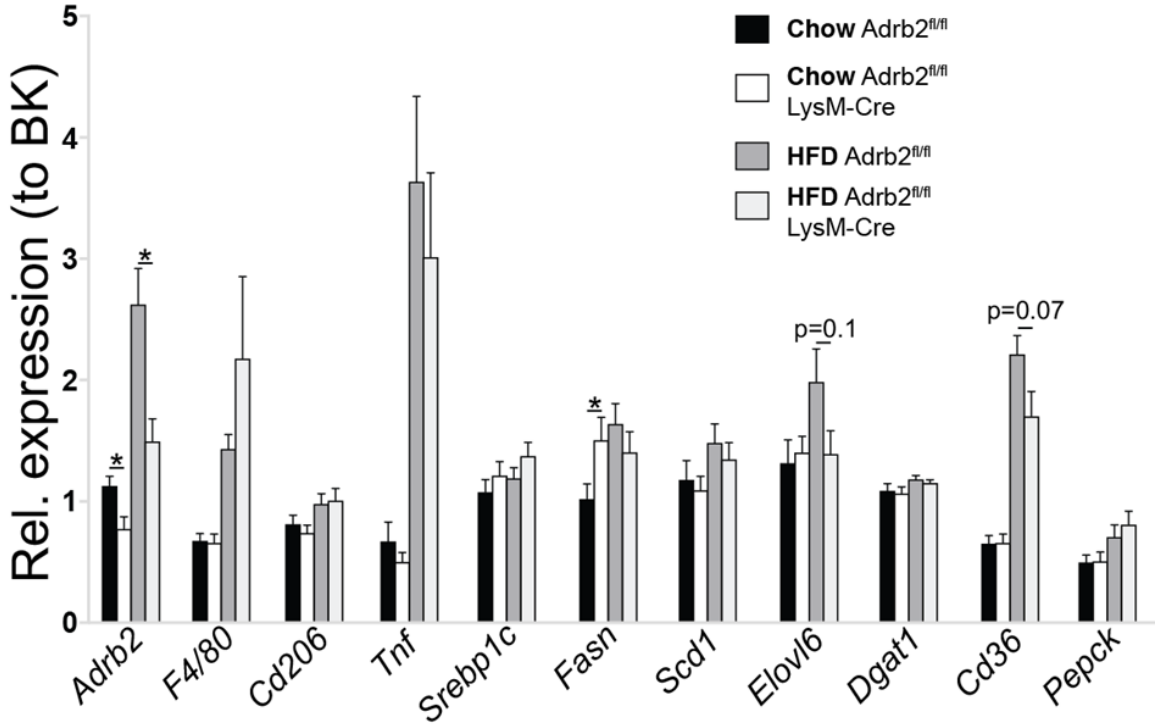

Figure 4-29. Gene expression analysis of livers isolated from chow and HFD-fed Adrb2$^{fl/fl}$ and LysM-Cre Adrb2$^{fl/fl}$ mice.

Adrb2, F4/80, Cd206, Tnf, Srebp1c, Fasn, Scd1, Elovl6, Dgat1, Cd36 and Pepck mRNA levels (normalised to BestKeeper) *in livers isolated from chow-fed Adrb2$^{fl/fl}$ (n=8, black bars), LysM-Cre Adrb2$^{fl/fl}$ (n=8, white bars) and HFD-fed Adrb2$^{fl/fl}$ (n=7, dark grey bars), LysM-Cre Adrb2$^{fl/fl}$ (n=7, light grey bars) 19-week-old male mice on a pure C57Bl/6J genetic background, culled in a random fed state. HFD-fed group received 60% kcal fat diet (D12492) from 8 weeks of age. * p < 0.05 compared to Adrb2$^{fl/fl}$ using student's t-test.*

4.2.2.12 Macrophage-specific *Adrb2* deletion reduced hepatic lipid accumulation in HFD-fed mice

Results. As the liver weight of HFD-fed LysM-Cre Adrb2$^{fl/fl}$ mice was reduced compared to the control group, I assessed the hepatic lipid content in order to determine whether the observed weight reduction resulted from decreased lipid accumulation in the liver. Indeed, while there were no genotype-dependent differences in hepatic lipid content on a chow diet, livers from HFD-fed LysM-Cre Adrb2$^{fl/fl}$ animals contained less lipid, indicating a lower degree of hepatic steatosis (Figure 4-30).

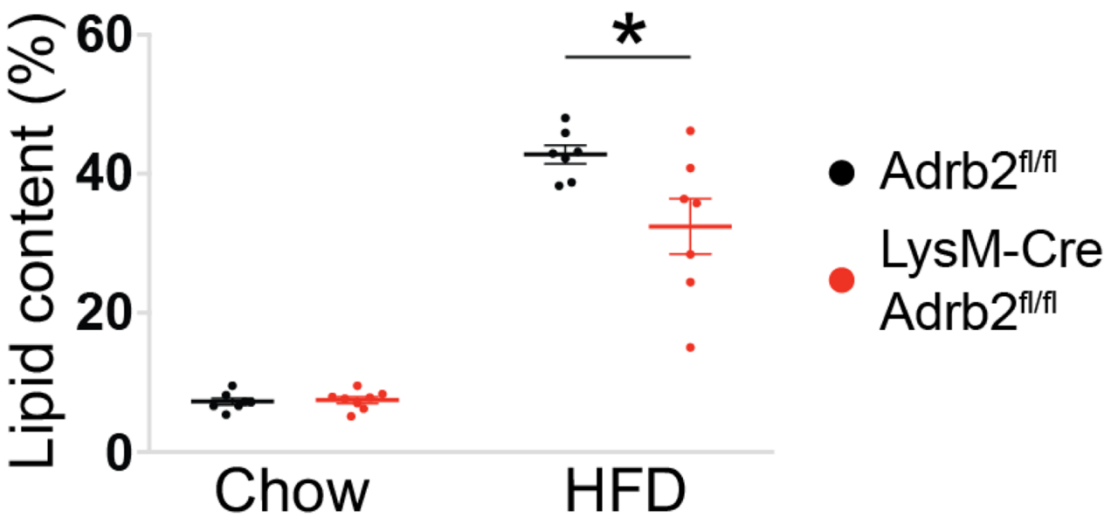

Figure 4-30. Hepatic lipid levels in chow and HFD-fed Adrb2$^{fl/fl}$ and LysM-Cre Adrb2$^{fl/fl}$ mice.

*Total lipid weight (as percentage of tissue weight) of the livers isolated from chow-fed Adrb2$^{fl/fl}$ (n=8, black dots), LysM-Cre Adrb2$^{fl/fl}$ (n=8, red dots) and HFD-fed Adrb2$^{fl/fl}$ (n=7, black dots), LysM-Cre Adrb2$^{fl/fl}$ (n=7, red dots) 19-week-old male mice on a pure C57Bl/6J genetic background, culled in a random fed state. HFD-fed group received 60% kcal fat diet (D12492) from 8 weeks of age. * p < 0.05 compared between genotypes using student's t-test.*

4.2.2.13 Macrophage-specific *Adrb2* deletion increased relative hepatic palmitate levels in chow-fed mice, but had no major impact on the hepatic fatty acid composition of HFD-fed mice

***Rationale*.** Intrigued by an increased *Fasn* expression in the chow-fed LysM-Cre Adrb2$^{fl/fl}$ animals compared to controls, I measured hepatic fatty acid composition of both chow- and HFD-fed groups. I fractionated total liver lipids into phospholipid and neutral lipid fractions and analysed them separately in order to identify specific changes in membrane remodelling or TG storage.

***Results*.** Relative palmitate levels were increased in the phospholipids of LysM-Cre Adrb2$^{fl/fl}$ animals compared to controls on a chow diet (Figure 4-31 A). Genotype had no effect on hepatic phospholipid fatty acid composition on a HFD (Figure 4-31 A). Similarly, hepatic TGs contained a higher proportion of palmitate in chow-fed LysM-Cre Adrb2$^{fl/fl}$ mice, but had normal levels of other measured fatty acid species compared to controls (Figure 4-31 B). On a HFD, β2AR deficiency in macrophages did not affect hepatic TG fatty acid composition (Figure 4-31 B).

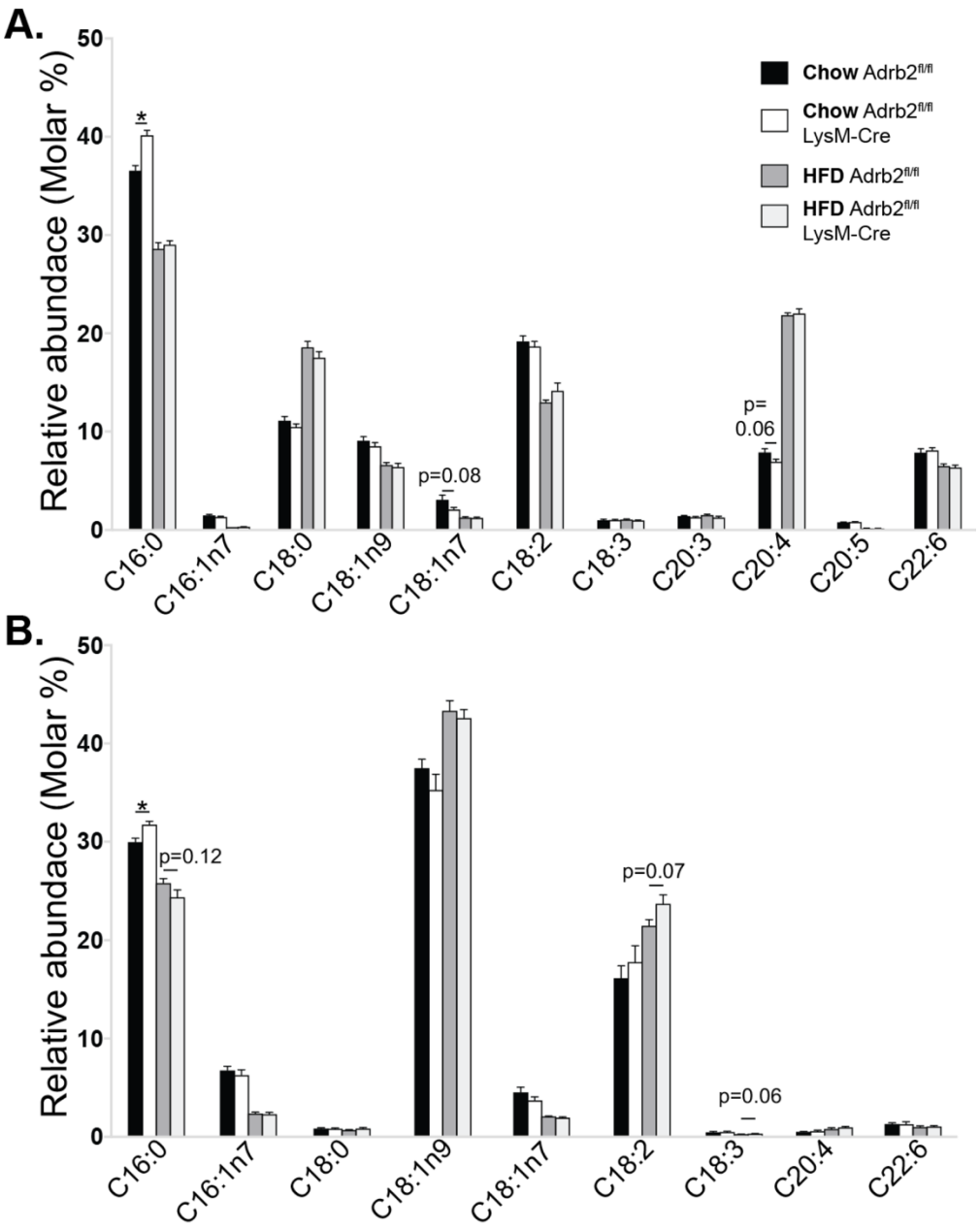

Figure 4-31. Hepatic fatty acid composition of chow and HFD-fed Adrb2$^{fl/fl}$ and LysM-Cre Adrb2$^{fl/fl}$ mice.

*Relative abundance of C16:0, C16:1n7, C18:0, C18:1n9, C18:1n7, C18:2, C18:3, C20:3, C20:4, C20:5, C22:6 (levels of C20:3 and C20:5 were below detection limit in **B**) fatty acids (expressed as molar percentages of each fatty acid relative to an overall fatty acid molar abundance in a given sample) in (**A**) phospholipid or (**B**) neutral lipid fraction of livers isolated from chow-fed Adrb2$^{fl/fl}$ (n=8, black bars), LysM-Cre Adrb2$^{fl/fl}$ (n=8, white bars) and HFD-fed Adrb2$^{fl/fl}$ (n=7, dark grey bars), LysM-Cre Adrb2$^{fl/fl}$ (n=7, light grey bars) 19-week-old male mice on a pure C57Bl/6J genetic background, culled in a random fed state. HFD-fed group received 60% kcal fat diet (D12492) from 8 weeks of age. * p < 0.05 compared between genotypes using student's t-test.*

4.2.2.14 Macrophage-specific *Adrb2* deletion did not affect the body weight, food intake or faecal excretion in mice on a chow diet, or during the initial 2 weeks of high-fat feeding

***Rationale*.** As I previously observed reduced body weight of LysM-Cre Adrb2$^{fl/fl}$ animals compared to controls after prolonged high-fat feeding without any obvious changes in energy expenditure or thermogenic markers in BAT and scWAT of these mice, I decided to assess whether β2AR deficiency in macrophages affects food intake or faecal excretion in chow- or HFD-fed animals. I therefore measured the body weight and assessed daily food intake in singly housed animals for 12 days on a chow-diet, before placing the same mice on a HFD and continuing the assessment for additional 12 days. I also measured faecal excretion during the last 5 days of each 12-day period.

***Results*.** Genotype had no effect on food intake or faecal excretion on a chow-diet, when mice demonstrated a stable body weight (Figure 4-32 A-C). LysM-Cre Adrb2$^{fl/fl}$ animals did not exhibit differences in the body weight gain, food intake or faecal excretion compared to controls during the first 12 days of HFD, indicating no genotype-dependent alterations in energy balance after a diet change (Figure 4-32 D-G).

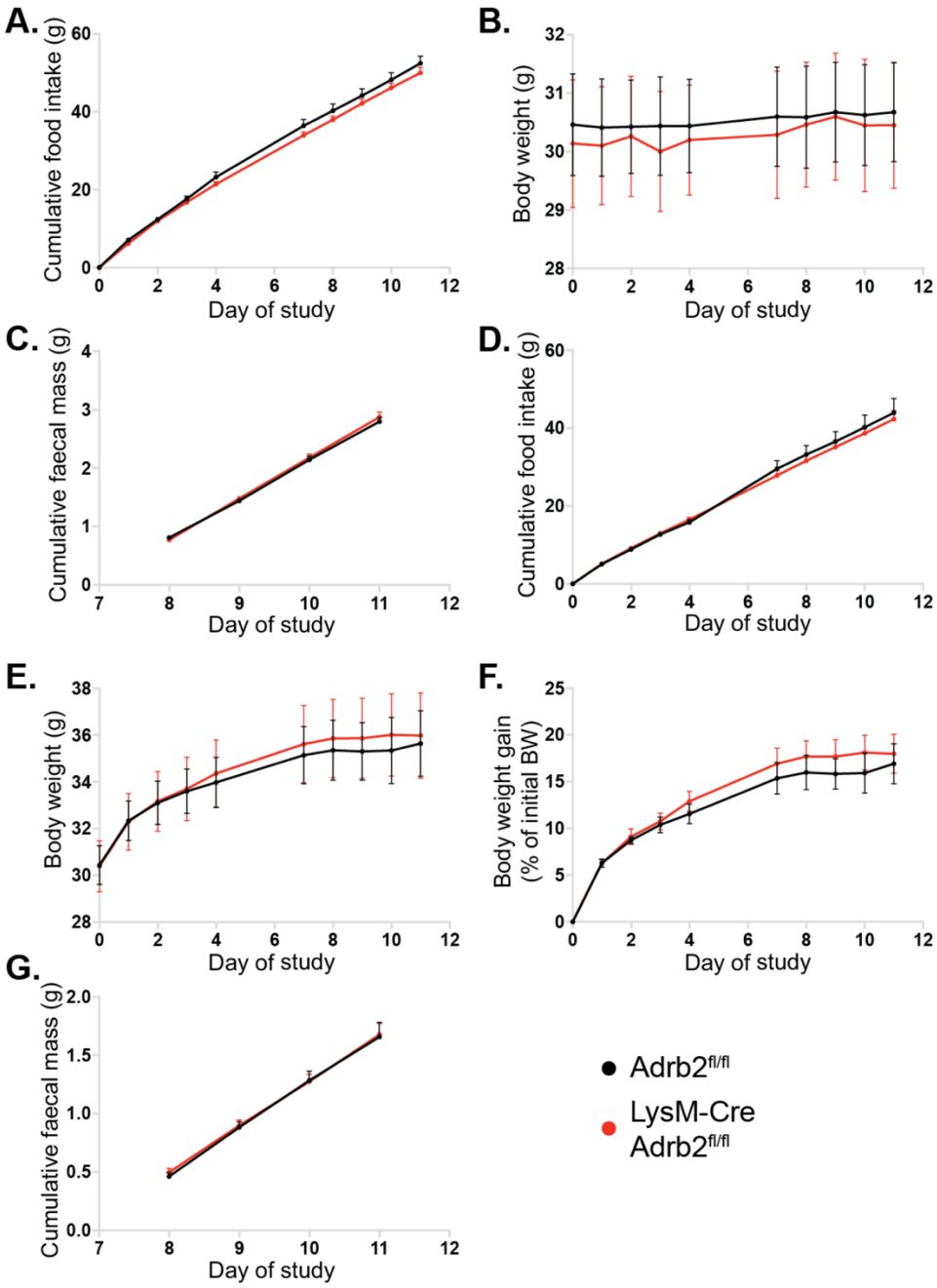

Figure 4-32. Body weight, food intake and excretion of faeces of chow and HFD-fed Adrb2$^{fl/fl}$ and LysM-Cre Adrb2$^{fl/fl}$ mice.

*(**A**) Cumulative food intake, (**B**) daily body weight measurements and (**C**) cumulative faecal weight assessed over 12 days (faecal weight was measured during last 5 days of the 12-day period) on chow diet, and (**D**) cumulative food intake, daily body weight measurements expressed as (**E**) absolute body weight or (**F**) percentage body weight increase from the start of HFD and cumulative faecal weight assessed over 12 days (faecal weight was measured during last 5 days of the 12-day period) on 60% kcal fat diet (D12492). N=8 Adrb2$^{fl/fl}$ (black lines) and n=8 LysM-Cre Adrb2$^{fl/fl}$ (red lines) male mice. 12 day-long chow diet intake analysis was initiated at 14 weeks of age and was immediately followed by 12-day long HFD intake analysis.*

4.2.2.15 Macrophage-specific *Adrb2* deletion increased blood glucose levels in the fed state after 2 weeks of HFD

Results. At the end of the food intake study, LysM-Cre Adrb2$^{fl/fl}$ animals and controls had similar body weight and BAT-, scWAT-, eWAT- and liver-to-body weight ratios (Figure 4-33 A, C-E). Interestingly, 2 weeks of high-fat feeding increased blood glucose levels in the fed state in LysM-Cre Adrb2$^{fl/fl}$ mice compared to controls (Figure 4-33 B, F).

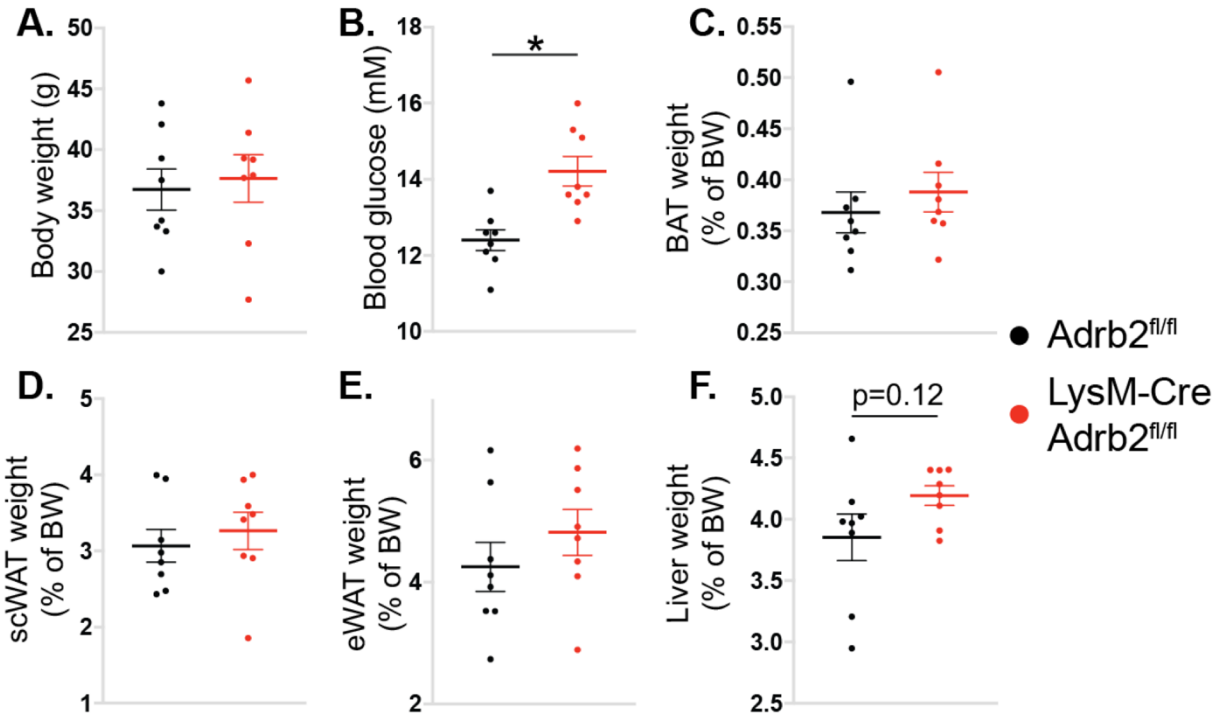

Figure 4-33. Tissue weights and blood glucose levels in Adrb2$^{fl/fl}$ and LysM-Cre Adrb2$^{fl/fl}$ mice after a short-term HFD.

*(**A**) Body weight, (**B**) blood glucose levels and weights of (**C**) BAT, (**D**) scWAT, (**E**) eWAT and (**F**) liver, expressed as a percentage of body weight of Adrb2$^{fl/fl}$ (n=7, black dots) and LysM-Cre Adrb2$^{fl/fl}$ (n=7, red dots) 19-week-old male mice on a pure C57Bl/6J background, fed a 60% kcal fat diet (D12492) from 8 weeks of age and culled in a random fed state. * p < 0.05 compared between genotypes using student's t-test.*

4.2.2.16 Macrophage-specific *Adrb2* deletion reduced glucose infusion rate during hyperinsulinaemic-euglycaemic clamp of chow-fed mice

***Rationale*.** As I observed increased blood glucose levels after 6 h fast, as well as elevated *Fasn* expression and relative palmitate levels in the livers of chow-fed LysM-Cre Adrb2$^{fl/fl}$ animals compared to controls, I decided to perform hyperinsulinaemic-euglycaemic clamps on chow- and HFD-fed animals in order to measure the rate of hepatic glucose production (HGP), and also to formally assess the impact of β2AR deficiency in macrophages on systemic insulin sensitivity in mice.

***Results*.** Chow-fed LysM-Cre Adrb2$^{fl/fl}$ group weighed similarly to controls leading up to the experiment (Figure 4-34 A). LysM-Cre Adrb2$^{fl/fl}$ mice that successfully undergone clamp procedure had a comparable body weight to controls (Figure 4-34 B). No difference in blood glucose levels after an overnight fast was observed between genotypes in this group, and all analysed mice were clamped within 1 mM range of their basal blood glucose levels (Figure 4-34 C). Interestingly, LysM-Cre Adrb2$^{fl/fl}$ mice required lower glucose infusion rate (GIR) to maintain stable blood glucose concentration in hyperinsulinaemic state compared to controls (Figure 4-34 D,E).

4.2.2.17 Macrophage-specific *Adrb2* deletion increased insulin-mediated glucose disposal during hyperinsulinaemic-euglycaemic clamp of HFD-fed mice

Results. Unlike my previous observation, β2AR deficiency in macrophages did not affect the body weight of mice during high-fat feeding (Figure 4-35 A). Successfully clamped mice had similar body weight, blood glucose concentration after overnight fast and required similar GIR to maintain stable blood glucose levels during the clamp (Figure 4-35 B, C,D, F). Interestingly, LysM-Cre Adrb2$^{fl/fl}$ animals showed increased glucose disposal during clamp, despite exhibiting similar clamp HGP compared to controls (Figure 4-35 E).

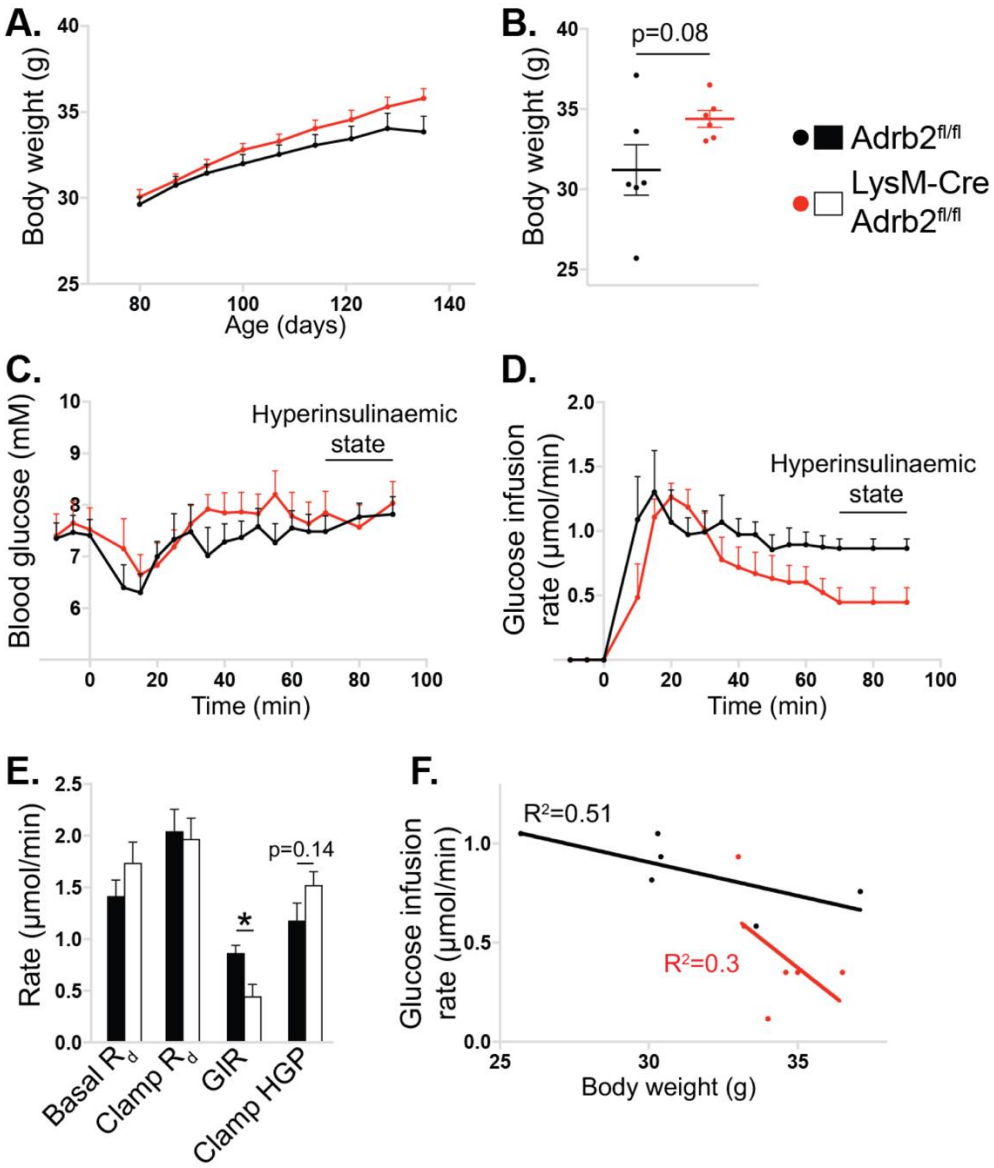

Figure 4-34. Hyperinsulinaemic-euglycaemic clamp analysis of chow-fed Adrb2$^{fl/fl}$ and LysM-Cre Adrb2$^{fl/fl}$ mice.

*(**A**) Weekly body weight measurements prior to the study (perfomed at 155 days of age), n=11 Adrb2$^{fl/fl}$ (black lines) and n=9 LysM-Cre Adrb2$^{fl/fl}$ (red lines) male mice on a pure C57Bl/6J background. (**B**) Body weights, (**C**) blood glucose levels and (**D**) glucose infusion rate during the clamp. Insulin was administered at T=0 min. Last 3 blood samples were considered as a hyperinsulinaemic ('clamped') state and were used for determining the clamp rate of glucose disposal (R_d) and HGP. Only the data from the animals that were successfully clamped is presented (n=6 mice/genotype). (**E**) Summary of the results (Adrb2$^{fl/fl}$, black bars and LysM-Cre Adrb2$^{fl/fl}$, white bars) and (**F**) the correlation between body weight and GIR. * $p < 0.05$ compared between genotypes using (**A**) two-way ANOVA with Bonferroni's multiple comparisons test, (**B, E**) student's t-test or (**F**) one-way ANCOVA. In (**F**), p=0.08. Experiment and data analysis was performed by Dr Sam Virtue and Dr Anne Mcgavigan.*

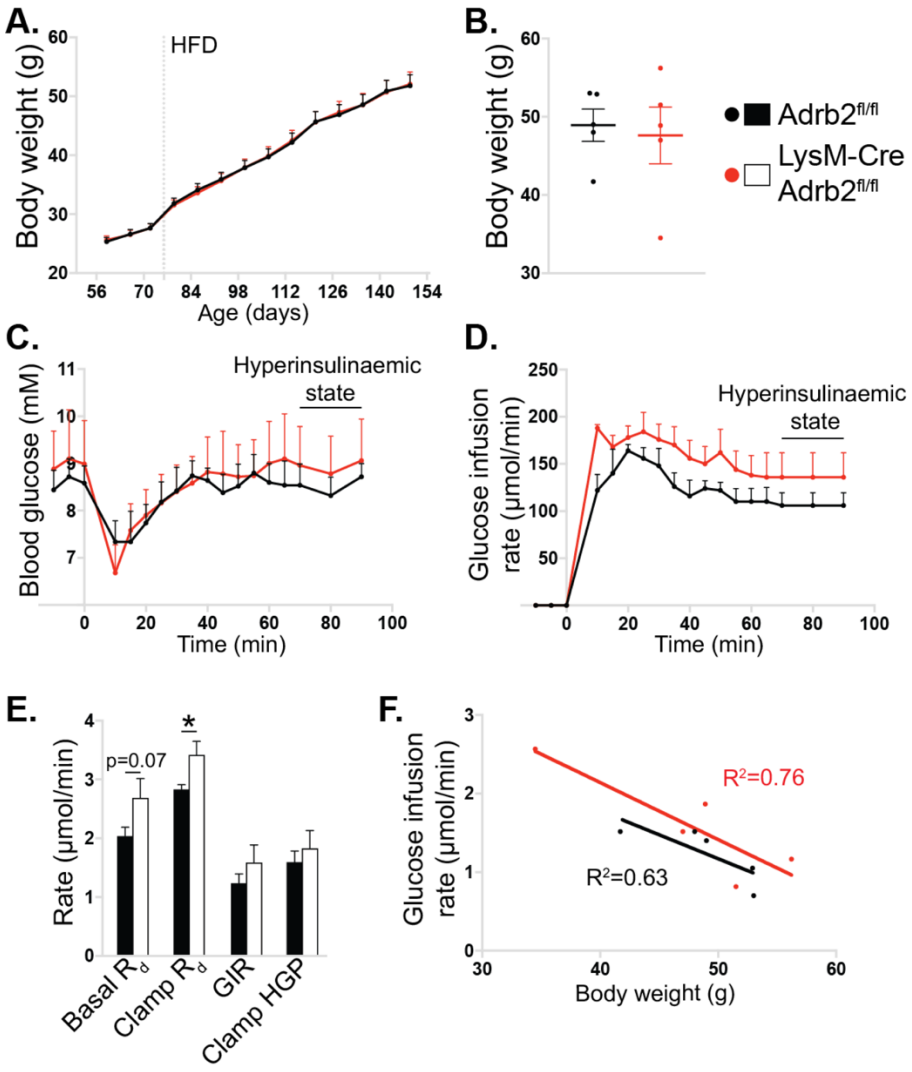

Figure 4-35. Hyperinsulinaemic-euglycaemic clamp analysis of HFD-fed Adrb2$^{fl/fl}$ and LysM-Cre Adrb2$^{fl/fl}$ mice.

*(**A**) Weekly body weight measurements prior to the study (perfomed at 155 days of age. Dotted line indicates the switch from chow to 60% kcal HFD (D12492)), n=10 Adrb2$^{fl/fl}$ (black lines) and n=11 LysM-Cre Adrb2$^{fl/fl}$ (red lines) male mice on a pure C57Bl/6J background. Duration of HFD was 12 weeks. (**B**) Body weights, (**C**) blood glucose levels and (**D**) glucose infusion rate during the clamp. Insulin was administered at T=0 min. Last 3 blood samples were considered as a hyperinsulinaemic ('clamped') state and were used for determining the clamp rate of glucose disposal (R_d) and HGP. Only the data from the mice that were successfully clamped is presented (n=5 mice/genotype). (**E**) Summary of the results (Adrb2$^{fl/fl}$, black bars and LysM-Cre Adrb2$^{fl/fl}$, white bars) and (**F**) the correlation between body weight and GIR. * $p < 0.05$ compared between genotypes using two-way ANOVA with Bonferroni's multiple comparisons test (**A**) student's t-test (**B, E**) or one-way ANCOVA (**F**). In (**F**), p=0.22. Experiment and data analysis was performed by Dr Sam Virtue and Dr Anne Mcgavigan.*

4.2.2.18 Systemic β2AR blockade reduced liver weight of mice after a short-term cold exposure

***Rationale*.** After completing the initial metabolic phenotyping experiments, I decided to investigate the effects of macrophage β2AR deficiency on the metabolic profile of mice exposed to cold, when SNS tone to adipose tissues is increased in order to enhance thermogenesis and to promote lipolysis to fuel increased lipid utilisation by UCP1-positive adipocytes.

I initially decided to use ICI-118,511 to block all β2ARs in mice before placing them from the room temperature to 10 °C. As the predominant NE receptor mediating lipolysis and thermogenesis in adipocytes is β3AR, I hypothesised that inhibiting β2AR would mostly affect macrophages and vascular smooth muscle cells.

***Results*.** Exposure of animals to 10 °C for 24 h did not affect their body weight independently of β2AR blockade (Figure 4-36 A). Core body temperature was reduced in cold to the same degree in both groups (Figure 4-36 B). Interestingly, while β2AR blockade during cold exposure did not impact the BAT-, scWAT- and eWAT-to-body weight ratios, it reduced the liver-to-body weight ratio compared to controls (Figure 4-36 C-F).

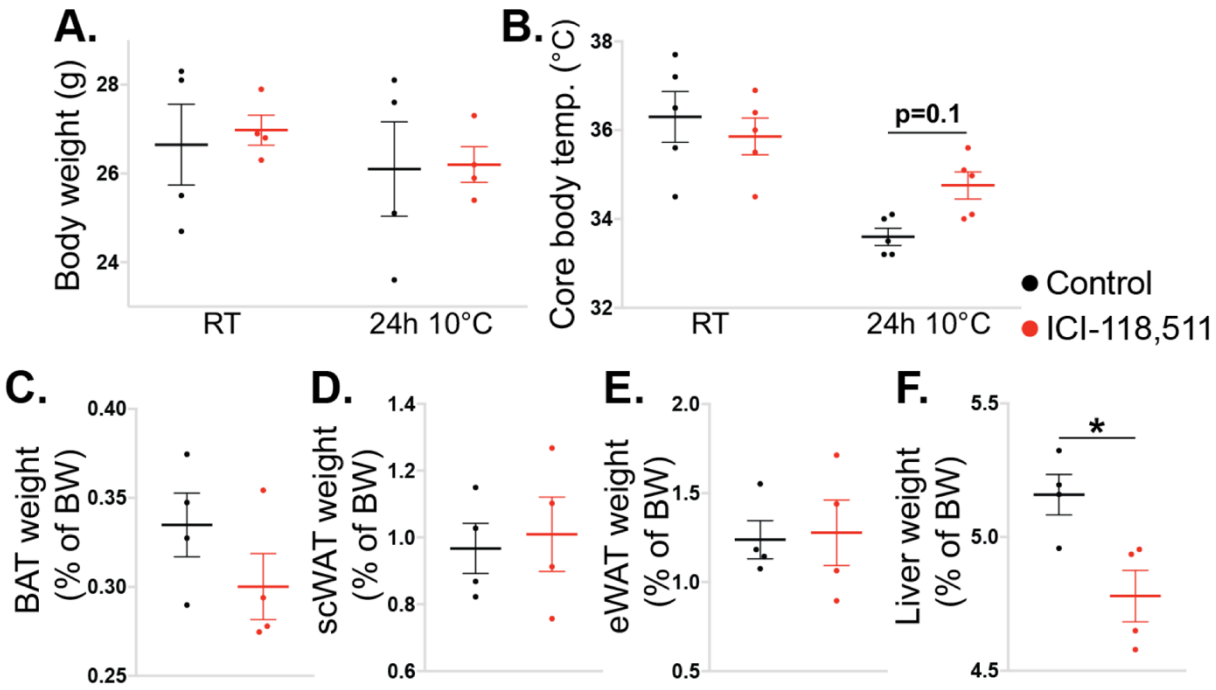

Figure 4-36. Body weight, core temperature and tissue weights of cold-exposed mice treated with β2AR blocker.

*(**A**) Body weight and (**B**) rectal temperature of 12-week-old male mice on a pure C57Bl/6J genetic background under the standard housing conditions (RT, both groups), or after an intraperitoneal bolus injection of ICI-118,511 (500 μg/mouse, red dots) and an immediate switch to the environmental temperature of 10 ℃ for 24 h (24h 10℃). Control mice were injected with PBS (black dots). Weights of (**C**) BAT, (**D**) scWAT, (**E**) eWAT and (**F**) liver, expressed as a percentage of body weight after 24 h at 10 ℃. N=5 mice/group for (**B**), and n=4 mice/group for (**A, C-F**). * $p < 0.05$ compared between genotypes using (**A, B**) two-way ANOVA with Bonferroni's multiple comparisons test or (**C-F**) student's t-test.*

4.2.2.19 Systemic β2AR blockade increased BAT *Ucp1* expression levels after a short-term cold exposure

Results. Animals injected with ICI-118,511 had higher *Ucp1* mRNA levels, indicating an increased BAT thermogenic function (Figure 4-37 A). The expression of beige adipocyte marker genes *Ucp1* and *Dio2* was similar, while *Elovl3* mRNA levels were higher in scWAT of cold exposed mice treated with β2AR-blocker compared to controls (Figure 4-37 B). Treatment with ICI-118,511 did not affect *Adrb2* mRNA levels in BAT or scWAT (Figure 4-37 A,B).

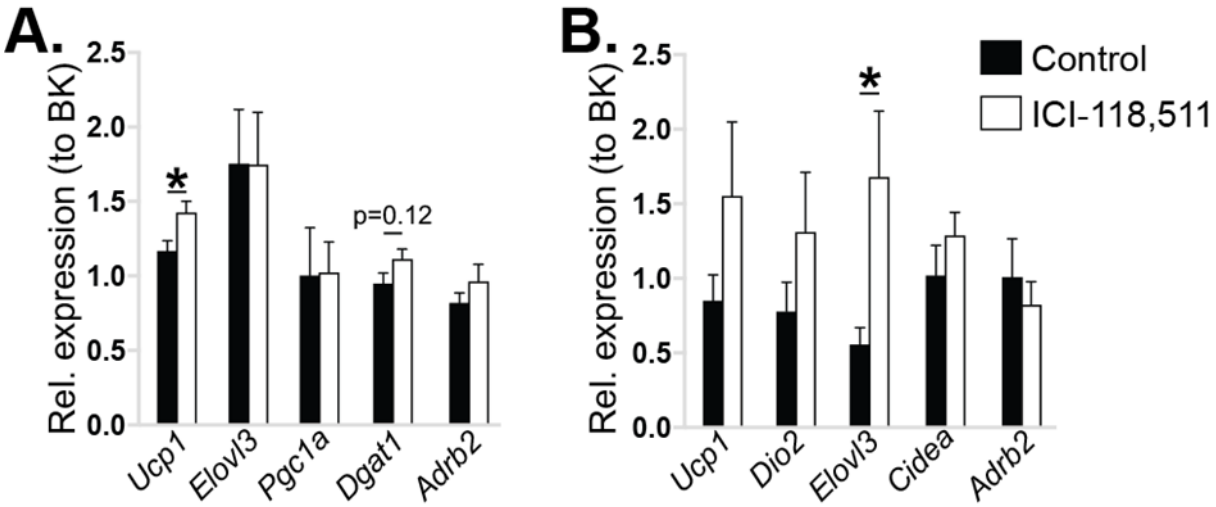

Figure 4-37. Gene expression analysis of BAT and scWAT isolated from cold-exposed mice treated with β2AR blocker.

*(**A**) Ucp1, Elovl3, Pgc1a, Dgat1 and Adrb2 mRNA levels* (normalised to BestKeeper) *in BAT, and (**B**) Ucp1, Dio2, Elovl3, Cidea and Adrb2 mRNA levels* (normalised to BestKeeper) *in scWAT of 12-week-old male mice on a pure C57Bl/6J genetic background, injected with PBS (n=5, black bars) or ICI-118,511 (500 μg/mouse, n=5, white bars) and placed at 10 ℃ for 24h. * p < 0.05 compared between genotypes using student's t-test.*

4.2.2.20 Macrophage-specific *Adrb2* deletion did not affect the systemic response to cold exposure

***Rationale*.** Next, I decided to investigate how mice carrying a macrophage-specific *Adrb2* deletion respond to a cold environment. To test this, I placed LysM-Cre Adrb2$^{fl/fl}$ and control animals at 5 °C and measured their body weight, core body temperature, circulating glucose and FFAs before and after 6, 24 and 72 h in a cold environment.

***Results*.** LysM-Cre Adrb2$^{fl/fl}$ mice exhibited comparable weight loss and core body temperature at 5 °C to controls (Figure 4-38 A,B). Cold exposure equally increased blood glucose concentration in both genotypes (Figure 4-38 C). While circulating FFA levels were higher in LysM-Cre Adrb2$^{fl/fl}$ animals compared to controls before cold exposure, atypically high serum FFA concentration indicated potential sample degradation, which could also explain observed decrease in serum FFA levels in both groups over the course of cold exposure, rather than the expected increase (Figure 4-38 D).

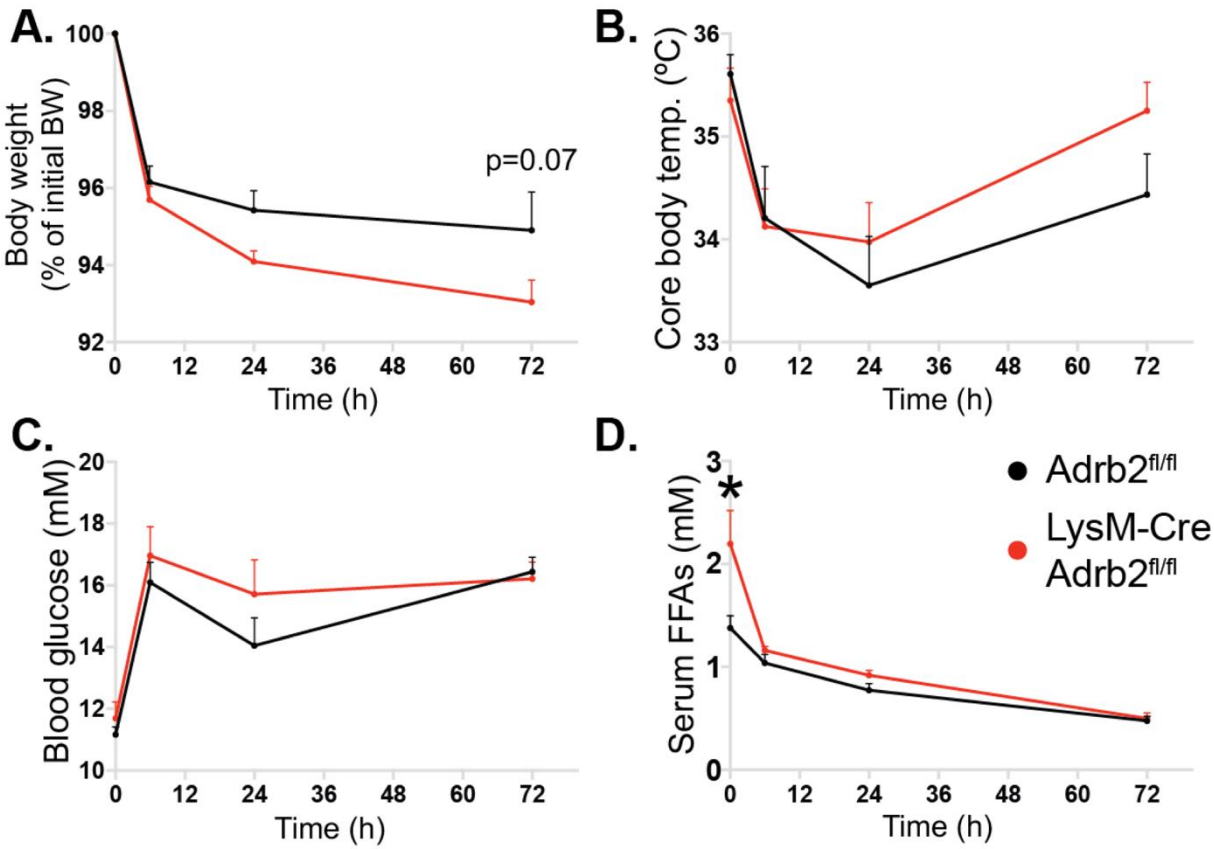

Figure 4-38. Body weight, core body temperature, circulating glucose and FFA levels in Adrb2$^{fl/fl}$ and LysM-Cre Adrb2$^{fl/fl}$ mice during cold exposure.

*(**A**) Body weight (expressed as percentage of the body weight at T=0), (**B**) rectal temperature, (**C**) blood glucose and (**D**) serum FFA levels measured after 6, 24 and 72 h of exposure to 5 ℃ environmental temperature in Adrb2$^{fl/fl}$ (n=11, black lines) and LysM-Cre Adrb2$^{fl/fl}$ (n=8, red lines) 16-week-old male mice on a pure C57Bl/6J genetic background. * p < 0.05 compared between genotypes at each time-point using two-way ANOVA with Bonferroni's multiple comparisons test.*

4.2.2.21 Macrophage-specific *Adrb2* deletion did not affect the weight of metabolic tissues of mice after 72 h of cold exposure

Results. There were no genotype-dependent differences in total body weight, and BAT-, scWAT-, eWAT-, and liver-to-body weight ratios after 72 h of cold exposure (Figure 4-39 A-E).

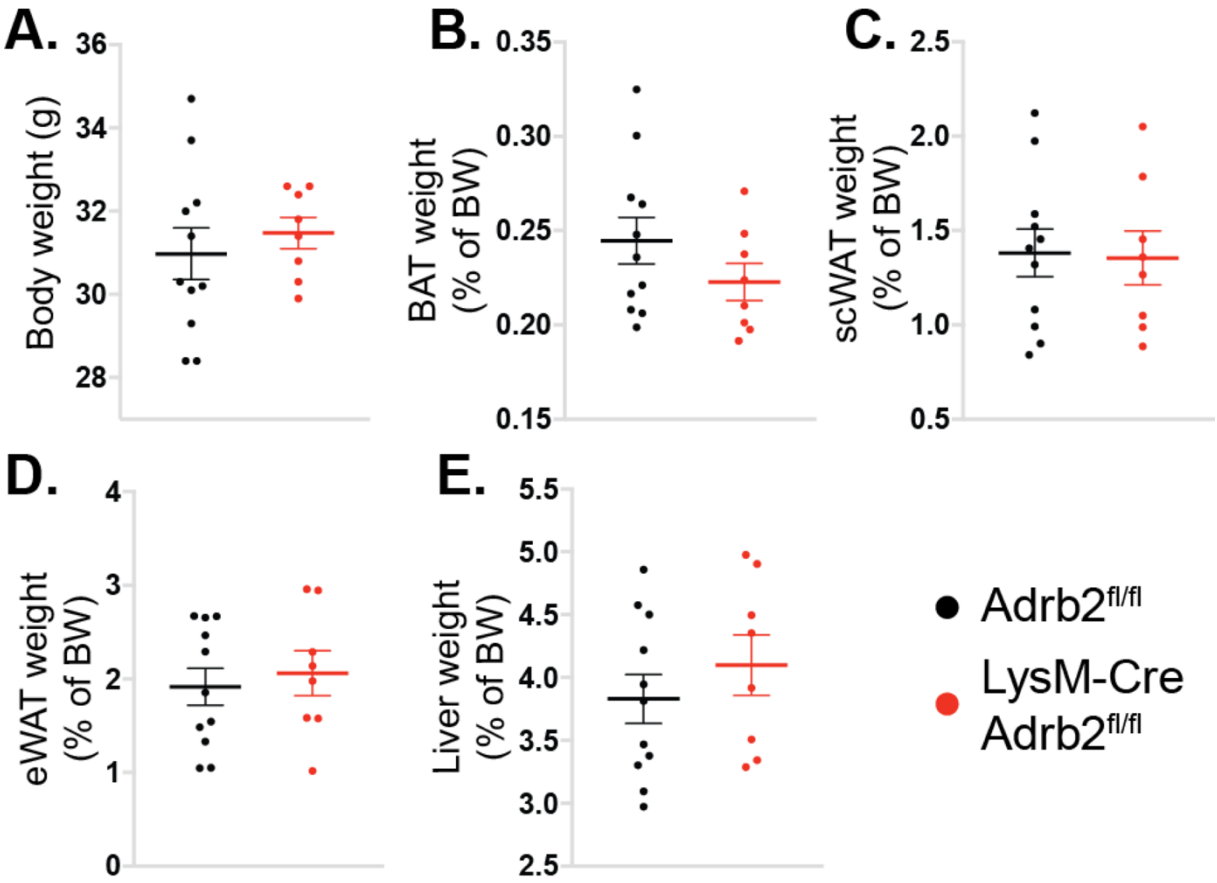

Figure 4-39. Tissue weights of Adrb2$^{fl/fl}$ and LysM-Cre Adrb2$^{fl/fl}$ mice after 72 h of cold exposure.

*(**A**) Body weight and weights of (**B**) BAT, (**C**) scWAT, (**D**) eWAT and (**E**) liver, expressed as a percentage of body weight of Adrb2$^{fl/fl}$ (n=11, black dots) and LysM-Cre Adrb2$^{fl/fl}$ (n=8, red dots) 16-week-old male mice on a pure C57Bl/6J genetic background, placed at 5 ℃ for 72 h. Statistical differences were compared between genotypes using student's t-test.*

4.2.2.22 Macrophage-specific *Adrb2* deletion did not affect scWAT gene expression after 72 h of cold exposure

Results. After 72 h at 5 °C, LysM-Cre Adrb2$^{fl/fl}$ and control animals had similar levels of *Ucp1*, *Pgc1a, Cidea, Elovl3, Atgl, Hsl, Adrb1, Adrb2, Adrb3, Cd11b, F4/80 and Cd206* mRNA in scWAT, indicating no genotype-dependent differences in scWAT browning or inflammation (Figure 4-40).

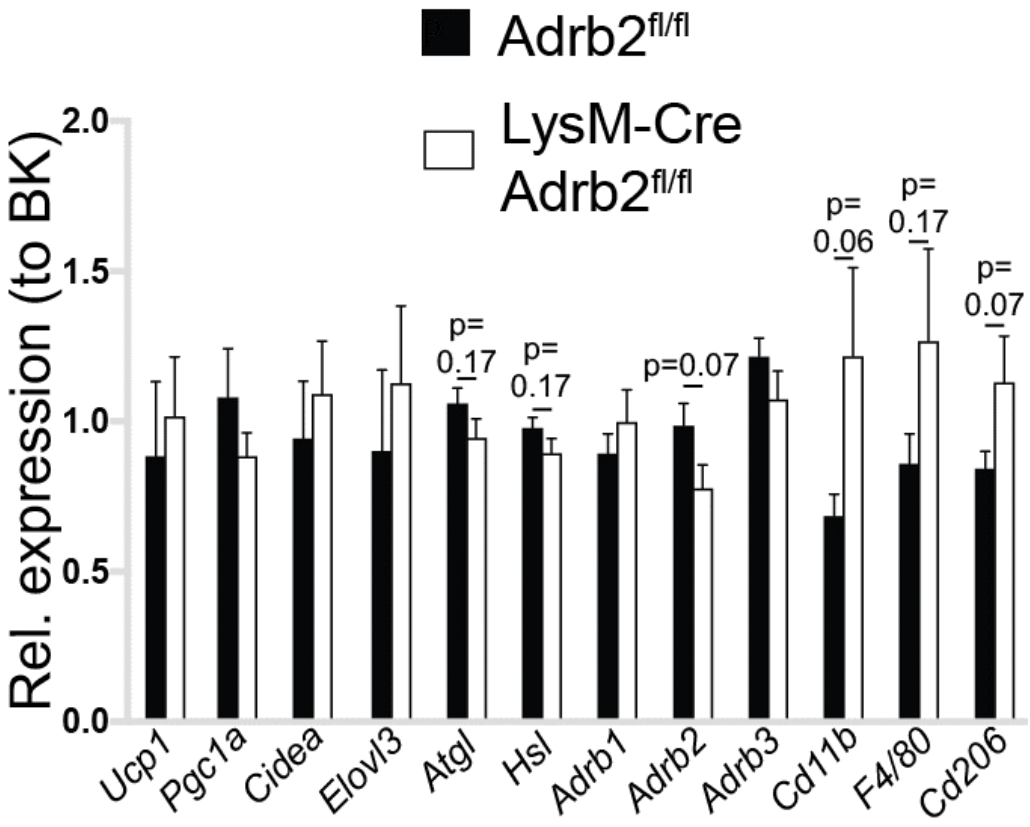

Figure 4-40. Gene expression analysis of scWAT isolated from Adrb2$^{fl/fl}$ and LysM-Cre Adrb2$^{fl/fl}$ mice after 72 h of cold exposure.

Ucp1, Pgc1a, Cidea, Elovl3, Atgl, Hsl, Adrb1, Adrb2, Adrb3, Cd11b, F4/80 and Cd206 mRNA levels (normalised to BestKeeper) *in scWAT isolated from Adrb2$^{fl/fl}$ (n=11, black dots) and LysM-Cre Adrb2$^{fl/fl}$ (n=8, red dots) 16-week-old male mice on a pure C57Bl/6J genetic background, placed at 5 ℃ for 72 h. Statistical differences were compared between genotypes using student's t-test.*

4.3 Discussion

This chapter describes how NE signalling via β2AR regulates TG metabolism in macrophages, and how the loss of macrophage β2AR signalling affects the metabolic health of a whole animal in lean and obese states. This study was initiated after β2AR stimulation had been found to reduce lipolysis and promote lipid accumulation in BMDMs. The main findings of this chapter were as follows:

1) β2AR activation enhanced TG storage in BMDMs by increasing *Dgat1* transcription.

2) LysM-Cre Adrb2$^{fl/fl}$ mice did not exhibit changes in WAT inflammation or systemic insulin sensitivity on a chow or HFD.

3) Both systemic inhibition of β2ARs and macrophage-specific *Adrb2* deletion did not alter the thermogenic response of mice to a cold environment challenge.

4.3.1 β2AR activation promoted FFA storage in BMDMs

In this chapter, I demonstrated that β2AR stimulation rapidly supressed lipolysis and enhanced TG storage in BMDMs via two independent mechanisms.

My lipolysis experiments have shown that the inhibitory effect on the oleate release from BMDMs occurs during 1-3 h post β2AR activation. Interestingly, such inhibition was not dependent on TG hydrolysis, oleate re-esterification to TGs or lipophagy. One potential reason for reduced appearance of radiolabelled oleate in the medium after stimulating lipid-laden BMDMs with β2AR agonist that was not tested in this chapter could be decreased rate of oleate oxidation, as observed independently during the measurement of FFA oxidation rates in response to NE stimulation. As the medium used in BMDM culture contain bicarbonate buffering system, CO_2 produced by BMDMs during complete β-oxidation of fatty acids will be initially trapped in the medium before equilibrating with atmospheric gas. Therefore, it is possible that a part of radioactivity released from radiolabelled oleate-laden BMDMs after the medium change does not correspond to liberated ^{14}C-oleate, but rather to $^{14}CO_2$ produced from the complete oxidation of ^{14}C-oleate. I will test such hypothesis in the future by performing lipid extraction on the supernatants of the lipolysis assay of BMDMs. If the inhibitory effect of β2AR activation on the oleate release from BMDMs are due to decreased ^{14}CO2

release, there should be equal amounts of radiolabel in the lipid phase of the supernatants from β2AR agonist-treated BMDMs and controls. Furthermore, I will investigate whether the inhibitory effect on the radiolabel appearance in the medium could be blocked by etomoxir.

Unlike inhibition of lipolysis, increased TG storage in BMDMs occur after prolonged β2AR activation and is predominantly mediated by up-regulated DGAT1 enzymatic activity. While increased TG esterification in response to β2AR agonism can be explained by a transcriptional activation of *Dgat1* gene, it is difficult to understand the biological importance of such process. Previous report has ascribed an anti-inflammatory role for DGAT1 in macrophages during treatments with LPS or palmitate[209]. However, the protective effects of DGAT1 during lipotoxicity are thought to be mediated by decreased intracellular concentrations of its substrate DAG[258]. My results showed that despite increased DGAT1 activity and TG synthesis, the absolute levels of DAG species in palmitate-treated BMDMs were not affected by β2AR activation or DGAT1 blockade. Consistent with such observation, anti-inflammatory effects of β2AR agonist in BMDMs during stimulation with palmitate were not mediated by increased DGAT1 activity, but likely by direct suppression of intracellular TLR signalling pathway, as described in other reports where β2AR stimulation inhibited NF-κB activation in LPS-treated macrophages[459,568].

4.3.2 Macrophage-specific *Adrb2* deletion did not lead to increased WAT inflammation during obesity

Current literature supports the anti-inflammatory role for macrophage β2AR in multiple tissues, including WAT. Gut luminal bacterial infection has been shown to rapidly activate gut extrinsic sympathetic innervation, leading to the activation of β2AR in the intestinal muscle macrophages and promoting their M2 polarisation, thus limiting the tissue inflammation[438]. Similarly, leptin-mediated increase in NE signalling in WAT has been suggested to reduce WAT inflammation through elevating cAMP levels in ATMs[460]. Furthermore, surgically denervating eWAT or BAT has been shown to increase their *Tnf* expression levels, supposedly due to decreased β2AR signalling in ATMs[459]. Finally, treating obese rats with β2AR agonist has attenuated inflammation and fibrosis in the kidneys and heart[569].

In the light of published reports, it is surprising that I did not observe elevated WAT inflammation in the macrophage-specific *Adrb2* knockout mice compared to controls after prolonged high-fat feeding. In fact, my results indicated a tendency towards a favourable metabolic phenotype in obese animals lacking β2ARs in macrophages, even when there was no difference in the total body-weight, as characterised by an increased rate in insulin-mediated glucose disposal compared to genotype controls in euglycaemic clamp experiment. It is important to emphasise that all the previous publications suggesting an anti-inflammatory role for β2AR signalling in ATMs did not utilise a macrophage-specific *Adrb2* knockout animal model, which is a best available tool to directly assess the importance of β2AR signalling in ATMs on the development of WAT inflammation. Both the activation of SNS by leptin[460], or surgical denervation of WAT[459] would directly affect the adipocytes by modulating their β3AR activation. Therefore, my results suggest that the anti-inflammatory properties of NE signalling in WAT observed in the previous studies are likely due to β-adrenergic stimulation of the adipocytes, which subsequently affect ATMs through a paracrine signalling that remains to be investigated.

The anti-inflammatory action of β2AR agonist observed during the palmitate treatment of BMDMs *in vitro* did not translate into elevated M1 or reduced M2 polarisation in β2AR-deficient ATMs *in vivo*. Such finding further emphasise the complexity of a physiological system and indicate that using canonical tools to study lipotoxicity in macrophages *in vitro* is not always a good model for processes occurring in the WAT. In the following results chapter (Chapter 5), I will describe a more detailed characterisation of the phenotype of β2AR agonist-treated BMDMs, which might help to explain the unexpected phenotype of LysM-Cre Adrb2$^{fl/fl}$ mice.

4.3.3 Macrophage-specific *Adrb2* deletion had a minor effect on hepatic glucose metabolism

Reduced body weight gain during high-fat feeding, and increased body weight loss following cold exposure in LysM-Cre Adrb2$^{fl/fl}$ animals could theoretically be explained by elevated SNS tone in BAT and/or scWAT. However, no changes in *Ucp1* or other genes that reflect increased BAT activity or scWAT browning were observed between genotypes on a HFD, or following cold exposure. Furthermore, the resistance to acquire body mass during obesity could not be replicated in two different cohorts of LysM-Cre Adrb2$^{fl/fl}$ mice. Finally, no differences in the overall energy balance were

found on a chow diet, or during the initial period of high-fat feeding between LysM-Cre Adrb2$^{fl/fl}$ animals and controls. Based on the presented evidence, it is difficult to identify the potential reasons for such discrepant *in vivo* findings in this chapter.

When compared to genotype controls, mice lacking β2AR in macrophages showed increased blood glucose levels in a fasted state on a chow diet and in a fed state after a short-term HFD; increased circulating liver enzyme AST on a chow diet; elevated hepatic *Fasn* expression and relative palmitate levels in the fed state on a chow diet. Furthermore, chow-fed LysM-Cre Adrb2$^{fl/fl}$ mice had reduced GIR during hyperinsulinaemic-euglycaemic clamp compared to controls, likely resulting from increased HGP during a clamp. In summary, macrophage-specific *Adrb2* deletion caused elevated HGP in multiple experimental settings. Interestingly, increased SNS tone in the liver is known to promote HGP[570,571]. Furthermore, hepatic SNS signalling has been shown to supress ketogenesis, which utilises FFAs, including palmitate, as substrates[572]. Therefore, it is possible that the observed changes in the liver profile of LysM-Cre Adrb2$^{fl/fl}$ mice are caused by reduced NE degradation by Kupffer cells, leading to increased hepatic SNS tone. In future, I will investigate such hypothesis by measuring NE concentration in the livers of LysM-Cre Adrb2$^{fl/fl}$ and control animals in the fed and fasted states. I will also isolate Kupffer cells from mice of both genotypes in order to assess the expression of genes encoding monoamine degradation enzymes.

As several *in vivo* findings in this chapter pointed to a role of macrophage β2AR in limiting SNS tone in liver, in future I will employ a more mechanistic approach to study the importance of macrophage β2AR for NE degradation *in vivo*. SLC6A2 deficiency in macrophages has been found to increase *Ucp1* levels in BAT and scWAT after 2 h of cold exposure of mice compared to controls[424]. Therefore, I will place LysM-Cre Adrb2$^{fl/fl}$ and control animals at 4 °C for 2 h in order to investigate the early SNS-mediated signalling events leading to increased BAT activation and scWAT browning in response to cold. It is possible that after 24 h of cold exposure, the physiological system adapts to a decreased rate of NE degradation by reducing SNS output to the adipose tissues. Such short-term regulatory mechanism could be physiologically important for the adaptation to circadian environmental temperature fluctuations, and my proposed experiment would provide the basis for the future studies in this area.

4.3.4 Conclusions

In this chapter, I found that NE, acting via β2AR, altered BMDM lipid metabolism by supressing oleate release and oxidation, and enhancing TG storage. While β2AR activation supressed palmitate-induced inflammatory activation of BMDMs, such suppression was not mediated by increased TG storage capacity. Despite the published and observed anti-inflammatory effects of β2AR agonism in BMDMs, macrophage-specific *Adrb2* knockout animals did not show differences in WAT inflammation or systemic insulin sensitivity compared to controls on a chow or HFD. Finally, mice lacking *Adrb2* in macrophages did not exhibit any differences in their response to a cold environment, but had a minor increase in HGP during fasting on a chow diet. In future, additional experiments will need to be performed in order to understand the importance of macrophage β2AR in regulating SNS signalling within different tissues.

5 The regulation of gene and protein expression in BMDMs in response to β2AR activation

5.1 Introduction

The *in vitro* studies presented in Chapter 4 predominantly focused on the molecular mechanisms mediating increased TG storage in BMDMs in response to β2AR stimulation. However, one finding that I did not discuss in Chapter 4 was the transcriptional regulation of *Dgat1* gene following β2AR agonism. All measured canonical CREB target genes had a similar pattern of expression in response to β2AR activation, characterised by a rapid increase in mRNA levels immediately after stimulation with fenoterol, a peak of expression at 1 h, and a decline to the basal mRNA levels at 2-3 h after β2AR activation (Figure 5-1). Interestingly, increase in *Dgat1* mRNA was delayed and only commenced at 1 h, peaked at 2-4 h, and returned to the baseline at 8 h post stimulation (Figure 5-1). Such finding indicated that DGAT1 and potentially other intracellular metabolic enzymes were under a different transcriptional control compared to the canonical CREB target genes in response to β2AR activation.

Subsequently in this chapter, the canonical CREB target genes that showed peak mRNA levels at 1 h after β2AR activation will be referred as **early phase genes**, and the transcripts that exhibited delayed up-regulation post stimulation, including *Dgat1* – as **late phase genes** (Figure 5-1).

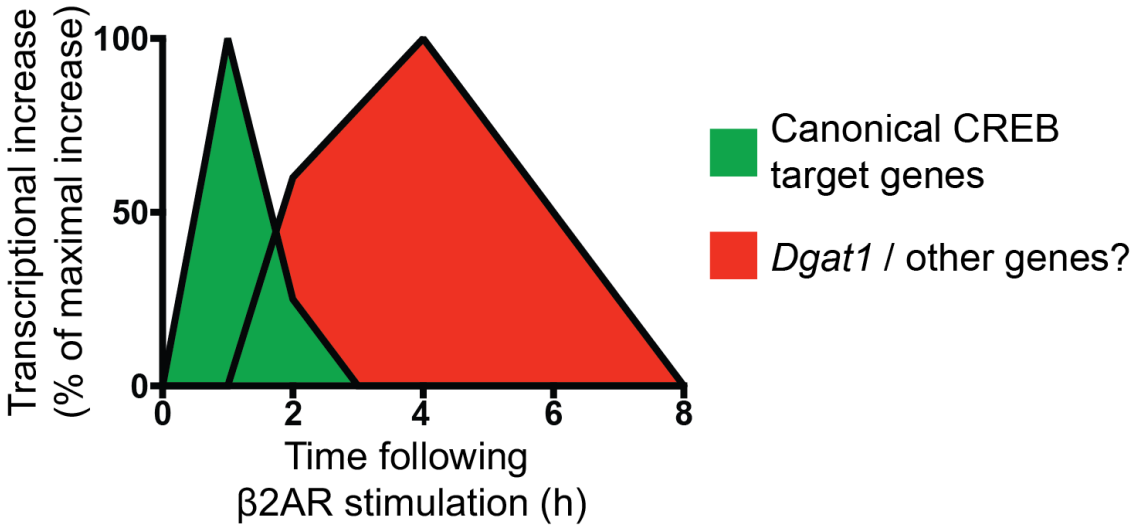

Figure 5-1. A hypothetical model of a biphasic induction of gene transcription following β2AR activation.

Furthermore, the *in vitro* studies of Chapter 4 focused only on β2AR agonism-elicited effects on BMDM fatty acid metabolism. Whether β2AR activation induces other changes to the intracellular BMDM nutrient metabolism is not yet known.

Based on my *in vitro* data presented in Chapter 4, I predict β2AR stimulation in macrophages to elicit a range of phenotypic changes. In part, these changes will be mediated by altered abundance of specific proteins. Therefore, in this chapter I propose the following research questions:

1) What is the identity of proteins induced by an acute β2AR stimulation in BMDMs? 2) What factors regulate the induction of these proteins in response to β2AR activation?

In this Chapter, I will aim to answer my research questions through the following objectives:

***Objective 1*. To characterise the changes in global protein expression elicited by β2AR agonism in BMDMs.** This will be performed using large-scale proteomic analysis of β2AR agonist-treated BMDMs. Based on the alterations in cellular proteome, bioinformatics tools will be utilised to predict the changes in metabolic and signalling pathways, as well as transcription factors that might mediate the BMDM phenotype induced by β2AR activation.

***Objective 2*. To validate the importance of predicted transcription factors in regulating gene transcription following β2AR stimulation in BMDMs.** Based on the results obtained in Objective 1, I will utilise pharmacological inhibitors and genetic cell models to identify signalling pathways and transcription factors regulating BMDM gene expression and lipid metabolism in response to β2AR activation alone or during inflammatory activation by LPS.

Expected impact. Overall, I expect that the results obtained in this chapter will help to explain the phenotype observed in LysM-Cre Adrb2$^{fl/fl}$ animals during obesity. Furthermore, the data from this chapter will contribute to the rapidly growing field investigating SNS-macrophage interactions by providing an insight into the effects of sympathetic nerve activation on the phenotype of neighbouring macrophages.

5.2 Results

5.2.1 Acute effects of β2AR activation on BMDM proteome

5.2.1.1 Acute β2AR activation induced profound changes in BMDM proteome

***Rationale*.** As my previous results indicated that fenoterol was specifically stimulating β2AR without any off-target effects on CREB phosphorylation, I decided to utilise it for β2AR activation in the proteomic analysis of BMDMs. Because of my primary interest in macrophage lipid metabolism, I used the kinetics of β2AR stimulation-induced *Dgat1* transcription to determine the appropriate time point for the proteome comparison. Since *Dgat1* mRNA levels peaked at approximately 4 h after β2AR activation, I chose to perform **6 h treatment** of BMDMs with fenoterol, accounting for the delay between gene transcription and protein expression.

***Results*.** In total, peptides corresponding to 5268 proteins were measured with a high degree of confidence. The coverage of proteome was incomplete, since multiple proteins that are known to be present in BMDMs, such as DGAT1, were not detected. The p value distribution analysis showed an enrichment in the abundance changes with a low p value (<0.05), indicating that β2AR activation for 6 h selectively modulated a specific set of measured proteins, and observed differences between two states were not due to a random distribution of protein amounts (Figure 5-2 A).

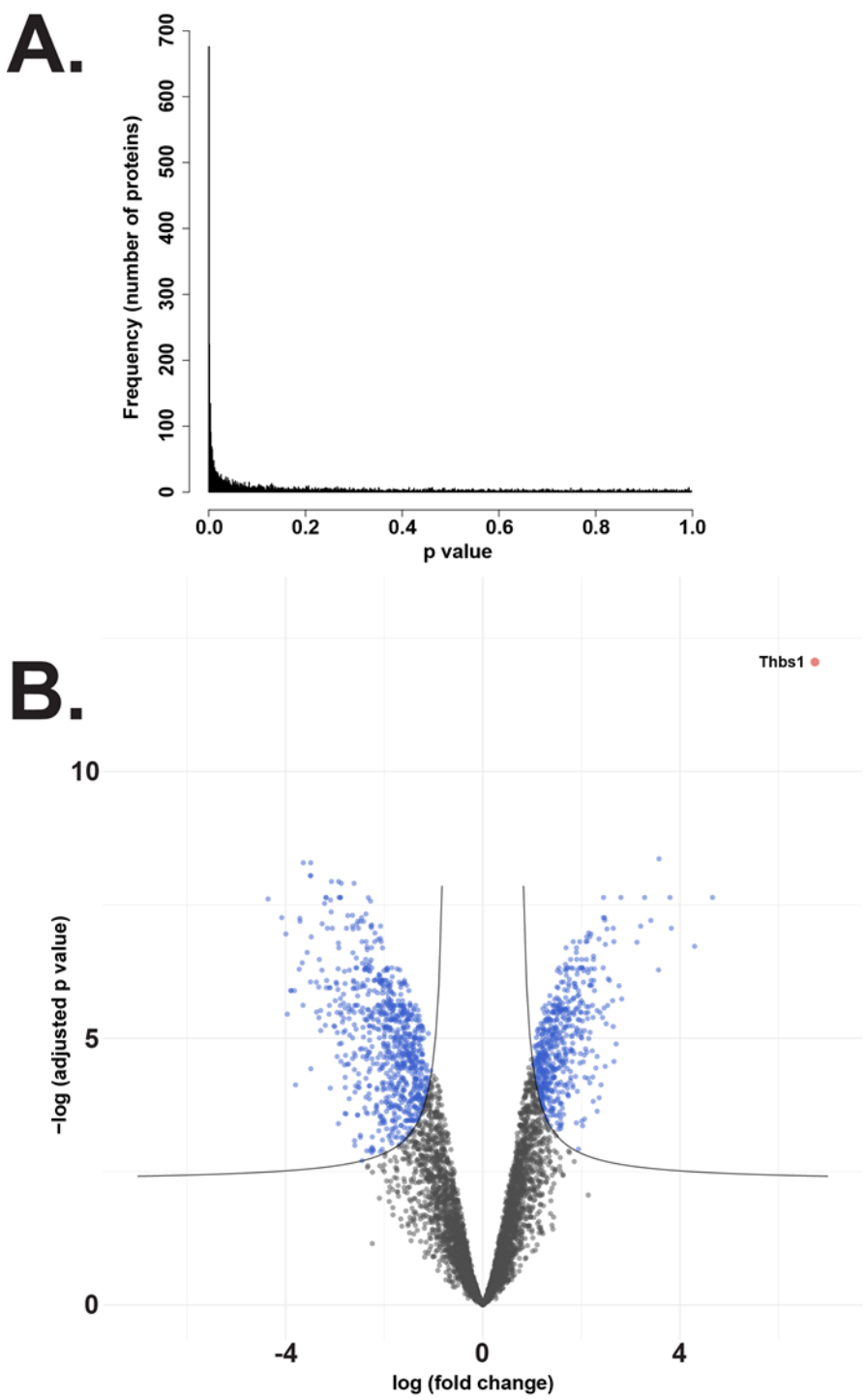

Figure 5-2. Visualisation of changes to BMDM proteome induced during 6 h following β2AR activation.

*(**A**) Frequency of proteins exhibiting a change in abundance at any degree of statistical significance and (**B**) the confidence and fold change in protein abundance between BMDMs treated with 1 μM fenoterol for 6 h and untreated controls. Hyperbolic cut-off lines and blue colouring in (**B**) is for visual comparison between up- and down-regulated proteins. Red dot corresponds to the most increased protein thrombospondin-1. N=3 mice. Data normalisation, analysis and visualisation was performed by PhD student Aurelien Dugourd from Prof. Rodriguez group.*

Plotting the confidence of change against the magnitude of change revealed that β2AR activation both increased and decreased the abundance of specific proteins, with a small bias towards down-regulating protein expression (Figure 5-2 B). Such observation is not uncommon for short-term cell stimulations, where agonist-induced protein degradation predominates over the synthesis of new proteins. Furthermore, one specific protein, **thrombospondin-1** (THBS1), exhibited a much greater increase upon β2AR activation than any other measured protein (Figure 5-2 B), and will be discussed further in this chapter.

5.2.1.2 Acute β2AR stimulation increased the activity of intracellular metabolic processes and pathways in BMDMs

***Rationale*.** Next, all measured proteins were analysed for biological trends in an unbiased manner based on the p value of changes between treated and non-treated groups (Figure 5-2 B, y axis). Gene Ontology (GO) database was utilised to identify proteins that are involved in the same biological processes, and Reactome, Kegg, NABA, Biocarta and PID databases were used to assign differentially expressed proteins to biological pathways.

***Results*.** Amongst all GO biological processes that had been up-regulated by β2AR stimulation, cellular metabolic processes were highly represented, including *carbohydrate, protein and lipid metabolism processes* (Figure 5-3 A). Similar trend was observed in the list of pathways showing elevated activity after β2AR activation, with the expression of proteins related metabolism of proteins, lipids and glucose being increased (Figure 5-4 A). Interestingly, despite fenoterol having no affinity to NE-degrading enzymes[573], the most up-regulated biological pathway in β2AR agonist-treated BMDMs was '*neuronal system*', which includes proteins involved in the *neurotransmitter uptake and degradation* (Figure 5-4 A). Finally, there was a clear trend for reduced activity of biological processes and pathways related to gene *transcription, mRNA processing and DNA replication* after β2AR activation in BMDMs (Figure 5-3 B, Figure 5-4 B).

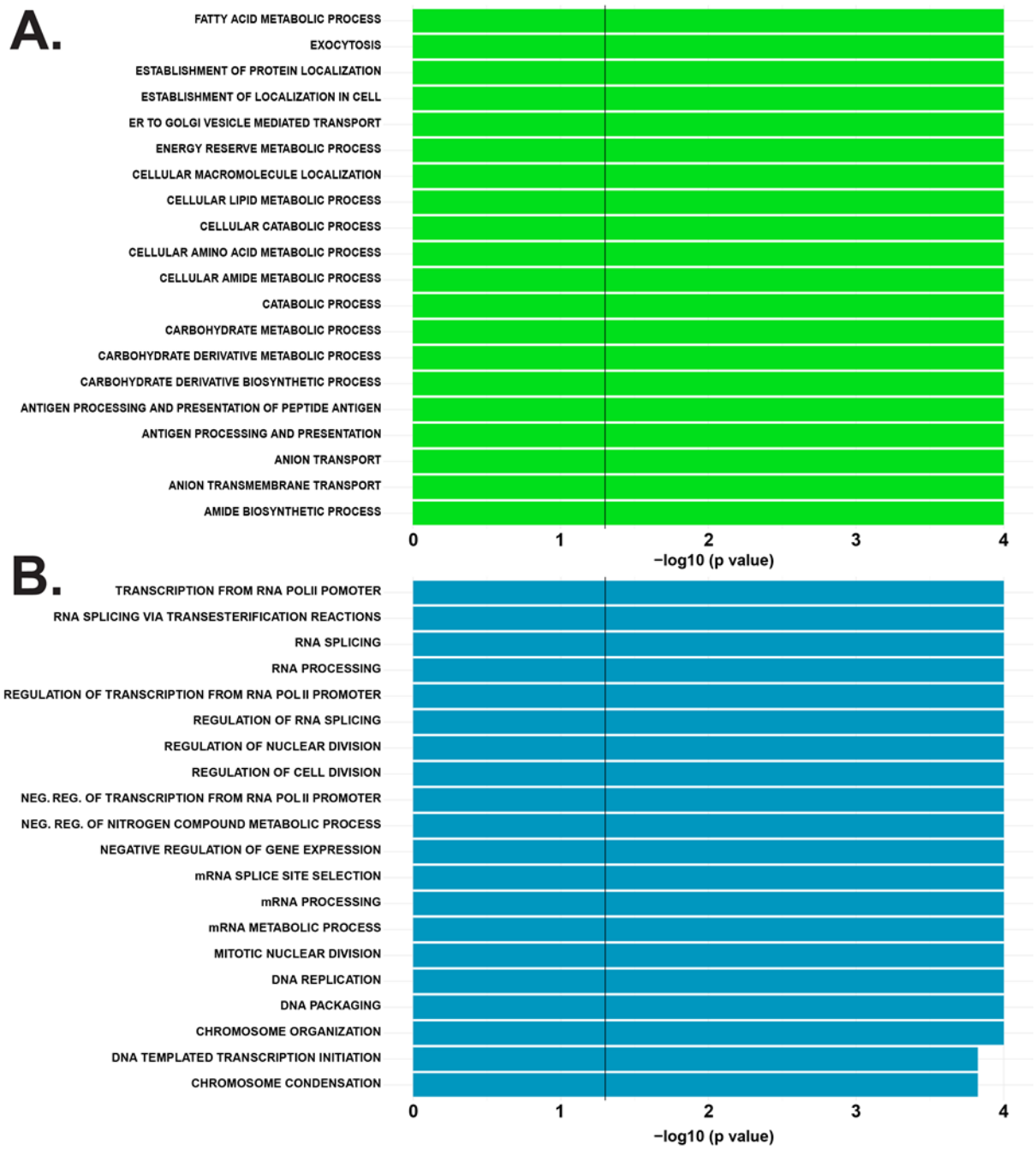

Figure 5-3. GO biological processes altered by β2AR activation in BMDMs.

*Lists of GO biological processes that were either (**A**) up-regulated (green bars) or (**B**) down-regulated (blue bars) in BMDMs stimulated with 1 μM fenoterol for 6 h. Processes within each list were ranked based on the confidence of change (expressed as –log10 (p value)). Due to the replicate number (n=3), the lowest possible p value obtained from the analysis was 0.0001. In cases where multiple processes had a p value of 0.0001, those processes were ranked based on the number of proteins contributing to the activity of that specific process. Data normalisation, analysis and visualisation was performed by PhD student Aurelien Dugourd from Prof. Rodriguez group.*

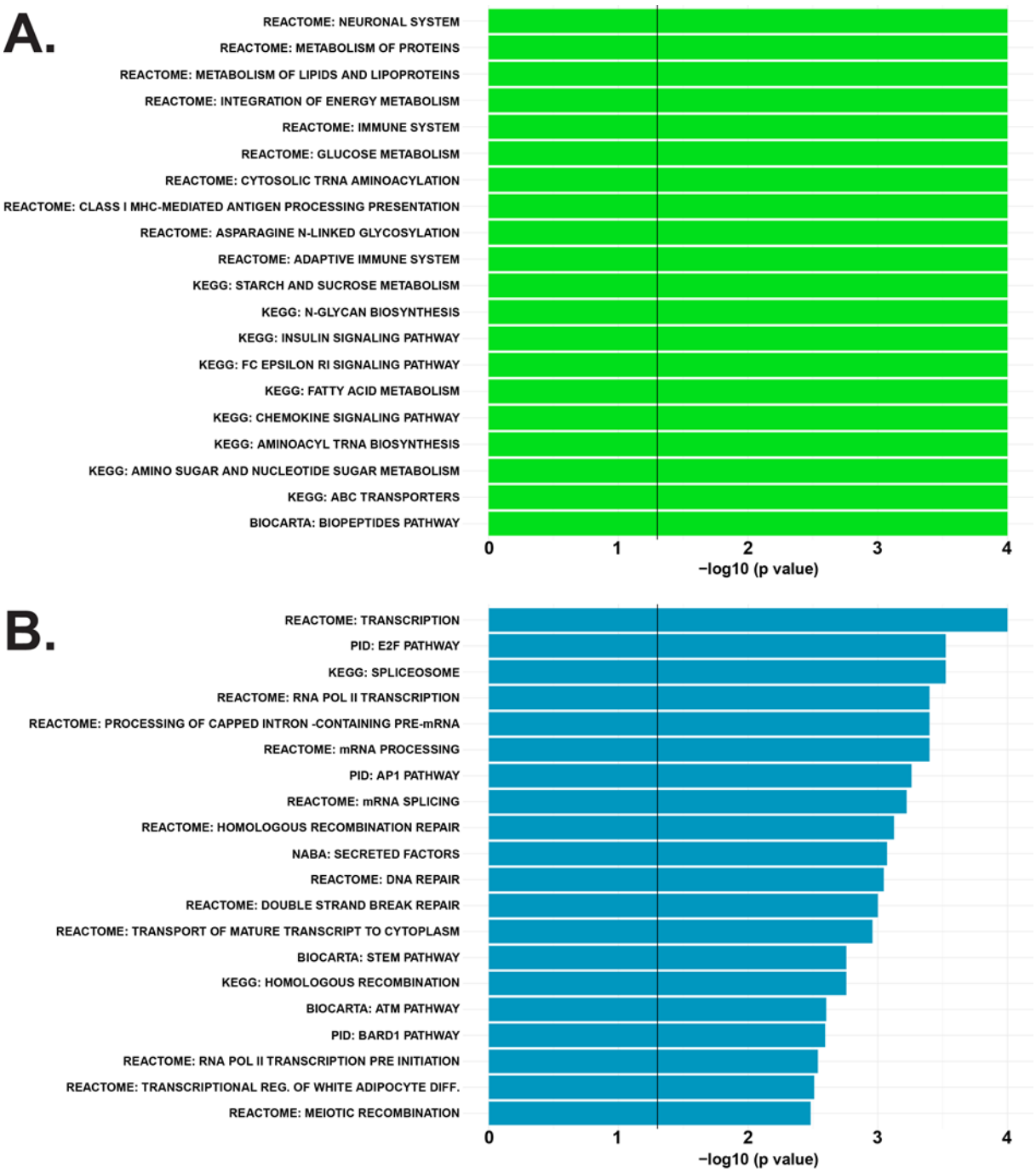

Figure 5-4. Biological pathways altered by β2AR activation in BMDMs.

*Lists of biological pathways from Reactome, Kegg, NABA, Biocarta and PID databases that were either (**A**) up-regulated (green bars) or (**B**) down-regulated (blue bars) in BMDMs stimulated with 1 μM fenoterol for 6 h. Pathways within each list were ranked based on the confidence of change (expressed as –log10 (p value)). Due to the replicate number (n=3), the lowest possible p value obtained from the analysis was 0.0001. In cases where multiple pathways had a p value of 0.0001, those pathways were ranked based on the number of proteins contributing to the activity of that specific pathway. Data normalisation, analysis and visualisation was performed by PhD student Aurelien Dugourd from Prof. Rodriguez group.*

5.2.1.3 Acute β2AR stimulation increased HIF1α-dependent protein expression

Rationale. All measured proteins were then subjected for transcription factor analysis, which predicted the likelihood of transcription factor activity based on the p value of their target gene product changes between treated and non-treated groups.

Results. Consistent with an increased abundance of proteins involved in lipid metabolism, β2AR stimulation was predicted to elevate the activity of SREBP1 and retinoid X receptor α (RXRα), which are known regulators of cellular lipid metabolism (Figure 5-5). Interestingly, HIF1α showed highest predicted transcriptional activity in BMDMs after β2AR stimulation (Figure 5-5). In line with this finding, the most up-regulated protein in response to β2AR activation, THBS1, is a known HIF target gene product[574].

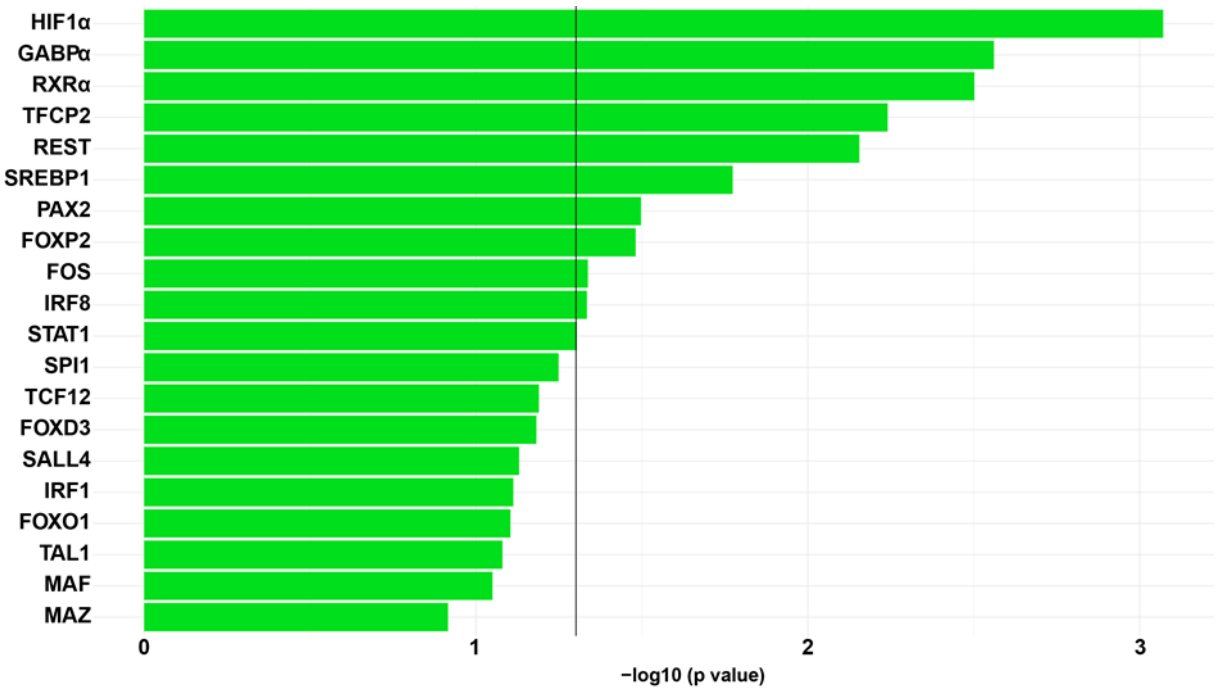

Figure 5-5. Transcription factors predicted to have elevated activity after β2AR activation in BMDMs.

List of transcription factors predicted to have increased activity in BMDMs stimulated with 1 μM fenoterol for 6 h. Transcription factors were ranked based on the confidence of change (expressed as –log10 (p value)). Data normalisation, analysis and visualisation was performed by PhD student Aurelien Dugourd from Prof. Rodriguez group.

5.2.1.4 Acute β2AR stimulation increased the expression of enzymes involved in catecholamine catabolism in BMDMs

Results. SAMs have been reported to express the enzymes involved in monoamine degradation, which are part of the '*neuronal system*' pathway. SAMs isolated from a healthy WAT were shown to express MAOA and SLC6A2[424], while aging also up-regulated the ATM genes encoding aldehyde dehydrogenase and aldo-keto reductase enzymes that catalyse the final step of NE breakdown[439]. Interestingly, treating cells with β2AR agonist fenoterol, which cannot be oxidised by MAOA[573], resulted in a small increase in all detected proteins involved in NE breakdown (Figure 5-6). Elevated levels of the enzymes involved in monoamine oxidation in β2AR-treated BMDMs were also accompanied by a large increase in NLRP3 protein, which has been described to drive the development of monoamine degradation transcriptional programme in the ATMs during aging[439] (Figure 5-6).

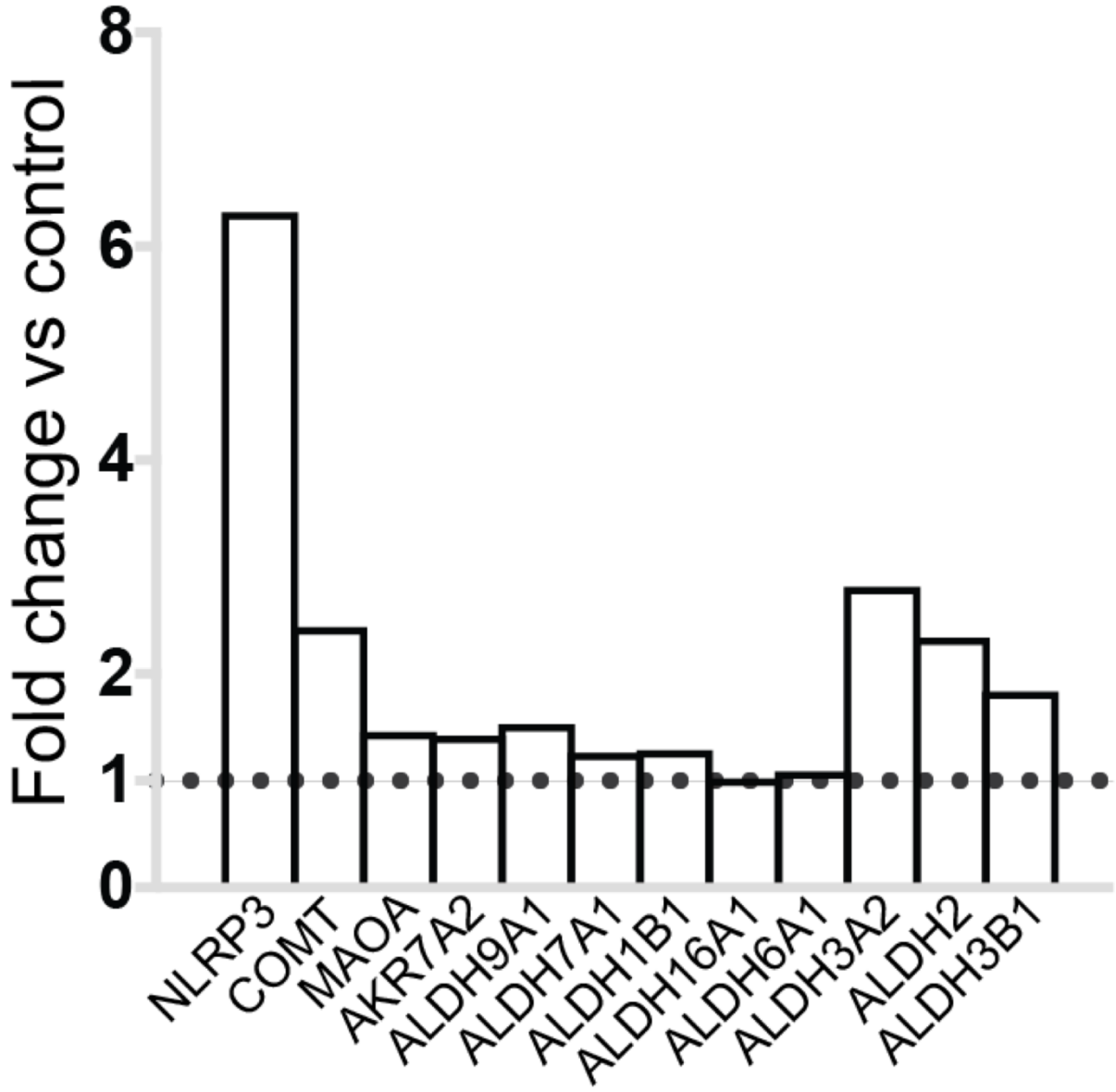

Figure 5-6. The effect of β2AR activation on the expression of proteins related to monoamine degradation in BMDMs.

Fold change in the abundance of indicated proteins between BMDMs treated with 1 μM fenoterol for 6 h and untreated controls, as described in 5.2.1.1. N=3 mice. Statistical differences are not indicated. Data normalisation and analysis was performed by PhD student Aurelien Dugourd.

5.2.2 Acute effects of β2AR activation on BMDM glucose metabolism

5.2.2.1 Acute β2AR stimulation promoted aerobic glycolysis in BMDMs

***Rationale*.** As glucose and lipid metabolism were amongst the top up-regulated pathways in the proteomic analysis of β2AR agonist-treated BMDMs, I decided to functionally assess BMDM nutrient utilisation in response to β2AR stimulation. Monocarboxylate transporter 4 (MCT4), responsible for transporting intracellular lactate outside of the cell, was highly up-regulated in BMDMs following fenoterol treatment (9.73 fold increase, adj. p value = 0.0005 compared to untreated controls). Based on this finding, I **hypothesised** that β2AR stimulation could increase lactate production through enhancing aerobic glycolysis in BMDMs. To test such hypothesis, real-time extracellular acidification rate (ECAR) was assessed after β2AR activation.

Results. Indeed, an increase in ECAR was readily observed 40 min after fenoterol treatment, reaching the peak ECAR increase of approximately 20% compared to control BMDMs at 80 min after β2AR activation (Figure 5-7 A). The observed ECAR increase was sustained throughout the duration of the assay (up to 3 h following fenoterol treatment), and was completely abolished when BMDMs were treated with 2-DG, indicating that the difference in the ECAR in response to β2AR agonism was driven entirely by glycolysis (Figure 5-7 A). Similar result was obtained in response to NE, and the increase in ECAR was diminished in β2AR-defficient BMDMs (Figure 5-7 B).

***Conclusion*.** β2AR activation rapidly increased the rate of aerobic glycolysis in BMDMs.

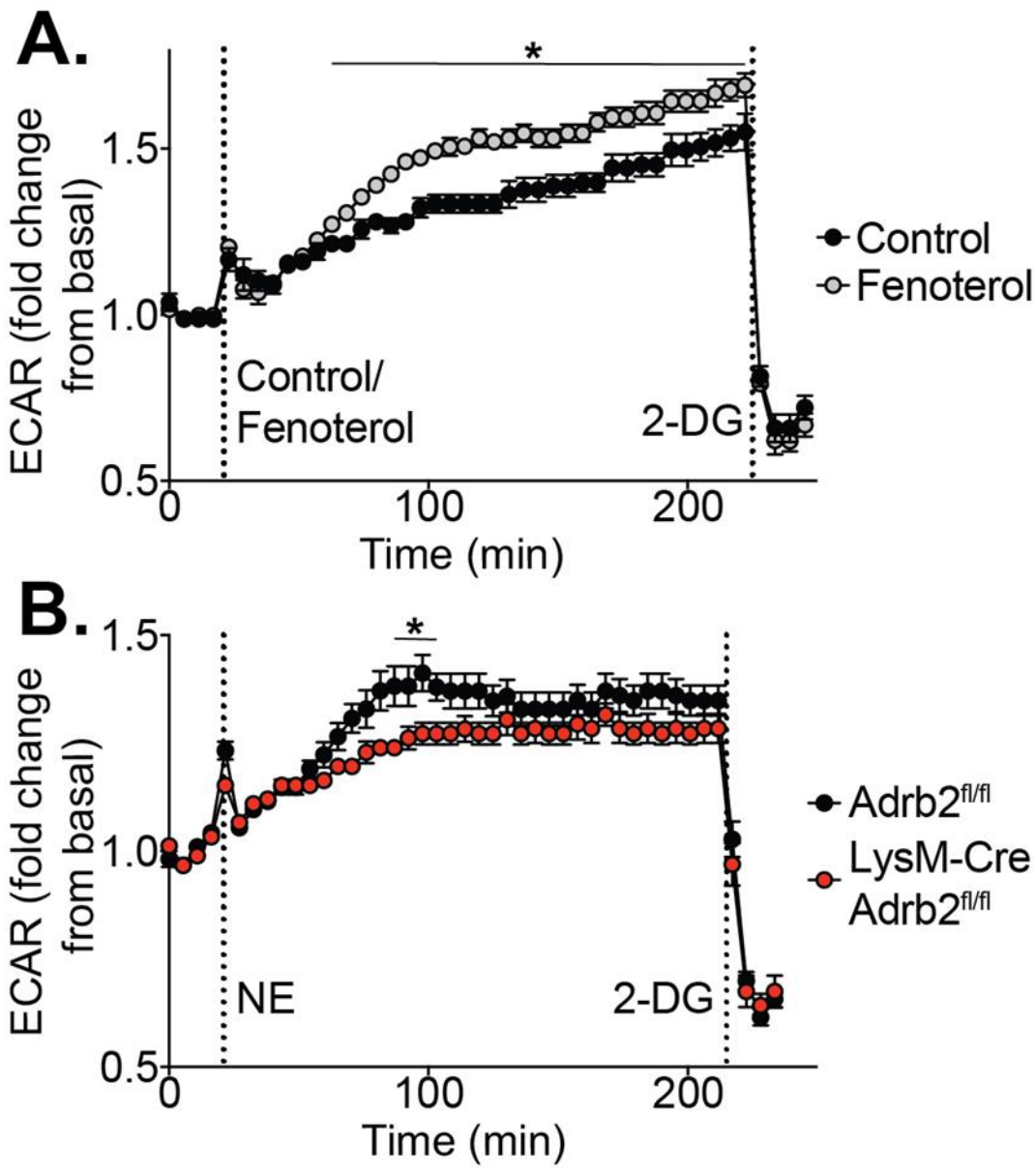

Figure 5-7. Extracellular acidification rate in response to β2AR activation in BMDMs.

*ECAR, expressed as fold change compared to initial 4 basal measurements, in (**A**) WT BMDMs (n=4 mice, 8 technical replicates per mouse per condition) treated with 10 μM fenoterol (grey dots represent treated cells, black dots – controls) at 21 min of the assay (as indicated by the dashed line in the graph), or in (**B**) Adrb2$^{fl/fl}$ (black dots) and LysM-Cre Adrb2$^{fl/fl}$ (red dots) BMDMs (n=4 mice/group, 8 technical replicates per mouse per condition) treated with 1 μM NE at 21 min of the assay (as indicated by the dashed line in the graph). At the end of the assay, glycolysis was inhibited by injecting 10 mM 2-DG (at the time indicated by the dashed line in the graphs). Experiments and data analysis was performed by Dr Guillaume Bidault. * $p < 0.05$ compared to control at each time-point using two-way ANOVA with Bonferroni's multiple comparisons test.*

5.2.2.2 Acute β2AR activation increased mitochondrial ROS in BMDMS

***Rationale*.** Prolonged treatment of macrophages with LPS results in enhanced aerobic glycolysis and decreased oxygen consumption rate (OCR), which is a consequence of mitochondrial repurposing from oxidative phosphorylation towards the production of ROS[110]. In order to assess whether mitochondrial function is affected in BMDMs in response to β2AR activation, I performed mitochondrial stress assay in BMDMs 1 h after NE stimulation, when ECAR was reaching its maximal increase compared to an unstimulated state. Mitochondrial function was assessed by measuring OCR in a basal state, and in response to a sequential injection of the following compounds: ATP synthase inhibitor oligomycin (where residual OCR represents the sum of ATP synthesis-independent mitochondrial proton leak and OCR from cellular processes other than electron transport chain), mitochondrial uncoupler FCCP (where OCR represents maximal mitochondrial respiratory capacity), FAO inhibitor etomoxir (where the difference in OCR between FCCP and etomoxir represents the rate of mitochondrial FAO) and electron transport chain complex I and III inhibitors rotenone and antimycin A (where the residual OCR represents oxygen-consuming cellular processes other than electron transport chain).

***Results*.** Contrary to LPS treatment, which results in increased basal ECAR and decreased basal OCR, no difference in basal OCR was detected in BMDMs treated with NE for 1 h, despite elevated basal ECAR (Figure 5-8 A, Figure 5-7 B). Surprisingly, maximal respiratory capacity was elevated in NE-treated BMDMs, and such increase was maintained after etomoxir injection, suggesting an FAO-independent effect (Figure 5-8 A). However, despite unimpaired mitochondrial respiration, mitochondrial ROS production was increased in BMDMs after acute β2AR activation (Figure 5-8 B).

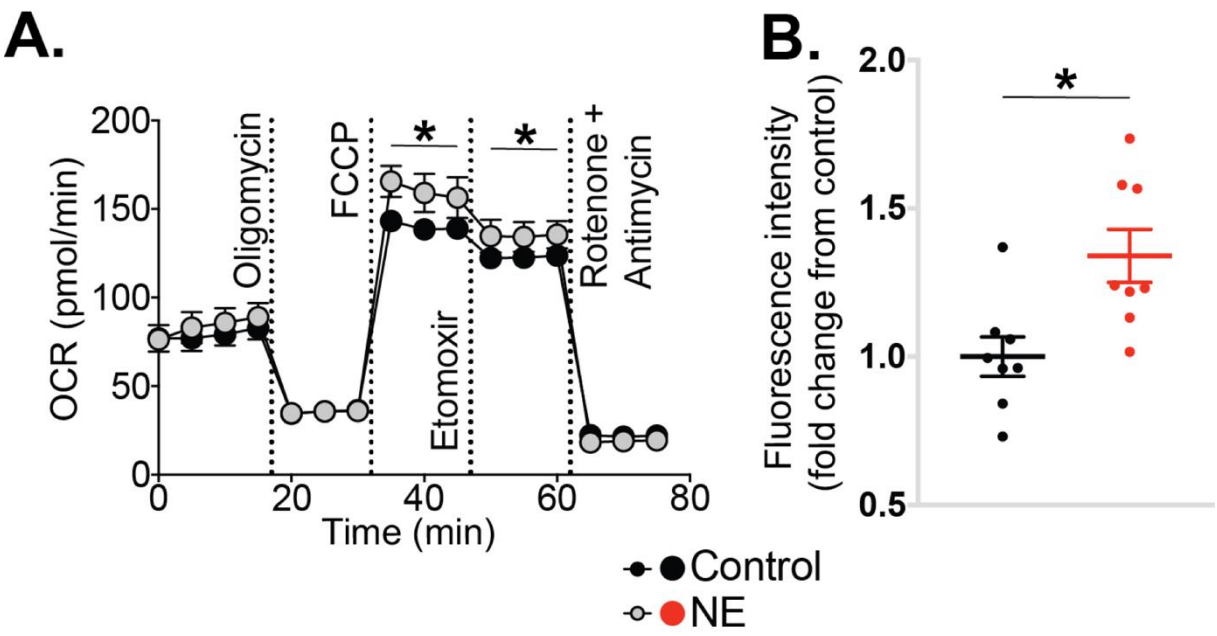

Figure 5-8. Mitochondrial respiration and ROS production in response to β2AR activation in BMDMs.

*(**A**) OCR, expressed as pmoles of oxygen/min, measured in WT BMDMs (n=4 mice, 8 technical replicates per mouse per conditions) pre-treated with 1 μM NE (grey dots represent treated cells, black dots – controls) for 1 h and subjected to mitochondrial stress assay involving sequential injections of 1 μM oligomycin, 1.5 μM FCCP, 40 μM etomoxir and 100 nM rotenone + 1 μM antimycin A at indicated time-points in the graph and 3 consecutive OCR measurements in between injections. (**B**) Mitochondrial ROS production in WT BMDMs (n=8 mice) treated with 1 μM NE for 1 h (red dots), normalised to untreated controls (black dots). Experiments and data analysis was performed by Dr Guillaume Bidault. * $p < 0.05$ compared to control (**A**) at each time-point using two-way ANOVA with Bonferroni's multiple comparisons test, (**B**) using student's t-test.*

5.2.3 The role of glycolysis and HIF transcription factors in the regulation of gene transcription in BMDMs in response to β2AR activation

5.2.3.1 Pharmacological inhibition of glycolysis prolonged the transcription of early phase genes, but diminished the late phase gene expression in BMDMs in response to β2AR activation

***Rationale*.** My results so far have established that β2AR activation induced a change in BMDM nutrient metabolism, characterised by a rapid increase in aerobic glycolysis and mitochondrial ROS production, increased flux of exogenous fatty acids towards TG storage and a decrease in oleate lipolysis and β-oxidation. Similar metabolic profile is observed when macrophages are activated by LPS, leading to an up-regulation of the aerobic glycolysis rate and increased fatty acid storage within lipid droplets[272]. Aerobic glycolysis in BMDMs has been previously shown to activate transcription factor HIF1α[111], and HIF1α itself is indispensable for ensuring an appropriate glycolytic flux and the maintenance of ATP levels in macrophages[301]. Consequently, genetic deletion of *Hif1a* gene in macrophages inhibits their inflammatory activation[103,301]. Furthermore, hypoxia is known to promote exogenous FFA accumulation within lipid droplets in multiple cell types (as summarised in the introduction), and HIF1α was shown to be instrumental in such process[297]. HIF1α activation has also been shown to promote cell cycle arrest[575,576], characterised by decreased DNA replication and gene transcription, which was also observed in BMDMs following β2AR activation (Figure 5-3 B, Figure 5-4 B). Finally, β2AR has recently been described to be involved in hypoxia sensing, and β2AR stimulation has been demonstrated to stabilise HIF1α[577].

Based on the high confidence of HIF1α transcriptional activation, as predicted by the proteomic analysis of fenoterol-treated BMDMs (Figure 5-5), and the cellular metabolic profile consistent with increased HIF1α activation, I decided to test whether HIF proteins were important for β2AR stimulation-induced gene expression.

***Results*.** As aerobic glycolysis has been shown to mediate HIF1α activation in macrophages, I initially stimulated BMDMs with β2AR agonist in the presence of 2-DG. Interestingly, I found that inhibiting glycolysis either unchanged or enhanced the expression of early phase genes at 1 h after β2AR activation (Figure 5-9 A). Furthermore, while the mRNA levels of early phase genes returned to their basal level after 4 h of stimulation with fenoterol, this transcriptional decrease was supressed by 2-DG (Figure 5-9 A). However, the expression of late phase genes, including *Thbs1* (encoding thrombospondin-1) was diminished when 2-DG was present during β2AR activation (Figure 5-9 B).

***Conclusion*.** Inhibiting glycolysis during β2AR stimulation prolonged the transcription of early phase genes, but supressed the expression of late phase genes in BMDMs.

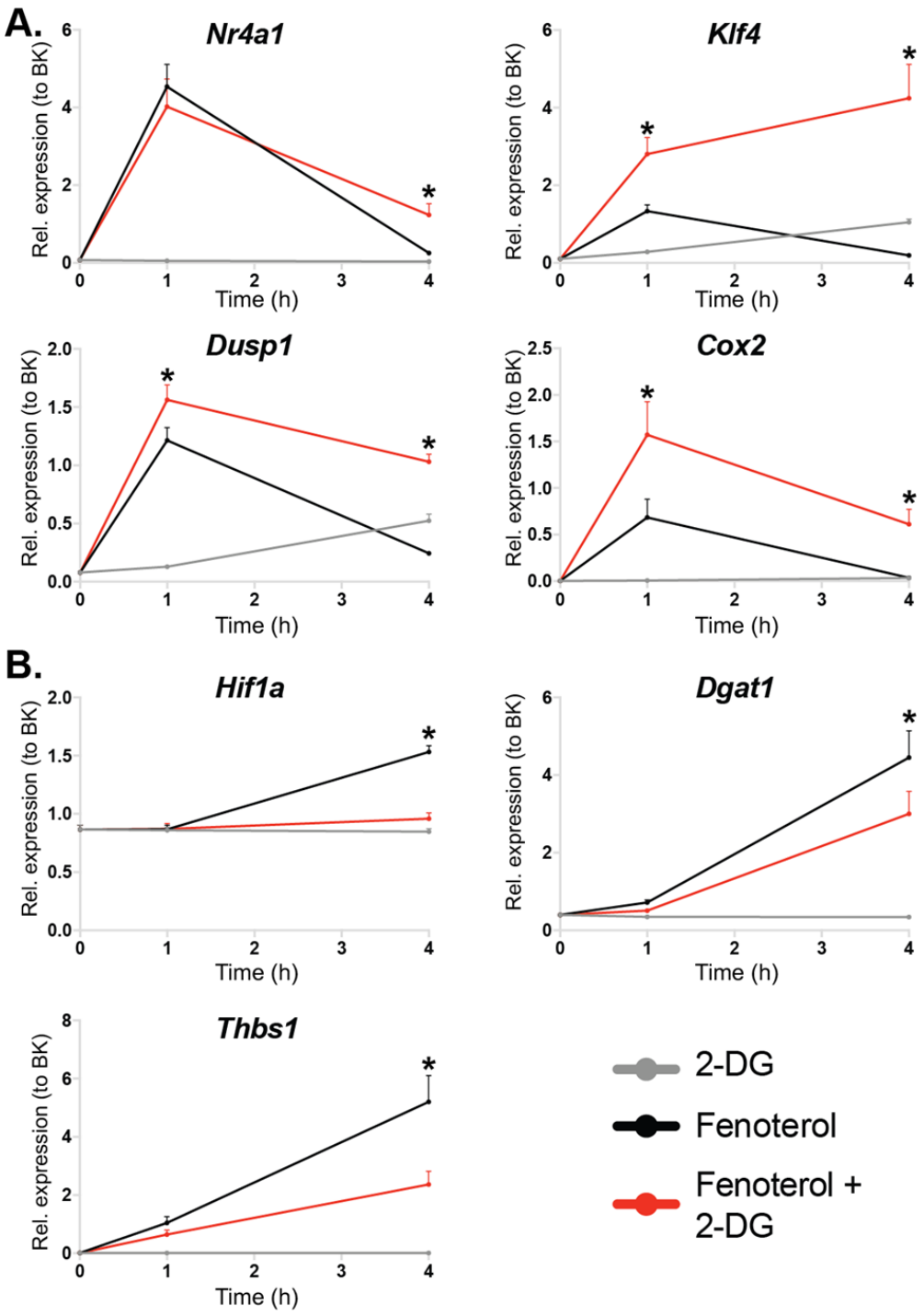

Figure 5-9. The effect of glycolysis inhibitor on β2AR agonism-mediated gene expression in BMDMs.

mRNA levels (normalised to BestKeeper) *of (**A**) early phase genes Nr4a1, Klf4, Dusp1 and Cox2, and (**B**) late phase genes Hif1a, Dgat1 and Thbs1 in BMDMs stimulated with 10 mM 2-deoxyglucose (grey lines), 1 μM fenoterol (black lines) or both compounds together (red lines) for 0, 1 and 4 h. N=4 mice. * $p < 0.05$ compared between fenoterol and fenoterol + 2-DG at each time-point using two-way ANOVA with Bonferroni's multiple comparisons test.*

5.2.3.1 Pharmacological inhibition of HIF transcription factors prolonged the transcription of early phase genes, but diminished the late phase gene expression in BMDMs in response to β2AR activation

***Rationale*.** Next, I decided to use a selective inhibitor of HIF transcription factors to further elucidate their role in β2AR agonism-mediated transcriptional response. Chetomin is a compound isolated from a large-scale screen, specifically targeting HIF interaction with its transcriptional co-activator p300, which is required for the activity of both HIF1α and HIF2α transcription factors[578]. Importantly, chetomin does not affect the interaction of p300 with its other partnering transcription factors, such as SREBP2[578].

***Results*.** When chetomin was present during β2AR stimulation, the induction of early phase genes was either unchanged or slightly diminished compared to controls at 1 h time-point, but the return of the early target gene mRNA to the basal levels was supressed at later time-points (Figure 5-10 A). Interestingly, while the induction of late phase genes *Hif1a* and *Thbs1* was inhibited, *Dgat1* transcription was enhanced by chetomin following β2AR activation (Figure 5-10 B).

***Conclusion*.** In summary, the results obtained using pharmacological HIF inhibitor chetomin were comparable to 2-DG, with the exception of *Dgat1* transcriptional induction.

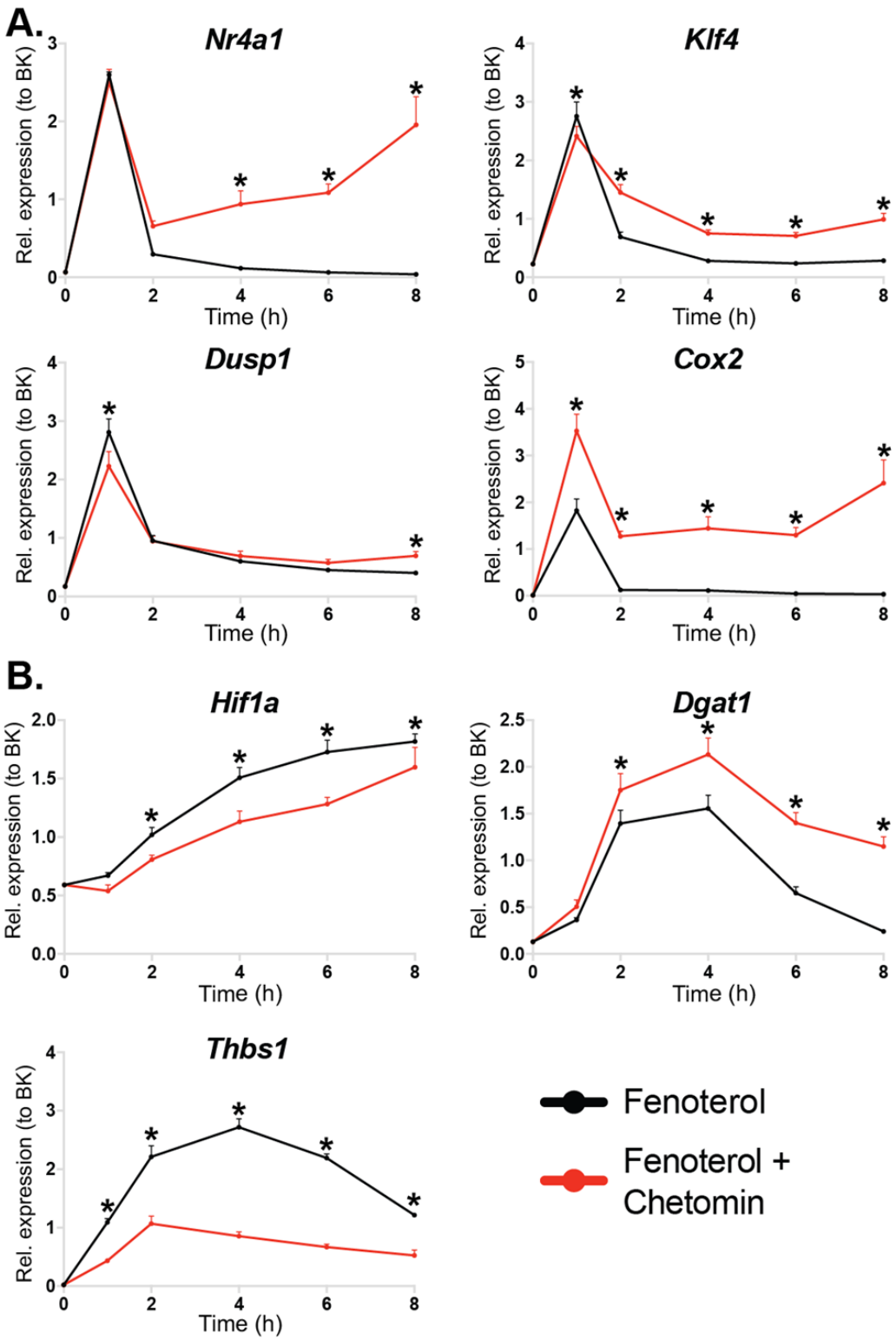

Figure 5-10. The effect of HIF1α-p300 protein complex inhibitor chetomin on β2AR agonism-mediated gene expression in BMDMs.

mRNA levels (normalised to BestKeeper) *of (**A**) early phase genes Nr4a1, Klf4, Dusp1 and Cox2, and (**B**) late phase genes Hif1a, Dgat1 and Thbs1 in BMDMs stimulated with 1 μM fenoterol in the presence (red lines) or absence (black lines) of 100 nM chetomin for 0, 1, 2, 4, 6 and 8 h. N=4 mice. * $p < 0.05$ compared between treatments at each time-point using two-way ANOVA with Bonferroni's multiple comparisons test.*

5.2.3.2 Genetic deletion of HIF1α or HIF2α DNA binding domain did not affect the induction of gene transcription in response to β2AR activation

Rationale. As my evidence for HIF1α activation in response to β2AR agonism has so far been based on the molecular observations and the use of pharmacological tools, I obtained BMDMs from animals that lack the exon 2 of *Hif1a* gene specifically in macrophages, encoding its DNA binding domain[579].

***Results*.** Similarly to the previously published observations[301], I measured approximately 85% deletion in the exon 2 of *Hif1a* gene in HIF1α-KO BMDMs, while the levels of remaining *Hif1a* transcript were slightly increased (Figure 5-11 A). Furthermore, the basal transcription of HIF1α target gene *Glut1* was diminished in HIF1α-deficient cells (Figure 5-11 A). However, unlike what has been described previously[301], I did not see a reduction in basal *Vegfa* mRNA levels in HIF1α-KO BMDMs compared to controls (Figure 5-11 A). Importantly, I did not observe an impairment in the fold induction of either canonical HIF1α target genes *Glut1* and *Vegfa* (Figure 5-11 A), or early and late phase genes *Nur77*, *Dgat1* and *Thbs1* in HIF1α-KO BMDMs compared to controls in response to β2AR activation (Figure 5-11 B).

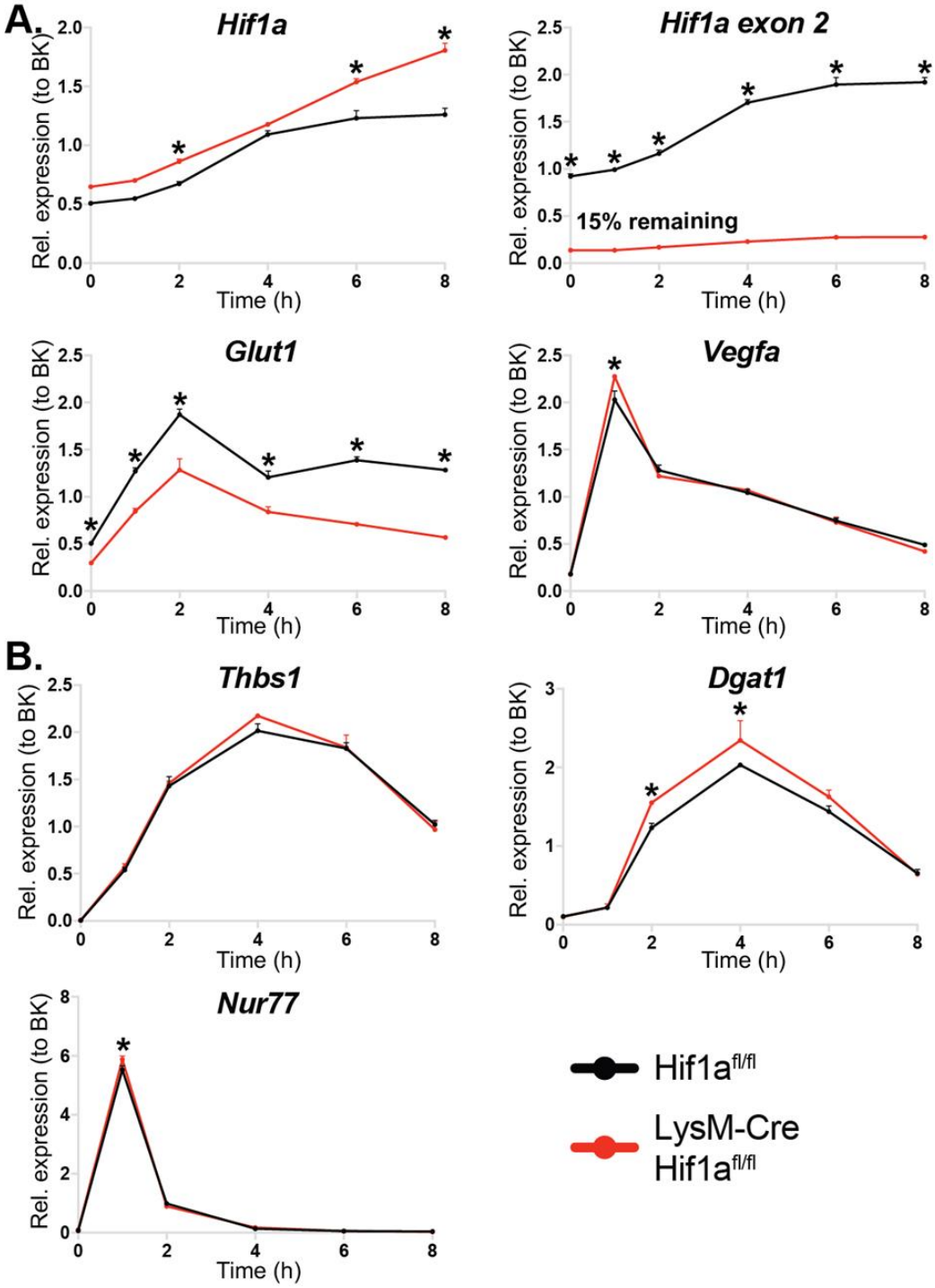

Figure 5-11. The importance of HIF1α DNA binding for β2AR agonism-mediated gene expression in BMDMs.

mRNA levels (normalised to BestKeeper) *of (**A**) Hif1a (measured using standard and exon 2-intron 2 boundary-spanning primer sets) and its target genes Glut1 and Vegfa, and of (**B**) Thbs1, Dgat1 and Nur77 in Hif1a exon2$^{fl/fl}$ (n=3, black lines) and LysM-Cre Hif1a exon2$^{fl/fl}$ (n=2, red lines) BMDMs stimulated with 1 μM fenoterol for 0, 1, 2, 4, 6 and 8 h. * p < 0.05 compared between genotypes at each time-point using two-way ANOVA with Bonferroni's multiple comparisons test.*

***Rationale*.** HIF2α has also been described to be important for macrophage inflammatory activation[537], but its role in regulating gene transcription during inflammation is thought to be substantially different than the role of HIF1α[580]. As *Thbs1* gene transcription has been previously shown to be dependent on HIF2α[581,582], I decided to investigate whether HIF2α mediates the induction of gene expression in response to β2AR activation. In order to do so, I obtained BMDMs from the animals with a macrophage specific deletion of *Epas1* exon 2, encoding the DNA binding domain of HIF2α[583].

***Results*.** The excision of exon 2 in HIF2α-KO BMDMs was verified by an observed reduction in the length of PCR amplicon containing exon 2 of *Epas1* gene (Figure 5-12 A). However, the induction of early and late phase genes in response to β2AR activation in BMDMs was not affected by the capacity of HIF2α to bind DNA (Figure 5-12 B). Interestingly, while there was only a minor impairment in the relative *Thbs1* transcriptional induction after 4 h of β2AR stimulation in HIF2α-KO BMDMs compared to controls, the basal level of *Thbs1* mRNA was approximately 3-fold increased, and it remained higher throughout the period of β2AR stimulation in HIF2α-KO BMDMs (Figure 5-12 B).

***Conclusion*.** Neither HIF1α, nor HIF2α transcriptional activity was required for β2AR agonism-mediated gene expression.

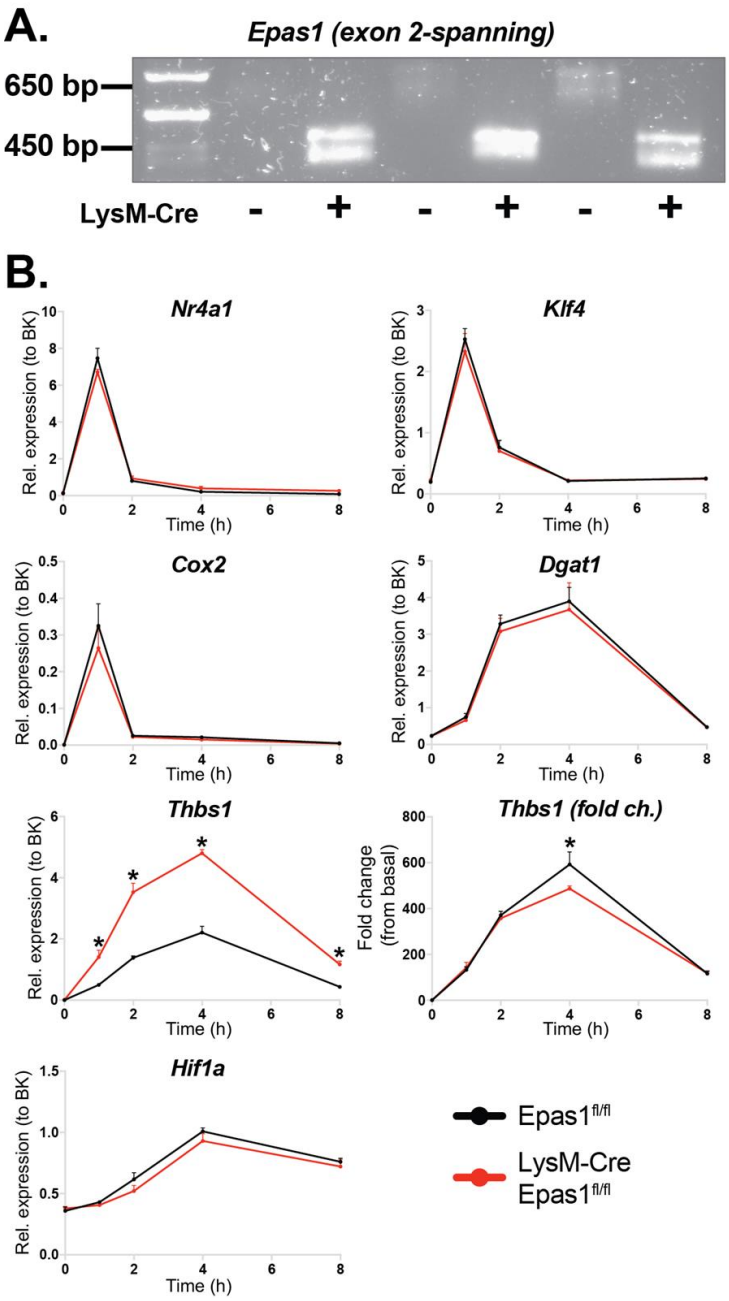

Figure 5-12. The importance of of HIF2α DNA binding for β2AR agonism-mediated gene expression in BMDMs.

*(**A**) PCR amplicon of exon 2 of Epas1 mRNA (generated using Epas1 exon 2-spanning primers), separated on 1.5% agarose gel and (**B**) mRNA levels* (normalised to BestKeeper) *of Nr4a1, Klf4, Cox2, Dgat1, Thbs1 (expressed both as a relative amount to the housekeeper genes and as a fold increase from unstimulated cells) and Hif1a in Epas1 exon2$^{fl/fl}$ (n=3, black lines) and LysM-Cre Epas1 exon2$^{fl/fl}$ (n=3, red lines) BMDMs stimulated with 1 μM fenoterol for 0, 1, 2, 4 and 8 h. * p < 0.05 compared between genotypes at each time-point using two-way ANOVA with Bonferroni's multiple comparisons test.*

5.2.4 The effects of β2AR activation on the inflammatory activation of BMDMs

5.2.4.1 β2AR activation mimicked the anti-inflammatory effects of salt-inducible kinase inhibition in BMDMs

***Rationale*.** CREB is a known regulator of *Il10* transcription in macrophages[584]. β2AR activation has been previously shown to promote *Il10* transcription in macrophages, both in CREB-dependent[585] and CREB-independent manner[457]. It has also been proposed that the transcriptional increase in *Il10* gene is largely responsible for the anti-inflammatory effects of β-adrenergic agonists in macrophages stimulated with LPS[586].

PGE2, an agonist of another $G_{\alpha s}$-linked GPCR, has been shown to elevate *Il10* transcription in LPS-treated macrophages by promoting the inhibitory phosphorylation of salt-inducible kinases (SIKs), leading to the formation of an active CREB-CRTC transcription factor complex[498]. Similarly, pharmacological inhibition of SIKs also showed a potent anti-inflammatory effect in macrophages by promoting CREB-dependent IL-10 production in response to LPS[497].

I therefore attempted to reproduce the reported anti-inflammatory effects of β2AR agonism in LPS-treated macrophages, and compare them to the effects of SIK inhibition. Furthermore, I wanted to investigate whether SIK blockade could potentiate the transcriptional response to β2AR agonism in BMDMs. To test this, I stimulated BMDMs with LPS in the presence of either fenoterol or SIK inhibitor HG-9-91-01, or with fenoterol and HG-9-91-01 in the absence of LPS.

***Results*.** I found that LPS alone potently increased *Tnf* gene expression after 1 h, while the induction in *Il10* transcription was only observed after 6 h, indicating an early pro-inflammatory response and a delayed autocrine signalling-mediated resolution phase in LPS-treated cells (Figure 5-13). Interestingly, both β2AR agonism and SIK inhibition elicited similar reduction in early phase *Tnf* transcription, while increasing *Il10* mRNA, which was likely driven by the formation of an active CREB-CRTC complex, as the transcription of a canonical CREB target gene *Nr4a1* was also potentiated by both fenoterol and HG-9-91-01 in LPS-treated BMDMs (Figure 5-13). Surprisingly, while both immunomodulators supressed *Tnf* transcription, they potently enhanced the expression of *Il1b* gene, which has a CRE sequence in its promoter[587] (Figure 5-13).

Finally, HG-9-91-01 diminished the induction of *Nr4a1*, but increased the expression of *Dgat1* and *Thbs1* in β2AR agonist-treated cells (Figure 5-13). LPS showed an opposite effect to HG-9-91-01 by enhancing *Nr4a1*, but supressing *Dgat1* and *Thbs1* transcriptional induction after fenoterol stimulation (Figure 5-13). Interestingly, both β2AR agonism and SIK blockade showed synergistic effects with LPS in increasing *Hif1a* gene expression (Figure 5-13).

***Conclusion*.** My results confirmed the anti-inflammatory effect of β2AR activation, likely mediated by an increased early phase *Il10* transcription. Furthermore, they also showed that LPS promoted the induction of early phase genes, but diminished the transcription of late phase genes in β2AR-agonist-treated BMDMs, while SIK inhibition had the opposite effect.

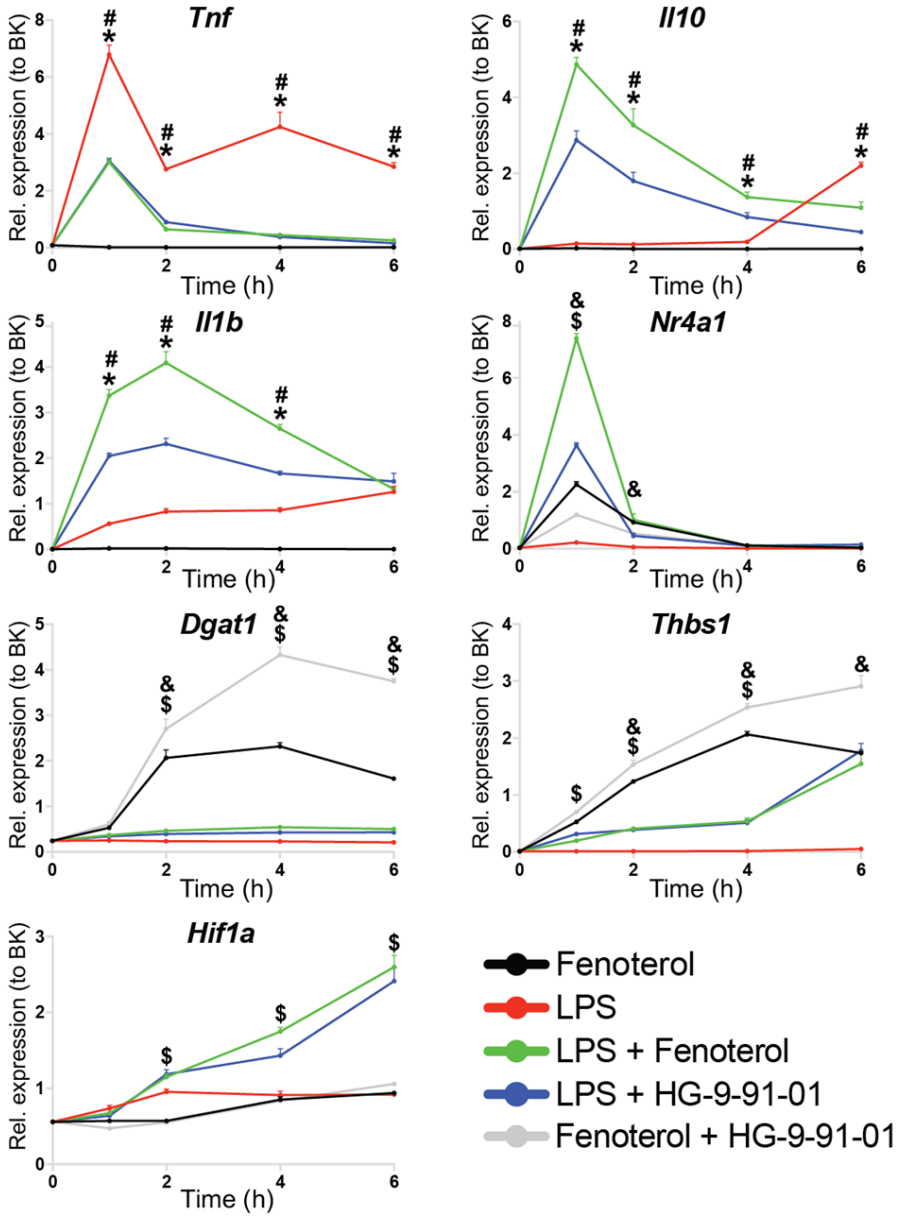

Figure 5-13. The effects of β2AR activation and salt-inducible kinase inhibition on LPS-induced gene transcription in BMDMs.

mRNA levels (normalised to BestKeeper) *of inflammatory genes Tnf, Il10 and Il1b, and β2AR-responsive genes Nr4a1, Dgat1, Thbs1 and Hif1a in BMDMs treated with 1 μM fenoterol (black lines), 100 ng/ml LPS (red lines), LPS + fenoterol (green lines), LPS + 100 nM HG-9-91-01 (blue lines) and fenoterol + HG-9-91-01 (grey lines) for 0, 1, 2, 4, and 6 h. N=4 mice. For genes Tnf, Il10 and Il1b: * p < 0.05 compared between LPS and LPS + fenoterol, and # p < 0.05 compared between LPS and LPS + HG-9-91-01 at each time-point using two-way ANOVA with Bonferroni's multiple comparisons test. For genes Nr4a1, Dgat1, Thbs1 and Hif1a: $ p < 0.05 compared between fenoterol and LPS + fenoterol, and & p <0.05 compared between fenoterol and fenoterol + HG-9-91-01 at each time-point using two-way ANOVA with Bonferroni's multiple comparisons test.*

5.2.4.2 β2AR activation enhanced inflammasome-dependent IL-1β secretion in BMDMs

***Rationale*.** Intrigued by the potentiating effects of β2AR agonism on *Il1b* transcription in LPS-treated BMDMs, I decided to evaluate whether β2AR stimulation alone could promote the expression of genes encoding IL-1β and NLRP3 inflammasome, which has recently been described to mediate the development of norepinephrine degradation pathway in ATMs during aging[439].

***Results*.** Indeed, β2AR activation rapidly increased *Il1b* and *Nlrp3* mRNA levels in BMDMs (Figure 5-14 A). Furthermore, while BMDMs treated with NE alone did not produce detectable IL-1β levels (data not shown), NE enhanced the release of IL-1β in the presence of canonical inflammasome activators LPS and ATP, and this potentiating effect was lost in β2AR-defficient BMDMs (Figure 5-14 B).

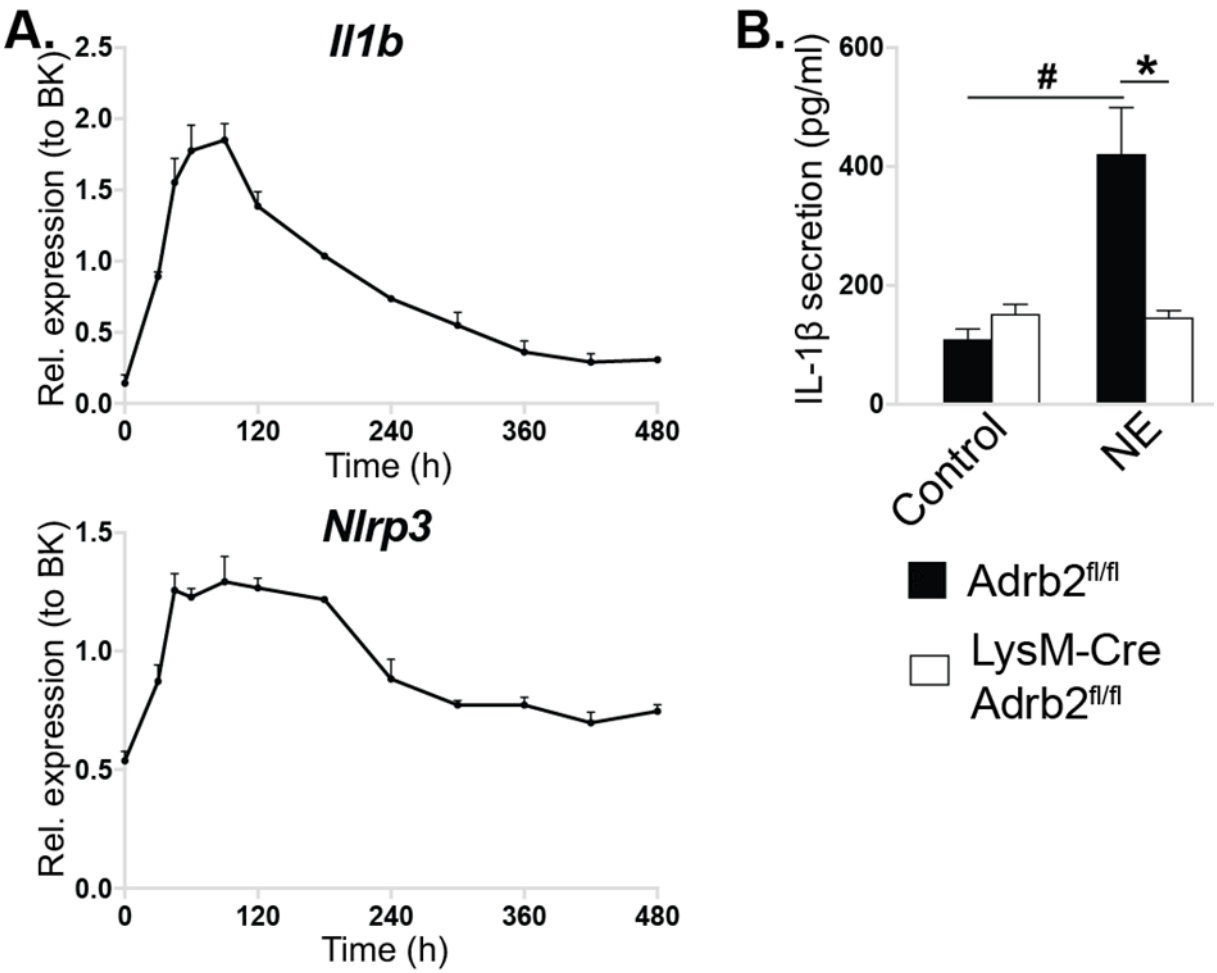

Figure 5-14. IL-1β secretion in response to β2AR activation in BMDMs.

*(**A**) Il1b and Nlrp3 mRNA levels* (normalised to BestKeeper) *in WT BMDMs treated with 1 μM fenoterol for 0, 30, 45, 60, 90, 120, 180, 240, 300, 360, 420 or 480 min. N=4 mice. Statistical differences were not assessed. (**B**) IL-1β levels (expressed in pg/ml of cell supernatant) in the medium of Adrb2$^{fl/fl}$ (n=4 mice, black bars) and LysM-Cre Adrb2$^{fl/fl}$ (n=4 mice, white bars) BMDMs treated sequentially with 1 μM NE for 1h (or left untreated for controls), then with 100 ng/ml LPS for 2 h, and then with 5 mM ATP for 30 min. * p < 0.05 compared genotypes, and # p < 0.05 compared between NE-treated and control cells using two-way ANOVA with Bonferroni's multiple comparisons test.*

5.3 Discussion

This chapter describes how NE signalling via β2AR regulates gene and protein expression, and cellular glucose metabolism in macrophages. The experiments described in the chapter aimed to gain a better understanding of the effects of β2AR activation on the phenotype of macrophages. The main finding of the chapter was that β2AR stimulation rapidly induced a hypoxic-like phenotype in BMDMs, characterised by aerobic glycolysis, increased lipid storage and elevated HIF-dependent gene transcription. Glycolysis was required for the appropriate induction of late phase gene transcription during β2AR activation. Furthermore, the molecular interaction between transcription factors HIF and p300, but not direct HIF1α or HIF2α transcriptional activity was mediating the transcription of late phase genes.

5.3.1 β2AR activation induced two phases of gene transcription in BMDMs

Phosphorylation of CREB and the induction of CREB-dependent gene transcription in response to β-adrenergic receptor stimulation has been described numerous times, and is widely accepted in cell signalling research[485]. However, in the current and previous chapters I found a novel property of β2AR-dependent CREB target gene induction in macrophages, characterised by two subsequent waves of gene transcription. It is important to emphasise that such observation would have not been possible without a frequent sampling during my experiments in order to obtain accurate gene transcription kinetics. The lack of knowledge on the kinetic properties of signalling is also a likely reason why such finding has not been made before in other labs, despite the studies on β2AR in macrophages dating back for over 2 decades[456]. Had I analysed only 1 h, 8 h or 24 h time-points following β2AR activation in BMDMs, I would have not found the induction of late phase genes, including *Dgat1*, and therefore would not have been able to design the proteomics study and identify the effects of β2AR stimulation on macrophage nutrient metabolism.

Despite the observed biphasic gene expression, the underlying mechanism that regulate such response is not completely clear. As summarised in the introduction, β2AR is known to act through the $G_{\alpha s}$, but also to engage β-arrestin-MAPK signalling axis. Furthermore, as β2AR has been shown to elicit both pro- and anti-inflammatory effects in macrophages, it has been suggested that G_{as} signalling is responsible for the immunomodulatory, and β-arrestin is driving the pro-inflammatory response in

macrophages[456]. It is therefore possible that the induction of early phase genes observed in this chapter is mediated by increased intracellular cAMP, leading to CREB phosphorylation and transcriptional activation, while the late phase gene transcription is dependent on β-arrestin signalling. In line with such hypothesis, I have recently obtained preliminary data in BMDMs showing that when CREB phosphorylation starts to diminish at 1 h following β2AR stimulation, there is an increase in ERK phosphorylation (data not shown), which is a known downstream event of a β-arrestin signalling pathway[588]. I am currently in the process of testing whether pharmacologically inhibiting β-arrestin signalling or ERK enzymes would diminish the induction of late phase genes in response to β2AR activation in BMDMs.

Another potential explanation for the biphasic gene expression is that some of the factors induced during the initial phase following β2AR activation in BMDMs are directly regulating the transcription of the second phase genes. Indeed, the product of *Nr4a1 gene*, which is highly and rapidly upregulated 1 hour post β2AR stimulation, has been described to control the expression of a subset of metabolic genes in macrophages [589]. I will attempt to adress this in future using cycloheximide, a pharmacological inhibitor of protein translation. If the proposed mechanism of regulation is true, the induction of the second phase of genes in response to β2AR activation should be lost in BMDMs pretreated with cycloheximide.

It is also difficult to pinpoint the exact role of HIF1α in regulating β2AR activation-dependent gene transcription in BMDMs. The results obtained from the proteomics experiment and metabolic analysis of β2AR-agonist treated BMDMs overwhelmingly indicate the activation of HIF1α-dependent gene expression. In line with this, blocking glycolysis, which is a known upstream event of HIF1α activation in macrophages, or utilising pharmacological HIF inhibitor diminished the induction of late phase genes in response to β2AR agonism in BMDMs. Therefore, perhaps the most unexpected result in this chapter was the conserved β2AR stimulation-dependent gene transcription in HIF1α-KO BMDMs. It is important to emphasise that due to the architecture of loxP sites surrounding *Hif1a* exon 2, its excision by Cre recombinase does not result in a frame shift or introduce a premature stop codon in the remaining 3' region of *Hif1a* mRNA[590]. It is not the case for the *Epas1* floxed allele, which produces an mRNA containing multiple premature stop codons after Cre-mediated excision[583]. While it has

not been verified, it is possible that HIF1α-KO cells may still produce a stable HIF1α protein that lacks its DNA binding domain, but retain the capacity to bind the transcriptional co-activators. Indeed, a published report utilising the same *Hif1a* exon 2-floxed genetic model crossed with a mouse expressing Cre recombinase in hepatocytes showed that despite lacking HIF1α-dependent transcriptional response, HIF1α-KO livers still contained a protein recognised by an anti-HIF1α antibody in a Western blot[591]. Another recent report has also identified a truncated form of HIF1α protein using anti-HIF1α antibody in a Western blot of hypoxic BMDMs from Tie2-Cre *Hif1a* exon 2-floxed mice[592].

Based on the opposing results obtained using pharmacological HIF inhibitor and a genetic model lacking HIF1α DNA binding domain, it is tempting to speculate that HIF1α mediates the transcription of the late phase genes in response to β2AR activation in BMDMs independently of its DNA binding. In line with such hypothesis, HIF inhibitor chetomin does not target HIF1α DNA binding domain, but disrupt the interaction between HIF1α and its transcriptional co-activator p300[578]. Interestingly, p300 also interacts with CREB, and CREB-p300-HIF1α transcriptional complex has been previously shown to be present in cells and bind to *Ldha* gene promoter[593] . Furthermore, late phase genes *Hif1a* and *Thbs1* have CRE sequences in their promoter, suggesting that CREB, rather that HIF1α binding to DNA might be important for their transcriptional induction in BMDMs in response to β2AR activation. Finally, it is unclear what role the glycolysis plays in the regulation of late phase gene transcription, but it could lead to the nuclear translocation of pyruvate kinase M2 (PKM2) isoform, similarly to what has been described in LPS- treated macrophages[594]. PKM2 is a part of glycolysis pathway, but has also been shown to translocate to the nucleus and facilitate the interaction between HIF1α and p300 when phosphorylated[595]. It is possible that inhibiting glycolysis in β2AR agonist-stimulated macrophages could disrupt the PKM2 nuclear translocation, therefore preventing HIF1α binding to p300.

Overall, my results from this chapter suggests a mechanism, where β2AR activation leads to a rapid phosphorylation of CREB by PKA and the induction of CREB target gene transcription within 30 min of stimulation (Figure 5-15). Simultaneously, β2AR agonism promotes aerobic glycolysis, which mediates HIF1α-dependent gene

transcription without the requirement of HIF1α DNA binding (Figure 5-15). Inhibiting glycolysis or the formation of a transcription factor complex containing HIF1α diminishes the induction of late phase gene transcription, but prolongs the expression of the early phase transcripts, suggesting that CREB is retained to the promoters of the early phase genes when the late phase of transcription is blocked (Figure 5-15). Interestingly, blocking HIF1α-p300 interaction also enhances *Dgat1* transcription, indicating that glycolysis also drives CREB interaction with transcriptional co-activators other than HIF1α. Overall, it seems that CREB or p300 availability is a limiting factor for the magnitude of both early and late phase gene transcription, and that glycolysis and potentially other intracellular signalling mechanisms redirect CREB-p300 complex from the early phase to the late phase gene promoters by catalysing its interaction with different transcriptional co-activators, such as HIF1α. Similar competition mechanisms for p300 availability have already been observed between HIF1α and p53[596], between SNIP1 and NF-κB[597], between AP-1 and CREB[598], between STAT-2 and NF-κB[599] and between ER and NF-κB[600] transcription factors.

I am currently in the process of validating the proposed mechanism in multiple steps. Firstly, total RNA sequencing of BMDMs treated with β2AR agonist for 1 h and 4 h is on-going. The results from a global transcription analysis will allow me to identify all early phase genes (showing an increase in mRNA levels at 1h compared to control before a reduction to the basal levels at 4 h post stimulation) and all late phase genes (showing an increase in mRNA levels at 4 h compared to control). Initially, transcription factor prediction analysis will be performed on all detected transcripts in order to confirm the role of CREB and HIF1α, but also to identify novel transcription factors mediating gene expression in response to β2AR stimulation. Next, the promoters of all up-regulated genes will be checked for the presence of CRE or other common response elements, in order to verify the mechanism of the relocation of the transcription factor complex from the early to late phase gene promoters. Finally, I will individually immunoprecipitate CREB, p300 and HIF1α from BMDMs treated with β2AR agonist for 30 min (corresponding to the highest rate of transcription of the early phase genes) and for 90 min (corresponding to the highest rate of transcription of the late phase genes) and assess bound chromatin for the promoter sequences of both early and late phase genes. If my proposed mechanism is correct, CREB-p300 complex should be predominantly localised at the early phase gene promoters at 30

min, while CREB-p300-HIF1α complex would be bound to the late phase gene promoters at 90 min post β2AR activation. Such redirection of CREB-p300 complex should be disrupted in the presence of HIF1α-p300 interaction inhibitor chetomin, but remain intact in BMDMs lacking DNA binding domain of HIF1α.

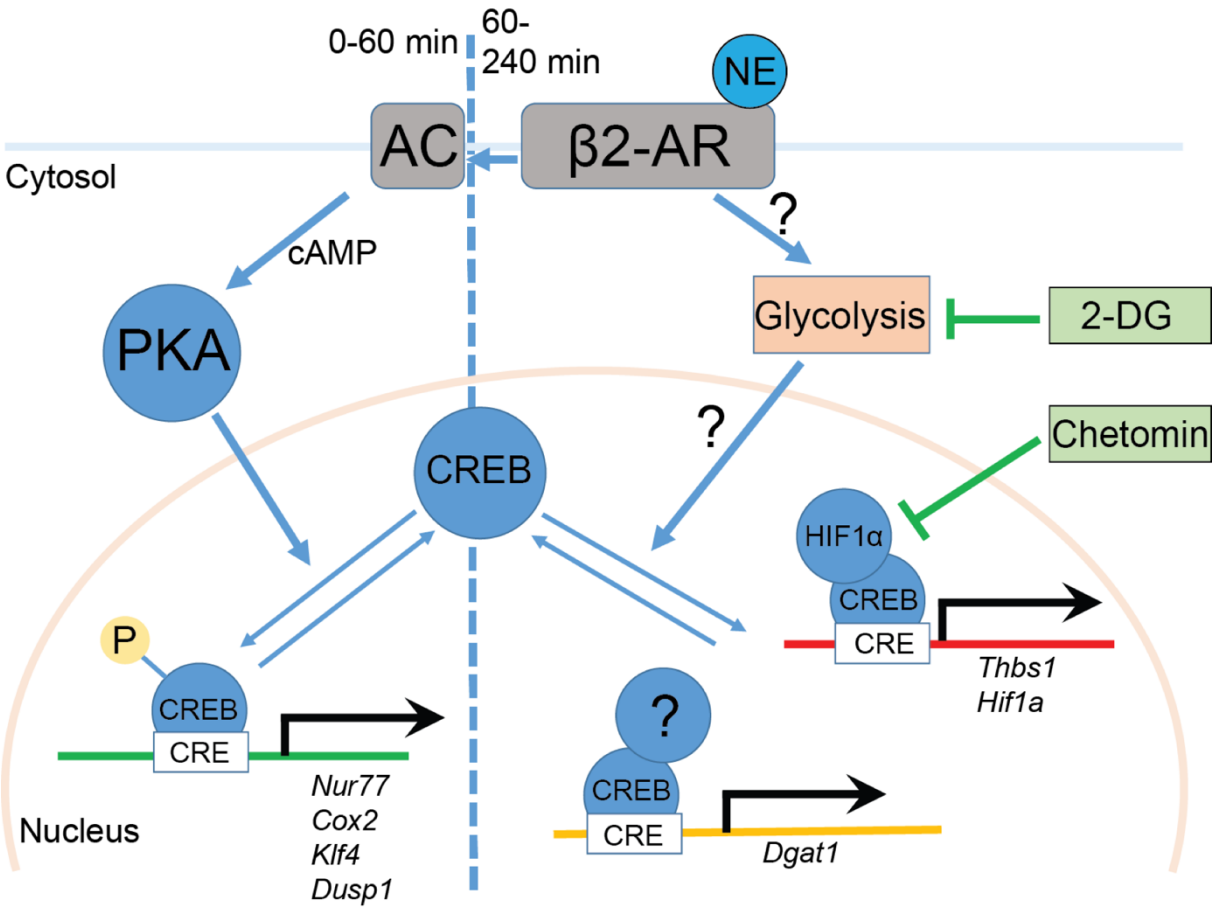

Figure 5-15. Proposed model of the induction of gene transcription by NE in BMDMs.

Molecular processes on the left side of the dashed line occur between 0-60 min after β2AR activation, while the ones on the right side – between 60 - 240 min.

While my experiments in this chapter did not indicate the identity of the transcription factor mediating *Dgat1* gene expression in response to β2AR activation, such regulator is also likely to be present in a complex with CREB-p300, as *Dgat1* promoter contains a CRE sequence. Interestingly, p300-ChREBP transcription factor complex has previously been described to regulate lipogenic gene expression in hepatocytes, including *Dgat1*[601,602]. Furthermore, SIK2 was shown to inhibit p300-ChREBP transcriptional activity by phosphorylating p300, and SIK2 genetic deletion enhanced

hepatic lipogenic gene expression[601]. I observed enhanced *Dgat1* expression in BMDMs following β2AR activation in the presence of SIK inhibitor, suggesting that CREB-p300-ChREBP could also be regulating lipogenic gene expression in macrophages. In future, I will obtain ChREBP-deficient BMDMs to verify the role of ChREBP in *Dgat1* transcription in response to β2AR activation.

Overall, most *in vitro* gene expression studies in this chapter were relatively basic and did not directly investigate the importance of β2AR activation in macrophages in the setting of lipotoxicity. However, understanding the role of glycolysis and HIF1α in response to β2AR stimulation is of high importance, because it indicates **the dependence of the β2AR signalling outcome on the cellular microenvironment**. In a healthy animal, characterised by adipose tissue normoxia and controlled blood glucose levels, β2AR activation in ATMs will favour the expression of early phase genes, predominantly encoding anti-inflammatory factors. However, obesity results in aberrant WAT expansion, leading to low oxygen levels in WAT and stabilisation of HIF1α in ATMs[603]. Furthermore, insulin resistance observed during obesity manifests in an impaired regulation of blood glucose concentration and prolonged periods of hyperglycaemia. In such hypoxic and hyperglycaemic adipose tissue environment, β2AR signalling in ATMs would favour the late phase gene transcription, leading to diminished anti-inflammatory response. Therefore, my results in this chapter will help to direct the future studies on the role of sympathetic nerve-ATM interactions in obesity.

Sympathetic nervous system is also known to regulate tumour microenvironment in multiple cancers, thus mediating the tumour growth and cancer progression[604]. A recent report has found that mice lacking *Adrb2* gene in the endothelial cells are protected against prostate cancer progression due to reduced angiogenesis[605]. While this study reported that macrophage-specific *Adrb2* deletion did not affect the prostate cancer development[605], β2AR in tumour-associated macrophages might be important for the progression of other cancer types. Importantly, tumour cells have been shown to compete for limited nutrient amounts present in the tumour microenvironment, and reduced tumour glucose availability has been described to inhibit the inflammatory activation of tumour growth-limiting T cells[606]. Similarly, reduced glucose availability in tumour-associated macrophages would favour the induction of early phase genes in response to β2AR signalling, therefore enhancing the anti-inflammatory response linked with an accelerated tumour growth[607]. Overall, my results in this chapter suggest

an additional mechanism for increased M2 polarisation of tumour-associated macrophages, leading to a faster progression of cancers associated with increased SNS activity, that could be investigated in future.

5.3.2 A potential link between mitochondrial ROS production and increased lipid storage in β2AR agonist-treated BMDMs

One potential reason for increased DGAT1 activity could be the elevated production of mitochondrial ROS, as observed in BMDMs after β2AR stimulation. ROS are known to oxidise double bonds in the fatty acids, which can be prevented by storing fatty acids as TGs in the lipid droplets[302]. As observed in the previous chapter in β2AR-treated BMDMs, DGAT1 inhibition completely blocked the increase in palmitate esterification, while enhanced storage of oleate as TGs was still observed even in the absence of DGAT1 enzymatic activity, suggesting alternative mechanisms that could selectively store unsaturated fatty acids in the lipid droplets, thus protecting them from oxidation. In future, I will investigate the mechanism of selective esterification of fatty acids based on their saturation using complex FFA mixtures that represent WAT fatty acid composition. I will treat BMDMs with β2AR agonist in the presence of WAT FFA mixture and analyse cellular neutral lipids using GC-MS in order to test whether β2AR activation could favour the storage of unsaturated FFAs. Furthermore, I will isolate ATMs from mice after prolonged fasting in order to measure their neutral lipid composition, and compare it to the fatty acid profile of the adipocytes for the differences in their relative saturation. Finally, I will investigate if co-treating BMDMS with β2AR agonist and WAT FFA mixture in the presence of DGAT1 inhibitor leads to increased formation of lipid peroxides. Overall, the presence of a selective storage of unsaturated FFAs in the ATMs in response to β2AR activation would indicate a similar mechanism as already observed in the microglia resident in the hypoxic areas of the developing brain, where glial lipid droplets have an antioxidant function[302]. Such finding could also lead to a new project aiming to describe the molecular mechanisms involved in the selective fatty acid storage in macrophage lipid droplets.

5.3.3 The role of macrophage β2AR in the interactions between macrophages and sympathetic nerves

My proteomic analysis revealed that the most up-regulated biological process in β2AR agonist-treated BMDMs was '*neuronal system'*, involving the cellular response to a neighbouring neuron. While such finding is perhaps expected, as β2AR is directly

stimulated by activated sympathetic nerves, it suggests a mechanism where macrophages could acquire the phenotype observed in SAMs *in vivo* through a continuous β2AR stimulation by NE released from the neighbouring nerves. While such mechanism will need to be investigated further in future, my results in this chapter point in its favour.

The protein showing the highest fold increase in response to β2AR activation in BMDMs is THBS1, which is known to promote TGFβ signalling, and thus mediate cell migration, attachment, proliferation and differentiation[608]. Interestingly, high levels of THBS1 have been found in the developing brain, where it has been shown to mediate synaptogenesis[609,610]. Circulating THBS1 concentration is increased following brain injury[611], when elevated brain NE turnover is also observed[612]. THBS1-deficient mice have worsened neurological outcomes than controls in response to traumatic brain injury[613]. Furthermore, THBS1 is important for neuronal migration in CNS[614], and has been shown to guide the regenerating peripheral nerve axons following injury[615]. Overall, it is possible that SAMs facilitate the sympathetic innervation of adipose tissues by secreting THBS1 in response to NE in a positive feedback manner.

At present, it is not clear whether BMDMs are capable of taking up and degrading NE, despite expressing the enzymes involved in the breakdown of monoamines. According to a recent report, the expression of SLC6A2 is required for NE import and degradation in SAMs[424]. Furthermore, out of all analysed tissue macrophage populations, *Slc6a2* gene expression is restricted to SAMs, suggesting that they are the only macrophages capable of NE breakdown[424]. However, an earlier study has found that cultured peritoneal macrophages can rapidly import and degrade NE, despite lacking *Slc6a2* expression[450]. Cocaine, a known inhibitor of SLC6A2 activity, did not block NE uptake into peritoneal macrophages, indicating a presence of alternative ways for cellular NE import[450]. Interestingly, the highest rate of NE import into peritoneal macrophages was observed at the concentration that I found to maximally activate β2AR in BMDMs (approximately 10 μM)[450], suggesting that β2AR might be important for NE uptake into macrophages.

Based on the detected proteins from my proteomic analysis, BMDMs predominantly express aldehyde dehydrogenases (mainly located in the mitochondria) over aldo-keto reductases (mainly cytosolic), suggesting that mitochondrial NE degradation pathway

plays a major role in macrophages. It is therefore possible that increased aerobic glycolysis and mitochondrial ROS, and decreased oleate β-oxidation observed in response to β2AR activation in BMDMs is a mechanism used to repurpose mitochondria for NE breakdown in an analogous way as mitochondrial repurposing for ROS production is achieved during LPS treatment[110]. In line with such hypothesis, MAOA enzymatic activity has been suggested to produce ROS at higher rate than any other mitochondrial ROS generators[616]. Therefore, similar OCR despite reduced mitochondrial oleate oxidation in NE-treated BMDMs could be explained by increased oxygen consumption by MAOA.

I am currently collaborating with Prof. Jeff Dalley's lab in setting up a liquid chromatography-electrochemical detection-based assay to simultaneously measure NE and its degradation products in BMDMs and their culture medium. Such assay will not only allow me to measure the rate of NE uptake and degradation in BMDMs, but also will be informative regarding the relative contribution of the activity of aldehyde dehydrogenases and aldo-keto reductases for NE breakdown in macrophages. I will utilise this assay to assess whether genetically or pharmacologically disrupting β2AR signalling would decrease the rate of NE uptake or degradation in BMDMs. If β2AR activation was found to be important for regulating NE breakdown, I will attempt to identify molecular mechanisms responsible for this effect. One potential way how β2AR could up-regulate NE degradation is through NLRP3-dependent increase in monoamine breakdown enzyme gene expression. I would therefore test whether the potentiating effects of β2AR agonism on NE degradation are lost in the presence of NLRP3 inhibitor. Interestingly, MAOA is also known to be regulated post-translationally[617,618], and MAOA activity is increased upon the phosphorylation of mitochondrial proteins by PKA in the presence of high cAMP levels[618]. As PKA activity is increased in response to β2AR activation, it could link β2AR signalling to NE degradation. Finally, β-adrenergic receptor activity has already been shown to be important for the clearance of circulating monoamines in humans[563]. It is therefore likely that NE clearance by SAMs also depends on β2AR signalling.

Lastly, SAMs have been demonstrated to contain high levels of *Adrb2* mRNA (Figure 5-16), and one of the most enriched pathways in SAMs compared to other tissue macrophages is cAMP signalling pathway[424]. Interestingly, the expression of genes

induced in response to β2AR stimulation in BMDMs is enriched in SAMs compared to other analysed tissue macrophage populations[424], suggesting an increased β2AR activation in SAMs *in vivo* (Figure 5-17). In future, it would be of interest to investigate the SAM abundance and morphology in LysM-Cre Adrb2$^{fl/fl}$ animals. Furthermore, to check whether β2AR deficiency in SAMs leads to a decreased expression of β2AR stimulation-responsive genes.

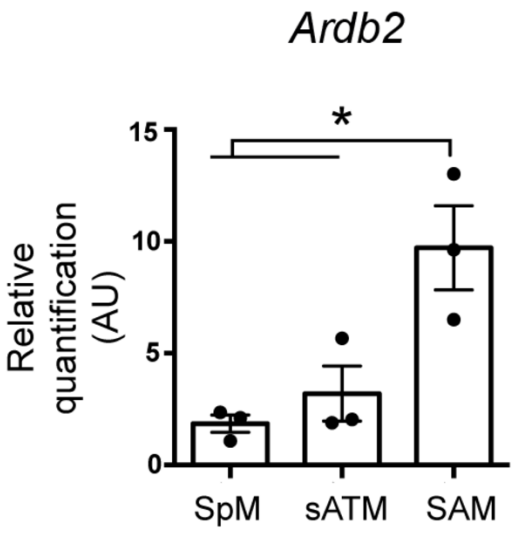

Figure 5-16. Adrb2 gene expression in spenic macrophages, scWAT macrophages, and scWAT SAMs.

Adrb2 mRNA in macrophages from spleen, scWAT or associated to SNS fibres in scWAT. N=3 pools of 10 mice/group. Graph was taken from a recent publication, where cell isolation and analysis was also described[424]*.*

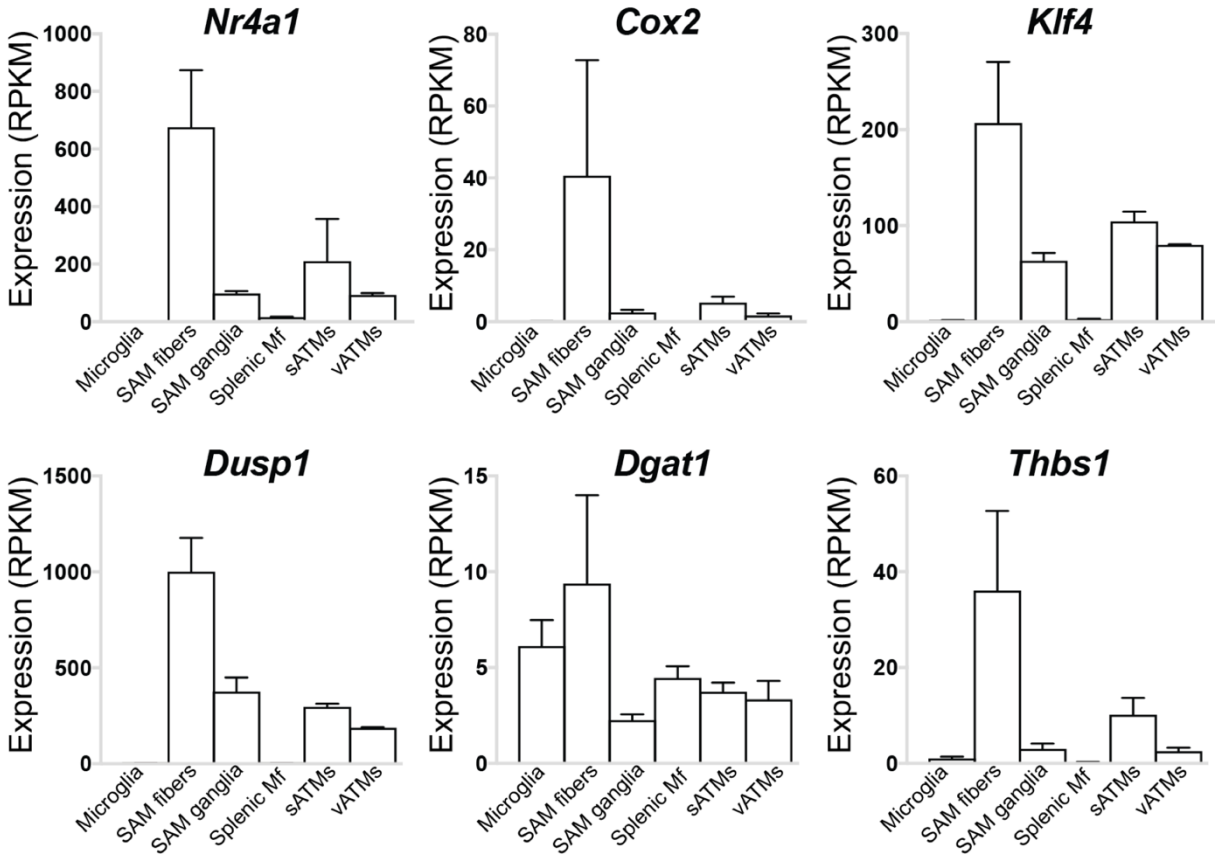

Figure 5-17. Expression of β2AR stimulation-responsive genes in different tissue macrophage populations.

The expression of Nr4a1, Cox2, Klf4, Dusp1, Dgat1 and Thbs1 genes in microglia (n=3), SAMs isolated from scWAT (SAM fibers) (n=2), SAMs isolated from superior cervical ganglia (SAM ganglia) (n=3), peritoneal (n=3), scWAT (n=2) and eWAT (n=2) ATMs. Macrophage populations were isolated and analysed as described in a recent report[424]*. Data was obtained from Gene Expression Omnibus database (GSE103847). Values are expressed as reads per kilobase of transcript per million of mapped reads (RPKM) + SEM. Statistical differences were not assessed.*

As β2AR signalling outcome was shown to be dependent on cellular glycolysis and oxygen sensing, it is possible that β2AR activation in the ATMs present in a hypertrophic WAT might be substantially different than in BMDMs and likely favour the induction of late phase genes. Interestingly, increased circulating levels of THBS1 protein, encoded by a late phase gene, has been found in obese patients, and its concentration in the serum correlated with WAT inflammation and systemic insulin resistance markers[619]. Furthermore, THBS1-deficient mice display reduced WAT inflammation and insulin resistance during obesity[620,621]. The large increase in THBS1 protein levels in β2AR agonist-treated BMDMs suggests a mechanism linking β2AR signalling in ATMs and THBS1-dependent inflammation in the WAT of obese mice. In future, I will measure THBS1 protein levels in WATs isolated from chow- and HFD-fed LysM-Cre Adrb2$^{fl/fl}$ and control animals to investigate whether β2AR deficiency in ATMs could reduce WAT THBS1 expression during obesity.

5.3.4 Conclusions

Overall, I found that NE, acting via β2AR, altered BMDM nutrient metabolism by increasing glycolysis, supressing oleate release and oxidation, and enhancing TG storage. My results also revealed a biphasic induction of gene transcription in response to β2AR activation in BMDMs, where a second phase of gene expression was dependent on glycolysis and the formation of HIF1α-p300 transcriptional complex. In future, additional experiments will need to be performed to further describe the intracellular signalling cascade downstream of β2AR and also to understand the importance of β2AR for NE catabolism in macrophages.

6 General discussion

6.1 Overview

This thesis presented two integrated projects with a common focus on the role of ATM lipid metabolism in mediating obesity-associated WAT inflammation. I have addressed two main objectives:

1) I have defined the role of *de novo* PC synthesis during palmitate-induced inflammation in cultured macrophages, and during obesity-induced WAT inflammation in ATMs.

2) I have characterised the molecular mechanisms responsible for NE signalling-dependent increase in macrophage TG storage capacity, and defined how NE signalling in ATMs impact the development of WAT inflammation and insulin resistance during obesity.

Both projects were executed with a common research strategy that involved an initial phase of BMDM phenotypic characterisation, and a subsequent validation of *in vitro* findings in a murine model of HFD-induced obesity and insulin resistance. Furthermore, both projects investigated relevant biological processes that were regulated pathophysiologically in murine ATMs, thus examining the causal relationship between the alterations in each process and the development of WAT inflammation during obesity. The experiments presented in Chapter 5 contained a broad descriptive analysis of BMDM cellular phenotype induced by adrenergic stimulation, the relevance of which extend beyond obesity-induced WAT inflammation, to other biological systems where SNS-macrophage interactions have been observed, such as gut bacterial infection or tumour development.

Since I have already discussed the main experimental findings and future work within the results chapters of this thesis, in this final chapter I will more generally discuss the limitations of the *in vitro* modelling systems utilised in this thesis, and I will propose alternative approaches to model ATMs and SAMs in physiological and pathophysiological states *in vitro*. Furthermore, here I will express my opinion

regarding the potential drugability of ATM lipid metabolism and GPCR signalling in treating obesity-induced WAT inflammation and insulin resistance.

6.2 Modelling ATMs and WAT inflammation *in vitro*

6.2.1 Cell culture model of ATMs

Like the majority of published reports that investigated macrophage genes involved in the development of obesity-induced WAT inflammation, I utilised BMDMs to model ATMs present in an obese animal. There are a few major advantages in working with BMDMs:

- They are relatively cheap to obtain and culture.
- One mouse yields enough BMDMs to perform virtually any experiment regardless of the amount of input material that is required.
- BMDMs are not immortalised, and thus represent a more physiological model cell type than immortalised macrophage-like cell lines, such as RAW264.7 or J774.2.

Peritoneal macrophages, which are also commonly utilised for the research in the area of adipose tissue inflammation, are considered to be another good primary macrophage model for *in vitro* work. The primary advantage of using peritoneal macrophages is that they differentiate *in vivo* and, when compared to BMDMs, are more similar to tissue macrophages. However, the yield of peritoneal macrophages is low when they are obtained from a healthy mouse. Inducing peritonitis by thioglycollate injection increases the yield of cells, but also skews the macrophages to M1 polarisation[622], making the experiments focusing on macrophage inflammatory activation difficult to interpret.

The main and the most critical downside in using BMDMs and peritoneal macrophages as model cells is that they do not resemble ATMs in terms of their global transcriptome[121]. Therefore, the way BMDMs and peritoneal macrophages metabolise lipids and behave in lipid-rich environments is likely to be substantially different compared to ATMs. This thesis provided a few examples where the cellular response observed in BMDMs *in vitro* did not occur in ATMs *in vivo*. In order to obtain more physiological conditions *in vitro*, one could either *work with isolated ATMs directly*, or

attempt to induce an ATM-like phenotype in BMDMs or peritoneal macrophages. Having a good *in vitro* model of ATMs would facilitate the discovery of different macrophage genes contributing to the development of WAT inflammation. Only the gene knockout models that show a phenotype in the *in vitro* culture model of ATMs could be further studied in mice *in vivo*, which would reduce the number of animals used, the time of the researcher and the cost of the study.

6.2.1.1 Culturing isolated ATMs

There are several publications that performed *in vitro* studies on cultured ATMs[160,284,623,624]. A recent report has found that ATMs isolated from obese mice secrete more IL-6 and CXCL1, but less TNFα in the medium compared to ATMs obtained from lean animals[623]. Furthermore, unlike classically activated macrophages, which reduce their oxidative phosphorylation rate and switch to aerobic glycolysis for ATP production, ATMs from obese mice exhibit an increase in both glycolysis and oxidative phosphorylation rates compared to ATMs isolated from lean animals[120]. These results suggest that the phenotype of ATMs during obesity does not resemble the phenotype of BMDMs induced by LPS or palmitate treatment *in vitro*, for reasons that are yet unknown. However, these findings might have been skewed by the cellular stress resulting from adipose tissue enzymatic digestion and subsequent column purification.

At the start of my PhD, I have made several attempts to culture isolated ATMs *in vitro*. However, I noticed that macrophages isolated using antibodies conjugated to magnetic beads did not exhibit a 'healthy morphology' under microscope. Furthermore, isolated ATMs start detaching from cell culture plates as early as 6 h post plating, indicating cell death.

One could argue that by using an optimised method of isolation and an optimised formulation of medium for subsequent culturing, ATMs could be maintained in a culture for a prolonged period without affecting cell viability. However, as macrophage is a plastic cell type, ATMs might quickly lose their native cellular identity after being placed in cell culture for a prolonged period, making them similar to BMDMs in terms of their phenotype and responsiveness to stimuli. Overall, I do not think that performing *in vitro* studies on isolated ATMs currently is, or could potentially be a viable approach for studying the mechanisms driving adipose tissue inflammation *in vitro*. While

comparative analyses of ATMs isolated from different genetically modified animal models in lean and obese states can be very informative, the methods of studying isolated ATMs in my opinion should be entirely analytic, such as flow cytometry and post-lysis RNA, protein and lipid analyses.

6.2.1.2 Differentiating macrophage progenitors into ATM-like cells

An alternative approach of studying ATM biology is to differentiate BMDMs into ATM-like cells. A similar approach is routinely used to model osteoclasts (macrophage-like bone cells that mediate bone degradation) *in vitro*, which involves adding a cytokine receptor activator of nuclear factor kappa-B ligand (RANKL) to a culture medium during BMDM differentiation[625]. Osteoclasts obtained in this manner are capable of resorbing bone after being plated on dentine or bone slices, thus phenotypically resembling their *in vivo* counterparts[625].

Several studies have modelled adipose tissue microenvironment by co-culturing adipocyte and macrophage cell lines[626-631]. However, the focus of most of these studies was adipocyte metabolism, thus the effect of the co-culture system on macrophages is poorly understood. One study has reported comparable effects between the direct presence of macrophages in the culture and the addition of macrophage-conditioned medium on the adipocyte metabolism, arguing that the majority of the intercellular communication effects results from the paracrine signalling[629]. On the other hand, another study has found that co-culturing adipocyte and macrophage cell lines induces phenotypic changes that cannot be explained by paracrine signalling alone[628].

A recent study has described a new protocol for obtaining ATM-like cells *in vitro* by differentiating BMDMs in the presence of WAT explants within the culture[284]. According to the study, the lipid metabolism of ATM-like cells differentiated in this manner was comparable to ATMs *in vivo*[284]. At the start of my PhD, I attempted to replicate this published protocol several times. While I found that BMDMs differentiating in WAT explant co-cultures contained more intracellular lipids than control BMDMs, the transcriptional signature of ATM-like cells was substantially different to ATMs isolated from WAT (data not shown, but described in my lent rotation project report). I thus concluded that such differentiation protocol was suboptimal and did not yield ATM-like cells.

Overall, existing co-culturing protocols suffer from the lack of knowledge regarding the molecular intercellular communication occurring within the culture, leading to poor reproducibility and control over the experiments. While the factors that shape the phenotype of macrophages in the adipocyte co-cultures can be investigated in order to improve the co-culturing protocols, it is arguably better to *direct that effort into understanding the developmental niche of ATMs*. As ATMs can be repopulated by bone marrow-derived progenitors *in vivo*, **there exists a defined physiological sequence of environmental stimuli that transform monocyte progenitors into ATMs**. Large scale -omics approaches can now enable us to investigate protein, lipid and small molecule factors present within the adipose tissues during ATM development, as well as to monitor the changes in the progenitor transcriptomes during their transition to ATMs. A thorough bioinformatics analysis linking the temporal presence of tissue factors to the activation of macrophage intracellular signalling pathways and transcriptional regulators could be used to formulate a protocol to differentiate bone marrow progenitor cells into ATMs *in vitro*. In my opinion, such protocol would be superior to existing macrophage-adipocyte co-culture methods because of its reproducibility, flexibility and relative simplicity.

Such approach could also be extended to obtain an *in vitro* model of SAMs. Like ATMs, SAMs can be repopulated by monocyte progenitors[424], suggesting that their *in vivo* differentiation conditions could be mimicked on bone marrow cells *in vitro*. SAMs and ATMs within WAT have similar developmental niches, with SAMs having one additional factor present – a neighbouring sympathetic nerve axon. Therefore, the paracrine factors released by sympathetic nerve axons in WAT could be identified and matched to the transcriptional changes of developing SAMs. As I have already suggested in this thesis, one of the factors mediating SAM development might be NE acting on surface β2ARs of the progenitor cells. However, it is likely that there are numerous other SNS-derived protein, lipid and small molecule mediators that influence SAM phenotype. The identity and molecular targets of these mediators could be investigated in future in order to increase our understanding of tissue macrophage biology, but also to aid the formulation of an *in vitro* SAM differentiation protocol.

Finally, the knowledge of environmental stimuli, leading to changes in transcription factor activity involved in shaping ATM phenotype will be crucial for the development of a successful platform of human induced pluripotent stem cell (iPSC) differentiation

into ATMs or SAMs. Human iPSC-derived ATMs and SAMs could be useful tools for studying human mutations associated with obesity, insulin resistance and dyslipidaemia, as well as to assess the effect of potential drugs targeting and adipose tissue inflammation and immune system-mediated BAT activation.

6.2.2 Modelling lipid-induced inflammation *in vitro*

The prevailing view within the scientific community is that saturated fatty acids drive the inflammatory activation of ATMs. This view was greatly influenced by numerous *in vitro* studies (many of which were summarised in the introduction of this thesis) showing that palmitate and other saturated FFAs induce ER stress and inflammation in cultured macrophages. The main problem in interpreting these studies is that under no physiological or pathophysiological conditions, the quantity of palmitate (or any other saturated fatty acid) is vastly overrepresented compared to other FFAs in any animal tissue. As the lipotoxic and inflammatory effects of saturated FFAs on virtually all cell types are abolished in the presence of unsaturated FFAs, it is difficult to envision how saturated FFAs alone could cause WAT inflammation during obesity.

The hypothesis that fatty acids induce inflammatory activation of macrophages has already been challenged by a recent study, which showed that fatty acids released from adipocyte lipolysis do not modulate inflammation in cultured macrophages[136]. During my PhD, I have also stimulated BMDMs with FFA mixtures that had been mixed according to their measured relative abundances in healthy WAT, as well as in WAT from HFD-fed and ob/ob mice. While the stimulations promoted intracellular TG accumulation, none of the FFA mixtures induced ER stress or inflammatory activation of BMDMs (data not shown). It is important to emphasise that like the mentioned study, the concentration of FFA mixtures that I used was approximately 250 μM[136]. However, the concentration of circulating FFAs in mice and humans is approximately 1 mM, and the intra-WAT concentration of FFAs might even exceed 1 mM during on-demand lipolysis or obesity. I have not attempted myself, or found any published studies that treated macrophages with individual FFAs or their mixtures in the millimolar concentration range. It is therefore plausible that ‘overloading’ macrophages with millimolar concentrations of FFA mixtures could induce ER stress and inflammation in a manner that is more similar to obesity-induced WAT inflammation, and could be tested in future.

6.3 Targeting ATMs to alleviate WAT inflammation during obesity

6.3.1 Targeting ATM lipid metabolism

There have been numerous attempts to target inflammatory pathways in order to alleviate insulin resistance in humans, and several clinical trials are currently ongoing (the main studies have been summarised in the introduction). However, with the aberrant ATM lipid metabolism emerging as the major initiator of WAT inflammation during obesity, insulin-sensitising interventions directed at normalising ATM lipid metabolism might be superior to existing generic anti-inflammatory drugs. For example, systemic administration of monoclonal antibody against lipid chaperone FABP4, which is highly expressed in macrophages, successfully alleviated diabetic symptoms in obese mouse models and could be a feasible approach for the treatment of metabolic disorders[632].

However, systemically inhibiting major intracellular metabolic pathways can have detrimental consequences for the patient health. Therefore, the major challenge in the development of macrophage metabolism-based therapeutics is to deliver them specifically to ATMs. Currently, multiple delivery systems, including liposomes, nanoparticles, carbon nanotubes and dendrimers, have been used to successfully deliver bioactives to the macrophages in mouse models *in vivo*[633]. With the rapid improvement of particle engineering technologies, as well as identification of new tissue macrophage-specific surface receptors that can be targeted for delivery, macrophage-aimed therapeutics should become widely applicable in the near future.

Paradoxically, lipid-centric view of ATM inflammatory activation and the development of WAT inflammation is a good argument *against* the *primary* targeting of ATM lipid metabolism in order to improve WAT function. As the accumulation of inflammatory lipid species in ATMs is a secondary event to the adipocyte lipid overload, pharmacologically manipulating macrophage lipid metabolism without normalising caloric intake or WAT storage capacity would still lead to the ectopic lipid accumulation and the development of metabolic complications. Therefore, once the ATM-specific targeting of lipid metabolism pathways is achieved, it should ideally be only used in conjunction with therapies aimed to enhance adipocyte lipid storage capacity. Such combined therapies would likely be faster and more effective at improving the

metabolic profile of obese individuals compared to adipocyte-targeting interventions alone.

6.3.2 Targeting ATM GPCRs

This thesis has illustrated how lipid metabolism in macrophages is regulated by β2AR signalling. Another example of GPCR signalling-mediated regulation of macrophage lipid metabolism is a recent report showing that melanocortin-1 receptor agonism promotes cholesterol efflux from macrophages both *in vitro* and *in vivo*[634]. It is likely that there are other GPCRs modulating lipid metabolism in macrophages, that could be exploited pharmaceutically.

The main advantage of pharmaceutical GPCR manipulation is their ease of targeting. As GPCRs are located extracellularly, cell-impermeable molecules can be utilised to alter their activity with relatively few off-target effects, which is not the case for the majority of drugs that act inside the cell. Furthermore, multiple GPCRs can be manipulated simultaneously, and a cocktail of GPCR-targeting drugs could be administered to elicit a desired effect on a phenotype of cells that express a specific set of GPCRs.

With the increasing number of studies analysing the ATM transcriptomes under different conditions, it should be possible to obtain a profile of G_s-linked GPCRs that are over-represented in the ATM population. Pharmacologically activating a subset of such ATM-specific GPCRs should increase intracellular cAMP concentration and promote a resolution phenotype in the ATM population during obesity, leading to reduced WAT inflammation. Finally, while macrophage-specific β2AR knockout mice did not exhibit increased WAT inflammation on chow or HFD compared to controls, it only indicated that the intrinsic SNS output to ATMs did not modulate their inflammatory status. A timed exogenous β2AR activation in ATMs could potentially alleviate WAT inflammation, and could be tested *in vivo* in future.

6.4 Summary and conclusions

Overall, our understanding of ATM biology and the development of WAT inflammation has greatly improved in the last several years. In particular, lipids and their intracellular metabolism are now considered as some of the main factors that drive the inflammatory activation of ATMs during obesity, leading to the development of WAT dysfunction and insulin resistance.

This thesis has described a link between the *de novo* PC biosynthesis capacity in macrophages and their inflammatory response to saturated fatty acids. In particular, macrophages with a reduced rate of *de novo* PC biosynthesis were protected against palmitate-induced inflammatory activation compared to control cells, likely because of increased expression of fatty acid remodelling enzymes. An inverse relationship between measured PC:PE ratio and the expression of fatty acid remodelling genes was also observed in ATMs *in vivo* – macrophages isolated from WAT of obese mice had higher PC:PE molar ratio and lower mRNA levels of fatty acid remodelling and anti-inflammatory genes than ATMs obtain from lean animals. While mice with a macrophage-specific deletion of *Pcyt1a*, a gene encoding the rate-limiting enzyme of *de novo* PC biosynthesis pathway, did not exhibit differences in WAT inflammation on a chow or HFD, they showed a minor improvement in the transcriptional profile of hepatic genes involved in nutrient metabolism compared to controls on HFD. More experiments are still required to understand the molecular mechanisms mediating the phenotype of mice lacking *Pcyt1a* in macrophages.

Furthermore, this thesis have identified a novel physiological regulator of TG metabolism in macrophages. In particular, I found that NE, acting on surface β2ARs, rapidly increases macrophage TG storage capacity by simultaneously supressing lipolysis and enhancing TG esterification. Such finding suggests that lipid accumulation in macrophages is not only a consequence of pathophysiological challenges, such as bacterial infection, WAT inflammation or atherosclerosis, but can also occur in a regulated manner. Future experiments designed to identify the biological purpose for such regulation will also improve our understanding of the mechanisms that drive lipid accumulation in ATMs during obesity.

7 References

1. Ng, M. *et al.* Global, regional, and national prevalence of overweight and obesity in children and adults during 1980-2013: a systematic analysis for the Global Burden of Disease Study 2013. *Lancet* **384,** 766–781 (2014).
2. Reaven, G. M. Banting lecture 1988. Role of insulin resistance in human disease. *Diabetes* **37,** 1595–1607 (1988).
3. Unwin, N. The metabolic syndrome. *J R Soc Med* **99,** 457–462 (2006).
4. Alberti, K. G. M. M. *et al.* Harmonizing the metabolic syndrome: a joint interim statement of the International Diabetes Federation Task Force on Epidemiology and Prevention; National Heart, Lung, and Blood Institute; American Heart Association; World Heart Federation; International Atherosclerosis Society; and International Association for the Study of Obesity. in **120,** 1640–1645 (American Heart Association, Inc., 2009).
5. World Health Organisation. *GLOBAL HEALTH RISKS*. 1–70 (2009).
6. Yanovski, S. Z. & Yanovski, J. A. Long-term drug treatment for obesity: a systematic and clinical review. *JAMA* **311,** 74–86 (2014).
7. Chang, S.-H. *et al.* The effectiveness and risks of bariatric surgery: an updated systematic review and meta-analysis, 2003-2012. *JAMA Surg* **149,** 275–287 (2014).
8. Ross, S. E., Flynn, J. I. & Pate, R. R. What is really causing the obesity epidemic? A review of reviews in children and adults. *J Sports Sci* **34,** 1148–1153 (2016).
9. Sethi, J. K. & Vidal-Puig, A. J. Thematic review series: adipocyte biology. Adipose tissue function and plasticity orchestrate nutritional adaptation. *The Journal of Lipid Research* **48,** 1253–1262 (2007).
10. Bellisari, A. Evolutionary origins of obesity. *Obesity Reviews* **9,** 165–180 (2008).
11. Neel, J. V. Diabetes Mellitus - a Thrifty Genotype Rendered Detrimental by Progress. *Am. J. Hum. Genet.* **14,** 353–& (1962).
12. Polderman, T. J. C. *et al.* Meta-analysis of the heritability of human traits based on fifty years of twin studies. *Nat. Genet.* **47,** 702–709 (2015).
13. Elks, C. E. *et al.* Variability in the heritability of body mass index: a systematic review and meta-regression. *Front Endocrinol (Lausanne)* **3,** 29 (2012).
14. Speakman, J. R. Thrifty genes for obesity, an attractive but flawed idea, and an alternative perspective: the |[lsquo]|drifty gene|[rsquo]| hypothesis. *International Journal of Obesity* **32,** 1611–1617 (2008).
15. Wang, G. & Speakman, J. R. Analysis of Positive Selection at Single Nucleotide Polymorphisms Associated with Body Mass Index Does Not Support the 'Thrifty Gene' Hypothesis. *Cell Metab.* **24,** 531–541 (2016).
16. LIMA, S. L. Predation Risk and Unpredictable Feeding Conditions - Determinants of

Body-Mass in Birds. *Ecology* **67,** 377–385 (1986).

17. MCNAMARA, J. M. & HOUSTON, A. I. The Value of Fat Reserves and the Tradeoff Between Starvation and Predation. *Acta Biotheoretica* **38,** 37–61 (1990).
18. Speakman, J. R. Why lipostatic set point systems are unlikely to evolve. *Mol Metab* (2017). doi:10.1016/j.molmet.2017.10.007
19. Blouet, C. & Schwartz, G. J. Hypothalamic nutrient sensing in the control of energy homeostasis. *Behavioural Brain Research* **209,** 1–12 (2010).
20. Locke, A. E. *et al.* Genetic studies of body mass index yield new insights for obesity biology. *Nature* **518,** 197–U401 (2015).
21. Fall, T. & Ingelsson, E. Genome-wide association studies of obesity and metabolic syndrome. *Molecular and Cellular Endocrinology* **382,** 740–757 (2014).
22. Tchkonia, T. *et al.* Mechanisms and metabolic implications of regional differences among fat depots. *Cell Metab.* **17,** 644–656 (2013).
23. Wang, W. & Seale, P. Control of brown and beige fat development. *Nat. Rev. Mol. Cell Biol.* **17,** 691–702 (2016).
24. Sacks, H. & Symonds, M. E. Anatomical Locations of Human trovvn Adipose Tissue Functional Relevance and Implications in Obesity and Type 2 Diabetes. *Diabetes* **62,** 1783–1790 (2013).
25. Symonds, M. E. *Adipose Tissue Biology*. (Springer, 2017).
26. Vance, J. E. & Vance, D. E. *Biochemistry of Lipids, Lipoproteins and Membranes*. (Elsevier, 2008).
27. Abdul-Ghani, M. A. & DeFronzo, R. A. Pathogenesis of Insulin Resistance in Skeletal Muscle. *Journal of Biomedicine and Biotechnology* **2010,** –19 (2010).
28. Goldberg, I. J., Eckel, R. H. & Abumrad, N. A. Regulation of fatty acid uptake into tissues: lipoprotein lipase- and CD36-mediated pathways. *The Journal of Lipid Research* **50 Suppl,** S86–90 (2009).
29. Duncan, R. E., Ahmadian, M., Jaworski, K., Sarkadi-Nagy, E. & Sul, H. S. Regulation of lipolysis in adipocytes. *Annual Review of Nutrition* **27,** 79–101 (2007).
30. Hastings, M. H., Reddy, A. B. & Maywood, E. S. A clockwork web: circadian timing in brain and periphery, in health and disease. *Nat. Rev. Neurosci.* **4,** 649–661 (2003).
31. Gooley, J. J. Circadian regulation of lipid metabolism. *Proceedings of the Nutrition Society* **75,** 440–450 (2016).
32. Martin, S. L. Mammalian hibernation: a naturally reversible model for insulin resistance in man? *Diab Vasc Dis Res* **5,** 76–81 (2008).
33. Kershaw, E. E. & Flier, J. S. Adipose tissue as an endocrine organ. *J. Clin. Endocrinol. Metab.* **89,** 2548–2556 (2004).
34. Zhang, Y. *et al.* Positional cloning of the mouse obese gene and its human homologue. *Nature* **372,** 425–432 (1994).

35. HALAAS, J. L. *et al.* Weight-Reducing Effects of the Plasma-Protein Encoded by the Obese Gene. *Science* **269,** 543–546 (1995).
36. PELLEYMOUNTER, M. A. *et al.* Effects of the Obese Gene-Product on Body-Weight Regulation in Ob/Ob Mice. *Science* **269,** 540–543 (1995).
37. Haynes, W. G., Morgan, D. A., Walsh, S. A., Mark, A. L. & Sivitz, W. I. Receptor-mediated regional sympathetic nerve activation by leptin. *J. Clin. Invest.* **100,** 270–278 (1997).
38. Zeng, W. *et al.* Sympathetic Neuro-adipose Connections Mediate Leptin-Driven Lipolysis. *Cell* **163,** 84–94 (2015).
39. Minokoshi, Y. *et al.* Leptin stimulates fatty-acid oxidation by activating AMP-activated protein kinase. *Nature* **415,** 339–343 (2002).
40. Takeda, S. *et al.* Leptin regulates bone formation via the sympathetic nervous system. *Cell* **111,** 305–317 (2002).
41. Montague, C. T. *et al.* Congenital leptin deficiency is associated with severe early-onset obesity in humans. *Nature* **387,** 903–908 (1997).
42. Farooqi, I. S. *et al.* Effects of recombinant leptin therapy in a child with congenital leptin deficiency. *N. Engl. J. Med.* **341,** 879–884 (1999).
43. Yamauchi, T. & Kadowaki, T. Physiological and pathophysiological roles of adiponectin and adiponectin receptors in the integrated regulation of metabolic and cardiovascular diseases. *International Journal of Obesity* **32,** S13–S18 (2008).
44. Kubota, N. *et al.* Disruption of adiponectin causes insulin resistance and neointimal formation. *Journal of Biological Chemistry* **277,** 25863–25866 (2002).
45. Peirce, V., Carobbio, S. & Vidal-Puig, A. The different shades of fat. *Nature* **510,** 76–83 (2014).
46. Harms, M. & Seale, P. Brown and beige fat: development, function and therapeutic potential. *Nature Publishing Group* **19,** 1252–1263 (2013).
47. Peirce, V. & Vidal-Puig, A. Regulation of glucose homoeostasis by brown adipose tissue. *Lancet Diabetes & Endocrinology* **1,** 353–360 (2013).
48. Villarroya, F. & Vidal-Puig, A. Beyond the Sympathetic Tone: The New Brown Fat Activators. *Cell Metab.* **17,** 638–643 (2013).
49. Frayn, K. N. Adipose tissue as a buffer for daily lipid flux. *Diabetologia* **45,** 1201–1210 (2002).
50. Lotta, L. A. *et al.* Integrative genomic analysis implicates limited peripheral adipose storage capacity in the pathogenesis of human insulin resistance. *Nat. Genet.* **49,** 17–26 (2017).
51. Virtue, S. & Vidal-Puig, A. Adipose tissue expandability, lipotoxicity and the Metabolic Syndrome--an allostatic perspective. *Biochim. Biophys. Acta* **1801,** 338–349 (2010).
52. Holt, R. I. G., Cockram, C., Flyvbjerg, A. & Goldstein, B. J. *Textbook of Diabetes*. (John

Wiley & Sons, 2016).

53. George, S. J. & Johnson, J. *Atherosclerosis*. (John Wiley & Sons, 2010).
54. Lavie, C. J., De Schutter, A. & Milani, R. V. Healthy obese versus unhealthy lean: the obesity paradox. *Nat Rev Endocrinol* **11,** 55–62 (2015).
55. Kim, J.-Y. *et al.* Obesity-associated improvements in metabolic profile through expansion of adipose tissue. *The Journal of Clinical Investigation* **117,** 2621–2637 (2007).
56. Huang-Doran, I., Sleigh, A., Rochford, J. J., O'Rahilly, S. & Savage, D. B. Lipodystrophy: metabolic insights from a rare disorder. *Journal of Endocrinology* **207,** 245–255 (2010).
57. Savage, D. B. Mouse models of inherited lipodystrophy. *Dis Model Mech* **2,** 554–562 (2009).
58. Choe, S. S., Huh, J. Y., Hwang, I. J., Kim, J. I. & Kim, J. B. Adipose Tissue Remodeling: Its Role in Energy Metabolism and Metabolic Disorders. *Front Endocrinol (Lausanne)* **7,** 30 (2016).
59. Weisberg, S. P. *et al.* Obesity is associated with macrophage accumulation in adipose tissue. *J. Clin. Invest.* **112,** 1796–1808 (2003).
60. Xu, H. *et al.* Chronic inflammation in fat plays a crucial role in the development of obesity-related insulin resistance. *J. Clin. Invest.* **112,** 1821–1830 (2003).
61. Reilly, S. M. & Saltiel, A. R. Adapting to obesity with adipose tissue inflammation. *Nat Rev Endocrinol* **13,** 633–643 (2017).
62. Zhou, L. *et al.* Insulin resistance and white adipose tissue inflammation are uncoupled in energetically challenged Fsp27-deficient mice. *Nat Commun* **6,** (2015).
63. Lackey, D. E. & Olefsky, J. M. Regulation of metabolism by the innate immune system. *Nat Rev Endocrinol* **12,** 15–28 (2016).
64. Biswas, S. K. & Mantovani, A. *Macrophages: Biology and Role in the Pathology of Diseases*. (Springer, 2014).
65. Fond, A. M. & Ravichandran, K. S. Clearance of Dying Cells by Phagocytes: Mechanisms and Implications for Disease Pathogenesis. *Adv. Exp. Med. Biol.* **930,** 25–49 (2016).
66. Bilzer, M., Roggel, F. & Gerbes, A. L. Role of Kupffer cells in host defense and liver disease. *Liver Int.* **26,** 1175–1186 (2006).
67. Whitsett, J. A., Wert, S. E. & Weaver, T. E. Alveolar Surfactant Homeostasis and the Pathogenesis of Pulmonary Disease. *Annual Review of Medicine* **61,** 105–119 (2010).
68. Parkhurst, C. N. *et al.* Microglia promote learning-dependent synapse formation through brain-derived neurotrophic factor. *Cell* **155,** 1596–1609 (2013).
69. Morris, G. P., Clark, I. A., Zinn, R. & Vissel, B. Microglia: A new frontier for synaptic plasticity, learning and memory, and neurodegenerative disease research. *Neurobiol*

Learn Mem **105,** 40–53 (2013).

70. van Furth, R. & Cohn, Z. A. The origin and kinetics of mononuclear phagocytes. *J. Exp. Med.* **128,** 415–435 (1968).
71. Yona, S. *et al.* Fate Mapping Reveals Origins and Dynamics of Monocytes and Tissue Macrophages under Homeostasis. *Immunity* **38,** 79–91 (2013).
72. Schulz, C. *et al.* A Lineage of Myeloid Cells Independent of Myb and Hematopoietic Stem Cells. *Science* **336,** 86–90 (2012).
73. Ginhoux, F. *et al.* Fate Mapping Analysis Reveals That Adult Microglia Derive from Primitive Macrophages. *Science* **330,** 841–845 (2010).
74. Hoeffel, G. *et al.* Adult Langerhans cells derive predominantly from embryonic fetal liver monocytes with a minor contribution of yolk sac-derived macrophages. *J. Exp. Med.* **209,** 1167–1181 (2012).
75. Hoeffel, G. *et al.* C-Myb(+) Erythro-Myeloid Progenitor-Derived Fetal Monocytes Give Rise to Adult Tissue-Resident Macrophages. *Immunity* **42,** 665–678 (2015).
76. Jakubzick, C. *et al.* Minimal differentiation of classical monocytes as they survey steady-state tissues and transport antigen to lymph nodes. *Immunity* **39,** 599–610 (2013).
77. Hashimoto, D. *et al.* Tissue-Resident Macrophages Self-Maintain Locally throughout Adult Life with Minimal Contribution from Circulating Monocytes. *Immunity* **38,** 792–804 (2013).
78. Guilliams, M. *et al.* Alveolar macrophages develop from fetal monocytes that differentiate into long-lived cells in the first week of life via GM-CSF. *J. Exp. Med.* **210,** 1977–1992 (2013).
79. Epelman, S. *et al.* Embryonic and Adult-Derived Resident Cardiac Macrophages Are Maintained through Distinct Mechanisms at Steady State and during Inflammation. *Immunity* **40,** 91–104 (2014).
80. Mass, E. *et al.* Specification of tissue-resident macrophages during organogenesis. *Science* **353,** –aaf4238 (2016).
81. Gomez Perdiguero, E. *et al.* Tissue-resident macrophages originate from yolk-sac-derived erythro-myeloid progenitors. *Nature* **518,** 547–551 (2015).
82. Sawai, C. M. *et al.* Hematopoietic Stem Cells Are the Major Source of Multilineage Hematopoiesis in Adult Animals. *Immunity* **45,** 597–609 (2016).
83. Bain, C. C. *et al.* Long-lived self-renewing bone marrow-derived macrophages displace embryo-derived cells to inhabit adult serous cavities. *Nat Commun* **7,** (2016).
84. Scott, C. L. *et al.* Bone marrow-derived monocytes give rise to self-renewing and fully differentiated Kupffer cells. *Nat Commun* **7,** 10321 (2016).
85. van de laar, L. *et al.* Yolk Sac Macrophages, Fetal Liver, and Adult Monocytes Can Colonize an Empty Niche and Develop into Functional Tissue-Resident Macrophages.

Immunity **44,** 755–768 (2016).

86. Lavin, Y. *et al.* Tissue-Resident Macrophage Enhancer Landscapes Are Shaped by the Local Microenvironment. *Cell* **159,** 1312–1326 (2014).
87. Ginhoux, F. & Jung, S. Monocytes and macrophages: developmental pathways and tissue homeostasis. *Nat. Rev. Immunol.* **14,** 392–404 (2014).
88. Guilliams, M. & Scott, C. L. Does niche competition determine the origin of tissue-resident macrophages? *Nat. Rev. Immunol.* **17,** 451–460 (2017).
89. Yu, Y.-R. A. *et al.* A Protocol for the Comprehensive Flow Cytometric Analysis of Immune Cells in Normal and Inflamed Murine Non-Lymphoid Tissues. *PLoS ONE* **11,** e0150606 (2016).
90. Kumar, H., Kawai, T. & Akira, S. Pathogen Recognition by the Innate Immune System. *International Reviews of Immunology* **30,** 16–34 (2011).
91. Murray, P. J. Macrophage Polarization. *Annu. Rev. Physiol.* **79,** 541–566 (2017).
92. Dinarello, C. A. A clinical perspective of IL-1β as the gatekeeper of inflammation. *Eur. J. Immunol.* **41,** 1203–1217 (2011).
93. Fink, S. L. & Cookson, B. T. Apoptosis, pyroptosis, and necrosis: Mechanistic description of dead and dying eukaryotic cells. *Infect. Immun.* **73,** 1907–1916 (2005).
94. He, Y., Hara, H. & Nunez, G. Mechanism and Regulation of NLRP3 Inflammasome Activation. *Trends in Biochemical Sciences* **41,** 1012–1021 (2016).
95. Rook, G. A. W., Martinelli, R. & Brunet, L. R. Innate immune responses to mycobacteria and the downregulation of atopic responses. *Curr Opin Allergy Clin Immunol* **3,** 337–342 (2003).
96. Anthony, R. M., Rutitzky, L. I., Urban, J. F. J., Stadecker, M. J. & Gause, W. C. Protective immune mechanisms in helminth infection. *Nat. Rev. Immunol.* **7,** 975–987 (2007).
97. Strachan, D. P. Hay fever, hygiene, and household size. *BMJ* **299,** 1259–1260 (1989).
98. Kilpelainen, M., Terho, E. O., Helenius, H. & Koskenvuo, M. Farm environment in childhood prevents the development of allergies. *Clin. Exp. Allergy* **30,** 201–208 (2000).
99. Rook, G. A Darwinian View of the Hygiene or 'Old Friends' Hypothesis. *Microbe* (2012).
100. Summers, R. W. *et al.* Trichuris suis seems to be safe and possibly effective in the treatment of inflammatory bowel disease. *American Journal of Gastroenterology* **98,** 2034–2041 (2003).
101. Weinstock, J. V. & Elliott, D. E. Translatability of helminth therapy in inflammatory bowel diseases. *International Journal for Parasitology* **43,** 245–251 (2013).
102. Summers, R. W., Elliott, D. E., Urban, J. F., Thompson, R. A. & Weinstock, J. V. Trichuris suis therapy for active ulcerative colitis: A randomized controlled trial.

Gastroenterology **128,** 825–832 (2005).

103. Kelly, B. & O'Neill, L. A. J. Metabolic reprogramming in macrophages and dendritic cells in innate immunity. *Cell Res.* **25,** 771–784 (2015).
104. Solaini, G., Baracca, A., Lenaz, G. & Sgarbi, G. Hypoxia and mitochondrial oxidative metabolism. *Biochimica Et Biophysica Acta-Bioenergetics* **1797,** 1171–1177 (2010).
105. Berg, J. M., Tymoczko, J. L. & Stryer, L. *Biochemistry*. (Macmillan, 2010).
106. SPURWAY, N. C. Aerobic Exercise, Anaerobic Exercise and the Lactate Threshold. *British Medical Bulletin* **48,** 569–591 (1992).
107. WARBURG, O. On the origin of cancer cells. *Science* **123,** 309–314 (1956).
108. Cairns, R. A., Harris, I. S. & Mak, T. W. Regulation of cancer cell metabolism. *Nat. Rev. Cancer* **11,** 85–95 (2011).
109. West, A. P. *et al.* TLR signalling augments macrophage bactericidal activity through mitochondrial ROS. *Nature* **472,** 476–480 (2011).
110. Mills, E. L. *et al.* Succinate Dehydrogenase Supports Metabolic Repurposing of Mitochondria to Drive Inflammatory Macrophages. *Cell* **167,** 457–470.e13 (2016).
111. Tannahill, G. M. *et al.* Succinate is an inflammatory signal that induces IL-1β through HIF-1α. *Nature* **496,** 238–242 (2013).
112. Vats, D. *et al.* Oxidative metabolism and PGC-1beta attenuate macrophage-mediated inflammation. *Cell Metab.* **4,** 13–24 (2006).
113. Rodriguez-Prados, J.-C. *et al.* Substrate Fate in Activated Macrophages: A Comparison between Innate, Classic, and Alternative Activation. *The Journal of Immunology* **185,** 605–614 (2010).
114. Galván-Peña, S. & O'Neill, L. A. J. Metabolic reprograming in macrophage polarization. *Front Immunol* **5,** 420 (2014).
115. Lai, X.-H., Xu, Y., Chen, X.-M. & Ren, Y. Macrophage cell death upon intracellular bacterial infection. *Macrophage (Houst)* **2,** e779 (2015).
116. Langston, P. K., Shibata, M. & Horng, T. Metabolism Supports Macrophage Activation. *Front Immunol* **8,** (2017).
117. Gaber, T., Strehl, C. & Buttgereit, F. Metabolic regulation of inflammation. *Nat Rev Rheumatol* **13,** 267–279 (2017).
118. Epelman, S., Lavine, K. J. & Randolph, G. J. Origin and Functions of Tissue Macrophages. *Immunity* **41,** 21–35 (2014).
119. Hassnain Waqas, S. F. *et al.* Adipose tissue macrophages develop from bone marrow-independent progenitors in Xenopus laevis and mouse. *Journal of Leukocyte Biology* **102,** 845–855 (2017).
120. Boutens, L. & Stienstra, R. Adipose tissue macrophages: going off track during obesity. *Diabetologia* **59,** 879–894 (2016).
121. Okabe, Y. & Medzhitov, R. Tissue-Specific Signals Control Reversible Program of

Localization and Functional Polarization of Macrophages. *Cell* **157,** 832–844 (2014).

122. Hotamisligil, G. S. Mechanisms of TNF-alpha-induced insulin resistance. *Exp. Clin. Endocrinol. Diabetes* **107,** 119–125 (1999).

123. Moller, D. E. Potential role of TNF-alpha in the pathogenesis of insulin resistance and type 2 diabetes. *Trends Endocrinol. Metab.* **11,** 212–217 (2000).

124. Stephens, J. M., Lee, J. & Pilch, P. F. Tumor necrosis factor-alpha-induced insulin resistance in 3T3-L1 adipocytes is accompanied by a loss of insulin receptor substrate-1 and GLUT4 expression without a loss of insulin receptor-mediated signal transduction. *Journal of Biological Chemistry* **272,** 971–976 (1997).

125. Hotamisligil, G. S., MURRAY, D. L., CHOY, L. N. & SPIEGELMAN, B. M. Tumor-Necrosis-Factor-Alpha Inhibits Signaling From the Insulin-Receptor. *Proc. Natl. Acad. Sci. U.S.A.* **91,** 4854–4858 (1994).

126. Jager, J., Grémeaux, T., Cormont, M., Le Marchand-Brustel, Y. & Tanti, J.-F. Interleukin-1beta-induced insulin resistance in adipocytes through down-regulation of insulin receptor substrate-1 expression. *Endocrinology* **148,** 241–251 (2007).

127. Gao, D. *et al.* Interleukin-1β mediates macrophage-induced impairment of insulin signaling in human primary adipocytes. *Am. J. Physiol. Endocrinol. Metab.* **307,** E289–304 (2014).

128. Kurebayashi, S., Sumitani, S., Kasayama, S., Jetten, A. M. & Hirose, T. TNF-alpha inhibits 3T3-L1 adipocyte differentiation without downregulating the expression of C/EBPbeta and delta. *Endocr. J.* **48,** 249–253 (2001).

129. Xing, H. *et al.* TNF alpha-mediated inhibition and reversal of adipocyte differentiation is accompanied by suppressed expression of PPARgamma without effects on Pref-1 expression. *Endocrinology* **138,** 2776–2783 (1997).

130. Cawthorn, W. P., Heyd, F., Hegyi, K. & Sethi, J. K. Tumour necrosis factor-alpha inhibits adipogenesis via a beta-catenin/TCF4(TCF7L2)-dependent pathway. *Cell Death Differ.* **14,** 1361–1373 (2007).

131. Odegaard, J. I. & Chawla, A. Pleiotropic Actions of Insulin Resistance and Inflammation in Metabolic Homeostasis. *Science* **339,** 172–177 (2013).

132. Hotamisligil, G. S. Inflammation, metaflammation and immunometabolic disorders. *Nature* **542,** 177–185 (2017).

133. Gautier, E. L. *et al.* HDL and Glut1 inhibition reverse a hypermetabolic state in mouse models of myeloproliferative disorders. *J. Exp. Med.* **210,** 339–353 (2013).

134. Delano, M. J. & Moldawer, L. L. The origins of cachexia in acute and chronic inflammatory diseases. *Nutr Clin Pract* **21,** 68–81 (2006).

135. Kosteli, A. *et al.* Weight loss and lipolysis promote a dynamic immune response in murine adipose tissue. *J. Clin. Invest.* **120,** 3466–3479 (2010).

136. Caspar-Bauguil, S. *et al.* Fatty acids from fat cell lipolysis do not activate an

inflammatory response but are stored as triacylglycerols in adipose tissue macrophages. *Diabetologia* **58,** 1–10 (2015).

137. Odegaard, J. I., Ganeshan, K. & Chawla, A. Adipose Tissue Macrophages: Amicus adipem? *Cell Metab.* **18,** 767–768 (2013).
138. Reilly, S. M. & Saltiel, A. R. Obesity: A complex role for adipose tissue macrophages. *Nat Rev Endocrinol* **10,** 193–194 (2014).
139. Hücking, K., Hamilton-Wessler, M., Ellmerer, M. & Bergman, R. N. Burst-like control of lipolysis by the sympathetic nervous system in vivo. *J. Clin. Invest.* **111,** 257–264 (2003).
140. Schoiswohl, G. *et al.* Impact of Reduced ATGL-Mediated Adipocyte Lipolysis on Obesity-Associated Insulin Resistance and Inflammation in Male Mice. *Endocrinology* **156,** 3610–3624 (2015).
141. Weisberg, S. P. *et al.* CCR2 modulates inflammatory and metabolic effects of high-fat feeding. *J. Clin. Invest.* **116,** 115–124 (2006).
142. Surmi, B. K. & Hasty, A. H. Macrophage infiltration into adipose tissue: initiation, propagation and remodeling. *Future Lipidology* **3,** 545–556 (2008).
143. Amano, S. U. *et al.* Local Proliferation of Macrophages Contributes to Obesity-Associated Adipose Tissue Inflammation. *Cell Metab.* **19,** 162–171 (2014).
144. Haase, J. *et al.* Local proliferation of macrophages in adipose tissue during obesity-induced inflammation. *Diabetologia* **57,** 562–571 (2014).
145. Zheng, C. *et al.* Local proliferation initiates macrophage accumulation in adipose tissue during obesity. *Cell Death Dis* **7,** –e2167 (2016).
146. Braune, J. *et al.* IL-6 Regulates M2 Polarization and Local Proliferation of Adipose Tissue Macrophages in Obesity. *The Journal of Immunology* **198,** 2927–2934 (2017).
147. Tardelli, M. *et al.* Osteopontin is a key player for local adipose tissue macrophage proliferation in obesity. *Mol Metab* **5,** 1131–1137 (2016).
148. Kamei, N. *et al.* Overexpression of monocyte chemoattractant protein-1 in adipose tissues causes macrophage recruitment and insulin resistance. *Journal of Biological Chemistry* **281,** 26602–26614 (2006).
149. Kanda, H. *et al.* MCP-1 contributes to macrophage infiltration into adipose tissue, insulin resistance, and hepatic steatosis in obesity. *J. Clin. Invest.* **116,** 1494–1505 (2006).
150. Kim, J. *et al.* Silencing CCR2 in Macrophages Alleviates Adipose Tissue Inflammation and the Associated Metabolic Syndrome in Dietary Obese Mice. *Mol Ther Nucleic Acids* **5,** 1–12 (2016).
151. Sullivan, T. J. *et al.* Experimental evidence for the use of CCR2 antagonists in the treatment of type 2 diabetes. *Metab. Clin. Exp.* **62,** 1623–1632 (2013).
152. Kitade, H. *et al.* CCR5 Plays a Critical Role in Obesity-Induced Adipose Tissue

Inflammation and Insulin Resistance by Regulating Both Macrophage Recruitment and M1/M2 Status. *Diabetes* **61,** 1680–1690 (2012).

153. Chavey, C. *et al.* CXC Ligand 5 Is an Adipose-Tissue Derived Factor that Links Obesity to Insulin Resistance. *Cell Metab.* **9,** 339–349 (2009).
154. Shah, R. *et al.* Fractalkine Is a Novel Human Adipochemokine Associated With Type 2 Diabetes. *Diabetes* **60,** 1512–1518 (2011).
155. Zheng, C. *et al.* CD11b regulates obesity-induced insulin resistance via limiting alternative activation and proliferation of adipose tissue macrophages. *Proc. Natl. Acad. Sci. U.S.A.* **112,** E7239–48 (2015).
156. Wensveen, F. M., Valentic, S., Sestan, M., Wensveen, T. T. & Polic, B. The 'Big Bang' in obese fat: Events initiating obesity-induced adipose tissue inflammation. *Eur. J. Immunol.* **45,** 2446–2456 (2015).
157. Wensveen, F. M. *et al.* NK cells link obesity-induced adipose stress to inflammation and insulin resistance. *Nature Immunology* **16,** 376–385 (2015).
158. Cinti, S. *et al.* Adipocyte death defines macrophage localization and function in adipose tissue of obese mice and humans. *The Journal of Lipid Research* **46,** 2347–2355 (2005).
159. Haka, A. S. *et al.* Exocytosis of macrophage lysosomes leads to digestion of apoptotic adipocytes and foam cell formation. *J. Lipid Res.* **57,** 980–992 (2016).
160. Coats, B. R. *et al.* Metabolically Activated Adipose Tissue Macrophages Perform Detrimental and Beneficial Functions during Diet-Induced Obesity. *CellReports* **20,** 3149–3161 (2017).
161. Alkhouri, N. *et al.* Adipocyte Apoptosis, a Link between Obesity, Insulin Resistance, and Hepatic Steatosis. *Journal of Biological Chemistry* **285,** 3428–3438 (2010).
162. Fischer-Posovszky, P., Wang, Q. A., Asterholm, I. W., Rutkowski, J. M. & Scherer, P. E. Targeted deletion of adipocytes by apoptosis leads to adipose tissue recruitment of alternatively activated M2 macrophages. *Endocrinology* **152,** 3074–3081 (2011).
163. Feng, D. *et al.* High-Fat Diet Induced Adipocyte Cell Death Occurs Through a Cyclophilin D Intrinsic Signaling Pathway Independent of Adipose Tissue Inflammation. *Diabetes* **60,** 2134–2143 (2011).
164. Shi, H. *et al.* TLR4 links innate immunity and fatty acid-induced insulin resistance. *J. Clin. Invest.* **116,** 3015–3025 (2006).
165. Vila, I. K. *et al.* Immune Cell Toll-like Receptor 4 Mediates the Development of Obesity-and Endotoxemia-Associated Adipose Tissue Fibrosis. *CellReports* **7,** 1116–1129 (2014).
166. Vandanmagsar, B. *et al.* The NLRP3 inflammasome instigates obesity-induced inflammation and insulin resistance. *Nature Publishing Group* **17,** 179–188 (2011).
167. Stienstra, R. *et al.* Inflammasome is a central player in the induction of obesity and

insulin resistance. *Proc. Natl. Acad. Sci. U.S.A.* **108,** 15324–15329 (2011).

168. Yu, M. *et al.* MyD88-dependent interplay between myeloid and endothelial cells in the initiation and progression of obesity-associated inflammatory diseases. *J. Exp. Med.* **211,** 887–907 (2014).
169. Castoldi, A. *et al.* Dectin-1 Activation Exacerbates Obesity and Insulin Resistance in the Absence of MyD88. *CellReports* **19,** 2272–2288 (2017).
170. Lim, A. K. H. *et al.* Role of MKK3-p38 MAPK signalling in the development of type 2 diabetes and renal injury in obese db/db mice. *Diabetologia* **52,** 347–358 (2009).
171. Han, M. S. *et al.* JNK Expression by Macrophages Promotes Obesity-Induced Insulin Resistance and Inflammation. *Science* **339,** 218–222 (2013).
172. Odegaard, J. I. *et al.* Macrophage-specific PPARgamma controls alternative activation and improves insulin resistance. *Nature* **447,** 1116–1120 (2007).
173. Liao, X. *et al.* Kruppel-like factor 4 regulates macrophage polarization. *J. Clin. Invest.* **121,** 2736–2749 (2011).
174. Reilly, S. M. *et al.* An inhibitor of the protein kinases TBK1 and IKK-ε improves obesity-related metabolic dysfunctions in mice. *Nature Publishing Group* **19,** 313–321 (2013).
175. Oral, E. A. *et al.* Inhibition of IKKε and TBK1 Improves Glucose Control in a Subset of Patients with Type 2 Diabetes. *Cell Metab.* **26,** 157–170.e7 (2017).
176. Goldfine, A. B. *et al.* Salicylate (salsalate) in patients with type 2 diabetes: a randomized trial. *Ann. Intern. Med.* **159,** 1–12 (2013).
177. Koska, J. *et al.* The effect of salsalate on insulin action and glucose tolerance in obese non-diabetic patients: results of a randomised double-blind placebo-controlled study. *Diabetologia* **52,** 385–393 (2009).
178. Barzilay, J. I. *et al.* The impact of salsalate treatment on serum levels of advanced glycation end products in type 2 diabetes. *Diabetes Care* **37,** 1083–1091 (2014).
179. Goldfine, A. B. *et al.* Use of salsalate to target inflammation in the treatment of insulin resistance and type 2 diabetes. *Clin Transl Sci* **1,** 36–43 (2008).
180. Solomon, D. H. *et al.* Association between disease-modifying antirheumatic drugs and diabetes risk in patients with rheumatoid arthritis and psoriasis. *JAMA* **305,** 2525–2531 (2011).
181. Paquot, N., Castillo, M. J., Lefèbvre, P. J. & Scheen, A. J. No increased insulin sensitivity after a single intravenous administration of a recombinant human tumor necrosis factor receptor: Fc fusion protein in obese insulin-resistant patients. *J. Clin. Endocrinol. Metab.* **85,** 1316–1319 (2000).
182. Dominguez, H. *et al.* Metabolic and vascular effects of tumor necrosis factor-alpha blockade with etanercept in obese patients with type 2 diabetes. *J. Vasc. Res.* **42,** 517–525 (2005).
183. van Asseldonk, E. J. P. *et al.* Treatment with Anakinra improves disposition index but

not insulin sensitivity in nondiabetic subjects with the metabolic syndrome: a randomized, double-blind, placebo-controlled study. *J. Clin. Endocrinol. Metab.* **96,** 2119–2126 (2011).

184. Dinarello, C. A., Simon, A. & van der Meer, J. W. M. Treating inflammation by blocking interleukin-1 in a broad spectrum of diseases. *Nat Rev Drug Discov* **11,** 633–652 (2012).
185. Kusminski, C. M., Bickel, P. E. & Scherer, P. E. Targeting adipose tissue in the treatment of obesity-associated diabetes. *Nat Rev Drug Discov* **15,** 639–660 (2016).
186. Hussaarts, L. *et al.* Chronic helminth infection and helminth-derived egg antigens promote adipose tissue M2 macrophages and improve insulin sensitivity in obese mice. *FASEB J.* **29,** 3027–3039 (2015).
187. Wu, D. *et al.* Eosinophils sustain adipose alternatively activated macrophages associated with glucose homeostasis. *Science* **332,** 243–247 (2011).
188. Wiria, A. E. *et al.* Infection with Soil-Transmitted Helminths Is Associated with Increased Insulin Sensitivity. *PLoS ONE* **10,** e0127746 (2015).
189. Tracey, E. F., McDermott, R. A. & McDonald, M. I. Do worms protect against the metabolic syndrome? A systematic review and meta-analysis. *Diabetes Res. Clin. Pract.* **120,** 209–220 (2016).
190. Toita, R., Kawano, T., Murata, M. & Kang, J.-H. Anti-obesity and anti-inflammatory effects of macrophage-targeted interleukin-10-conjugated liposomes in obese mice. *Biomaterials* **110,** 81–88 (2016).
191. Yan, S. *et al.* Long-chain acyl-CoA synthetase in fatty acid metabolism involved in liver and other diseases: an update. *World J. Gastroenterol.* **21,** 3492–3498 (2015).
192. Matsuzaka, T. & Shimano, H. Elovl6: a new player in fatty acid metabolism and insulin sensitivity. *J. Mol. Med.* **87,** 379–384 (2009).
193. Paton, C. M. & Ntambi, J. M. Biochemical and physiological function of stearoyl-CoA desaturase. *Am. J. Physiol. Endocrinol. Metab.* **297,** E28–37 (2009).
194. Hotamisligil, G. S. & Bernlohr, D. A. Metabolic functions of FABPs--mechanisms and therapeutic implications. *Nat Rev Endocrinol* **11,** 592–605 (2015).
195. Steimle, A., Autenrieth, I. B. & Frick, J.-S. Structure and function: Lipid A modifications in commensals and pathogens. *Int. J. Med. Microbiol.* **306,** 290–301 (2016).
196. KRAUSS, J. H., SEYDEL, U., WECKESSER, J. & MAYER, H. Structural-Analysis of the Nontoxic Lipid-a of Rhodobacter-Capsulatus 37b4. *Eur. J. Biochem.* **180,** 519–526 (1989).
197. MUNFORD, R. S. & HALL, C. L. Detoxification of Bacterial Lipopolysaccharides (Endotoxins) by a Human Neutrophil Enzyme. *Science* **234,** 203–205 (1986).
198. Suganami, T. *et al.* Role of the Toll-like receptor 4/NF-kappaB pathway in saturated fatty acid-induced inflammatory changes in the interaction between adipocytes and

macrophages. *Arterioscler. Thromb. Vasc. Biol.* **27,** 84–91 (2007).

199. Nguyen, M. T. A. *et al.* A subpopulation of macrophages infiltrates hypertrophic adipose tissue and is activated by free fatty acids via toll-like receptors 2 and 4 and JNK-dependent pathways. *Journal of Biological Chemistry* **282,** 35279–35292 (2007).
200. Davis, J. E., Gabler, N. K., Walker-Daniels, J. & Spurlock, M. E. Tlr-4 deficiency selectively protects against obesity induced by diets high in saturated fat. *Obesity (Silver Spring)* **16,** 1248–1255 (2008).
201. Holland, W. L. *et al.* Lipid-induced insulin resistance mediated by the proinflammatory receptor TLR4 requires saturated fatty acid-induced ceramide biosynthesis in mice. *J. Clin. Invest.* **121,** 1858–1870 (2011).
202. Saberi, M. *et al.* Hematopoietic Cell-Specific Deletion of Toll-like Receptor 4 Ameliorates Hepatic and Adipose Tissue Insulin Resistance in High-Fat-Fed Mice. *Cell Metab.* **10,** 419–429 (2009).
203. Erridge, C. & Samani, N. J. Saturated fatty acids do not directly stimulate Toll-like receptor signaling. *Arterioscler. Thromb. Vasc. Biol.* **29,** 1944–1949 (2009).
204. Pal, D. *et al.* Fetuin-A acts as an endogenous ligand of TLR4 to promote lipid-induced insulin resistance. *Nature Medicine* **18,** 1279–+ (2012).
205. Steinberg, S. F. Structural basis of protein kinase C isoform function. *Physiol. Rev.* **88,** 1341–1378 (2008).
206. Castrillo, A. *et al.* Protein kinase C epsilon is required for macrophage activation and defense against bacterial infection. *J. Exp. Med.* **194,** 1231–1242 (2001).
207. Loegering, D. J. & Lennartz, M. R. Protein kinase C and toll-like receptor signaling. *Enzyme Res* **2011,** 537821–7 (2011).
208. Erion, D. M. & Shulman, G. I. Diacylglycerol-mediated insulin resistance. *Nature Medicine* **16,** 400–402 (2010).
209. Koliwad, S. K. *et al.* DGAT1-dependent triacylglycerol storage by macrophages protects mice from diet-induced insulin resistance and inflammation. *J. Clin. Invest.* **120,** 756–767 (2010).
210. Imamura, F. *et al.* Effects of Saturated Fat, Polyunsaturated Fat, Monounsaturated Fat, and Carbohydrate on Glucose-Insulin Homeostasis: A Systematic Review and Meta-analysis of Randomised Controlled Feeding Trials. *PLoS Med.* **13,** (2016).
211. Milligan, G., Alvarez-Curto, E., Hudson, B. D., Prihandoko, R. & Tobin, A. B. FFA4/GPR120: Pharmacology and Therapeutic Opportunities. *Trends Pharmacol. Sci.* **38,** 809–821 (2017).
212. Oh, D. Y. *et al.* GPR120 is an omega-3 fatty acid receptor mediating potent anti-inflammatory and insulin-sensitizing effects. *Cell* **142,** 687–698 (2010).
213. Ichimura, A. *et al.* Dysfunction of lipid sensor GPR120 leads to obesity in both mouse and human. *Nature* **483,** 350–354 (2012).

214. Miyamoto, J. *et al.* Nutritional Signaling via Free Fatty Acid Receptors. *Int J Mol Sci* **17,** 450 (2016).
215. Wahli, W. & Michalik, L. PPARs at the crossroads of lipid signaling and inflammation. *Trends Endocrinol. Metab.* **23,** 351–363 (2012).
216. Zelcer, N. & Tontonoz, P. Liver X receptors as integrators of metabolic and inflammatory signaling. *J. Clin. Invest.* **116,** 607–614 (2006).
217. Varin, A. *et al.* Liver X receptor activation promotes polyunsaturated fatty acid synthesis in macrophages: relevance in the context of atherosclerosis. *Arterioscler. Thromb. Vasc. Biol.* **35,** 1357–1365 (2015).
218. Li, P. *et al.* NCoR Repression of LXRs Restricts Macrophage Biosynthesis of Insulin-Sensitizing Omega 3 Fatty Acids. *Cell* **155,** 200–214 (2013).
219. Erbay, E. *et al.* Reducing endoplasmic reticulum stress through a macrophage lipid chaperone alleviates atherosclerosis. *Nature Publishing Group* **15,** 1383–1391 (2009).
220. Oishi, Y. *et al.* SREBP1 Contributes to Resolution of Pro-inflammatory TLR4 Signaling by Reprogramming Fatty Acid Metabolism. *Cell Metab.* **25,** 412–427 (2017).
221. Shimano, H. & Sato, R. SREBP-regulated lipid metabolism: convergent physiology - divergent pathophysiology. *Nat Rev Endocrinol* **13,** 710–730 (2017).
222. Hetz, C. The unfolded protein response: controlling cell fate decisions under ER stress and beyond. *Nat. Rev. Mol. Cell Biol.* **13,** 89–102 (2012).
223. Hou, N. S. *et al.* Activation of the endoplasmic reticulum unfolded protein response by lipid disequilibrium without disturbed proteostasis in vivo. *Proc. Natl. Acad. Sci. U.S.A.* **111,** E2271–80 (2014).
224. Volmer, R. & Ron, D. Lipid-dependent regulation of the unfolded protein response. *Curr. Opin. Cell Biol.* **33,** 67–73 (2015).
225. Volmer, R., van der Ploeg, K. & Ron, D. Membrane lipid saturation activates endoplasmic reticulum unfolded protein response transducers through their transmembrane domains. *Proc. Natl. Acad. Sci. U.S.A.* **110,** 4628–4633 (2013).
226. Fu, S. *et al.* Aberrant lipid metabolism disrupts calcium homeostasis causing liver endoplasmic reticulum stress in obesity. *Nature* **473,** 528–531 (2011).
227. Fonseca, S. G., Burcin, M., Gromada, J. & Urano, F. Endoplasmic reticulum stress in beta-cells and development of diabetes. *Curr Opin Pharmacol* **9,** 763–770 (2009).
228. Kawasaki, N., Asada, R., Saito, A., Kanemoto, S. & Imaizumi, K. Obesity-induced endoplasmic reticulum stress causes chronic inflammation in adipose tissue. *Scientific Reports 2015 5:null* **2,** 799 (2012).
229. Gregor, M. F. & Hotamisligil, G. S. Adipocyte stress: the endoplasmic reticulum and metabolic disease. *The Journal of Lipid Research* **48,** 1905–1914 (2007).
230. Ramirez, S. & Claret, M. Hypothalamic ER stress: A bridge between leptin resistance and obesity. *FEBS Lett.* **589,** 1678–1687 (2015).

231. Shan, B. *et al.* The metabolic ER stress sensor IRE1α suppresses alternative activation of macrophages and impairs energy expenditure in obesity. *Nature Immunology* **18,** 519–529 (2017).
232. Biden, T. J., Boslem, E., Chu, K. Y. & Sue, N. Lipotoxic endoplasmic reticulum stress, β cell failure, and type 2 diabetes mellitus. *Trends Endocrinol. Metab.* **25,** 389–398 (2014).
233. Robblee, M. M. *et al.* Saturated Fatty Acids Engage an IRE1α-Dependent Pathway to Activate the NLRP3 Inflammasome in Myeloid Cells. *Cell Reports* **14,** 2611–2623 (2016).
234. Suzuki, T. *et al.* ER Stress Protein CHOP Mediates Insulin Resistance by Modulating Adipose Tissue Macrophage Polarity. *CellReports* **18,** 2045–2057 (2017).
235. Tufanli, O. *et al.* Targeting IRE1 with small molecules counteracts progression of atherosclerosis. *Proc. Natl. Acad. Sci. U.S.A.* **114,** E1395–E1404 (2017).
236. Namgaladze, D. & Brüne, B. Macrophage fatty acid oxidation and its roles in macrophage polarization and fatty acid-induced inflammation. *Biochim. Biophys. Acta* **1861,** 1796–1807 (2016).
237. Huang, S. C.-C. *et al.* Metabolic Reprogramming Mediated by the mTORC2-IRF4 Signaling Axis Is Essential for Macrophage Alternative Activation. *Immunity* **45,** 817–830 (2016).
238. Huang, S. C.-C. *et al.* Cell-intrinsic lysosomal lipolysis is essential for alternative activation of macrophages. *Nature Immunology* **15,** 846–855 (2014).
239. Nomura, M. *et al.* Fatty acid oxidation in macrophage polarization. *Nature Immunology* **17,** 216–217 (2016).
240. Bruce, C. R. *et al.* Overexpression of Carnitine Palmitoyltransferase-1 in Skeletal Muscle Is Sufficient to Enhance Fatty Acid Oxidation and Improve High-Fat Diet-Induced Insulin Resistance. *Diabetes* **58,** 550–558 (2009).
241. Monsenego, J. *et al.* Enhancing liver mitochondrial fatty acid oxidation capacity in obese mice improves insulin sensitivity independently of hepatic steatosis. *J. Hepatol.* **56,** 632–639 (2012).
242. Malandrino, M. I. *et al.* Enhanced fatty acid oxidation in adipocytes and macrophages reduces lipid-induced triglyceride accumulation and inflammation. *Am. J. Physiol. Endocrinol. Metab.* **308,** E756–69 (2015).
243. Namgaladze, D. *et al.* Inhibition of macrophage fatty acid β-oxidation exacerbates palmitate-induced inflammatory and endoplasmic reticulum stress responses. *Diabetologia* **57,** 1067–1077 (2014).
244. Gonzalez-Hurtado, E. *et al.* Loss of macrophage fatty acid oxidation does not potentiate systemic metabolic dysfunction. *Am. J. Physiol. Endocrinol. Metab.* **312,** E381–E393 (2017).

245. Walther, T. C., Chung, J. & Farese, R. V. Lipid Droplet Biogenesis. *Annu. Rev. Cell Dev. Biol.* **33,** 491–510 (2017).
246. Krahmer, N., Farese, R. V. & Walther, T. C. Balancing the fat: lipid droplets and human disease. *EMBO Mol Med* **5,** 973–983 (2013).
247. Wilfling, F., Haas, J. T., Walther, T. C. & Farese, R. V. Lipid droplet biogenesis. *Curr. Opin. Cell Biol.* **29,** 39–45 (2014).
248. Yen, C.-L. E., Monetti, M., Burri, B. J. & Farese, R. V. The triacylglycerol synthesis enzyme DGAT1 also catalyzes the synthesis of diacylglycerols, waxes, and retinyl esters. *The Journal of Lipid Research* **46,** 1502–1511 (2005).
249. Sachdev, V. *et al.* Novel role of a triglyceride-synthesizing enzyme: DGAT1 at the crossroad between triglyceride and cholesterol metabolism. *Biochim. Biophys. Acta* **1861,** 1132–1141 (2016).
250. Yen, C.-L. E., Stone, S. J., Koliwad, S., Harris, C. & Farese, R. V. Thematic review series: glycerolipids. DGAT enzymes and triacylglycerol biosynthesis. *The Journal of Lipid Research* **49,** 2283–2301 (2008).
251. Listenberger, L. L. *et al.* Triglyceride accumulation protects against fatty acid-induced lipotoxicity. *Proc. Natl. Acad. Sci. U.S.A.* **100,** 3077–3082 (2003).
252. Zhang, X. & Zhang, K. Endoplasmic Reticulum Stress-Associated Lipid Droplet Formation and Type II Diabetes. *Biochem Res Int* **2012,** 247275–5 (2012).
253. Lee, A.-H., Scapa, E. F., Cohen, D. E. & Glimcher, L. H. Regulation of hepatic lipogenesis by the transcription factor XBP1. *Science* **320,** 1492–1496 (2008).
254. Smith, S. J. *et al.* Obesity resistance and multiple mechanisms of triglyceride synthesis in mice lacking Dgat. *Nat. Genet.* **25,** 87–90 (2000).
255. Streeper, R. S. *et al.* Deficiency of the lipid synthesis enzyme, DGAT1, extends longevity in mice. *Aging (Albany NY)* **4,** 13–27 (2012).
256. Lee, B., Fast, A. M., Zhu, J., Cheng, J.-X. & Buhman, K. K. Intestine-specific expression of acyl CoA:diacylglycerol acyltransferase 1 reverses resistance to diet-induced hepatic steatosis and obesity in Dgat1-/- mice. *J. Lipid Res.* **51,** 1770–1780 (2010).
257. Tsuda, N. *et al.* Intestine-targeted DGAT1 inhibition improves obesity and insulin resistance without skin aberrations in mice. *PLoS ONE* **9,** e112027 (2014).
258. Liu, L. *et al.* Upregulation of myocellular DGAT1 augments triglyceride synthesis in skeletal muscle and protects against fat-induced insulin resistance. *J. Clin. Invest.* **117,** 1679–1689 (2007).
259. Liu, L. *et al.* DGAT1 Expression Increases Heart Triglyceride Content but Ameliorates Lipotoxicity. *Journal of Biological Chemistry* **284,** 36312–36323 (2009).
260. Chen, H. C., Stone, S. J., Zhou, P., Buhman, K. K. & Farese, R. V. Dissociation of obesity and impaired glucose disposal in mice overexpressing acyl coenzyme

a:diacylglycerol acyltransferase 1 in white adipose tissue. *Diabetes* **51,** 3189–3195 (2002).

261. Monetti, M. *et al.* Dissociation of hepatic steatosis and insulin resistance in mice overexpressing DGAT in the liver. *Cell Metab.* **6,** 69–78 (2007).
262. Wurie, H. R., Buckett, L. & Zammit, V. A. Diacylglycerol acyltransferase 2 acts upstream of diacylglycerol acyltransferase 1 and utilizes nascent diglycerides and de novo synthesized fatty acids in HepG2 cells. *FEBS J.* **279,** 3033–3047 (2012).
263. Irshad, Z., Dimitri, F., Christian, M. & Zammit, V. A. Diacylglycerol acyltransferase 2 links glucose utilization to fatty acid oxidation in the brown adipocytes. *The Journal of Lipid Research* **58,** 15–30 (2017).
264. Li, C. *et al.* Roles of Acyl-CoA: Diacylglycerol Acyltransferases 1 and 2 in Triacylglycerol Synthesis and Secretion in Primary Hepatocytes. *Arterioscler. Thromb. Vasc. Biol.* **35,** 1080–1091 (2015).
265. Qi, J. *et al.* The use of stable isotope-labeled glycerol and oleic acid to differentiate the hepatic functions of DGAT1 and-2. *The Journal of Lipid Research* **53,** 1106–1116 (2012).
266. Wilfling, F. *et al.* Triacylglycerol synthesis enzymes mediate lipid droplet growth by relocalizing from the ER to lipid droplets. *Developmental Cell* **24,** 384–399 (2013).
267. Stone, S. J. *et al.* Lipopenia and skin barrier abnormalities in DGAT2-deficient mice. *Journal of Biological Chemistry* **279,** 11767–11776 (2004).
268. Melo, R. C. N. *et al.* Lipid bodies in inflammatory cells: structure, function, and current imaging techniques. *J. Histochem. Cytochem.* **59,** 540–556 (2011).
269. Melo, R. C. N. & Weller, P. F. Lipid droplets in leukocytes: Organelles linked to inflammatory responses. *Exp. Cell Res.* **340,** 193–197 (2016).
270. Kiechl, S. *et al.* Toll-like receptor 4 polymorphisms and atherogenesis. *N. Engl. J. Med.* **347,** 185–192 (2002).
271. Funk, J. L., Feingold, K. R., Moser, A. H. & Grunfeld, C. Lipopolysaccharide stimulation of RAW 264.7 macrophages induces lipid accumulation and foam cell formation. *Atherosclerosis* **98,** 67–82 (1993).
272. Feingold, K. R. *et al.* Mechanisms of triglyceride accumulation in activated macrophages. *Journal of Leukocyte Biology* **92,** 829–839 (2012).
273. Lu, M., Kho, T. & Munford, R. S. Prolonged triglyceride storage in macrophages: pHo trumps pO2 and TLR4. *J. Immunol.* **193,** 1392–1397 (2014).
274. Huang, Y.-L. *et al.* Toll-like receptor agonists promote prolonged triglyceride storage in macrophages. *J. Biol. Chem.* **289,** 3001–3012 (2014).
275. Lopes-Virella, M. F., Klein, R. L. & Stevenson, H. C. Low density lipoprotein metabolism in human macrophages stimulated with microbial or microbial-related products. *Arteriosclerosis* **7,** 176–184 (1987).

276. Kazemi, M. R., McDonald, C. M., Shigenaga, J. K., Grunfeld, C. & Feingold, K. R. Adipocyte fatty acid-binding protein expression and lipid accumulation are increased during activation of murine macrophages by toll-like receptor agonists. *Arterioscler. Thromb. Vasc. Biol.* **25,** 1220–1224 (2005).
277. Haka, A. S. *et al.* Macrophages create an acidic extracellular hydrolytic compartment to digest aggregated lipoproteins. *Mol. Biol. Cell* **20,** 4932–4940 (2009).
278. Norris, P. C. & Dennis, E. A. A lipidomic perspective on inflammatory macrophage eicosanoid signaling. *Adv Biol Regul* **54,** 99–110 (2014).
279. Bozza, P. T. *et al.* Leukocyte lipid body formation and eicosanoid generation: cyclooxygenase-independent inhibition by aspirin. *Proc. Natl. Acad. Sci. U.S.A.* **93,** 11091–11096 (1996).
280. Bozza, P. T., Payne, J. L., Goulet, J. L. & Weller, P. F. Mechanisms of platelet-activating factor-induced lipid body formation: requisite roles for 5-lipoxygenase and de novo protein synthesis in the compartmentalization of neutrophil lipids. *J. Exp. Med.* **183,** 1515–1525 (1996).
281. Bozza, P. T. *et al.* Eosinophil lipid bodies: specific, inducible intracellular sites for enhanced eicosanoid formation. *J. Exp. Med.* **186,** 909–920 (1997).
282. Pacheco, P. *et al.* Lipopolysaccharide-induced leukocyte lipid body formation in vivo: innate immunity elicited intracellular Loci involved in eicosanoid metabolism. *The Journal of Immunology* **169,** 6498–6506 (2002).
283. Prieur, X. *et al.* Differential lipid partitioning between adipocytes and tissue macrophages modulates macrophage lipotoxicity and M2/M1 polarization in obese mice. *Diabetes* **60,** 797–809 (2011).
284. Xu, X. *et al.* Obesity Activates a Program of Lysosomal-Dependent Lipid Metabolism in Adipose Tissue Macrophages Independently of Classic Activation. *Cell Metab.* **18,** 816–830 (2013).
285. Gabriel, T. L. *et al.* Lysosomal stress in obese adipose tissue macrophages contributes to MITF-dependent Gpnmb induction. *Diabetes* **63,** 3310–3323 (2014).
286. Toker, A. The biology and biochemistry of diacylglycerol signalling. Meeting on molecular advances in diacylglycerol signalling. *EMBO Rep.* **6,** 310–314 (2005).
287. Morad, S. A. F. & Cabot, M. C. Ceramide-orchestrated signalling in cancer cells. *Nat. Rev. Cancer* **13,** 51–65 (2013).
288. Vujic, N. *et al.* Acyl-CoA:Diacylglycerol Acyltransferase 1 Expression Level in the Hematopoietic Compartment Impacts Inflammation in the Vascular Plaques of Atherosclerotic Mice. *PLoS ONE* **11,** e0156364 (2016).
289. Gordon, G. B., Barcza, M. A. & Bush, M. E. Lipid accumulation of hypoxic tissue culture cells. *Am. J. Pathol.* **88,** 663–678 (1977).
290. Mylonis, I. *et al.* Hypoxia causes triglyceride accumulation by HIF-1-mediated

stimulation of lipin 1 expression. *J. Cell. Sci.* **125,** 3485–3493 (2012).

291. Cao, R. *et al.* Hypoxia induces dysregulation of lipid metabolism in HepG2 cells via activation of HIF-2α. *Cell. Physiol. Biochem.* **34,** 1427–1441 (2014).
292. Beloribi-Djefaflia, S., Vasseur, S. & Guillaumond, F. Lipid metabolic reprogramming in cancer cells. *Oncogenesis* **5,** e189–e189 (2016).
293. Furuta, E. *et al.* Fatty acid synthase gene is up-regulated by hypoxia via activation of Akt and sterol regulatory element binding protein-1. *Cancer Res.* **68,** 1003–1011 (2008).
294. Lewis, C. A. *et al.* SREBP maintains lipid biosynthesis and viability of cancer cells under lipid- and oxygen-deprived conditions and defines a gene signature associated with poor survival in glioblastoma multiforme. *Oncogene* **34,** 5128–5140 (2015).
295. Kamphorst, J. J. *et al.* Hypoxic and Ras-transformed cells support growth by scavenging unsaturated fatty acids from lysophospholipids. *Proc. Natl. Acad. Sci. U.S.A.* **110,** 8882–8887 (2013).
296. Crucet, M. *et al.* Hypoxia enhances lipid uptake in macrophages: role of the scavenger receptors Lox1, SRA, and CD36. *Atherosclerosis* **229,** 110–117 (2013).
297. Bensaad, K. *et al.* Fatty acid uptake and lipid storage induced by HIF-1α contribute to cell growth and survival after hypoxia-reoxygenation. *CellReports* **9,** 349–365 (2014).
298. Du, W. *et al.* HIF drives lipid deposition and cancer in ccRCC via repression of fatty acid metabolism. *Nat Commun* **8,** 1769 (2017).
299. Dengler, V. L., Galbraith, M. & Espinosa, J. M. Transcriptional regulation by hypoxia inducible factors. *Crit. Rev. Biochem. Mol. Biol.* **49,** 1–15 (2014).
300. Courtnay, R. *et al.* Cancer metabolism and the Warburg effect: the role of HIF-1 and PI3K. *Mol. Biol. Rep.* **42,** 841–851 (2015).
301. Cramer, T. *et al.* HIF-1alpha is essential for myeloid cell-mediated inflammation. *Cell* **112,** 645–657 (2003).
302. Bailey, A. P. *et al.* Antioxidant Role for Lipid Droplets in a Stem Cell Niche of Drosophila. *Cell* **163,** 340–353 (2015).
303. Liou, G.-Y. & Storz, P. Reactive oxygen species in cancer. *Free Radic. Res.* **44,** 479–496 (2010).
304. Bell, E. L. *et al.* The Qo site of the mitochondrial complex III is required for the transduction of hypoxic signaling via reactive oxygen species production. *The Journal of Cell Biology* **177,** 1029–1036 (2007).
305. Brigelius-Flohé, R. & Maiorino, M. Glutathione peroxidases. *Biochim. Biophys. Acta* **1830,** 3289–3303 (2013).
306. Yang, W. S. *et al.* Regulation of ferroptotic cancer cell death by GPX4. *Cell* **156,** 317–331 (2014).
307. Hangauer, M. J. *et al.* Drug-tolerant persister cancer cells are vulnerable to GPX4

inhibition. *Nature* **551,** 247–250 (2017).

308. Reo, N. V., Adinehzadeh, M. & Foy, B. D. Kinetic analyses of liver phosphatidylcholine and phosphatidylethanolamine biosynthesis using (13)C NMR spectroscopy. *Biochim. Biophys. Acta* **1580,** 171–188 (2002).

309. Zhang, D. *et al.* Macrophages deficient in CTP:Phosphocholine cytidylyltransferase-alpha are viable under normal culture conditions but are highly susceptible to free cholesterol-induced death. Molecular genetic evidence that the induction of phosphatidylcholine biosynthesis in free cholesterol-loaded macrophages is an adaptive response. *Journal of Biological Chemistry* **275,** 35368–35376 (2000).

310. Hjelmstad, R. H., Morash, S. C., McMaster, C. R. & Bell, R. M. Chimeric enzymes. Structure-function analysis of segments of sn-1,2-diacylglycerol choline- and ethanolaminephosphotransferases. *Journal of Biological Chemistry* **269,** 20995–21002 (1994).

311. Henneberry, A. L. & McMaster, C. R. Cloning and expression of a human choline/ethanolaminephosphotransferase: synthesis of phosphatidylcholine and phosphatidylethanolamine. *Biochem. J.* **339 (Pt 2),** 291–298 (1999).

312. Henneberry, A. L., Wistow, G. & McMaster, C. R. Cloning, genomic organization, and characterization of a human cholinephosphotransferase. *Journal of Biological Chemistry* **275,** 29808–29815 (2000).

313. Vance, J. E. Phospholipid synthesis and transport in mammalian cells. *Traffic* **16,** 1–18 (2015).

314. Sundler, R., Arvidson, G. & Akesson, B. Pathways for the incorporation of choline into rat liver phosphatidylcholines in vivo. *Biochim. Biophys. Acta* **280,** 559–568 (1972).

315. Sundler, R. & Akesson, B. Regulation of phospholipid biosynthesis in isolated rat hepatocytes. Effect of different substrates. *Journal of Biological Chemistry* **250,** 3359–3367 (1975).

316. Vance, D. E., Trip, E. M. & Paddon, H. B. Poliovirus increases phosphatidylcholine biosynthesis in HeLa cells by stimulation of the rate-limiting reaction catalyzed by CTP: phosphocholine cytidylyltransferase. *Journal of Biological Chemistry* **255,** 1064–1069 (1980).

317. Infante, J. P. Rate-limiting steps in the cytidine pathway for the synthesis of phosphatidylcholine and phosphatidylethanolamine. *Biochem. J.* **167,** 847–849 (1977).

318. Houweling, M., Tijburg, L. B., Vaartjes, W. J. & van Golde, L. M. Phosphatidylethanolamine metabolism in rat liver after partial hepatectomy. Control of biosynthesis of phosphatidylethanolamine by the availability of ethanolamine. *Biochem. J.* **283 (Pt 1),** 55–61 (1992).

319. Snider, S. Choline transport links phospholipid metabolism and inflammation in

macrophages. 1–109 (2017).

320. Pulido, S. A. *et al.* Insights into the phosphatidylcholine and phosphatidylethanolamine biosynthetic pathways in Leishmania parasites and characterization of a choline kinase from Leishmania infantum. *Comp. Biochem. Physiol. B, Biochem. Mol. Biol.* **213,** 45–54 (2017).

321. Hishikawa, D. *et al.* Discovery of a lysophospholipid acyltransferase family essential for membrane asymmetry and diversity. *Proc. Natl. Acad. Sci. U.S.A.* **105,** 2830–2835 (2008).

322. Shindou, H., Hishikawa, D., Harayama, T., Eto, M. & Shimizu, T. Generation of membrane diversity by lysophospholipid acyltransferases. *J. Biochem.* **154,** 21–28 (2013).

323. Harayama, T. *et al.* Lysophospholipid acyltransferases mediate phosphatidylcholine diversification to achieve the physical properties required in vivo. *Cell Metab.* **20,** 295–305 (2014).

324. Rong, X. *et al.* LXRs regulate ER stress and inflammation through dynamic modulation of membrane phospholipid composition. *Cell Metab.* **18,** 685–697 (2013).

325. Gibellini, F. & Smith, T. K. The Kennedy pathway--De novo synthesis of phosphatidylethanolamine and phosphatidylcholine. *IUBMB Life* **62,** 414–428 (2010).

326. Sugimoto, H., Banchio, C. & Vance, D. E. Transcriptional regulation of phosphatidylcholine biosynthesis. *Prog. Lipid Res.* **47,** 204–220 (2008).

327. Jackowski, S. & Fagone, P. CTP: Phosphocholine cytidylyltransferase: paving the way from gene to membrane. *Journal of Biological Chemistry* **280,** 853–856 (2005).

328. Karim, M., Jackson, P. & Jackowski, S. Gene structure, expression and identification of a new CTP:phosphocholine cytidylyltransferase beta isoform. *Biochim. Biophys. Acta* **1633,** 1–12 (2003).

329. Fagone, P. & Jackowski, S. Phosphatidylcholine and the CDP-choline cycle. *Biochim. Biophys. Acta* **1831,** 523–532 (2013).

330. Wang, L., Magdaleno, S., Tabas, I. & Jackowski, S. Early embryonic lethality in mice with targeted deletion of the CTP:phosphocholine cytidylyltransferase alpha gene (Pcyt1a). *Molecular and Cellular Biology* **25,** 3357–3363 (2005).

331. Jackowski, S. *et al.* Disruption of CCTbeta2 expression leads to gonadal dysfunction. *Molecular and Cellular Biology* **24,** 4720–4733 (2004).

332. Yamamoto, G. L. *et al.* Mutations in PCYT1A cause spondylometaphyseal dysplasia with cone-rod dystrophy. *Am. J. Hum. Genet.* **94,** 113–119 (2014).

333. Testa, F. *et al.* Mutations in the PCYT1A gene are responsible for isolated forms of retinal dystrophy. *Eur. J. Hum. Genet.* **25,** 651–655 (2017).

334. Hoover-Fong, J. *et al.* Mutations in PCYT1A, encoding a key regulator of phosphatidylcholine metabolism, cause spondylometaphyseal dysplasia with cone-

rod dystrophy. *Am. J. Hum. Genet.* **94,** 105–112 (2014).

335. Payne, F. *et al.* Mutations disrupting the Kennedy phosphatidylcholine pathway in humans with congenital lipodystrophy and fatty liver disease. *Proc. Natl. Acad. Sci. U.S.A.* **111,** 8901–8906 (2014).

336. Cornell, R. B. & Ridgway, N. D. CTP:phosphocholine cytidylyltransferase: Function, regulation, and structure of an amphitropic enzyme required for membrane biogenesis. *Prog. Lipid Res.* **59,** 147–171 (2015).

337. Pelech, S. L., Pritchard, P. H., Brindley, D. N. & Vance, D. E. Fatty acids promote translocation of CTP:phosphocholine cytidylyltransferase to the endoplasmic reticulum and stimulate rat hepatic phosphatidylcholine synthesis. *Journal of Biological Chemistry* **258,** 6782–6788 (1983).

338. Pelech, S. L., Cook, H. W., Paddon, H. B. & Vance, D. E. Membrane-bound CTP:phosphocholine cytidylyltransferase regulates the rate of phosphatidylcholine synthesis in HeLa cells treated with unsaturated fatty acids. *Biochim. Biophys. Acta* **795,** 433–440 (1984).

339. Pelech, S. L., Paddon, H. B. & Vance, D. E. Phorbol esters stimulate phosphatidylcholine biosynthesis by translocation of CTP:phosphocholine cytidylyltransferase from cytosol to microsomes. *Biochim. Biophys. Acta* **795,** 447–451 (1984).

340. Sleight, R. & Kent, C. Regulation of phosphatidylcholine biosynthesis in cultured chick embryonic muscle treated with phospholipase C. *Journal of Biological Chemistry* **255,** 10644–10650 (1980).

341. Kalmar, G. B., Kay, R. J., Lachance, A., Aebersold, R. & Cornell, R. B. Cloning and expression of rat liver CTP: phosphocholine cytidylyltransferase: an amphipathic protein that controls phosphatidylcholine synthesis. *Proc. Natl. Acad. Sci. U.S.A.* **87,** 6029–6033 (1990).

342. Cornell, R. B. *et al.* Functions of the C-terminal domain of CTP: phosphocholine cytidylyltransferase. Effects of C-terminal deletions on enzyme activity, intracellular localization and phosphorylation potential. *Biochem. J.* **310 (Pt 2),** 699–708 (1995).

343. Sleight, R. & Kent, C. Regulation of phosphatidylcholine biosynthesis in mammalian cells. III. Effects of alterations in the phospholipid compositions of Chinese hamster ovary and LM cells on the activity and distribution of CTP:phosphocholine cytidylyltransferase. *Journal of Biological Chemistry* **258,** 836–839 (1983).

344. Jamil, H., Yao, Z. M. & Vance, D. E. Feedback regulation of CTP:phosphocholine cytidylyltransferase translocation between cytosol and endoplasmic reticulum by phosphatidylcholine. *Journal of Biological Chemistry* **265,** 4332–4339 (1990).

345. Utal, A. K., Jamil, H. & Vance, D. E. Diacylglycerol signals the translocation of CTP:choline-phosphate cytidylyltransferase in HeLa cells treated with 12-O-

tetradecanoylphorbol-13-acetate. *Journal of Biological Chemistry* **266,** 24084–24091 (1991).

346. Davies, S. M., Epand, R. M., Kraayenhof, R. & Cornell, R. B. Regulation of CTP: phosphocholine cytidylyltransferase activity by the physical properties of lipid membranes: an important role for stored curvature strain energy. *Biochemistry* **40,** 10522–10531 (2001).

347. Attard, G. S., Templer, R. H., Smith, W. S., Hunt, A. N. & Jackowski, S. Modulation of CTP:phosphocholine cytidylyltransferase by membrane curvature elastic stress. *Proc. Natl. Acad. Sci. U.S.A.* **97,** 9032–9036 (2000).

348. Watkins, J. D. & Kent, C. Phosphorylation of CTP:phosphocholine cytidylyltransferase in vivo. Lack of effect of phorbol ester treatment in HeLa cells. *Journal of Biological Chemistry* **265,** 2190–2197 (1990).

349. Wang, Y. & Kent, C. Effects of altered phosphorylation sites on the properties of CTP:phosphocholine cytidylyltransferase. *Journal of Biological Chemistry* **270,** 17843–17849 (1995).

350. Jamil, H., Utal, A. K. & Vance, D. E. Evidence that cyclic AMP-induced inhibition of phosphatidylcholine biosynthesis is caused by a decrease in cellular diacylglycerol levels in cultured rat hepatocytes. *Journal of Biological Chemistry* **267,** 1752–1760 (1992).

351. Agassandian, M. *et al.* Oxysterols inhibit phosphatidylcholine synthesis via ERK docking and phosphorylation of CTP:phosphocholine cytidylyltransferase. *Journal of Biological Chemistry* **280,** 21577–21587 (2005).

352. Shiratori, Y., Houweling, M., Zha, X. & Tabas, I. Stimulation of CTP:phosphocholine cytidylyltransferase by free cholesterol loading of macrophages involves signaling through protein dephosphorylation. *Journal of Biological Chemistry* **270,** 29894–29903 (1995).

353. Fagone, P. *et al.* Phospholipid biosynthesis program underlying membrane expansion during B-lymphocyte differentiation. *Journal of Biological Chemistry* **282,** 7591–7605 (2007).

354. Mallampalli, R. K., Ryan, A. J., Salome, R. G. & Jackowski, S. Tumor necrosis factor-alpha inhibits expression of CTP:phosphocholine cytidylyltransferase. *Journal of Biological Chemistry* **275,** 9699–9708 (2000).

355. Banchio, C., Schang, L. M. & Vance, D. E. Phosphorylation of Sp1 by cyclin-dependent kinase 2 modulates the role of Sp1 in CTP:phosphocholine cytidylyltransferase alpha regulation during the S phase of the cell cycle. *Journal of Biological Chemistry* **279,** 40220–40226 (2004).

356. Banchio, C., Schang, L. M. & Vance, D. E. Activation of CTP:phosphocholine cytidylyltransferase alpha expression during the S phase of the cell cycle is mediated

by the transcription factor Sp1. *Journal of Biological Chemistry* **278,** 32457–32464 (2003).

357. Golfman, L. S., Bakovic, M. & Vance, D. E. Transcription of the CTP:phosphocholine cytidylyltransferase alpha gene is enhanced during the S phase of the cell cycle. *Journal of Biological Chemistry* **276,** 43688–43692 (2001).
358. Cornell, R., Grove, G. L., Rothblat, G. H. & Horwitz, A. F. Lipid requirement for cell cycling. The effect of selective inhibition of lipid synthesis. *Exp. Cell Res.* **109,** 299–307 (1977).
359. Tercé, F., Brun, H. & Vance, D. E. Requirement of phosphatidylcholine for normal progression through the cell cycle in C3H/10T1/2 fibroblasts. *The Journal of Lipid Research* **35,** 2130–2142 (1994).
360. Morgan, C., Pollard, J. W. & Stanley, E. R. Isolation and characterization of a cloned growth factor dependent macrophage cell line, BAC1.2F5. *J. Cell. Physiol.* **130,** 420–427 (1987).
361. Tessner, T. G., Rock, C. O., Kalmar, G. B., Cornell, R. B. & Jackowski, S. Colony-stimulating factor 1 regulates CTP: phosphocholine cytidylyltransferase mRNA levels. *Journal of Biological Chemistry* **266,** 16261–16264 (1991).
362. Lagace, T. A., Storey, M. K. & Ridgway, N. D. Regulation of phosphatidylcholine metabolism in Chinese hamster ovary cells by the sterol regulatory element-binding protein (SREBP)/SREBP cleavage-activating protein pathway. *Journal of Biological Chemistry* **275,** 14367–14374 (2000).
363. Kast, H. R., Nguyen, C. M., Anisfeld, A. M., Ericsson, J. & Edwards, P. A. CTP:phosphocholine cytidylyltransferase, a new sterol- and SREBP-responsive gene. *The Journal of Lipid Research* **42,** 1266–1272 (2001).
364. Ryan, A. J., McCoy, D. M., Mathur, S. N., Field, F. J. & Mallampalli, R. K. Lipoprotein deprivation stimulates transcription of the CTP:phosphocholine cytidylyltransferase gene. *The Journal of Lipid Research* **41,** 1268–1277 (2000).
365. Mallampalli, R. K., Ryan, A. J., Carroll, J. L., Osborne, T. F. & Thomas, C. P. Lipid deprivation increases surfactant phosphatidylcholine synthesis via a sterol-sensitive regulatory element within the CTP:phosphocholine cytidylyltransferase promoter. *Biochem. J.* **362,** 81–88 (2002).
366. Ridgway, N. D. & Lagace, T. A. Regulation of the CDP-choline pathway by sterol regulatory element binding proteins involves transcriptional and post-transcriptional mechanisms. *Biochem. J.* **372,** 811–819 (2003).
367. Krahmer, N. *et al.* Phosphatidylcholine Synthesis for Lipid Droplet Expansion Is Mediated by Localized Activation of CTP:Phosphocholine Cytidylyltransferase. *Cell Metab.* **14,** 504–515 (2011).
368. Sriburi, R., Jackowski, S., Mori, K. & Brewer, J. W. XBP1: a link between the unfolded

protein response, lipid biosynthesis, and biogenesis of the endoplasmic reticulum. *The Journal of Cell Biology* **167,** 35–41 (2004).

369. Sriburi, R. *et al.* Coordinate regulation of phospholipid biosynthesis and secretory pathway gene expression in XBP-1(S)-induced endoplasmic reticulum biogenesis. *Journal of Biological Chemistry* **282,** 7024–7034 (2007).
370. Ecker, J. *et al.* Induction of fatty acid synthesis is a key requirement for phagocytic differentiation of human monocytes. *Proc. Natl. Acad. Sci. U.S.A.* **107,** 7817–7822 (2010).
371. García Gil, M., Alonso, F., Alvarez Chiva, V., Sánchez Crespo, M. & Mato, J. M. Phospholipid turnover during phagocytosis in human polymorphonuclear leucocytes. *Biochem. J.* **206,** 67–72 (1982).
372. Rosales, C. *Molecular Mechanisms of Phagocytosis*. (Springer Science & Business Media, 2008).
373. Tian, Y. *et al.* Cytokine secretion requires phosphatidylcholine synthesis. *The Journal of Cell Biology* **181,** 945–957 (2008).
374. Jacobs, R. L., Devlin, C., Tabas, I. & Vance, D. E. Targeted deletion of hepatic CTP:phosphocholine cytidylyltransferase alpha in mice decreases plasma high density and very low density lipoproteins. *Journal of Biological Chemistry* **279,** 47402–47410 (2004).
375. Tian, Y., Zhou, R., Rehg, J. E. & Jackowski, S. Role of phosphocholine cytidylyltransferase alpha in lung development. *Molecular and Cellular Biology* **27,** 975–982 (2007).
376. van der Veen, J. N. *et al.* The critical role of phosphatidylcholine and phosphatidylethanolamine metabolism in health and disease. *Biochim. Biophys. Acta* **1859,** 1558–1572 (2017).
377. Tabas, I. Macrophage apoptosis in atherosclerosis: consequences on plaque progression and the role of endoplasmic reticulum stress. *Antioxid. Redox Signal.* **11,** 2333–2339 (2009).
378. Lundberg, B. Chemical composition and physical state of lipid deposits in atherosclerosis. *Atherosclerosis* **56,** 93–110 (1985).
379. Small, D. M., Bond, M. G., Waugh, D., Prack, M. & Sawyer, J. K. Physicochemical and histological changes in the arterial wall of nonhuman primates during progression and regression of atherosclerosis. *J. Clin. Invest.* **73,** 1590–1605 (1984).
380. Rapp, J. H., Connor, W. E., Lin, D. S., Inahara, T. & Porter, J. M. Lipids of human atherosclerotic plaques and xanthomas: clues to the mechanism of plaque progression. *The Journal of Lipid Research* **24,** 1329–1335 (1983).
381. Haley, N. J., Shio, H. & Fowler, S. Characterization of lipid-laden aortic cells from cholesterol-fed rabbits. I. Resolution of aortic cell populations by metrizamide density

gradient centrifugation. *Lab. Invest.* **37,** 287–296 (1977).

382. Warner, G. J., Stoudt, G., Bamberger, M., Johnson, W. J. & Rothblat, G. H. Cell toxicity induced by inhibition of acyl coenzyme A:cholesterol acyltransferase and accumulation of unesterified cholesterol. *Journal of Biological Chemistry* **270,** 5772–5778 (1995).

383. Tabas, I., Marathe, S., Keesler, G. A., Beatini, N. & Shiratori, Y. Evidence that the initial up-regulation of phosphatidylcholine biosynthesis in free cholesterol-loaded macrophages is an adaptive response that prevents cholesterol-induced cellular necrosis. Proposed role of an eventual failure of this response in foam cell necrosis in advanced atherosclerosis. *Journal of Biological Chemistry* **271,** 22773–22781 (1996).

384. Rader, D. J. & Puré, E. Lipoproteins, macrophage function, and atherosclerosis: beyond the foam cell? *Cell Metab.* **1,** 223–230 (2005).

385. Lagace, T. A. Phosphatidylcholine: Greasing the Cholesterol Transport Machinery. *Lipid Insights* **8,** 65–73 (2015).

386. Shiratori, Y., Okwu, A. K. & Tabas, I. Free cholesterol loading of macrophages stimulates phosphatidylcholine biosynthesis and up-regulation of CTP: phosphocholine cytidylyltransferase. *Journal of Biological Chemistry* **269,** 11337–11348 (1994).

387. Tabas, I. Phospholipid metabolism in cholesterol-loaded macrophages. *Curr. Opin. Lipidol.* **8,** 263–267 (1997).

388. Murray, R. Z. & Stow, J. L. Cytokine Secretion in Macrophages: SNAREs, Rabs, and Membrane Trafficking. *Front Immunol* **5,** 538 (2014).

389. Brügger, B. Lipidomics: analysis of the lipid composition of cells and subcellular organelles by electrospray ionization mass spectrometry. *Annu. Rev. Biochem.* **83,** 79–98 (2014).

390. Manchekar, M. *et al.* Apolipoprotein B-containing lipoprotein particle assembly: lipid capacity of the nascent lipoprotein particle. *Journal of Biological Chemistry* **279,** 39757–39766 (2004).

391. Rusiñol, A., Verkade, H. & Vance, J. E. Assembly of rat hepatic very low density lipoproteins in the endoplasmic reticulum. *Journal of Biological Chemistry* **268,** 3555–3562 (1993).

392. Verkade, H. J., Fast, D. G., Rusiñol, A. E., Scraba, D. G. & Vance, D. E. Impaired biosynthesis of phosphatidylcholine causes a decrease in the number of very low density lipoprotein particles in the Golgi but not in the endoplasmic reticulum of rat liver. *Journal of Biological Chemistry* **268,** 24990–24996 (1993).

393. Fisher, E. A. *et al.* The degradation of apolipoprotein B100 is mediated by the ubiquitin-proteasome pathway and involves heat shock protein 70. *Journal of Biological Chemistry* **272,** 20427–20434 (1997).

394. Yao, Z. M. & Vance, D. E. Reduction in VLDL, but not HDL, in plasma of rats deficient in choline. *Biochem. Cell Biol.* **68,** 552–558 (1990).

395. Rizki, G. *et al.* Mice fed a lipogenic methionine-choline-deficient diet develop hypermetabolism coincident with hepatic suppression of SCD-1. *The Journal of Lipid Research* **47,** 2280–2290 (2006).

396. Rinella, M. E. & Green, R. M. The methionine-choline deficient dietary model of steatohepatitis does not exhibit insulin resistance. *J. Hepatol.* **40,** 47–51 (2004).

397. Zeisel, S. H. *et al.* Choline, an essential nutrient for humans. *FASEB J.* **5,** 2093–2098 (1991).

398. Buchman, A. L. *et al.* Choline deficiency: a cause of hepatic steatosis during parenteral nutrition that can be reversed with intravenous choline supplementation. *Hepatology* **22,** 1399–1403 (1995).

399. Jacobs, R. L., Lingrell, S., Zhao, Y., Francis, G. A. & Vance, D. E. Hepatic CTP:phosphocholine cytidylyltransferase-alpha is a critical predictor of plasma high density lipoprotein and very low density lipoprotein. *Journal of Biological Chemistry* **283,** 2147–2155 (2008).

400. Li, Z. *et al.* The ratio of phosphatidylcholine to phosphatidylethanolamine influences membrane integrity and steatohepatitis. *Cell Metab.* **3,** 321–331 (2006).

401. Walker, A. K. *et al.* A Conserved SREBP-1/Phosphatidylcholine Feedback Circuit Regulates Lipogenesis in Metazoans. *Cell* **147,** 840–852 (2011).

402. Smulan, L. J. *et al.* Cholesterol-Independent SREBP-1 Maturation Is Linked to ARF1 Inactivation. *Cell Reports* **16,** 9–18 (2016).

403. Martínez-Uña, M. *et al.* Excess S-adenosylmethionine reroutes phosphatidylethanolamine towards phosphatidylcholine and triglyceride synthesis. *Hepatology* **58,** 1296–1305 (2013).

404. van der Veen, J. N., Lingrell, S. & Vance, D. E. The membrane lipid phosphatidylcholine is an unexpected source of triacylglycerol in the liver. *J. Biol. Chem.* **287,** 23418–23426 (2012).

405. Lu, S. C. *et al.* Methionine adenosyltransferase 1A knockout mice are predisposed to liver injury and exhibit increased expression of genes involved in proliferation. *Proc. Natl. Acad. Sci. U.S.A.* **98,** 5560–5565 (2001).

406. Kim, Y.-C. *et al.* AhR and SHP regulate phosphatidylcholine and S-adenosylmethionine levels in the one-carbon cycle. *Nat Commun* **9,** 540 (2018).

407. Sezgin, E., Levental, I., Mayor, S. & Eggeling, C. The mystery of membrane organization: composition, regulation and roles of lipid rafts. *Nat. Rev. Mol. Cell Biol.* **18,** 361–374 (2017).

408. Wei, X. *et al.* Fatty acid synthesis configures the plasma membrane for inflammation in diabetes. *Nature* **539,** 294–298 (2016).

409. Holzer, R. G. *et al.* Saturated fatty acids induce c-Src clustering within membrane subdomains, leading to JNK activation. *Cell* **147,** 173–184 (2011).
410. Jung, S. Macrophages and monocytes in 2017: Macrophages and monocytes: of tortoises and hares. *Nat. Rev. Immunol.* **18,** 85–86 (2018).
411. Benschop, R. J., Rodriguez-Feuerhahn, M. & Schedlowski, M. Catecholamine-induced leukocytosis: early observations, current research, and future directions. *Brain Behav. Immun.* **10,** 77–91 (1996).
412. Nance, D. M. & Sanders, V. M. Autonomic innervation and regulation of the immune system (1987-2007). *Brain Behav. Immun.* **21,** 736–745 (2007).
413. Kenney, M. J. & Ganta, C. K. *Autonomic Nervous System and Immune System Interactions*. 1177–1200 (John Wiley & Sons, Inc., 2011). doi:10.1002/cphy.c130051
414. Bergquist, J., Tarkowski, A., Ekman, R. & Ewing, A. Discovery of endogenous catecholamines in lymphocytes and evidence for catecholamine regulation of lymphocyte function via an autocrine loop. *Proc. Natl. Acad. Sci. U.S.A.* **91,** 12912–12916 (1994).
415. Brown, S. W. *et al.* Catecholamines in a macrophage cell line. *J. Neuroimmunol.* **135,** 47–55 (2003).
416. Flierl, M. A. *et al.* Phagocyte-derived catecholamines enhance acute inflammatory injury. *Nature* **449,** 721–U8 (2007).
417. Shaked, I. *et al.* Transcription factor Nr4a1 couples sympathetic and inflammatory cues in CNS-recruited macrophages to limit neuroinflammation. *Nature Immunology* **16,** 1228–1234 (2015).
418. Nguyen, K. D. *et al.* Alternatively activated macrophages produce catecholamines to sustain adaptive thermogenesis. *Nature* **480,** 104–U272 (2011).
419. Qiu, Y. *et al.* Eosinophils and type 2 cytokine signaling in macrophages orchestrate development of functional beige fat. *Cell* **157,** 1292–1308 (2014).
420. Abdullahi, A. *et al.* Alternatively Activated Macrophages Drive Browning of White Adipose Tissue in Burns. *Ann. Surg.* 1 (2017). doi:10.1097/SLA.0000000000002465
421. Spadaro, O. *et al.* IGF1 Shapes Macrophage Activation in Response to Immunometabolic Challenge. *CellReports* **19,** 225–234 (2017).
422. Hui, X. *et al.* Adiponectin Enhances Cold-Induced Browning of Subcutaneous Adipose Tissue via Promoting M2 Macrophage Proliferation. *Cell Metab.* **22,** 279–290 (2015).
423. Fischer, K. *et al.* Alternatively activated macrophages do not synthesize catecholamines or contribute to adipose tissue adaptive thermogenesis. *Nature Medicine* **23,** 623–+ (2017).
424. Pirzgalska, R. M. *et al.* Sympathetic neuron–associated macrophages contribute to obesity by importing and metabolizing norepinephrine. *Nature Publishing Group* 1–19 (2017). doi:10.1038/nm.4422

425. Wolf, Y. *et al.* Brown-adipose-tissue macrophages control tissue innervation and homeostatic energy expenditure. *Nature Immunology* **18,** 665–674 (2017).
426. Slavin, B. G. & Ballard, K. W. Morphological studies on the adrenergic innervation of white adipose tissue. *Anat. Rec.* **191,** 377–389 (1978).
427. Vitali, A. *et al.* The adipose organ of obesity-prone C57BL/6J mice is composed of mixed white and brown adipocytes. *J. Lipid Res.* **53,** 619–629 (2012).
428. Jiang, H., Ding, X., Cao, Y., Wang, H. & Zeng, W. Dense Intra-adipose Sympathetic Arborizations Are Essential for Cold-Induced Beiging of Mouse White Adipose Tissue. *Cell Metab.* **26,** 686–+ (2017).
429. Mosser, C.-A., Baptista, S., Arnoux, I. & Audinat, E. Microglia in CNS development: Shaping the brain for the future. *Prog. Neurobiol.* **149-150,** 1–20 (2017).
430. Rosenberg, A. F., Wolman, M. A., Franzini-Armstrong, C. & Granato, M. In Vivo Nerve-Macrophage Interactions Following Peripheral Nerve Injury. *J. Neurosci.* **32,** 3898–3909 (2012).
431. Mokarram, N., Merchant, A., Mukhatyar, V., Patel, G. & Bellamkonda, R. V. Effect of modulating macrophage phenotype on peripheral nerve repair. *Biomaterials* **33,** 8793–8801 (2012).
432. Mokarram, N. *et al.* Immunoengineering nerve repair. *Proc. Natl. Acad. Sci. U.S.A.* **114,** E5077–E5084 (2017).
433. Cattin, A.-L. *et al.* Macrophage-Induced Blood Vessels Guide Schwann Cell-Mediated Regeneration of Peripheral Nerves. *Cell* **162,** 1127–1139 (2015).
434. Chen, P., Piao, X. & Bonaldo, P. Role of macrophages in Wallerian degeneration and axonal regeneration after peripheral nerve injury. *Acta Neuropathol.* **130,** 605–618 (2015).
435. Qian, L. & Flood, P. M. Microglial cells and Parkinson's disease. *Immunol. Res.* **41,** 155–164 (2008).
436. Sarlus, H. & Heneka, M. T. Microglia in Alzheimer's disease. *J. Clin. Invest.* **127,** 3240–3249 (2017).
437. Muller, P. A. *et al.* Crosstalk between Muscularis Macrophages and Enteric Neurons Regulates Gastrointestinal Motility. *Cell* **158,** 1210 (2014).
438. Gabanyi, I. *et al.* Neuro-immune Interactions Drive Tissue Programming in Intestinal Macrophages. *Cell* **164,** 378–391 (2016).
439. Camell, C. D. *et al.* Inflammasome-driven catecholamine catabolism in macrophages blunts lipolysis during ageing. *Nature* 1–24 (2017). doi:10.1038/nature24022
440. Meiser, J., Weindl, D. & Hiller, K. Complexity of dopamine metabolism. *Cell Commun. Signal* **11,** 34 (2013).
441. Torres, G. E., Gainetdinov, R. R. & Caron, M. G. Plasma membrane monoamine transporters: structure, regulation and function. *Nat. Rev. Neurosci.* **4,** 13–25 (2003).

442. Häggström, M. Medical gallery of Mikael Häggström 2014. *Wiki J Med* **1,** 1–53 (2014).
443. Delgado, P. L. Depression: the case for a monoamine deficiency. *J Clin Psychiatry* **61 Suppl 6,** 7–11 (2000).
444. Youdim, M. B. H., Edmondson, D. & Tipton, K. F. The therapeutic potential of monoamine oxidase inhibitors. *Nat. Rev. Neurosci.* **7,** 295–309 (2006).
445. Sulzer, D. How addictive drugs disrupt presynaptic dopamine neurotransmission. *Neuron* **69,** 628–649 (2011).
446. McDermott, R., Tingley, D., Cowden, J., Frazzetto, G. & Johnson, D. D. P. Monoamine oxidase A gene (MAOA) predicts behavioral aggression following provocation. *Proc. Natl. Acad. Sci. U.S.A.* **106,** 2118–2123 (2009).
447. Eslami Amirabadi, M. R. *et al.* Monoamine oxidase a gene polymorphisms and bipolar disorder in Iranian population. *Iran Red Crescent Med J* **17,** e23095 (2015).
448. Buades-Rotger, M. & Gallardo-Pujol, D. The role of the monoamine oxidase A gene in moderating the response to adversity and associated antisocial behavior: a review. *Psychol Res Behav Manag* **7,** 185–200 (2014).
449. Ma, Y. *et al.* Extracellular norepinephrine clearance by the norepinephrine transporter is required for skeletal homeostasis. *J. Biol. Chem.* **288,** 30105–30113 (2013).
450. Balter, N. J. & Schwartz, S. L. Accumulation of norepinephrine by macrophages and relationships to known uptake processes. *J. Pharmacol. Exp. Ther.* **201,** 636–643 (1977).
451. Czech, M. P. Macrophages dispose of catecholamines in adipose tissue. *Nature Publishing Group* **23,** 1255–1257 (2017).
452. Cotecchia, S. The α1-adrenergic receptors: diversity of signaling networks and regulation. *J. Recept. Signal Transduct. Res.* **30,** 410–419 (2010).
453. Giovannitti, J. A., Thoms, S. M. & Crawford, J. J. Alpha-2 adrenergic receptor agonists: a review of current clinical applications. *Anesth Prog* **62,** 31–39 (2015).
454. Wachter, S. B. & Gilbert, E. M. Beta-adrenergic receptors, from their discovery and characterization through their manipulation to beneficial clinical application. *Cardiology* **122,** 104–112 (2012).
455. Collins, S. β-Adrenoceptor Signaling Networks in Adipocytes for Recruiting Stored Fat and Energy Expenditure. *Front Endocrinol (Lausanne)* **2,** 102 (2011).
456. Lorton, D. & Bellinger, D. L. Molecular Mechanisms Underlying beta-Adrenergic Receptor-Mediated Cross-Talk between Sympathetic Neurons and Immune Cells. *Int J Mol Sci* **16,** 5635–5665 (2015).
457. Grailer, J. J., Haggadone, M. D., Sarma, J. V., Zetoune, F. S. & Ward, P. A. Induction of M2 regulatory macrophages through the β2-adrenergic receptor with protection during endotoxemia and acute lung injury. *J Innate Immun* **6,** 607–618 (2014).
458. Kox, M. *et al.* Voluntary activation of the sympathetic nervous system and attenuation

of the innate immune response in humans. *Proc. Natl. Acad. Sci. U.S.A.* **111,** 7379–7384 (2014).

459. Tang, L. *et al.* Sympathetic Nerve Activity Maintains an Anti-inflammatory State in Adipose Tissue in Male Mice by Inhibiting TNF-α Gene Expression in Macrophages. *Endocrinology* EN.2015–1096–14 (2015). doi:10.1210/EN.2015-1096

460. Luan, B. *et al.* Leptin-mediated increases in catecholamine signaling reduce adipose tissue inflammation via activation of macrophage HDAC4. *Cell Metab.* **19,** 1058–1065 (2014).

461. Spengler, R. N., Allen, R. M., Remick, D. G., Strieter, R. M. & Kunkel, S. L. Stimulation of alpha-adrenergic receptor augments the production of macrophage-derived tumor necrosis factor. *The Journal of Immunology* **145,** 1430–1434 (1990).

462. Miksa, M. *et al.* Pivotal role of the alpha(2A)-adrenoceptor in producing inflammation and organ injury in a rat model of sepsis. *PLoS ONE* **4,** e5504 (2009).

463. Tan, K. S. *et al.* Beta2 adrenergic receptor activation stimulates pro-inflammatory cytokine production in macrophages via PKA- and NF-kappaB-independent mechanisms. *Cell. Signal.* **19,** 251–260 (2007).

464. Mutlu, G. M. *et al.* Ambient particulate matter accelerates coagulation via an IL-6-dependent pathway. *J. Clin. Invest.* **117,** 2952–2961 (2007).

465. Chiarella, S. E. *et al.* β_2-Adrenergic agonists augment air pollution-induced IL-6 release and thrombosis. *J. Clin. Invest.* **124,** 2935–2946 (2014).

466. Méndez-Ferrer, S., Lucas, D., Battista, M. & Frenette, P. S. Haematopoietic stem cell release is regulated by circadian oscillations. *Nature* **452,** 442–447 (2008).

467. Lucas, D., Battista, M., Shi, P. A., Isola, L. & Frenette, P. S. Mobilized hematopoietic stem cell yield depends on species-specific circadian timing. *Cell Stem Cell* **3,** 364–366 (2008).

468. Heidt, T. *et al.* Chronic variable stress activates hematopoietic stem cells. *Nature Publishing Group* **20,** 754–758 (2014).

469. Straub, R. H. *et al.* Neurotransmitters of the sympathetic nerve terminal are powerful chemoattractants for monocytes. *Journal of Leukocyte Biology* **67,** 553–558 (2000).

470. Grisanti, L. A. *et al.* β2-Adrenergic receptor-dependent chemokine receptor 2 expression regulates leukocyte recruitment to the heart following acute injury. *Proc. Natl. Acad. Sci. U.S.A.* **113,** 15126–15131 (2016).

471. Grisanti, L. A. *et al.* Leukocyte-Expressed β2-Adrenergic Receptors Are Essential for Survival After Acute Myocardial Injury. *Circulation* **134,** 153–167 (2016).

472. Yang, T. *et al.* Shifts in the Gut Microbiota Composition Due to Depleted Bone Marrow Beta Adrenergic Signaling Are Associated with Suppressed Inflammatory Transcriptional Networks in the Mouse Colon. *Front Physiol* **8,** 220 (2017).

473. Chruscinski, A. J. *et al.* Targeted disruption of the beta2 adrenergic receptor gene.

Journal of Biological Chemistry **274,** 16694–16700 (1999).

474. Jiang, Y. *et al.* β2-adrenergic receptor knockout mice exhibit A diabetic retinopathy phenotype. *PLoS ONE* **8,** e70555 (2013).

475. Fernandes, G. W. *et al.* Inactivation of the adrenergic receptor 2 disrupts glucose homeostasis in mice. *Journal of Endocrinology* **221,** 381–390 (2014).

476. Santulli, G. *et al.* Age-related impairment in insulin release: the essential role of β(2)-adrenergic receptor. *Diabetes* **61,** 692–701 (2012).

477. Elefteriou, F. *et al.* Leptin regulation of bone resorption by the sympathetic nervous system and CART. *Nature* **434,** 514–520 (2005).

478. Fu, L., Patel, M. S., Bradley, A., Wagner, E. F. & Karsenty, G. The molecular clock mediates leptin-regulated bone formation. *Cell* **122,** 803–815 (2005).

479. Bonnet, N. *et al.* Doping dose of salbutamol and exercise training: impact on the skeleton of ovariectomized rats. *J. Appl. Physiol.* **103,** 524–533 (2007).

480. Erraji-Benchekroun, L. *et al.* Overexpression of beta2-adrenergic receptors in mouse liver alters the expression of gluconeogenic and glycolytic enzymes. *Am. J. Physiol. Endocrinol. Metab.* **288,** E715–22 (2005).

481. Saccà, L., Vigorito, C., Cicala, M., Corso, G. & Sherwin, R. S. Role of gluconeogenesis in epinephrine-stimulated hepatic glucose production in humans. *Am. J. Physiol.* **245,** E294–302 (1983).

482. Ghosh, P. M. *et al.* Role of β-adrenergic receptors in regulation of hepatic fat accumulation during aging. *J. Endocrinol.* **213,** 251–261 (2012).

483. Shi, Y. *et al.* β2-Adrenergic receptor ablation modulates hepatic lipid accumulation and glucose tolerance in aging mice. *Exp. Gerontol.* **78,** 32–38 (2016).

484. McCorry, L. K. Physiology of the autonomic nervous system. *Am J Pharm Educ* **71,** 78 (2007).

485. Altarejos, J. Y. & Montminy, M. CREB and the CRTC co-activators: sensors for hormonal and metabolic signals. *Nat. Rev. Mol. Cell Biol.* **12,** 141–151 (2011).

486. McKnight, G. S. Cyclic AMP second messenger systems. *Curr. Opin. Cell Biol.* **3,** 213–217 (1991).

487. Brasaemle, D. L. Thematic review series: adipocyte biology. The perilipin family of structural lipid droplet proteins: stabilization of lipid droplets and control of lipolysis. *The Journal of Lipid Research* **48,** 2547–2559 (2007).

488. Kraemer, F. B. & Shen, W.-J. Hormone-sensitive lipase: control of intracellular tri-(di-)acylglycerol and cholesteryl ester hydrolysis. *The Journal of Lipid Research* **43,** 1585–1594 (2002).

489. Ritter, S. L. & Hall, R. A. Fine-tuning of GPCR activity by receptor-interacting proteins. *Nat. Rev. Mol. Cell Biol.* **10,** 819–830 (2009).

490. Bystrom, J. *et al.* Resolution-phase macrophages possess a unique inflammatory

phenotype that is controlled by cAMP. *Blood* **112,** 4117–4127 (2008).

491. Kim, C. *et al.* Antiinflammatory cAMP signaling and cell migration genes co-opted by the anthrax bacillus. *Proc. Natl. Acad. Sci. U.S.A.* **105,** 6150–6155 (2008).

492. Medzhitov, R. & Horng, T. Transcriptional control of the inflammatory response. *Nat. Rev. Immunol.* **9,** 692–703 (2009).

493. Ollivier, V., Parry, G. C., Cobb, R. R., de Prost, D. & Mackman, N. Elevated cyclic AMP inhibits NF-kappaB-mediated transcription in human monocytic cells and endothelial cells. *Journal of Biological Chemistry* **271,** 20828–20835 (1996).

494. Parry, G. C. & Mackman, N. Role of cyclic AMP response element-binding protein in cyclic AMP inhibition of NF-kappaB-mediated transcription. *The Journal of Immunology* **159,** 5450–5456 (1997).

495. Platzer, C. *et al.* Cyclic adenosine monophosphate-responsive elements are involved in the transcriptional activation of the human IL-10 gene in monocytic cells. *Eur. J. Immunol.* **29,** 3098–3104 (1999).

496. Ananieva, O. *et al.* The kinases MSK1 and MSK2 act as negative regulators of Toll-like receptor signaling. *Nature Immunology* **9,** 1028–1036 (2008).

497. Clark, K. *et al.* Phosphorylation of CRTC3 by the salt-inducible kinases controls the interconversion of classically activated and regulatory macrophages. *Proc. Natl. Acad. Sci. U.S.A.* **109,** 16986–16991 (2012).

498. MacKenzie, K. F. *et al.* PGE(2) induces macrophage IL-10 production and a regulatory-like phenotype via a protein kinase A-SIK-CRTC3 pathway. *J. Immunol.* **190,** 565–577 (2013).

499. Luan, B. *et al.* CREB pathway links PGE2 signaling with macrophage polarization. *Proc. Natl. Acad. Sci. U.S.A.* **112,** 15642–15647 (2015).

500. Luttrell, L. M. *et al.* Beta-arrestin-dependent formation of beta2 adrenergic receptor-Src protein kinase complexes. *Science* **283,** 655–661 (1999).

501. Krasel, C., Bünemann, M., Lorenz, K. & Lohse, M. J. Beta-arrestin binding to the beta2-adrenergic receptor requires both receptor phosphorylation and receptor activation. *Journal of Biological Chemistry* **280,** 9528–9535 (2005).

502. Witherow, D. S., Garrison, T. R., Miller, W. E. & Lefkowitz, R. J. beta-Arrestin inhibits NF-kappaB activity by means of its interaction with the NF-kappaB inhibitor IkappaBalpha. *Proc. Natl. Acad. Sci. U.S.A.* **101,** 8603–8607 (2004).

503. Gao, H. *et al.* Identification of beta-arrestin2 as a G protein-coupled receptor-stimulated regulator of NF-kappaB pathways. *Mol. Cell* **14,** 303–317 (2004).

504. Sun, J. & Lin, X. Beta-arrestin 2 is required for lysophosphatidic acid-induced NF-kappaB activation. *Proc. Natl. Acad. Sci. U.S.A.* **105,** 17085–17090 (2008).

505. Cianfrocca, R. *et al.* β-Arrestin 1 is required for endothelin-1-induced NF-κB activation in ovarian cancer cells. *Life Sci.* **118,** 179–184 (2014).

506. Kang, J. *et al.* A nuclear function of beta-arrestin1 in GPCR signaling: regulation of histone acetylation and gene transcription. *Cell* **123,** 833–847 (2005).
507. Wang, Y. *et al.* Association of beta-arrestin and TRAF6 negatively regulates Toll-like receptor-interleukin 1 receptor signaling. *Nature Immunology* **7,** 139–147 (2006).
508. Fan, H. *et al.* Beta-arrestin 2 negatively regulates sepsis-induced inflammation. *Immunology* **130,** 344–351 (2010).
509. Cheung, R. *et al.* An arrestin-dependent multi-kinase signaling complex mediates MIP-1beta/CCL4 signaling and chemotaxis of primary human macrophages. *Journal of Leukocyte Biology* **86,** 833–845 (2009).
510. Zhuang, L.-N., Hu, W.-X., Xin, S.-M., Zhao, J. & Pei, G. Beta-arrestin-1 protein represses adipogenesis and inflammatory responses through its interaction with peroxisome proliferator-activated receptor-gamma (PPARgamma). *J. Biol. Chem.* **286,** 28403–28413 (2011).
511. Zhuang, L.-N. *et al.* Beta-arrestin-1 protein represses diet-induced obesity. *J. Biol. Chem.* **286,** 28396–28402 (2011).
512. Luan, B. *et al.* Deficiency of a beta-arrestin-2 signal complex contributes to insulin resistance. *Nature* **457,** 1146–1149 (2009).
513. Zhu, L. *et al.* Hepatic β-arrestin 2 is essential for maintaining euglycemia. *J. Clin. Invest.* **127,** 2941–2945 (2017).
514. Litonjua, A. A. *et al.* Very important pharmacogene summary ADRB2. *Pharmacogenetics and Genomics* **20,** 64–69 (2010).
515. Green, S. A., Turki, J., Innis, M. & Liggett, S. B. Amino-terminal polymorphisms of the human beta 2-adrenergic receptor impart distinct agonist-promoted regulatory properties. *Biochemistry* **33,** 9414–9419 (1994).
516. Green, S. A., Turki, J., Bejarano, P., Hall, I. P. & Liggett, S. B. Influence of beta 2-adrenergic receptor genotypes on signal transduction in human airway smooth muscle cells. *Am. J. Respir. Cell Mol. Biol.* **13,** 25–33 (1995).
517. Green, S. A., Cole, G., Jacinto, M., Innis, M. & Liggett, S. B. A polymorphism of the human beta 2-adrenergic receptor within the fourth transmembrane domain alters ligand binding and functional properties of the receptor. *Journal of Biological Chemistry* **268,** 23116–23121 (1993).
518. Gjesing, A. P. *et al.* Studies of the associations between functional beta2-adrenergic receptor variants and obesity, hypertension and type 2 diabetes in 7,808 white subjects. *Diabetologia* **50,** 563–568 (2007).
519. Chang, T.-J. *et al.* The Arg16Gly polymorphism of human beta2-adrenoreceptor is associated with type 2 diabetes in Taiwanese people. *Clin. Endocrinol. (Oxf)* **57,** 685–690 (2002).
520. Pereira, A. C. *et al.* Beta2 adrenoceptor functional gene variants, obesity, and blood

pressure level interactions in the general population. *Hypertension* **42,** 685–692 (2003).

521. Hayakawa, T. *et al.* Gln27Glu and Arg16Gly polymorphisms of the beta2-adrenergic receptor gene are not associated with obesity in Japanese men. *Metab. Clin. Exp.* **49,** 1215–1218 (2000).

522. Ishiyama-Shigemoto, S., Yamada, K., Yuan, X., Ichikawa, F. & Nonaka, K. Association of polymorphisms in the beta2-adrenergic receptor gene with obesity, hypertriglyceridaemia, and diabetes mellitus. *Diabetologia* **42,** 98–101 (1999).

523. Ikarashi, T. *et al.* Genotype Gly/Gly of the Arg16Gly polymorphism of the beta2-adrenergic receptor is associated with elevated fasting serum insulin concentrations, but not with acute insulin response to glucose, in type 2 diabetic patients. *Diabetes Res. Clin. Pract.* **63,** 11–18 (2004).

524. Masuo, K. *et al.* Beta2-adrenoceptor polymorphisms relate to insulin resistance and sympathetic overactivity as early markers of metabolic disease in nonobese, normotensive individuals. *Am. J. Hypertens.* **18,** 1009–1014 (2005).

525. Wu, H.-M. *et al.* [Analysis of beta2-adrenergic receptor gene (beta2AR) Arg16Gly polymorphism in patients with endogenous hypertriglyceridemia in Chinese population]. *Zhonghua Yi Xue Yi Chuan Xue Za Zhi* **25,** 50–54 (2008).

526. Yamada, K. *et al.* Polymorphism in the 5'-leader cistron of the beta2-adrenergic receptor gene associated with obesity and type 2 diabetes. *J. Clin. Endocrinol. Metab.* **84,** 1754–1757 (1999).

527. Pinelli, M. *et al.* Beta2-adrenergic receptor and UCP3 variants modulate the relationship between age and type 2 diabetes mellitus. *BMC Med. Genet.* **7,** 85 (2006).

528. Carlsson, M., Orho-Melander, M., Hedenbro, J. & Groop, L. C. Common variants in the beta2-(Gln27Glu) and beta3-(Trp64Arg)--adrenoceptor genes are associated with elevated serum NEFA concentrations and type II diabetes. *Diabetologia* **44,** 629–636 (2001).

529. Kim, S.-H. *et al.* Significance of beta2-adrenergic receptor gene polymorphism in obesity and type 2 diabetes mellitus in Korean subjects. *Metab. Clin. Exp.* **51,** 833–837 (2002).

530. Large, V. *et al.* Human beta-2 adrenoceptor gene polymorphisms are highly frequent in obesity and associate with altered adipocyte beta-2 adrenoceptor function. *J. Clin. Invest.* **100,** 3005–3013 (1997).

531. Lange, L. A. *et al.* Association of adipose tissue deposition and beta-2 adrenergic receptor variants: the IRAS family study. *International Journal of Obesity* **29,** 449–457 (2005).

532. Corbalán, M. S., Marti, A., Forga, L., Martínez-González, M. A. & Martínez, J. A. Beta(2)-adrenergic receptor mutation and abdominal obesity risk: effect modification

by gender and HDL-cholesterol. *Eur J Nutr* **41,** 114–118 (2002).

533. Jalba, M. S., Rhoads, G. G. & Demissie, K. Association of codon 16 and codon 27 beta 2-adrenergic receptor gene polymorphisms with obesity: a meta-analysis. *Obesity (Silver Spring)* **16,** 2096–2106 (2008).

534. Thomsen, M., Dahl, M., Tybjærg-Hansen, A. & Nordestgaard, B. G. β2-adrenergic receptor Thr164Ile polymorphism, obesity, and diabetes: comparison with FTO, MC4R, and TMEM18 polymorphisms in more than 64,000 individuals. *J. Clin. Endocrinol. Metab.* **97,** E1074–9 (2012).

535. Clausen, B. E., Burkhardt, C., Reith, W., Renkawitz, R. & Förster, I. Conditional gene targeting in macrophages and granulocytes using LysMcre mice. *Transgenic Res.* **8,** 265–277 (1999).

536. Hinoi, E. *et al.* The sympathetic tone mediates leptin's inhibition of insulin secretion by modulating osteocalcin bioactivity. *The Journal of Cell Biology* **183,** 1235–1242 (2008).

537. Imtiyaz, H. Z. *et al.* Hypoxia-inducible factor 2alpha regulates macrophage function in mouse models of acute and tumor inflammation. *J. Clin. Invest.* **120,** 2699–2714 (2010).

538. Weir, J. B. *New methods for calculating metabolic rate with special reference to protein metabolism. 1949. Nutrition (Burbank, Los Angeles County, Calif.)* **6,** 213–221 (1990).

539. Huynh, F. K., Green, M. F., Koves, T. R. & Hirschey, M. D. Measurement of fatty acid oxidation rates in animal tissues and cell lines. *Meth. Enzymol.* **542,** 391–405 (2014).

540. FOLCH, J., LEES, M. & SLOANE STANLEY, G. H. A simple method for the isolation and purification of total lipides from animal tissues. *Journal of Biological Chemistry* **226,** 497–509 (1957).

541. Greer, M. S., Zhou, T. & Weselake, R. J. A novel assay of DGAT activity based on high temperature GC/MS of triacylglycerol. *Lipids* **49,** 831–838 (2014).

542. Christoforou, A. *et al.* A draft map of the mouse pluripotent stem cell spatial proteome. *Nat Commun* **7,** 8992 (2016).

543. Huber, W., Heydebreck, von, A., Sültmann, H., Poustka, A. & Vingron, M. Variance stabilization applied to microarray data calibration and to the quantification of differential expression. *Bioinformatics* **18 Suppl 1,** S96–104 (2002).

544. Ritchie, M. E. *et al.* limma powers differential expression analyses for RNA-sequencing and microarray studies. *Nucleic Acids Res.* **43,** e47–e47 (2015).

545. Väremo, L., Nielsen, J. & Nookaew, I. Enriching the gene set analysis of genome-wide data by incorporating directionality of gene expression and combining statistical hypotheses and methods. *Nucleic Acids Res.* **41,** 4378–4391 (2013).

546. Cubuk, C. *et al.* Differential metabolic activity and discovery of therapeutic targets using summarized metabolic pathway models. *bioRxiv* 367334 (2018).

doi:10.1101/367334

547. Gillet, C. *et al.* Oleate Abrogates Palmitate-Induced Lipotoxicity and Proinflammatory Response in Human Bone Marrow-Derived Mesenchymal Stem Cells and Osteoblastic Cells. *Endocrinology* **156,** 4081–4093 (2015).

548. Tabas, I. & Kitakaze, M. The Role of Endoplasmic Reticulum Stress in the Progression of Atherosclerosis. *Circulation Research* **107,** 839–850 (2010).

549. Lund-Katz, S. & Phillips, M. C. High density lipoprotein structure-function and role in reverse cholesterol transport. *Subcell. Biochem.* **51,** 183–227 (2010).

550. Schmitz, G., Beuck, M., Fischer, H., Nowicka, G. & Robenek, H. Regulation of phospholipid biosynthesis during cholesterol influx and high density lipoprotein-mediated cholesterol efflux in macrophages. *The Journal of Lipid Research* **31,** 1741–1752 (1990).

551. Ghosn, E. E. B. *et al.* Two physically, functionally, and developmentally distinct peritoneal macrophage subsets. *Proc. Natl. Acad. Sci. U.S.A.* **107,** 2568–2573 (2010).

552. Huang, S. *et al.* Saturated fatty acids activate TLR-mediated proinflammatory signaling pathways. *J. Lipid Res.* **53,** 2002–2013 (2012).

553. Clemons-Miller, A. R., Cox, G. W., Suttles, J. & Stout, R. D. LPS Stimulation of TNF-Receptor Deficient Macrophages: a Differential Role for TNF-α Autocrine Signaling in the Induction of Cytokine and Nitric Oxide Production. *Immunobiology* **202,** 477–492 (2000).

554. Shindou, H. & Shimizu, T. Acyl-CoA:lysophospholipid acyltransferases. *Journal of Biological Chemistry* **284,** 1–5 (2009).

555. Akagi, S. *et al.* Lysophosphatidylcholine acyltransferase 1 protects against cytotoxicity induced by polyunsaturated fatty acids. *FASEB J.* **30,** 2027–2039 (2016).

556. Rong, X. *et al.* ER phospholipid composition modulates lipogenesis during feeding and in obesity. *J. Clin. Invest.* **127,** (2017).

557. Chakraborty, M. *et al.* Myeloid cell–specific serine palmitoyltransferase subunit 2 haploinsufficiency reduces murine atherosclerosis. *The Journal of Clinical Investigation* **123,** 1784–1797 (2013).

558. Camell, C. D. *et al.* Macrophage-specific de Novo Synthesis of Ceramide Is Dispensable for Inflammasome-driven Inflammation and Insulin Resistance in Obesity. *J. Biol. Chem.* **290,** 29402–29413 (2015).

559. Tan, C. Y. *et al.* Adipose tissue fatty acid chain length and mono-unsaturation increases with obesity and insulin resistance. *Scientific Reports 2015 5:null* **5,** srep18366 (2015).

560. RICQUIER, D. *et al.* Expression of Uncoupling Protein Messenger-Rna in Thermogenic or Weakly Thermogenic Brown Adipose-Tissue - Evidence for a Rapid Beta-Adrenoceptor-Mediated and Transcriptionally Regulated Step During Activation

of Thermogenesis. *Journal of Biological Chemistry* **261,** 13905–13910 (1986).

561. Thorp, A. A. & Schlaich, M. P. Relevance of Sympathetic Nervous System Activation in Obesity and Metabolic Syndrome. *J Diabetes Res* **2015,** 341583–11 (2015).

562. Collins, S., Daniel, K. W. & Rohlfs, E. M. Depressed expression of adipocyte beta-adrenergic receptors is a common feature of congenital and diet-induced obesity in rodents. *Int. J. Obes. Relat. Metab. Disord.* **23,** 669–677 (1999).

563. Cryer, P. E., Rizza, R. A., Haymond, M. W. & Gerich, J. E. Epinephrine and norepinephrine are cleared through beta-adrenergic, but not alpha-adrenergic, mechanisms in man. *Metab. Clin. Exp.* **29,** 1114–1118 (1980).

564. Clutter, W. E., Bier, D. M., Shah, S. D. & Cryer, P. E. Epinephrine plasma metabolic clearance rates and physiologic thresholds for metabolic and hemodynamic actions in man. *J. Clin. Invest.* **66,** 94–101 (1980).

565. Liu, X. *et al.* Mechanism of intracellular allosteric β2AR antagonist revealed by X-ray crystal structure. *Nature* **548,** 480–484 (2017).

566. Bruno, N. E. *et al.* Creb coactivators direct anabolic responses and enhance performance of skeletal muscle. *The EMBO Journal* **33,** 1027–1043 (2014).

567. Hodenberg, von, E., Khoo, J. C., Jensen, D., Witztum, J. L. & Steinberg, D. Mobilization of stored triglycerides from macrophages as free fatty acids. *Arteriosclerosis* **4,** 630–635 (1984).

568. Ye, R. D. beta-Adrenergic agonists regulate NF-kappaB activation through multiple mechanisms. *Am. J. Physiol. Lung Cell Mol. Physiol.* **279,** L615–7 (2000).

569. Noh, H. *et al.* Beta 2-adrenergic receptor agonists are novel regulators of macrophage activation in diabetic renal and cardiovascular complications. *Kidney Int.* **92,** 101–113 (2017).

570. Yi, C.-X., la Fleur, S. E., Fliers, E. & Kalsbeek, A. The role of the autonomic nervous liver innervation in the control of energy metabolism. *Biochim. Biophys. Acta* **1802,** 416–431 (2010).

571. Chu, C. A. *et al.* The direct effects of catecholamines on hepatic glucose production occur via alpha(1)- and beta(2)-receptors in the dog. *Am. J. Physiol. Endocrinol. Metab.* **279,** E463–73 (2000).

572. Ishii-Iwamoto, E. L., Ferrarese, M. L., Constantin, J., Salgueiro-Pagadigorria, C. & Bracht, A. Effects of norepinephrine on the metabolism of fatty acids with different chain lengths in the perfused rat liver. *Mol. Cell. Biochem.* **205,** 13–23 (2000).

573. Brès, J., Clauzel, A. M., Pistre, M. C., Rachmat, H. & Bressolle, F. [Metabolism of beta-adrenergic substances. Therapeutic implications]. *Bull Eur Physiopathol Respir* **21,** 19s–34s (1985).

574. Zhao, C., Isenberg, J. S. & Popel, A. S. Transcriptional and Post-Transcriptional Regulation of Thrombospondin-1 Expression: A Computational Model. *PLoS Comput.*

Biol. **13,** e1005272 (2017).

575. Koshiji, M. *et al.* HIF-1alpha induces cell cycle arrest by functionally counteracting Myc. *The EMBO Journal* **23,** 1949–1956 (2004).

576. Koshiji, M. *et al.* HIF-1alpha induces genetic instability by transcriptionally downregulating MutSalpha expression. *Mol. Cell* **17,** 793–803 (2005).

577. Cheong, H. I. *et al.* Hypoxia sensing through β-adrenergic receptors. *JCI Insight* **1,** e90240 (2016).

578. Kung, A. L. *et al.* Small molecule blockade of transcriptional coactivation of the hypoxia-inducible factor pathway. *Cancer Cell* **6,** 33–43 (2004).

579. Ryan, H. E. *et al.* Hypoxia-inducible factor-1alpha is a positive factor in solid tumor growth. *Cancer Res.* **60,** 4010–4015 (2000).

580. Takeda, N. *et al.* Differential activation and antagonistic function of HIF-{alpha} isoforms in macrophages are essential for NO homeostasis. *Genes Dev.* **24,** 491–501 (2010).

581. Labrousse-Arias, D. *et al.* HIF-2α-mediated induction of pulmonary thrombospondin-1 contributes to hypoxia-driven vascular remodelling and vasoconstriction. *Cardiovasc. Res.* **109,** 115–130 (2016).

582. Kumar, R. *et al.* TGF-β activation by bone marrow-derived thrombospondin-1 causes Schistosoma- and hypoxia-induced pulmonary hypertension. *Nat Commun* **8,** 15494 (2017).

583. Gruber, M. *et al.* Acute postnatal ablation of Hif-2alpha results in anemia. *Proc. Natl. Acad. Sci. U.S.A.* **104,** 2301–2306 (2007).

584. Saraiva, M. & O'Garra, A. The regulation of IL-10 production by immune cells. *Nat. Rev. Immunol.* **10,** 170–181 (2010).

585. Avni, D., Ernst, O., Philosoph, A. & Zor, T. Role of CREB in modulation of TNFalpha and IL-10 expression in LPS-stimulated RAW264.7 macrophages. *Mol. Immunol.* **47,** 1396–1403 (2010).

586. Suberville, S. *et al.* Regulation of interleukin-10 production by beta-adrenergic agonists. *Eur. J. Immunol.* **26,** 2601–2605 (1996).

587. Gray, J. G. *et al.* A CRE/ATF-like site in the upstream regulatory sequence of the human interleukin 1 beta gene is necessary for induction in U937 and THP-1 monocytic cell lines. *Molecular and Cellular Biology* **13,** 6678–6689 (1993).

588. Shenoy, S. K. *et al.* beta-arrestin-dependent, G protein-independent ERK1/2 activation by the beta2 adrenergic receptor. *Journal of Biological Chemistry* **281,** 1261–1273 (2006).

589. Koenis, D. S. *et al.* Nuclear Receptor Nur77 Limits the Macrophage Inflammatory Response through Transcriptional Reprogramming of Mitochondrial Metabolism. *CellReports* **24,** 2127–2140.e7 (2018).

590. Ryan, H. E., Lo, J. & Johnson, R. S. HIF-1α is required for solid tumor formation and embryonic vascularization. *The EMBO Journal* **17,** 3005–3015 (1998).

591. Nath, B. *et al.* Hepatocyte-specific hypoxia-inducible factor-1α is a determinant of lipid accumulation and liver injury in alcohol-induced steatosis in mice. *Hepatology* **53,** 1526–1537 (2011).

592. Maier, A. *et al.* Hypoxia-inducible protein 2 Hig2/Hilpda mediates neutral lipid accumulation in macrophages and contributes to atherosclerosis in apolipoprotein E-deficient mice. *FASEB J.* **31,** 4971–4984 (2017).

593. Ebert, B. L. & Bunn, H. F. Regulation of transcription by hypoxia requires a multiprotein complex that includes hypoxia-inducible factor 1, an adjacent transcription factor, and p300/CREB binding protein. *Molecular and Cellular Biology* **18,** 4089–4096 (1998).

594. Palsson-McDermott, E. M. *et al.* Pyruvate kinase M2 regulates Hif-1α activity and IL-1β induction and is a critical determinant of the warburg effect in LPS-activated macrophages. *Cell Metab.* **21,** 65–80 (2015).

595. Luo, W. *et al.* Pyruvate kinase M2 is a PHD3-stimulated coactivator for hypoxia-inducible factor 1. *Cell* **145,** 732–744 (2011).

596. Ruas, J. L. *et al.* Complex regulation of the transactivation function of hypoxia-inducible factor-1 alpha by direct interaction with two distinct domains of the CREB-binding protein/p300. *J. Biol. Chem.* **285,** 2601–2609 (2010).

597. Kim, R. H. *et al.* SNIP1 inhibits NF-kappa B signaling by competing for its binding to the C/H1 domain of CBP/p300 transcriptional co-activators. *Journal of Biological Chemistry* **276,** 46297–46304 (2001).

598. Kamei, Y. *et al.* A CBP integrator complex mediates transcriptional activation and AP-1 inhibition by nuclear receptors. *Cell* **85,** 403–414 (1996).

599. Hottiger, M. O., Felzien, L. K. & Nabel, G. J. Modulation of cytokine-induced HIV gene expression by competitive binding of transcription factors to the coactivator p300. *The EMBO Journal* **17,** 3124–3134 (1998).

600. Nettles, K. W. *et al.* CBP Is a dosage-dependent regulator of nuclear factor-kappaB suppression by the estrogen receptor. *Mol. Endocrinol.* **22,** 263–272 (2008).

601. Bricambert, J. *et al.* Salt-inducible kinase 2 links transcriptional coactivator p300 phosphorylation to the prevention of ChREBP-dependent hepatic steatosis in mice. *J. Clin. Invest.* **120,** 4316–4331 (2010).

602. Benhamed, F. *et al.* The lipogenic transcription factor ChREBP dissociates hepatic steatosis from insulin resistance in mice and humans. *J. Clin. Invest.* **122,** 2176–2194 (2012).

603. Fujisaka, S. *et al.* Adipose tissue hypoxia induces inflammatory M1 polarity of macrophages in an HIF-1α-dependent and HIF-1α-independent manner in obese mice. *Diabetologia* **56,** 1403–1412 (2013).

604. Cole, S. W., Nagaraja, A. S., Lutgendorf, S. K., Green, P. A. & Sood, A. K. Sympathetic nervous system regulation of the tumour microenvironment. *Nat. Rev. Cancer* **15,** 563–572 (2015).
605. Zahalka, A. H. *et al.* Adrenergic nerves activate an angio-metabolic switch in prostate cancer. *Science* **358,** 321–326 (2017).
606. Chang, C.-H. *et al.* Metabolic Competition in the Tumor Microenvironment Is a Driver of Cancer Progression. *Cell* **162,** 1229–1241 (2015).
607. Chanmee, T., Ontong, P., Konno, K. & Itano, N. Tumor-associated macrophages as major players in the tumor microenvironment. *Cancers (Basel)* **6,** 1670–1690 (2014).
608. Murphy-Ullrich, J. E. & Poczatek, M. Activation of latent TGF-beta by thrombospondin-1: mechanisms and physiology. *Cytokine Growth Factor Rev.* **11,** 59–69 (2000).
609. Christopherson, K. S. *et al.* Thrombospondins are astrocyte-secreted proteins that promote CNS synaptogenesis. *Cell* **120,** 421–433 (2005).
610. Risher, W. C. & Eroglu, C. Thrombospondins as key regulators of synaptogenesis in the central nervous system. *Matrix Biol.* **31,** 170–177 (2012).
611. Wang, J.-L. *et al.* Plasma thrombospondin-1 and clinical outcomes in traumatic brain injury. *Acta Neurol. Scand.* **134,** 189–196 (2016).
612. Dunn-Meynell, A. A., Hassanain, M. & Levin, B. E. Norepinephrine and traumatic brain injury: a possible role in post-traumatic edema. *Brain Res.* **800,** 245–252 (1998).
613. Cheng, C. *et al.* Thrombospondin-1 Gene Deficiency Worsens the Neurological Outcomes of Traumatic Brain Injury in Mice. *Int J Med Sci* **14,** 927–936 (2017).
614. Blake, S. M. *et al.* Thrombospondin-1 binds to ApoER2 and VLDL receptor and functions in postnatal neuronal migration. *The EMBO Journal* **27,** 3069–3080 (2008).
615. Hoffman, J. R. & O'Shea, K. S. Thrombospondin expression in nerve regeneration I. Comparison of sciatic nerve crush, transection, and long-term denervation. *Brain Res. Bull.* **48,** 413–420 (1999).
616. Zorov, D. B., Juhaszova, M. & Sollott, S. J. Mitochondrial reactive oxygen species (ROS) and ROS-induced ROS release. *Physiol. Rev.* **94,** 909–950 (2014).
617. Cao, X., Wei, Z., Gabriel, G. G., Li, X. & Mousseau, D. D. Calcium-sensitive regulation of monoamine oxidase-A contributes to the production of peroxyradicals in hippocampal cultures: implications for Alzheimer disease-related pathology. *BMC Neurosci* **8,** 73 (2007).
618. Famulski, K. S., Nałecz, M. J. & Wojtczak, L. Phosphorylation of mitochondrial membrane proteins: effect of the surface potential on monoamine oxidase. *FEBS Lett.* **157,** 124–128 (1983).
619. Matsuo, Y. *et al.* Thrombospondin 1 as a novel biological marker of obesity and metabolic syndrome. *Metab. Clin. Exp.* **64,** 1490–1499 (2015).
620. Kong, P. *et al.* Thrombospondin-1 regulates adiposity and metabolic dysfunction in

diet-induced obesity enhancing adipose inflammation and stimulating adipocyte proliferation. *Am. J. Physiol. Endocrinol. Metab.* **305,** E439–50 (2013).

621. Li, Y., Tong, X., Rumala, C., Clemons, K. & Wang, S. Thrombospondin1 deficiency reduces obesity-associated inflammation and improves insulin sensitivity in a diet-induced obese mouse model. *PLoS ONE* **6,** e26656 (2011).
622. Cook, A. D., Braine, E. L. & Hamilton, J. A. The phenotype of inflammatory macrophages is stimulus dependent: implications for the nature of the inflammatory response. *The Journal of Immunology* **171,** 4816–4823 (2003).
623. Boutens, L. *et al.* Unique metabolic activation of adipose tissue macrophages in obesity promotes inflammatory responses. *Diabetologia* **2,** e30–12 (2018).
624. Kratz, M. *et al.* Metabolic dysfunction drives a mechanistically distinct proinflammatory phenotype in adipose tissue macrophages. *Cell Metab.* **20,** 614–625 (2014).
625. Marino, S., Logan, J. G., Mellis, D. & Capulli, M. Generation and culture of osteoclasts. *Bonekey Rep* **3,** 570 (2014).
626. Nagasaki, H. *et al.* Inflammatory changes in adipose tissue enhance expression of GPR84, a medium-chain fatty acid receptor: TNFα enhances GPR84 expression in adipocytes. *FEBS Lett.* **586,** 368–372 (2012).
627. Furuhashi, M. *et al.* Adipocyte/macrophage fatty acid-binding proteins contribute to metabolic deterioration through actions in both macrophages and adipocytes in mice. *J. Clin. Invest.* **118,** 2640–2650 (2008).
628. Nitta, C. F. & Orlando, R. A. Crosstalk between Immune Cells and Adipocytes Requires Both Paracrine Factors and Cell Contact to Modify Cytokine Secretion. *PLoS ONE* **8,** (2013).
629. Lumeng, C. N., Deyoung, S. M. & Saltiel, A. R. Macrophages block insulin action in adipocytes by altering expression of signaling and glucose transport proteins. *Am. J. Physiol. Endocrinol. Metab.* **292,** E166–E174 (2007).
630. Sárvári, A. K. *et al.* Interaction of differentiated human adipocytes with macrophages leads to trogocytosis and selective IL-6 secretion. *Cell Death Dis* **6,** e1613–e1613 (2015).
631. Xie, L., Ortega, M. T., Mora, S. & Chapes, S. K. Interactive Changes between Macrophages and Adipocytes. *Clin. Vaccine Immunol.* **17,** 651–659 (2010).
632. Burak, M. F. *et al.* Development of a therapeutic monoclonal antibody that targets secreted fatty acid-binding protein aP2 to treat type 2 diabetes. *Sci Transl Med* **7,** 319ra205–319ra205 (2015).
633. Jain, N. K., Mishra, V. & Mehra, N. K. Targeted drug delivery to macrophages. *Expert Opin Drug Deliv* **10,** 353–367 (2013).
634. Rinne, P. *et al.* Melanocortin 1 Receptor Signaling Regulates Cholesterol Transport in Macrophages. *Circulation* **136,** 83–97 (2017).